





Université de Montréal

**Manganese, Copper and Zinc catalysts in *rac*-lactide polymerization**

par Pargol Daneshmandkashani

Département de Chimie  
Faculté des Arts et des Sciences

Thèse présentée  
en vue de l'obtention du grade de  
*Philosophiæ Doctor* (Ph.D)  
en chimie

Juillet 2018

© Pargol Daneshmandkashani, 2018



## Abstract

Diiminopyrrolide ligands bearing two chiral *N*-methylbenzyl substituents were prepared by a condensation reaction of the 1*H*-pyrrole-2,5-dicarbaldehyde and *S*-methylbenzylamine. Reaction of the ligand with Cu(OMe)<sub>2</sub> in the presence of 2 equiv of pyridylmethanol or dimethylaminoethanol yielded the dimeric Cu(II) catalysts L<sub>2</sub>Cu<sub>2</sub>(μ-OR)<sub>2</sub>. Application of these complexes in *rac*-lactide polymerization gave isotactic ( $P_m = 0.73$ ) and atactic ( $P_m = 0.50$ ) PLA, respectively. Kinetic studies conducted on these two complexes indicated the presence of two different active species. GPC results obtained for the copper catalyst containing two pyridylmethoxide bridges indicate the growth of only one chain per dimer (thus one alkoxide remains as a spectator ligand), while in the complex bearing two dimethylaminoethoxides both alkoxides inserted lactide. A ligand mediated chain-end control mechanism, which is accomplished by the epimerization of the catalytic site based on the chirality of the last inserted unit, is proposed. The presence of a coordinated and an uncoordinated imine “arms” facilitates epimerization since it requires only dissociation/re-coordination. The effects of the ligand framework (steric bulk) on activity and stereocontrol of the catalyst were investigated by variation of the imine substituents to benzyl, bromobenzyl, xylyl, diphenylmethyl and cyclohexyl. Benzyl, bromobenzyl and cyclohexyl were the only imine substituents providing the desired dimeric copper catalyst with pyridylmethoxide. Benzyl and cyclohexyl substituted complexes produced isotactic PLA. Substituent chirality was thus not required for stereocontrol. The bromobenzyl-substituted complex was the only one providing an atactic catalytic site with both imines coordinated and produced atactic PLA.

Monoiminopyrrolide copper(II) complexes with pyridylmethoxide ligands were prepared with naphthyl, diphenylmethyl, xylyl and 2,6-diisopropylphenyl *N*-substituents. They showed reduced stereocontrol which is assumed to be due to slower epimerization (rotation around the Cu-pyrrole bond is now required). All complexes provided isotactic PLA, but the stereocontrol did not surpass that of the

diiminopyrrolide complexes. Substitution of the 5-position of the pyrrole by chloride led to loss of activity while a methyl substituent provided atactic PLA.

Phenoxy-imine ligands were prepared by a condensation reaction of the salicylaldehyde derivative and the desired amine (benzyl, cyclohexyl, xylyl and diphenylmethyl). Their complexes bearing either dimethylaminoethoxide or pyridylmethoxide ligands were structurally similar to the iminopyrrolide complexes. All complexes were active in *rac*-lactide polymerization, but although GPC results indicated the growth of only one chain per dimer for the pyridylmethoxide complexes and thus indicated a similar active species, only atactic PLA was produced.

A zinc analog of the isotactic copper complex with the *N,N'*-bis(methylbenzyl)diiminopyrrolide ligand was prepared and structurally characterized, but produced heterotactic PLA ( $P_r = 0.75$ ). Zinc complexes with 2,4-di-*tert*-butyl-6-aminomethyl-phenol ligands with amino = *N,N,N',N'*-tetramethyldiethylenetriamine or di-(2-picolyl)amine substituents were prepared and structurally characterized. They showed a chiral tetrahedral zinc center with one coordinated and one uncoordinated for the ethylenediamine substituents and a five-coordinated zinc center with both amino groups coordinated for picolylamine. NMR investigations indicated fast epimerization of the metal center on the NMR time scale. Both zinc complexes are highly active in lactide polymerization and reach full conversion in only a few minutes, placing them among the most active zinc catalysts known. Slightly isotactic PLA ( $P_m$  up to 0.6) was obtained for both complexes, showing in proof-of-principle the advantage of introducing catalytic site epimerization. The picolylamine-substituted complex showed a suppression of stereocontrol at high catalyst concentrations, which is not fully understood.

Bulk polymerization of lactide was conducted with manganese diamino-diphenolate complexes following a coordination-insertion mechanism. Their activity was low and only heterotactic PLA was obtained. Tri/tetradentate phenoxy-imine copper complexes were likewise used in bulk polymerization, following an activated monomer mechanism with benzyl alcohol as co-initiator. Polymerizations were stable in air and in the presence of water or acetic acid, but polymer molecular weight

control was low with evidence for facile intramolecular transesterification reactions. Surprisingly high heterotacticities were obtained in molten monomer ( $P_r$  up to 0.85), but there was no evidence that the additional basic site on the ligand participates in stereocontrol.

**Keywords:** Catalysis, Copper complexes, Manganese complexes, polylactic acid, lactide polymerization, mechanism, isotactic stereocontrol.





## Résumé

Des ligands diiminopyrrolides portant deux substituants *N*-méthylbenzyle chiraux ont été préparés par condensation du 1*H*-pyrrole-2,5-dicarbaldéhyde et de la *S*-méthylbenzylamine. La réaction de ce ligand avec du Cu(OMe)<sub>2</sub> en présence de 2 équivalents de pyridylméthanol ou de diméthylaminoéthanol a donné les catalyseurs dimériques de Cu(II) L<sub>2</sub>Cu<sub>2</sub>(μ-OR)<sub>2</sub>. L'application de ces complexes dans la polymérisation du *rac*-lactide a permis d'obtenir respectivement des PLA isotactiques ( $P_m = 0,73$ ) et atactiques ( $P_m = 0,50$ ). Les études cinétiques menées sur ces deux complexes ont indiqué la présence de deux espèces actives différentes. Les résultats de GPC obtenus pour le catalyseur cuivrique contenant deux pyridylméthoxyde pontant indiquent la croissance d'une seule chaîne par dimère (un des alcoolates reste en tant que ligand spectateur), alors que dans le cas du complexe portant deux diméthylaminoéthoxydes, les deux alcoolates attaquent le lactide. Un mécanisme de "ligand mediated chain-end control", se faisant par l'épimérisation du site catalytique par rapport à la chiralité de la dernière molécule de lactide insérée, est proposé. La présence d'un "bras" iminé coordonné et non coordonné facilite l'épimérisation car celle-ci ne nécessite qu'une dissociation / ré-coordination. Les effets du ligand (encombrement stérique) sur l'activité et le stéréocontrôle du catalyseur ont été étudiés par utilisations de divers substituants sur l'imine : benzyle, bromobenzyle, xylyle, diphenylméthyle et cyclohexyle. Les substituants imino-benzyle, -bromobenzyle et -cyclohexyle ont été les seuls fournissant les catalyseurs de cuivre dimérique désiré avec le pyridylméthoxyde. Les complexes portant les groupes benzyle et cyclohexyle ont produit du PLA isotactique. La chiralité portée par le ligand n'était donc pas requise pour le stéréocontrôle. Le complexe bromobenzyl-substitué a été le seul à fournir un site catalytique achirale avec les deux imines coordonnées et produit un PLA atactique.

Des complexes monoiminopyrrolidiques de cuivre(II) avec des ligands pyridylméthoxydes ont été préparés avec des substituants imino *N*-naphtyle, -diphenylméthyle, -xylyle et -2,6-diisopropylphényle. Ils ont démontré un stéréocontrôle réduit, qui est présumé due à une épimérisation plus lente (une rotation autour de la liaison Cu-pyrrole est désormais nécessaire). Tous les complexes

ont fourni des PLA isotactiques, mais le stéréocontrôle obtenu n'a pas dépassé celui des complexes diiminopyrrolidiques. La substitution de la position 5 du pyrrole par un Chlore conduit à une perte d'activité tandis qu'un substituant méthyle fournit un PLA atactique.

Les ligands phénoxy-imine ont été préparés par condensation de dérivée de salicyldaldéhydes et d'une amine (benzyle, cyclohexyle, xylyle et diphenylméthyle). Leurs complexes de Cuivre(II) portant soit un ligand diméthylaminoéthoxyde ou pyridylméthoxyde étaient structurellement similaires aux complexes iminopyrrolidiques. Tous les complexes étaient actifs dans la polymérisation du *rac*-lactide, mais bien que les résultats GPC indiquaient la croissance d'une seule chaîne par dimère pour les complexes de pyridylméthoxyde et ainsi une espèce active similaire, seul du PLA atactique était produit.

Un analogue de zinc du complexe de cuivre isotactique avec le ligand N,N'-bis (méthylbenzyl-diiminopyrrolide) a été préparé et structurellement caractérisé, mais a produit du PLA hétérotactique ( $P_r = 0,75$ ). Les complexes de zinc de 2,4-di-tert-butyl-6-aminométhylphénol, où les substituants amino sont le N,N,N',N'-tétraméthyl-diéthylènetriamine ou le di-(2-picolyl)amine ont été préparés et structurellement caractérisés. Ils ont montré un centre zincique tétraédrique chiral avec un "bras" coordonné et un non coordonné pour l'éthylènediamine et un centre zincique pentacoordiné avec les deux groupes picolylamine. Les analyses par RMN ont indiqué une épimérisation rapide du centre métallique, sur l'échelle de temps de la RMN.

Les deux complexes de zinc sont hautement actifs dans la polymérisation du lactide et atteignent une conversion complète en seulement quelques minutes, les plaçant parmi les catalyseurs de zinc les plus actifs connus à ce jour. Un PLA légèrement isotactique ( $P_m$  jusqu'à 0,6) a été obtenu pour les deux complexes, démontrant en principe l'avantage de l'introduction d'un site catalytique capable de s'épimériser. Le complexe substitué par le ligand picolylaminique présentait une suppression du stéréocontrôle à des concentrations élevées de catalyseur, qui n'est pas entièrement compris.

La polymérisation en masse du lactide a été réalisée avec des complexes de manganèse diamino-diphénolate suivant un mécanisme de coordination-insertion. Leur activité était faible et seul un PLA hétérotactique a été obtenu. Des complexes tri / tétradentate de phénoxy-imine-cuivrique ont également été utilisés dans la polymérisation en masse, en suivant un mécanisme de monomère activé et utilisant de l'alcool benzylique en tant que co-initiateur. Les polymérisations étaient stables dans l'air et en présence d'eau ou d'acide acétique, mais le contrôle du poids moléculaire du polymère était faible du à des réactions de transestérification intramoléculaire aisées. Des PLA hétérotactiques étonnamment élevées ont été obtenues dans le monomère fondu ( $P_r$  jusqu'à 0,85), mais il n'y avait aucune preuve que le site basique additionnel des ligands participe au stéréocontrôle.

**Mots clés :** Catalyse, complexes de cuivre, complexes de manganèse, acide polylactique, polymérisation de lactide, mécanisme, stéréocontrôle isotactique.



**Table of Content**

Abstract .....	v
Résumé .....	ix
Table of Content .....	xiii
Table list .....	xix
Figure list .....	xxi
Scheme list .....	xxix
Abreviation list .....	xxxix
Acknowledgment .....	xxxvii
<b>Chapter 1 . Introduction .....</b>	<b>1</b>
1. History of polymers .....	3
2. Different types of polymers .....	4
2.1. Natural and semi-synthetic polymers .....	5
2.2. Synthetic polymers .....	6
3. Biodegradation .....	8
4. Bioplastics .....	9
4.1. Polyhydroxybutyrate (PHB) .....	10
4.2. Polycaprolactone (PCL) .....	10
4.3. Polylactic acid (PLA) .....	10
4.3.1. Production of lactic acid .....	13
4.3.2. Production of PLA .....	14
4.3.3. Lactide .....	17
5. Effects determining the molecular weight of polymer chains .....	18
6. Living and immortal polymerization .....	20

7. Stereocontrol .....	21
7.1. Stereocontrol mechanisms .....	24
7.1.1. Catalytic-site mediated chain-end control mechanism .....	25
8. Catalysts used in the ROP of lactide .....	27
8.1. Most popular catalysts for the production of PLA.....	27
8.1.1. Aluminum.....	27
8.1.2. Tin.....	28
8.1.3. Zinc.....	29
8.2. Catalysts applied to the ROP of lactide based on their ligand frame.....	30
8.2.1. Salen and Salan ligands .....	30
8.2.2. Tetradentate and tridentate Schiff-base ligands.....	33
8.2.3. $\beta$ -Diketiminato ligands .....	37
8.2.4. Amino(bisphenolato) and amino(trisphenolato) ligands .....	39
8.3. Copper catalysts used in lactide polymerisation.....	41
9. Aim of this work .....	47
References Chapter 1 .....	49
<b>Chapter 2 . Exploring the Reactivity of Manganese(III) Complexes with Diphenolate-diamino Ligands in <i>rac</i>-Lactide Polymerization .....</b>	<b>57</b>
Abstract .....	59
Introduction.....	60
Results and Discussion.....	61
Synthesis.....	61
UV/vis-spectra.....	63
Magnetic moments.....	64
Solid-state structures.....	64

Lactide polymerization.....	67
Experimental section .....	73
References Chapter 2.....	79
<b>Chapter 3 . Mechanism and Stereocontrol in Isotactic <i>rac</i>-Lactide Polymerization with Copper(II) complexes .....</b>	<b>85</b>
Abstract .....	87
Introduction .....	88
Results and Discussion.....	90
Schlenk equilibria.....	90
Polymerization kinetics.....	90
Nuclearity of the active species in 3.1.....	93
EPR measurements.....	100
Influence of the bridging ligand on stereocontrol.....	104
Solvent dependence of stereocontrol.....	109
Origin of stereocontrol.....	110
Influence of the pending imine.....	112
Conclusions .....	115
Experimental Section .....	116
References Chapter 3.....	126
<b>Chapter 4 . Diiminopyrrolide Copper Complexes: Synthesis, Structures and <i>rac</i>- Lactide-Polymerization Activity. ....</b>	<b>131</b>
Abstract .....	133
Introduction .....	134
Results and discussion.....	136

Ligand synthesis.....	136
Attempted synthesis of copper alkoxide complexes. ....	137
Reactions with chelating alcohols. ....	142
<i>rac</i> -Lactide polymerization – activity. ....	153
Polymer molecular weight control. ....	157
Stereocontrol. ....	161
Mechanism of stereocontrol. ....	164
Conclusions.....	165
Experimental section.....	166
References Chapter 4 .....	184
<b>Chapter 5 . Catalytic-site-mediated chain-end control in the polymerization of <i>rac</i>-lactide with copper iminopyrrolide complexes .....</b>	<b>191</b>
Abstract.....	193
Introduction.....	193
Results and discussion.....	197
Impact of sterically bulky ligands on stereocontrol. ....	197
Lactide polymerization.....	200
Impact of site-epimerization on stereocontrol.....	203
Impact of catalytic-site symmetry on stereocontrol. ....	204
Conclusion.....	206
Experimental section.....	207
References Chapter 5 .....	214



**Chapter 6 . Dinuclear iminophenoxide copper complexes in *rac*-Lactide polymerisation 227**

Abstract .....	229
Introduction .....	229
Results and discussion.....	232
Iminophenols - ligand and general complex synthesis.....	237
Salicylaldehyde-based ligands. ....	239
4,6-di(tert-butyl)salicylaldehyde-based ligands. ....	244
1,3-dichlorosalicylaldehyde-based ligands. ....	247
Conclusion.....	248
Experimental .....	248
References Chapter 6.....	261

**Chapter 7 . Configurationally Flexible Zinc Complexes as Catalysts for *rac*-Lactide Polymerisation ..... 271**

Abstract .....	273
Introduction .....	274
Results and discussion.....	276
Diiminopyrrolide complexes.....	276
Synthesis and structure.....	276
<i>rac</i> -Lactide polymerisation. ....	278
Triaminophenolate complexes .....	279
Syntheses and structures.....	281
<i>rac</i> -Lactide polymerisation. ....	285
Conclusions .....	292
Experimental .....	292

References Chapter 7 .....	301
<b>Chapter 8 . Tetradentate aminophenolate copper complexes in <i>rac</i>-lactide polymerization .....</b>	<b>309</b>
Abstract .....	311
Introduction .....	311
Results and discussions .....	314
Conclusions .....	327
Experimental section .....	327
References Chapter 8 .....	335
<b>Chapter 9 . Conclusions .....</b>	<b>341</b>
Annexes .....	349
Supporting information Chapter 2 .....	xxxix
Supporting information Chapter 3 .....	xlvi
Supporting information Chapter 4 .....	lxv
Supporting information Chapter 5 .....	lxxxv
Supporting information Chapter 6 .....	xcv
Supporting information Chapter 7 .....	cv
Supporting information Chapter 8 .....	cxiii

## Table list

<b>Table 2.I.</b> Selected bond distances [ $\text{\AA}$ ] and bond angles [ $^\circ$ ] from X-ray diffraction studies.....	66
<b>Table 2.II.</b> <i>rac</i> -lactide polymerization with <b>2.3a</b> , <b>2.3b</b> and <b>2.5a</b> ·MeOH <sup>a</sup> .....	68
<b>Table 2.III.</b> <i>Rac</i> -lactide polymerization with <b>2.5a</b> ·MeOH in the presence of protic impurities <sup>a</sup> .....	70
<b>Table 2.IV.</b> Effect of additional alcohol on <i>rac</i> -lactide conversion at different reaction times <sup>a</sup> .....	72
<b>Table 2.V.</b> Details of X-ray diffraction studies.....	77
<b>Table 3.I.</b> <i>rac</i> -Lactide polymerization catalyzed by <b>3.1</b> – <b>3.11</b> .....	92
<b>Table 3.II.</b> Selected bond distances ( $\text{\AA}$ ) and bond angles ( $^\circ$ ) for <b>3.5</b> , <b>3.6</b> and <b>3.8</b> – <b>3.11</b> .....	98
<b>Table 3.III.</b> Stereocontrol ( $P_m$ ) in polymerizations with benzyl alcohol as chain-transfer reagent.....	112
<b>Table 3.IV.</b> Experimental and simulated distributions of stereoerror tetrads.....	113
<b>Table 3.V.</b> Details of X-ray Diffraction Studies.....	123
<b>Table 4.I.</b> Selected bond lengths ( $\text{\AA}$ ) and angles ( $^\circ$ ) of <b>4.1c</b> and <b>4.4c</b> .....	140
<b>Table 4.II.</b> Selected geometric data for pyridylmethoxide complexes <b>4.1</b> , <b>4.5</b> , and <b>4.7-4.11</b> <sup>a</sup> .....	146
<b>Table 4.III.</b> Selected geometric data for dimethylaminoethoxide complexes <b>4.3b</b> and <b>4.5b-4.11b</b> <sup>a</sup> .....	152
<b>Table 4.IV.</b> Apparent first-order rate constants for <i>rac</i> -lactide polymerization with complexes <b>4.1-4.11</b> and <b>4.1b-4.11b</b> .....	156
<b>Table 4.V.</b> Selected results for <i>rac</i> -lactide polymerization with <b>4.5-4.11</b> and <b>4.3b-4.11b</b> <sup>a</sup> .....	160
<b>Table 4.VI.</b> Stereocontrol by <i>in-situ</i> formation of pyridylmethoxide species.....	163
<b>Table 4.VII.</b> Details of X-ray Diffraction Studies.....	178
<b>Table 5.I.</b> Bond distances [ $\text{\AA}$ ] and bond angles [ $\text{deg}$ ] in iminopyrrolide copper complexes.....	199
<b>Table 5.II.</b> <i>Rac</i> -lactide polymerizations with <b>5.2-5.5</b> and <b>5.9</b> . <sup>a</sup> .....	201

<b>Table 5.III.</b> <i>rac</i> -Lactide polymerization with <b>5.4</b> at different lactide concentrations. <sup>a</sup>	204
<b>Table 5.IV.</b> Details of X-ray diffraction experiments.	212
<b>Table 6.I.</b> Bond distances [Å] in crystal structures of <b>6.2a</b> , <b>6.3b</b> and <b>6.4a</b>	234
<b>Table 6.II.</b> <i>rac</i> -lactide polymerizations <sup>a</sup>	235
<b>Table 6.III.</b> Selected geometric data for heteroleptic copper complexes	242
<b>Table 6.IV.</b> Details of X-ray Diffraction Studies	259
<b>Table 7.I.</b> Selected geometric data for pyridylmethoxide complexes <b>7.1</b> and <b>7.2</b> <sup>a</sup>	278
<b>Table 7.II.</b> Geometrical details for the X-ray structures of <b>7.8-7.10</b> .	283
<b>Table 7.III.</b> <i>rac</i> -Lactide polymerisation with <b>7.7</b> and <b>7.10</b> .	287
<b>Table 7.IV.</b> Experimental details of X-ray diffraction studies	300
<b>Table 8.I.</b> Bond lengths in the X-ray structures of <b>8.1-8.6</b>	316
<b>Table 8.II.</b> Summary of <i>rac</i> -lactide polymerizations with <b>8.1-8.6</b> /1 equiv benzyl alcohol <sup>a</sup>	318
<b>Table 8.III.</b> Details of X-ray Diffraction Studies	332

## Figure list

<b>Figure 1.1.</b> Jöns Jakob Berzelius (left) and Hermann Staudinger (right) (taken from an open access source). <sup>7</sup> .....	3
<b>Figure 1.2.</b> Different types of polymer sources and their examples. <sup>9</sup> .....	4
<b>Figure 1.3</b> Cellulose (top) and starch (bottom). .....	6
<b>Figure 1.4.</b> Wallace Carothers (taken from an open access source). <sup>7</sup> .....	7
<b>Figure 1.5.</b> Poly(ethylene terephthalate). .....	7
<b>Figure 1.6.</b> Polyhydroxybutyrate (PHB). .....	10
<b>Figure 1.7.</b> Polycaprolactone (PCL). .....	10
<b>Figure 1.8.</b> Different applications of PLA (taken from an open access source). <sup>7</sup> .....	11
<b>Figure 1.9.</b> Pollution caused by plastics (taken from an open access source). <sup>7</sup> .....	12
<b>Figure 1.10.</b> Edmonton composting facility (taken from an open access source). <sup>7</sup> ...	12
<b>Figure 1.11.</b> The two configurations of lactic acid. ....	14
<b>Figure 1.12.</b> Coordination-insertion ROP mechanism. ....	16
<b>Figure 1.13.</b> Different stereoisomers of lactide. ....	17
<b>Figure 1.14.</b> The effect of the $k_{\text{propagation}}/k_{\text{initiation}}$ ratio on the molecular weight of the obtained polymer chains. ....	19
<b>Figure 1.15.</b> Intramolecular and intermolecular transesterification. ....	19
<b>Figure 1.16.</b> Living and immortal polymerization. ....	21
<b>Figure 1.17.</b> <i>meso</i> and <i>racemic</i> diads. ....	22
<b>Figure 1.18.</b> Isotactic, syndiotactic and heterotactic diads. ....	23
<b>Figure 1.19.</b> Different stereoselectivities of produced PLA chains. ....	24
<b>Figure 1.20.</b> Catalytic-site control and chain-end control mechanism. ....	25
<b>Figure 1.21.</b> Okuda Scandium complex. ....	25
<b>Figure 1.22.</b> Tin(II) bis(2-ethylhexanoate). ....	28
<b>Figure 1.23.</b> The structure of catalysts <b>1</b> and <b>2</b> . ....	30
<b>Figure 1.24.</b> The structure of catalyst <b>3</b> . ....	31
<b>Figure 1.25.</b> The structure of catalysts <b>4</b> and <b>5</b> . ....	31
<b>Figure 1.26.</b> The structure of catalysts <b>6</b> and <b>7</b> . ....	32
<b>Figure 1.27.</b> The structure of catalyst <b>8</b> . ....	32
<b>Figure 1.28.</b> The structure of catalysts <b>9</b> , <b>10</b> , <b>11</b> and <b>12</b> . ....	33

<b>Figure 1.29.</b> The structure of catalysts <b>13</b> and <b>14</b> .	33
<b>Figure 1.30.</b> The structures of catalysts <b>15</b> , <b>16</b> and <b>17</b> .	34
<b>Figure 1.31.</b> The structure of catalyst <b>18</b> .	34
<b>Figure 1.32.</b> The structures of catalysts <b>19</b> and <b>20</b> .	35
<b>Figure 1.33.</b> The structure of catalyst <b>21</b> .	35
<b>Figure 1.34.</b> The structure of catalyst <b>22</b> .	36
<b>Figure 1.35.</b> The structure of catalyst <b>23</b> .	36
<b>Figure 1.36.</b> The structure of catalyst <b>24</b> .	37
<b>Figure 1.37.</b> The structure of catalyst <b>25</b> .	37
<b>Figure 1.38.</b> The structures of catalysts <b>26</b> and <b>27</b> .	38
<b>Figure 1.39.</b> The structure of catalyst <b>28</b> .	39
<b>Figure 1.40.</b> The structure of catalysts <b>29</b> , <b>30</b> , <b>31</b> and <b>32</b> .	39
<b>Figure 1.41.</b> The structure of catalyst <b>33</b> .	40
<b>Figure 1.42.</b> The structure of catalysts <b>34</b> , <b>35</b> and <b>36</b> .	40
<b>Figure 1.43.</b> The structure of catalyst <b>37</b> .	41
<b>Figure 1.44.</b> The structure of catalyst <b>38</b> .	42
<b>Figure 1.45.</b> The structure of catalysts <b>39</b> , <b>40</b> and <b>41</b> .	42
<b>Figure 1.46.</b> The structure of catalysts <b>42</b> , <b>43</b> , <b>44</b> and <b>45</b> .	43
<b>Figure 1.47.</b> The structure of catalyst <b>46</b> .	43
<b>Figure 1.48.</b> The structure of catalyst <b>47</b> .	44
<b>Figure 1.49.</b> The structure of catalyst <b>48</b> .	45
<b>Figure 1.50.</b> The structure of catalyst <b>49</b> .	45
<b>Figure 1.51.</b> The structure of catalysts <b>50</b> , <b>51</b> and <b>52</b> .	46
<b>Figure 1.52.</b> The structure of catalysts <b>53</b> , <b>54</b> , <b>55</b> and <b>56</b> .	46
<b>Figure 1.53.</b> The structure of catalysts <b>57</b> and <b>58</b> .	47
<b>Figure 2.1.</b> UV/vis spectra in methanol of manganese complexes <b>2.3a</b> (solid bold), <b>2.3b</b> (solid thin), <b>2.4b</b> ·MeOH (dashed bold), <b>2.4b</b> ·MeOH (dashed thin) and <b>5a</b> ·MeOH (dotted).	64
<b>Figure 2.2.</b> X-ray structure of <b>2.3a</b> (top left), <b>2.5a</b> ·MeOH (top right), <b>2.4a</b> ·MeOH (bottom left), and <b>2.4b</b> ·MeOH (bottom right). Thermal ellipsoids are drawn at 50%	

probability. Hydrogen atoms (except those on methanol or water molecules) omitted for clarity. ....	67
<b>Figure 3.1.</b> Polymerization kinetics of <b>3.1</b> (circles) and <b>3.2</b> (triangles). Two independent experiments (filled and hollow symbols) are shown for each catalyst. The left inset shows an enlargement of the first two hours, the right inset the linearized plot according to a pseudo-first order rate law. Conditions: [catalyst] = 2 mM, [ <i>rac</i> -lactide] = 200 mM, C <sub>6</sub> D <sub>6</sub> , ambient temperature. ....	91
<b>Figure 3.2.</b> Polymer molecular weight in <i>rac</i> -lactide polymerizations with <b>3.1</b> in the presence of benzyl alcohol (spheres), pyridyl methanol (triangles) or trityl alcohol (diamond) and with <b>3.2</b> in the presence or absence of benzyl alcohol (squares). Polymer molecular weights were extrapolated to full conversion, i. e. $M_{n,corrected} = M_n / \text{yield}$ . The two lines correspond to the theoretical polymer molecular weight expected if either 1 or 2 alkoxide groups per catalyst initiate polymerization. ....	94
<b>Figure 3.3.</b> Improved molecular weight control upon addition of trityl alcohol as a chain-transfer reagent. ....	95
<b>Figure 3.4.</b> Crystal structure of <b>3.5</b> (left) and <b>3.6</b> (right). Thermal ellipsoids are shown at the 50% probability level. Hydrogen atoms were omitted for clarity. Complex <b>3.5</b> cocrystallized with (3.L)Cu <sub>2</sub> (OR) <sub>2</sub> Cl (L = diiminopyrrole, Fig. 3.S7, omitted here for clarity), which is not expected to participate in polymerization (see sup. inf.). ....	100
<b>Figure 3.5.</b> Experimental (bold line) and simulated (thin line) EPR-spectra of polymerization reactions with <b>3.1</b> and <b>3.2</b> . ....	102
<b>Figure 3.6.</b> Crystal structures of <b>3.8–3.10</b> . Thermal ellipsoids are drawn at the 50% probability level. Hydrogen atoms and the minor components of rotational disorder of the <i>N</i> -substituent at N3 (8) and N6 (10) were omitted for clarity. ....	108
<b>Figure 3.7.</b> Titration of <b>3.1</b> with pyridine. Solid lines represent experimental spectra, dotted lines are simulated spectra. Equilibrium constant <i>K</i> and the spectrum of the pyridine adduct were obtained by non-linear regression analysis using all spectra assuming a 1:1 equilibrium. A scale factor was added to allow for complex decomposition and refined to ±1% for 1 – 100 equiv pyridine, –3% for 200 and –6% for 400 equiv pyridine. ....	109

- Figure 3.8.**  $P_m$ -values determined for polymerizations with **3.1** at different conversions..... 111
- Figure 3.9.** Crystal structure of **3.11**. Thermal ellipsoids are drawn at the 50% probability level. Hydrogen atoms, minor component of the disorder at N3 and the second, independent molecule of similar geometry in the unit cell were omitted for clarity..... 114
- Figure 4.1.** X-ray structures of **4.1c** (left) and **4.4c** (right). Hydrogen atoms were omitted for clarity. Thermal ellipsoids were drawn at the 50% probability level..... 139
- Figure 4.2.** X-ray structures of **4.2d** and **4.3d**. Thermal ellipsoids are drawn at 50% probability. Hydrogen atoms, other independent molecules (**4.3d**) and minor components of disordered *N*-substituents (**4.3d**) were omitted for clarity..... 141
- Figure 4.3.** X-ray structures of **4.5**, **4.7**, and **4.9-4.11**. Thermal ellipsoids are drawn at the 50% probability level. Hydrogen atoms, toluene solvent (**4.11**) and a second independent molecule of similar geometry (**4.10** and **4.11**) omitted for clarity..... 145
- Figure 4.4.** Crystal structure of **4.1e**, **4.4e** and **4.6e**. Hydrogen atoms and two of the three independent molecules in **6e** were omitted for clarity. Thermal ellipsoids were drawn at the 50% probability level. .... 148
- Figure 4.5.** X-ray structures of **4.3b** and **4.5b – 4.11b**. Thermal ellipsoids are drawn at the 50% probability level. Hydrogen atoms and disorder of the *N*-substituent (**4.3b**, **4.8b**) omitted for clarity. .... 151
- Figure 4.6.** Conversion/time plots for addition of several batches of monomer over several days. Black arrows indicate time of monomer addition. Top left, blue circles: **4.8**, [**4.8**] = 1 mM in C<sub>6</sub>D<sub>6</sub>, addition of 200, 200 and 25 equiv of *rac*-lactide. Top right, blue circles: **4.8**, 3 mM, 300, 200, 100 equiv. Middle, red circles: **4.8b**, 3 mM, 300, 200, 100 equiv. Bottom left, blue triangles: **4.9**, 3 mM, 300, 100, 100, 200 equiv. Bottom right, blue triangles: **4.9b**, 3 mM, 300, 100, 200 equiv. Solid lines are based on pseudo-first-order rate constants determined in the first addition..... 154
- Figure 4.7.** Polymer molecular weights in *rac*-lactide polymerizations with **4.8** (blue circles) and **4.8b** (red squares) in the presence of benzyl alcohol. Polymer molecular weights were corrected for yield ( $M_{n,corr.} = M_n / \text{yield}$ ) to allow comparison with the theoretical values. Blue solid line: polymer molecular weight expected for one



- alkoxide per catalyst dimer initiating. Red dashed line: for both alkoxides initiating. Hollow circles and squares show the respective polydispersities (right axis). ..... 159
- Figure 4.8.** Isotacticities ( $P_m$ , left axis, black circles) and polymer molecular weights ( $M_n$ , right axis, blue squares) obtained for polymerizations of *rac*-lactide with **4.1b** in the presence of varying amounts of pyridylmethanol. The solid lines represent values expected if reaction of **4.1b** or **4.1b\*** with pyridylmethanol first forms **4.1**, to then initiate polymerization to form the active species **4.1\***. The dashed lines show the values expected if reaction with pyridylmethanol directly forms the active species **4.1\*** without passing via **4.1**. ..... 162
- Figure 5.1.** Crystal structures of **5.2-5.5**. Thermal ellipsoids are drawn at 50% probability (at 30% for **5.2**). Hydrogen atoms, a second independent molecule (**5.4**) and the minor component of *N*-aryl disorder (**5.4**) omitted for clarity..... 199
- Figure 5.2.** Semi-logarithmic conversion-time plot for *rac*-lactide polymerizations with **5.2** (circles), **5.3** (squares), **5.4** (triangles) and **5.5** (diamonds). ..... 200
- Figure 5.3.**  $^{13}\text{C}\{^1\text{H}\}$ -NMR of PLA obtained with **5.4**. Left: carbonyl region, right: methine region. Tetrad assignments according to ref. <sup>113, 114</sup>. ..... 202
- Figure 5.4.** Crystal structure of **5.9**. Hydrogen atoms and the minor part of the disorder omitted for clarity. Thermal ellipsoids shown at the 50% probability level. .... 206
- Figure 6.1.** X-ray structures of **6.2a**, **6.3b** and **6.4a**. Thermal displacements are shown at the 50% probability level. Hydrogen atoms and the minor part of the aminoethoxide disorder in **6.4a** were omitted for clarity. .... 233
- Figure 6.2.** Conversion-time profiles for *rac*-lactide polymerization with **6.4a** (diamonds), **6.5a** (squares), **6.6a** (circles) and **6.6b** (triangles). Conditions:  $\text{C}_6\text{D}_6$ , RT, 0.2 M lactide, 2 mM [cat.]. The inset shows the semi-logarithmic plot. Solid lines represent in both graphics theoretical conversions with the values obtained in linear regression analysis: **6.4a**:  $k_{\text{app}} = 0.604(2) \text{ h}^{-1}$ ,  $t_0 = -4 \text{ min}$ , **6.5a**:  $k_{\text{app}} = 0.080(1) \text{ h}^{-1}$ ,  $t_0 = -1 \text{ min}$ . ..... 237
- Figure 6.3.** X-ray structures of **6.5a**, **6.6a**, **6.6b**, and **6.16a** and **6.16b**. Thermal displacements are shown at the 50% probability level. Hydrogen atoms were omitted for clarity. Only one of two independent molecules shown for **6.5a**. ..... 240

**Figure 6.4.** X-ray structures of **6.8b**, **6.9a**, **6.10a**, and **6.11b** and **6.12b**. Thermal displacements are shown at the 50% probability level. Hydrogen atoms and solvent (**6.8b**) were omitted for clarity. Only one of two independent molecules shown for **6.8b**.....245

**Figure 6.5.** Conversion-time profiles for *rac*-lactide polymerization with **6.8b** (squares), **6.9a** (circles) and **6.11b** (triangles). Conditions: C<sub>6</sub>D<sub>6</sub>, RT, 0.2 M lactide, 2 mM cat.. The inset shows the semi-logarithmic plot. Solid lines represent in both graphics theoretical conversions with the values obtained in linear regression analysis: **6.8b**:  $k_{app} = 0.57(2) \text{ h}^{-1}$ ,  $t_0 = 102 \text{ min}$ , **6.9a**:  $k_{app} = 0.078(1) \text{ h}^{-1}$ ,  $t_0 = -19 \text{ min}$ , **11b**:  $k_{app} = 1.1(1) \text{ h}^{-1}$ ,  $t_0 = 23 \text{ min}$ . .....246

**Figure 7.1.** X-ray structure of **7.2**. Thermal ellipsoids are drawn at the 50% probability level. Hydrogen atoms omitted for clarity. ....278

**Figure 7.2.** Conversion-time profile for *rac*-lactide polymerisation with **7.2**. The inset shows the semi-logarithmic plot. Solid lines represent theoretical curves based on linear regression of the linear region in the semi-logarithmic plot. ....279

**Figure 7.3.** X-ray structure of **7.8**. Thermal ellipsoids are drawn at the 50% probability level. Hydrogen atoms and minor fractions of disorder in *tert*-butyl and dimethylaminoethylene substituents omitted for clarity. ....282

**Figure 7.4.** X-ray structure of **7.9**. Thermal ellipsoids are drawn at the 50% probability level. Hydrogen atoms and the second, independent molecule in the asymmetric unit omitted for clarity. ....285

**Figure 7.5.** Conversion-time profiles for *rac*-lactide polymerisation with **7.7**. Conditions: C<sub>6</sub>D<sub>6</sub>, RT, **7.7**:lactide = 1:100. The inset shows the semi-logarithmic plot. Solid lines correspond to theoretical conversions based on rate constants obtained from linear regression: Black triangles:  $[7.7] = 2.0 \text{ mM}$ ,  $k_{obs} = 4.1(1) \text{ h}^{-1}$ ,  $t_0 = -5 \text{ min}$ , final conversion after >7 h: 99%; blue diamonds:  $[7.7] = 0.5 \text{ mM}$ ,  $k_{obs} = 0.73(1) \text{ h}^{-1}$ ,  $t_0 = -5 \text{ min}$ , final conversion after >7 h: 67%. The negative axis intercept might indicate partial catalyst decomposition in the first 5 min of the reaction, inhomogeneous starting conditions or – although unlikely – experimental error. ....286

- Figure 7.6.** Variation of polymer microstructure ( $P_m$ ) in dependence of conversion or time in *rac*-lactide polymerisations with **7.7**. Black triangles:  $[7.7] = 2.0$  mM, blue diamonds:  $[7.7] = 0.5$  mM. With  $[7.7] = 0.5$  mM, conversion plateaued at 67%. ....288
- Figure 7.7.** X-ray structure of **7.11**. Thermal ellipsoids are drawn at the 50% probability level. Hydrogen atoms, and the second, independent molecule in the asymmetric unit omitted for clarity. ....289
- Figure 8.1.** X-ray structures of **8.1** (left), **8.2** (middle) and **8.3** (right). Thermal ellipsoids are drawn at 50% probability. Hydrogen atoms other than those of water, non-coordinated anions, the second independent molecule for **8.3**, and the minor fraction of the disordered nitrate in **8.3** omitted for clarity. ....315
- Figure 8.2.** Conversion-time plot for the polymerization of *rac*-lactide with **8.1**/benzyl alcohol at 140 °C. lactide: **8.1**:BnOH = 100:1:1. Black squares: single experiment with aliquots taken at desired times. Reaction was exposed to air during sampling. Blue diamonds: Series of 5 independent polymerization experiments quenched after 2, 4, 7 and 24 h. Reactions were not exposed to air. The inset shows the semi-logarithmic plot. Solid lines are theoretical conversions using the apparent first-order rate constant determined from the linear region of the semi-logarithmic plot. ....317
- Figure 8.3.** *rac*-Lactide polymerization with **8.1**/BnOH with different ratios of benzyl alcohol. Conditions: 140 °C, neat monomer, lactide: **8.1** = 100:1, BnOH: **8.1** = 1 (blue diamonds, 5 separate experiments), 1 (brown squares), 2 (black triangles), 4 (blue hollow diamonds), and 8 (red circles). The solid lines are theoretical conversions based on the pseudo-first-order rate constant determined from the linear region of the semilogarithmic plot (conversion < 70%). Left: Conversion-time plots, Upper Right: Semilogarithmic plots, Lower Right: Dependence of the observed pseudo-first-order rate constant on benzyl alcohol concentration. ....319
- Figure 8.4.** Conversion-time plot for the polymerization of *rac*-lactide with **8.2** (blue diamonds). Data for **8.1** under identical conditions is provided for comparison (black squares). Conditions: 140 °C, lactide:[Cu]:BnOH = 100:1:1. The inset shows the semilogarithmic plot. Solid lines represent theoretical conversions based on the

pseudo-first-order rate constant determined by linear regression of the semilogarithmic plots. .... 320

**Figure 8.5.** Conversion-time plot for the polymerization of *rac*-lactide with **8.1** in the presence of ammonium salts: 1 equiv [NEt<sub>4</sub>]Cl (black triangle), 4 equiv [NEt<sub>4</sub>]Cl (hollow triangle), 1 equiv [NEt<sub>3</sub>H][TsO] (red circle), 4 equiv [NEt<sub>3</sub>H][TsO] (hollow circle). Conditions: 140 °C, lactide:[Cu]:BnOH = 100:1:1. The inset shows the semilogarithmic plot. Solid lines represent theoretical conversions based on the pseudo-first-order rate constant determined by linear regression of the semilogarithmic plots for  $t > 120$  min. .... 321

**Figure 8.6.** Conversion-time plot and the semilogarithmic plot for *rac*-lactide polymerizations with **8.3**. Conditions: lactide:3:BnOH = 100:1:1 (blue diamonds), 100:1:4 (red circles). .... 322

**Figure 8.7.** X-ray structures of **8.4-8.6**. Thermal ellipsoids drawn at 50% probability level. Hydrogen atoms, the second independent molecule in 5 and the anion disorder in 4 omitted for clarity. .... 324

**Figure 8.8.** Conversion-time plot and the semilogarithmic plot for *rac*-lactide polymerizations with **8.4**. Conditions: lactide:4:BnOH = 100:1:1. Hollow diamonds are independent reactions quenched after 0.5, 2, 4, and 7 h without exposing the reaction to air. In the remaining four experiments samples were taken in the desired intervals, exposing the reaction to air. Two reactions were conducted with twice (diamonds) or half (triangles) the total amount of reactants to verify the influence of external impurities. .... 325

**Figure 8.9.** Conversion-time plot and the semilogarithmic plot for *rac*-lactide polymerizations with **8.6**. Conditions: lactide:6:BnOH = 100:1:1 (squares, triangles), 100:1:4 (circles). Lines represent theoretical conversions calculated from the pseudo-first-order rate constants obtained from the linear regions of the semilogarithmic plot. .... 326

**Figure 9.1.** Proposed air stable copper complexes for *rac*-lactide polymerization. . 347

## Scheme list

<b>Scheme 1.1.</b> Anionic ROP mechanism.....	15
<b>Scheme 1.2.</b> Activated monomer ROP mechanism.....	16
<b>Scheme 1.3.</b> Two-step reaction for the synthesis of lactide.....	18
<b>Scheme 1.4.</b> The synthesis of the Scandium complex with the bulkiest substituents.....	26
<b>Scheme 1.5.</b> The proposed stereocontrol mechanism.....	27
<b>Scheme 1.6.</b> Coordination-insertion mechanism for the Al( <i>Oi</i> -Pr) <sub>3</sub> -catalyzed ROP of lactide.....	28
<b>Scheme 2.1.</b> .....	61
<b>Scheme 2.2.</b> .....	62
<b>Scheme 2.3.</b> .....	63
<b>Scheme 2.4.</b> .....	71
<b>Scheme 3.1.</b> Dependence of stereocontrol on the initiating group in polymerizations with <b>3.1</b> and <b>3.2</b> .....	89
<b>Scheme 3.2.</b> Potential Schlenk-equilibrium for <b>3.1</b> .....	90
<b>Scheme 3.3.</b> Attempted preparation of <b>3.4</b> .....	96
<b>Scheme 3.4.</b> Preparation of <b>3.5</b> and <b>3.6</b> .....	100
<b>Scheme 3.5.</b> Proposed mechanism for lactide polymerization with <b>3.1</b> and <b>3.2</b> . The structures proposed for <b>3.1b/3.2b</b> are representative examples of a possible structure. ....	105
<b>Scheme 3.6.</b> Preparation of <b>3.7a</b> and <b>3.8</b> .....	107
<b>Scheme 3.7.</b> Preparation of <b>3.9</b> – <b>3.11</b> .....	111
<b>Scheme 3.8.</b> Interplay of catalytic-site inversion and stereoerror insertion. The <i>C</i> , <i>C</i> , <i>R/A</i> , <i>A</i> , <i>S</i> – configuration was arbitrarily chosen as a stereomatch between catalytic site and chain end. ....	114
<b>Scheme 4.1.</b> .....	134
<b>Scheme 4.2.</b> .....	136
<b>Scheme 4.3.</b> .....	137
<b>Scheme 4.4.</b> .....	138
<b>Scheme 4.5.</b> .....	142
<b>Scheme 4.6.</b> .....	143

<b>Scheme 4.7.</b> .....	149
<b>Scheme 4.8.</b> .....	162
<b>Scheme 4.9.</b> .....	166
<b>Scheme 5.1.</b> .....	195
<b>Scheme 5.2.</b> .....	195
<b>Scheme 5.3.</b> Catalyst systems showing catalytic-site mediated chain-end control. <i>RR</i> and <i>SS</i> denote <i>R,R</i> - and <i>S,S</i> -lactide .....	196
<b>Scheme 5.4.</b> .....	198
<b>Scheme 5.5.</b> .....	205
<b>Scheme 6.1.</b> .....	230
<b>Scheme 6.2.</b> .....	232
<b>Scheme 6.3.</b> .....	233
<b>Scheme 6.4.</b> .....	239
<b>Scheme 6.5.</b> .....	241
<b>Scheme 6.6.</b> .....	247
<b>Scheme 7.1.</b> .....	274
<b>Scheme 7.2.</b> .....	275
<b>Scheme 7.3.</b> .....	277
<b>Scheme 7.4.</b> .....	281
<b>Scheme 7.5.</b> .....	282
<b>Scheme 7.6.</b> .....	284
<b>Scheme 7.7.</b> .....	289
<b>Scheme 7.8.</b> .....	290
<b>Scheme 8.1.</b> .....	313
<b>Scheme 8.2.</b> .....	314
<b>Scheme 8.3.</b> .....	315
<b>Scheme 8.4.</b> .....	323

**Abbreviation list**

Ac	acetyl
Ar	aryl
Bn	benzyl
br	broad
<i>tert</i> -Bu	<i>tert</i> -butyl
CCVC	Centre en Chimie Verte et Catalyse
CIF	crystallographic information file
$\delta$	chemical shift (in ppm)
d	doublet
DCM	dichloromethane
diip	2,6-diisopropylphenyl
eq.	equivalent
Et	ethyl
EPR	electron paramagnetic resonance
GPC	gel permeation chromatography
HMBC	heteronuclear multiple bond correlation
HMDS	bis(trimethylsilyl)amide
HRMS	high resolution mass spectrometry
HSQC	heteronuclear single quantum coherence
J	coupling constant (in NMR)
$\lambda$	wavelength
L	ligand

m	multiplet
<i>m</i>	<i>meso</i>
MALDI	matrix-assisted laser desorption ionization
Me	methyl
MLCT	metal-ligand charger transfer
$M_n$	number-average molar mass
MS	mass spectrometry
$M_w$	weight-average molar mass
nacnac	$\beta$ -diketiminato
NMR	nuclear magnetic resonance
NSERC	National Science and Engineering Research Council
PDI	polydispersity index
Ph	phenyl
PLA	polylactic acid
$P_m$	probability for a <i>meso</i> diads insertion
$P_r$	probability for a <i>racemic</i> diads insertion
ppm	part per million
<i>i</i> Pr	iso-propyl
Py	pyridine
R	alkyl group
<i>r</i>	<i>racemic</i>
<i>rac</i>	<i>racemic</i>
ROP	Ring-Opening Polymerization



s	singlet (in NMR)
sqp	square pyramidal
t	triplet
tbp	trigonal bipyramidal
THF	tetrahydrofuran
Ts	Tosyl
UV-vis	ultraviolet-visible
q	quadruplet
xylyl	2,6-dimethylphenyl



*To Shally, Maëlia, Setila Douchez*



## **Acknowledgment**

I would like to begin by thanking my supervisor, Prof. Frank Schaper, who not only helped me to become a good chemist, but also gave me a lot of valuable life lessons. During these past five years, not only did I learn a lot about chemistry under his supervision, specially in the field of catalyst design (what has become my passion), but I have also gained a lot of self-confidence. I will forever be grateful to have been a part of Schaper's group.

I would like to thank the past and present members of the group, Ibrahim, Todd and Valérie with whom I experienced a very good working environment. A special thanks to Arek who always had my back and brought a smile on my lips even during the hardest of times.

I am thankful to have had the opportunity to work with nine young chemists, Dhruv, Nathan, Marie Luise, Cédric, Leena, Ina, Maxime, José and Aurélie with whom I got the chance to share my knowledge with. You guys definitely made my Ph.D. very memorable and I can only wish you nothing but the best.

I will always consider myself super lucky to have learnt so much from Francine in the field of crystallography and I will not be able to thank her enough for all of her help! You are one of the most amazing people I have met. I would also like to thank Thierry and Michel for all of their support. We have one of the most amazing crystallography groups at UdeM! A very special thank you to Elena for all of the elemental analysis she passed for me. We all know how annoying it is to work with air and moisture sensitive compounds! And a big thank you to Pierre and Sylvain who gave me a formation to be able to use the GPC and also to Cedric that is always ready to help with the NMR! It's not an exaggeration to say that because of all of you guys my Ph.D. turned into an amazing experience.

I would like to acknowledge the UdeM support teams. The MS people, Marie-Christine, Karine and Alexandra who have patiently helped me with all the MALDIs I needed and also all of the last minute HRMS. And I would also like to thank all the support people in the university from the security guys to the secretaries of the department which made UdeM a comfortable and safe environment to work in.

I would like to thank Prof. Zargarian, Prof. Reber and Prof. Hanan and their group members for their help and support during these past five years.

A big thank you to Prof. van der Est from Brock University who gave me the opportunity to pass my samples on the EPR and patiently answered all of my questions and taught me a lot.

A very special thank you to my husband's parents, Patricia and Francis, and also his two sisters, Gaëlle and Noémie, for all of their support and love during these past five years. I am very lucky to have had the chance to become a part of your family!

I will never be able to thank my parents enough for all they have done for me, specially my mom, who is not only my best friend but is also my world. We have gone through a lot together and I will never be able to tell you how much I love you! You will forever have a very special place in my heart. As we say in Persian, heaven belongs to mothers. This is true! You are my Angel! Thank you again for everything you have done for me in my life! Without you I would not be standing here in my life! You are the best mother a child could ask for!

Last but not least, a huge thank you to the love of my life, Antoine. I cannot believe that we met and got married at the beginning of our Ph.D. and now after four years we are leaving UdeM with our sweet princess Shally. Antoine, you are my soulmate and I love you more than anything in this world! I truly believe we are one soul in two bodies! I cannot thank you enough for all of the support you have given me these past few years we have been together! All I can say is that you are the sweetest person I know and that our daughter and I are very lucky to have you!

## **Chapter 1 . Introduction**





## 1. History of polymers

The word “polymer” was first used in 1833 by Jöns Jakob Berzelius (Figure 1.1), a renowned Swedish Chemist, coming from the Greek “polys meros” meaning many identical parts.<sup>1,2</sup> For example, he considered benzene ( $C_6H_6$ ) to be a polymer of ethylene ( $C_2H_2$ ). This term was later modified by the German chemist Hermann Staudinger (Figure 1.1), also known as the father of polymer chemistry (laureate of the Nobel Prize in 1953).<sup>3,4</sup> Staudinger defined polymerization as a process in which two or more small molecules come together to produce a product with higher molecular weight while having the same composition. There are two main polymerization routes: a) condensation polymerization or step-growth polymerization, in which polymers are synthesized by the reaction of bi-functional or multifunctional monomers in order to produce dimers, trimers, oligomers and long chain polymers, b) chain-growth polymerization or addition polymerization, where polymers are formed by the addition of monomers to the active site (chain-ends) of the growing polymer one at a time.<sup>5</sup> Hermann Staudinger found it necessary to coin the word “macromolecule” in 1922 to describe chains of organic molecules with more than 10 000 units that are covalently bonded together since the original term (polymer) did not imply anything about the size.<sup>2,6</sup>



**Figure 1.1.** Jöns Jakob Berzelius (left) and Hermann Staudinger (right) (taken from an open access source).<sup>7</sup>

It is necessary to point out that polymer and macromolecule refer to very different concepts. Not all polymers are macromolecules (i.e.  $S_3O_9$  is a trimer of  $SO_3$ ) and vice versa (such as copolymers that don't have the same repeating unit). Most chemists ignore this difference in concept and consider polymers macromolecular chains of organic molecules that are covalently bonded. This definition does not cover all ranges of existing polymers such as inorganic polymers. A lot of inorganic polymers are not covalently bonded or might contain infinitely polymerized layers or framework structures as well as chains.<sup>2,8</sup>

## 2. Different types of polymers

Polymers in general can be divided into three groups:

- 1) Natural polymers, which are found in nature and can be obtained from plants and animal based sources.
- 2) Semi-synthetic polymers which are natural polymers, chemically treated in order to have enhanced physical properties.
- 3) Synthetic polymers which are produced in the laboratory by the polymerization of simple molecules.

Some examples of each of these three types of polymers are given below (Figure 1.2).<sup>9</sup>

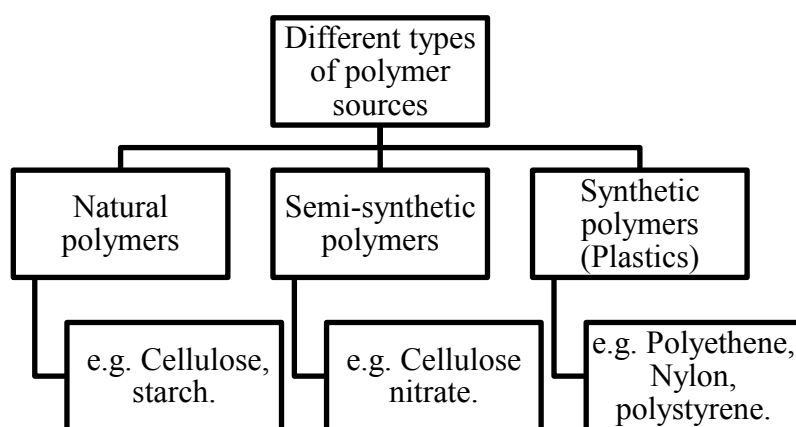


**Figure 1.2.** Different types of polymer sources and their examples.<sup>9</sup>

## 2.1. Natural and semi-synthetic polymers

Natural polymers or in other words *biopolymers*, are polymers that are produced under natural conditions within organisms. These polymers are synthesized inside living cells by complicated metabolic processes. Natural polymers, especially plant based polymers are very much valued because they are *economical*, *readily available* and *non-toxic*. These polymers are *biodegradable* (ASTM D 6400-99), if degradation occurs through microorganisms such as bacteria, and *biocompatible*,<sup>10</sup> if there is no harmful relationship between the polymer and the organism to which the polymer is applied. However, one should not assume that these polymers degrade easily in the environment just due to their natural origin. The rate of degradation for these polymers depends on the complexity of their structure and the conditions of the environment in which they will degrade. Besides the degradation process of these polymers, their production can also be challenging. Their isolation and purification is often slow and expensive due to the complex mixtures in which they are found.<sup>11</sup>

Two of the most important natural/semi-synthetic polymers that are widely used are cellulose and starch. Both of which are made from the same monomer, *glucose*. The difference between these two similar polymers is the orientation of the repeating glucose monomer. In starch all monomer units are directed in the same direction while in cellulose there is a 180 degrees rotation around the axis of the polymer chain backbone relative to the last repeating monomer unit. This difference can also be defined based on the type of linkage between the glucose units present in the two polymers. Cellulose consists of  $\alpha$ -linkages while in starch the monomers are connected via  $\beta$ -linkages. The two polymers have completely different physical properties (Figure 1.3). Unlike starch, cellulose cannot be digested in our body. It is a much better polymer for practical application than starch, due to its higher strength and degree of crystallinity (increase in roughness), as well as its insolubility in water.<sup>11,12</sup>

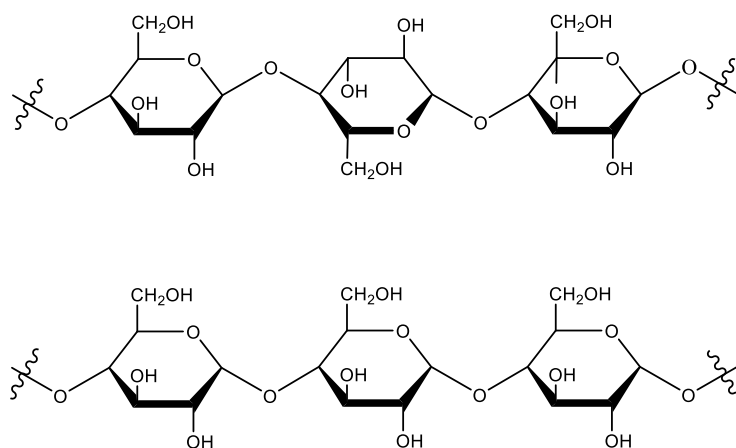


**Figure 1.3** Cellulose (top) and starch (bottom).

## 2.2. Synthetic polymers

The majority of polymer production and application, around 62% of all plastic materials, consist of synthetic polymers and in particular polyolefins which are the simplest synthetic polymers.<sup>13</sup> Polyolefins are produced by opening the double bonds of the monomer in a chain growth polymerization reaction. The first commercially available polyolefin with high molecular weight was polyisobutylene (PIB) which was first synthesized by Farben in 1931. PIB is a very tough, rubber-like polymer and is used as the base of chewing gums, in adhesives, etc.<sup>13,14</sup>

Polyethylene (PE), first synthesized by German chemist Hans von Pechmann in 1888, is the most known polyolefin and produced from ethylene monomers. The most common catalyst used for this purpose is titanium(III) chloride also known as Ziegler catalyst. Polyethylene can be classified based on its density and branching. Linear PE or high-density PE (HDPE) has the simplest structure consisting of a long chain of carbons with two hydrogen atoms on each carbon.<sup>15</sup>

Nylon is the generic term for another big family of synthetic polymers known as aliphatic polyamides. These polyamides were first produced at DuPont's research facility in 1935 by Wallace Carothers (Figure 1.4). Carothers is most famous for the synthesis of synthetic polymers of Nylon and glycol esters through condensation polymerization. Nylon is one of the most important thermoplastics, plastics that soften upon heating and reharden upon cooling in a reversible manner without any

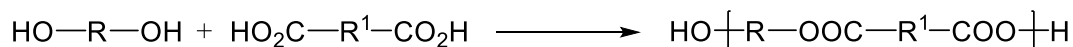
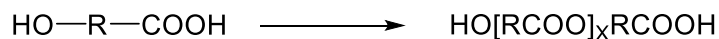
change in their properties.<sup>16</sup> Nylons have different chemical structures and are known by different brand names.<sup>5</sup>



**Figure 1.4.** Wallace Carothers (taken from an open access source).<sup>7</sup>

There are two main synthetic paths for the production of Nylon. 1) The reaction of a dicarboxylic acid with a diamine. 2) The polymerization of aminoacids. This polymerization will lead to a chain with  $(-\text{NH}-[\text{CH}_2]_n-\text{CO}-)_x$  as its repeating unit.<sup>5</sup>

As for nylons, polyesters can be obtained by condensation polymerization of hydroxyl acids or from reaction between diacids and diols:<sup>17</sup>



The most popular man-made polyester is polyethylene terephthalate (PET) or mostly known as poly(ethylene terephthalate) (Figure 1.5). PET is a thermoplastic, nonbiodegradable synthetic polymer.

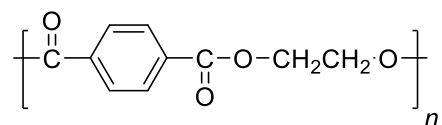


**Figure 1.5.** Poly(ethylene terephthalate).

Polyesters have a general chemical formula of  $-(\text{COOR})_x-$ . By changing the R groups the chemical and physical properties of the polyesters will change accordingly. Polyethylene terephthalates contain an aromatic ring in their main chain

structure, which is the main reason that causes these polyesters to be nonbiodegradable.<sup>5</sup>

An average of 140 million tones of synthetic polymers is produced every year. The land waste produced from these polymers as well as the amount of plastic waste found in the oceans, are a source of environmental pollution. It is estimated that the plastic wastes are responsible for 8% of the weight and 20% of the volume of wastes in landfills.<sup>18</sup> The very slow rate or lack of biodegradation of synthetic polymers has drawn a lot of interest towards biodegradable polymers.

### 3. Biodegradation

A biodegradable plastic is a polymer that degrades in a limited amount of time, through a natural process by microorganisms (such as bacteria, fungi and algae) without ecotoxic effects.<sup>19</sup> In a complete biodegradation the polymer degrades into biomass through aerobic or anaerobic biodegradation. Aerobic or anaerobic biodegradation differ in whether oxygen is present or not and which gases are produced:

a) Aerobic biodegradation:



b) Anaerobic biodegradation:



Environmental conditions, such as temperature, oxygen, humidity, etc. as well as physical and physico-mechanical properties of the polymer such as molecular weight, elasticity and morphology (crystalline or amorphous) greatly affect the biodegradability of the polymer.<sup>19</sup>

It is worth to note that biodegradable polymers mostly come from renewable resources. However, this does not necessarily mean that renewable resources should be favored over non-renewable resources. To make this judgment a lot of factors have to be taken into account:

- 1) To produce the desired crops there is a need for fertilizers, herbicides and pesticides that could in turn have a negative impact on the environment.
- 2) The soil used for the agriculture of the crops is depleted of nutrients or requires fertilizers, which are obtained from fossil resources (Haber-Bosch process).
- 3) All the chemical and biochemical procedures that are required to purify the polymer should be taken into account.  
  
They require water, energy and additives that produce waste that in turn requires specific treatment and disposal.
- 4) Most importantly, if edible crops are used as sources for biodegradable polymers then the cost of food would increase, which is not desired.

A possible solution to the stated problems is to use:

- 1) Raw materials that are less valuable (such as industrial or agricultural food wastes).
- 2) Nonedible plants, eventually cultivated in areas that are not suitable for the production of food.

On the whole, despite some drawbacks related to biodegradable plastics, they have become an important target for industrial purposes.<sup>20,21,22</sup>

#### **4. Bioplastics**

The most common bioplastics currently marketed can be categorized into three groups:<sup>23</sup>

- 1) Extracted directly from biomass such as cellulose and starch.
- 2) Synthesized from microorganisms or genetically modified bacteria such as polyhydroxybutyrate (PHB) and polycaprolactone (PCL).
- 3) Chemically synthesized from renewable bio-derived monomers such as polylactic acid (PLA).

#### 4.1. Polyhydroxybutyrate (PHB)

Polyhydroxybutyrate (PHB, Figure 1.6) was first discovered by Lemoigne in 1926 at Pasteur Institute in France, and can be synthesized through ester formation between  $\beta$ -hydroxybutyryl–CoA monomers. Microbes are known to be the main source of production for this polymer. PHB comes from the family of polyhydroxylalkanoates. It is biodegradable while having properties resembling synthetic polymers, which makes it a very attractive biopolymer.<sup>24</sup>

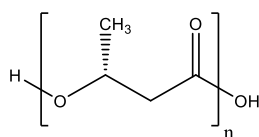


**Figure 1.6.** Polyhydroxybutyrate (PHB).

#### 4.2. Polycaprolactone (PCL)

Polycaprolactone (PCL, Figure 1.7) was one of the first biodegradable polymers synthesized by Carothers in the 1930s. What makes the usage of this polymer very interesting is its miscibility with a wide range of other monomers. Besides biosynthesis via microbes, polycaprolactone can be prepared by a ring-opening polymerization of  $\epsilon$ -caprolactone using catalysts such as stannous octoate.<sup>25</sup>

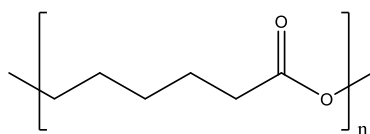


**Figure 1.7.** Polycaprolactone (PCL).

#### 4.3. Polylactic acid (PLA)

Polylactic acid (PLA) was first discovered by Carothers in 1932 who obtained a low molecular weight product through the heating of lactic acid under vacuum. In the beginning, its low molecular weight, high cost of production and lack of availability made it only suitable for medical and pharmaceutical purposes. Nowadays, PLA has a very wide range of applications ranging from industrial packaging to medical applications, where PLA is used as a biocompatible and/or bioabsorbable polymer.



<sup>26,27,28,29</sup> A biocompatible polymer is a polymer that does not produce any toxic or harmful products as well as no immune response in a biological system.<sup>30</sup> A bioabsorbable polymer is a polymer that dissolves over time and is absorbed by the body. For example, in bone implants, the implants can be engineered to dissolve at the same rate as a new bone growing thus making them suitable materials for prosthetics (Figure 1.8.)<sup>31</sup> Compared to other biopolymers, PLA has some advantages:<sup>29</sup>

- 1) It is biodegradable.
- 2) PLA production is beneficial to the agricultural economy.
- 3) Through hydrolysis the produced PLA could be recycled back to lactic acid.
- 4) Considered to be safe by the United States Food and Drug Administration (FDA) for food packaging, thus there has also been increased interest in using PLA for medical applications.



**Figure 1.8.** Different applications of PLA (taken from an open access source).<sup>7</sup>

Besides many advantages associated to the application of PLA, it should be mentioned that its usage is not without drawbacks:<sup>32,33</sup>

- 1) Slow rate of degradation. If PLA is placed in a “controlled composting environment at 140 °C in the presence of digestive bacteria” it could take three months to decompose into water and carbon dioxide. Unfortunately the

same cannot happen in a compost bin or in landfills where there is very little oxygen available as the biodegradable polymer is packed very tightly. Thus it might take PLA up to 1000 years to degrade in any nonindustrial environment. Unfortunately this is also true for oceans, where an accumulation of plastics causes harm to the marine organisms (Figure 1.9).



**Figure 1.9.** Pollution caused by plastics (taken from an open access source).<sup>7</sup>

- 2) PLA does not fit into the established recycling stream and has to be kept separate or be separated and sent to a composting facility. (Figure 1.10).



**Figure 1.10.** Edmonton composting facility (taken from an open access source).<sup>7</sup>

- 3) Nowadays, there is a lot of focus on genetically modified corn for the production of PLA. The purpose of this modification is to produce corn in much higher yields. Unfortunately there is not much known about the future

side effects of these modifications on the environment and also the human health, which can cause problems with public acceptance.

On the whole advantages of PLA overweigh the disadvantages of using PLA as a replacement for regular plastics. Even though PLA might not be able to degrade at a fast rate in landfills, it still has a higher degradation rate compared to conventional plastics. The replacement of harmful plastics by PLA which is a corn-based biodegradable polymer is fast increasing. It should be kept in mind there is yet “no evidence” on harmful side effects caused by genetically modified corn, while the higher yields obtained from this modification could actually solve ethical issues related to the misuse of human food resources for the production of plastic. In recent years, much effort has been made to work out the disposal means of PLA. This is not only achieved by building more facilities suitable for this goal, but also by educating people more about the different sources used to produce plastics and as a consequence how the addition of PLA to the recycling stream could be harmful.<sup>32</sup>

#### **4.3.1. Production of lactic acid**

Lactic acid is industrially prepared by the fermentation of carbohydrates, mostly corn starch.<sup>34</sup> The fermentation is a metabolic process consisting of two different paths:

- 1) Homofermentation: conversion of a six-carbon sugar molecule into two lactic acid molecules. In the process the released energy is stored into two ATP molecules.
- 2) Heterofermentation: conversion of one mole of glucose to one mole of lactate. In the process byproducts such as CO<sub>2</sub>, acetic acid and ethanol can also be produced.

Homofermentation is the more used route since it yields the highest amounts of lactic acid with the minimum amount of side products.<sup>35</sup>

PLA is based on lactic acid (2-hydroxypropionic acid, HOCH(CH<sub>3</sub>)COOH) as its monomer. Lactic acid has two optically active configurations (Figure 1.11), L(+) and D(-).<sup>29</sup>

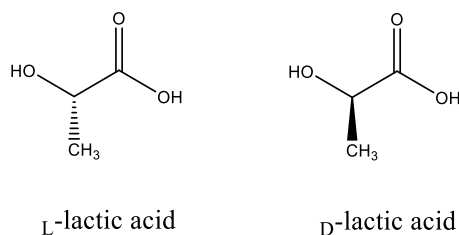


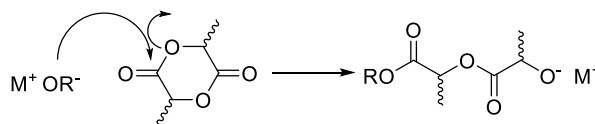
**Figure 1.11.** The two configurations of lactic acid.

### 4.3.2. Production of PLA

There are three general ways to polymerize lactic acid:

- 1) Direct condensation polymerization: In the presence of high vacuum and high temperatures without the presence of any solvent, esterification of the monomers occurs while molecules of water are being removed. The biggest problem of this technique is the removal of the water at the end of the polymerization when the viscosity of the polymer melt increases. Consequently, this technique does not produce PLA chains with high molecular weights.<sup>35</sup> Yamaguchi and co-workers have synthesized PLA chains with high molecular weights using molecular sieves in the reaction media. Unfortunately this technique still requires high temperatures and long reaction times which makes the production of polymers with high molecular weights complicated.<sup>36,37</sup>
- 2) Polycondensation in an azeotropic solution: The azeotropic solution actually helps to decrease the distillation pressure which in turn helps ease the separation of the PLA from the water, increasing the molecular weight of the PLA chains to around  $6.6 \times 10^4$  Da.<sup>35</sup>
- 3) Ring-opening polymerization (ROP) of lactide: Lactide is the cyclic dimeric anhydride of lactic acid and can be polymerized to polylactic acid through three different mechanisms:
  - a) Anionic ROP mechanism: This mechanism involves the nucleophilic attack of an anionic group on the carbonyl group of a lactide monomer. Strongly basic anions might generate the nucleophile by deprotonation of the monomer. Bond cleavage will in turn form another alkoxide at the

chain-end. The only counter cation that has been studied in larger extent is lithium, since it has been the only metal that has shown a significant stereocontrol in lactide polymerization (Scheme 1.1).<sup>38</sup> In comparison to the other following methods, activities are typically high, due to the strong nucleophilic nature of the initiating group.



**Scheme 1.1.** Anionic ROP mechanism.

- b) Coordination-insertion ROP mechanism: This mechanism, also known as a pseudo-anionic mechanism, is based on metal salts and coordination complexes in which the ring-opening polymerization of lactide is achieved through the coordination of the carbonyl group of the lactide monomer to the open coordination site of the catalyst. This coordination is followed by the insertion of the lactide into the metal-alkoxide bond of the catalyst resulting in the formation of a new alkoxide chain on the metal center. This new chain now acts as an initiator for the next lactide (Figure 1.12).<sup>39</sup> Catalysts applied in a coordination-insertion mechanism provide the highest degree of control during polymerization, due to the tight metal-centered transition states causing the ligand system to have a direct effect on transition state energies.

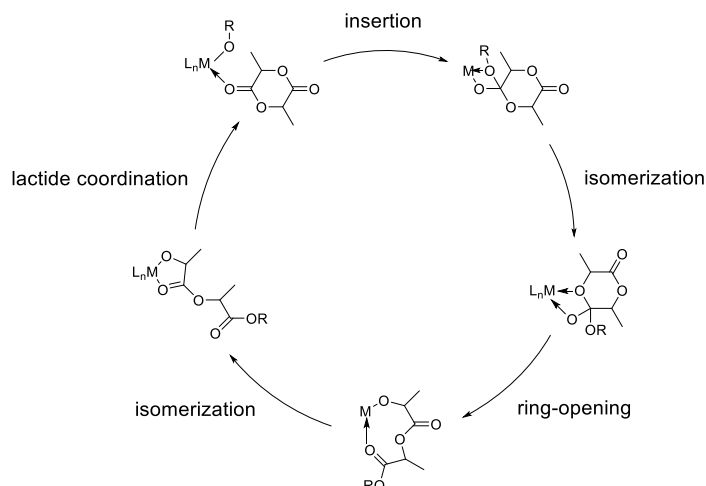
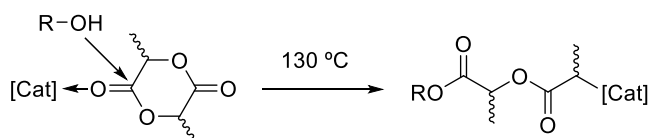


**Figure 1.12.** Coordination-insertion ROP mechanism.

- c) **Activated monomer ROP mechanism:** This mechanism is very similar to the coordination-insertion mechanism; the only difference is the absence of an initiating group (alkoxide). Thus the reaction requires the addition of an external alcohol. In this polymerization, the lactide monomer coordinates to the Lewis-acidic metal center and is attacked by an external alcohol, leading to the opening of the lactide cycle. Typically, polymerizations are performed at high temperature (>130 °C) in the absence of solvent (Scheme 1.2). Catalysts for an activated monomer mechanism are the most stable compared to the other three ROP mechanisms discussed, and can polymerize lactide in the presence of water and possibly lactic acid.



**Scheme 1.2.** Activated monomer ROP mechanism.

- d) **Organocatalytic ROP mechanism:** Organocatalysts are a group of small organic molecules applied for the ROP of lactide. The mechanism is similar to anionic polymerization and can be combined with an activated monomer mechanism. *N*-heterocyclic carbenes (NHCs) are one of the most popular organocatalysts used to date.<sup>40</sup>

For the rest of the introduction, I will discuss mostly coordination-insertion polymerization.

### 4.3.3. Lactide

As seen in the structure of lactic acid, lactic acid consists of one chiral center, thus lactide itself contains two chiral centers. There are three stereoisomers possible for lactide : *L*-lactide (with two times the *L*- configuration), *D*-lactide (with two times the *D*- configuration) and *meso*-lactide (with both the *L*- and the *D*- configuration, Figure 1.13)<sup>41</sup>

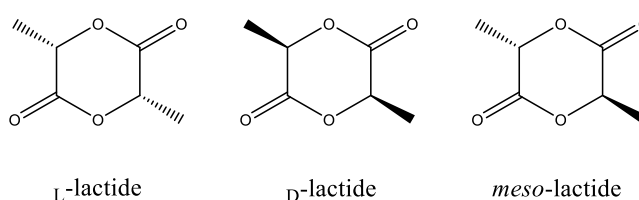


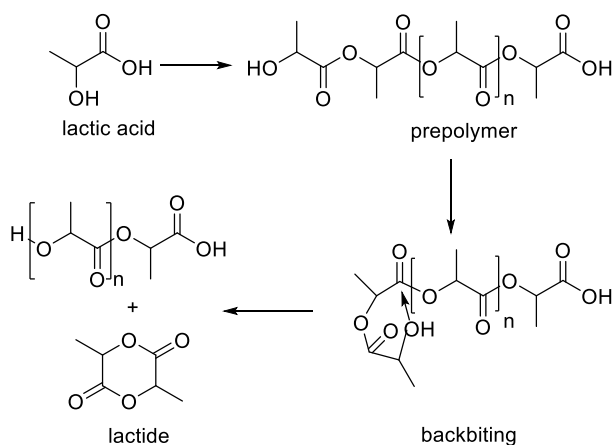
**Figure 1.13.** Different stereoisomers of lactide.

There are several mechanisms for the production of lactide using lactic acid:<sup>41</sup>

- 1) The two-step synthesis of lactide (industrial process).
- 2) The gas-phase synthesis of lactide over packed beds of solid catalyst.
- 3) The one-step liquid-phase conversion of lactic acid to lactide.
- 4) The synthesis of enantiopure lactide from racemic lactate through enzymatic strategies.

In this introduction only the two-step synthesis will be discussed. This synthesis was first reported by Wislicenus in 1878.<sup>42</sup> He detected the presence of lactide as he was synthesizing lactic acid through a polycondensation process. The lactide was formed at 130 °C before increasing the temperature to 150 °C. The two-step lactide synthesis is a polymerization-depolymerization process (Scheme 1.3), in which the molecular weight of the prepolymer is very important. The shorter the prepolymer the lower its viscosity would be, which in turn will cause a faster heat transfer for the depolymerization step leading to a faster formation of the lactide from the

prepolymer. A sufficiently high temperature of about 180 °C is needed for the water removal.<sup>41</sup>



**Scheme 1.3.** Two-step reaction for the synthesis of lactide.

## 5. Effects determining the molecular weight of polymer chains

One of the main goals of polymer chemists is to produce polymer chains with high molecular weights and narrow polydispersities. The molecular weight control of the chain depends on different criteria:<sup>43,44,45</sup>

- 1) The  $k_{propagation}/k_{initiation}$  ratio: If the rate of propagation is much higher than the rate of initiation, then active species will form at different points leading to the growth of polymer chains with different molecular weight. Thus the obtained polydispersity will be broad. If initiation is much faster than propagation, all active species form at the same time, leading to the growth of all polymer chains at the same time. As a consequence a very narrow molecular weight distribution is obtained (Figure 1.14).



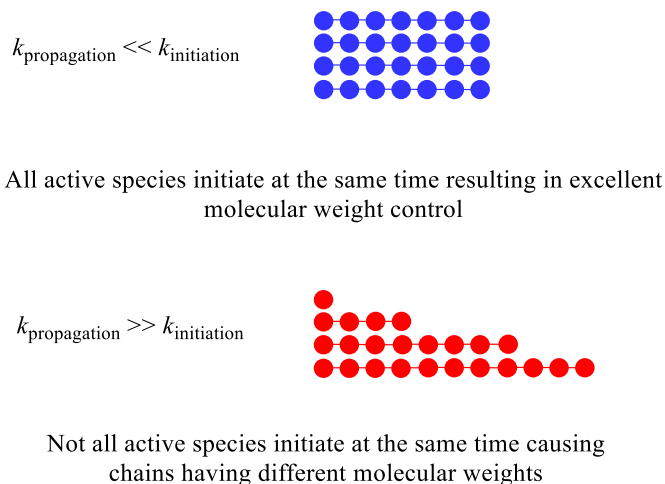


**Figure 1.14.** The effect of the  $k_{\text{propagation}}/k_{\text{initiation}}$  ratio on the molecular weight of the obtained polymer chains.

- 2) The effects of side reactions that occur during the polymerization of lactide. One of these side reactions is transesterification (Figure 1.15). The two major mechanisms for transesterification are:
- Intramolecular: through backbiting which leads to macrocyclic structures and shorter chains.
  - Intermolecular: through chain redistribution.

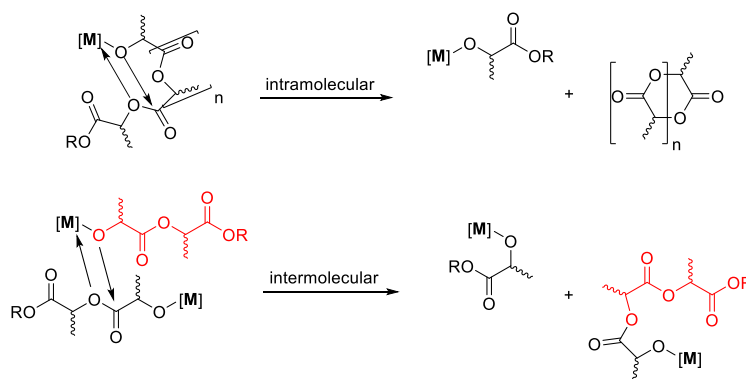


**Figure 1.15.** Intramolecular and intermolecular transesterification.

Both of these transesterification side reactions result in a broadened molecular weight distribution and potentially in irreproducible polymer molecular weights.

## 6. Living and immortal polymerization

Living polymerization is a type of chain-growth polymerization in which chain termination and chain transfer reactions are absent. The molecular weight of the growing chain is proportional to the monomer/initiator ratio. Thus living polymerizations can be used for the production of polymers with high molecular weights and narrow polydispersities.<sup>46,47</sup> An immortal polymerization is a living polymerization in which polymer chains with highly controlled molecular weights and narrow molecular weight distributions are being generated, while exceeding the number of initiating groups due to a fast chain exchange. For lactide polymerization, this is the reaction between the alkoxide on the metal center and alcohol in the polymerization media. In general, chain transfer reactions are side reactions in which the growth of a polymer molecule is terminated while the growth of a new polymer begins. In an immortal polymerization the chain transfer reaction is reversible and, if faster than chain growth, leads to narrow molecular weight distributions. A living (or immortal) polymerization can be “killed” or in other words terminated. In lactide polymerization, addition of a protic compound which does not form initiating groups on the metal center, such as water, terminates polymerization (Figure 1.16).<sup>47,48</sup>

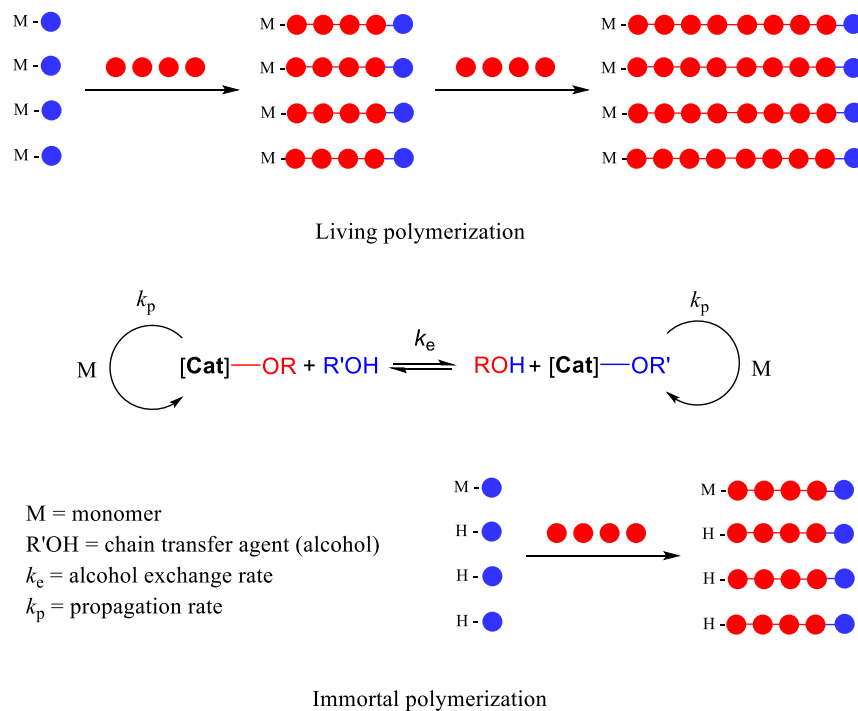


**Figure 1.16.** Living and immortal polymerization.

## 7. Stereocontrol

The lactide monomer contains two stereocenters and exist in three diastereomers:  $DD$ -,  $LL$ - and  $DL$ - (*meso*-lactide). The chiral isomers besides being commercially available as single enantiomers, can also be purchased as a racemic mixture (*rac*-lactide). With the opening of the lactide ring through polymerization, polymer chains are generated that also contain these stereocenters. Depending on the type of lactide monomer used and the alignment of the stereocenters next to each other in the chain, polymers have different microstructures.<sup>39</sup>

Tacticity is the stereochemistry of chiral centers positioned right next to each other in a polymer chain. The regularity of the stereochemistry of the polymer chain dictates to which degree the structure is rigid and crystalline or flexible and amorphous. Two stereocenters in a polymer chain constitute a diad. If both centers have the same orientation, the diad is called *meso*; if the centers are oriented opposite to each other, the diad is called *racemic* (Figure 1.17).<sup>39,49</sup> The nomenclature originates from propylene polymerization. For lactide, it is counterintuitive, since the *meso*-diad contains two identical stereocenters ( $RR$ ) or ( $SS$ ), while the racemic one two centers

of different chirality (*RS*) or (*SR*). For this reason, several authors prefer the use of isotactic and syndiotactic diads (*i* and *s*). In this thesis, I remain with the *rac/meso* nomenclature, but I will use the terms *m*-diad and *r*-diad, instead of *meso/rac* to avoid confusion.

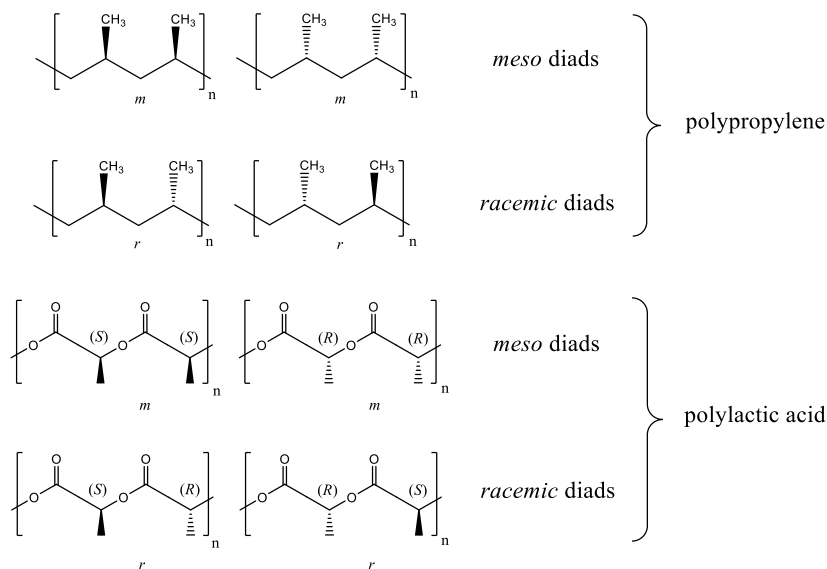


**Figure 1.17.** *meso* and *racemic* diads.

To delve a bit deeper into the stereochemistry of a polymer chain, triads can be described. Triads consist of three stereocenters positioned next to each other. Three different triads are possible (Figure 1.18):<sup>49,50</sup>

- 1) Isotactic triad: In which two *meso* diads are adjacent to each other (*mm*)
- 2) Syndiotactic triad: In which two *racemic* diads are adjacent to each other (*rr*)
- 3) Heterotactic triad: In which a *racemic* diad is adjacent to a *meso* diad (*rm* or *mr*)

Tetrads, pentads and hexads are defined analogously.

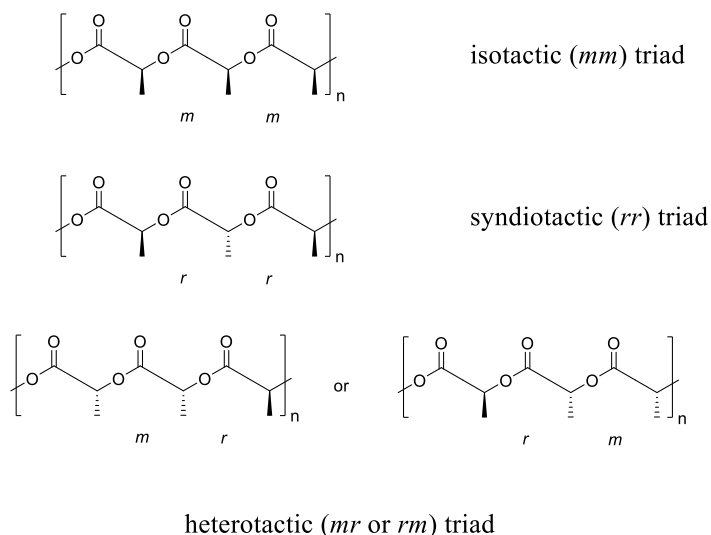


**Figure 1.18.** Isotactic, syndiotactic and heterotactic diads.

To show the degree of stereocontrol, two parameters are generally used,  $P_m$  (*meso*) and  $P_r$  (*racemic*).  $P_m$  is the probability by which a *meso* (isotactic) diad is formed by insertion, while  $P_r$  shows the probability by which a *racemic* (syndiotactic) diad is formed. In *rac*-lactide polymerization,  $P_m = 1$  ( $P_r = 0$ ) results in a completely isotactic PLA,  $P_m = 0$  ( $P_r = 1$ ) indicates the formation of a completely heterotactic PLA, and  $P_m = P_r = 0.50$  points to an atactic PLA chain.<sup>39</sup>

Depending on the type of lactide used, different microstructures can be obtained (Figure 1.19):<sup>39</sup>

- 1) Enantiopure lactide (*SS* or *RR*) can form only isotactic PLA ( $P_m = 1$ ,  $P_r = 0$ ).
- 2) *rac*-Lactide (the stereocenters are presented as a 1:1 mixture of *RR* and *SS*) forms:
  - (1) Isotactic PLA ( $P_m = 1$ ,  $P_r = 0$ ).
  - (2) Heterotactic PLA ( $P_m = 0$ ,  $P_r = 1$ ).
  - (3) Atactic PLA ( $P_m = P_r = 0.5$ ).
- 3) *meso*-Lactide (the stereocenters are presented as *RS* or *SR*) forms:
  - (1) Heterotactic PLA ( $P_m = 1$ ,  $P_r = 0$ ).
  - (2) Syndiotactic PLA ( $P_m = 0$ ,  $P_r = 1$ ).

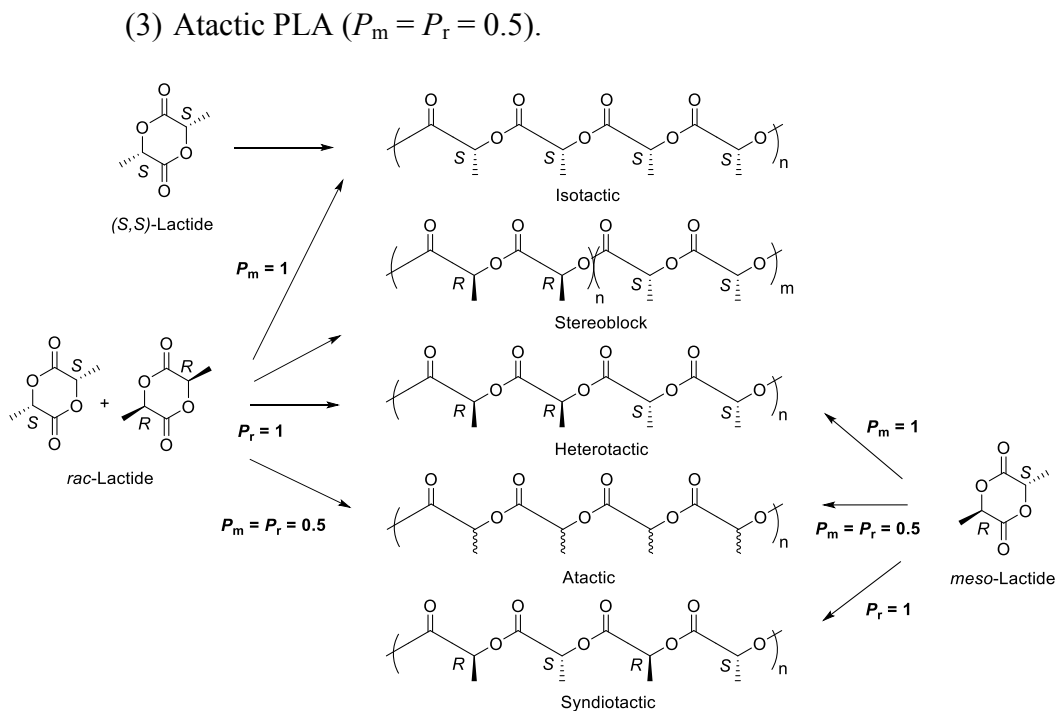


**Figure 1.19.** Different stereoselectivities of produced PLA chains.

### 7.1. Stereocontrol mechanisms

There are two main mechanisms by which the stereoregularity of a PLA chain can be controlled (Figure 1.20):<sup>39</sup>

- 1) Chain-end control mechanism: the chirality of the last monomer inserted into the growing PLA chain determines the chirality of the next lactide monomer to be inserted.
- 2) Catalytic-site control mechanism: the chirality of the Lewis-acid metallic center determines the chirality of the next monomer to be inserted into the propagating chain.

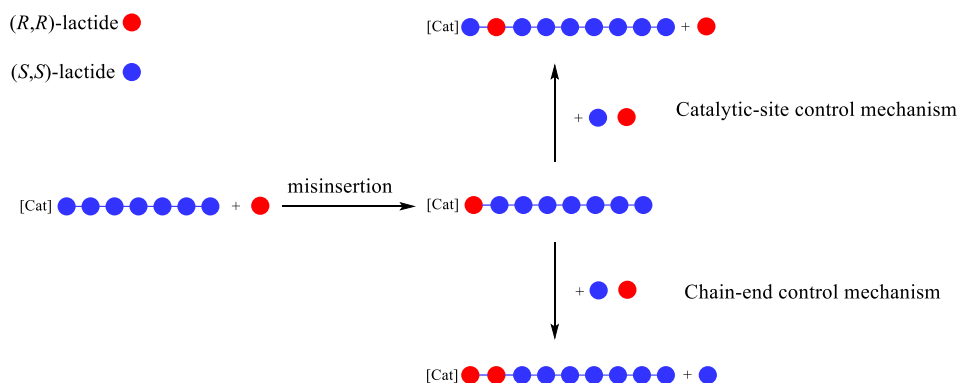


**Figure 1.20.** Catalytic-site control and chain-end control mechanism.

### 7.1.1. Catalytic-site mediated chain-end control mechanism

In some cases, stereocontrol was obtained through a chain-end control mechanism but with the assistance of the spectator ligand, called a “catalytic-site mediated chain-end control mechanism” or “ligand-mediated chain-end control mechanism”. This mechanism was first proposed by Okuda and co-workers in 2006.<sup>51</sup> They designed a new series of scandium complexes with 1, $\omega$ -dithia-alkanediyl-bridged bisphenolato (OSSO)-type ligands. The difference in this ligand system was the flexibility in the bridge (Figure 1.21).

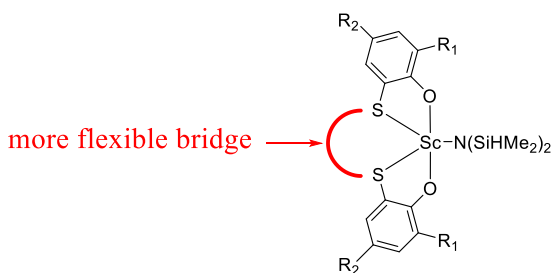
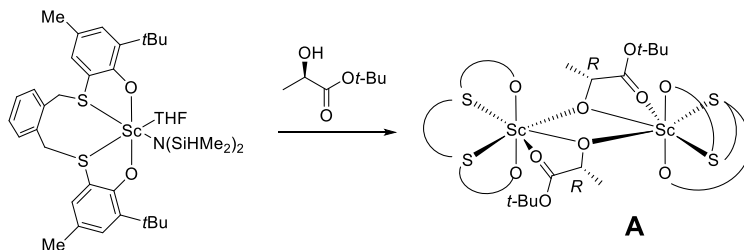


**Figure 1.21.** Okuda Scandium complex.

Previously such ligand systems with more rigid bridges had only shown a slight heterotactic preference for the ROP of *rac*-lactide. Okuda and co-workers studied the effect of increasing the steric bulk on the ligand system (both the bridge and the two phenolate arms), on the stereocontrol during ROP of *rac*-lactide. They observed that they only had a drastic increase in heterotacticity (from  $P_r = 0.78$  to  $P_r = 0.95$ ) when the bridge became more sterically bulky. To study this observation in more detail and find the source of the stereocontrol, the complex with the bulkiest substituents and

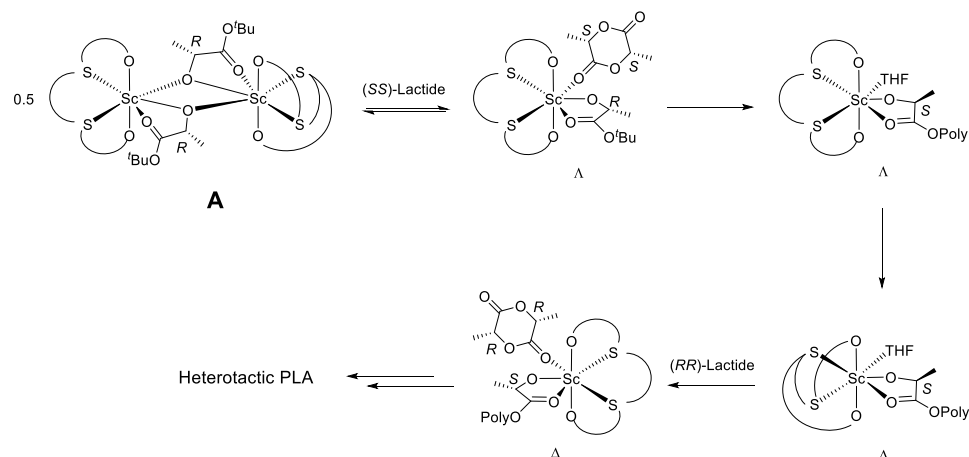
bridge was chosen. As seen below the chosen catalyst was reacted with (*R*)-*tert*-butyl lactate (a single opened half monomer for lactide with an *R* stereocenter) to yield the desired dimer, **A**, with a  $\Delta,\Delta$  configuration (Scheme 1.4).



**Scheme 1.4.** The synthesis of the Scandium complex with the bulkiest substituents.

The presence of a dimeric structure has been confirmed by an X-ray diffraction study. The obtained dimer was then reacted with *rac*-lactide in  $[\text{D}_8]\text{THF}$ . In the presence of excess lactide, the dimer is broken into monomers and the open coordination site will be filled with a lactide. Based on these interactions and repulsions obtained from DFT calculations, it has been concluded that the  $\Delta$ -Sc has a preference for an (*S,S*)-lactide to coordinate. Thus after the insertion of the  $\text{L}$ -lactide, there will be a repulsion between the  $\alpha$ -methyl of the opened ring and the upper *tert*-butyl of the ligand system. To lower this repulsion, the upper *tert*-butyl will move away resulting in a change in the configuration of the catalyst from  $\Delta$  to  $\Delta$ . Thus now the  $\Delta$ -Sc will have a preference for a  $\text{D}$ -lactide. As seen in the mechanism, the chirality of the last inserted monomer dictates the chirality of the catalyst which then selects the monomer. Due to the influence of the ligand system on the stereocontrol, the mechanism is called a “ligand-mediated chain-end control mechanism” (Scheme 1.5).<sup>51</sup>





**Scheme 1.5.** The proposed stereocontrol mechanism.

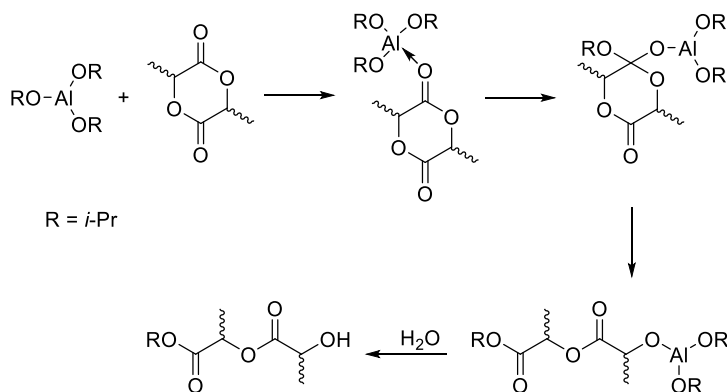
## 8. Catalysts used in the ROP of lactide

Coordination-insertion ring-opening polymerization of lactide, unlike the activated monomer mechanism and anionic mechanism, contains metal-centered transition states. The direct influence of the catalyst enables higher control during the course of the polymerization. Consequently the amount of side reactions (such as transesterification) occurring during the polymerization is typically less than the other two mechanisms. The coordination-insertion mechanism is a metal-mediated ROP. Since catalysts used in industry (tin(II) and aluminum alkoxides) do not provide any stereocontrol, there is a lot of interest in academia to design catalysts that are able to produce highly isotactic PLA from *rac*-lactide.<sup>37</sup>

### 8.1. Most popular catalysts for the production of PLA

#### 8.1.1. Aluminum

The coordination-insertion mechanism for the ring-opening polymerization of lactide was first proposed by Dittrich and Schulz in 1971,<sup>52,43</sup> and was proven experimentally by Kricheldorf,<sup>53,43</sup> and Teyssié,<sup>54,43</sup> in the late 1980s, using  $\text{Al}(\text{O}i\text{-Pr})_3$  as the catalyst (Scheme 1.6).



**Scheme 1.6.** Coordination-insertion mechanism for the  $\text{Al}(\text{O}i\text{-Pr})_3$ -catalyzed ROP of lactide.

Unfortunately there are many disadvantages in using  $\text{Al}(\text{O}i\text{-Pr})_3$  as a catalyst for lactide polymerization:<sup>43,55</sup>

- 1) Very low activity: The polymerization can reach full conversion in several days in bulk conditions, at temperatures ranging between 125–180 °C.
- 2) The molecular weights obtained for the polymer chains are normally much lower than  $10^5$  Da.
- 3) Aluminum ions in general are not considered to be safe for the human body due to concerns of the relationship between this element and Alzheimer's disease.

### 8.1.2. Tin

Later on it was shown that  $\text{Sn}(\text{Oct})_2$  has a higher activity compared to  $\text{Al}(\text{O}i\text{-Pr})_3$ .<sup>56</sup> In the presence of a protic reagent such as an external alcohol, activities increased further and polymer molecular weight was similar to the Al(III) complex. Nowadays,  $\text{Sn}(\text{Oct})_2$  (tin(II) octanoate, tin(II) bis(2-ethylhexanoate)) has become the most widely used catalyst in industry for the polymerization of lactide (Figure 1.22).<sup>43</sup>

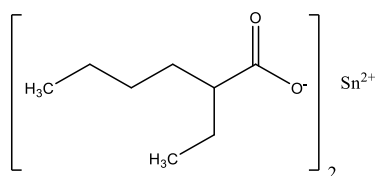
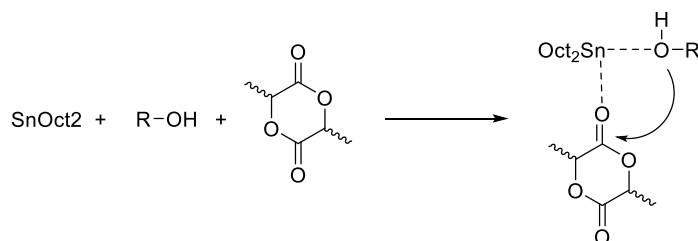


**Figure 1.22.** Tin(II) bis(2-ethylhexanoate).

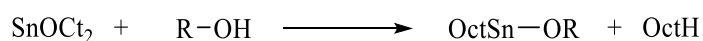
Its attractiveness to industry stems from its availability, easy handling and solubility in most organic solvents as well as in molten monomer. Tin(II) octanoate is an active catalyst which can reach full conversion in only a few hours in bulk polymerization at temperatures between 140–180 °C, but unfortunately is very prone to transesterification.<sup>57</sup> One drawback of this catalyst is concerns about its toxicity, even though its usage has been accepted in the food industry by the U.S. FDA.<sup>43,55</sup>

Contrary to  $\text{Al}(\text{O}i\text{-Pr})_3$  that clearly follows a coordination-insertion mechanism,  $\text{Sn}(\text{Oct})_2$  has raised a lot of controversy. Two slightly different pathways have been proposed for the coordination-insertion mechanism of tin(II) octanoate:

- 1) Kricheldorf and co-workers have suggested a mechanism in which the propagation step involves the coordination of both the alcohol and the monomer to the  $\text{SnOct}_2$ -complex.<sup>58</sup>



- 2) Penczek and co-workers have proposed the conversion of the tin(II) octanoate into a tin-alkoxide before the ROP of the monomer.<sup>59</sup>



### 8.1.3. Zinc

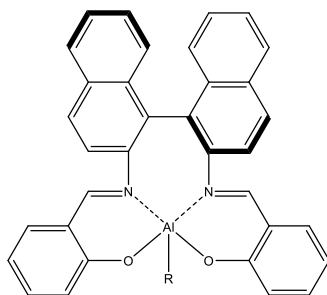
As stated before the biggest drawback of using  $\text{Sn}(\text{Oct})_2$  are concerns about the toxicity of tin(II). Thus there has been a lot of interest to find a nontoxic replacement such as zinc derivatives. Initially zinc powder was used a lot in polymerization, but due to its low activity and bad molecular weight control the usage of other zinc catalysts such as  $\text{Zn}(\text{Lact})_2$  has been very much favored.  $\text{Zn}(\text{Lact})_2$  is easily synthesized from  $\text{ZnO}$  and ethyl lactate or lactide, and yields polymers with very good molecular weight control. Compared to  $\text{Al}(\text{O}i\text{-Pr})_3$  and  $\text{Sn}(\text{Oct})_2$ , the mechanism of  $\text{Zn}(\text{Lact})_2$  is much less studied. Similar to what had been seen for  $\text{Sn}(\text{Oct})_2$ , the

presence of an external alcohol seems to be essential in order to obtain higher activities and a better molecular weight control.<sup>43,60,61</sup>

## 8.2. Catalysts applied to the ROP of lactide based on their ligand frame

### 8.2.1. Salen and Salan ligands

Tetradentate iminophenolate (salicaldimine or salen) and aminophenolates (salicaldamine or salan) ligands have been widely used in *rac*-lactide polymerization and showed very high degrees of stereocontrol with Al centers. Spassky designed an enantiomerically pure aluminum methoxide catalyst, **1** (Figure 1.23), which had a 19 times higher preference for (*R,R*)-lactide than (*S,S*)-lactide. When the insertion of (*R,R*)-lactide was completed, insertion of (*S,S*)-lactide led to the production of a stereoblock PLA. This was the first time that highly isotactic PLA was obtained from *rac*-lactide.<sup>37,62</sup> Coates and Ovitt reproduced **1** and prepared **2**. The compounds were only different in the nature of the initiator, as **1** contained a methoxide and **2** contained an isopropoxide (Figure 1.23). It was reported that both catalysts were active in solution at 70 °C while producing a stereoblock PLA. As expected, changing the initiator did not have any effect on the stereocontrol, since after the first insertion it will be placed at the end of the growing polymer chain.<sup>63,64</sup>



R = OMe, **1**; O<sup>i</sup>Pr, **2**.

**Figure 1.23.** The structure of catalysts **1** and **2**.

Feijen and co-workers continued the investigations on salen aluminum complexes by adding bulky *tert*-butyl groups on the phenolates and using a chiral bridge. **3** (Figure 1.24) showed to be active in *rac*-lactide polymerization with a very strong preference for (*S,S*)-lactide and producing stereoblock PLA ( $P_m = 0.93$ ). The most amazing result Feijen observed with this catalyst was obtaining the same excellent

stereocontrol in *bulk polymerization* ( $P_m = 0.88$ ). This was the first time a catalyst was able to produce a highly isotactic PLA from *rac*-lactide at 130 °C.<sup>65,66</sup>

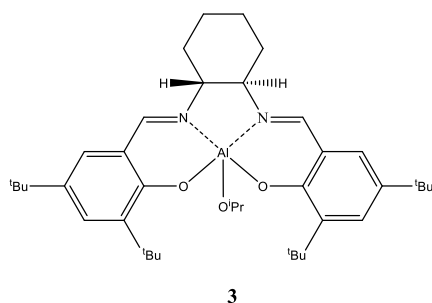


**Figure 1.24.** The structure of catalyst **3**.

Later, Nomura and co-workers reported the synthesis of **4** and **5** (Figure 1.25) which contained more flexible bridges compared to those used before. The alkoxide version of these two catalysts was formed *in situ* in the presence of benzyl alcohol. Catalysts **4** and **5** both produced highly isotactic PLA, while **5** provided an even higher degree of stereocontrol ( $P_m = 0.91$ ) due to its more flexible bridge.<sup>67</sup>

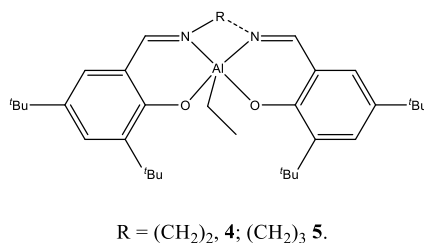


**Figure 1.25.** The structure of catalysts **4** and **5**.

Chen and co-workers, prepared **6** (Figure 1.26) very similar to **5**, in which they kept the more flexible propyl as the bridge while placing two methyl groups on the middle carbon, making it more sterically bulky. The alkoxide version of **6** was also prepared *in situ* (in the presence of isopropanol) and as also seen for **5**, a highly isotactic stereoblock PLA was obtained. They also prepared **7** (Figure 1.26), with exactly the same ligand frame but with an isopropoxide coordinated to the aluminum center. **7** gave the same exact stereocontrol as well as rate constant seen for **6**.<sup>68</sup> Nomura and co-workers also used **7** in bulk polymerization and they were able to obtain a high degree of isotacticity.<sup>69</sup>

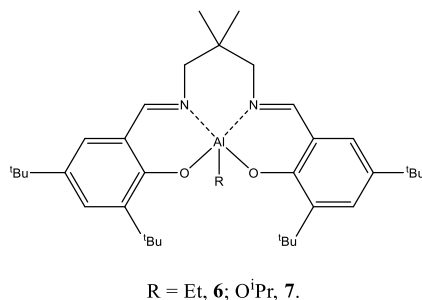


**Figure 1.26.** The structure of catalysts **6** and **7**.

Nomura and co-workers, kept the same ligand frame used for **7** while replacing the *tert*-butyls with much bulkier *tert*-BuMe<sub>2</sub>Si substituents on the phenolates, **8** (Figure 1.27). Increasing the steric bulk on the *ortho* and *para* positions of the phenol groups led to a high increase in the isotacticity of the obtained PLA chains.<sup>70</sup>

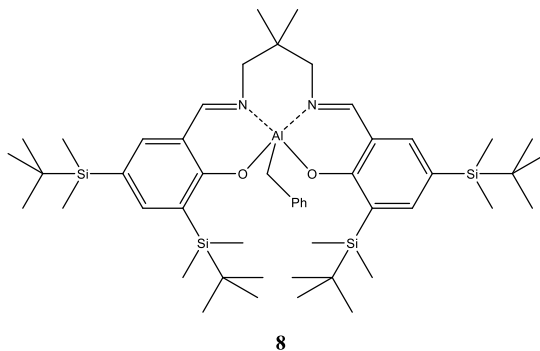


**Figure 1.27.** The structure of catalyst **8**.

Gibson and co-workers, prepared a series of aluminum methyl complexes with tetradentate aminophenoxide ligands containing different substituents on the phenol groups. Unfortunately this ligand system did not produce PLA with very high degrees of stereocontrol as had been seen for salen type ligands. In the presence of methyl (**9**) and isopropyl (**10**) as the substituents on the phenol rings a moderate isotacticity of 0.73 and 0.65 was observed respectively. Replacing the substituents with a bulkier *tert*-butyl group (**11**) produced a heterotactic PLA while placing two chlorides (**12**) as an electron withdrawing group on the phenolates, completely killed the stereocontrol of the obtained PLA chain (Figure 1.28).<sup>71</sup>

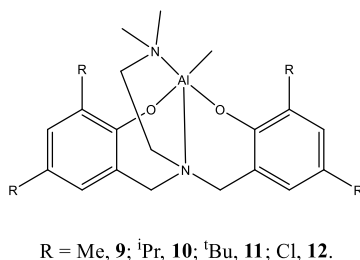


**Figure 1.28.** The structure of catalysts **9**, **10**, **11** and **12**.

Gibson and co-workers, extended their studies to aminophenoxide ligand systems (Salan) by preparing catalysts **13** and **14** (Figure 1.29). In the presence of benzyl alcohol, **13** showed a very high isotacticity of  $P_m = 0.88$  while placing chlorides (**14**) on the phenolates produced a highly heterotactic PLA with a  $P_r$  value of 0.96, being the first aluminum catalyst to show such a high degree of heterotacticity. Such a dramatic switch in tacticity solely due to small changes of substituents on the ligand frame are unfortunately typical for lactide polymerization. Kol showed that the mechanism most likely grows through an activated/deactivated species which continues polymerization only after chain transfer to a catalytic site of opposite chirality.<sup>72,73</sup>

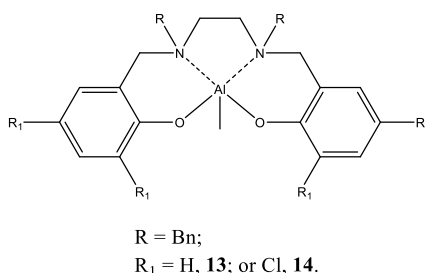


**Figure 1.29.** The structure of catalysts **13** and **14**.

### 8.2.2. Tetradentate and tridentate Schiff-base ligands

Besides salen/salan type ligand systems, tetradentate and tridentate Schiff-base ligands have been applied widely to the ROP of lactide. Feijen and co-workers showed that achiral bis(pyrroline) Schiff-base aluminum alkoxides, **15**, are able to produce isotactic PLA from *rac*-lactide. The degree of stereocontrol is less than what was obtained with salen ligands ( $P_m = 0.75$ ).<sup>74</sup> Jing and co-workers have synthesized enolic tetradentate Schiff-base aluminum catalysts (**16**) that behave very similar to **15**

( $P_m = 0.80$ ).<sup>75</sup> Carpentier and co-workers modified the ligand system used for **15** by replacing the phenyl groups adjacent to the alkoxides with electron withdrawing trifluoromethyl groups (**17**), but no significant change occurred in the tacticity of the obtained PLA (Figure 1.30). High degrees of sterecontrol were observed, a  $P_m$  value of 0.83–0.87.<sup>76</sup>

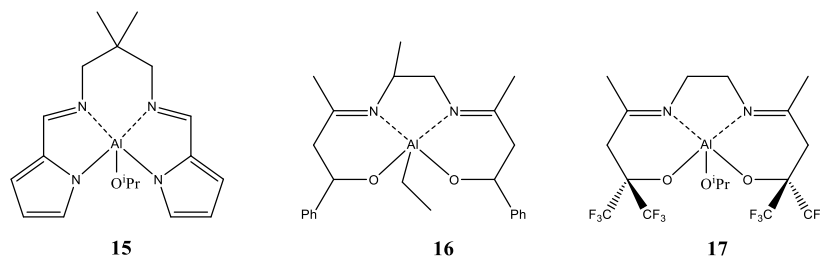


**Figure 1.30.** The structures of catalysts **15**, **16** and **17**.

In an attempt to retain the stereoselectivity of Al, but to increase activity, Mehrkhodavandi and co-workers prepared a catalyst with an NNO-ligand system, a cyclohexyl arm, and with indium as the Lewis-acidic metal center (**18**, Figure 1.31). The catalyst is dimeric, with a chloride and an ethoxide bridging ligand. **18** provides an isotactically enriched PLA ( $P_m \sim 0.6$ ) at room temperature in  $CD_2Cl_2$  in only 30 min, much faster than aluminum salen complexes that require several hours and high temperature to reach full conversion.<sup>77,78,79,80</sup> Mehrkhodavandi studied several variations of this catalyst, in particular the relationship between complex nuclearity and stereocontrol. While isotacticities could be improved, they unfortunately did not reach the values observed for Al.<sup>81,82</sup>

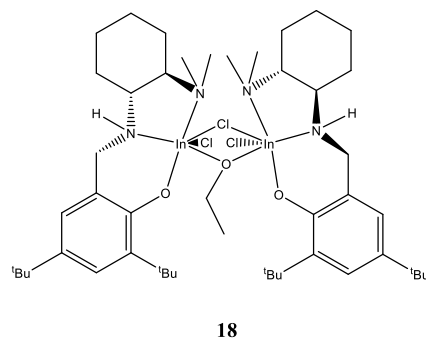


**Figure 1.31.** The structure of catalyst **18**.



Besides aluminum complexes that have been studied thoroughly, other metal centers, such as zinc and calcium also produce PLA with high degrees of stereocontrol, bearing tridentate Schiff-base ligands (NNO). Lin and co-workers have designed zinc complexes with such ligand systems (**19**) that show very high degrees of heterotacticity ( $P_r = 0.91$ ). Further investigations have shown that reducing the steric bulk of the ligand system will lead to a reduction of the heterotacticity ( $P_r = 0.59$ – $0.65$ ).<sup>83</sup> Behuvanesh and co-workers replaced the zinc in **19** with a calcium to obtain **20**. This complex provided only moderate stereocontrol at  $-33\text{ }^\circ\text{C}$  ( $P_r = 0.73$ ) (Figure 1.32).<sup>84</sup>

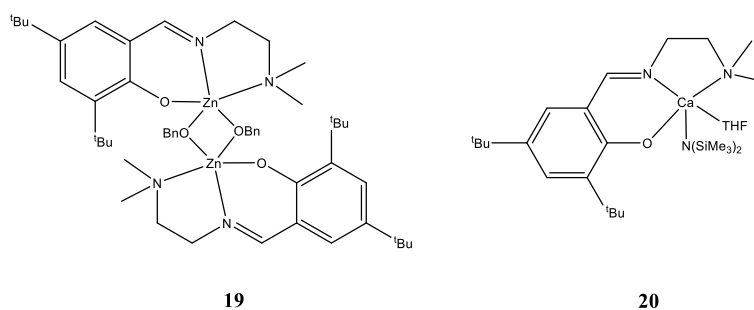


**Figure 1.32.** The structures of catalysts **19** and **20**.

Hillmyer and Tolman investigated a dinuclear zinc complex with a phenolate ligand bearing two ethylenediamine arms (**21**, Figure 1.33). This catalyst was able to reach full conversion in around 30 min, in dichloromethane at room temperature.<sup>85</sup>

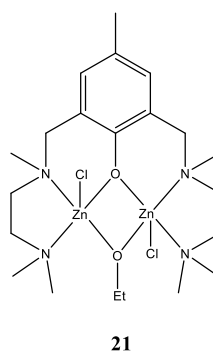


**Figure 1.33.** The structure of catalyst **21**.

Hillmyer and Tolman continued their investigations on a very similar catalyst with a single ethylene diamine arm (**22**, Figure 1.34). X-ray diffraction studies show the presence of a dimer in solid state while NMR and mass spectrometric analysis point

towards a monomer present in the solution. Catalyst **22** has been able to polymerize *rac*-lactide at a rate 8 times faster than **21** (reaching full conversion in just a few minutes), thus becoming one of the fastest zinc catalysts known to date. However, **22** has not been able to provide any stereocontrol.<sup>86</sup>

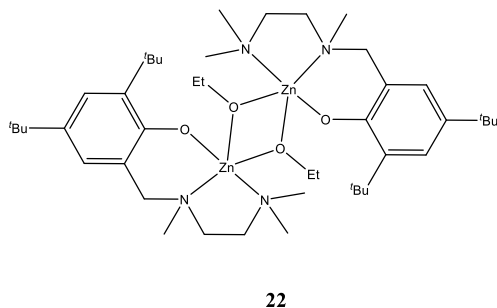


**Figure 1.34.** The structure of catalyst **22**.

In hopes of improving stereocontrol, Mehrkhodavandi and co-workers later designed a zinc catalyst with the same ligand frame as **22**, while incorporating a chiral cyclohexyl arm on the ligand (**23**, Figure 1.35). However, the more rigid ligand led to severe loss of activity (full conversion in a few days), and it did not provide any stereocontrol.<sup>87</sup>

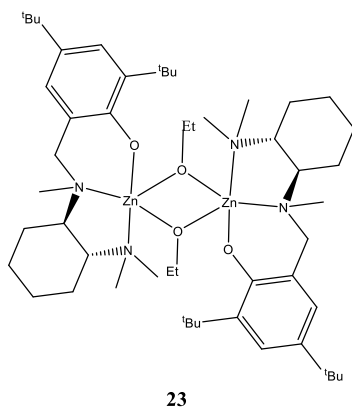
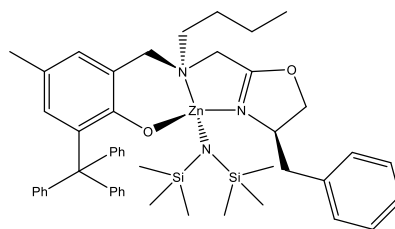


**Figure 1.35.** The structure of catalyst **23**.

In 2017, Ma and co-workers prepared a series of zinc complexes with oxazolinyll/benzoxazolyl based aminophenolate ligands. Of all the complexes they reported, **24**, showed the highest isoselectivity ( $P_m = 0.86$ ) as well as being the most active, reaching 94% conversion in only 14 min. **24** is one of the most active and isotactic catalysts reported to date (Figure 1.36).<sup>88</sup>

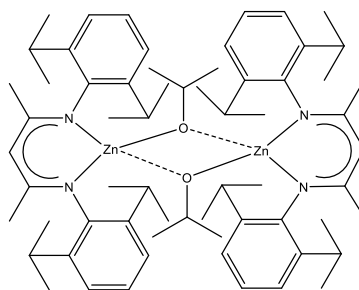


24

**Figure 1.36.** The structure of catalyst **24**.

### 8.2.3. $\beta$ -Diketiminato ligands

$\beta$ -Diketiminato (BDI) ligand frames have also been widely used to prepare catalysts for lactide polymerization. Coates and co-workers designed a dimeric ( $\beta$ -diketiminato)zinc catalyst with two bridging isopropoxide groups (**25**, Figure 1.37), that reached full conversion in about 20 min while providing a very high degree of heterotacticity ( $P_r = 0.94$ ).<sup>89</sup> Further studies conducted on these types of ligand systems have shown that changing the substituent on the  $\beta$ -diketiminato affects the stereocontrol of the obtained PLA chain during the polymerization reaction. For instance, changing the substituents on the *ortho* position of the phenyl ring to ethyl or *n*-propyl will consequently decrease the heterotacticity to  $P_r = 0.79$  or  $P_r = 0.76$ , respectively.<sup>90</sup>



25

**Figure 1.37.** The structure of catalyst **25**.

Based on the work of Williams and Phomhrai, it has been shown that tin(II) and magnesium based complexes with  $\beta$ -diketiminato also provide heterotactic stereocontrol for the ROP of *rac*-lactide. A heterotacticity of 0.7 and 0.9 has been reported for tin(II) (**26**) and magnesium(II) (**27**) respectively (Figure 1.38).<sup>91,92</sup> It is important to note that this high degree of heterotacticity for **27** is only observed when

THF is used for polymerization. In dichloromethane and benzene no stereocontrol is provided. The behavior of zinc (**25**) is completely contrary to magnesium, as it can provide high degrees of stereocontrol in dichloromethane, THF and benzene. Chisholm and co-workers, investigated the differences between the magnesium and zinc  $\beta$ -diketiminato complexes in more detail.<sup>93,94</sup> In the case of the zinc complex the coordinated THF is dissociated in solution at a very high rate, even at very low temperatures such as  $-80$  °C. In contrast, for the magnesium complex both coordinated and free THF have been observed in the NMR spectra. Based on the obtained results, it has been proposed that the steric hindrance caused by the coordination of the THF to magnesium center is required for stereocontrol.

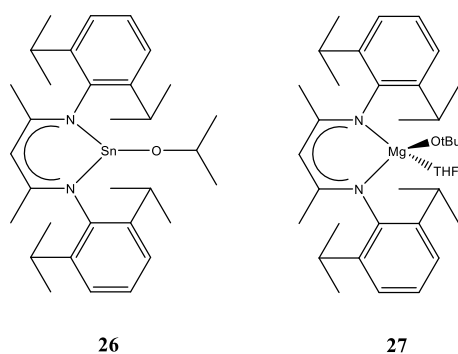
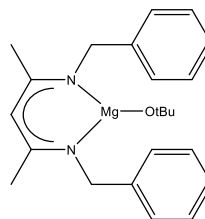


**Figure 1.38.** The structures of catalysts **26** and **27**.

Diketiminato complexes typically do not provide isotactic PLA. Chisholm attempted to introduce chirality in the catalytic site by the use of mono-substituted aryl diketiminates.<sup>94,95</sup> Schaper and co-workers attempted the same by the use of aliphatic N-substituents, providing either a chiral ligand or a flexible ligand able to form chiral catalytic sites.<sup>96</sup> In all cases, different degrees of heterotacticity were observed.

The only evidence for isotactic preference in diketiminato catalysts was observed by Schaper for the respective Mg complexes, **28** (Figure 1.39). While interesting as proof of principle, the low degree of isotacticity ( $P_m = 0.55$  at  $-23$  °C) which could not be improved upon, did not encourage further optimization of these catalysts.<sup>97</sup>

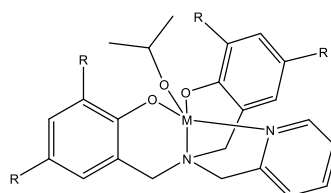


28

**Figure 1.39.** The structure of catalyst **28**.

#### 8.2.4. Amino(bisphenolato) and amino(trisphenolato) ligands

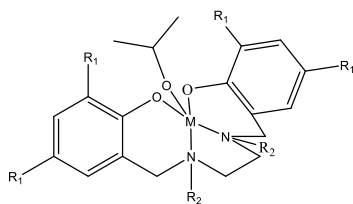
Tetradentate amino(bisphenolato) and amino(trisphenolato) ligand systems have also been studied with a wide range of metal centers for the ROP of lactide while providing high degrees of stereocontrol. Davidson and co-workers studied the behavior of amino(trisphenolato) ligands with zirconium (**29**), hafnium (**30**) and germanium (**31**) in both melt conditions at 130 °C and in solution at room temperature.<sup>98,99</sup> In both conditions, very high degrees of heterotacticity were observed,  $P_r = 0.96$ ,  $P_r = 0.88$  and  $P_r = 0.80$  for Zr, Hf and Ge respectively. Davidson and co-workers also applied titanium (**32**) to the ROP of lactide, but they were not able to obtain any stereocontrol which they attributed to the large amount of chain transfer they observed in the polymerization (Figure 1.40).<sup>100</sup>



**29:** M = Zr, R = <sup>t</sup>Bu  
**30:** M = Hf, R = <sup>t</sup>Bu  
**31:** M = Ge, R = Me  
**32:** M = Ti, R = <sup>t</sup>Bu

**Figure 1.40.** The structure of catalysts **29**, **30**, **31** and **32**.

Davidson and co-workers continued their investigations on group IV metals by changing the ligand system to a diamine(bisphenolate), thus instead of  $C_s$  symmetric chiral complex they prepared a  $C_2$  symmetric achiral catalyst. This resulted in isotactic PLA. The highest degree of isotacticity was observed for **33** which contained a zirconium as the metal center (Figure 1.41).<sup>100</sup>



33: X : M = Zr, R<sub>1</sub> = R<sub>2</sub> = Me

**Figure 1.41.** The structure of catalyst **33**.

Mountford and co-workers broadened the scope of diamino-bis(phenoxy) ligands in lactide polymerization, by designing dimeric borohydride complexes containing rare earth metals such as yttrium (**34**), samarium (**35**) and neodymium (**36**). All three complexes provided PLA chains with very high degrees of stereocontrol,  $P_r = 0.87$ ,  $P_r = 0.72$  and  $P_r = 0.64$ , for Y, Sm and Nd respectively (Figure 1.42).<sup>101</sup>

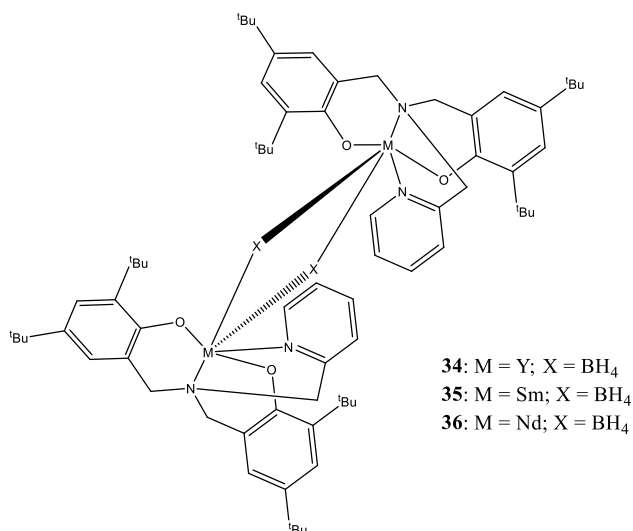
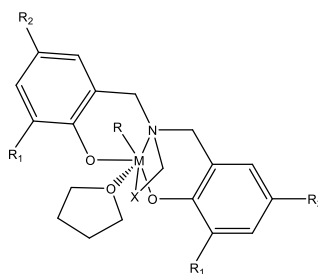


**Figure 1.42.** The structure of catalysts **34**, **35** and **36**.

Carpentier and co-workers also studied rare earth metals such as lanthanum, yttrium and neodymium but with an achiral tetradentate alkoxyaminobis(phenolate) ligand system. Yttrium based complexes, **37** (Figure 1.43), showed the highest degree of stereocontrol with a  $P_r$  value of 0.90. It has been observed that the nature of the solvent and the metallic center as well as the steric bulk of the substituents on the ligand frame have a great influence on the stereocontrol of the obtained PLA chain. It has also been shown that increasing the steric bulk on these ligands especially in the *ortho* position could result in a decrease of the rate of polymerization. Although it

should be mentioned that these catalysts are very active in lactide polymerization and are able to reach full conversion in around 20 min at room temperature.<sup>102</sup> Carpentier has also been able to show that these catalysts can form the alkoxide complex *in situ* as seen previously for the aluminum catalysts. These polymerizations proved to be immortal in the presence of an external alcohol. By adding 50 equivalents of an alcohol 50 chains could be produced while always obtaining a high degree of heterotacticity ( $P_r = 0.90$ ), an excellent molecular weight control and very narrow polydispersities of 1.08.<sup>103</sup>



37: M = Y; R = N(SiHMe<sub>2</sub>); R<sub>1</sub> = R<sub>2</sub> = C(Me<sub>2</sub>)Ph; X=OMe

**Figure 1.43.** The structure of catalyst **37**.

### 8.3. Copper catalysts used in lactide polymerisation

Most of the transition metals that have been studied have  $d^0$ - or  $d^{10}$ - electronic configuration. Other transition metals such as Cr,<sup>104</sup> Mn,<sup>105,106,107,108,109</sup> Ni,<sup>110,111,112,113,114</sup> and Co,<sup>107,115,116,117</sup> have been largely left unstudied. Prior to 2013, catalysts based on group 5-11, with the exception of iron and copper, provided typically low to moderate activities and no or slightly heterotactic stereocontrol. The one exception were several iron complexes, which showed high activities (but no stereocontrol). Jeong showed in 2015 that Cu(II) catalysts can provide highly heterotactic PLA.<sup>118</sup> Very recently, Chen showed an impressive degree of isotactic stereocontrol in Fe-based catalysts.<sup>119</sup> Copper catalysts that have been used in both *rac*- and *L*-lactide polymerization will be discussed in more detail below. Prior to work in the Schaper and Jeong groups, Cu-based catalysts were based on either copper carboxylate salts or on copper salen or phenoxyimine complexes. In 2011, Charkraborty and co-workers studied Cu(OAc)<sub>2</sub> in bulk polymerization conditions, in

the presence and absence of water. In both cases they were able to obtain very good molecular weight control as well as very narrow molecular weight distributions. Unfortunately no stereocontrol was observed in the presence of *rac*-lactide.<sup>120</sup>

In 2001, Liang and co-workers reported the preparation of  $K[CuL] \cdot nH_2O$ , **38** (Figure 1.44), where *L*-aspartic acid-salicylidene was used as the ligand. They only observed activity in molten monomer. Unfortunately no stereocontrol or molecular weight control was observed.<sup>121</sup>

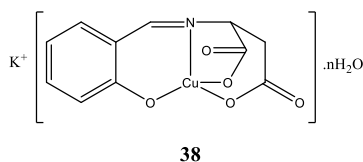


**Figure 1.44.** The structure of catalyst **38**.

In 2002, Ghosh and co-workers prepared three homoleptic copper catalysts, **39**, **40** and **41**, with phenoxy-ketimine ligands as shown below (Figure 1.45). The polymerizations were conducted in pressure tubes in molten monomer. All three catalysts produced PLA with rather good molecular weight control and somewhat narrow polydispersities. Lower molecular weights obtained with **40** compared to **39** and **41**, were attributed to the distortion observed in its square planar geometry.<sup>110</sup>

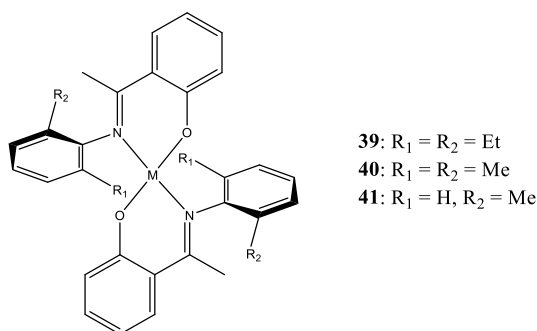


**Figure 1.45.** The structure of catalysts **39**, **40** and **41**.

In 2010, Nordlander and co-workers investigated phenoxyimine copper catalysts with substituents such as *tert*-Bu and Cl on the phenolate ring, **42**, **43**, **44** and **45** (Figure 1.46). They realized that the activity of the catalyst depended on the electronic nature of the substituents. In the presence of electron donating *tert*-Bu groups the catalyst was able to reach full conversion. They attributed this result to the increased electron



density on the oxygen of the phenolate group due to this electron donating substituents, thus increasing its  $\pi$ -donating ability which will in turn weaken the copper-oxygen bond and thus will facilitate the insertion of the lactide into this bond. As a result an improvement in the activity of the catalyst is observed.<sup>122</sup>

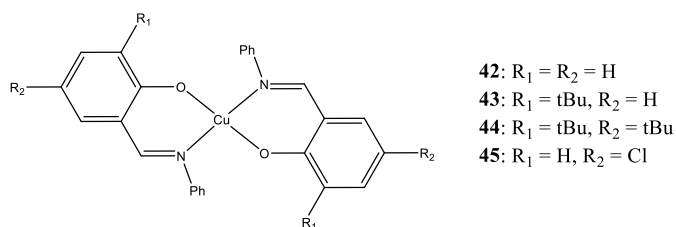


**Figure 1.46.** The structure of catalysts **42**, **43**, **44** and **45**.

In 2010, Jin and co-workers synthesized a mononuclear copper(II) catalyst bearing a salen-type Schiff–base ligand as shown below, **46** (Figure 1.47). The catalyst was active at 130 °C in bulk polymerization. The polymerization took a few days to reach about 70 % conversion. With time the polymer molecular weight increased and narrow polydispersities were observed but after almost 24 h the polymer molecular weight started to decrease while higher polydispersities were obtained, indicating the presence of transesterification during the polymerization.<sup>123</sup>

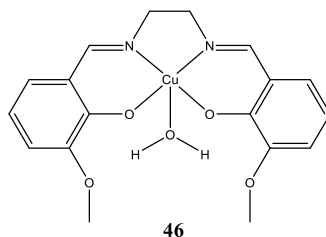
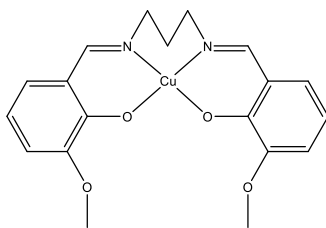


**Figure 1.47.** The structure of catalyst **46**.

In 2015, Sutar and co-workers prepared a copper(II) catalyst very similar to what was shown just previously, but with a more flexible bridge between the two imines, **47** (Figure 1.48). The catalyst had no initiating group, thus the polymerization was conducted in the presence of BnOH. The catalyst showed to be active in dichloromethane at RT, reaching higher than 90% conversion in about 24 h while producing PLA chains with a relatively good molecular weight control. The very high

activity in an activated monomer mechanism was surprising, in particular since these Cu/salen complexes without BnOH required 12 h in molten monomer.<sup>124</sup>



47

**Figure 1.48.** The structure of catalyst **47**.

In 2013, Schaper and co-workers reported a copper catalyst with a  $\beta$ -diketiminato ligand frame (**48**, Figure 1.49) for the polymerization of *rac*-lactide. In contrast to previous Cu-based complexes, catalyst **48** contains an alkoxide initiating group, suitable for a coordination-insertion mechanism. Polymerizations with **48** reached full conversion in a few minutes at room temperature in dichloromethane. Polymer chains with excellent molecular weight control and polydispersities under 1.1 were obtained. Unfortunately while being the most active copper catalyst, no stereocontrol was obtained. The biggest limitation of this catalyst system is the size of the substituent on the  $\beta$ -diketiminato ligand. It has been shown that only in the presence of a benzyl group as the substituent the heteroleptic catalyst can be obtained, while in the presence of bulkier groups the homoleptic complexes will be formed, which are inactive in lactide polymerization. In the presence of even more sterically hindered groups, such as 2,6-diisopropylphenol, even the homoleptic complex could not be formed, and the complex decomposed through a  $\beta$ -H elimination from the isopropoxide forming an unstable Cu(II)-hydride complex.<sup>125</sup>

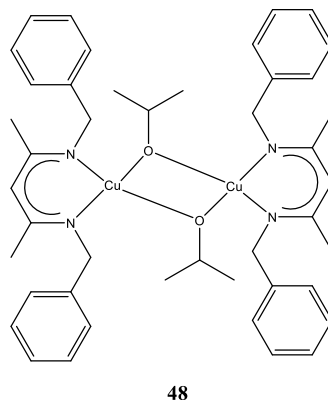


**Figure 1.49.** The structure of catalyst **48**.

Later on, Schaper and co-workers reported that homoleptic complexes such as **49** (Figure 1.50), can be activated *in situ* by the addition of an excess of an external alcohol. The preparation of catalysts with bulkier substituents, however still remain unsuccessful due to steric bulk.<sup>126</sup>

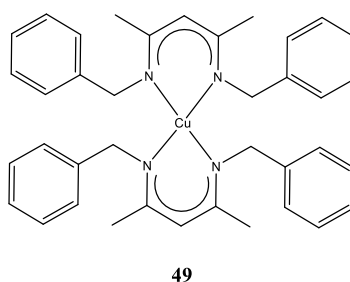


**Figure 1.50.** The structure of catalyst **49**.

Homoleptic copper(II) benzotriazole phenoxide catalysts, comparable to iminophenoxide systems, **50**, **51** and **52** (Figure 1.51), were reported by Huang and co-workers in 2013. These catalysts were active in toluene at 110 °C and were able to polymerize *L*-lactide in the presence of different external alcohols bearing two to three alcohol arms. All the arms showed to be able to insert into the lactide monomer and thus two to three polymer chains grew per alcohol.<sup>127</sup>

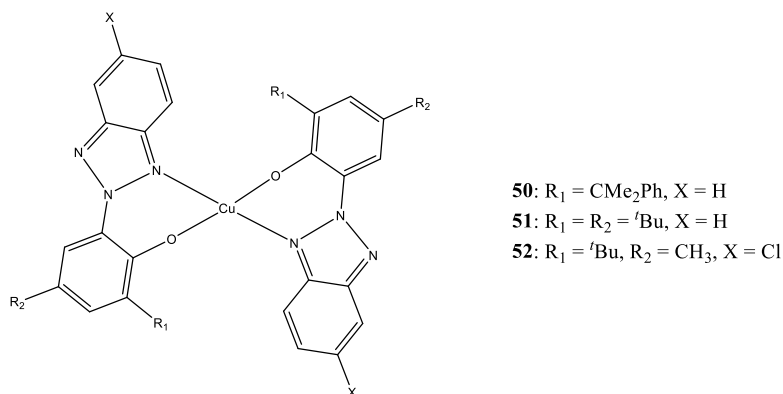


**Figure 1.51.** The structure of catalysts **50**, **51** and **52**.

In 2014, Darkwa and co-workers synthesized a series of copper complexes bearing a bis(3,5-dimethylpyrazole) ligand and two coordinated benzyl carboxylates with different substituents on the benzyl rings, **53**, **54**, **55** and **56** (Figure 1.52). Interestingly all four catalysts behaved the same way in *rac*-lactide polymerization, producing heterotactic PLA chains with lower than expected molecular weights and moderate polydispersities.<sup>128</sup>

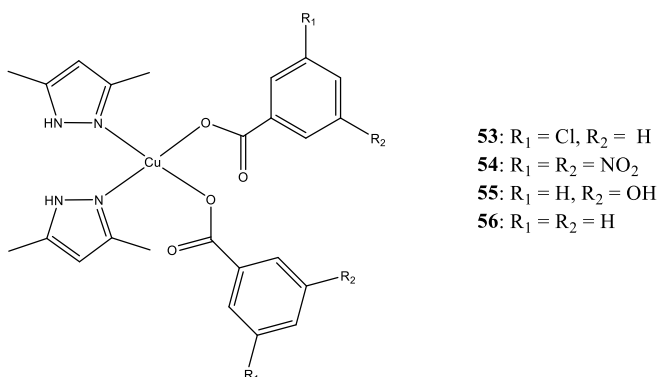


**Figure 1.52.** The structure of catalysts **53**, **54**, **55** and **56**.

In 2015, Jeong and co-workers reported the synthesis of two of the most active copper catalysts in the ROP of lactide with methyl-naphthalenylmethyl-(*R,R*)-1,2-diaminocyclohexanes ligand frames, **57** and **58** (Figure 1.53). The complexes were prepared by the addition of the ligand to  $\text{CuCl}_2 \cdot 2\text{H}_2\text{O}$  in which the chloride was later replaced in situ by the addition of lithium isopropoxide in the course of the polymerization. **57** went to full conversion in only 10 s at room temperature while it took **58** a few seconds longer to reach 100% conversion. This difference of rate has

been attributed to the less sterically bulky ligand frame of **57**. Both catalysts provided very good molecular weight control with narrow polydispersities and very high degrees of heterotacticity,  $P_r = 0.88$  and  $P_r = 0.90$  respectively.<sup>118</sup>

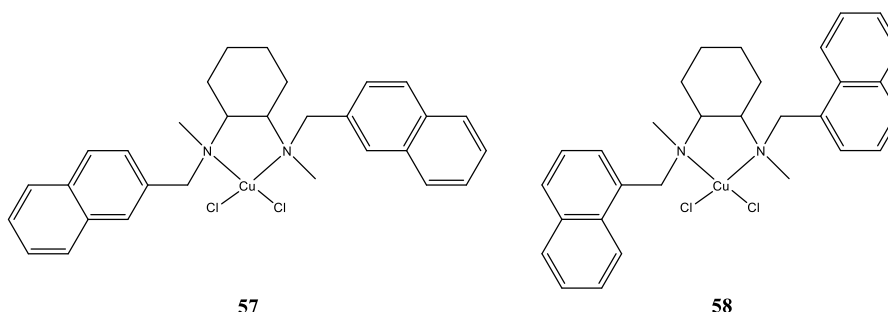


**Figure 1.53.** The structure of catalysts **57** and **58**.

## 9. Aim of this work

Since there are not that many catalysts reported with manganese that undergo a coordination-insertion mechanism for the ROP of lactide, in chapter 2 I report a series of Mn(III) bisphenolate complexes that show such a mechanism in bulk polymerization.

Cu(II) complexes with a  $\beta$ -diketiminato ligand framework, previously synthesized in the group, had a high preference for the formation of the homoleptic complex, which is not active in *rac*-lactide polymerization. In order to overcome the Schlenk equilibrium, a catalyst with a new ligand containing a pyrrole and two coordinating imine arms was designed. In the original design, the complex was supposed to have an isopropoxide as the initiator and an open coordination site for the coordination of the lactide monomer. All attempts to prepare this catalyst failed.

In chapter 3, the stereocontrol mechanism of these dimeric Cu(II) diiminopyrrolide complexes is studied in detail.

Chapter 4 and 5 continue the study of such dimeric Cu(II) catalysts with the presence of different substituents to investigate the effect of steric bulk and electronegativity on the activity and stereocontrol of the complexes in ROP of lactide.

Chapter 6 takes this investigation one step further and discusses phenoxy-imine ligand frameworks instead of diiminopyrrolides.

In chapter 7, the copper center is being replaced by a zinc and the effects on the activity and stereocontrol of the catalyst is being studied. The same mechanism that has proven to cause stereocontrol in chapter 4 is being applied to a series of zinc complexes through a specially designed ligand framework.

In chapter 8, completely different from what has been discussed until now, a series of Cu(II) complexes with different tri/tetradentate phenoxy-imine ligand frameworks are investigated for bulk polymerization with an activated monomer mechanism.

## References Chapter 1

1. Jensen, W. B. *J. Chem. Educ.* **2006**, 83 (6), 838.
2. Jensen, W. B. *J. Chem. Educ.* **2008**, 85 (5), 624.
3. Nicholson, J. W. *Educ. Chem.* **1991**, 70 (28).
4. Feldman, D. *Des. Monomers Polym.* **2008**, 11 (1), 1-15.
5. Zhang, C. Biodegradable Polyesters: Synthesis, Properties, Applications. In *Biodegradable Polyesters*, Fakirov, S., Ed. Wiley-VCH Verlag GmbH & Co. KGaA: 2015.
6. Staudinger., H.; Fritschi, J. *Helv. Chim. Acta* **1922**, 5 (5), 785-806.
7. *Wikimedia Commons* (commons.wikimedia.org).
8. Larsen, L. V. *Chem. Eng. News* **1984**, 62 (Jan. 23), 58.
9. Kusum Kaushik, R. B. S.; Agarwal, S. *Int. J. Pharm. Sci. Rev. Res.* **2016**, 37 (2), 30-36.
10. de Moraes Porto, I. C. C. **2012**.
11. (Gajre)Kulkarni, V.; Butte, K.; Rathod, S. *Natural Polymers- A comprehensive Review*. 2012; Vol. 3, p 1597-1613.
12. Zouai, F. Z. B. F. *Alg. J. Nat. Prod.* **2016**, 4 (3), 348-357.
13. Stefano, T. *J. Appl. Polym. Sci.* **2013**, 127 (2), 837-837.
14. Hutley, T. J.; Ouederni, M. Polyolefins—The History and Economic Impact. In *Polyolefin Compounds and Materials: Fundamentals and Industrial Applications*, Al-Ali AlMa'adeed, M.; Krupa, I., Eds. Springer International Publishing: Cham, 2016; pp 13-50.
15. Aggarwal, S. L.; Sweeting, O. J. *Chem. Rev.* **1957**, 57 (4), 665-742.
16. Biron, M. Chapter 3 - Basic criteria for the selection of thermoplastics. In *Thermoplastics and Thermoplastic Composites*, Elsevier: Oxford, 2007; pp 155-216.
17. Carothers, W. H. *J. Am. Chem. Soc.* **1929**, 51 (8), 2548-2559.
18. Gopal Rao, M.; Bharathi, P.; Akila, Rm. *Sci. Revs. Chem. Comm.* **2014**, 4 (2), 61-68.
19. Katarzyna Leja, G. L. *Polish J. of Environ. Stud.* **2010**, 19, 255-266.
20. Gironi, F.; Piemonte, V. *Energ. Sources. Part A* **2011**, 33 (21), 1949-1959.
21. Ren, X. *J. Clean. Prod.* **2003**, 11 (1), 27-40.

22. Rujnić-Sokele, M.; Pilipović, A. *Waste Manag. Res.* **2017**, *35* (2), 132-140.
23. Tănase, E. E.; Rapa, M.; Popa, O. *Scientific Bulletin. Series F. Biotechnologies* **2014**, *XVIII*, 188-195.
24. Bharti, S. N.; Swetha, G. *J. Pet. Environ. Biotechnol.* **2016**, *07* (02).
25. Woodruff, M. A.; Hutmacher, D. W. *Prog. Polym. Sci.* **2010**, *35* (10), 1217-1256.
26. Lipinsky, E. S.; Sinclair, R. G. *Chem. Eng. Prog.* 1986; Vol. 82, p 26-32.
27. Vert, M.; Schwarch, G.; Coudane, J. *J. Macromol. Sci., Part A: Pure Appl. Chem.* **1995**, *32* (4), 787-796.
28. Lunt, J. *Polylactic acid polymers for fibers and nonwovens.* 2000; Vol. 15, p 48-52.
29. Avinc, O.; Khoddami, A. *Fibre Chemistry* **2009**, *41* (6), 391-401.
30. Wickramasinghe, N.; Geisler, E. *Encyclopedia of Healthcare Information Systems* **2008**, *3*, 1566.
31. Cho, J.; Nayab, S.; Jeong, J. H. *Polyhedron* **2016**, *113*, 81-87.
32. Gibson, V. C.; Marshall, E. L.; Navarro-Llobet, D.; White, A. J. P.; Williams, D. J. *J. Chem. Soc., Dalton Trans.* **2002**, (23), 4321-4322.
33. Kershaw, D. P. J. *United Nations Environment Programme (UNEP), Nairobi.* **2015**.
34. Ghaffar, T.; Irshad, M.; Anwar, Z.; Aqil, T.; Zulifqar, Z.; Tariq, A.; Kamran, M.; Ehsan, N.; Mehmood, S. *J. Radiat. Res. Appl. Sci.* **2014**, *7* (2), 222-229.
35. Majid, J.; Arab, T. E.; Muhammad, I.; Muriel, J.; Stéphane, D. *Compr. Rev. Food Sci. F. Saf.* **2010**, *9* (5), 552-571.
36. Masanobu, A.; Katashi, E.; Kazuhiko, S.; Akihiro, Y. *Bull. Chem. Soc. Jpn.* **1995**, *68* (8), 2125-2131.
37. Xuan, P.; Xiuli, Z.; Zhaohui, T.; Xuesi, C. *Biotechnol. J.* **2010**, *5* (11), 1125-1136.
38. Garlotta, D. *J. Polym. Environ.* **2001**, *9* (2), 63-84.
39. Stanford, M. J.; Dove, A. P. *Chem. Soc. Rev.* **2010**, *39* (2), 486-494.
40. Dove, A. P. *ACS Macro Lett.* **2012**, *1* (12), 1409-1412.



41. Pieter, V. W.; Michiel, D.; Evelien, V.; Bert, S. *ChemSusChem* **2016**, *9* (9), 907-921.
42. Van Wouwe, P.; Dusselier, M.; Vanleeuw, E.; Sels, B. *ChemSusChem* **2016**, *9* (9), 907-21.
43. Dechy-Cabaret, O.; Martin-Vaca, B.; Bourissou, D. *Chem. Rev.* **2004**, *104* (12), 6147-6176.
44. Jolanta, B.; Andrzej, D.; Adam, K.; Ryszard, S.; Stanislaw, P. *Macromol. Symp.* **1997**, *123* (1), 93-101.
45. Stanislaw, P.; Andrzej, D.; Ryszard, S. *Macromol. Symp.* **1998**, *132* (1), 441-449.
46. Szwarc., M. *J. Polym. Sci., Part A: Polym. Chem.* **1998**, *36* (1), IX-XV.
47. Aida, T.; Inoue, S. *Acc. Chem. Res.* **1996**, *29* (1), 39-48.
48. Wang, L.; Poirier, V.; Ghiotto, F.; Bochmann, M.; Cannon, R. D.; Carpentier, J.-F.; Sarazin, Y. *Macromolecules* **2014**, *47* (8), 2574-2584.
49. Young, R. J. *Introduction to Polymers*. Chapman and Hall: 1981.
50. Chisholm, M. H.; Iyer, S. S.; McCollum, D. G.; Pagel, M.; Werner-Zwanziger, U. *Macromolecules* **1999**, *32* (4), 963-973.
51. Haiyan, M.; P., S. T.; Jun, O. *Angew. Chem. Int. Ed.* **2006**, *45* (46), 7818-7821.
52. Dittrich, W. S., R. C. *Angew. Makromol. Chem.* **1971**, *15*, 109.
53. Kricheldorf, H. R.; Berl, M.; Scharnagl, N. *Macromolecules* **1988**, *21* (2), 286-293.
54. Dubois, P.; Jacobs, C.; Jerome, R.; Teyssie, P. *Macromolecules* **1991**, *24* (9), 2266-2270.
55. Philippe, D.; Robert, J.; Sven, J.; Hans-Gerhard, F. *Macromol. Symp.* **1999**, *144* (1), 289-302.
56. Dege'e, P. D., P.; Jero^me, R.; Jacobsen, S.; Fritz, H.-G. *Macromol. Symp.* **1999**, (144), 289-302.
57. Maciej, B.; Barbara, C.; Piotr, D.; Henryk, J.; Janusz, K. *Macromol. Chem. Phys.* **1999**, *200* (4), 911-916.

58. Kricheldorf, H. R.; Kreiser-Saunders, I.; Boettcher, C. *Polymer* **1995**, *36* (6), 1253-1259.
59. Adam, K.; Andrzej, D.; Stanislaw, P. *Macromol. Rapid Comm.* **1998**, *19* (11), 567-572.
60. Ingrid, K. S.; R., K. H. *Macromol. Chem. Phys.* **1998**, *199* (6), 1081-1087.
61. Kricheldorf, H. R.; Damrau, D.-O. *Macromol. Chem. Phys.* **1997**, *198* (6), 1753-1766.
62. Nicolas, S.; Muriel, W.; Christian, P.; Alain, L. B. *Macromol. Chem. Phys.* **1996**, *197* (9), 2627-2637.
63. Coates, G. W., Ovitt, T. M. *Abstr. Pap. Am. Chem. Soc.* **2000**, *219*, 4-POLY.
64. Ovitt, T. M., Coates, G. W. *J. Am. Chem. Soc.* **2002**, *124*, 1316-1326.
65. Zhiyuan, Z.; J., D. P.; Jan, F. *Angew. Chem. Int. Ed.* **2002**, *41* (23), 4510-4513.
66. Zhong, Z.; Dijkstra, P. J.; Feijen, J. *J. Am. Chem. Soc.* **2003**, *125* (37), 11291-11298.
67. Nomura, N.; Ishii, R.; Akakura, M.; Aoi, K. *J. Am. Chem. Soc.* **2002**, *124* (21), 5938-5939.
68. Tang, Z.; Chen, X.; Pang, X.; Yang, Y.; Zhang, X.; Jing, X. *Biomacromolecules* **2004**, *5* (3), 965-970.
69. Ishii, R.; Nomura, N.; Kondo, T. *Polym. J.* **2004**, *36*, 261.
70. Nobuyoshi, N.; Ryohei, I.; Yoshihiko, Y.; Tadao, K. *Chem.-Eur. J.* **2007**, *13* (16), 4433-4451.
71. Tang, Z.; Gibson, V. C. *Eur. Polym. J.* **2007**, *43* (1), 150-155.
72. Hormnirun, P.; Marshall, E. L.; Gibson, V. C.; White, A. J. P.; Williams, D. J. *J. Am. Chem. Soc.* **2004**, *126* (9), 2688-2689.
73. Konstantin, P.; Israel, G.; Moshe, K. *Angew. Chem. Int. Ed.* **2015**, *54* (49), 14858-14861.
74. Du, H.; Velders, A. H.; Dijkstra, P. J.; Zhong, Z.; Chen, X.; Feijen, J. *Macromolecules* **2009**, *42* (4), 1058-1066.
75. Pang, X.; Chen, X.; Du, H.; Wang, X.; Jing, X. *J. Organomet. Chem.* **2007**, *692* (25), 5605-5613.

76. Bouyahyi, M.; Grunova, E.; Marquet, N.; Kirillov, E.; Thomas, C. M.; Roisnel, T.; Carpentier, J.-F. *Organometallics* **2008**, *27* (22), 5815-5825.
77. Osten, K. M.; Mehrkhodavandi, P. *Acc. Chem. Res.* **2017**, *50* (11), 2861-2869.
78. Douglas, A. F.; Patrick, B. O.; Mehrkhodavandi, P. *Angew. Chem.* **2008**, *120* (12), 2322-2325.
79. Aluthge, D. C.; Ahn, J. M.; Mehrkhodavandi, P. *Chem. Sci.* **2015**, *6* (9), 5284-5292.
80. Osten, K. M.; Aluthge, D. C.; Mehrkhodavandi, P. *Dalton Trans.* **2015**, *44* (13), 6126-6139.
81. Aluthge, D. C.; Patrick, B. O.; Mehrkhodavandi, P. *Chem. Commun.* **2013**, *49* (39), 4295-4297.
82. Aluthge, D. C.; Yan, E. X.; Ahn, J. M.; Mehrkhodavandi, P. *Inorg. Chem.* **2014**, *53* (13), 6828-6836.
83. Chen, H.-Y.; Tang, H.-Y.; Lin, C.-C. *Macromolecules* **2006**, *39* (11), 3745-3752.
84. Darensbourg, D. J.; Choi, W.; Karroonnirun, O.; Bhuvanesh, N. *Macromolecules* **2008**, *41* (10), 3493-3502.
85. Williams, C. K.; Brooks, N. R.; Hillmyer, M. A.; Tolman, W. B. *Chem. Commun.* **2002**, (18), 2132-2133.
86. Williams, C. K.; Breyfogle, L. E.; Choi, S. K.; Nam, W.; Young, V. G.; Hillmyer, M. A.; Tolman, W. B. *J. Am. Chem. Soc.* **2003**, *125* (37), 11350-11359.
87. Labourdette, G.; Lee, D. J.; Patrick, B. O.; Ezhova, M. B.; Mehrkhodavandi, P. *Organometallics* **2009**, *28* (5), 1309-1319.
88. Kan, C.; Hu, J.; Huang, Y.; Wang, H.; Ma, H. *Macromolecules* **2017**, *50* (20), 7911-7919.
89. Cheng, M.; Moore, D. R.; Reczek, J. J.; Chamberlain, B. M.; Lobkovsky, E. B.; Coates, G. W. *J. Am. Chem. Soc.* **2001**, *123* (36), 8738-8749.
90. Cheng, M.; Attygalle, A. B.; Lobkovsky, E. B.; Coates, G. W. *J. Am. Chem. Soc.* **1999**, *121* (49), 11583-11584.
91. Dove, A. P.; Gibson, V. C.; Marshall, E. L.; White, A. J. P.; Williams, D. J. *Chem. Commun.* **2001**, (3), 283-284.

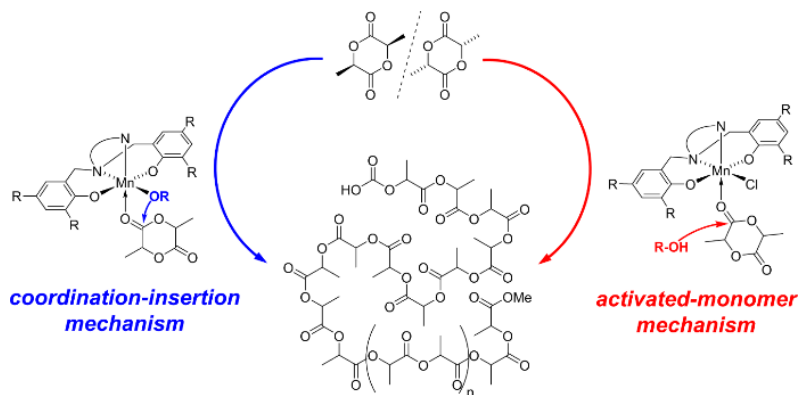
92. Dove, A. P.; Gibson, V. C.; Marshall, E. L.; Rzepa, H. S.; White, A. J. P.; Williams, D. J. *J. Am. Chem. Soc.* **2006**, *128* (30), 9834-9843.
93. Chisholm, M. H.; Gallucci, J.; Phomphrai, K. *Inorg. Chem.* **2002**, *41* (10), 2785-2794.
94. Chisholm, M. H.; Phomphrai, K. *Inorg. Chim. Acta* **2003**, *350*, 121-125.
95. Chisholm, M. H.; Gallucci, J. C.; Phomphrai, K. *Inorg. Chem.* **2005**, *44* (22), 8004-8010.
96. Drouin, F.; Oguadinma, P. O.; Whitehorne, T. J. J.; Prud'homme, R. E.; Schaper, F. *Organometallics* **2010**, *29* (9), 2139-2147.
97. Drouin, F.; Whitehorne, T. J. J.; Schaper, F. *Dalton Trans.* **2011**, *40* (6), 1396-1400.
98. Chmura, A. J.; Davidson, M. G.; Frankis, C. J.; Jones, M. D.; Lunn, M. D. *Chem. Commun.* **2008**, (11), 1293-1295.
99. Chmura, A. J.; Chuck, Ch. J.; Davidson, M. G.; Jones, M. D.; Lunn, M. D.; Bull, S. D.; Mahon, M. F. *Angew. Chem. Int. Ed.* **2007**, *46* (13), 2280-2283.
100. Chmura, A. J.; Davidson, M. G.; Jones, M. D.; Lunn, M. D.; Mahon, M. F.; Johnson, A. F.; Khunkamchoo, P.; Roberts, S. L.; Wong, S. S. F. *Macromolecules* **2006**, *39* (21), 7250-7257.
101. Bonnet, F.; Cowley, A. R.; Mountford, P. *Inorg. Chem.* **2005**, *44* (24), 9046-9055.
102. Cai, C.-X.; Amgoune, A.; Lehmann, C. W.; Carpentier, J.-F. *Chem. Commun.* **2004**, (3), 330-331.
103. Amgoune, A.; Thomas, Ch. M.; Carpentier, J.-F. *Macromol. Rapid Comm.* **2007**, *28* (6), 693-697.
104. Balasanthiran, V.; Chatterjee, C.; Chisholm, M. H.; Harrold, N. D.; RajanBabu, T. V.; Warren, G. A. *J. Am. Chem. Soc.* **2015**, *137* (5), 1786-1789.
105. Kricheldorf, H. R.; Schwarz, G. *J. Macromol. Sci., Part A: Pure Appl. Chem.* **2007**, *44* (6), 625-649.
106. Idage, B. B.; Idage, S. B.; Kasegaonkar, A. S.; Jadhav, R. V. *Mater. Sci. Eng., B* **2010**, *168* (1), 193-198.
107. Rajashekhar, B.; Chakraborty, D. *Polymer Bulletin* **2014**, *71* (9), 2185-2203.

108. Daneshmand, P.; Schaper, F. *Dalton Trans.* **2015**, 44 (47), 20449-20458.
109. Rathore, A.; Kaur, H.; Luque, R. *J. Polym. Res.* **2018**; Vol. 25.
110. John, A.; Katiyar, V.; Pang, K.; Shaikh, M. M.; Nanavati, H.; Ghosh, P. *Polyhedron* **2007**, 26 (15), 4033-4044.
111. Ding, L.; Jin, W.; Chu, Z.; Chen, L.; Lü, X.; Yuan, G.; Song, J.; Fan, D.; Bao, F. *Inorg. Chem. Commun.* **2011**, 14 (8), 1274-1278.
112. Jin, W.-J.; Ding, L.-Q.; Chu, Z.; Chen, L.-L.; Lü, X.-Q.; Zheng, X.-Y.; Song, J.-R.; Fan, D.-D. *J. Mol. Catal. A: Chem.* **2011**, 337 (1), 25-32.
113. Xiao, G.; Yan, B.; Ma, R.; Jin, W. J.; Lu, X. Q.; Ding, L. Q.; Zeng, C.; Chen, L. L.; Bao, F. *Polym. Chem.* **2011**, 2 (3), 659-664.
114. Routaray, A.; Mantri, S.; Nath, N.; Sutar, A. K.; Maharana, T. *Polyhedron* **2016**, 119, 335-341.
115. Tschan, M. J. L.; Guo, J.; Raman, S. K.; Brule, E.; Roisnel, T.; Rager, M.-N.; Legay, R.; Durieux, G.; Rigaud, B.; Thomas, C. M. *Dalton Trans.* **2014**, 43 (11), 4550-4564.
116. Shin, S.; Nayab, S.; Lee, H. *Polyhedron* **2018**, 141, 309-321.
117. Jianing, Z.; Baolong, W.; Liying, W.; Junmin, S.; Yongfeng, Z.; Zhenzhu, C.; Zhenqiang, W. *Appl. Organomet. Chem.* **2018**, 32 (2), e4077.
118. Kwon, K. S.; Cho, J.; Nayab, S.; Jeong, J. H. *Inorg. Chem. Commun.* **2015**, 55, 36-38.
119. Duan, R.; Hu, C.; Li, X.; Pang, X.; Sun, Z.; Chen, X.; Wang, X. *Macromolecules* **2017**, 50 (23), 9188-9195.
120. Gowda, R. R.; Chakraborty, D. *J. Mol. Catal. A: Chem.* **2011**, 349 (1), 86-93.
121. Junquan, S.; Weiliang, S.; Deyu, C.; Chengfeng, L. *J. Appl. Polym. Sci.* **2002**, 86 (13), 3312-3315.
122. Suraj, B.; Jane, M.; Archana, B. L.; Selwyn, M.; Juanita, V. W.; James, D.; Ebbe, N. *Appl. Organomet. Chem.* **2011**, 25 (2), 133-145.
123. Lei-Lei, C.; Li-Qin, D.; Chu, Z.; Yong, L.; Xing-Qiang, L.; Ji-Rong, S.; Dai-Di, F.; Wen-Juan, J. *Appl. Organomet. Chem.* **2011**, 25 (4), 310-316.
124. Routaray, A.; Nath, N.; Maharana, T.; Sutar, A. K. *J. Macromol. Sci., Part A: Pure Appl. Chem.* **2015**, 52 (6), 444-453.

125. Whitehorne, T. J. J.; Schaper, F. *Inorg. Chem.* **2013**, *52* (23), 13612-13622.
126. Whitehorne, T. J. J.; Schaper, F. *Can. J. Chem.* **2013**, *92* (3), 206-214.
127. Chen-Yu, L.; Shi-Jie, H.; Chin-lung, L.; Chen-Yen, T.; Jun-Han, W.; Bao-Tsan, K.; Chia-Her, L.; Hsi-Ya, H. *J. Polym. Sci., Part A: Polym. Chem.* **2013**, *51* (18), 3840-3849.
128. Appavoo, D.; Omondi, B.; Guzei, I. A.; van Wyk, J. L.; Zinyemba, O.; Darkwa, J. *Polyhedron* **2014**, *69*, 55-60.

## Chapter 2 . Exploring the Reactivity of Manganese(III) Complexes with Diphenolate-diamino Ligands in *rac*-Lactide Polymerization

Daneshmand, P.; Schaper F. Exploring the Reactivity of Manganese(III) Complexes with Diphenolate-diamino Ligands in *rac*-Lactide Polymerization. *Dalton Trans.* **2015**, *44*, 20449-20458.



Reproduced by permission of the Royal Society of Chemistry.

Contributions of F. Schaper: A first draft was provided by me with major modification from Prof. Frank Schaper.





# Exploring the Reactivity of Manganese(III) Complexes with Diphenolate-diamino Ligands in *rac*-Lactide Polymerization

*Pargol Daneshmand, Frank Schaper\**

*Centre in Green Chemistry and Catalysis, Department of chemistry, Université de Montréal, C. P. 6128 Succ. Centre-Ville, Montréal, QC, H3T 3J7, Canada.*

*Email: Frank.Schaper@umontreal.ca*

*Electronic Supplementary Information (ESI) available: [Additional details on polymerization reactions, MALDI-spectra, X-ray structure determinations (CIF)].*

## **Abstract**

Manganese(III) complexes of tetradentate diphenolate-diamino (NNOO<sup>2-</sup>) ligands were prepared from aerobic reaction of MnCl<sub>2</sub> with the respective ligands in basic methanolic solution. Methoxide complexes (NNOO)Mn(OMe)(MeOH)<sub>0-1</sub> were obtained for three ligands, while others only provided the respective chloride complexes (NNOO)Mn(Cl)(MeOH). Complexes were analyzed by X-ray diffraction studies and octahedral complexes showed evidence of Jahn-Teller distortions. Magnetic moments determined in MeOD were indicative of high-spin Mn(III)-*d*<sup>4</sup> complexes ( $\mu_{\text{eff}} = 4.2 - 4.6 \mu_{\text{B}}$ ). Methoxide complexes were active in the coordination-insertion polymerization of *rac*-lactide (130 °C, 0.33 – 1.0 mol-% catalyst loading) to yield atactic polylactic acid with moderate molecular weight control. Polymerization activity was reduced, but not suppressed by the presence of protic impurities. Chloride complexes showed less activity and only in the presence of external alcohol, indicative of an activated-monomer mechanism.

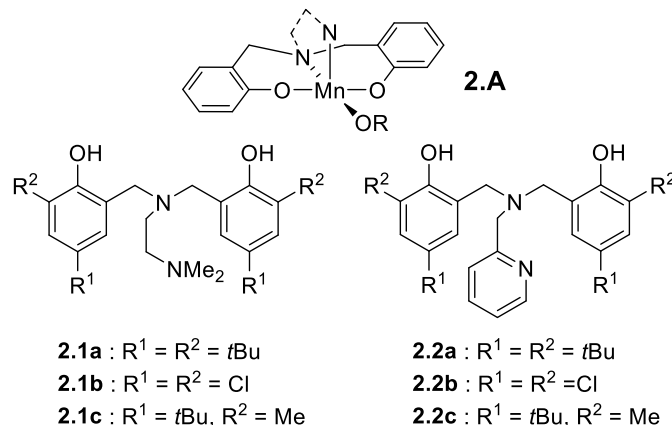
## Introduction

Interest in bio-degradable polymers and materials obtained from renewable resources<sup>1, 2</sup> sparked a large number of investigations in the coordination-insertion polymerization of *rac*-lactide.<sup>3-16</sup> Catalysts with desirable characteristics such as high activity, isoselectivity, perfect molecular weight control, absence of side reactions or chemical robustness have been reported, even though combining all of these in one catalytic system still remains challenging. Most of the investigated catalyst systems are based on metals with an empty *d*-shell (group 1-4 and rare earth metals)<sup>3, 7, 13-23</sup> or a filled *d*-shell (Zn, group 13-14).<sup>4-6, 11, 14, 15, 24, 25</sup>

Of catalysts based on mid-range transition metals, only iron<sup>26-42</sup> and copper<sup>43-54</sup> have been studied in somewhat more detail. Copper catalysts originally showed low to moderate activities,<sup>43-47</sup> but choosing the right ligand system recently provided catalysts with very high activities,<sup>48-54</sup> and even in one case isoselectivity.<sup>54</sup> Catalysts based on Cr,<sup>55</sup> Mn,<sup>38, 56, 57</sup> Ni,<sup>44, 58-60</sup> or Co,<sup>57</sup> remain curiously understudied. Of the three studies employing Mn catalysts for lactide polymerization, two relied on the use of manganese salts, such as MnCl<sub>2</sub> or Mn(OAc)<sub>2</sub>, acting essentially as simple Lewis acids.<sup>56, 57</sup> Idage et al. employed a Mn(III) salen chloride complex and achieved moderate activities and good polymer molecular weight control.<sup>38</sup> A coordination-insertion mechanism was reported, although no nucleophile other than the ligand was present.

Given the promising activities and the limited number of studies with Mn-based catalysts, we decided to further explore the performance of air- and moisture-stable manganese complexes in lactide polymerization. In particular, we were interested in complexes of type **A** (Scheme 2.1), which are designed to follow a coordination-insertion mechanism. To provide stability at ambient atmosphere, Mn(III) complexes were targeted, which required a dianionic spectator ligand. Diamino-diphenolate ligands are readily synthesized, can be easily modified, provide good hydrolytic stability and have been introduced in lactide polymerization by Carpentier for group 3 metals,<sup>18</sup> by Kol for group 4,<sup>61</sup>

by Gibson for group 13,<sup>62</sup> and by Cui and Mountford for lanthanides.<sup>63, 64</sup> We thus explored ligands **1** and **2** as spectator ligands for Mn-catalysed lactide polymerizations.

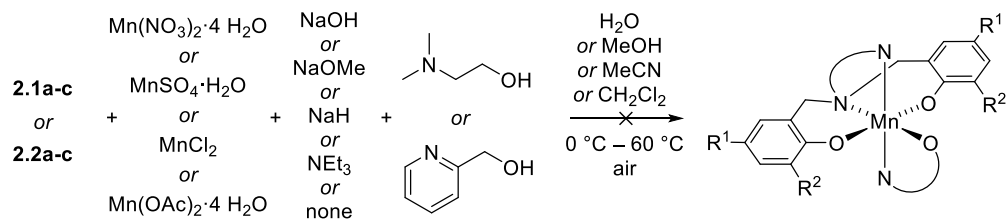


**Scheme 2.1.**

## Results and Discussion

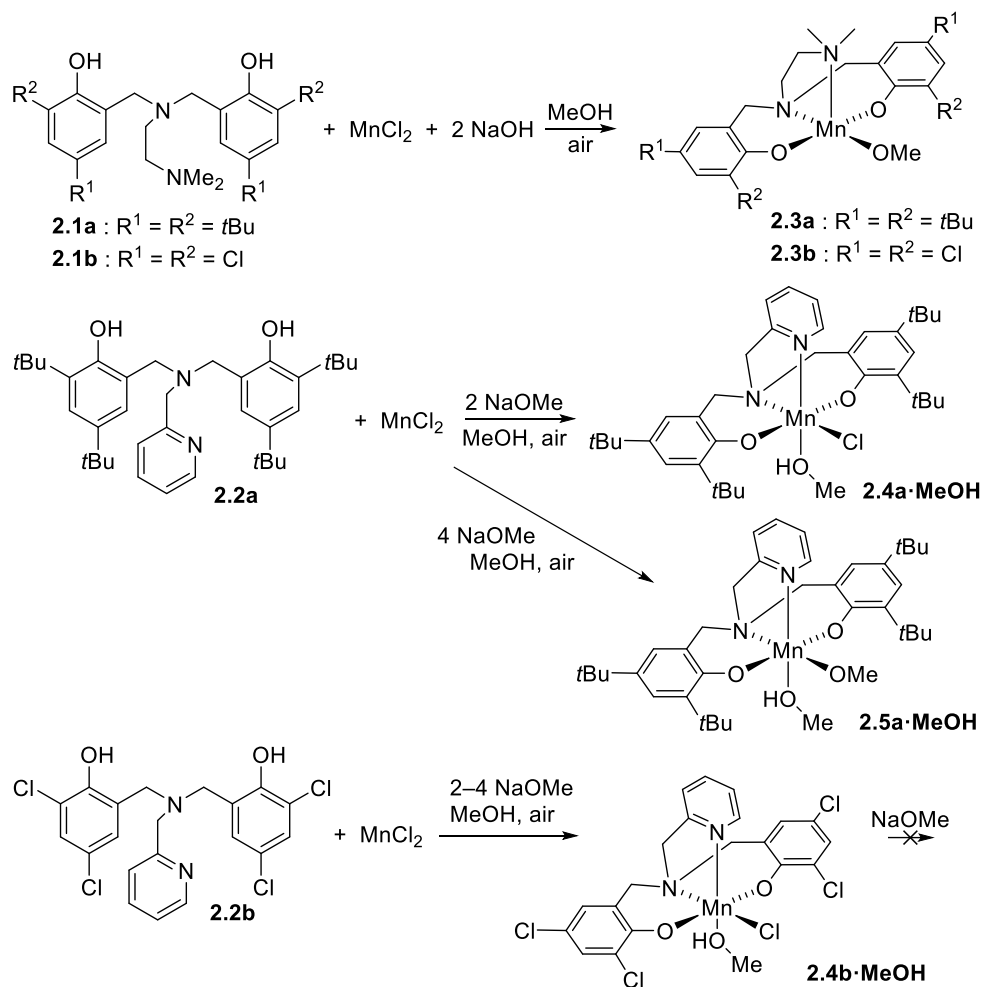
### Synthesis.

Ligands **2.1** and **2.2** were prepared with slight variations of literature protocols (see Experimental Section). Manganese(III) complexes with ligands identical or similar to those employed here have been reported with the ancillary ligand being carboxylates,<sup>65-68</sup> azide or thiocyanate,<sup>69, 70</sup> or planar, bidentate ligands such as acetylacetonate.<sup>68, 71</sup> Since in all cases octahedral complexes had been reported, initial attempts concentrated on the preparation of complexes containing a chelating alcohol, such as pyridyl methoxide or dimethylamino ethoxide, to provide octahedral complexes and to suppress potential  $\beta$ -H elimination reactions in the presence of an open coordination site. Consistent colour changes to red-brown in these reactions seem to indicate ligand coordination to manganese, but despite numerous attempts and variations in Mn source, solvent, base and temperature, neither crystalline material nor powders showing correct combustion analyses could be obtained (Scheme 2.2).



### Scheme 2.2.

A recurrent trend in the obtained combustion analyses were low nitrogen values, indicating a lack of coordination of the chelating alcohol. Replacement of the chelating alcohol by a mixture of methoxide/acetonitrile gave indeed small amounts of a methoxide complex, which did not, however, contain acetonitrile. In an optimized procedure, ligands **2.1a** and **2.1b** were then reacted with  $\text{MnCl}_2$  and 2 equiv  $\text{NaOH}$  in methanol and provided the five-coordinated methoxide complexes **2.3a** and **2.3b** (Scheme 2.3). Reactions of **2.2a** and **2.2b** under the same conditions did not yield crystalline material and the base was switched to sodium methoxide. Reaction of **2.2a** with  $\text{MnCl}_2$  in the presence of two equivalents of  $\text{NaOMe}$  provided only the chloride complex **2.4a**· $\text{MeOH}$ . To encourage chloride/methoxide exchange, the reaction was repeated with four equivalents of  $\text{NaOMe}$  and yielded the methoxide complex **2.5a**· $\text{MeOH}$ . Both complexes were obtained as hexacoordinated complexes with an additional methanol ligand.



### Scheme 2.3.

Reactions of ligand **2.2b** with  $\text{MnCl}_2$  and 2-4 equiv of sodium methoxide under various reaction temperatures did not provide a methoxide complex, but the chloride complex **2.4b·MeOH**. Reaction of the isolated chloride complex **2.4b·MeOH** with sodium methoxide was likewise unsuccessful (Scheme 2.3). Variation of the manganese source to  $\text{MnBr}_2$  or  $\text{MnI}_2$  did not provide any improvement, neither did variation of the base ( $\text{NaOH}$  or  $\text{NEt}_3$ ) or of the solvent. Ligands **2.1c** or **2.2c** failed to produce any isolable or characterizable material, regardless of the conditions employed.

### UV/vis-spectra.

In addition to high-intensity transitions below 300 nm, all Mn complexes display several peaks in the visible region with intensities indicative of charge-

transfer transitions (Fig. 2.1). Based on the hypsochromic displacement observed when the *tert*-butyl substituents in **2.3a** (330, 381 and 512 nm) are replaced by chloride in **2.3b** (293, 370, and 484 nm) or, likewise, in **2.4a**·MeOH (376 and 518 nm) and **2.4b**·MeOH (360 and 470 nm), we tentatively assign these as LMCT transitions from MeO<sup>-</sup> or Cl<sup>-</sup> to Mn. Bathochromic shifts of the two low-energy transitions when replacing the Mn-bound chloride in **2.4a**·MeOH against methoxide in **2.5a**·MeOH (376/518 nm and 410/540 nm, respectively) are in agreement with this assignment.

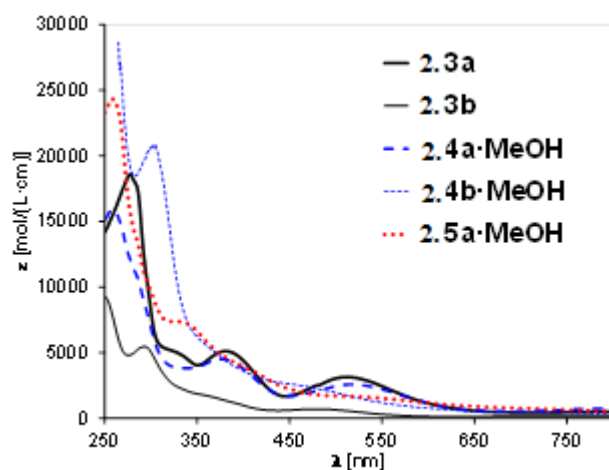


**Figure 2.1.** UV/vis spectra in methanol of manganese complexes **2.3a** (solid bold), **2.3b** (solid thin), **2.4b**·MeOH (dashed bold), **2.4b**·MeOH (dashed thin) and **5a**·MeOH (dotted).

### Magnetic moments.

Magnetic susceptibilities were determined using the Evans NMR method at ambient temperature in MeOD and yielded the expected values for high-spin Mn(III) with  $\mu_{\text{eff}} = 4.2 - 4.6 \mu_{\text{B}}$ .<sup>72, 73</sup>

### Solid-state structures.

Crystals for diffraction studies were obtained for all complexes, but **2.3b** (Fig. 2.2, Table 2.I). The complexes show a wide diversity of conformations due to the flexibility of the tetradentate ligand. In **2.3a**, the two oxametallacycles formed by the phenolate ligands display a boat-conformation, with one aryl

ring oriented towards the dimethylamino ligand (endo), the other oriented away from this ligand (exo). The exo-oriented aryl ring most likely prevents coordination of a sixth ligand. Complex **2.3a** has a geometry intermediate between square-pyramidal and trigonal-bipyramidal ( $\tau = 0.4$ ), but can be considered square-pyramidal with N2 in the apical position for the following discussion. The remaining complexes complete octahedral geometry by coordination of methanol solvent. The equatorial plane contains the phenolate oxygen atoms O1 and O2 and the nitrogen bridgehead atom N1 with Mn-O distances of 1.86 – 1.94 Å and Mn-N1 distances of 2.13 – 2.18 Å (Table 2.I). The N2 atom of the pyridine ligand is found in the apical position with Mn-N2 distances of 2.22 – 2.34 Å, slightly longer than Mn-N1 due to Jahn-Teller distortions expected for high-spin Mn(III) complexes. In **2.4a**·MeOH and **2.5a**·MeOH, the methanol ligand is found in the apical position trans to N2, while in **2.4b**·MeOH, the chloride ligand is found trans to N2, with an increased Mn-Cl bond length (2.498(1) Å in **2.4b** vs. 2.370(2) in **2.4a**), again due to Jahn-Teller distortions. Similar Mn-Cl distances are observed in octahedral Mn(III) chloride complexes with salen and related ligands, which force the chloride ligand in an apical position due to ligand planarity (Mn-Cl = 2.43 – 2.68 Å,  $n = 41$ ).<sup>74</sup> As expected, the methanol ligand shows the reversed trend with a shorter Mn-O distance in **2.4b**·MeOH (2.086(2) Å, trans to N1) then in **2.4a**·MeOH or **2.5a**·MeOH (2.257(5) and 2.273(3) Å, trans to N2).

There is no obvious steric explanation for the placement of the anionic vs. methanol ligand. Neither does it correlate with the conformation of the oxametallacycles (Table 2.I), i. e. a half-chair/endo-boat conformation is observed both for **2.5a**·MeOH and **2.4b**·MeOH. The only structural correlation consists in the evidence of  $\pi$ -stacking to pyridine: a bending of pyridine towards the phenolate ring in **2.4a**·MeOH and **2.5a**·MeOH (Fig. 2.2) is indicative of weak  $\pi$ -stacking interactions between the electron-rich bis-*tert*-butyl phenol and pyridine (aryl-aryl angle = 32°,  $d(\text{atom-plane})$  2.9-4.3 Å). As a consequence, the pyridine ring is no longer perpendicular to the equatorial plane (67°). In **2.4b**·MeOH, there is no approach of the pyridine ring towards

the less electron-rich dichlorophenolate (aryl-aryl angle = 51°) and the pyridine ring remains perpendicular to the equatorial plane (88°). Placement of chloride trans to pyridine in **2.4b**·MeOH might thus be related to better  $\pi$ -interaction of the pyridine with the metal *d*-orbitals.

**Table 2.I.** Selected bond distances [ $\text{\AA}$ ] and bond angles [ $^\circ$ ] from X-ray diffraction studies

	<b>2.3a</b>	<b>2.5a</b> ·MeOH	<b>2.4a</b> ·MeOH	<b>2.4b</b> ·MeOH
Mn-OAr	1.896(2), 1.926(2)	1.884(2), 1.894(2)	1.895(4), 1.936(4)	1.858(2), 1.871(2)
Mn-N1	2.125(2)	2.132(3)	2.178(5)	2.142(2)
Mn-N2	2.254(2)	2.342(3)	2.226(5)	2.224(2)
Mn-X	1.856(2) (OMe)	1.896(3) (OMe)	2.370(2) (Cl)	2.498(1) (Cl)
Me-O(H)Me		2.273(3)	2.262(5)	2.086(2)
ArO-Mn-OAr	151.54(7)	176.06(10)	171.4(2)	176.65(8)
ArO-Mn-N1	89.29(7), 90.18(7)	88.01(10), 90.81(10)	88.8(2), 91.1(2)	88.54(8), 94.05(8)
N1-Mn-Y <sup>a</sup>	174.83(8)	176.50(11)	174.7(1)	166.45(8)
Ring conformations	exo-boat, endo-boat	half-chair, endo-boat	endo-boat, endo-boat	half-chair, endo-boat

<sup>a</sup> Y (ligand trans to N1) = O3 (OMe<sup>-</sup>; **2.3a**, **2.5a**·MeOH), Cl1 (**2.4a**·MeOH), O3 (MeOH; **2.4b**·MeOH)



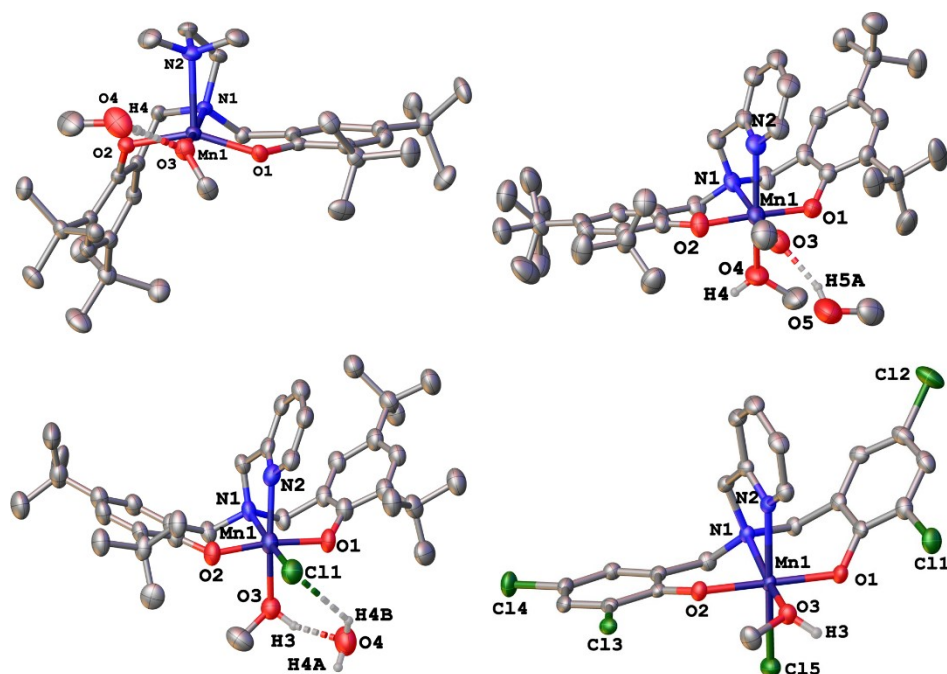


**Figure 2.2.** X-ray structure of **2.3a** (top left), **2.5a**·MeOH (top right), **2.4a**·MeOH (bottom left), and **2.4b**·MeOH (bottom right). Thermal ellipsoids are drawn at 50% probability. Hydrogen atoms (except those on methanol or water molecules) omitted for clarity.

### Lactide polymerization.

Alkoxide complexes **2.3a**, **2.3b** and **2.5a**·MeOH were tested for the polymerization of *rac*-lactide in solution, but proved to be inactive in dichloromethane at ambient temperature or toluene at 70 °C. In molten monomer at 130 °C all catalysts were moderately active and maximum conversion was reached in 4 – 6 hours (Tables 2.II and 2.S1). Polymerizations with **2.3a** showed evidence for catalyst decomposition: appr. 50% conversion was reached after 2 h, but prolongation of the polymerization time did not lead to higher conversions (with exception of one outlier experiment). Conversion was independent from catalyst concentration and decomposition is likely caused by thermal degradation of the active species rather than by impurities in the monomer. Irregular and large disagreements between calculated and observed molecular weights indicate chain termination reactions, in line with thermal degradation of the catalyst. Complex **2.3b** likewise did not show a

notable difference in conversion between 2 and 4 h of reaction time, indicating that the active species was largely decomposed at this time. In contrast to **2.3a**, matching calculated and observed molecular weights and polydispersities of 1.2 – 1.3 indicate improved polymerization control despite catalyst degradation. Increased yields at higher catalyst loadings, together with the better polymer weight control, indicate a slightly higher thermal stability of **2.3b**.

**Table 2.II.** *rac*-lactide polymerization with **2.3a**, **2.3b** and **2.5a**·MeOH <sup>a</sup>

Catalyst	Lactide : Mn	Reaction time / h	Conversion 100	$M_n$ (calc.) mol/kg <sup>b</sup>	$M_n$ (GPC) mol/kg <sup>c</sup>	$M_w/M_n$
<b>2.3a</b>	100:1	2	49	3.5	1.5	1.1
<b>2.3a</b>	100:1	4	52	4.0	2.5	1.2
<b>2.3a</b>	100:1	6	47	3.5	6.5	1.4
<b>2.3a</b>	100:1	6	91	6.5	3.0	1.3
<b>2.3a</b>	300:1	2	53	11.0	11.0	1.3
<b>3a</b>	300:1	4	43	9.5	2.0	1.1
<b>2.3a</b>	300:1	6	51	11.0	29.0	1.5
<b>2.3a</b>	300:1	6	56	12.0	2.5	1.2
<b>2.3b</b>	100:1	4	71	10.5	11.0	1.3
<b>2.3b</b>	100:1	6	81	11.5	13.5	1.3
<b>2.3b</b>	200:1	4	38	11.0	7.5	1.2
<b>2.3b</b>	200:1	6	48	14.0	11.0	1.2
<b>2.5a</b> ·MeOH	100:1	2	41	3.0	3.5	1.1
<b>2.5a</b> ·MeOH	100:1	4	90	6.5	5.0	1.5
<b>2.5a</b> ·MeOH	200:1	2	51	7.5	2.0	1.1
<b>2.5a</b> ·MeOH	200:1	4	88	13.0	15.5	1.4
<b>2.5a</b> ·MeOH	300:1	2	56	12.0	12.0	1.3
<b>2.5a</b> ·MeOH	300:1	4	88	19.0	16.0	1.6

<sup>a</sup> Conditions: 130 °C, sealed tube under N<sub>2</sub>. <sup>b</sup> Calculated from  $m_{\text{lactide}}/(n_{\text{catalyst}}+n_{\text{alcohol}})\cdot\text{conversion}+M_{\text{MeOH}}\cdot n_{\text{alcohol}}$  was determined from the elemental analysis, since in all complexes but **2.3a** co-crystallized solvent was lost on drying, while coordinated methanol was retained. Thus,  $n_{\text{alcohol}} = n_{\text{catalyst}}$  for **2.3a** and **2.5a**·MeOH and  $n_{\text{alcohol}} = 0$  for **2.3b**. Values were rounded to  $\pm 0.5$  kg/mol. <sup>c</sup> Determined by GPC (see experimental part). Values were rounded to  $\pm 0.5$  kg/mol.

Complex **2.5a**·MeOH showed less evidence of catalyst decomposition and polymerizations continue after 2 h to reach appr. 90% conversion after 4 h of

reaction. The greater rigidity of the pyridyl-containing metallacycle in **2.5a**·MeOH might be responsible for the enhanced thermal stability. Assuming the typically observed first-order dependence of the rate on lactide concentration, the curvature of the logarithmic plot of conversion vs. time indicates slow polymerization initiation (Fig. 2.S1), but the general experimental error is too large to draw a definitive conclusion. Polymerizations with **2.5a**·MeOH showed narrow polydispersities of 1.1 – 1.3 at 2 h reaction time and 50% conversion, which increased to 1.4 – 1.6 at 4 h and 90% conversion (Table 2.II). The latter is indicative of transesterification side reactions, which become more evident at higher conversions. MALDI spectra of polymers obtained with **2.5a**·MeOH after 2 and 4 h showed indeed a series of peaks with  $\Delta m/z = 72$ , indicative of transesterification reactions (Fig. 2.S2). The intensity of peaks originating from transesterification increases in the polymer obtained after 4 h of polymerization, in agreement with the observed increase of polydispersity. PLA produced by all three complexes was atactic to slightly heterotactic (**2.3a**:  $P_r = 0.67$ - $0.68$  (lactide:Mn = 300:1), **2.3b**: 0.70-0.73 (200:1), **2.5a**: 0.60-0.62 (300:1)).

Given the air-stability of the complexes, it seemed of interest to verify the performance of **2.5a**·MeOH under less rigorous exclusion of moisture. Thus a sample of **2.5a**·MeOH was washed with water, dried and used in *rac*-lactide polymerization under standard conditions (Table 2.III). The activity was only slightly lower than that of the untreated catalyst and polydispersities remained narrow. Obtained polymer molecular weights showed a lower number of polymer chains produced per manganese, which might indicate (partial) loss of coordinated methanol upon washing. Alternatively, three equivalents of water were added to polymerizations with **2.5a**·MeOH without any notable effect on polymerization activity. Polymerization of unpurified lactide resulted in a more drastic decrease of polymerization activity and only 26% conversion was observed after 4 h (Table 2.III). Narrow polydispersities and good agreements of expected and calculated polymer molecular weights indicate that coordinated methanol and methoxide are liberated upon catalyst degradation.

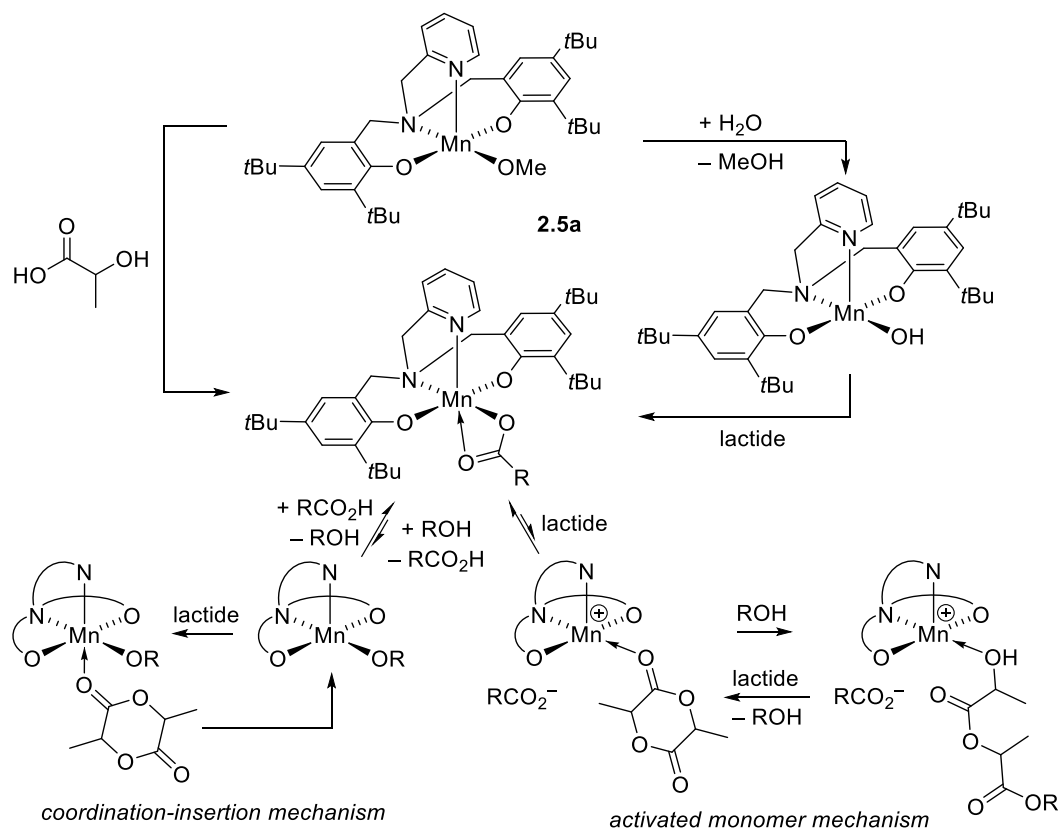
The most likely deactivation path is thus protonation of the methoxide in **2.5a**·MeOH by lactic acid to form a less reactive/unreactive lactate complex. Polymerization with purified lactide under ambient atmosphere proceeded with a comparable loss of activity (Table 2.III). An increased number of polymer chains per manganese indicate that water absorbed from the atmosphere might act as a chain-transfer reagent.

**Table 2.III.** *Rac*-lactide polymerization with **2.5a**·MeOH in the presence of protic impurities <sup>a</sup>

Conditions	Reaction time / h	Conversion 100	$M_n$ (calc.) · mol/kg <sup>b</sup>	$M_n$ (GPC) · mol/kg <sup>c</sup>	$M_w/M_n$	Polymer chains per Mn <sup>d</sup>
Purified lactide, sealed tube under N <sub>2</sub>	2	46	12	12	1.3	2.0
	4	88	19	16	1.6	2.3
Catalyst washed with H <sub>2</sub> O, purified lactide, sealed tube under N <sub>2</sub>	2	14	3	4	1.3	1.6
	4	70	15	29	1.3	1.0
Unpurified lactide, sealed tube under N <sub>2</sub>	2	12	2.5	4.5	1.1	1.2
	4	26	6	6	1.1	1.9
Purified lactide, ambient atmosphere	2	8	3.5	0.5	1.0	6.5
	4	38	8.5	3.5	1.1	4.8

<sup>a</sup> Conditions: 130 °C, lactide:catalyst = 300:1. <sup>b</sup> Calculated from  $m_{\text{lactide}}/(n_{\text{catalyst}}+n_{\text{alcohol}})\cdot\text{conversion}+M_{\text{MeOH}}$ , with  $n_{\text{alcohol}} = n_{\text{catalyst}}$ . <sup>c</sup> Determined by GPC (see experimental part). <sup>d</sup> Calculated from  $(m_{\text{lactide}}/n_{\text{catalyst}}\cdot\text{conversion}+M_{\text{MeOH}})/M_n(\text{GPC})$ .

Lowered, but still notable activity in the presence of impurities might indicate a (reversible) deactivation by lactic acid (water might form dilactic acid on first insertion, Scheme 2.4) or that polymerization follows an activated-monomer mechanism instead of a coordination-insertion mechanism (Scheme 2.4). In fact, previous reports on Mn-catalyzed lactide polymerization employed catalyst structures lacking good initiating groups and are either likely<sup>56, 57</sup> or proven<sup>38</sup> to follow an activated-monomer mechanism.



**Scheme 2.4.**

To verify the presence of a coordination-insertion mechanism in the reactions studied here, the activity of **2.5a**·MeOH and its chloro-derivative **2.4a**·MeOH was investigated in the presence of varying amounts of external alcohol (Table 2.IV). Employing methanol as external alcohol, advantageous since it is already present in the employed catalysts, led to variable results, probably due to competition between incorporation of methanol in the polymer chain and its evaporation into the head space of the reaction. Additional experiments were thus conducted using benzyl alcohol. Overall, the activity of **2.5a**·MeOH is significantly higher than that of **2.4a**·MeOH. The opposite would have been expected for an activated-monomer mechanism, which should favour the more Lewis-acidic **2.4a**·MeOH. Further, the activity of **2.5a**·MeOH remained unchanged upon addition of five equivalents of alcohol (Table 2.IV). Polymerizations with **2.5a**·MeOH thus clearly follow a coordination-insertion mechanism. Catalyst **2.4a**·MeOH, on the other hand, shows increased

conversions in the presence of external alcohol (Table 2.IV). When large amounts of external alcohol were added (35-95 equiv), conversions of 90% were achieved in 30 min (Table 2.S1). Polymerization of **2.4a**·MeOH are thus in agreement with simple Lewis-acid activation of the monomer. Activities observed for **2.4a**·MeOH are in the range of error comparable to those observed for **2.5a**·MeOH in the presence of protic impurities (Table 2.III) and both mechanisms are possible for the deactivated form of **2.5a**·MeOH.

**Table 2.IV.** Effect of additional alcohol on *rac*-lactide conversion at different reaction times <sup>a</sup>

Time / min	<b>2.5a</b> ·MeOH	<b>2.5a</b> ·MeOH + 5 BnOH	<b>2.4a</b> ·MeOH	<b>2.4a</b> ·MeOH + 5 BnOH
30	7 – 18 (2)	17	5 – 10 (3)	
60		19 – 27 (2)	6	16 – 22 (2)
120	51	30	7	32
240	88	95		43

Time / min	<b>2.4a</b> ·MeOH	<b>2.4a</b> ·MeOH + 1 MeOH	<b>2.4a</b> ·MeOH + 2 MeOH	<b>2.4a</b> ·MeOH + 1 NaOMe
15	7 – 8 (2)	4 – 18 (3)	4 – 49 (4)	
30	5 – 10 (3)	0 – 8 (4)	14 – 47 (2)	
60	6		17 – 61 (3)	27
120	7		39 – 88 (2)	13

<sup>a</sup> Conversion in %, numbers in parenthesis indicate the number of polymerization experiments. Conditions: *rac*-lactide : catalyst = 200 : 1, 130 °C, sealed tube.

Polymerization of **2.4a**·MeOH in the presence of sodium methoxide was expected to provide activities comparable to the directly prepared methoxide derivative. Activities remained, however, well below those of to **2.5a**·MeOH (Table 2.IV), indicating that in-situ preparation of the active species is inefficient in this system. Complex **2.4b**·MeOH was likewise applied to the polymerization of lactide in the presence of either 2 equivalents of methanol or one equivalent of sodium methoxide, but proved to be unreactive (< 7% conversion after 1 or 2 h, Table 2.S1).

## Conclusions

Manganese complexes of type **2.A** (Scheme 2.1) are air-stable and are moderately active catalysts for the polymerization of *rac*-lactide. While neither of the presented catalysts represents a significant improvement over existing systems using other metal centers, they compare well to other Mn-based catalysts. Polymerization activities were higher than those of simple  $\text{MnX}_2$  salts, such as  $\text{MnCl}_2$  or  $\text{Mn}(\text{OAc})_2$ ,<sup>56, 57</sup> which required several days at 145 °C. In the presence of larger amounts of external alcohol and following an activated monomer mechanism,<sup>57</sup> activities were similar to those observed for **2.4a**·MeOH. For **2.5a**·MeOH, polymerization was shown to proceed via a coordination-insertion mechanism. Polymerization activities were similar to the Mn salen chloride catalyst reported by Idage,<sup>38</sup> for which the polymerization mechanism is unclear. Although reports on lactide polymerization with Mn so far do not indicate a significant advantage of Mn over other mid-range transition metals, the observed coordination-insertion mechanism offers the chance to improve catalyst activity and polymer molecular weight control for manganese-based catalysts by correct choice of ligand design.

## Experimental section

**General considerations.** Ligand and complex synthesis was performed under ambient atmosphere. Polymerization reactions were carried out under  $\text{N}_2$  atmosphere in a sealed tube if not stated otherwise. Ligands **2.1a-2.1c** and **2.2a-2.2c** were prepared following literature protocols with small variations in some cases:<sup>75-77</sup> **2.1a**, **2.2a**: reflux for 24 h instead of reaction at ambient temperature; **2.1c**, **2.2c**: reflux in water for 24 h instead of methanol. *rac*-Lactide (98%) was purchased from Sigma–Aldrich, purified by 3x recrystallization from dry ethyl acetate and kept at -30 °C. All other chemicals were purchased from common commercial suppliers and used without further purification.  $^1\text{H}$  spectra were acquired on a Bruker AVX 400 spectrometer. The chemical shifts were referenced to the residual signals of the deuterated solvents ( $\text{CDCl}_3$ ;  $^1\text{H}$ :  $\delta$  7.26 ppm). Magnetic moments were determined using

the Evans method at ambient temperature in 10% SiMe<sub>4</sub>/MeOD.<sup>72, 73</sup> Elemental analyses were performed by the Laboratoire d'analyse élémentaire (Université de Montréal). Most compounds contained co-crystallized solvent according to the X-ray diffraction analyses, but combustion analysis indicated that these solvents were mostly removed on drying (see sup. information).

**(*t*Bu<sub>2</sub>ArO-CH<sub>2</sub>)<sub>2</sub>N(C<sub>2</sub>H<sub>4</sub>NMe<sub>2</sub>)Mn(OMe), 2.3a.** Ligand **2.1a** (0.52 g, 0.99 mmol) was added to a solution of MnCl<sub>2</sub> (0.13 g, 1.0 mmol) in methanol (30 ml) and stirred at ambient temperature for 1 h. A solution of NaOH (40 mg, 0.7 mmol) in MeOH (7 ml) was then added dropwise. Stirring was continued for another hour. The obtained solution was concentrated to 1/3 of its volume to yield purple crystals (546 mg, 86%).

Anal. Calcd for C<sub>35</sub>H<sub>57</sub>MnN<sub>2</sub>O<sub>3</sub>·MeOH : C, 67.47; H, 9.60; N, 4.37. Found C, 67.00; H, 9.26; N, 4.44. (One molecule of co-crystallized methanol was observed in the crystal structure.) UV/vis (MeOH, 1.64·10<sup>-4</sup> mol/L) [ $\lambda_{\max}$ , nm ( $\epsilon$ , mol<sup>-1</sup> cm<sup>2</sup>): 278 (19 000), 330 (sh, 4900), 381 (5100), 512 (3100).  $\mu_{\text{eff}}$ (MeOD) = 4.4  $\mu_{\text{B}}$ .

**(Cl<sub>2</sub>ArO-CH<sub>2</sub>)<sub>2</sub>N(C<sub>2</sub>H<sub>4</sub>NMe<sub>2</sub>)Mn(OMe), 2.3b.** Analogous to **2.3a**, ligand **2.1b** (0.39 g, 0.89 mmol), MnCl<sub>2</sub> (0.11 g, 0.90 mmol) and NaOH (36 mg, 0.9 mmol) in methanol (7 ml) afforded **2.3b** as brown powder (223 mg, 48%).

Anal. Calcd for C<sub>19</sub>H<sub>21</sub>Cl<sub>4</sub>MnN<sub>2</sub>O<sub>3</sub> : C, 43.71; H, 4.05; N, 5.37. Found : C, 43.35; H, 3.67; N, 5.38. UV/vis (MeOH, 1.92·10<sup>-4</sup> mol/L) [ $\lambda_{\max}$ , nm ( $\epsilon$ , mol<sup>-1</sup> cm<sup>2</sup>): 293 (5500), 370 (sh, 1600), 484 (700), 735 (150).  $\mu_{\text{eff}}$ (MeOD) = 4.6  $\mu_{\text{B}}$ .

**(*t*Bu<sub>2</sub>ArO-CH<sub>2</sub>)<sub>2</sub>N(CH<sub>2</sub>C<sub>6</sub>H<sub>4</sub>N)MnCl(MeOH), 2.4a·MeOH.** Analogous to **2.3a**, ligand **2.2a** (0.48 g, 0.88 mmol), MnCl<sub>2</sub> (0.11 g, 0.90 mmol) and NaOMe (100 mg, 1.8 mmol) in methanol (7 ml) afforded **2.4a**·MeOH as purple crystals (481 mg, 82%).

Anal. Calcd for C<sub>36</sub>H<sub>50</sub>ClMnN<sub>2</sub>O<sub>2</sub>·MeOH<sub>0.5</sub>: C, 67.53; H, 8.07; N, 4.31. Found: C, 67.72; H, 8.14; N, 4.29. (Co-crystallized solvent observed in X-ray structure, but partly lost on drying.) UV/vis (MeOH, 1.51·10<sup>-4</sup> mol/L) [ $\lambda_{\max}$ ,



nm ( $\epsilon$ , mol<sup>-1</sup> cm<sup>2</sup>): 259 (16 000), 376 (4500), 518 (2600).  $\mu_{\text{eff}}(\text{MeOD}) = 4.3 \mu_{\text{B}}$ .

**(Cl<sub>2</sub>ArO-CH<sub>2</sub>)<sub>2</sub>N(CH<sub>2</sub>C<sub>6</sub>H<sub>4</sub>N)MnCl(MeOH), 2.4b·MeOH.** Ligand **2.2b** (0.38 g, 0.83 mmol) was added to a solution of MnCl<sub>2</sub> (0.11 g, 0.90 mmol) in methanol (30 ml) and stirred for 1 h. A solution of NaOMe (100 mg, 1.8 mmol) in methanol (7 ml) was added dropwise and the reaction heated at reflux for 12 h. The resulting solution was cooled to room temperature and concentrated to 1/3 of its volume to yield red crystals (364 mg, 76%).

Anal. Calcd for C<sub>21</sub>H<sub>18</sub>Cl<sub>5</sub>MnN<sub>2</sub>O<sub>3</sub>: C, 43.60; H, 3.14; N, 4.84. Found : C, 43.49; H, 2.95; N, 4.62. (Two additional molecules of methanol were found in the crystal structure, but lost on drying.) UV/vis (MeOH, 1.51·10<sup>-4</sup> mol/L) [ $\lambda_{\text{max}}$ , nm ( $\epsilon$ , mol<sup>-1</sup> cm<sup>2</sup>): 302 (21 000), 360 (sh, 5500), 470 (sh, 2400), 760 (sh, 400).  $\mu_{\text{eff}}(\text{MeOD}) = 4.2 \mu_{\text{B}}$ .

**(tBu<sub>2</sub>ArO-CH<sub>2</sub>)<sub>2</sub>N(CH<sub>2</sub>C<sub>6</sub>H<sub>4</sub>N)Mn(OMe)(MeOH), 2.5a·MeOH.** Ligand **2.2a** (0.48 g, 0.88 mmol) was added to a solution of MnCl<sub>2</sub> (0.11 g, 0.90 mmol) in methanol (30 ml) and stirred for 1 h at ambient temperature. A solution of NaOMe (150 mg, 2.7 mmol) in methanol (10 ml) was added dropwise and stirring continued for one day. A second portion of NaOMe (50 mg, 0.90 mmol) in methanol (3 ml) was added dropwise and stirring continued for a further day. Concentration of the solution to 1/3 of its volume afforded after one day purple crystals of **2.5a**·MeOH (494 mg, 85%).

Anal. Calcd for C<sub>38</sub>H<sub>57</sub>MnN<sub>2</sub>O<sub>4</sub> : C, 69.07; H, 8.69; N, 4.24. Found : C, 69.10; H, 8.58; N, 4.34. UV/vis (MeOH, 1.64·10<sup>-4</sup> mol/L) [ $\lambda_{\text{max}}$ , nm ( $\epsilon$ , mol<sup>-1</sup> cm<sup>2</sup>): 259 (24 000), 342 (sh, 7100), 410 (sh, 3600), 540 (sh, 1600).  $\mu_{\text{eff}}(\text{MeOD}) = 4.5 \mu_{\text{B}}$ .

**Lactide polymerization.** In a glovebox under an N<sub>2</sub> atmosphere, a pressure tube was charged with 400 – 450 mg of *rac*-lactide. The required amount of catalyst was added to obtain the desired catalyst loading of 0.33 – 1.0 mol-% and, if desired, several  $\mu\text{L}$  of a solution of MeOH or BnOH in toluene. The pressure tube was sealed, removed from the glove box and immersed in an oil

bath pre-heated to 130 °C. The polymerization was conducted under light stirring for the desired time, the pressure tube removed from the oil bath and cooled for appr. 5 min. A solution of acetic acid in CDCl<sub>3</sub> (1 M, 3 – 4 drops) was added to quench the reaction. After cooling to room temperature, the polymer was dissolved in CDCl<sub>3</sub> and filtered through a short silica plug, which was rinsed with additional CDCl<sub>3</sub>. In the absence of external alcohol, the solution was analyzed by NMR and then evaporated to dryness. In the presence of added alcohol, the solution was immediately evaporated and samples were re-dissolved for NMR analysis. All isolated polymers were kept at –80 °C between analyses.

Conversion was determined from <sup>1</sup>H NMR in CDCl<sub>3</sub> by comparison to remaining lactide.  $P_r$  was determined from decoupled <sup>1</sup>H NMR by  $P_r = 2 \cdot I_1 / (I_1 + I_2)$ , with  $I_1 = 5.20 - 5.25$  ppm (*rmr*, *mmr/rmm*),  $I_2 = 5.13 - 5.20$  ppm (*mmr/rmm*, *mmm*, *mrm*). Molecular weight analyses were performed on a Waters 1525 gel permeation chromatograph equipped with three Phenomenex columns and a refractive index detector at 35 °C. THF was used as the eluent at a flow rate of 1.0 mL·min<sup>-1</sup> and polystyrene standards (Sigma–Aldrich, 1.5 mg·mL<sup>-1</sup>, prepared and filtered (0.2 mm) directly prior to injection) were used for calibration. Obtained molecular weights were corrected by a Mark-Houwink factor of 0.58.<sup>78</sup>

**X-ray diffraction studies.** Single crystals were obtained directly from isolation of the products as described above. Diffraction data were collected on a Bruker Microstar with a rotating anode source (Cu K $\alpha$ ), on a Bruker Smart APEX with a microsource (Cu K $\alpha$ ) or on a Bruker Venture metaljet diffractometer (Ga K $\alpha$ ) using the APEX2 software package.<sup>79</sup> Data reduction was performed with SAINT,<sup>80</sup> absorption corrections with SADABS.<sup>81</sup> Structures were solved using intrinsic phasing (SHELXT).<sup>82</sup> All non-hydrogen atoms were refined anisotropic using full-matrix least-squares on  $F^2$  and hydrogen atoms refined with fixed isotropic U using a riding model (SHELXL97).<sup>83</sup> Only weakly diffracting crystals could be obtained for

**2.4a**·MeOH and **2.5a**·MeOH, which resulted in increased  $R_{\sigma}$  and  $R1$  values. Two strongly disordered co-crystallized methanol molecules could be identified, but not refined in **2.4b**·MeOH and were removed using the solvent mask routine in OLEX2. Disordered *tert*-butyl groups in **2.3a** and **2.5a**·MeOH were refined using appropriate restraints (SADI, RIGU). Complex **2.4a**·MeOH was found to be non-merohedrally twinned (80:20) and refined using an HKLF 5 file obtained from PLATON/TWINROT.MAT.<sup>84</sup> Further experimental details can be found in Table 2.V and in the supporting information (CIF).

**Table 2.V.** Details of X-ray diffraction studies

	<b>2.3a</b>	<b>2.4a</b> ·MeOH	<b>2.4b</b> ·MeOH	<b>2.5a</b> ·MeOH
Formula	C <sub>35</sub> H <sub>57</sub> MnN <sub>2</sub> O <sub>3</sub> ·MeOH	C <sub>37</sub> H <sub>54</sub> ClMnN <sub>2</sub> O <sub>3</sub> ·H <sub>2</sub> O	C <sub>21</sub> H <sub>18</sub> Cl <sub>3</sub> MnN <sub>2</sub> O <sub>3</sub> ·2 MeOH	C <sub>38</sub> H <sub>57</sub> MnN <sub>2</sub> O <sub>4</sub> ·MeOH
$M_w$ (g/mol); $d_{\text{calcd}}$ (g/cm <sup>3</sup> )	640.80; 1.180	683.22; 1.226	578.56; 1.549	692.83; 1.154
$T$ (K); F(000)	150; 1392	150; 1464	100; 1312	150; 748
Crystal System	orthorhombic	monoclinic	monoclinic	triclinic
Space Group	<i>Pna</i> 2 <sub>1</sub>	<i>P</i> 2 <sub>1</sub> / <i>c</i>	<i>P</i> 2 <sub>1</sub> / <i>c</i>	<i>P</i> -1
Unit Cell: $a$ (Å)	12.3705(4)	15.2595(8)	12.7413(7)	10.5736(8)
$b$ (Å)	10.8698(4)	15.9590(9)	13.0938(7)	12.2554(9)
$c$ (Å)	26.8207(9)	15.8429(9)	16.8087(9)	16.4321(13)
$\alpha$ (°)				104.320(5)
$\beta$ (°)		106.365(4)	100.589(2)	103.352(5)
$\gamma$ (°)				92.336(5)
$V$ (Å <sup>3</sup> ); $Z$	3606.4(2); 4	3701.9(4); 4	2756.5(3); 4	1996.6(3); 2
$\square$ (mm <sup>-1</sup> ); Abs. Corr.	3.26; multi-scan	2.54; multi-scan	8.67; multi-scan	1.97; multi-scan
$\theta$ range (°); completeness	1.6 – 67.7; 1.00	3.5 – 60.9; 0.99	3.5 – 67.7; 1.00	3.3 – 53.6; 1.00
collected reflections;	71267; 0.038	50921; 0.13	38130; 0.030	33228; 0.078
$R_{\square}$				
unique reflections; $R_{\text{int}}$	6675; 0.053	8498; 0.19	5371; 0.049	9145; 0.087
observed reflections;	6432; 0.039	4189; 0.100	4930; 0.039	5223; 0.073
$R1(F)$				
wR( $F^2$ ) (all data);	0.078; 1.03	0.31; 1.038	0.112; 1.044	0.22; 1.03
GoF( $F^2$ )				
Residual electron density	0.25; -0.32	1.1; -0.92	0.89; -0.71	0.65; -0.53

**Acknowledgements**

Support by Francine Bélanger (X-ray) and Marie-Christine Tang (MALDI) is gratefully acknowledged. Funding was supplied by the NSERC – Discovery Program.

## References Chapter 2

1. S. Slomkowski, S. Penczek and A. Duda, *Polym. Adv. Technol.*, 2014, **25**, 436-447.
2. M. Singhvi and D. Gokhale, *RSC Advances*, 2013, **3**, 13558-13568.
3. A. Sauer, A. Kapelski, C. Fliedel, S. Dagorne, M. Kol and J. Okuda, *Dalton Trans.*, 2013, **42**, 9007-9023.
4. R. Jianming, X. Anguo, W. Hongwei and Y. Hailin, *Des. Monomers Polym.*, 2013, **17**, 345-355.
5. B. H. Huang, S. Dutta and C. C. Lin, in *Comprehensive Inorganic Chemistry II (Second Edition)*, ed. J. R. Poeppelemeier, Elsevier, Amsterdam, 2013, DOI: <http://dx.doi.org/10.1016/B978-0-08-097774-4.00146-7>, pp. 1217-1249.
6. S. Dagorne, M. Normand, E. Kirillov and J.-F. Carpentier, *Coord. Chem. Rev.*, 2013, **257**, 1869-1886.
7. J.-F. Carpentier, B. Liu and Y. Sarazin, in *Advances in Organometallic Chemistry and Catalysis*, John Wiley & Sons, Inc., 2013, DOI: 10.1002/9781118742952.ch28, pp. 359-378.
8. I. dos Santos Vieira and S. Herres-Pawlis, *Eur. J. Inorg. Chem.*, 2012, **2012**, 765-774.
9. S. Dutta, W.-C. Hung, B.-H. Huang and C.-C. Lin, in *Synthetic Biodegradable Polymers*, eds. B. Rieger, A. Künkel, G. W. Coates, R. Reichardt, E. Dinjus and T. A. Zevaco, Springer-Verlag, Berlin, 2011, pp. 219-284.
10. P. J. Dijkstra, H. Du and J. Feijen, *Polym. Chem.*, 2011, **2**, 520-527.
11. N. Ajellal, J.-F. Carpentier, C. Guillaume, S. M. Guillaume, M. Helou, V. Poirier, Y. Sarazin and A. Trifonov, *Dalton Trans.*, 2010, **39**, 8363.
12. M. D. Jones, in *Heterogenized Homogeneous Catalysts for Fine Chemicals Production*, eds. P. Barbaro and F. Liguori, Springer Netherlands, 2010, vol. 33, pp. 385-412.
13. A. K. Sutar, T. Maharana, S. Dutta, C.-T. Chen and C.-C. Lin, *Chem. Soc. Rev.*, 2010, **39**, 1724-1746.
14. C. M. Thomas, *Chem. Soc. Rev.*, 2010, **39**, 165.

15. J.-F. Carpentier, *Macromol. Rapid Comm.*, 2010, **31**, 1696-1705.
16. C. A. Wheaton, P. G. Hayes and B. J. Ireland, *Dalton Trans.*, 2009, 4832 - 4846.
17. H. Ma and J. Okuda, *Macromolecules*, 2005, **38**, 2665-2673.
18. A. Amgoune, C. M. Thomas, T. Roisnel and J.-F. Carpentier, *Chem.-Eur. J.*, 2006, **12**, 169-179.
19. E. M. Broderick and P. L. Diaconescu, *Inorg. Chem.*, 2009, **48**, 4701-4706.
20. Z. Zhang and D. Cui, *Chem.-Eur. J.*, 2011, **17**, 11520-11526.
21. C. Bakewell, T.-P.-A. Cao, N. Long, X. F. Le Goff, A. Auffrant and C. K. Williams, *J. Am. Chem. Soc.*, 2012, **134**, 20577-20580.
22. C.-Y. Tsai, H.-C. Du, J.-C. Chang, B.-H. Huang, B.-T. Ko and C.-C. Lin, *RSC Advances*, 2014, **4**, 14527-14537.
23. A. Stopper, J. Okuda and M. Kol, *Macromolecules*, 2012, **45**, 698-704.
24. C. A. Wheaton and P. G. Hayes, *Comments Inorg. Chem.*, 2011, **32**, 127-162.
25. M. Cheng, A. B. Attygalle, E. B. Lobkovsky and G. W. Coates, *J. Am. Chem. Soc.*, 1999, **121**, 11583-11584.
26. H. R. Kricheldorf and D.-O. Damrau, *Macromol. Chem. Phys.*, 1997, **198**, 1767-1774.
27. A. Södergård and M. Stolt, *Macromol. Symp.*, 1998, **130**, 393-402.
28. M. Stolt and A. Södergård, *Macromolecules*, 1999, **32**, 6412-6417.
29. B. J. O'Keefe, S. M. Monnier, M. A. Hillmyer and W. B. Tolman, *J. Am. Chem. Soc.*, 2001, **123**, 339-340.
30. V. C. Gibson, E. L. Marshall, D. Navarro-Llobet, A. J. P. White and D. J. Williams, *J. Chem. Soc., Dalton Trans.*, 2002, DOI: 10.1039/B209703F, 4321-4322.
31. B. J. O'Keefe, L. E. Breyfogle, M. A. Hillmyer and W. B. Tolman, *J. Am. Chem. Soc.*, 2002, **124**, 4384-4393.
32. D. S. McGuinness, E. L. Marshall, V. C. Gibson and J. W. Steed, *J. Polym. Sci., Part A: Polym. Chem.*, 2003, **41**, 3798-3803.
33. A. B. Biernesser, B. Li and J. A. Byers, *J. Am. Chem. Soc.*, 2013, **135**, 16553-16560.

34. C. M. Manna, H. Z. Kaplan, B. Li and J. A. Byers, *Polyhedron*, 2014, **84**, 160-167.
35. J. L. Gorczynski, J. Chen and C. L. Fraser, *J. Am. Chem. Soc.*, 2005, **127**, 14956-14957.
36. X. Wang, K. Liao, D. Quan and Q. Wu, *Macromolecules*, 2005, **38**, 4611-4617.
37. J. Chen, J. L. Gorczynski, G. Zhang and C. L. Fraser, *Macromolecules*, 2010, **43**, 4909-4920.
38. B. B. Idage, S. B. Idage, A. S. Kasegaonkar and R. V. Jadhav, *Mater. Sci. Eng., B*, 2010, **168**, 193-198.
39. Y. Y. Kang, H.-R. Park, M. H. Lee, J. An, Y. Kim and J. Lee, *Polyhedron*, 2015, **95**, 24-29.
40. A. Keuchguerian, B. Mougang-Soume, F. Schaper and D. Zargarian, *Can. J. Chem.*, 2015, **93**, 594-601.
41. A. Kundys, A. Plichta, Z. Florjańczyk, A. Frydrych and K. Żurawski, *J. Polym. Sci., Part A: Polym. Chem.*, 2015, **53**, 1444-1456.
42. A. C. Silvino, A. L. C. Rodrigues and J. A. L. C. Resende, *Inorg. Chem. Commun.*, 2015, **55**, 39-42.
43. J. Sun, W. Shi, D. Chen and C. Liang, *J. Appl. Polym. Sci.*, 2002, **86**, 3312-3315.
44. A. John, V. Katiyar, K. Pang, M. M. Shaikh, H. Nanavati and P. Ghosh, *Polyhedron*, 2007, **26**, 4033-4044.
45. S. Bhunora, J. Mugo, A. Bhaw-Luximon, S. Mapolie, J. Van Wyk, J. Darkwa and E. Nordlander, *Appl. Organomet. Chem.*, 2011, **25**, 133-145.
46. L.-L. Chen, L.-Q. Ding, C. Zeng, Y. Long, X.-Q. Lü, J.-R. Song, D.-D. Fan and W.-J. Jin, *Appl. Organomet. Chem.*, 2011, **25**, 310-316.
47. R. R. Gowda and D. Chakraborty, *J. Molec. Catal. A: Chem.*, 2011, **349**, 86-93.
48. T. J. J. Whitehorne and F. Schaper, *Chem. Commun. (Cambridge, U. K.)*, 2012, **48**, 10334-10336.
49. T. J. J. Whitehorne and F. Schaper, *Inorg. Chem.*, 2013, **52**, 13612-13622.

50. T. J. J. Whitehorne and F. Schaper, *Can. J. Chem.*, 2014, **92**, 206-214.
51. T. J. J. Whitehorne, B. Vabre and F. Schaper, *Dalton Trans.*, 2014, **43**, 6339-6352.
52. K. S. Kwon, J. Cho, S. Nayab and J. H. Jeong, *Inorg. Chem. Commun.*, 2015, **55**, 36-38.
53. A. Routaray, N. Nath, T. Maharana and A. k. Sutar, *J. Macromol. Sci., Part A: Pure Appl.Chem.*, 2015, **52**, 444-453.
54. S. Fortun, P. Daneshmand and F. Schaper, *Angew. Chem., Int. Ed. Engl.*, 2015, **in print**, 10.1002/ange.201505674.
55. V. Balasanthiran, C. Chatterjee, M. H. Chisholm, N. D. Harrold, T. V. RajanBabu and G. A. Warren, *J. Am. Chem. Soc.*, 2015, **137**, 1786-1789.
56. H. R. Kricheldorf and D.-O. Damrau, *J. Macromol. Sci., Part A: Pure Appl.Chem.*, 1998, **35**, 1875-1887.
57. B. Rajashekhar and D. Chakraborty, *Polym. Bull.*, 2014, **71**, 2185-2203.
58. L. Ding, W. Jin, Z. Chu, L. Chen, X. Lü, G. Yuan, J. Song, D. Fan and F. Bao, *Inorg. Chem. Commun.*, 2011, **14**, 1274-1278.
59. W.-J. Jin, L.-Q. Ding, Z. Chu, L.-L. Chen, X.-Q. Lü, X.-Y. Zheng, J.-R. Song and D.-D. Fan, *J. Molec. Catal. A: Chem.*, 2011, **337**, 25-32.
60. G. Xiao, B. Yan, R. Ma, W. J. Jin, X. Q. Lu, L. Q. Ding, C. Zeng, L. L. Chen and F. Bao, *Polym. Chem.*, 2011, **2**, 659-664.
61. S. Gendler, S. Segal, I. Goldberg, Z. Goldschmidt and M. Kol, *Inorg. Chem.*, 2006, **45**, 4783-4790.
62. Z. Tang and V. C. Gibson, *European Polymer Journal*, 2007, **43**, 150-155.
63. X. Liu, X. Shang, T. Tang, N. Hu, F. Pei, D. Cui, X. Chen and X. Jing, *Organometallics*, 2007, **26**, 2747-2757.
64. H. E. Dyer, S. Huijser, A. D. Schwarz, C. Wang, R. Duchateau and P. Mountford, *Dalton Trans.*, 2008, DOI: 10.1039/B714583G, 32-35.
65. M. Hirotsu, M. Kojima and Y. Yoshikawa, *Bull. Chem. Soc. Jpn.*, 1997, **70**, 649-657.
66. M. Hirotsu, M. Kojima, W. Mori and Y. Yoshikawa, *Bull. Chem. Soc. Jpn.*, 1998, **71**, 2873-2884.

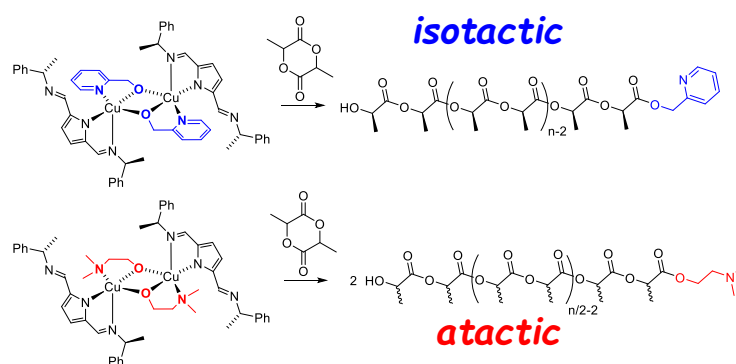


67. E. Chard, L. N. Dawe and C. M. Kozak, *Acta Crystallogr., Sect. E: Struct. Rep. Online*, 2010, **66**, m771.
68. R. van Gorkum, J. Berding, A. M. Mills, H. Kooijman, D. M. Tooke, A. L. Spek, I. Mutikainen, U. Turpeinen, J. Reedijk and E. Bouwman, *Eur. J. Inorg. Chem.*, 2008, **2008**, 1487-1496.
69. D. Maity, W. S. Sheldrick, H. M.-F. Mayer-Figge and M. Ali, *Indian J. Chem., Sect A*, 2007, **46**, 1057-1062.
70. N. Noshiranzadeh, M. Emami, R. Bikas, K. Ślepokura and T. Lis, *Polyhedron*, 2014, **72**, 56-65.
71. N. Reddig, D. Pursche, B. Krebs and A. Rompel, *Inorg. Chim. Acta*, 2004, **357**, 2703-2712.
72. D. F. Evans, *J. Chem. Soc.*, 1959, DOI: 10.1039/JR9590002003, 2003-2005.
73. E. M. Schubert, *J. Chem. Educ.*, 1992, **69**, 62.
74. F. H. Allen, *Acta Crystallogr., Sect. B: Struct. Sci.*, 2002, **B58**, 380-388.
75. E. Y. Tshuva, I. Goldberg, M. Kol and Z. Goldschmidt, *Organometallics*, 2001, **20**, 3017-3028.
76. S. Groysman, I. Goldberg, M. Kol, E. Genizi and Z. Goldschmidt, *Organometallics*, 2004, **23**, 1880-1890.
77. A. J. Nielson and J. M. Waters, *Polyhedron*, 2010, **29**, 1715-1726.
78. M. Save, M. Schappacher and A. Soum, *Macromol. Chem. Phys.*, 2002, **203**, 889-899.
79. *APEX2*, Release 2.1-0; Bruker AXS Inc.: Madison, USA, 2006.
80. *SAINT*, Release 7.34A; Bruker AXS Inc.: Madison, USA, 2006.
81. G. M. Sheldrick *SADABS*, Bruker AXS Inc.: Madison, USA, 1996 & 2004.
82. G. Sheldrick, *Acta Crystallographica Section A*, 2015, **71**, 3-8.
83. G. M. Sheldrick, *Acta Crystallogr.*, 2008, **A64**, 112-122.
84. A. Spek, *Acta Cryst. D*, 2009, **65**, 148-155.



### Chapter 3 . Mechanism and Stereocontrol in Isotactic *rac*-Lactide Polymerization with Copper(II) complexes

Daneshmand, P.; van der Est, A.; Schaper, F. Mechanism and Stereocontrol in Isotactic *rac*-Lactide Polymerization with Copper(II) complexes. *ACS Catal.* **2017**, *7*, 6289–6301.



Reprinted with permission from *ACS Catalysis*. Copyright 2017 American Chemical Society.

Contributions of F. Schaper: A first draft was provided by me with major modification from Prof. Frank Schaper.

Contributions of A. van der Est: EPR measurements and interpretation.



# Mechanism and Stereocontrol in Isotactic *rac*-Lactide Polymerization with Copper(II) complexes

Pargol Daneshmand,<sup>a</sup> Art van der Est,<sup>b</sup> Frank Schaper<sup>a,\*</sup>

<sup>a</sup> *Centre in Green Chemistry and Catalysis, Department of Chemistry, Université de Montréal, C. P. 6128 Succ. Centre-Ville, Montréal, QC, H3T 3J7, Canada.* <sup>b</sup> *Department of Chemistry, Brock University, St. Catharines, ON, L2S 3A1, Canada.*

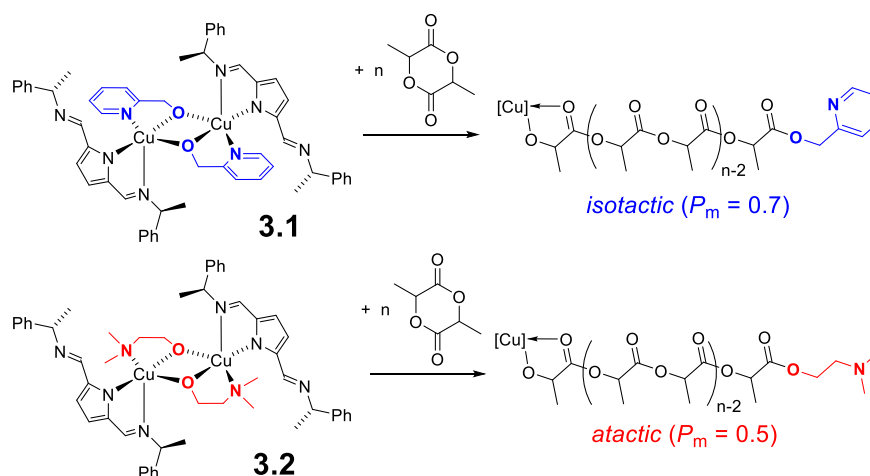
## Abstract

Reaction of *N*-R,*N'*-R'-2,5-diiminopyrroles (R = R' = *S*-CH(Me)Ph; R = R' = CH<sub>2</sub>Ph; R = *S*-CH(Me)Ph, R' = H) with Cu(OMe)<sub>2</sub> in the presence of chelating alcohols, ROH (R1 = C<sub>2</sub>H<sub>4</sub>NMe<sub>2</sub>, R2 = C<sub>2</sub>H<sub>4</sub>Py, R3 = CH<sub>2</sub>Py, R4 = CMe<sub>2</sub>Py), yielded dinuclear, alkoxide-bridged complexes 3.L<sub>2</sub>Cu<sub>2</sub>(OR)<sub>2</sub>. The complexes catalyze the polymerization of *rac*-lactide at room temperature with catalyst concentrations of 1 – 3 mM in 4 – 24 h ( $v = k \cdot [\text{cat}] \cdot [\text{monomer}]$  with  $k = 2.3(5) \cdot 10^2 - 6.5(6) \cdot 10^2 \text{ M}^{-1} \text{ h}^{-1}$ ). EPR- and mechanistic studies indicate that the complexes remain dinuclear during the polymerization reaction. In complexes with OR1, both alkoxides of the dimer initiate polymerization, with OR2 or OR3 only one alkoxide initiates polymerization, and OR4 is inactive in polymerization. The nature of the bridging ligand in the dinuclear complex determines stereocontrol. Independent of the spectator ligand L, complexes which retain an OR3 or OR4 bridging ligand in the active species show preference for isotactic polymerizations ( $P_m = 0.60 - 0.75$ ), while those with only polymeryloxo-bridges or OR2 as the bridging ligand provide atactic polymer. Stereocontrol follows a chain-end control mechanism, with the catalytic site likely adapting to the configuration of the chain end.

*Keywords: copper(II) complexes, catalysis, polymerization, lactide, polylactide, stereocontrol, isotacticity, EPR*

## Introduction

The controlled polymerization of *rac*-lactide has become the focus of a large number of academic studies, partly due to the economic success of polylactic acid (PLA),<sup>1</sup> and partly since enantioselectivity in *rac*-lactide polymerization presents "*a challenging goal that molecular chemists could gratifyingly tackle*".<sup>2</sup> Two decades after the ground-laying work in the 90's,<sup>3</sup> stereocontrol in coordination-insertion polymerization of lactide still remains below the level taken for granted in  $\alpha$ -olefin polymerizations. Catalysts with  $P_m > 0.9$  ( $P_m$  = probability of isotactic insertion) remain rare and – most importantly – their catalytic performance often changes unpredictably with minor changes in the catalyst structure, making gradual improvements difficult. The latter problem is related to the multitude of mechanistic pathways in the polymerization of lactide: Polymerizations can be under either thermodynamic or kinetic control, stereocontrol can be achieved either at the state of monomer coordination, insertion, or ring-opening, and possible mechanisms include not only catalytic-site as well as chain-end control, but also more "esoteric" mechanistic steps such as the involvement of fast and selective chain-transfer<sup>4</sup> or catalyst auto-inhibition.<sup>5</sup> We were thus intrigued when we observed different stereocontrol in two diiminopyrrole copper complexes, **1** and **2**, which differ only in the initiating alkoxide (Scheme 3.1).<sup>6</sup> In a typical coordination-insertion mechanism, the initiating group on the pre-catalyst is found at the end of the polymeryl chain and is not expected to exert any influence on the polymerization beyond the first insertion step.



**Scheme 3.1.** Dependence of stereocontrol on the initiating group in polymerizations with **3.1** and **3.2**.

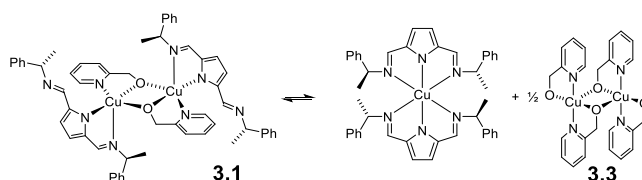
Catalyst systems explored for lactide polymerization have been based almost exclusively on  $d^0$ -metals (groups 1-4 + lanthanides, in particular Mg, Y and Zr)<sup>7</sup> and  $d^{10}$ -metals (group 12 + main group, in particular Zn, Al and Sn).<sup>7c, 7g-k, 8</sup> In contrast to  $\alpha$ -olefins,  $d^n$ -transition metals have not been used extensively in lactide polymerization. Of these, iron-based catalysts received the most attention, including some highly active catalysts,<sup>9</sup> and, more recently, switchable catalysts.<sup>10</sup> Cu(II) complexes represent the second-most investigated  $d^n$ -metal. Most work concentrated on coordination complexes,  $L_mCuX_n$ , best suited to an activated monomer mechanism.<sup>11</sup> These catalysts are in general more robust against temperature or moisture than catalysts optimized for coordination-insertion polymerization, but activities are typically low, polymer molecular weight control is often difficult (with some exceptions<sup>11b, 11h</sup>), and there is no stereocontrol.  $L_mCu(OR)_n$  complexes, suitable for coordination-insertion polymerization, are more difficult to prepare and more sensitive to temperature and protic impurities, but display higher activities (by orders of magnitude) and excellent polymer molecular weight control.<sup>6, 12</sup> They also represent the first examples of stereocontrol with Cu(II)-based catalysts, either to the heterotactic polymer,<sup>12d, 12e</sup> or, in the case of **3.1**, but not **3.2**, to isotactic PLA.<sup>6</sup> The following presents a discussion of the mechanism of *rac*-lactide polymerization by

**3.1** and **3.2**, a determination of the origin of stereocontrol and an explanation how the initiating group can determine isoselectivity.

## Results and Discussion

### *Schlenk equilibria.*

A trivial explanation of the observed impact of the initiating group on stereocontrol is ligand re-distribution into the homoleptic complexes and that the actual catalyst in polymerizations with **3.1** is the homoleptic complex **3.3** (Scheme 3.2). We independently prepared **3.3**, which crystallizes as a dimer with a structure similar to **3.1** (Fig. 3.S1). Complex **3.3** was slightly more active in lactide polymerization than **3.1**, with no notable induction period and produced an essentially atactic polymer ( $P_m = 0.42 - 0.55$ , Table 3.S1). Schlenk equilibria are thus not responsible for the difference in stereocontrol between **3.1** and **3.2**.



**Scheme 3.2.** Potential Schlenk-equilibrium for **3.1**

### *Polymerization kinetics.*

To investigate differences in active species and or the polymerization mechanism between **3.1** and **3.2**, polymerization reactions were followed by  $^1\text{H}$  NMR spectroscopy. Complex **3.1** displayed a notable induction period of variable length (Table 3.S2), but followed a pseudo-first order rate-law afterwards (Fig. 3.1). The length of the induction period was highly influenced by the presence of protic impurities and the observed variations are unrelated to the reaction mechanism (see supp. Inform., Fig. 3.S2, 3.S3). No notable induction period was noticed for **3.2**. While there was some indication of catalyst decomposition (Fig. 3.1, right inset), all polymerizations reached completion. In fact, additional batches of monomer added



after 3 and 4 days, respectively, were polymerized with identical activity and stereocontrol (Fig. 3.S4, Table 3.S3, entries 11-13).

In agreement with different active species for both catalysts, different rate constants were obtained for **3.1** and **3.2**, the latter being approximately twice as active as **3.1** (Table 3.I).<sup>13</sup> Polymerization reactions at different catalyst concentrations revealed a first-order dependence of the rate law on catalyst concentration for both catalysts ( $k_1 = 2.6(5) \cdot 10^2 \text{ M}^{-1}\text{h}^{-1}$ ,  $k_2 = 6.5(6) \cdot 10^2 \text{ M}^{-1}\text{h}^{-1}$ , Fig. 3.S5). There is thus no evidence for any association/dissociation equilibria from the kinetic data.

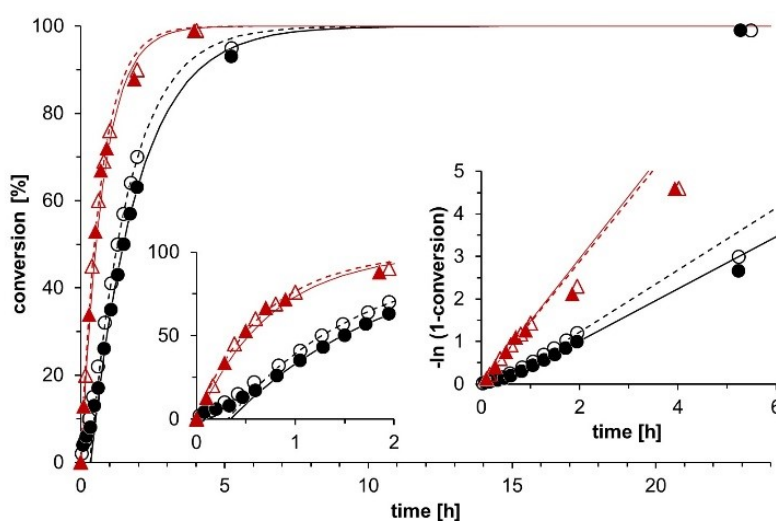


**Figure 3.1.** Polymerization kinetics of **3.1** (circles) and **3.2** (triangles). Two independent experiments (filled and hollow symbols) are shown for each catalyst. The left inset shows an enlargement of the first two hours, the right inset the linearized plot according to a pseudo-first order rate law. Conditions: [catalyst] = 2 mM, [*rac*-lactide] = 200 mM,  $\text{C}_6\text{D}_6$ , ambient temperature.

**Table 3.I.** *rac*-Lactide polymerization catalyzed by **3.1 – 3.11**

Catalyst	Conversion after 24 h	$k_{\text{obs}}$ at [cat.] = 2 mM	$M_{\text{n, GPC}}^{\text{a}}$	$M_{\text{n, calc}}^{\text{b}}$	Chains per catalyst <sup>c</sup>	$M_{\text{w}}/M_{\text{n}}$	$P_{\text{m}}^{\text{d}}$
<b>3.1</b>	98 – 99%	$0.6 \pm 0.1 \text{ h}^{-1}$	11 – 31 kDa	7.2 kDa	0.5 – 1.4	1.3 – 1.7	$0.72 \pm 0.02$
<b>3.1</b> / 1 – 3 Ph <sub>3</sub> COH	98 – 99%	$0.7 \pm 0.3 \text{ h}^{-1}$	$13 \pm 3 \text{ kDa}$	7.2 kDa	$1.1 \pm 0.2$	1.2 – 1.3	$0.71 \pm 0.02$
<b>3.2</b>	98 – 99%	$1.4 \pm 0.2 \text{ h}^{-1}$	$5 \pm 1.5 \text{ kDa}$	7.2 kDa	$2.5 \pm 0.5$	1.1 – 1.3	$0.48 \pm 0.02$
<b>3.2</b> / 0.5 – 2.3 PyCH <sub>2</sub> OH	95 – 99%	$0.5 – 1.4 \text{ h}^{-1}$	4.6 – 6.3 kDa	3.4 – 4.9 kDa	2.2 – 3.1	1.2	0.58 – 0.66
<b>3.5</b>	0%						
<b>3.6</b>	97 / 98%	$0.13 \text{ h}^{-1}$	15 / 23 kDa	7.2 kDa	0.6 / 0.9	1.2	$0.74 \pm 0.01$
<b>3.8</b>	61 / 71%	$0.55 \pm 0.1 \text{ h}^{-1}$	6.1 / 6.8 kDa	4.5 / 5.2 kDa	1.5	1.1 / 1.2	$0.50 \pm 0.01$
<b>3.9</b>	97 – 99%	$0.65 \pm 0.1 \text{ h}^{-1}$	7 – 28 kDa	6.4 – 7.2 kDa	0.5 – 2	1.4 – 1.5	$0.67 \pm 0.02$
<b>3.10</b>	72 – 89 %	$0.6 \pm 0.1 \text{ h}^{-1}$	3.3 – 7.3 kDa	5.3 – 6.5 kDa	1.6 – 3.3	1.1 – 1.3	$0.47 \pm 0.03$
<b>3.11</b>	98 – 99%	$1.3 \pm 0.1 \text{ h}^{-1}$	11 – 17 kDa	6.9 – 7.2 kDa	$1.0 \pm 0.2$	1.3 – 2.2	$0.61 \pm 0.02$

Cited values are averages of 2 to 9 polymerizations. For detailed information, see Tables 3.S3 - 3.S5 in the supporting information. Conditions: C<sub>6</sub>D<sub>6</sub>, ambient temperature. [cat.] = 1 – 3 mM, [lactide]/[cat.] = 100 – 300. Concentrations and ratios always provided per catalyst dimer, i. e. for 3.L<sub>2</sub>Cu<sub>2</sub>(OR)<sub>2</sub>. <sup>a</sup>  $M_{\text{n}}$  and  $M_{\text{w}}$  determined by size exclusion chromatography vs. polystyrene standards, with a Mark-Houwink correction factor of 0.58. <sup>b</sup>  $M_{\text{n}}$  expected if all alkoxides initiate polymerization, calculated from  $[\text{lactide}]/(2 \cdot [\text{cat}] + [\text{ROH}]) \cdot \text{conversion} \cdot M_{\text{lactide}} + M_{\text{ROH}}$ . <sup>c</sup> Number of chains per catalyst dimer, calculated from the ratio of expected and obtained polymer molecular weight. <sup>d</sup>  $P_{\text{m}}$  determined from decoupled <sup>1</sup>H NMR by  $P_{\text{m}} = 1 - 2 \cdot I_1 / (I_1 + I_2)$ , with  $I_1 = 5.20 - 5.25 \text{ ppm}$  (*rmr*, *mmr/rmm*),  $I_2 = 5.13 - 5.20 \text{ ppm}$  (*mmr/rmm*, *mmm*, *mr*).  $P_{\text{m}}$ -values obtained this way were typically consistent to  $\pm 1\%$  over the course of one experiment and  $\pm 3\%$  between different experiments under identical conditions.

### Nuclearity of the active species in **3.1**.

Next to the differences in stereocontrol, the main difference in polymerizations with **3.1** and **3.2** is the difference in the obtained polymer molecular weight (Table 3.I, 3.S3, 3.S4). Polymerizations with **3.2** yielded polymer molecular weights only slightly lower than the theoretical values expected if all alkoxide groups initiate chain growth. Depression of polymer molecular weight in lactide polymerization is often observed as a consequence of intramolecular transesterification reactions leading to cyclic oligomers. Indeed, MALDI spectra of polymers obtained with **3.2** showed evidence of intramolecular transesterification (Fig. 3.S6), in agreement with polydispersities of 1.1 – 1.3.

Polymerizations with **3.1**, on the other hand, consistently yielded polymer molecular weights higher than expected (Table 3.I, 3.S3). This indicates that not all alkoxide groups initiate polymerization, despite the fact that clean first-order kinetics after 30% conversion clearly show that all catalysts have initiated polymerization at this point. The isoselective active species thus contains pyridyl methoxide ligands, most likely in a polynuclear species. Unfortunately, the obtained molecular weights differed widely between 11 – 31 kDalton in polymerizations with identical lactide:catalyst ratios (Table 3.I), making it impossible to reliably determine which fraction of alkoxide groups initiates chain growth and thus the nuclearity of the active species. Polymerization under immortal conditions, i. e. in the presence of external alcohol acting as a reversible chain-transfer reagent, can restore molecular weight control either by shortening induction periods (exchange of a slowly initiating group by a faster reacting one) or by enforcing chain transfer between active and deactivated species. Immortal polymerizations in the presence of 0.25 – 4 equivalents (per catalyst dimer) of benzyl alcohol or pyridyl methanol showed strongly reduced polydispersities (1.1 – 1.2 vs. 1.3 – 1.7 with **3.1** alone, Table 3.S3, entries 14-20 and 34-36) and the obtained polymer molecular weights are in good agreement with the theoretical values expected if only one pyridyl methoxide group in **3.1** initiates chain growth (Fig. 3.2). There is no correlation between the induction period and polydispersities or obtained molecular weight (Table 3.S2). The advantageous effect of external alcohol on polymer molecular weight control is thus not due to

improvement of the initiation step, but most likely due to enforced chain-shuttling between active and inactive centers.

To obtain the best estimate for the number of initiating pyridyl methoxide groups without generating additional chains, chain-shuttling was enforced with the aid of an alcohol which would not undergo insertion. Trityl alcohol was chosen, since its  $pK_A$  enables protonation of pyridyl methoxide, but it is unlikely to insert lactide for steric as well as electronic reasons. Indeed, polymerizations in the presence of increasing amounts (0.5, 1 or 2 equivalents) of trityl alcohol did not show any reduction of polymer molecular weight (Fig. 3.3, Table 3.I, 3.S3, entries 21-29). Polymer molecular weight control was, however, drastically improved: in 9 polymerizations, polymer molecular weight was in the range of 9 – 15 kDalton, with an average of 13.0 kDalton. Catalyst **3.1** thus undergoes partial deactivation during polymerization, but the alkoxide groups of the deactivated species are accessible to chain-transfer.<sup>14</sup>

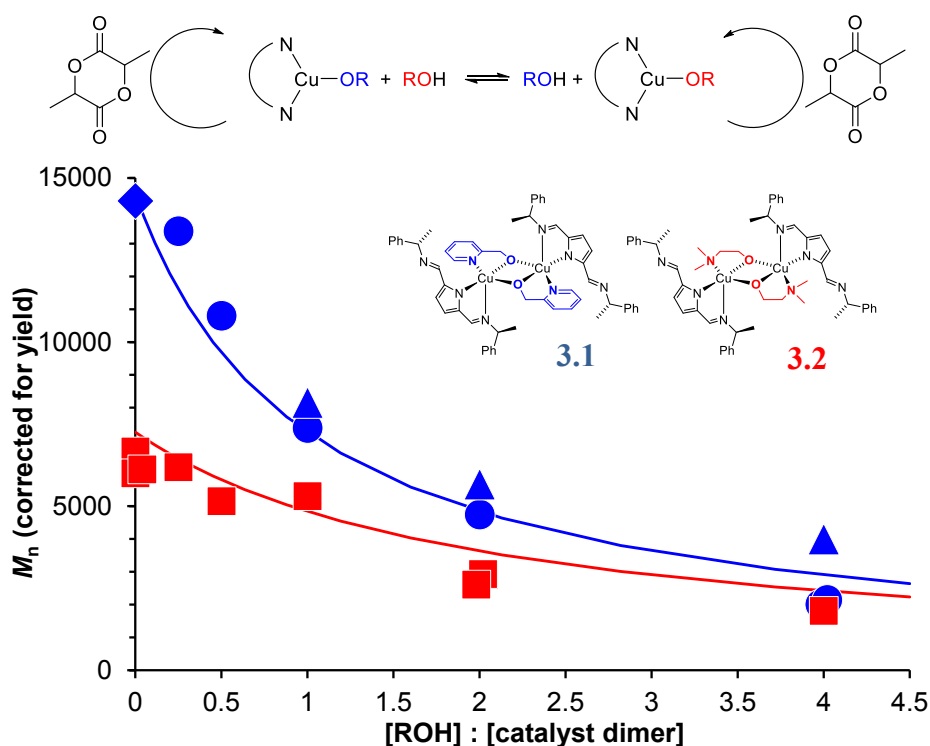


**Figure 3.2.** Polymer molecular weight in *rac*-lactide polymerizations with **3.1** in the presence of benzyl alcohol (spheres), pyridyl methanol (triangles) or trityl alcohol (diamond) and with **3.2** in the presence or absence of benzyl alcohol (squares).

Polymer molecular weights were extrapolated to full conversion, i. e.  $M_{n,corrected} = M_n / \text{yield}$ . The two lines correspond to the theoretical polymer molecular weight expected if either 1 or 2 alkoxide groups per catalyst initiate polymerization.

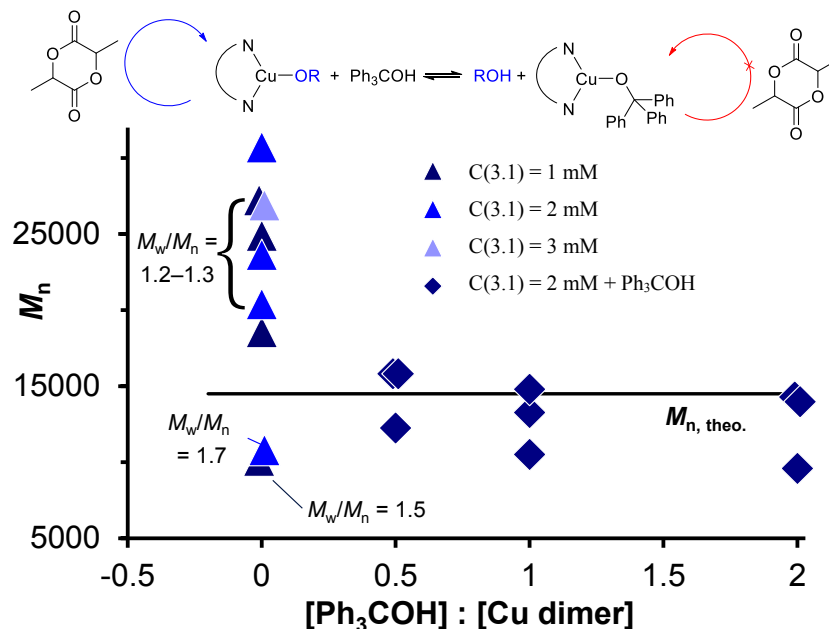
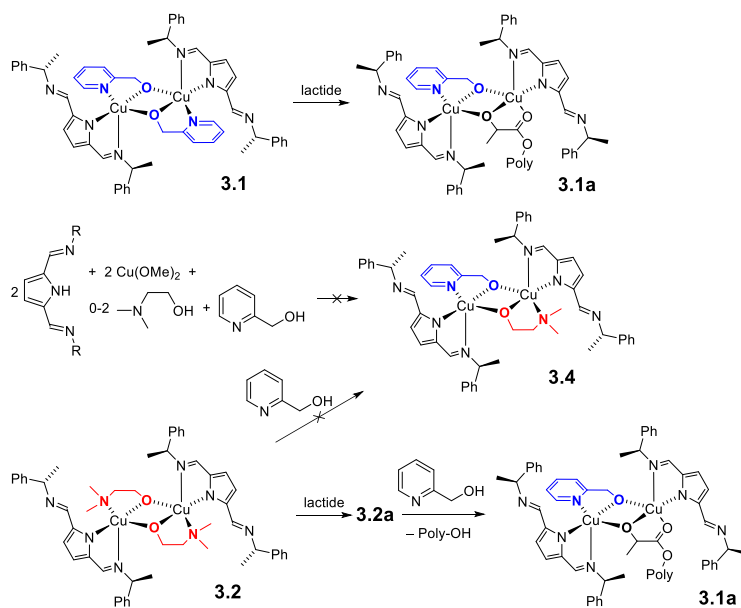


**Figure 3.3.** Improved molecular weight control upon addition of trityl alcohol as a chain-transfer reagent.

Polymer molecular weight data for immortal polymerizations with **3.1** in the presence of benzyl alcohol, pyridyl methanol or trityl alcohol are in close agreement with the theoretical values expected if only one in two alkoxide groups initiates chain growth (Fig. 3.2). For **3.2**, on the other hand, polymer molecular weights obtained in the presence and in the absence of benzyl alcohol agree well with those expected if both alkoxide groups initiate.

From the kinetic and polymer molecular weight data, we can conclude that **3.1** and **3.2** form different active species, **3.1a** and **3.2a**, and that the isoselective active species **3.1a** contains one pyridyl methoxide ligand per two copper centers. We had tentatively proposed species **3.1a** to be a dinuclear complex, formed by insertion of lactide into only one of the two pyridyl methoxide groups (Scheme 3.3).<sup>6</sup> To test this hypothesis, we attempted to prepare a complex containing one pyridyl methoxide and

one dimethylamino ethoxide group, **3.4**, which should provide the same active species **3.1a** in polymerization (Scheme 3.3). Unfortunately, **3.4** could not be obtained with either dimethylamino ethoxide, methyl lactate or methoxide as the fast-initiating group. *In-situ* generation of **3.1a** from **3.2a** by addition of 1 equiv of pyridyl methanol to polymerizations with **3.2**, was only partially successful. With increasing addition of pyridyl methanol to polymerizations with **3.2**, polymerizations became increasingly isoselective, polymer molecular weights were slightly higher than expected (in contrast to other polymerizations with **3.2**), and activities were reduced to those observed for **3.1**. (Table 3.I, 3.S4, Entries 19-25). While this strongly indicates that **3.1a** is indeed formed under these conditions, stereocontrol remained lower than in **3.1**, even when excess pyridyl methanol was used. The data thus does not allow us to distinguish whether **3.1a** is formed directly from reaction of **3.2a** with one equiv of pyridyl methanol, supporting that **3.1a** contains one bridging pyridyl methoxide per two copper centers, or if **3.1a** is obtained trivially via formation of **3.1** (from **3.2a** + two pyridyl methanol) and subsequent reaction with lactide.



**Scheme 3.3.** Attempted preparation of **3.4**

Since it was not possible to prepare a complex containing pyridyl methoxide and a fast-initiating group, complexes containing non-initiating alkoxide ligands were investigated. Complexes **3.5** and **3.6** contain one or two 2-pyridyl-2-propoxide

ligands (Scheme 3.4), which, being tertiary alcohols, were expected to react with lactide only very slowly or not at all. Both complexes were characterized by X-ray diffraction (Fig. 3.4, Table 3.II)

**Table 3.II.** Selected bond distances (Å) and bond angles (°) for **3.5**, **3.6** and **3.8** – **3.11**.

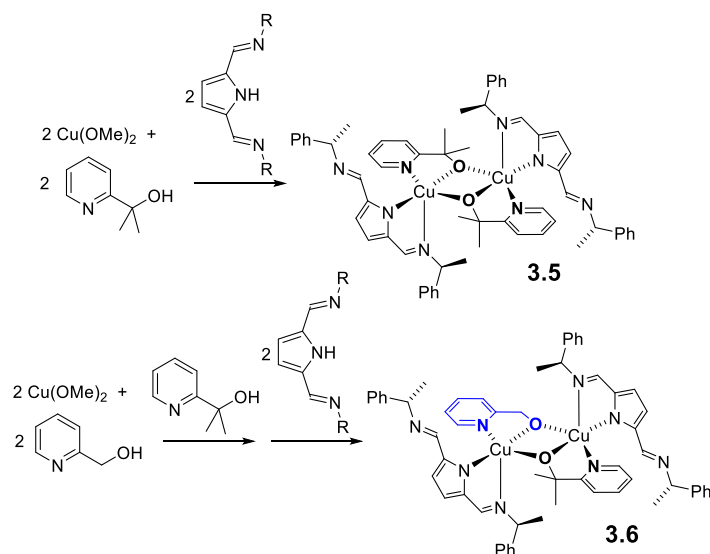
	<b>3.5</b>	<b>3.6</b>	<b>3.8</b>	<b>3.9</b>	<b>3.10</b>	<b>3.11</b>
Cu-O <sub>short</sub>	1.936(2), 1.939(2)	1.915(4), 1.931(4)	1.917(6), 1.938(7)	1.9483(15)	1.9319(16)	1.9594(13) 1.9271(11), 1.9306(11)
Cu-O <sub>long</sub>	1.958(2), 1.967(2)	1.938(4), 1.986(4)	1.954(6), 1.967(6)	1.9853(15)	1.9640(15)	1.9898(11) 1.9507(11), 1.9507(11)
Cu-N <sub>pyrrole</sub>	1.961(3), 1.971(3)	1.954(5), 1.958(5)	1.956(8), 1.977(7)	1.9551(18)	1.9522(19)	1.9744(16) 1.9309(13), 1.9347(13)
Cu-N <sub>imine</sub>	2.427(3), 2.463(3)	2.350(5), 2.479(5)	2.414(8), 2.490(10)	2.0765(19)	2.2143(19)	2.0435(16) 2.3170(15), 2.3976(13)
Cu-N <sub>pyridine/amine</sub>	2.002(3), 2.008(3)	1.993(5), 2.033(5)	2.020(8), 2.039(7)	2.1529(19)	2.0334(18)	2.2815(16) 2.0222(13), 2.0261(13)
Cu-Cu	3.0 (6)	3.0	3.1	3.0	3.0	3.0 3.0, 3.1
Cu-O-Cu	101.32(9), 101.53(10)	100.8(2), 103.6(2)	103.9(3), 105.2(3)	100.76(6)	101.40(7)	97.59(5) 104.36(5)
N <sub>pyrrole</sub> -Cu-O	102.05(10), 102.69(10)	101.0(2), 104.3(2)	93.7(3), 97.2(3)	100.45(7)	99.06(7)	99.95(6) 100.42(5), 102.81(5)
N <sub>pyrid./amine</sub> -Cu-O	80.63(10), 81.34(10)	81.4(2), 81.7(2)	92.6(3), 93.0(3)	80.76(7)	81.68(7)	82.83(6) 80.74(5), 81.23(5)
N <sub>pyrrole</sub> -Cu-N <sub>pyrid./amine</sub>	95.62(11), 96.81(11)	94.8(2), 97.6(2)	93.6(3), 97.6(3)	99.46(7)	100.83(8)	97.15(6) 98.72(5), 100.12(6)
O-Cu-O	78.42(9), 78.72(9)	77.3(2), 78.0(2)	75.4(3), 75.5(3)	79.24(6)	78.60(7)	82.40(5) 75.64(5), 76.91(5)
τ	0.4, 0.4	0.4, 0.4	0.2, 0	0.6	0.6	0.4 0.4, 0.4
Ligand in apical position	imine	imine	imine	pyridine	imine	NMe <sub>2</sub> imine

Structures of **3.5** and **3.6** are, unsurprisingly, very similar to that of **3.1**: the two copper-centers form a dimer with nearly symmetric ( $\Delta d_{\text{Cu-O}} < 0.06$  Å)  $\mu$ -alkoxo bridges. Both copper centers are penta-coordinated and have opposite chirality.



Although  $\tau$ -values around 0.4 would indicate a coordination geometry intermediate between sqp and tbp,<sup>15</sup> the large  $\tau$ -values are a consequence of the constrained O-Cu-O angle (77-79°) and the geometry is best described as distorted square-pyramidal. In agreement with this, the Cu-N bond of the imino group occupying the apical position is significantly elongated compared to the pyridine ligand in equatorial position ( $\Delta d_{\text{Cu-N}} \approx 0.4 \text{ \AA}$ ). The chiral N-substituent does not notably affect the coordination environment around copper: although there is a mismatch between ligand chirality (always *S,S*) and metal chirality (either *C* or *A*) for one of the copper centers, coordination geometries around copper are identical within  $\pm 0.03 \text{ \AA}$  and  $\pm 2^\circ$ . The only exceptions are the Cu-N<sub>imine</sub> bonds in **3.6**, which is a result of the non-symmetric substitution of the pyridyl methanol ligand: Cu-imine distances are 2.24 – 2.29 Å in **3.1**, 2.43– 2.45 Å in **3.5**, and 2.35 and 2.48 Å in **3.6**.

Complex **3.5** was inactive towards lactide polymerization and no conversion was observed even after 24 h (Table 3.I, 3.S5, entries 1+2), thus confirming the low tendency of 2-pyridyl-2-propoxide to initiate polymerization. Catalysis with the mixed alkoxide complex **3.6**, however, yielded results practically identical to those with **3.1** (Table 3.I and 3.S5, entries 3+4): full conversion, albeit with notably lower activities;  $P_m = 0.75$ , slightly higher than for **3.1**; and polymer molecular weights in agreement with only one alkoxide group initiating polymerization. MALDI analysis of the polymer showed a series of peaks corresponding to  $n \cdot 144 + M(\text{pyridyl methanol}) + M(\text{Na})$ , but no respective series with  $M(\text{pyridyl propanol})$ . We can thus conclude with high confidence that **3.1a**, the active species in isotactic *rac*-lactide polymerizations with **3.1**, is a dinuclear complex containing one growing polymer chain and one pyridyl methoxide ligand.



**Scheme 3.4.** Preparation of **3.5** and **3.6**

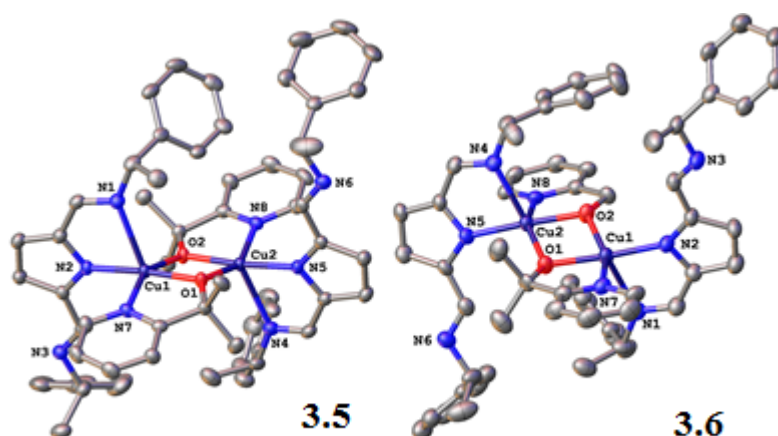


**Figure 3.4.** Crystal structure of **3.5** (left) and **3.6** (right). Thermal ellipsoids are shown at the 50% probability level. Hydrogen atoms were omitted for clarity. Complex **3.5** cocrystallized with  $(3.L)\text{Cu}_2(\text{OR})_2\text{Cl}$  ( $L = \text{diiminopyrrole}$ , Fig. 3.S7, omitted here for clarity), which is not expected to participate in polymerization (see sup. inf.).

#### *EPR measurements.*

To investigate the nuclearity of **3.1a** and **3.2a** in more detail, we conducted EPR experiments under polymerization conditions. Solutions of **3.1** or **3.2** were reacted

with 100 equiv of lactide to 55% – 95% conversion to assure complete transformation into the active species. The reactions were transferred to EPR tubes and rapidly cooled to 100 K. X-band EPR spectra were recorded of the frozen solutions at 100 K, representing snapshots of the polymerization. The EPR spectra of **3.1** and **3.2**, in the absence of lactide (Fig. 3.5a+d), displayed only a small EPR signal (5% – 10% of the expected total intensity, determined by comparison with a mononuclear Cu(II) standard). The very weak EPR signal suggests that complexes **3.1** and **3.2** remain dimeric in solution, with strong antiferromagnetic coupling between the copper centers, a situation generally observed for dinuclear copper complexes with two  $\mu$ -alkoxo or aryloxo bridges.<sup>16</sup>

After addition of lactide, additional signals can be observed (Fig. 3.5). The total intensity remains below the expected values and indicate the continued presence of an EPR-silent species, **A**, in the polymerization mixture.<sup>17</sup> The EPR-spectra can be fitted as a sum of contributions from two EPR-active species: the triplet state of a dinuclear Cu(II) complex **B** (Fig. 3.5g) and a mono-nuclear Cu(II) complex **C** (Fig. 3.5h). We did not observe any signal at half-field strength for the  $\Delta M = 2$  transition of the triplet state in the experimental spectra, but the simulated intensity of this signal was weak and it is likely that it is too weak to be observed. The  $g$ -factors and Cu hyperfine splitting of **B** show considerable anisotropy. The  $g$ -tensor of the triplet state is an average of the  $g$ -tensors of the two Cu(II) centers and the anisotropy suggests that they are probably not coaxial and may have different principal values. This would imply that the two copper centers have different coordination environments. However, some of the apparent anisotropy may be a result of a breakdown of the assumption in the simulation that all of the magnetic tensors of the triplet state share a common set of principal axes.

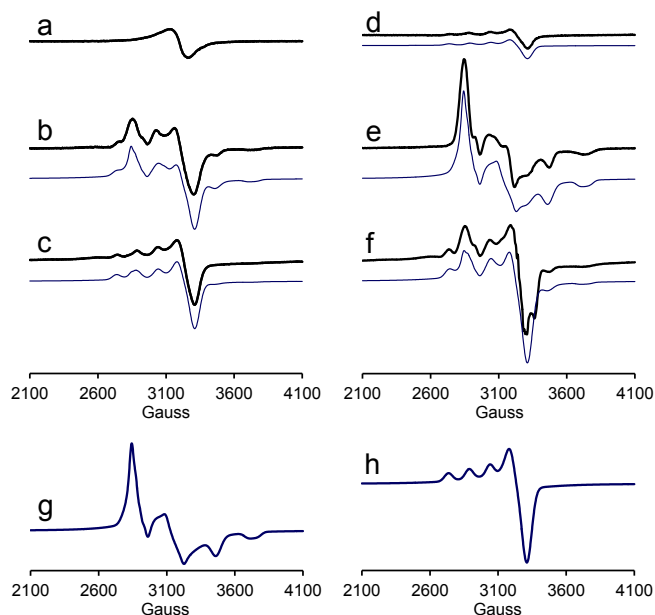


**Figure 3.5.** Experimental (bold line) and simulated (thin line) EPR-spectra of polymerization reactions with **3.1** and **3.2**.

The provided percentages are the relative contributions of B, C and an EPR silent species (by comparison of integrated intensity to a monomeric Cu(II) reference compound): (a) **3.1** without lactide, 90% EPR-silent; (b) **3.1** + 100 lactide, conversion = 55-70%,  $P_m = 0.71$ , fit: 60% EPR silent, 20% **B**, 20% **C**; (c) **3.1** + 100 lactide, conversion = 75-85%,  $P_m = 0.70$ , fit: 75% EPR silent, 5% **B**, 20% **C**; (d) **3.2** without lactide, fit: 95% EPR-silent, 5% **C**; (e) **3.2** + 100 lactide, conversion = 80-90%,  $P_m = 0.50$ , fit: 35% EPR silent, 60% **B**, 5% **C**; (f) **3.2** + 100 lactide, conversion = 90-95%,  $P_m = 0.49$ , fit: 45% EPR silent, 15% **B**, 40% **C**; (g) Simulated spectrum **B**:  $S = 1$ ,  $g_{xx} = 2.192$ ,  $g_{yy} = 2.104$ ,  $g_{zz} = 2.031$ ,  $A_{xx} = 33 \cdot 10^{-4} \text{ cm}^{-1}$ ,  $A_{yy} = 8 \cdot 10^{-4} \text{ cm}^{-1}$ ,  $A_{zz} = 28 \cdot 10^{-4} \text{ cm}^{-1}$ ,  $D = -0.043 \text{ cm}^{-1}$ ,  $E = -0.0057 \text{ cm}^{-1}$ . The principal axes  $g$ -,  $A$ - and zero-field splitting tensors are assumed to be parallel. (h) Simulated spectrum **C**:  $S = \frac{1}{2}$ ,  $g_{xx} = 2.036$ ,  $g_{yy} = 2.070$ ,  $g_{zz} = 2.247$ ,  $A_{xx} = A_{yy} = 17 \cdot 10^{-4} \text{ cm}^{-1}$ ,  $A_{zz} = 150 \cdot 10^{-4} \text{ cm}^{-1}$ .

The fact that species **A** is EPR-silent suggests that it retains two  $\mu$ -oxo bridges and is strongly antiferromagnetically coupled, similar to **3.1** and **3.2** and most doubly alkoxo-bridged copper complexes.<sup>16</sup> The triplet species **B** has likely lost one or two  $\mu$ -oxo bridges. In the latter case, a  $\kappa_{\text{O}^-}$ ,  $\kappa'_{\text{N}}$ -pyridyl methoxide bridged species could

be formed. However, magnetic coupling between the copper centers in this complex would probably be weaker than the coupling observed in the EPR spectra. A non-chelating pyridyl methoxide should also be readily replaced by external pyridine, but addition of excess pyridine had no impact on stereoselectivities of polymerizations with either **3.1** or **3.2** (Table 3.S3, entries 30-32; 3.S4, entries 9-11). Species **B** thus most likely retains one  $\mu$ -oxo bridge. Exchange coupling in mono- $\mu$ -oxo copper complexes can vary between  $2J = +26 - (-1100) \text{ cm}^{-1}$  depending on the presence and type of other bridging ligands.<sup>18</sup> Changes from an EPR-silent species to a weakly coupled species have been reported for doubly  $\mu$ -oxo-bridged dinuclear copper complexes upon dissociation of one  $\mu$ -oxo-bridge.<sup>19</sup> The zero-field splitting value of  $|D| = 0.043 \text{ cm}^{-1}$  is likewise comparable to those observed for singly  $\mu$ -oxo-bridged copper complexes ( $|D| = 0.04 - 0.08 \text{ cm}^{-1}$ ).<sup>19b, 19c, 20</sup> Under the assumption that only dipolar interactions contribute to  $D$  and using the point-dipole approximation, the Cu-Cu distance can be estimated to  $\approx 4 \text{ \AA}$ ,<sup>21</sup> significantly longer than the Cu-Cu distance in **3.1** or **3.2** ( $3.0 \text{ \AA}$ )<sup>6</sup> and in agreement with the average Cu-Cu distances in mono- $\mu$ -oxo dinuclear copper complexes ( $3.7 \text{ \AA}$ ).<sup>22,23</sup> Species **B** is thus assigned to a dinuclear copper complex retaining a single  $\mu$ -alkoxo bridge.

The simulation of species **C** shows a nearly axial EPR spectrum with Cu-hyperfine splitting (Fig. 3.5h) and is typical for a monomeric Cu(II) complex with square-planar, square-pyramidal or Jahn-Teller distorted octahedral geometry. Although this species is present throughout the polymerization, other experimental observations do not support the involvement of a mononuclear species in the catalytic cycle for **3.1**: (i) Relative concentrations of species **C** are arbitrary and do not seem to correlate with the nature of the catalyst or conversion. (ii) The presence of pyridyl methoxide is essential for stereocontrol, which is thus achieved in a dinuclear complex. (iii) The presence of dissociation equilibria would allow formation of  $(\mathbf{3.1})_{1/2}(\mathbf{3.2})_{1/2}$ , **3.4**, from **3.1** and **3.2**. Complex **3.4** would display the same stereocontrol as **1**. Polymerizations of equal mixtures of **3.1** and **3.2**, however, yield PLA consistent with independent polymerization from both catalysts (Table 3.S5, entry 5. (iv) The observed first-order dependence of the rate law on catalyst concentration excludes participation of a dinuclear-monomer equilibrium in the catalytic cycle. (v) Insertion into the first

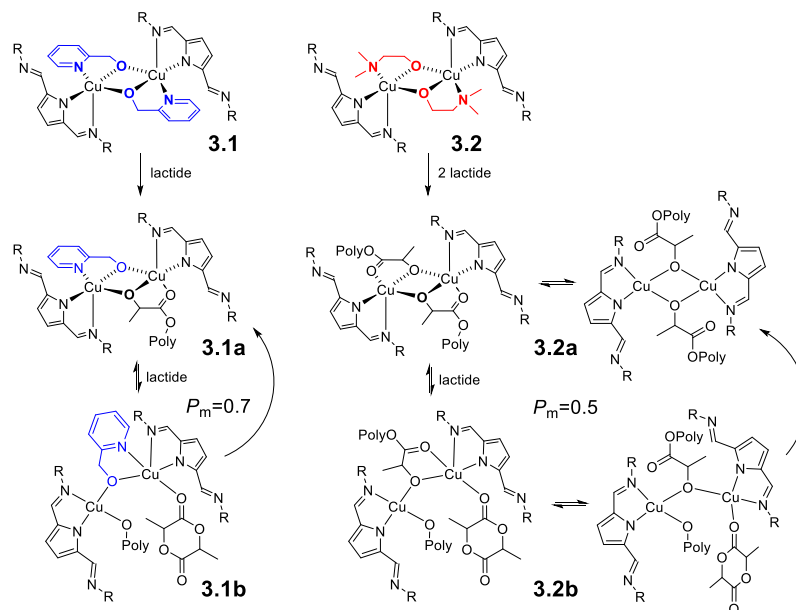
pyridyl methoxide ligand is completed in less than 1 h, while no insertion into the second pyridyl methoxide is observed. In sum, we cannot conceive any polymerization mechanism involving mononuclear species which could account for all of these observations in the case of **3.1**. The monomeric species **C** is thus putatively assigned to a decomposition or deactivation product.<sup>24</sup>

Several mechanistic conclusions can be drawn from the EPR results: (i) The continued presence of EPR-silent species throughout the polymerization indicate the presence of strongly antiferromagnetically coupled dinuclear species **3.1a** and **3.2a** for both catalysts. (ii) Complexes **3.1** and **3.2** display essentially identical changes in their EPR spectra upon addition of lactide and can be fitted using the same dinuclear intermediate **B**. The species present in polymerization are thus most likely identical with regard to nuclearity and magnetic coupling for **3.1** and **3.2**. (iii) The relative concentration of the weakly coupled dinuclear species **3.1b** and **3.2b** decreases with decreasing concentration of lactide, and **3.2b** forms easier than **3.1b**. Based on these results we propose the mechanism depicted in scheme 3.5: Initial insertion of lactide into **3.1** or **3.2** yields the dinuclear complexes **3.1a** and **3.2a**, containing two bridging alkoxide groups. Both initial alkoxides undergo insertion in **3.2**, while in **3.1** only one pyridyl methoxide reacts with lactide. EPR-silent **3.1a/3.2a** reversibly coordinate lactide to yield the EPR-active species **3.1b/3.2b**. From EPR data we can estimate equilibrium constants of  $3 \pm 2 \text{ M}^{-1}$  for coordination of lactide to **3.1a**, and  $40 \pm 20 \text{ M}^{-1}$  for **3.2a**, respectively. Species **3.1b/3.2b** reform **3.1a/3.2a** upon insertion and the active species is dinuclear in isotactic polymerizations with **3.1** as well as in atactic polymerizations with **3.2**.

*Influence of the bridging ligand on stereocontrol.*

The EPR results disagree with the initial proposal that a difference in nuclearity of the active species **3.1a** and **3.2a** is responsible for the differences in stereocontrol.<sup>6</sup> The only difference between the two active species seems to be the nature of the bridging ligand: pyridyl methoxide in **3.1a** promotes isotactic selectivity while polymeryl alkoxide in **3.2a** does not. Based on the presence of an induction period for the reaction of **3.1** with lactide and 10x lower tendency of **3.1a** to coordinate lactide

compared to **3.2a**, pyridyl methoxide presents a more rigid coordination environment than polymeryl alkoxide, which seems to be required for stereocontrol.



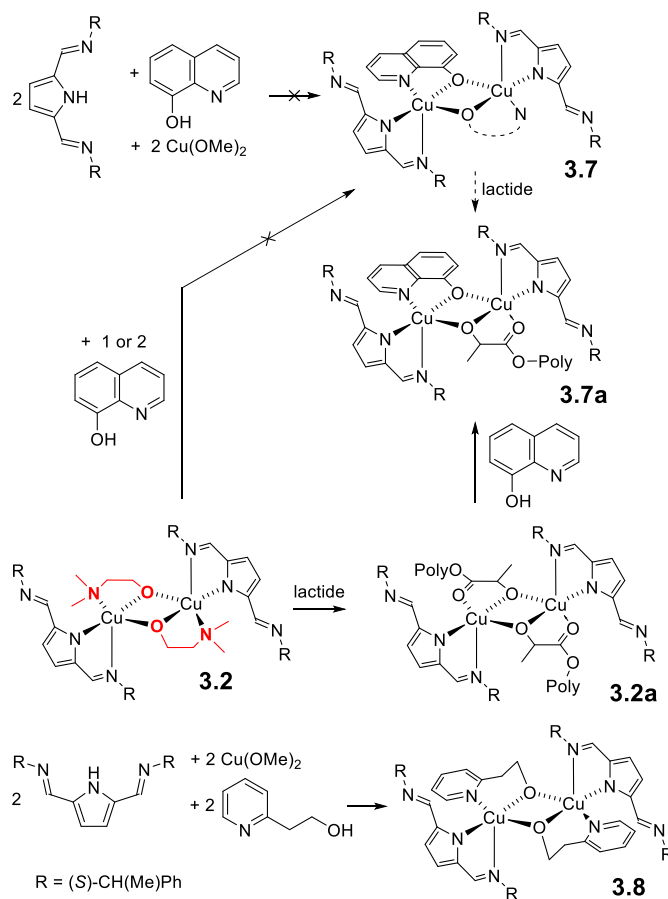
**Scheme 3.5.** Proposed mechanism for lactide polymerization with **3.1** and **3.2**. The structures proposed for **3.1b/3.2b** are representative examples of a possible structure.

To explore this concept in more detail, hydroxyquinoline and pyridyl ethanol were investigated as possible bridging ligands (Scheme 3.6). Both alcohols are sterically similar to pyridyl methanol, but provide an either less or more rigid/stable chelate ring. The rigid hydroxyquinoline ligand should increase stereocontrol, but we were unable to prepare the corresponding  $(3.1L)_2Cu_2(\text{hydroxyquinoline})_2$  complex, **3.7**, or a complex containing only one hydroxyquinoline ligand. The respective active species **3.7a** was thus generated *in situ* by addition of hydroxyquinoline to polymerizations with **3.2**. The latter species was inactive in polymerization: a mixture of **3.2** with 1 equiv of hydroxyquinoline per catalyst dimer (thus hydroxyquinoline:Cu = 1:2) did not display any activity in polymerization of lactide. Polymerization with less than 1 equiv per catalyst dimer showed reduced activity to atactic ( $P_m = 0.43$ ) PLA, in agreement with polymerization solely from unreacted **3.2** (Table 3.S4, entries 26-28). Other phenol-based ligands, such as phenol, 2-aminophenol, 2-iminophenol and 2-aminothiophenol likewise quenched activity upon addition of 1 equiv ligand per catalyst dimer **3.2**. A dinuclear copper complex,

$LX_2Cu_2(OMe)$  ( $L$  = diiminophenolate), recently prepared in our group, also proved to be unreactive in lactide polymerization.<sup>25</sup> Bridging ligands which stabilize a planar  $Cu_2O_2$ -core, such as  $sp^2$ -hybridized aryloxides, are thus detrimental to activity, probably by preventing dissociation of a  $\mu$ -oxo bridge and coordination of lactide.

Preparation of complex **3.8** containing pyridyl ethoxide bridges was achieved analogous to that of **3.1** (Scheme 3.6) and its crystal structure is presented in Figure 6. The structure of **3.8** is again similar to that of **3.1**, **3.5**, or **3.6** (Table 3.II): square pyramidal-coordination around copper with the imine group in apical position. Ring-expansion of the chelate ring led to O-Cu-N<sub>Pyridine</sub> angles closer to ideal geometry ( $93^\circ$  in **3.8**,  $81$ - $82^\circ$  in **3.1**, **3.5**, or **3.6**) and smaller  $\tau$ -values. Either the closer resemblance to ideal sqp geometry or the increase of the steric bulk in the  $Cu_2O_2$ -plane caused by the additional  $CH_2$  group resulted in an elongation of the Cu-N<sub>imine</sub> distances. The crystal structure shows a disorder of *R*- and *S*-methylbenzyl at N3. Based on the total quantity of *R*-methylbenzyl in isolated **3.8**, it is possible that it originates from *R*-methylbenzylamine impurities in the starting material (98% ee *S*). It is more likely, however, that partial racemization occurred during complex synthesis (basic conditions). Polymerizations with **3.8** proceeded with rates similar to those with **3.1** under identical conditions (Fig. 3.S8, Table 3.I, 3.S5, entries 6+7), but suffered from catalyst decomposition. While an induction period was present, it was smaller than any observed for **3.1**. Polymer molecular weights, obtained in the presence or absence of trityl alcohol as a chain transfer reagent, indicate that – similar to **3.1** – not all alkoxides initiate chain transfer and that one pyridyl ethoxide bridge is retained in the active species. Although polymerizations with **3.8** thus closely resemble those with **3.1**, the produced polymer is atactic ( $P_m = 0.49 - 0.52$ ) over the whole conversion range (Fig. 3.S9). In agreement with the above mechanistic proposal, increased flexibility of the bridging alkoxide thus reduced stereocontrol.





Scheme 3.6. Preparation of 3.7a and 3.8.

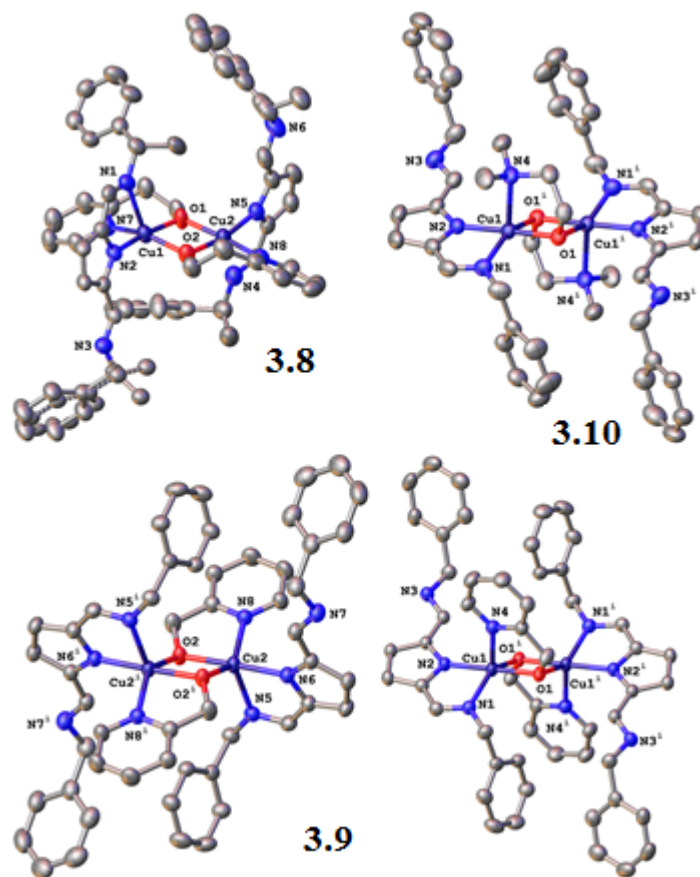


**Figure 3.6.** Crystal structures of **3.8–3.10**. Thermal ellipsoids are drawn at the 50% probability level. Hydrogen atoms and the minor components of rotational disorder of the *N*-substituent at N3 (**8**) and N6 (**10**) were omitted for clarity.

UV/vis-titration of **3.1**, **3.2**, **3.2**/hydroxyquinoline and **3.7** with pyridine allowed to characterize the rigidity of the bridging alkoxides at least in a qualitative manner (Fig. 3.7). The obtained equilibrium constant for pyridine coordination is higher for **3.2** than for **3.1** (**3.1**:  $K = 3 \cdot 10^2 \text{ M}^{-1}$ , **3.2**:  $K = 1.3 \cdot 10^3 \text{ M}^{-1}$ ), which correlates with the easier coordination of lactide to **3.2a** compared to **3.1a** observed in the EPR spectra. Spectra of **3.2**+hydroxyquinoline before and after addition of pyridine were identical to those of **3.2**. Introduction of hydroxyquinoline is thus possible in the active species, but not in precatalyst **3.2**. This is in line with failed synthetic attempts to replace the amino ethoxide in **3.2** by hydroxyquinoline or other bridging ligands (Scheme 3.6). Pyridine coordination to **3.7** ( $K = 2.5 \cdot 10^4 \text{ M}^{-1}$ ) is much more favorable than to **3.1**, in agreement with pyridyl ethoxide affording higher flexibility in the

dinuclear complex. The lack of stereocontrol in **3.2** and **3.7** is thus related to a higher flexibility of the dinuclear complex and/or a weaker coordination of the bridging ligand.

*Solvent dependence of stereocontrol.*

Since stereocontrol seems to correlate with the stability/rigidity of the dinuclear complex, influence of solvent polarity was investigated briefly. No stereocontrol was observed for *rac*-lactide polymerizations with **3.1** in either THF or dichloromethane (Table 3.S3, entry 42+43). While GPC data of PLA obtained in THF indicated extensive intramolecular transesterification and the nature of the active species is unclear, polymer molecular weights obtained in dichloromethane agree with only one pyridyl methoxide initiating polymerization. The active species in dichloromethane is thus most likely identical to the one in benzene.<sup>26</sup> However, UV/vis spectra of **3.1** and **3.9** in toluene and dichloromethane, respectively, differ notably (Fig. 3.S10): the  $\pi$ - $\pi^*$  transition around 260 nm in toluene is displaced bathochromically to 275 nm and reduced to half its intensity, while the weak transition visible as a shoulder at 470 nm vanishes completely. Difference in solvent polarity thus seem to be sufficient to affect the electronic structure of **3.1** and **3.9**, and apparently also stereocontrol.<sup>27</sup>

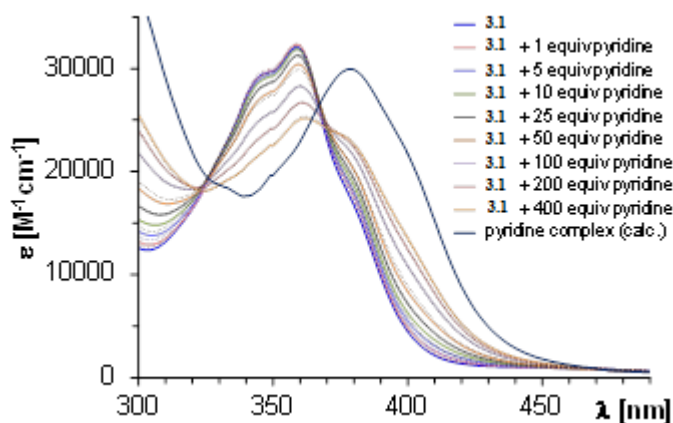
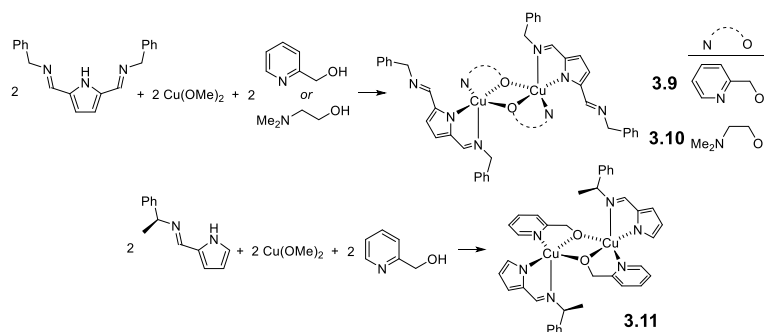


**Figure 3.7.** Titration of **3.1** with pyridine. Solid lines represent experimental spectra, dotted lines are simulated spectra. Equilibrium constant  $K$  and the spectrum of the pyridine adduct were obtained by non-linear regression analysis using all spectra assuming a 1:1 equilibrium. A scale factor was added to allow for complex

decomposition and refined to  $\pm 1\%$  for 1 – 100 equiv pyridine,  $-3\%$  for 200 and  $-6\%$  for 400 equiv pyridine.

#### *Origin of stereocontrol.*

Despite its crucial nature to achieve stereocontrol, pyridyl methoxide itself cannot be the source of chirality in isotactic lactide polymerizations with **1**. The most obvious source of chirality would be the chiral, enantiopure *S,S*-diiminopyrrole ligand employed. Kinetic resolution by a homochiral catalyst would lead to conversion-dependent isoselectivities.<sup>28</sup>  $P_m$  values were however independent from conversion (Fig. 3.8). To clarify the importance of a chiral *N*-substituent, we prepared complexes **3.9** and **3.10**, incorporating achiral benzyl substituents on the imino group instead of *S*-methylbenzyl (Scheme 3.7). Structures of both complexes in the solid state showed the recurrent motif of the dinuclear, five-coordinated copper complex (Fig. 3.6, Table 3.II). The absence of the chiral *N*-substituent now allows **3.9** and **3.10** to crystallize with a crystallographic inversion center. The structure of **3.9** displays two independent molecules in the unit cell, one with pyridine, one with an imino group in the apical position. In **3.10**, only the  $\text{NMe}_2$  group occupies the apical position. There is no apparent electronic or steric reason why coordination of the bridging ligand in the apical position should be preferred in **3.9** or **3.10**. Both structural motifs are thus likely to be close in energy and interconversion between them is expected to be facile in solution. The coordination environment in **3.1** – **3.10** is thus highly flexible and adapts easily even to small changes. Polymerizations with **3.9** and **3.10** are again first-order in monomer and catalyst concentration, and rate constants are within the margin of error identical to that of **1** ( $k_9 = 2.5(7) \cdot 10^2 \text{ M}^{-1}\text{h}^{-1}$ ,  $k_{10} = 2.3(5) \cdot 10^2 \text{ M}^{-1}\text{h}^{-1}$ , Fig. 3.S11 and 3.S12, Table 3.I and 3.S5, entries 8-27). Dimethylamino ethoxy complex **3.10** yielded atactic PLA while pyridyl methoxide complex **3.9** provided isoselectivity ( $P_m = 0.67$ , Fig. 3.S13 and 3.S14) very similar to **3.1**, despite the absence of a chiral ligand.



**Scheme 3.7.** Preparation of **3.9** – **3.11**

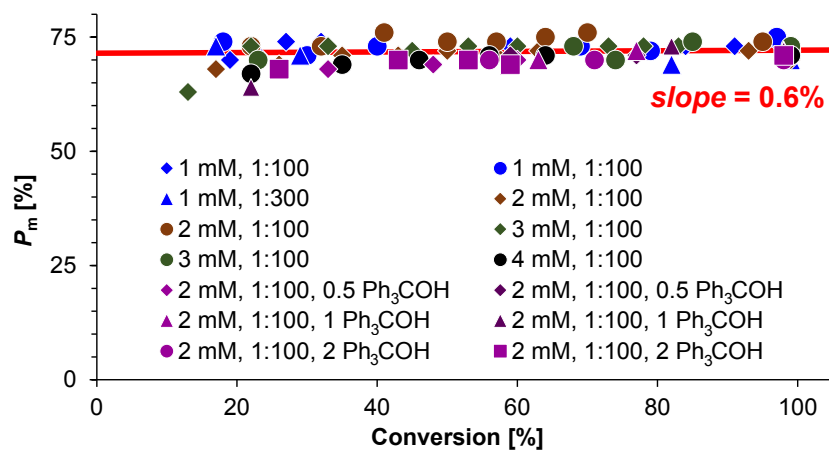


**Figure 3.8.**  $P_m$ -values determined for polymerizations with **3.1** at different conversions.

**Table 3.III.** Stereocontrol ( $P_m$ ) in polymerizations with benzyl alcohol as chain-transfer reagent.

Catalyst	no BnOH	+1 equiv BnOH	+2 equiv BnOH	+4 equiv BnOH
<b>3.1</b>	0.72(1)	0.70(1)	0.69(2)	0.70(1)
<b>3.9</b>	0.67(1)		0.64(2)	0.66(2)
<b>3.11</b>	0.64(1)	0.62(1)	0.59(2)	0.58(1)

Insertion into one pyridyl methoxide ligand leads to pairs of diastereomeric (for **3.1**) or enantiomeric (for **3.9**) dinuclear complexes and catalytic-site as well as chain-end control are possible mechanisms for stereocontrol in **3.1** or **3.9**. The complete retention of stereocontrol in immortal polymerizations (Table 3.III), i. e. in the presence of fast chain-exchange, indicates chain-end control as the most likely stereocontrol mechanism. The latter is supported by  $^{13}\text{C}$  analysis of stereoerrors of PLA produced with **3.6**. Integration of the carbonyl and the methine regions (Fig. 3.S15)<sup>29</sup> afforded values for all tetrads with the single assumption that *mmr*- and *rmm*-tetrads have equal intensity. The obtained distribution is in very good agreement with those simulated for a chain-end control mechanism (Table 3.IV).<sup>4, 30</sup>

#### *Influence of the pending imine.*

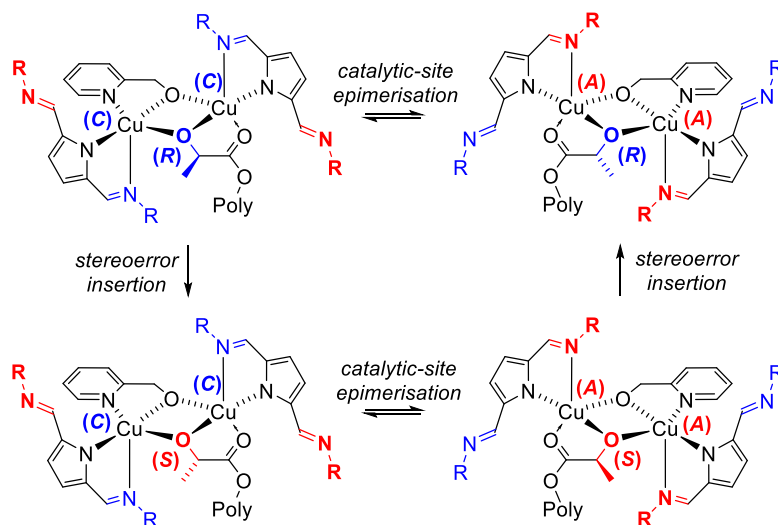
The presence of the pending imine substituent facilitates catalytic-site epimerization, since no rotation around the pyrrole-Cu bond is required. While detrimental in catalytic-site control, site epimerization can be advantageous in chain-end control by removing site/chain-end mismatches after stereoerror insertion (Scheme 3.8).<sup>31</sup> Substitution of one imine substituent in **3.1** by hydrogen afforded complex **3.11** (Scheme 3.7). The crystal structure of **3.11** (Fig. 3.9, Table 3.II) is essentially identical to that of **3.1** and the removal of the pending imine substituent did not have a major effect on the overall structure.<sup>32</sup> Cu-pyrrole bond lengths in **3.11** are slightly shorter than in **3.1** either for electronic or steric reasons. Consequently, Cu-imine

bonds are slightly elongated in **3.11**. Polymerizations with **3.11** were approximately twice as fast as with **3.1** at the same catalyst loading (Table 3.I, 3.S5, entries 28-40). Polymer molecular weights in the presence or absence of added benzyl alcohol are in good agreement with one polymer chain per catalyst dimer. While otherwise comparable to **3.1**, removal of the imino substituent resulted in reduced isotacticity ( $P_m = 0.61$ , Table 3.I). This is in agreement with facile site epimerization being advantageous in chain-end control, but we cannot exclude that it is simply a consequence of steric or electronic effects.

**Table 3.IV.** Experimental and simulated distributions of stereoerror tetrads.

<b>Tetrad</b>	<sup>13</sup> C <sup>a</sup>	<b>Chain-end control</b> <sup>b</sup>	<b>Catalytic-site control</b> <sup>b</sup>
rmr	2.7%	3.0%	6.7%
rmm	9.4%	9.3%	6.7%
mmr	9.4%	9.3%	6.7%
mmm	66.0%	66.0%	66.3%
mrm	12.4%	12.3%	13.5%
$P_m / \alpha$	75%	75.3%	83.9%

<sup>a</sup> Obtained from integration of the carbonyl and the methine regions. <sup>b</sup> Best fit with the experimental values upon optimization of  $P_m$ .



**Scheme 3.8.** Interplay of catalytic-site inversion and stereoerror insertion. The *C*, *C*, *R/A*, *A*, *S* – configuration was arbitrarily chosen as a stereomatch between catalytic site and chain end.

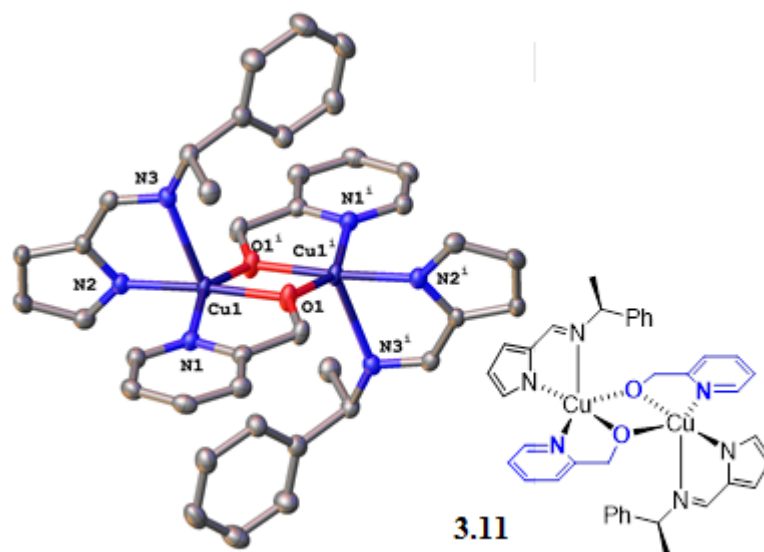


**Figure 3.9.** Crystal structure of **3.11**. Thermal ellipsoids are drawn at the 50% probability level. Hydrogen atoms, minor component of the disorder at N3 and the second, independent molecule of similar geometry in the unit cell were omitted for clarity.



## Conclusions

The diiminopyrrole complex **3.1** and the derivatives presented herein are the only reported Cu-based catalysts with an isoselective preference for lactide insertion. Resting states and active species are dinuclear and there is no evidence that mononuclear copper complexes are involved in the catalytic cycle (other than as possible products of decomposition/deactivation). Stereocontrol is achieved via chain-end control and it is likely amplified by the flexible catalytic site following the "ligand-mediated chain-end control" mechanism proposed by Okuda.<sup>33</sup> This adaptation of the catalytic site to chain-end chirality in a dinuclear complex might explain why isotactic chain-end control is observed for **3.1**, while previous Cu-based catalysts show no stereocontrol<sup>11-12</sup> or a heterotactic bias.<sup>12d-f</sup>

Although diiminopyrrole copper complexes show modest to good activities, preference for isotactic insertion, remain active under polymerization conditions over several days and provide good polymer weight control in the presence of chain-transfer reagents, they do not present, as such, major improvements on successful catalyst systems based on other metals. They also suffer from their serendipitous origin, which requires pyridyl methoxide to act as initiating group and essential spectator ligands *at the same time*. Of interest, however, is the importance of nuclearity for stereocontrol. Complex nuclearity has been reported previously to influence stereocontrol in lactide polymerization either by an enhancement of catalytic-site control by a chiral ligand in dinuclear indium complexes,<sup>34</sup> by a (slight) enhancement of stereocontrol already present in the respective monomeric zirconium complexes,<sup>35</sup> or by loss of stereocontrol upon dimerization of an yttrium complex.<sup>36</sup> In diiminopyrrole copper complexes, catalyst nuclearity itself seems to be essential to enable isotactic chain-end control.

The nature of the bridging ligand was found to play a crucial role in stereocontrol and activity and some design principles can be deduced: Ligand chirality is not required, but the catalyst should be dinuclear in solution, sufficiently flexible to allow dissociation of a  $\mu$ -polymeryloxo bridge upon lactide coordination, but rigid enough

to enforce stereoselectivity on monomer selection. We are currently exploring new Cu-based ligand systems incorporating these design principles and whether the factors granting isoselectivity in Cu(II)-catalyzed polymerizations can be transferred to other transition metals.

## Experimental Section

**General considerations.** All reactions were carried out using Schlenk or glove box techniques under nitrogen atmosphere.  $\text{Cu}(\text{OMe})_2$ ,<sup>37</sup> 1*H*-pyrrole-2,5-dicarbaldehyde,<sup>38</sup> and **3.L3**<sup>39</sup> were prepared according to literature. Solvents were dried by passage through activated aluminum oxide (MBraun SPS), de-oxygenated by repeated extraction with nitrogen, and stored over molecular sieves.  $\text{C}_6\text{D}_6$  was dried over molecular sieves. *rac*-Lactide (98%) was purchased from Sigma–Aldrich, purified by 3x recrystallization from dry ethyl acetate and kept at  $-30\text{ }^\circ\text{C}$ . All other chemicals were purchased from common commercial suppliers and used without further purification.  $^1\text{H}$  and  $^{13}\text{C}$  NMR spectra were acquired on Bruker Avance 300 and 400 spectrometers. Chemical shifts were referenced to the residual signals of the deuterated solvents ( $\text{C}_6\text{D}_6$ :  $^1\text{H}$ :  $\delta$  7.16 ppm,  $^{13}\text{C}$ :  $\delta$  128.38 ppm,  $\text{CDCl}_3$ :  $^1\text{H}$ :  $\delta$  7.26 ppm,  $^{13}\text{C}$ :  $\delta$  77.16). Elemental analyses were performed by the Laboratoire d'analyse élémentaire (Université de Montréal). Molecular weight analyses were performed on a Waters 1525 gel permeation chromatograph equipped with three Phenomenex columns and a refractive index detector at  $35\text{ }^\circ\text{C}$ . THF was used as the eluent at a flow rate of  $1.0\text{ mL}\cdot\text{min}^{-1}$  and polystyrene standards (Sigma–Aldrich,  $1.5\text{ mg}\cdot\text{mL}^{-1}$ , prepared and filtered (0.2 mm) directly prior to injection) were used for calibration. Obtained molecular weights were corrected by a Mark-Houwink factor of 0.58.<sup>40</sup> EPR-spectra were measured using a Bruker Elexsys E580 spectrometer operating in cw mode. The simulation of the spectra was carried out using EasySpin.<sup>41</sup>

**2,5-Bis(*S*-methylbenzyl)aldimino)pyrrole, 3.L1.** 1*H*-pyrrole-2,5-dicarbaldehyde (1.0 g, 8.1 mmol) was dissolved in dry toluene (25 ml), treated with  $\text{MgSO}_4$  (5.0 g), a catalytic amount of Amberlyst 15 and *S*-methylbenzylamine (2.0 g, 16 mmol, 98% ee). The reaction was left to stir overnight at RT. The brown suspension was filtered,

dried and treated with hexane (20 ml), resulting in a light orange powder. The powder was separated by filtration and dried under vacuum (1.09 g, 41%).

$^1\text{H}$  NMR ( $\text{C}_6\text{D}_6$ , 300 MHz):  $\delta$  7.72 (d,  $J = 1$  Hz, 2H, (N=C)H), 7.33 – 7.26 (m, 4H, aromatic H), 7.25 – 6.97 (m, 6H, Ph), 6.30 (s, 2H, pyrrole), 4.18 (q,  $J = 7$  Hz, 2H, CH(Me)Ph), 1.43 (d,  $J = 7$  Hz, 6H, Me).  $^{13}\text{C}\{^1\text{H}\}$  NMR ( $\text{C}_6\text{D}_6$ , 75 MHz):  $\delta$  149.6 ((N=)CH), 145.7 (*ipso*-Ph), 133.3 (2,5-pyrrole), 128.7 (m-Ph), 127.9 (o-Ph), 127.0 (p-Ph), 114.5 (3,4-pyrrole), 69.9 (CH(Me)Ph), 25.3 (Me). ESI-HRMS ( $m/z$ ):  $[\text{M}+\text{H}]^+$  ( $\text{C}_{22}\text{H}_{24}\text{N}_3$ ) calcd 330.1965; found 330.1974.

**2,5-Di(benzylaldimino)pyrrole, 3.L2.** Analogous to **3.L1**, from 1*H*-pyrrole-2,5-dicarbaldehyde (0.5 g, 4.1 mmol), dry toluene (25 ml),  $\text{MgSO}_4$  (5.0 g), a catalytic amount of Amberlyst 15, and benzylamine (0.87 g, 8.2 mmol) to yield a light pink, crystalline powder (380 mg, 31%).

$^1\text{H}$  NMR ( $\text{CDCl}_3$ , 300 MHz):  $\delta$  8.14 (s, 2H, (N=)CH), 7.36 – 7.18 (m, 10H, Ph), 6.48 (s, 2H, pyrrole), 4.71 (s, 4H,  $\text{CH}_2$ ).  $^{13}\text{C}\{^1\text{H}\}$  NMR ( $\text{CDCl}_3$ , 75 MHz):  $\delta$  151.9 ((N=)C), 139.4 (*ipso*-Ph), 132.9 (2,5-pyrrole), 128.6 (o-Ph), 128.1 (m-Ph), 127.2 (p-Ph), 114.8 (3,4-pyrrole), 64.8 ( $\text{CH}_2$ ). ESI-HRMS ( $m/z$ ):  $[\text{M}+\text{H}]^+$  ( $\text{C}_{20}\text{H}_{20}\text{N}_3$ ) calcd 302.1651; found 302.1659.

**(3.L1) $_2$ Cu $_2$ ( $\mu$ -O, $\kappa$  $_N$ -OCH $_2$ Py) $_2$ , 3.1.**<sup>6</sup> A previous preparation has been optimized as follows:  $\text{Cu}(\text{OMe})_2$  (38 mg, 0.30 mmol) was suspended in toluene (3 ml). 2-Pyridylmethanol (58  $\mu\text{L}$ , 0.61 mmol) was added to the blue suspension, which was left to stir for 45 min. A freshly prepared orange solution of **3.L1** (100 mg, 0.30 mmol) in toluene (2 ml) was added dropwise, resulting in a dark green solution. The reaction was stirred 24 hours at RT, filtered to remove trace impurities (syringe filter), concentrated to 1/3 of the volume, diluted with hexane (18 ml) and kept at  $-30^\circ\text{C}$  for 4 hours, resulting in a light green powder. The powder was separated by decantation, suspended in hexane (20 ml) and left at RT for one day to give green crystals, which were separated by decantation (74 mg, 48%).

$^1\text{H}$  NMR (400 MHz,  $\text{C}_6\text{D}_6$ )  $\delta$  47.2, 44.2, 41.2, 24.3, 20.5, 17.1, 13.9, 11.6, 9.5, 8.1, 8.0, 7.4, 7.2, 7.0, 3.2, 2.4. UV-vis (toluene,  $2.3 \cdot 10^{-5}$  M) [ $\lambda_{\text{max}}$ , nm ( $\epsilon$ ,  $\text{mol}^{-1} \text{cm}^2$ ): 331

(sh), 347 (29500), 358 (32000), 382 (sh), 463 (sh). An analytically pure sample was obtained by diffusion of hexane into a dichloromethane solution. Anal. Calcd for  $C_{56}H_{56}Cu_2N_8O_2 \cdot \frac{1}{4}CH_2Cl_2$ : C, 66.14; H, 5.58; N, 10.97; Found: C, 66.06; H, 5.79; N, 11.15. (Presence of dichloromethane confirmed by NMR.)

**(3.L1)<sub>2</sub>Cu<sub>2</sub>( $\mu$ -O, $\kappa$ <sub>N</sub>-OC<sub>2</sub>H<sub>4</sub>NMe<sub>2</sub>)<sub>2</sub>, 3.2.** Analogous to **3.1**, from Cu(OMe)<sub>2</sub> (38 mg, 0.30 mmol) in toluene (3 mL), dimethylamino ethanol (60  $\mu$ L, 0.61 mmol), **3.L1** (100 mg, 0.33 mmol) in toluene (2 mL). The filtered and concentrated (1/3 of the volume) green solution was diluted with hexane (18 mL) and kept at  $-30$  °C for 4 h. Decantation and washing with hexane (3 x 10 mL) afforded 93 mg (64%) of green X-ray quality crystals.

<sup>1</sup>H NMR (400 MHz, C<sub>6</sub>D<sub>6</sub>)  $\delta$  31.3, 28.5, 23.0, 21.7, 20, 8.2, 7.4, 3.1. UV-vis (toluene,  $2.3 \cdot 10^{-5}$  M) [ $\lambda_{max}$ , nm ( $\epsilon$ , mol<sup>-1</sup> cm<sup>2</sup>): 332 (sh), 349 (32700), 361 (35000), 381 (sh), 459 (sh). Anal. Calcd for C<sub>52</sub>H<sub>64</sub>Cu<sub>2</sub>N<sub>8</sub>O<sub>2</sub>: C, 65.04; H, 6.72; N, 11.67; Found: C, 64.66; H, 6.87; N, 11.66.

**Cu<sub>2</sub>(OCH<sub>2</sub>Py)<sub>4</sub>·2(PyCH<sub>2</sub>OH), 3.3.** Cu(OMe)<sub>2</sub> (30 mg, 0.24 mmol) was suspended in toluene (3 mL). 2-pyridinemethanol (45  $\mu$ L, 0.48 mmol) was added to the blue suspension, which was left to stir for overnight. The dark purple solution was filtered to remove trace impurities, treated with hexane (18 mL) and left to slowly evaporate, resulting in dark blue crystals, suitable for X-ray diffraction studies. The crystals were separated by decantation and washed with hexane (3 x 10 mL) to yield 18 mg (26%) of the pyridyl methanol adduct (confirmed by crystal structure).

UV-vis (toluene,  $2.3 \cdot 10^{-5}$  M) [ $\lambda_{max}$ , nm ( $\epsilon$ , mol<sup>-1</sup> cm<sup>2</sup>): 409 (sh), 477 (2650). An analytically pure sample was obtained by diffusion of hexane into a dichloromethane solution. Anal. Calcd for C<sub>24</sub>H<sub>24</sub>Cu<sub>2</sub>N<sub>4</sub>O<sub>4</sub>·2(C<sub>5</sub>H<sub>4</sub>NCH<sub>2</sub>OH)·1.33(CH<sub>2</sub>Cl<sub>2</sub>): C, 50.44; H, 4.38; N, 9.45; Found: C, 50.71; H, 4.38; N, 9.77. (Presence of dichloromethane confirmed by NMR.)

**(3.L1)<sub>2</sub>Cu<sub>2</sub>( $\mu$ -O, $\kappa$ <sub>N</sub>-OCMe<sub>2</sub>Py)<sub>2</sub>·(3.L1)(Cl)Cu<sub>2</sub>( $\mu$ -O, $\kappa$ <sub>N</sub>-OCMe<sub>2</sub>Py)<sub>2</sub>, 3.5.**

Analogous to **3.1**, from Cu(OMe)<sub>2</sub> (38 mg, 0.30 mmol) in toluene (3 mL), 2-pyridyl-

propan-2-ol (84 mg, 0.61 mmol), **3.L1** (100 mg, 0.33 mmol) in toluene (2 mL). The filtered and concentrated (1/3 of the volume) green solution was diluted with hexane (18 mL) and left to slowly evaporate at RT for overnight, resulting in green crystals. The crystals were separated by decantation and recrystallized by diffusion of hexane into dichloromethane (1:3) to afford 32 mg (24%) of X-ray quality crystals.

$^1\text{H}$  NMR (400 MHz,  $\text{C}_6\text{D}_6$ )  $\delta$  37.7, 33.2, 25, 22.2, 19.8, 17.8, 17.3, 15.1, 13.7, 13.5, 10.7, 9.3, 7.7, 7.1, 5.4, 4.8, 3.7, 3.1, 2.6, 2.2. UV-vis (toluene,  $2.3 \cdot 10^{-5}$  M) [ $\lambda_{\text{max}}$ , nm ( $\epsilon$ ,  $\text{mol}^{-1} \text{ cm}^2$ ): 325 (sh), 341 (54000), 356 (56800), 377 (sh). Anal. Calcd for  $\text{C}_{98}\text{H}_{106}\text{ClCu}_4\text{N}_{13}\text{O}_4 \cdot \frac{1}{4}\text{CH}_2\text{Cl}_2$ : C, 64.69; H, 5.87; N, 10.01; Found: C, 64.66; H, 6.04; N, 10.23.

**(3.L1)<sub>2</sub>Cu<sub>2</sub>( $\mu$ -O, $\kappa$ <sub>N</sub>-OCMe<sub>2</sub>Py)( $\mu$ -O, $\kappa$ <sub>N</sub>-OCH<sub>2</sub>Py), 3.6.** Cu(OMe)<sub>2</sub> (38 mg, 0.30 mmol) was suspended in toluene (3 mL). 2-pyridylmethanol (58  $\mu\text{L}$ , 0.61 mmol) was added to the blue suspension, which was left to stir for 30 minutes, followed by the addition of 2-(pyridine-2-yl)propan-2-ol (41 mg, 0.30 mmol). A freshly prepared orange solution of **3.1** (100 mg, 0.30 mmol) in dichloromethane (2 mL) was added. The reaction was stirred 24 hours at RT, filtered to remove trace impurities, concentrated to 1/3 of the volume, diluted with hexane (18 mL). After standing at room temperature for 24 hours, green crystals (28 mg, 18%), suitable for X-ray diffraction studies, separated from the solution.

UV-vis (toluene,  $2.3 \cdot 10^{-5}$  M) [ $\lambda_{\text{max}}$ , nm ( $\epsilon$ ,  $\text{mol}^{-1} \text{ cm}^2$ ): 317 (sh), 343 (sh), 359 (15000), 379 (sh). Anal. Calcd for  $\text{C}_{58}\text{H}_{60}\text{Cu}_2\text{N}_8\text{O}_2 \cdot \frac{1}{4}\text{CH}_2\text{Cl}_2$ : C, 66.66; H, 5.81; N, 10.68; Found: C, 66.55; H, 5.88; N, 10.91. (Presence of dichloromethane confirmed by NMR.)

**(3.L1)<sub>2</sub>Cu<sub>2</sub>( $\mu$ -O, $\kappa$ <sub>N</sub>-OC<sub>2</sub>H<sub>4</sub>Py)<sub>2</sub>, 3.8.** Analogous to **3.1**, from Cu(OMe)<sub>2</sub> (38 mg, 0.30 mmol) in toluene (3 mL), 2-pyridine-2-yl-ethanol (69  $\mu\text{L}$ , 0.61 mmol), **3.L1** (100 mg, 0.33 mmol) in toluene (2 mL). The filtered and concentrated (1/3 of the volume) dark green solution was diluted with hexane (18 mL) and kept at  $-30$  °C for 4 hours. Decantation and washing with hexane (3 x 10 mL) afforded 38 mg (24%) of X-ray quality, green crystals.

$^1\text{H}$  NMR (400 MHz,  $\text{C}_6\text{D}_6$ )  $\delta$  21.7, 15.7, 12.6, 10.5, 9.9, 8.9, 7.5, 7.0, 6.1, 5.7, 2.4, 1.93. UV-vis (toluene,  $2.3 \cdot 10^{-5}$  M) [ $\lambda_{\text{max}}$ , nm ( $\epsilon$ ,  $\text{mol}^{-1} \text{cm}^2$ ): 329 (sh), 345 (34000); 359 (36000), 379 (sh). An analytically pure sample was obtained by diffusion of hexane into a dichloromethane solution. Anal. Calcd for  $\text{C}_{58}\text{H}_{60}\text{Cu}_2\text{N}_8\text{O}_2 \cdot \frac{1}{4}\text{CH}_2\text{Cl}_2$ : C, 66.66; H, 5.81; N, 10.68; Found: C, 66.78; H, 6.26; N, 10.79. (Presence of dichloromethane confirmed by NMR.)

**(3.L2) $_2$ Cu $_2$ ( $\mu$ -O, $\kappa$ <sub>N</sub>-OCH $_2$ Py) $_2$ , 3.9.** Analogous to **3.1**, from  $\text{Cu}(\text{OMe})_2$  (42 mg, 0.33 mmol) in toluene (3 mL), 2-pyridine-methanol (64  $\mu\text{L}$ , 0.66 mmol), **3.L2** (100 mg, 0.33 mmol) in toluene (2 mL). The filtered and concentrated (1/3 of the volume) dark green solution was diluted with hexane (18 mL) and slowly evaporated at RT overnight to yield green crystals, which were separated by decantation and recrystallized by hexane diffusion into dichloromethane (1:3) (42 mg, 26% of X-ray quality green crystals).

$^1\text{H}$  NMR (400 MHz,  $\text{C}_6\text{D}_6$ )  $\delta$  64.5, 60.6, 55, 46.6, 26.8, 22.1, 18.8, 14.0, 11.8, 10.1, 8.6, 7.1. UV-vis (toluene,  $2.3 \cdot 10^{-5}$  M) [ $\lambda_{\text{max}}$ , nm ( $\epsilon$ ,  $\text{mol}^{-1} \text{cm}^2$ ): 331 (sh), 346 (20500), 359 (22000), 386 (sh), 467 (sh). Anal. Calcd for  $\text{C}_{52}\text{H}_{48}\text{Cu}_2\text{N}_8\text{O}_2$ : C, 66.16; H, 5.12; N, 11.87; Found: C, 66.02; H, 5.26; N, 12.05.

**(3.L2) $_2$ Cu $_2$ ( $\mu$ -O, $\kappa$ <sub>N</sub>-OC $_2$ H $_4$ NMe $_2$ ) $_2$ , 3.10.** Analogous to **3.1**, from  $\text{Cu}(\text{OMe})_2$  (42 mg, 0.33 mmol) in toluene (3 mL), dimethylamino ethanol (67  $\mu\text{L}$ , 0.66 mmol), **3.L2** (100 mg, 0.33 mmol) in toluene (2 mL). The filtered and concentrated (1/3 of the volume) dark green solution was diluted with hexane (18 mL) and kept at  $-30$  °C for 4 h. Decantation and washing with hexane (3 x 10 mL) afforded X-ray quality green crystals (62 mg, 42%).

$^1\text{H}$  NMR (400 MHz,  $\text{C}_6\text{D}_6$ )  $\delta$  32.93, 28.5, 23.3, 8.2, 7.5, 7.2. UV-vis (toluene,  $2.3 \cdot 10^{-5}$  M) [ $\lambda_{\text{max}}$ , nm ( $\epsilon$ ,  $\text{mol}^{-1} \text{cm}^2$ ): 363 (12800), 388 (sh), 469 (sh). Anal. Calcd for  $\text{C}_{48}\text{H}_{56}\text{Cu}_2\text{N}_8\text{O}_2$ : C, 63.77; H, 6.24; N, 12.39; Found: C, 63.87; H, 6.45 N, 12.52.

**(3.L3) $_2$ Cu $_2$ ( $\mu$ -O, $\kappa$ <sub>N</sub>-OCH $_2$ Py) $_2$ , 3.11.** Analogous to **3.1**, from  $\text{Cu}(\text{OMe})_2$  (63 mg, 0.50 mmol) in toluene (3 mL), 2-pyridine-methanol (97  $\mu\text{L}$ , 1.0 mmol), **3.L3** (100 mg,

0.50 mmol) in toluene (2 mL). The filtered and concentrated (1/3 of the volume) dark green solution was diluted with hexane (18 mL) and kept at  $-30\text{ }^{\circ}\text{C}$  for 4 hours. Decantation and washing with hexane (3 x 10 mL) afforded 72 mg (38%) of X-ray quality, green crystals.

$^1\text{H}$  NMR (400 MHz,  $\text{C}_6\text{D}_6$ )  $\delta$  56.7, 49.3, 33.9, 24.0, 22.9, 20.2, 18.6, 11.4, 8.5. UV-vis (toluene,  $2.3 \cdot 10^{-5}$  M) [ $\lambda_{\text{max}}$ , nm ( $\epsilon$ ,  $\text{mol}^{-1} \text{cm}^2$ ): 342 (17800), 427 (sh), 483 (sh). Anal. Calcd for  $\text{C}_{38}\text{H}_{38}\text{Cu}_2\text{N}_6\text{O}_2$ : C, 61.86; H, 5.19; N, 11.39; Found: C, 61.68; H, 5.41; N, 11.45.

***rac*-Lactide polymerization.** In a glove box, the desired amount of *rac*-lactide was placed into a J.-Young tube together with  $\text{C}_6\text{D}_6$ . If required, a stock solution of an additive (benzyl alcohol, trityl alcohol, etc. was added, followed by a stock solution of the catalyst ( $\approx 20$  mM in  $\text{C}_6\text{D}_6$ ). The reaction was followed by  $^1\text{H}$  NMR. The reaction was quenched by addition of  $\approx 5$  equiv of a  $\text{CDCl}_3$  solution of acetic acid (5 mM). The volatiles were immediately evaporated and solid polymer samples were stored at  $-80\text{ }^{\circ}\text{C}$  for further analysis. Conversion was determined from  $^1\text{H}$  NMR by comparison to remaining lactide.  $P_m$  values were determined from homodecoupled  $^1\text{H}$  NMR spectra and calculated from  $P_m = 1 - 2 \cdot I_1 / (I_1 + I_2)$ , with  $I_1 = 5.15 - 5.21$  ppm (*rmr*, *mmr/rmm*),  $I_2 = 5.21 - 5.25$  ppm (*mmr/rmm*, *mmm*, *mr*). The integration of the left multiplet and right multiplet ( $I_1$  and  $I_2$ ) required only one, very reproducible dividing point of the integration, which was always taken as the minimum between the two multiplets.  $P_m$ -values obtained this way were typically consistent to  $\pm 1\%$  over the course of one experiment and  $\pm 3\%$  between different experiments under identical conditions.

**X-ray diffraction.** Single crystals were obtained directly from isolation of the products as described above. Diffraction data were collected on a Bruker Venture METALJET diffractometer (Ga  $\text{K}\alpha$  radiation) or a Bruker APEXII with a Cu microsource/Quazar MX using the APEX2 software package.<sup>42</sup> Data reduction was performed with SAINT,<sup>43</sup> absorption corrections with SADABS.<sup>44</sup> Structures were solved by dual-space refinement (SHELXT).<sup>45</sup> All non-hydrogen atoms were refined

anisotropic using full-matrix least-squares on  $F^2$  and hydrogen atoms refined with fixed isotropic U using a riding model (SHELXL97).<sup>46</sup> Further experimental details can be found in Table 3.V and in the supporting information (CIF).



**Table 3.V.** Details of X-ray Diffraction Studies

	<b>3.5</b>	<b>3.6</b>	<b>3.8</b>
Formula	C <sub>98</sub> H <sub>106</sub> ClCu <sub>4</sub> N <sub>13</sub> O <sub>4</sub>	C <sub>58</sub> H <sub>60</sub> Cu <sub>2</sub> N <sub>8</sub> O <sub>2</sub>	C <sub>58</sub> H <sub>60</sub> Cu <sub>2</sub> N <sub>8</sub> O <sub>2</sub>
$M_w$ (g/mol); $d_{\text{calcd}}$	1819.56; 1.328	1028.22; 1.326	1028.22; 1.304
$T$ (K); F(000)	100; 3800	100; 2152	100; 1076
Crystal System	orthorhombic	orthorhombic	monoclinic
Space Group	$P2_12_12_1$	$P2_12_12_1$	$P2_1$
Unit Cell:			
$a$ (Å)	10.1680(2)	10.0964(4)	9.9536(8)
$b$ (Å)	11.6795(2)	13.6786(6)	11.6038(8)
$c$ (Å)	76.6231(12)	37.2880(16)	22.8593(15)
$\alpha$ (°)	90	90	90
$\beta$ (°)	90	90	97.224(4)
$\gamma$ (°)	90	90	90
$V$ (Å <sup>3</sup> ); $Z$	9099.5(3); 4	5149.6(4); 4	2619.3(3); 2
$\mu$ (mm <sup>-1</sup> )	1.779	4.714	1.389
$\theta$ range (°); completeness	2.3 - 71.1; 0.97	3.5 - 55.4; 0.98	3.9 - 64.7; 0.96
collected reflections; $R_{\sigma}$	61301; 0.0357	68232; 0.0802	36152; 0.0614
unique reflections; $R_{\text{int}}$	17326; 0.0352	11643; 0.1000	9919; 0.0654
$R1(F)$ ( $I > 2\sigma(I)$ )	0.0350	0.0664	0.0852
$wR(F^2)$ (all data)	0.0913	0.1725	0.2332
GoF( $F^2$ ); Flack-x	1.045; 0.11(6)	0.990; 0.48(6)	1.069; 0.01(2)
Res. electron density	0.40; -0.36	1.39; -0.71	1.62; -1.08

	3.9	3.10	3.11
Formula	C <sub>52</sub> H <sub>48</sub> Cu <sub>2</sub> N <sub>8</sub> O <sub>2</sub>	C <sub>48</sub> H <sub>56</sub> Cu <sub>2</sub> N <sub>8</sub> O <sub>2</sub>	C <sub>38</sub> H <sub>38</sub> Cu <sub>2</sub> N <sub>6</sub> O <sub>2</sub>
$M_w$ (g/mol); $d_{\text{calcd}}$	944.06; 1.373	904.08	737.82
$T$ (K); F(000)	100; 980	150; 948	100; 764
Crystal System	triclinic	monoclinic	triclinic
Space Group	$P-1$	$P2_1/c$	$P-1$
Unit Cell:			
$a$	9.8736(6)	9.6823(5)	8.4786(3)
$b$ (Å)	14.8316(9)	16.6306(8)	12.6946(4)
$c$ (Å)	15.8958(10)	14.4263(7)	16.1937(6)
$\alpha$ (°)	88.899(2)	90	79.417(2)
$\beta$ (°)	89.403(2)	103.175(2)	89.851(2)
$\gamma$ (°)	78.773(2)	90	88.804(2)
$V$ (Å <sup>3</sup> ); $Z$	2282.8(2); 2	2261.8(2); 2	1712.9(1); 2
$\mu$ (mm <sup>-1</sup> )	1.545	5.323	6.924
$\theta$ range (°); completeness	3.0 - 71.9; 0.97	4.7 - 61.0; 0.95	2.4 - 60.7; 1.00
collected reflections; $R_\sigma$	104020; 0.0270	38871; 0.0379	42498; 0.0254
unique reflections; $R_{\text{int}}$	8683; 0.0563	4996; 0.0630	7847; 0.0254
$R1(F)$ ( $I > 2\sigma(I)$ )	0.0423	0.0360	0.0315
wR( $F^2$ ) (all data)	0.1215	0.0929	0.0831
GoF( $F^2$ ); Flack-x	1.075; -	1.046; -	1.06; -
Res. electron density	0.74; -0.48	0.34; -0.16	0.42; -0.21

**Supporting Information**

Additional figures, full listing of polymerization results, crystal structure data (CIF). This material is available free of charge via the Internet at <http://pubs.acs.org>.

**Acknowledgment**

D. Kapoor contributed to the preparation of **11** during his internship in the group. S. Fortun contributed an initial preparation of **9**. We like to thank F. Bélanger for support with X-ray diffraction and M.-C. Tang and A. Furtos for MS-analyses.

**Corresponding Author**

\* [Frank.Schaper@umontreal.ca](mailto:Frank.Schaper@umontreal.ca)

**Funding Sources**

NSERC Discovery Grant RGPIN-2016-04953 and the Centre for Green Chemistry and Catalysis (FQRNT).

### References Chapter 3

- (1) (a) Nagarajan, V.; Mohanty, A. K.; Misra, M. *ACS Sustainable Chem. Eng.* **2016**, *4*, 2899-2916. (b) Castro-Aguirre, E.; Iñiguez-Franco, F.; Samsudin, H.; Fang, X.; Auras, R. *Adv. Drug Delivery Rev.* **2016**, *107*, 333-366. (c) Slomkowski, S.; Penczek, S.; Duda, A. *Polym. Adv. Technol.* **2014**, *25*, 436-447.
- (2) Guillaume, S. M.; Kirillov, E.; Sarazin, Y.; Carpentier, J.-F. *Chem.-Eur. J.* **2015**, *21*, 7988-8003.
- (3) (a) Chisholm, M. H.; Eilerts, N. W. *Chem. Commun. (Cambridge, U. K.)* **1996**, 853-854. (b) Spassky, N.; Wisniewski, M.; Pluta, C.; Le Borgne, A. *Macromol. Chem. Phys.* **1996**, *197*, 2627-2637. (c) Chamberlain, B. M.; Sun, Y.; Hagadorn, J. R.; Hemmesch, E. W.; Young, V. G.; Pink, M.; Hillmyer, M. A.; Tolman, W. B. *Macromolecules* **1999**, *32*, 2400-2402. (d) Cheng, M.; Attygalle, A. B.; Lobkovsky, E. B.; Coates, G. W. *J. Am. Chem. Soc.* **1999**, *121*, 11583-11584.
- (4) Ovitt, T. M.; Coates, G. W. *J. Am. Chem. Soc.* **2002**, *124*, 1316-1326.
- (5) Press, K.; Goldberg, I.; Kol, M. *Angew. Chem., Int. Ed.* **2015**, *54*, 14858-14861.
- (6) Fortun, S.; Daneshmand, P.; Schaper, F. *Angew. Chem. Int. Ed.* **2015**, *54*, 13669-13672.
- (7) (a) Sauer, A.; Kapelski, A.; Fliedel, C.; Dagorne, S.; Kol, M.; Okuda, J. *Dalton Trans.* **2013**, *42*, 9007-9023. (b) Carpentier, J.-F.; Liu, B.; Sarazin, Y. In *Advances in Organometallic Chemistry and Catalysis*, John Wiley & Sons, Inc.: 2013; Vol. pp 359-378. (c) Wheaton, C. A.; Hayes, P. G. *Comments Inorg. Chem.* **2011**, *32*, 127-162. (d) Thomas, C. M. *Chem. Soc. Rev.* **2010**, *39*, 165. (e) Sutar, A. K.; Maharana, T.; Dutta, S.; Chen, C.-T.; Lin, C.-C. *Chem. Soc. Rev.* **2010**, *39*, 1724-1746. (f) Carpentier, J.-F. *Macromol. Rapid Comm.* **2010**, *31*, 1696-1705. (g) Wheaton, C. A.; Hayes, P. G.; Ireland, B. J. *Dalton Trans.* **2009**, 4832 - 4846. (h) O'Keefe, B. J.; Hillmyer, M. A.; Tolman, W. B. *J. Chem. Soc., Dalton Trans.* **2001**, 2215-2224. (i) Platel, R. H.; Hodgson, L. M.; Williams, C. K. *Polym. Rev.* **2008**, *48*, 11 - 63. (j) Dutta, S.; Hung, W.-C.; Huang, B.-H.; Lin, C.-C. In *Synthetic Biodegradable Polymers*, Rieger, B.; Künkel, A.; Coates, G. W.; Reichardt, R.; Dinjus, E.; Zevaco, T. A., Eds. Springer-Verlag: Berlin, 2011; Vol. pp 219-284. (k)

Paul, S.; Zhu, Y.; Romain, C.; Brooks, R.; Saini, P. K.; Williams, C. K. *Chem. Commun. (Cambridge, U. K.)* **2015**, *51*, 6459-6479.

(8) (a) Jianming, R.; Anguo, X.; Hongwei, W.; Hailin, Y. *Des. Monomers Polym.* **2013**, *17*, 345-355. (b) Huang, B. H.; Dutta, S.; Lin, C. C. In *Comprehensive Inorganic Chemistry II (Second Edition)*, Poeppelemeier, J. R., Ed. Elsevier: Amsterdam, 2013; Vol. pp 1217-1249. (c) Dagherne, S.; Normand, M.; Kirillov, E.; Carpentier, J.-F. *Coord. Chem. Rev.* **2013**, *257*, 1869-1886.

(9) (a) Gibson, V. C.; Marshall, E. L.; Navarro-Llobet, D.; White, A. J. P.; Williams, D. J. *J. Chem. Soc., Dalton Trans.* **2002**, 4321-4322. (b) O'Keefe, B. J.; Breyfogle, L. E.; Hillmyer, M. A.; Tolman, W. B. *J. Am. Chem. Soc.* **2002**, *124*, 4384-4393. (c) Gorczynski, J. L.; Chen, J.; Fraser, C. L. *J. Am. Chem. Soc.* **2005**, *127*, 14956-14957.

(10) (a) Biernesser, A. B.; Delle Chiaie, K. R.; Curley, J. B.; Byers, J. A. *Angew. Chem., Int. Ed.* **2016**, *55*, 5251-5254. (b) Biernesser, A. B.; Li, B.; Byers, J. A. *J. Am. Chem. Soc.* **2013**, *135*, 16553-16560.

(11) (a) Appavoo, D.; Omondi, B.; Guzei, I. A.; van Wyk, J. L.; Zinyemba, O.; Darkwa, J. *Polyhedron* **2014**, *69*, 55-60. (b) Li, C.-Y.; Hsu, S.-J.; Lin, C.-I.; Tsai, C.-Y.; Wang, J.-H.; Ko, B.-T.; Lin, C.-H.; Huang, H.-Y. *J. Polym. Sci., Part A: Polym. Chem.* **2013**, *51*, 3840-3849. (c) Gowda, R. R.; Chakraborty, D. *J. Molec. Catal. A: Chem.* **2011**, *349*, 86-93. (d) Chen, L.-L.; Ding, L.-Q.; Zeng, C.; Long, Y.; Lü, X.-Q.; Song, J.-R.; Fan, D.-D.; Jin, W.-J. *Appl. Organomet. Chem.* **2011**, *25*, 310-316. (e) Bhunora, S.; Mugo, J.; Bhaw-Luximon, A.; Mapolie, S.; Van Wyk, J.; Darkwa, J.; Nordlander, E. *Appl. Organomet. Chem.* **2011**, *25*, 133-145. (f) John, A.; Katiyar, V.; Pang, K.; Shaikh, M. M.; Nanavati, H.; Ghosh, P. *Polyhedron* **2007**, *26*, 4033-4044. (g) Sun, J.; Shi, W.; Chen, D.; Liang, C. *J. Appl. Polym. Sci.* **2002**, *86*, 3312-3315. (h) Routaray, A.; Nath, N.; Maharana, T.; Sutar, A. k. *J. Macromol. Sci., Part A: Pure Appl. Chem.* **2015**, *52*, 444-453. (i) Akpan, E. D.; Ojwach, S. O.; Omondi, B.; Nyamori, V. O. *New Journal of Chemistry* **2016**, *40*, 3499-3510. (j) Routaray, A.; Nath, N.; Maharana, T.; Sahoo, P. K.; Das, J. P.; Sutar, A. K. *J Chem Sci* **2016**, *128*, 883-891.

(12) (a) Whitehorne, T. J. J.; Schaper, F. *Chem Commun.* **2012**, *48*, 10334-10336. (b) Whitehorne, T. J. J.; Schaper, F. *Inorg. Chem.* **2013**, *52*, 13612-13622. (c) Whitehorne, T. J. J.; Schaper, F. *Can. J. Chem.* **2014**, *92*, 206-214. (d) Kwon, K. S.; Cho, J.; Nayab, S.; Jeong, J. H. *Inorg. Chem. Commun.* **2015**, *55*, 36-38. (e) Cho, J.; Nayab, S.; Jeong, J. H. *Polyhedron* **2016**, *113*, 81-87. (f) Ahn, S. H.; Chun, M. K.; Kim, E.; Jeong, J. H.; Nayab, S.; Lee, H. *Polyhedron* **2017**, *127*, 51-58.

(13) Pseudo-first order rate constants obtained in preliminary investigations (ref. 6) were identical within the margin of error for both complexes. However, both complexes showed evidence of up to 50% catalyst decomposition during the polymerization reaction. To obtain more reliable kinetic data, the preparation of ligands and complexes was optimized (see Exp. Section) to minimize the possibility of impurities and the kinetic analysis repeated in more detail. In line with improved purity, the obtained rate constants were higher than those obtained in the preliminary communication and complex decomposition significantly reduced.

(14) The kinetic data does not show evidence for notable catalyst decomposition and there is no correlation of polymer molecular weight or polydispersity with catalyst activity. Deactivation of **3.1** is thus either reversible, but slow enough to lead to inhomogeneities in the polymer molecular weight distribution, or irreversible, but negligible compared to the experimental error in the determination of reaction kinetics.

(15) Addison, A. W.; Rao, T. N.; Reedijk, J.; van Rijn, J.; Verschoor, G. C. *J. Chem. Soc., Dalton Trans.* **1984**, 1349-1356.

(16) Ruiz, E.; Alemany, P.; Alvarez, S.; Cano, J. *J. Am. Chem. Soc.* **1997**, *119*, 1297-1303.

(17) Reduced intensity might also be a consequence of partial occupation of the triplet state in a weakly coupled species. In this case, the ratio **A:B** should be constant, however, which was not observed.

(18) (a) McKee, V.; Zvagulis, M.; Dagdigian, J. V.; Patch, M. G.; Reed, C. A. *J. Am. Chem. Soc.* **1984**, *106*, 4765-4772. (b) Satcher, J. H.; Balch, A. L. *Inorg. Chem.* **1995**, *34*, 3371-3373.

(19) (a) Dalgaard, P.; Hazell, A.; McKenzie, C. J.; Moubaraki, B.; Murray, K. S. *Polyhedron* **2000**, *19*, 1909-1915. (b) Torelli, S.; Belle, C.; Gautier-Luneau, I.; Pierre, J. L.; Saint-Aman, E.; Latour, J. M.; Le Pape, L.; Luneau, D. *Inorg. Chem.* **2000**, *39*, 3526-3536. (c) Michel, F.; Torelli, S.; Thomas, F.; Duboc, C.; Philouze, C.; Belle, C.; Hamman, S.; Saint-Aman, E.; Pierre, J.-L. *Angew. Chem., Int. Ed.* **2005**, *44*, 438-441.

(20) Li, L.; Murthy, N. N.; Telser, J.; Zakharov, L. N.; Yap, G. P. A.; Rheingold, A. L.; Karlin, K. D.; Rokita, S. E. *Inorg. Chem.* **2006**, *45*, 7144-7159.

(21) Weil, J. A.; Bolton, J. R. In *Electron Paramagnetic Resonance*, John Wiley & Sons, Inc.: 2006; Vol. p 187.

(22) Based on 39 structures in the CSD with only an alkoxy or aryloxy group bridging two copper centers:  $d(\text{Cu-Cu}) = 3.1 - 4.8 \text{ \AA}$ , average: 3.7(4).

(23) Groom, C. R.; Bruno, I. J.; Lightfoot, M. P.; Ward, S. C. *Acta Crystallographica Section B* **2016**, *72*, 171-179.

(24) For experimental reasons, solutions had to be exposed to ambient atmosphere during shock-freezing.

(25) Hardouin Duparc, V.; Schaper, F. *unpublished results*,

(26) One reviewer posed the question of possible aggregation of the complexes to explain the observed solvent dependence of stereocontrol. While we cannot exclude this, there is no evidence for complex aggregation: kinetics are first order in catalyst concentration and the same stereocontrol was achieved with 1, 2 and 3 mM catalyst concentration (Table 4.S3, entries 1-11).

(27) Even a stoichiometric amount of dichloromethane (from co-crystallized solvent in the catalyst) notably reduced stereocontrol (Table 4.S3, entry 37-41). The reason for this strong response to dichloromethane is unclear, since the presence of pyridine is well tolerated (Table 4.S3, entry 30-32).

(28) Aluthge, D. C.; Patrick, B. O.; Mehrkhodavandi, P. *Chem. Commun. (Cambridge, U. K.)* **2013**, *49*, 4295-4297.

(29) (a) Kasperczyk, J. E. *Polymer* **1999**, *40*, 5455-5458. (b) Kasperczyk, J. E. *Macromolecules* **1995**, *28*, 3937-3939.

(30) Chamberlain, B. M.; Cheng, M.; Moore, D. R.; Ovitt, T. M.; Lobkovsky, E. B.; Coates, G. W. *J. Am. Chem. Soc.* **2001**, *123*, 3229-3238.

(31) Jones, M. D.; Hancock, S. L.; McKeown, P.; Schafer, P. M.; Buchard, A.; Thomas, L. H.; Mahon, M. F.; Lowe, J. P. *Chem. Commun. (Cambridge, U. K.)* **2014**, *50*, 15967-15970.

(32) Despite the use of enantiopure (98% ee) amine, an inversion-symmetric complex containing two ligands of opposite chirality was obtained in 38% yield, indicative of severe racemization of the methylbenzyl substituent under the basic preparative conditions.

(33) Ma, H.; Spaniol, T. P.; Okuda, J. *Angew. Chem., Int. Ed.* **2006**, *45*, 7818-7821.

(34) (a) Douglas, A. F.; Patrick, B. O.; Mehrkhodavandi, P. *Angew. Chem., Int. Ed.* **2008**, *47*, 2290-2293. (b) Yu, I.; Acosta-Ramírez, A.; Mehrkhodavandi, P. *J. Am. Chem. Soc.* **2012**, *134*, 12758-12773.

(35) Hu, M.; Wang, M.; Zhu, H.; Zhang, L.; Zhang, H.; Sun, L. *Dalton Trans.* **2010**, *39*, 4440-4446.

(36) Platel, R. H.; White, A. J. P.; Williams, C. K. *Chem. Commun. (Cambridge, U. K.)* **2009**, 4115-4117.

(37) Singh, J. V.; Baranwal, B. P.; Mehrotra, R. C. *Z. Anorg. Allg. Chem.* **1981**, *477*, 235-240.

(38) Knizhnikov, V. A.; Borisova, N. E.; Yurashevich, N. Y.; Popova, L. A.; Chernyad'ev, A. Y.; Zubreichuk, Z. P.; Reshetova, M. D. *Russ. J. Org. Chem.* **2007**, *43*, 855-860.

(39) Kerr, W. J.; Middleditch, M.; Watson, A. J. B. *Synlett* **2011**, *2011*, 177-180.

(40) Save, M.; Schappacher, M.; Soum, A. *Macromol. Chem. Phys.* **2002**, *203*, 889-899.

(41) Stoll, S.; A. Schweiger *J. Magn. Reson.* **2006**, *178*, 42-55.

(42) *APEX2*, Release 2.1-0; Bruker AXS Inc.: Madison, USA, 2006.

(43) *SAINTE*, Release 7.34A; Bruker AXS Inc.: Madison, USA, 2006.

(44) Sheldrick, G. M. *SADABS*, Bruker AXS Inc.: Madison, USA, 1996 & 2004.

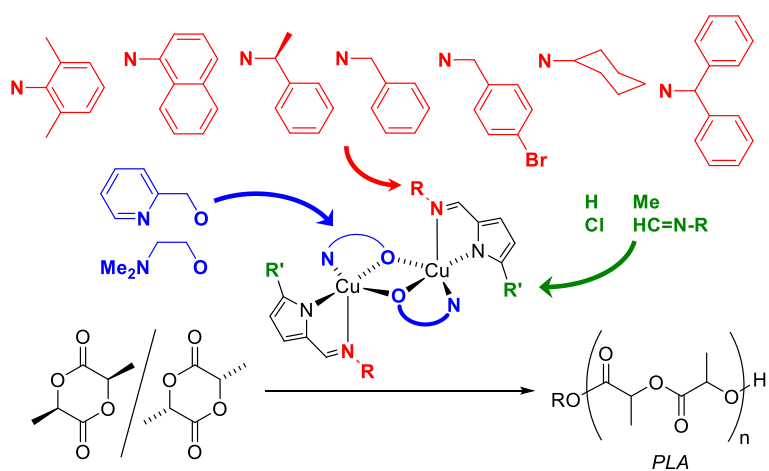
(45) Sheldrick, G. *Acta Crystallogr. Sect. A: Found. Crystallogr.* **2015**, *71*, 3-8.

(46) Sheldrick, G. M. *Acta Crystallogr.* **2008**, *A64*, 112-122.



## Chapter 4 . Diiminopyrrolide Copper Complexes: Synthesis, Structures and *rac*-Lactide-Polymerization Activity.

Daneshmand, P.; Fortun, S.; Schaper F. Diiminopyrrolide Copper Complexes: Synthesis, Structures and *rac*-Lactide-Polymerization Activity. *Organometallics*, 2017, 36, 3860–3877.



Reprinted with permission from *Organometallics*. Copyright 2017 American Chemical Society.

Contributions of F. Schaper: A first draft was provided by me with major modification from Prof. Frank Schaper.

Contributions of S. Fortun: Preparation of the homoleptic and Cu(I) complexes.



# Diiminopyrrolide Copper Complexes: Synthesis, Structures and *rac*-Lactide- Polymerization Activity

Pargol Daneshmand, Solène Fortun, Frank Schaper\*

*Centre in Green Chemistry and Catalysis, Department of chemistry, Université de Montréal, C. P. 6128 Succ. Centre-Ville, Montréal, QC, H3T 3J7, Canada*

*Supporting Information Placeholder*

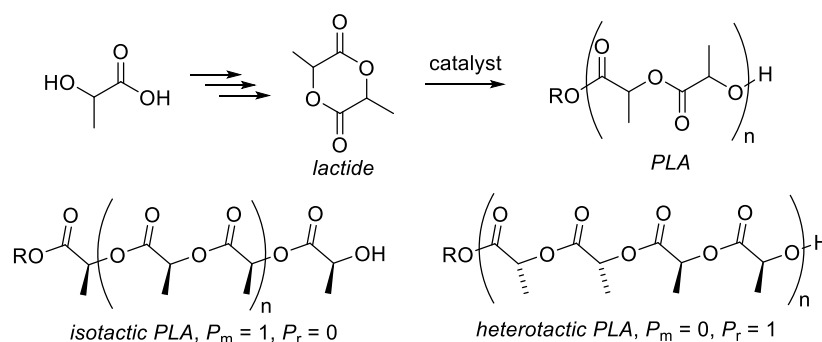
## Abstract

2,5-Diiminopyrrole ligands with *N*-xylyl (4.L3), *N*-naphtyl (4.L4), *N*-cyclohexyl (4.L5), *N*-diphenylmethyl (4.L6), and *N*-*para*-bromobenzyl (4.L7), as well as the 5-*R*-2-iminopyrroles with *N*-*S*-methylbenzyl (4.L8: *R*=H, 4.L10: *R*=Me, and 4.L11: *R*=Cl) and *N*-benzyl (*R*=H, 4.9) were reacted with Cu(OMe)<sub>2</sub> and pyridylmethanol (R1OH) or dimethylaminoethanol (R2OH) to yield the corresponding dinuclear complexes 4.L<sub>2</sub>Cu<sub>2</sub>(μ-OR)<sub>2</sub>. Reactions in the absence of chelating R1OH or R2OH only yielded homoleptic 4.L<sub>2</sub>Cu or 4.L<sub>2</sub>Cu<sub>2</sub>. Complexes with R2OH were obtained with all ligands but 4.L4, complexes with R1OH for all ligands but 4.L3, 4.L4 and 4.L6. All complexes but those with 4.L7 displayed dinuclear crystal structures with pentacoordinated copper centers and bridging alkoxy groups. The alkoxy group and the pyrrolide ligand were consistently found in equatorial positions. Either imine, pyridine or amine occupied the axial position. 4.L7 coordinated both iminogroups to copper yielding a distorted octahedral coordination geometry. All complexes containing R1OH, with the exception of 4.L7, showed an isotactic bias in the polymerization of *rac*-lactide, with a maximum *P<sub>m</sub>* of 0.7. Complexes containing R2OH provided atactic PLA or, in the case of 4.L3 and 4.L6, heterotactic PLA. Reduced stereocontrol in monoiminopyrrolide copper complexes and lack of

stereocontrol with octahedrally coordinated 4.L7 indicate that the catalytic site needs to adapt to chain-end chirality and is participating in enantiomer selection.

## Introduction

Poly lactide or polylactic acid (PLA) is one of the most successful biodegradable polymers marketed today.<sup>1</sup> PLA is currently obtained on a commercial scale by unselective chain-growth, ring-opening polymerization of lactide, the dimeric anhydride of lactic acid (Scheme 4.1). To achieve the desired isotactic PLA, enantiopure lactide, obtained by fermentation of corn starch, is employed.<sup>2</sup> Given its economic importance and in analogy to  $\alpha$ -olefin polymerization, a large number of studies were dedicated to the development of single-site, coordination-insertion catalysts for the polymerization of lactide, which ideally would enable control of the polymer microstructure via the catalyst instead of the monomer.<sup>3</sup> While high selectivity towards the heterotactic polymer is obtained comparatively easily, high selectivity towards isotactic PLA is difficult and very few, if any catalyst systems combine high isoselectivity, high activity and high catalyst stability.<sup>4</sup>



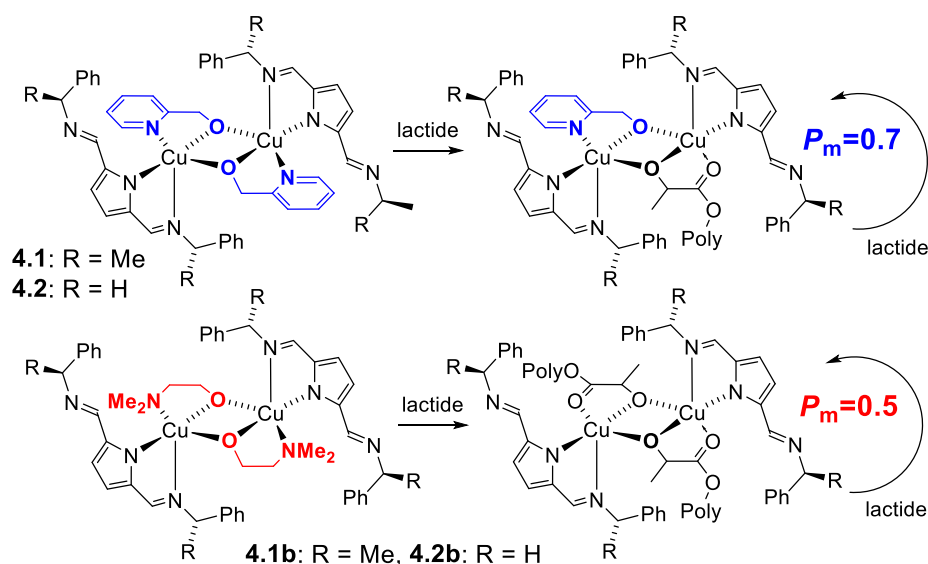
### Scheme 4.1.

For the major part, catalysts for the coordination-insertion polymerization of lactide are based on either  $d^0$ - or  $d^{10}$ -metals, such as alkaline and earth alkaline metals,<sup>3j, 3k, 3p-s</sup> group 3 and rare earth metals,<sup>3f, 3j, 3m</sup> group 4 metals,<sup>3j, 3m, 3t, 3u</sup> zinc,<sup>3b, 3j-m, 3p-r</sup> or group 13 metals.<sup>3f, 3i-m, 3p, 3v-aa</sup> The chemistry of mid-to-late transition metals with partially filled  $d$ -shells, on the other hand, remains little explored. Of these, iron<sup>5</sup> and copper<sup>6</sup> received the most attention. Work on iron-based catalysts by Gibson, Tolman, and Hillmyer resulted in some highly active catalysts,<sup>5s-v</sup> but was

not much pursued further, mostly because of the lack of stereocontrol. More current work from the Byers group concentrates on the possibility to control the polymerization by switching the redox state of the iron center.<sup>5c-e, 5m, 5n</sup> Copper-based systems were initially investigated to replace stannous octoate in molten-monomer polymerizations and were either simple carboxylate salts<sup>6d, 6l, 6n, 6r</sup> or complexes with phenoxyimine or salen ligands.<sup>6e-g, 6m, 6o-q</sup> Activities were typically moderate, requiring several hours or days at elevated temperatures or in the melt to reach completion. Copper catalysts often displayed, however, very good polymer molecular weight control.<sup>6e-g, 6l-r</sup> Kumar and Maharana reported a surprisingly active copper salen/benzyl alcohol catalyst, which polymerized lactide in 12 – 24 h at room temperature in solution.<sup>6e-g</sup> In the absence of benzyl alcohol, the complex was inactive. The same salen copper complex had been used previously without additional alcohol in melt polymerizations, and required 24 h at  $T > 140\text{ }^{\circ}\text{C}$  for polymerizations to reach completion.<sup>6o</sup> In 2012, we reported a discrete copper alkoxide complex carrying a diketiminate spectator ligand, *nacnac*CuOiPr, which was highly active in the coordination-insertion polymerization of lactide, completing polymerization in less than 2 min at ambient temperature.<sup>6i-k</sup> As with all other copper catalysts reported before, PLA produced with (*nacnac*)CuOiPr was atactic. Shortly after, Jeong reported similar high activities with a diamino copper catalyst formed *in situ* from the respective copper chloride complex and lithium alkoxide.<sup>6a-c</sup> In addition to high activities, these catalysts showed preference for heterotactic monomer insertion ( $P_r = 0.65 - 0.88$ ), the first time notable stereocontrol was observed for copper-based catalysts.

In continuation of our work on copper diketiminate complexes, we prepared copper diiminopyrrolide complexes **4.1** and **4.2**.<sup>6h</sup> The complexes showed good polymerization activity (3 – 8 h at room temperature to completion). More importantly, they provided isotactically enriched PLA from *rac*-lactide ( $P_m = 0.7$ ), the first copper-based catalysts showing the desired preference for isotactic insertion (Scheme 4.2).<sup>6h</sup> In an unexpected dependence of stereocontrol on the initiating group, the respective complexes **4.1b** and **4.2b**, which contain dimethylaminoethoxide instead of pyridylmethoxide ligands, provided atactic PLA. The polymerization

mechanism was investigated in detail and showed that all complexes remain dinuclear throughout the polymerization reaction.<sup>7</sup> Depending on the initiating alkoxide, either one or both alkoxides initiate chain growth, and stereocontrol depends strongly on the bridging ligand in the dinuclear active species (Scheme 4.2).<sup>7</sup> Stereocontrol was independent from ligand chirality and only minor differences were observed between **4.1** and **4.2**. In the current study we explore how further variations of the iminopyrrole spectator ligand affect reactivity and stereocontrol in *rac*-lactide polymerization.

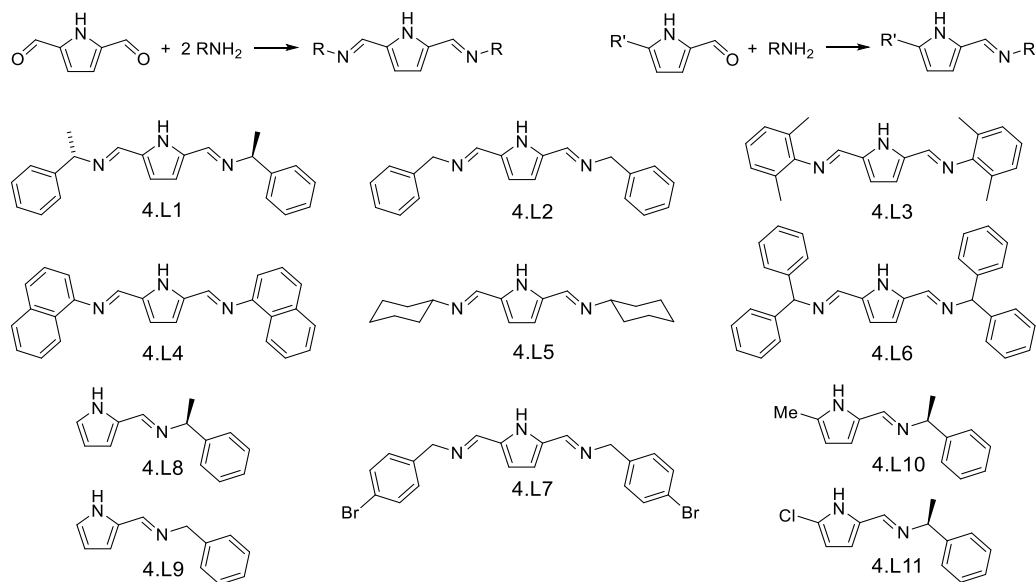


**Scheme 4.2.**

## Results and discussion

### Ligand synthesis.

Known and new diiminopyrroles **4.L1**-**4.L7** and iminopyrroles **4.L9**-**4.L11** were prepared by condensation of diformyl- or monoformylpyrrole with the respective amines, using techniques described previously for **4.L1**,<sup>7</sup> **4.L2**,<sup>7</sup> **4.L3**,<sup>8</sup> **4.L8**,<sup>9</sup> or **4.L9**<sup>10</sup> (Scheme 4.3).

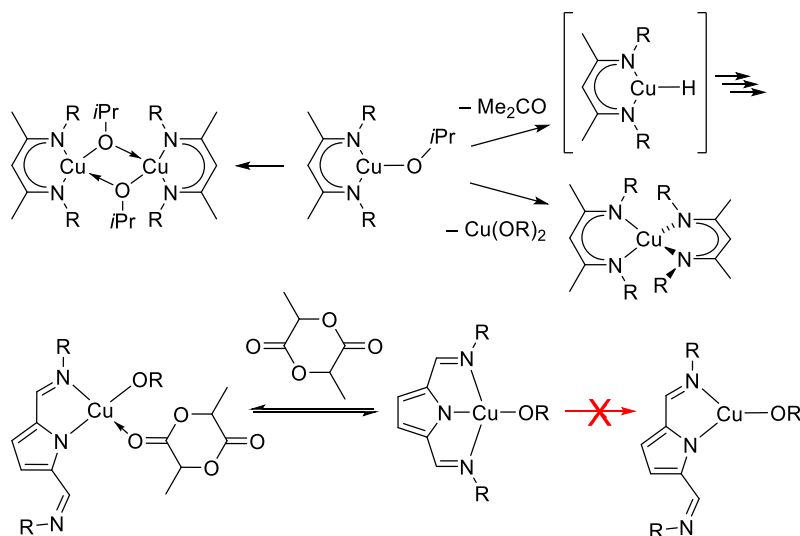


### Scheme 4.3.

#### Attempted synthesis of copper alkoxide complexes.

Previous work on copper diketiminate complexes revealed difficulties in preparing the desired heteroleptic LCuOR complexes.<sup>6j</sup> When saturation of the open coordination site required for polymerization activity was not possible by dimerization of the complex, the latter decomposed either by ligand exchange to the homoleptic copper(II) complex or by  $\beta$ -H elimination from the isopropoxide ligand (Scheme 4.4). Diiminopyrrolide ligands, such as 4.L1-4.L7, are tridentate ligands, but formation of two adjacent five-membered metallacycles is disfavoured for metals with small atomic radii. Consequently, approximately half of the diiminopyrrolide metal complexes characterized by X-ray diffraction studies show bidentate coordination of diiminopyrrolide, with one uncoordinated imino group.<sup>11</sup> In the case of copper as a central metal, Baley et al. reported the synthesis of a homoleptic  $\text{L}_2\text{Cu}$  complex ( $\text{L}_2$  = macrocyclic bis(diiminopyrrolide) ligand) with bidentate coordination of the diiminopyrrolide moieties, and of putative LCu(OR) complexes which were not structurally characterized.<sup>12</sup> Babu et al. reported  $(\text{L}^{\text{diip}})_2\text{Cu}(\text{MeOH})$ ,  $\text{L}^{\text{diip}}$  = 2,5-bis(diisopropylphenylimino)pyrrolide, which interestingly showed bidentate coordination of one and tridentate coordination of the other diiminopyrrolide ligand.<sup>13</sup> Diiminopyrrolide complexes have not been used in lactide polymerization, but

diiminopyrrolide yttrium and lanthanide complexes were active in the polymerization of  $\epsilon$ -caprolactone.<sup>8, 14</sup> We speculated that diiminopyrrolide ligands would be able to stabilize the open coordination site in a square-planar copper alkoxide complex, thus avoiding the decomposition reactions observed for copper diketiminates. In the presence of lactide monomer they would likely easily isomerize to bidentate coordination (Scheme 4.4).



**Scheme 4.4.**

A large number of attempts to prepare heteroleptic  $\text{LCuOiPr}$  complexes by reaction of  $\text{Cu(OiPr)}_2$  with 4.L1-4.L4 were unsuccessful. Neither variation of reaction solvent (toluene, ether, THF, dichloromethane, acetonitrile), reaction temperature (RT or 50 °C), order of addition, or stoichiometry (0.45 – 1.2 equiv  $\text{Cu(OR)}_2$ ) yielded the desired complexes. Several reactions yielded crystalline material (Table 4.S1), which allowed to trace the outcome of these reactions:<sup>15</sup> Homoleptic bis(diiminopyrrolide) complexes 4.L<sub>2</sub>Cu, **4.1c** and **4.4c**, were isolated from reactions of 4.L1 and 4.L4 with  $\text{Cu(OiPr)}_2$ . The crystal structure of **4.1c** (Fig. 4.1, Table 4.I) shows octahedral coordination of copper by two tridentate diiminopyrrolide ligands. The complex is highly symmetric with the copper atom on the intersection of three crystallographic  $C_2$ -axes, and all  $\text{Cu-N}_{\text{imine}}$  distances are thus crystallographically equivalent. The steric constraints of the diiminopyrrolide ligand result in some deviations from ideal octahedral geometry. Thus,  $\text{Cu-N}_{\text{imine}}$  distances are significantly ( $\approx 0.7 \text{ \AA}$ ) longer than



Cu-N<sub>pyrrole</sub> distances. Due to crystallographic symmetry, all N<sub>imine</sub>-Cu-N<sub>pyrrole</sub> angles are equal, but deviate from ideal octahedral symmetry (73.38(9)°). The coordination is highly similar to the  $\kappa^3$ -coordinated diiminopyrrole ligand in L<sup>diip</sup><sub>2</sub>Cu(MeOH) (Table 4.I).<sup>13</sup> Complex **1c** appeared initially to be one of the few examples of Cu(II) complexes where Jahn-Teller distortion results in a compressed octahedral geometry instead of the more typical elongated geometry.<sup>16</sup> Closer inspection of the thermal displacement parameters, however, reveal that they contain an unusually large component parallel to the Cu-imine bond. It seems thus likely that the complex actually adopts an elongated octahedral geometry, with two trans-positioned Cu-imine bonds elongated. Disorder of the elongation direction then complies with crystallographic symmetry. Apparent compressed octahedral geometry by disorder of an elongated geometry is an often observed phenomenon, for example in Cu(II) bisterpyridine complexes.<sup>17</sup>

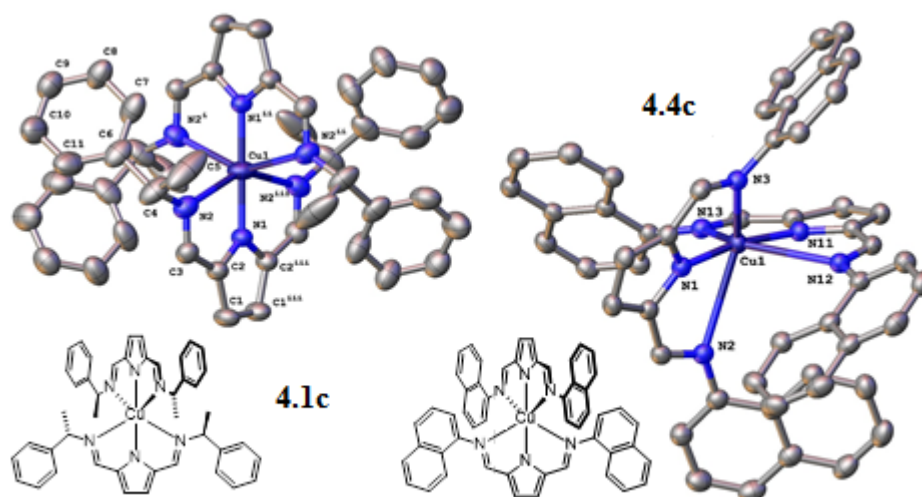


**Figure 4.1.** X-ray structures of **4.1c** (left) and **4.4c** (right). Hydrogen atoms were omitted for clarity. Thermal ellipsoids were drawn at the 50% probability level.

**Table 4.I.** Selected bond lengths (Å) and angles (°) of **4.1c** and **4.4c**.

	<b>4.1c</b>	<b>4.4c</b>	<b>L<sup>diip</sup><sub>2</sub>Cu(MeOH)<sup>a</sup></b>	
			<b>κ<sup>3</sup>-L<sup>diip</sup></b>	<b>κ<sup>2</sup>-L<sup>diip</sup></b>
Cu-N <sub>pyrrole</sub>	1.860(4)	1.882(2), 1.883(2)	1.941(3)	2.013(3)
Cu-N <sub>imine,1</sub>	2.537(4)	2.151(2), 2.184(2)	2.738(3)	2.023(3)
Cu-N <sub>imine,2</sub>	2.537(4)	2.950(2), 2.998(2)	2.738(3)	5.1
N <sub>py</sub> -Cu-N <sub>im,1</sub> <sup>b</sup>	73.38(9)	80.55(6), 80.52(6)	70.8	83.1(1)
N <sub>py</sub> -Cu-N <sub>im,2</sub> <sup>c</sup>	73.38(9)	64.87(6), 64.47(6)	70.8	33.9

<sup>a</sup> Data taken from ref <sup>13</sup>. L<sup>diip</sup> = 2,5-bis(diisopropylphenylimino)pyrrolide. <sup>b</sup> **4.1c**: N1-Cu1-N2, **4.4c**: N1-Cu1-N3, N11-Cu2-N13. <sup>c</sup> **4.1c**: N1-Cu1-N2, **4.4c**: N1-Cu1-N2, N11-Cu2-N12.

The coordination of the pyrrolide ligand in **4.4c** seems to be intermediate between κ<sup>2</sup>- and κ<sup>3</sup>-coordination (Fig. 4.1): The difference in Cu-N<sub>imine,1</sub> and Cu-N<sub>pyrrole</sub> is reduced to half, while the two Cu-N<sub>imine</sub> distances and N<sub>imine</sub>-Cu-N<sub>pyrrole</sub> angles become notably different (Table 4.I). Based on the Cu-N<sub>imine,2</sub> distances of 2.950(2) and 2.998(2) Å, which are comparable to the sum of the vdW-radii (2.95 Å), N<sub>imine,2</sub> might be considered non-bonding and the coordination mode κ<sup>2</sup>. The resulting coordination geometry around copper would be highly distorted, intermediate between square-planar and tetrahedral coordination (τ<sub>4</sub> = 0.5),<sup>18</sup> but not unprecedented for copper. However, N<sub>imine,2</sub> in **4.4c** retains the *s-trans* conformation of the κ<sup>3</sup>-coordination mode instead of the sterically favorable *s-cis* conformation of the κ<sup>2</sup>-coordination,<sup>13</sup> which would also allow for a less distorted square-planar geometry. Despite the long distances, there thus seem to be stabilizing interactions of N<sub>imine,2</sub> with copper and

**4.4c** is best described as a strongly distorted octahedral coordination geometry. While pseudo-octahedral coordination geometries with two elongated cis-ligands have been reported for Cu(II), the distortion is typically much weaker. The only example in the Cambridge Structural Database of a Cu(II) complex with four short ( $< 2.4 \text{ \AA}$ ) and two long, cis-ligands ( $> 2.8 \text{ \AA}$ , angle  $90^\circ \pm 30^\circ$ ) shows a similar geometry but with two large selenium atoms occupying the weak coordination side.<sup>19</sup> Complex **4.4c** thus seems to be an extreme example for this type of octahedral distortion.

Alternatively, reactions of 4.L1-4.L4 with Cu(OiPr)<sub>2</sub> sometimes yielded dinuclear Cu(I) complexes, 4.L<sub>2</sub>Cu<sub>2</sub> (Table 4.S1), in yields ranging from traces to 70%. Figure 2 shows the structures obtained for **4.2d** and **4.3d**. Coordination chemistry around copper is best described as a linear coordination to one pyrrolide and one iminogroup, both with identical Cu-N distances of 1.88 – 1.91 Å (Table 4.S2). An additional weak coordination of another iminogroup with notable longer Cu-N distances (2.4 – 2.5 Å) and an intramolecular copper-copper interaction is likewise present. Cu-Cu distances in **4.2d** and **4.3d** are 2.60 Å and are in the typical range of cuprophilic interactions in dinuclear Cu(I) complexes ( $d_{\text{Cu-Cu}} = 2.55(5) \text{ \AA}$ , based on 78 structures in the CSD).<sup>11</sup>

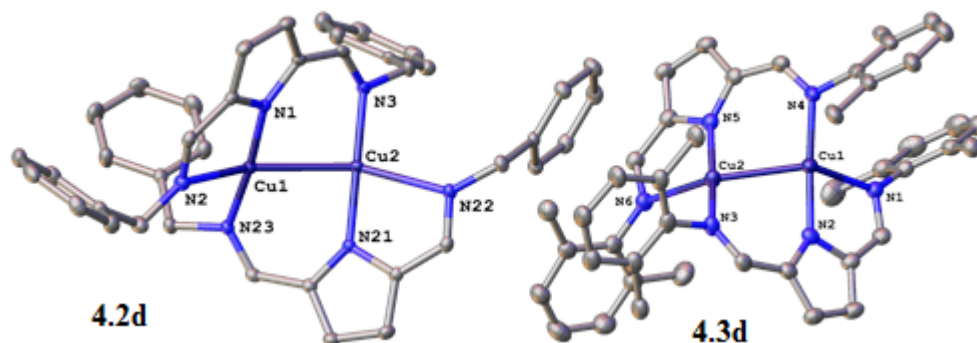
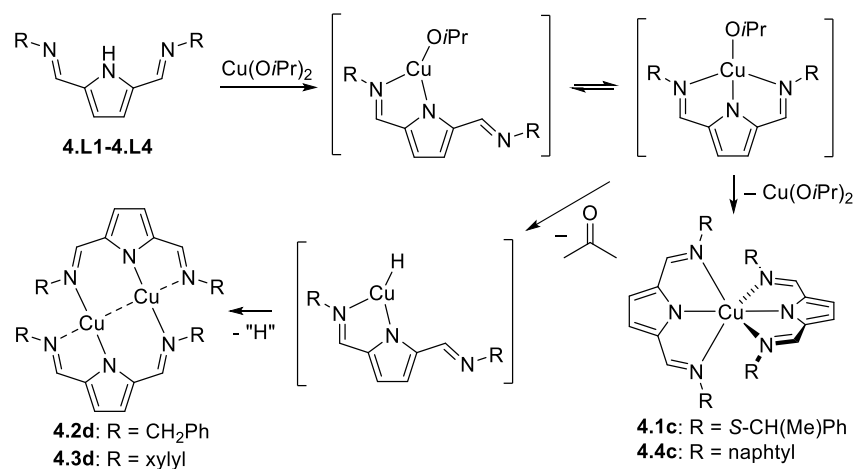


**Figure 4.2.** X-ray structures of **4.2d** and **4.3d**. Thermal ellipsoids are drawn at 50% probability. Hydrogen atoms, other independent molecules (**4.3d**) and minor components of disordered *N*-substituents (**4.3d**) were omitted for clarity.

The combination of these results allowed us to trace the probable reaction pathway for reactions with copper isopropoxide (Scheme 4.5). Protonation of one isopropoxide group likely yields the desired heteroleptic complex LCuOiPr. Although

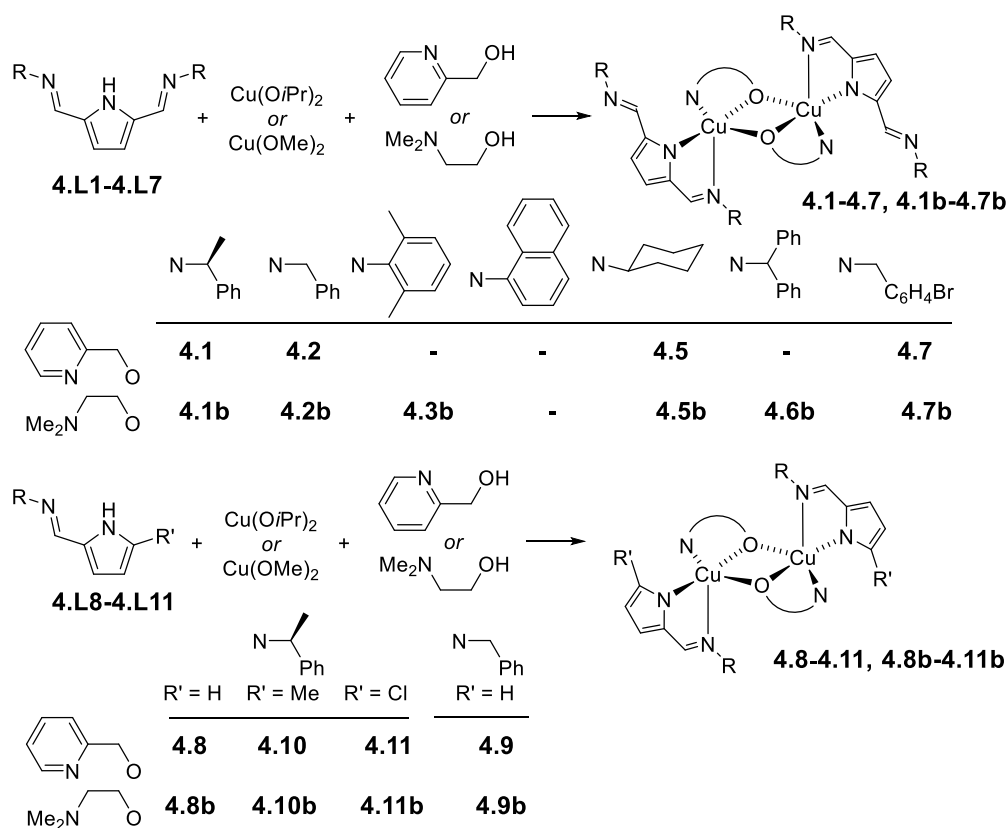
three-coordinate coordination is observed in **4.1c** and **4.4c**, it is either not present in  $\text{LCuOiPr}$  or in thermally accessible equilibrium with the  $\kappa^2$ -coordination mode. Similar to the observed reactivity of diketiminate complexes,  $(\kappa^2\text{-L})\text{CuOiPr}$  allows either reaction to the homoleptic complex (most likely by ligand exchange) or succumbs to  $\beta$ -H elimination of the isopropoxide ligand. The copper(II) hydrides thus formed are not stable and undergo homolytic bond cleavage to the respective Cu(I) complexes.



### Scheme 4.5.

#### Reactions with chelating alcohols.

Since tridentate coordination of diiminopyrrolide was too weak to stabilize the desired heteroleptic copper complexes, alcohols carrying a functional group able to coordinate to copper were employed. Methyl lactate shows the strongest resemblance to the growing polymer chain, but none of numerous attempts to prepare a  $\text{LCu(methyl lactate)}$  complex were successful. This is somewhat surprising, given the strong similarity of polymeryloxy and methyl lactate ligands and the stability of the complexes in this study under polymerization conditions (*vide infra*). Likewise unsuccessful were attempts to prepare  $\text{LCuOR}$  with ROH being 2-iminophenol or dipyridylmethanol. Reactions with  $\text{Cu(OMe)}_2$  or  $\text{Cu(OiPr)}_2$  in the presence of pyridylmethanol, on the other hand, yielded the desired diiminopyrrolide complexes **4.1**, **4.2**, **4.5** and **4.7**, and the monoiminopyrrolide complexes **4.8-4.11** (Scheme 4.6).



### Scheme 4.6.

All complexes were characterized by X-ray diffraction studies (Figure 3, synthesis and structures of **4.1**, **4.2**, and **4.8** were reported previously).<sup>6h, 7</sup> Although square-planar coordination is sterically possible, all complexes crystallize as oxygen-bridged, penta-coordinated dimers. While  $\tau$ -values<sup>20</sup> indicate a coordination geometry intermediate between square-pyramidal and trigonal-bipyramidal (Table 4.II), observed bond distances are in better agreement with square-pyramidal coordination: short bond lengths are observed for the two  $\mu$ -oxy ligands and for two of the nitrogen ligands (1.9 – 2.0 Å), while the remaining nitrogen ligand in the apical position shows elongated Cu-N distances of 2.2 – 2.4 Å (Table 4.II). Deviations of the  $\tau$ -value from 0 is thus likely caused by the small bite angle of the five-membered metallacycles, but the bonding situation around copper represents square-pyramidal geometry. The anionic ligands (pyrrolide and bridging oxygen atoms) occupy an equatorial position in all complexes. Bridging coordination of an alkoxide ligand is

thus preferred over the coordination of the iminogroup, which explains the motivation for the formation of penta-coordinated dimers instead of square-planar monomers.

A larger structural flexibility is observed in the general coordination geometry. As long as the general requirement of square-pyramidal coordination with anionic pyrrolide and alkoxy ligands in the equatorial plane is respected, several possible isomers were observed. Complexes **4.10** and **4.11** show the same geometry as **4.1**: inversion symmetry of the copper coordination environment with the imine group in apical position. Complex **4.9** shows the same inversion-symmetric coordination environment (which due to the absence of the chiral *N*-substituent now coincides with crystallographic inversion symmetry), but the pyridine ligand is occupying the axial position. In previously reported **4.2**,<sup>7</sup> the asymmetric unit contains two molecules, one showing the pyridine, the other the imine in apical position. In complex **4.5**, imine occupies the apical position, but the coordination geometry is now  $C_2$ -symmetric, with identical chirality of the copper centers and both pyridine groups on the same side of the  $Cu_2O_2$ -plane. This allowed for one, but not both of the diiminopyrrole ligands in **4.5** to adopt an *s-cis*, *s-cis* conformation and a weak (Cu-N = 3.4 Å) interaction of the second imino group with copper. Complex **4.7**, which only differs from **4.2** by the presence of a *para*-bromine on the *N*-benzyl substituent, shows an *s-cis*, *s-cis* conformation and tridentate coordination of both diiminopyrrole ligands. Although the Cu-N distance of the second imino group (2.9 Å) is barely below the sum of the vdW-radii, the coordination geometry around copper should now be considered octahedral. There are no obvious steric reasons for the observed variations in coordination geometry. Complex **4.7**, for example, is clearly stabilized by triple-decker  $\pi$ -stacking between the *N*-benzyl substituents and pyridylmethoxide (angle between planes: 7° and 16°, shortest atom-plane distance: 3.6 Å), but it is unclear why such stacking interactions should be more favorable for bromine-substituted **4.7** than for unsubstituted **4.2**.

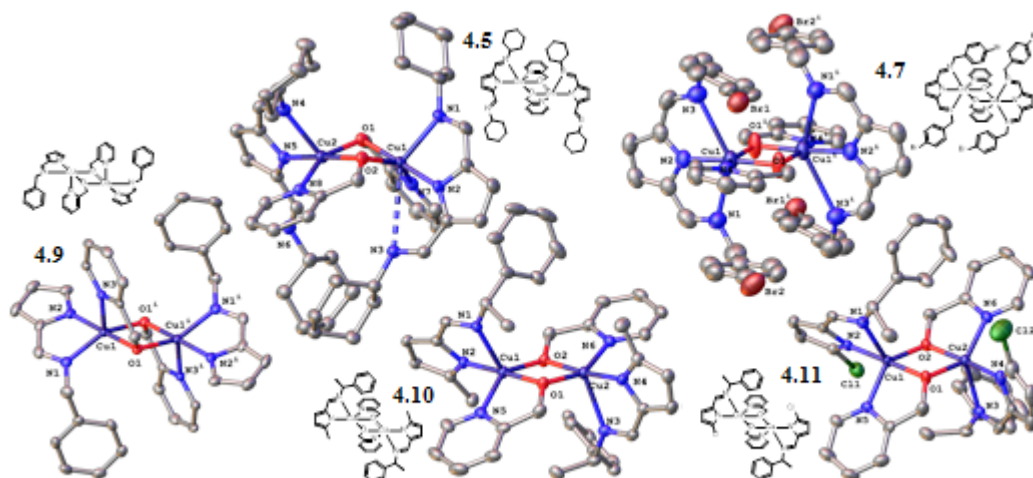


**Figure 4.3.** X-ray structures of **4.5**, **4.7**, and **4.9-4.11**. Thermal ellipsoids are drawn at the 50% probability level. Hydrogen atoms, toluene solvent (**4.11**) and a second independent molecule of similar geometry (**4.10** and **4.11**) omitted for clarity.

**Table 4.II.** Selected geometric data for pyridylmethoxide complexes **4.1**, **4.5**, and **4.7-4.11**<sup>a</sup>

	4.1 <sup>b</sup>	4.5	4.7	4.8 <sup>c</sup>	4.9	4.10	4.10	4.11	4.11
Cu-	1.945(2),	1.955(2),	1.936(9)	1.9309(13),	1.960(2)	1.923(4),	1.948(4),	1.953(4),	1.940(4),
N <sub>pyrrole</sub>	1.964(2)	1.978(2)		1.9347(13)		1.934(4)	1.934(4)	1.959(4)	1.950(4)
Cu-	2.294(3),	2.288(3),	2.484(11),	2.3170(15),	2.047(2)	2.274(4),	2.251(4),	2.286(4),	2.296(4),
N <sub>imine</sub>	2.242(3)	2.343(3)	2.862(11)	2.3976(13)		2.390(4)	2.248(4)	2.273(4)	2.415(4)
Cu-O <sub>short</sub>	1.915(2), 1.944(2)	1.941(2), 1.949(2)	1.908(7)	1.9271(11), 1.9306(11)	1.974(2)	1.915(3), 1.933(3)	1.922(3), 1.935(3)	1.926(3), 1.926(3)	1.922(3), 1.924(3)
Cu-O <sub>long</sub>	1.960(2), 1.960(2)	1.982(2), 1.966(2)	1.940(7)	1.9507(11), 1.9507(11)	1.986(2)	1.972(3), 1.936(3)	1.998(3), 2.000(3)	1.981(3), 1.992(3)	1.959(3), 1.937(3)
Cu-	2.025(3),	2.024(3),	2.011(8)	2.0222(13),	2.173(2)	2.028(4),	2.056(4),	2.040(4),	2.029(4),
N <sub>pyridine</sub>	1.995(3)	2.008(2)		2.0261(13)		1.989(4)	1.993(5)	2.028(4)	1.989(4)
Cu-Cu	3.025(5)	2.9199(6)	3.018(3)	3.0628(5), 3.0395(4)	2.992(1)	3.0267(10)	3.035(1)	3.019(1)	3.018(1)
τ	0.6, 0.4	0.6, 0.4		0.4, 0.4	0.6, 0.6	0.6, 0.4	0.7, 0.5	0.7, 0.5	0.6, 0.3
Chirality at Cu	C, A	C, C		C, A / C, A	A, C	C, A	C, A	C, A	C, A
Atom in apical position	Imine, Imine	Imine, Imine		Imine, Imine	Pyridine, Pyridine	Imine, Imine	Imine, Imine	Imine, Imine	Imine, Imine

<sup>a</sup> The second values cited refers to the second copper center of the dimer, if crystallographically inequivalent. Two columns are used for molecules having two independent molecules in the asymmetric unit. <sup>b</sup> taken from ref 6h for comparison. <sup>c</sup> taken from ref 7 for comparison.

Pyridylmethoxide complexes could not be prepared for sterically demanding ligands 4.L3, 4.L4 and 4.L6. In the case of 4.L6, a mixed dinuclear complex 4.LCu(μ-OCH<sub>2</sub>Py)<sub>2</sub>CuCl, **4.6e**, was obtained (Figure 4.4, Table 4.S3). The absence of a diiminopyrrole ligand on the other copper center allows a weak coordination of the second iminogroup to the copper center (Cu-N = 2.6 – 3.1 Å) and the ligand adopts the *s-cis*, *s-cis* conformation observed in **7**, instead of the *s-cis*, *s-trans*-conformation in the other 4.L<sub>2</sub>Cu(OR)<sub>2</sub> complexes, which orients the second imino group away from the metal. Tridentate coordination is further stabilized by weak hydrogen



bonding between the aromatic protons of the diphenylmethyl substituent with the heteroatoms in the equatorial plane. However, similar weak hydrogen bonds were observed also in the  $4.L_2Cu(OR)_2$  complexes above. Unsurprisingly, coordination of the second imino group leads to further elongation of the Cu-N<sub>imino</sub> distance, but the effects seems to be subtle: The structure of **4.6e** contains three independent molecules. One shows different Cu-N<sub>imino</sub> distances of 2.6 and 3.1 Å and is best described as square-pyramidal with an additional weak interaction. On the other extreme, one of the molecules shows equal Cu-N<sub>imino</sub> distances of 2.7 and 2.8 Å and should be considered a Jahn-Teller-distorted octahedral coordination. The presence of such a wide range of distances in the same asymmetric unit indicates that interactions of Cu with the ligands in the apical positions are very weak. The copper center containing the chloride ligand shows square-planar coordination geometry and is unaffected by the observed variation in the coordination mode of diiminopyrrolide.

A complex similar to **4.6e**, **4.1e**, has been obtained in early synthetic attempts from reactions of chloride-contaminated Cu(O*i*Pr)<sub>2</sub>. The structure of **4.1e** is similar to that **4.6e**. Again, the all *s-cis* conformation of the ligand allows a weak (Cu-N = 3.1 Å) coordination of the second imino group (Fig. 4.4, Table 4.S3). In the case of **4.6e**, the Cu(OMe)<sub>2</sub> starting material was analytically pure and chloride impurities cannot explain the obtained crystallized yield of 29%. Most likely, the inability to form the stabilized dimer **4.6** resulted in (partial) decomposition to a Cu(I) complex, similar to reactions in the absence of pyridylmethanol. Upon recrystallisation of the oily reaction mixture in dichloromethane, copper(I) species were re-oxidized by abstraction of a chlorine from the solvent and **4.6e** was formed by reaction with pyridylmethanol (or copperbispyridylmethoxide) present in the reaction mixture. (Scheme 4.7). Complexes **4.1e** and **4.6e** did not initiate lactide polymerization at room temperature (no conversion even after 48 h) and will not be discussed further.

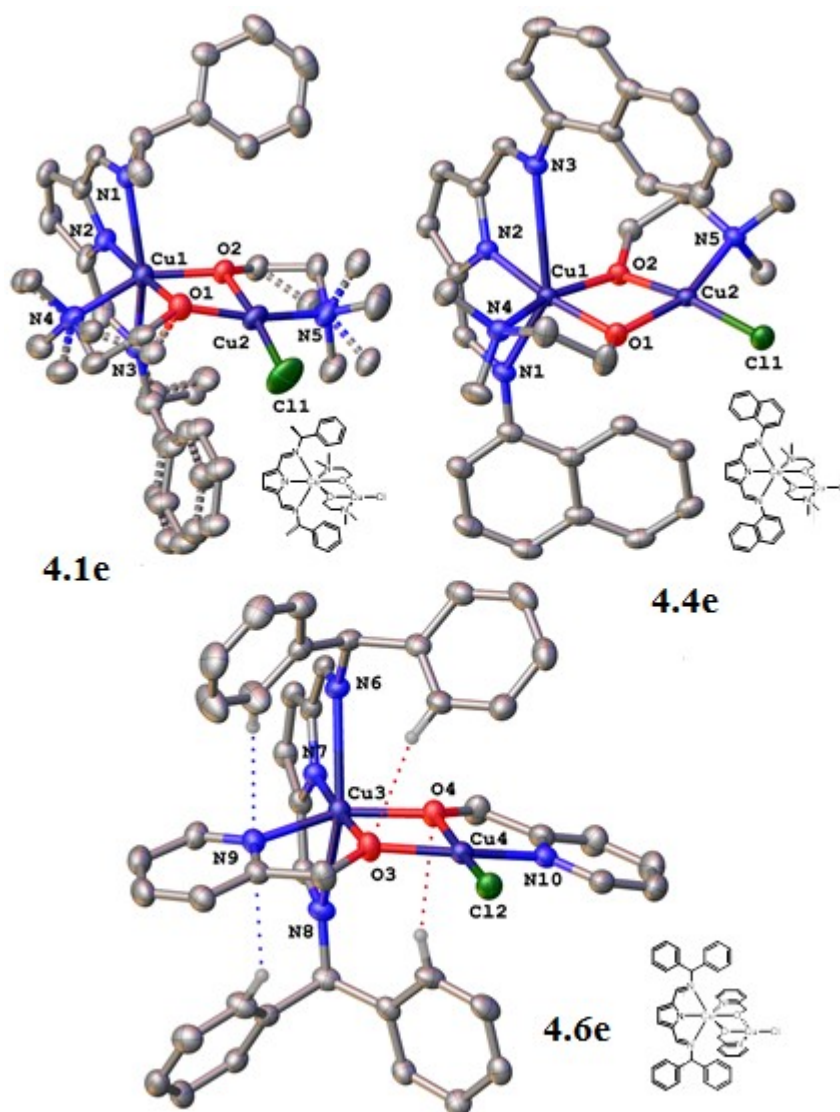
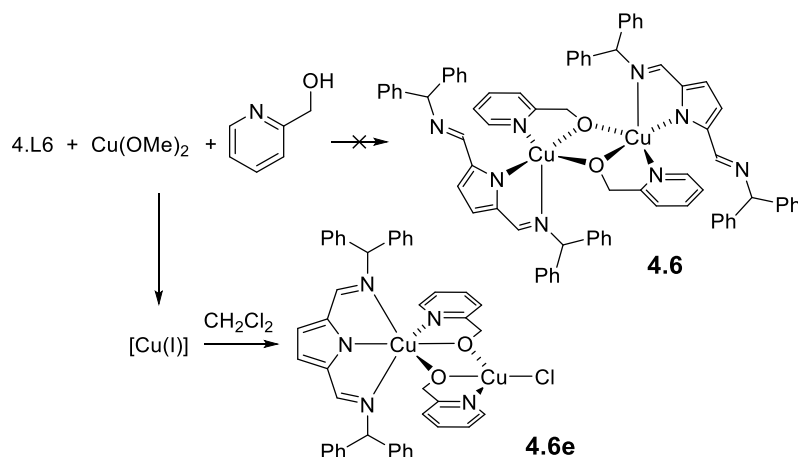


**Figure 4.4.** Crystal structure of **4.1e**, **4.4e** and **4.6e**. Hydrogen atoms and two of the three independent molecules in **6e** were omitted for clarity. Thermal ellipsoids were drawn at the 50% probability level.



**Scheme 4.7.**

Similar reactivity as for pyridylmethanol was observed for reactions of  $\text{Cu}(\text{OMe})_2$  with 4.L1-4.L11 in the presence of dimethylaminoethanol (Scheme 4.6). The latter seems to be sterically less demanding and dinuclear  $4.L_2\text{Cu}_2(\mu\text{-OC}_2\text{H}_4\text{NMe}_2)_2$  complexes **4.1b** – **4.11b** were obtained for all ligands but 4.L4. In the latter case, the respective mixed complex  $(4.L4)\text{Cu}(\mu\text{-OR})_2\text{CuCl}$ , **4.4e**, was obtained instead after recrystallisation from dichloromethane, the crystal structure of which is similar to that of **4.1e** and **4.6e** (Fig. 4.4, Table 4.S3). Analogous to **4.6e** (Scheme 4.7), we suspect that inability to form dimeric **4.4b** led to partial decomposition of  $(4.L4)\text{Cu}(\text{OC}_2\text{H}_4\text{NMe}_2)$ .

Since aminoethoxide complexes showed to be more easily accessible we attempted to prepare **4.3** and **4.6** by reaction of **4.3b** and **4.6b** with pyridylmethanol. However, none of these attempts (nor attempts to obtain **4.1** from **4.1b**) were successful. It seems thus not possible to replace the chelating alkoxide ligand once the dinuclear complex is formed.

Complexes **4.1b**–**4.3b** and **4.5b**–**4.11b** yield very similar dinuclear structures (Fig. 4.5, Table 4.III, synthesis and structures of **4.1b** and **4.2b** have been reported previously).<sup>6h, 7</sup> Compared to the respective pyridylmethoxide complexes, the amino group has a slightly higher tendency to coordinate to the apical position, e.g. **4.2** (pyridyl or imine in the apical position) vs. **4.2b** (amine), **4.5** (imine) vs. **4.5b** (amine). The weaker coordination of the amino group to copper compared to pyridyl

indicated by the X-ray structures is in line with lactide reactivity (vide infra), in which pyridylmethoxide complexes in general show longer induction periods. Bond distances of the equatorial ligands, Cu-N<sub>pyrrole</sub> and Cu-O, in **4.1b–4.11b** differ by less than 5 pm from those of the respective pyridylmethanol complexes **4.1–4.11** (Table 4.III). Variation of the pyrrole substituent in **4.8**, **4.10** and **4.11** or **4.8b**, **4.10b** and **4.11b** between H, Me, and Cl likewise does not seem to have an impact on structural features: bond distances to Cu differ by less than 3 pm for Cu-N<sub>pyrrole</sub> and Cu-O and there is no evident correlation with electronic or steric factors. The nature of the imino substituent also shows little impact on Cu-X bond lengths: Cu-N<sub>pyrrole</sub> (1.92 – 1.98 Å), C-O<sub>short</sub> (1.90 – 1.97 Å) and Cu-O<sub>long</sub> (1.94 – 2.01 Å) differ by only 6 – 7 pm for all dinuclear complexes regardless of the nature of the imino substituent or the complex geometry, and again without evident correlation to steric or electronic factors. Changing the nature of the bridge, variation of the imino-N-substituent or even complete replacement of the imino group by methyl or chloride thus does not have any significant effect on equatorial Cu-X bond distances.

The only exception is again **4.L7**, where the seemingly minor variation of bromination in the *para*-benzyl position led to a notably different structure. Complex **4.7b** has a  $\tau$ -value of 0.8. More importantly, the imine and the amine ligand in **4.7b** are found with essentially identical Cu-N bond distances of 2.162(7) and 2.130(7) Å, while 0.2 – 0.4 Å differences are observed for the other aminoethoxide complexes. The coordination geometry in **4.7b** is thus trigonal-bipyramidal instead of the square-pyramidal geometry observed in all other cases.

Given the wide variety of coordination geometries, the lack of obvious correlation with steric or electronic factors and essentially invariant Cu-X bond distances, the different coordination isomers are probably very close in energy, so that even small effects can lead to the observed geometries. In solution, the coordination geometry likely adapts easily to even small changes in the complex environment.

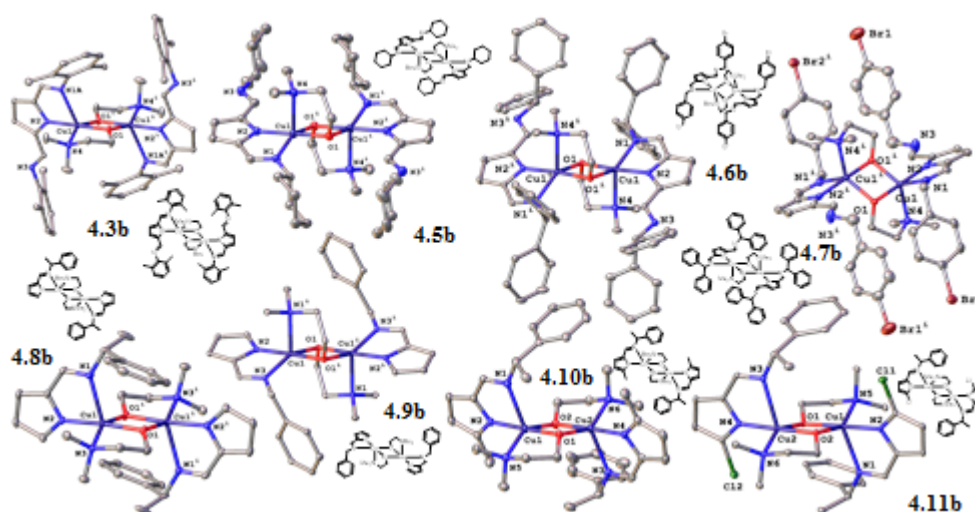


**Figure 4.5.** X-ray structures of **4.3b** and **4.5b – 4.11b**. Thermal ellipsoids are drawn at the 50% probability level. Hydrogen atoms and disorder of the *N*-substituent (**4.3b**, **4.8b**) omitted for clarity.

**Table 4.III.** Selected geometric data for dimethylaminoethoxide complexes **4.3b** and **4.5b-4.11b**<sup>a</sup>

	<b>4.1b</b> <sup>b</sup>	<b>4.3b</b>	<b>4.5b</b>	<b>4.6b</b>	<b>4.7b</b>
Cu-N <sub>pyrrole</sub>	1.924(12), 1.924(12)	1.9617(12)	1.9609(15)	1.9621(15)	1.954(7)
Cu-N <sub>imine</sub>	2.327(11), 2.244(10)	2.535(8)	2.0184(14)	2.0697(15)	2.163(7)
Cu-O <sub>short</sub>	1.896(9), 1.896(8)	1.9295(11)	1.9607(12)	1.9510(12)	1.934(6)
Cu-O <sub>long</sub>	1.965(8), 1.993(9)	1.9542(11)	1.9817(12)	2.0138(13)	1.995(6)
Cu-N <sub>amine</sub>	2.048(12), 2.056(14)	2.0785(13)	2.3100(17)	2.2409(16)	2.124(7)
Cu-Cu	3.014(2)	3.0770(8)	2.9753(5)	2.9824(5)	2.952(2)
$\tau$	0.5, 0.5	0.4, 0.4	0.4, 0.4	0.5, 0.5	0.8, 0.8
Chirality at Cu	A, C	C, A	C, A	A, C	A, C
Atom in apical position	Imine, Imine	Imine, Imine	Amine, Amine	Amine, Amine	tbp geometry

Table 4.III. to be continued

	<b>4.8b</b>	<b>4.9b</b>	<b>4.10b</b>	<b>4.11b</b>
Cu-N <sub>pyrrole</sub>	1.9507(12)	1.9639(9)	1.964(4), 1.961(4)	1.969(3), 1.944(3)
Cu-N <sub>imine</sub>	2.3361(13)	2.0444(8)	2.382(4), 2.343(4)	2.339(3), 2.458(3)
Cu-O <sub>short</sub>	1.9206(11)	1.9615(7)	1.930(3), 1.943(3)	1.923(3), 1.922(3)
Cu-O <sub>long</sub>	1.9628(11)	1.9847(7)	1.954(3), 1.975(3)	1.956(3), 1.958(3)
Cu-N <sub>amine</sub>	2.0731(14)	2.2628(9)	2.094(4), 2.082(4)	2.062(3), 2.088(3)
Cu-Cu	3.0325(4)	2.9579(3)	3.0219(8)	3.0026(7)
$\tau$	0.3, 0.3	0.4, 0.4	0.6, 0.5	0.4, 0.5
Chirality at Cu	C, A	C, A	C, A	A, C
Atom in apical position	Imine, Imine	Amine, Amine	Imine, Imine	Imine, Imine

<sup>a</sup> The second values cited refers to the second copper center of the dimer, if crystallographically inequivalent. Two columns are used for molecules having two independent molecules in the asymmetric unit. b taken from ref 6h for comparison.

### ***rac*-Lactide polymerization – activity.**

Complexes **4.5**, **4.7-4.11** and **4.3b – 4.11b** were tested for activity in *rac*-lactide polymerization and compared to previously studied **4.1/4.1b** and **4.2/4.2b** to determine the influence of the ligand substitution pattern on reactivity and selectivity. All complexes tested were active for the polymerization of lactide at room temperature in benzene solution with catalyst concentrations of 1 – 3 mM. Polymerizations reached completion for all complexes but **4.6b**, **4.11** and **4.11b** (Table 4.S4), although polymerization kinetics indicated some catalyst decomposition for **4.5b** (Fig. 4.S13, 4.S14). General catalyst stability under polymerization conditions was tested for **4.8/4.8b** and **4.9/4.9b** (Fig. 4.6). All four complexes retained sufficient activity to enable complete monomer conversion even after 3 – 4 days, i. e. 50 – 150 half-lives of the reaction. Similar stability at prolonged reaction

times had been observed for **4.1**.<sup>7</sup> GPC analysis of these multi-addition experiments showed significantly reduced polymer molecular weights compared to theory and broadened polydispersities (Table 4.S4, entries 4, 7, 16, 33, and 44).  $P_m$ -values show a steady increase in these long-term reactions, likewise an indication for transesterification side-reactions ( $rr$ -triads formed in transesterification overlap with  $mmm$ , thus artificially leading to an increased  $P_m$  value).<sup>21</sup> For copper pyrrolide complexes, transesterification side-reactions thus become noticeable at these long reaction times, while the related copper diketimate complexes did not show evidence for transesterification even over >1000 half-lives.<sup>6k</sup>

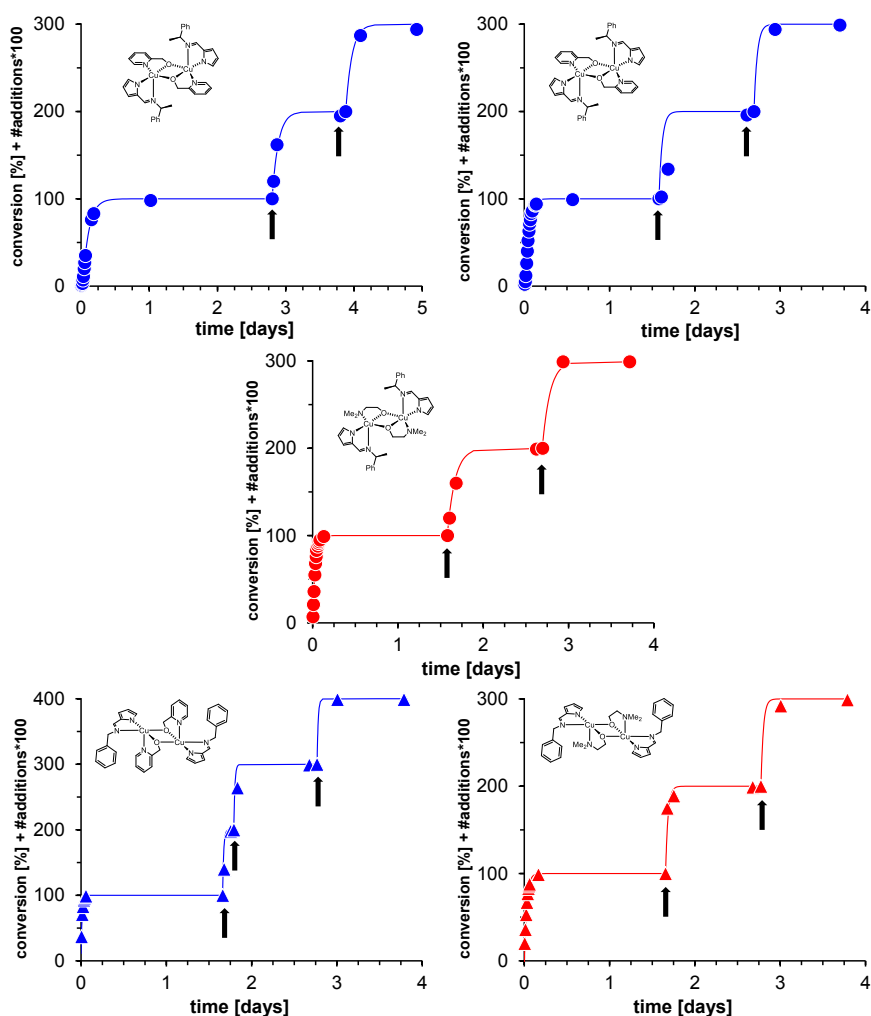


**Figure 4.6.** Conversion/time plots for addition of several batches of monomer over several days. Black arrows indicate time of monomer addition. Top left, blue circles:



**4.8**, [**4.8**] = 1 mM in C<sub>6</sub>D<sub>6</sub>, addition of 200, 200 and 25 equiv of *rac*-lactide. Top right, blue circles: **4.8**, 3 mM, 300, 200, 100 equiv. Middle, red circles: **4.8b**, 3 mM, 300, 200, 100 equiv. Bottom left, blue triangles: **4.9**, 3 mM, 300, 100, 100, 200 equiv. Bottom right, blue triangles: **4.9b**, 3 mM, 300, 100, 200 equiv. Solid lines are based on pseudo-first-order rate constants determined in the first addition.

Table 4.IV compares the activity of complexes **4.1-4.11** and **4.1b-4.11b**. More detailed kinetic analyses and a complete listing of polymerization results is available in the supporting information (Table 4.S4, Fig. 4.S1-4.S17). Mechanistic investigations on the polymerization of *rac*-lactide with **4.1/4.1b** and **4.2/4.2b** have shown that complexes remain dinuclear during polymerization (Scheme 4.2).<sup>7</sup> Complexes **4.1** and **4.2** retain one pyridylmethoxide as a spectator ligand in the active species, while both alkoxides initiate in **4.1b** and **4.2b**. Although both complexes thus form different active species with potentially different kinetics, the impact of the bridging alkoxide on polymerization activity is very subtle. Pseudo-first order rate constants for **4.1/4.1b**, **4.2/4.2b**, **4.5/4.5b** and **4.8-4.11/4.8b-4.11b** differ by a factor of two at the maximum and are identical within the margin of error in half of the cases. From the pairs with notable differences (**4.1** < **4.1b**, **4.5** > **4.5b**, and **4.10** < **4.10b**), there is no conclusion whether pyridylmethoxide or dimethylaminoethoxide provides the more active catalyst.

**Table 4.IV.** Apparent first-order rate constants for *rac*-lactide polymerization with complexes **4.1-4.11** and **4.1b-4.11b**.

N-R / N-R, R'	OR = OCH <sub>2</sub> Py		OR = OC <sub>2</sub> H <sub>4</sub> NMe <sub>2</sub>	
		<i>k</i> <sub>obs</sub> (h <sup>-1</sup> )		<i>k</i> <sub>obs</sub> (h <sup>-1</sup> )
NCH(Me)Ph <sup>a</sup>	<b>4.1</b>	0.6 ± 0.1	<b>4.1b</b>	1.4 ± 0.2
NCH <sub>2</sub> Ph <sup>a</sup>	<b>4.2</b>	0.7 ± 0.1	<b>4.2b</b>	0.6 ± 0.1
N-xylyl			<b>4.3b</b>	0.05 <sup>b</sup>
N- <i>cyc</i> -C <sub>6</sub> H <sub>11</sub>	<b>4.5</b>	1.8 ± 0.2	<b>4.5b</b>	0.8 <sup>b</sup>
N-CHPh <sub>2</sub>			<b>4.6b</b>	0.07 <sup>b</sup>
NCH <sub>2</sub> C <sub>6</sub> H <sub>4</sub> Br	<b>4.7</b>	1.0 <sup>b</sup>		
NCH(Me)Ph, H <sup>a</sup>	<b>4.8</b>	1.2 ± 0.3	<b>4.8b</b>	1.4 ± 0.1
NCH <sub>2</sub> Ph, H	<b>4.9</b>	1.1 <sup>b</sup>	<b>4.9b</b>	0.8 <sup>b</sup>
NCH(Me)Ph, Me	<b>4.10</b>	0.4 ± 0.3	<b>4.10b</b>	0.9 ± 0.1
NCH(Me)Ph, H	<b>4.11</b>	0.004 <sup>b</sup>	<b>4.11b</b>	0.003 <sup>b</sup>

Conditions: [catalyst] = 2 mM, C<sub>6</sub>D<sub>6</sub>, ambient temperature, lactide:catalyst = 100:1 – 300:1. The provided error is the biggest deviation from the average in multiple experiments. <sup>a</sup> Data for **4.1**, **4.1b**, **4.2**, **4.2b** and **4.8** from ref. <sup>7</sup>. <sup>b</sup> Single experiment.

With regard to the steric bulk of the imino substituent, complexes with secondary alkyl imines (**4.1**, **4.1b**, **4.5**, **4.5b**, **4.8** or **4.8b**) react as fast as or even faster than those with benzyl imines (**4.2**, **4.2b**, **4.7**, **4.9** or **4.9b**). The highest activity is observed for cyclohexyl-substituted **4.5**, which makes us suspect that  $\pi$ -stacking of benzyl or methylbenzyl substituents with pyridylmethoxide (Fig. 4.3) might be detrimental to activity. However, complex **7**, for which  $\pi$ -stacking was most evident in its crystal structure, does not show any reduced activity.  $\pi$ -Stacking interactions are thus unlikely to be a structural element important to activity. Larger differences are

observed for complexes **4.3b** and **4.6b**, carrying sterically very demanding ligands, whose activities are about one order of magnitude lower than **4.1/4.1b**.

Monoiminopyrrolide complexes **4.8/4.8b** and **4.9/4.9b**, lacking the second, dangling iminosubstituent, show slightly higher activities than the respective diiminopyrrolide complexes **4.1/4.1b** and **4.2/4.2b**. The respective 5-methyl substituted monoiminopyrrolide complexes **4.10/4.10b**, on the other hand, show slightly lower activities. Relative activities of **4.8** > **4.1** > **4.10** and **4.8b** > **4.1b** > **4.10b** correlate with the steric, but not the electronic nature of the pyrrole substituent.<sup>22</sup> Chloride-substituted monoiminopyrrolide complexes **4.11/4.11b** were investigated to gain closer insight into potential electronic effects, but they proved to be barely active and reactions did not reach completion even after several days. Such a large impact on reactivity is unlikely considering the minor variations between **4.1/4.1b**, **4.8/4.8b** and **4.10/4.10b** and the low activities are probably due to complex decomposition rather than due to an electronic influence of the chloride substituent. In agreement with this, complex **4.11** did not show any stereocontrol, while a preference for isotactic enchainment was observed in **4.8-4.10** (Table 4.V, 4.S4).

In summary, the activity of iminopyrrolide complexes seems insensitive towards most changes of the substitution pattern of the pyrrole ring, substitution of the imino position, removal of the pending imino substituent or the nature of the bridging alkoxide. Apparent first-order rate constants of pyridylmethoxide complexes **4.1**, **4.2**, **4.5** and **4.7-4.10** ranged from 0.4 h<sup>-1</sup> to 1.2 h<sup>-1</sup>, those of the respective complexes **4.1b**, **4.2b**, **4.5b** and **4.8b-4.10b** from 0.6 h<sup>-1</sup> to 1.4 h<sup>-1</sup> (Table 4.IV). Only large *N*-substituents in 4.L3 and 4.L6 showed a more notable impact on activities, indicative of increased steric crowding of the metal center.

### **Polymer molecular weight control.**

Polymer molecular weights in **4.1/4.1b** and **4.2/4.2b** were indicative of the polymerization mechanism and stereocontrol: Generation of one chain per catalyst dimer in **4.1** and **4.2** indicated continued presence of a pyridylmethoxide in the active species, which was essential for isotactic stereocontrol. Initiation of both alkoxide

groups in **4.1b** and **4.2b** led to active species containing a less rigid polymeryl alkoxy bridge and loss of stereocontrol (Scheme 4.2). The same correlation is complicated in **4.5/4.5b** and **4.8-4.11/4.8b-4.11b** by depression of polymer molecular weight by transesterification reactions. For example, in immortal polymerizations with **4.8/4.8b**, complex **4.8** consistently provides higher polymer molecular weights than **4.8b**, in agreement with one pyridylmethoxide ligand in **4.8** not initiating polymerization. Polymer molecular weights for both catalysts are, however, depressed from their theoretical values (Fig. 4.7, Table 4.S4, entries 6, 8-12, 32 and 34-38). Complex **4.8** provides 1.1 – 1.5 chains per catalyst dimer, while 2.9 – 7.5 chains per dimer are observed for **4.8b**, accompanied by slightly increased polydispersities. MALDI spectra of **4.8** show the presence of peaks with  $m/z = n \cdot 72 + M(\text{Na}^+)$ , in agreement with intramolecular transesterification reactions (Fig. 4.S18). Monoiminopyrrolide complexes **4.8/4.8b** seem thus more prone to transesterification than their respective diiminopyrrolide analogues **4.1/4.1b**. Unsurprisingly, transesterification side reactions thus increase when the steric demand is reduced.

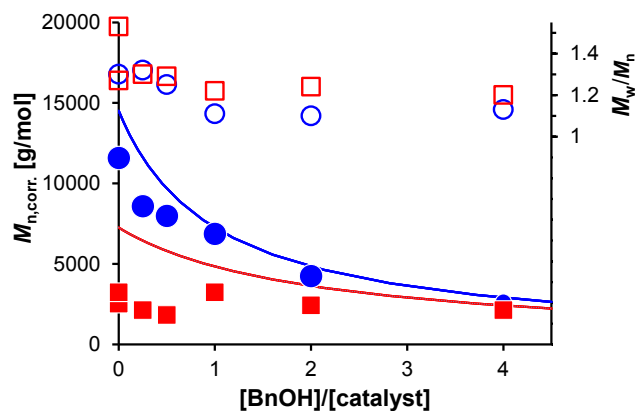


**Figure 4.7.** Polymer molecular weights in *rac*-lactide polymerizations with **4.8** (blue circles) and **4.8b** (red squares) in the presence of benzyl alcohol. Polymer molecular weights were corrected for yield ( $M_{n,corr.} = M_n / \text{yield}$ ) to allow comparison with the theoretical values. Blue solid line: polymer molecular weight expected for one alkoxide per catalyst dimer initiating. Red dashed line: for both alkoxides initiating. Hollow circles and squares show the respective polydispersities (right axis).

While transesterification leads to a calculated number of polymer chains per catalyst dimer higher than the theoretical value, pyridylmethoxide complexes consistently provide higher molecular weight than the respective aminoethoxide complexes (Table 4.V). They also consistently show an isotactic bias, while aminoethoxide complexes do not. The same correlation of only one initiating alkoxide and isotactic stereocontrol in pyridylmethoxide complexes and two initiating alkoxides without stereocontrol in aminoethoxide complexes is thus likewise observed for **4.5-4.10** and **4.5b-4.10b**, and they follow the same stereocontrol mechanism as **4.1/4.1b** and **4.2/4.2b**.

Chloride-substituted **4.11** displays in addition of drastically reduced activity (3 orders of magnitude) and lack of stereocontrol, also a large number of chains produced per catalyst dimer (Table 4.V), reinforcing the interpretation that the active species in this catalyst differs from those in **4.1-4.10**, i. e. catalyst decomposition.

**Table 4.V.** Selected results for *rac*-lactide polymerization with **4.5-4.11** and **4.3b-4.11b**<sup>a</sup>

	<b>Convers., time</b> <sup>b</sup>	<b><math>k_{\text{obs}}</math> [h<sup>-1</sup>]</b>	<b><math>P_m</math></b> <sup>c</sup>	<b><math>M_n</math> [kDa]</b> <sup>d</sup>	<b><math>M_w/M_n</math></b>	<b><math>n_{\text{PLA}}/n_{\text{cat}}</math></b> <sup>e</sup>
<b>4.1</b> <sup>f</sup>	99%, 24 h	0.6 ± 0.1	0.72	13	1.3	1.1
<b>4.1b</b> <sup>f</sup>	99%, 24 h	1.4 ± 0.2	0.49	5	1.2	2.5
<b>4.2</b> <sup>f</sup>	99%, 28 h	0.65±0.1	0.67	7 - 28	1.4	0.5-2
<b>4.2b</b> <sup>f</sup>	72-89%, 28 h	0.6 ± 0.1	0.47	4 - 7	1.2	1.6-3.3
<b>4.3b</b>	95%, 75 h	0.046(1)	0.33	8.6	1.4	1.6
<b>4.5</b>	99%, 23 h	1.75(2)	0.71	17.3	1.5	0.8
<b>4.5b</b>	88%, 28 h	0.82(6)	0.46	5.6	1.2	2.3
<b>4.6b</b>	81%, 23 h	0.074(2)	0.43	6.5	1.2	1.8
<b>4.7</b>	96%, 6 h	1.02(2)	0.53	6.1	1.7	2.3
<b>4.8</b>	99%, 10 h	1.29(1)	0.64	16.9	2.2	0.8
<b>4.8b</b>	99%, 34 h	1.41(1)	0.46	3.2	1.3	4.5
<b>4.9</b>	99%, 32 h	1.06(4)	0.59	7.0	2	2.1
<b>4.9b</b>	99%, 32 h	0.80(2)	0.46	3.9	1.3	3.7
<b>4.10</b>	99%, 27 h	0.52(3)	0.59	12.5	1.5	1.1
<b>4.10b</b>	97%, 5 h	1.00(3)	0.44	7.1	1.3	2
<b>4.11</b>	76%, 16 d	0.0021(2)	0.44	1.6	1.2	6.9
<b>4.11b</b>	64%, 16 d	0.0027(3)	0.43	3.5	1.4	2.7

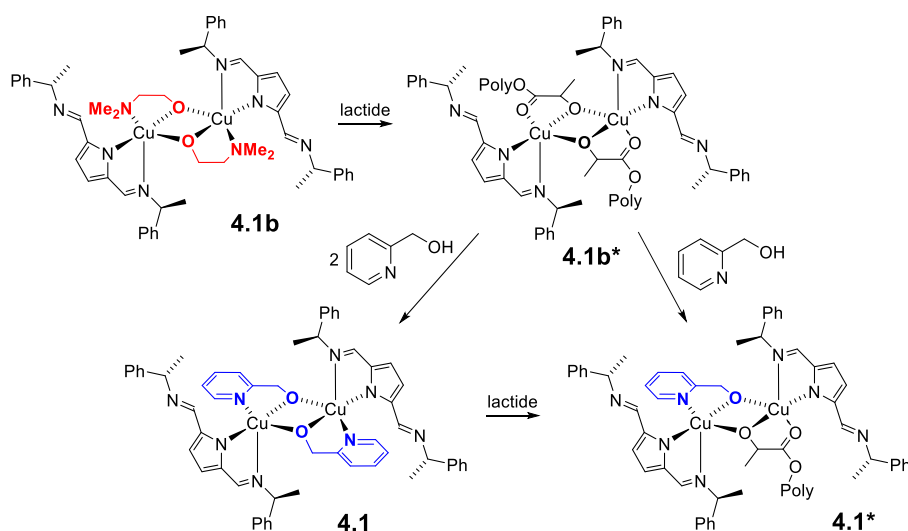
<sup>a</sup> [cat.] = 2 mM, lactide:catalyst = 100:1, C<sub>6</sub>D<sub>6</sub>, ambient temperature. For a full list of polymerization results see Table 4.S4. <sup>b</sup> Time at which the reaction was quenched. This time is not indicative of activity (see  $k_{\text{obs}}$  and Table 4.IV). <sup>c</sup> Determined from decoupled <sup>1</sup>H NMR spectra (see Exp. Section). <sup>d</sup> Determined by GPC (see Exp. Section). <sup>e</sup> number of polymer chains per catalyst dimer calculated from  $n_{\text{PLA}}/n_{\text{cat}} = ([\text{lactide}]/[\text{cat.}] \cdot M_{\text{lact.}} \cdot \text{conversion} + M_{\text{ROH}})/M_n$ . <sup>f</sup> Data from ref. <sup>7</sup>. Data are averages of several experiments.  $P_m$ -values obtained this way were typically consistent to ±1% over the course of one experiment and ±3% between different experiments under identical conditions.

### Stereocontrol.

Increasing the steric demand of a spectator ligand is a textbook tool in catalyst optimization, since it typically leads to tightening of the catalytic pocket, stronger differentiation of transition states and thus increased selectivities. Unfortunately, the isoselective pyridylmethoxide complexes were synthetically not accessible for sterically very demanding ligands 4.L3, 4.L4 and 4.L6. The high activities of cyclohexyl-substituted **4.5** (Table 4.IV) already indicated that its steric demand is not notably higher than in **4.1** or **4.2**, and consequently **4.5** provided the same isotactic stereocontrol (Table 4.V).

Aminoethoxide complexes **4.3b-4.10b** did not provide isotactic PLA in agreement with the polymerization mechanism proposed for **4.1/4.1b** (Table 4.V, Scheme 4.2). The sterically crowded complex **4.3b** afforded a heterotactic bias of  $P_m = 0.33$ , while all other complexes were essentially atactic. This indicates that bulky *N*-substituents can indeed increase the steric pressure in the transition state sufficiently to increase selectivity. Pyridylmethoxide complexes with ligands 4.L3 and 4.L6 could not be prepared from the respective aminoethoxide complexes (*vide supra*), but the polymerylalkoxide ligand in the active species should be less stabilized than aminoethoxide. We thus investigated whether a pyridylmethoxide spectator ligand could be introduced *in situ* by protonation of the active bis(polymerylalkoxide) species (Scheme 4.8). Polymerizations with **4.1b** in the presence of pyridylmethanol showed indeed the induction period normally associated with polymerizations with **4.1** and provided isotactically enriched PLA, indicative of incorporation of a pyridylmethoxide ligand into the active species. Reaction with pyridylmethanol might either involve direct formation of **4.1\***, the active species of **4.1**, by reaction with one equivalent of pyridylmethanol, or formation of **4.1** by reaction with two equivalents of alcohol (Scheme 4.8). In the former case, polymerizations of **4.1b**/PyCH<sub>2</sub>OH (1:1) are indistinguishable from polymerizations with **4.1**, in the latter case we obtain polymerization from a 1:1 mixture of **4.1** and **4.1b** and a polymer of intermediate characteristics.<sup>23</sup> Obtained  $P_m$  values and polymer molecular weights in polymerizations of *rac*-lactide with **4.1b** in the presence of varying amounts of

pyridylmethanol indicate that reactions of **4.1b**\* with pyridylmethanol provide **4.1** rather than **4.1**\* (Fig. 4.8). This agrees with the observed induction periods in **4.1b**/PyCH<sub>2</sub>OH systems, which should be absent if **4.1**\* is formed directly. Reactions are not well controlled and the full isotacticity observed for **4.1** could not be restored even by addition of more than two equivalents of pyridylmethanol to **4.1b**.



**Scheme 4.8.**

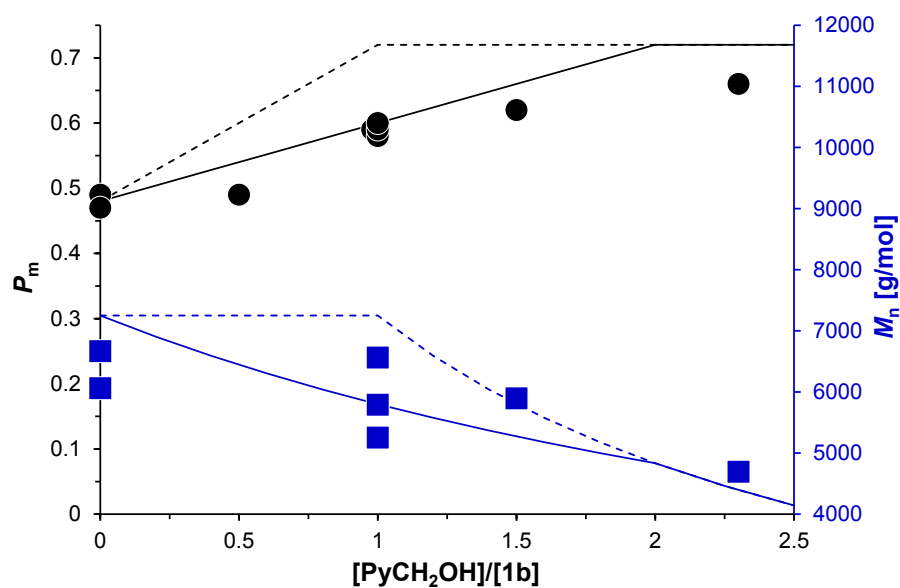


**Figure 4.8.** Isotacticities ( $P_m$ , left axis, black circles) and polymer molecular weights ( $M_n$ , right axis, blue squares) obtained for polymerizations of *rac*-lactide with **4.1b** in the presence of varying amounts of pyridylmethanol. The solid lines represent values



expected if reaction of **4.1b** or **4.1b\*** with pyridylmethanol first forms **4.1**, to then initiate polymerization to form the active species **4.1\***. The dashed lines show the values expected if reaction with pyridylmethanol directly forms the active species **4.1\*** without passing via **4.1**.

Table 4.VI compares isotacticities of aminoethoxide complexes obtained in the presence of additional pyridylmethanol. For **4.1b**, **4.2b** and **4.5b** isotacticities obtained in polymerizations in the presence of 1 equiv of pyridylmethanol correspond well with the isotacticities expected from a 1:1 mixture of the respective aminoethoxide and pyridylmethoxide complexes. Addition of pyridylmethanol to **4.3b** or **4.6b**, however, did not provide polymer with an isotactic bias. In the case of **4.3b**, the polymer became notably more atactic, but polymerizations with **4.3b/PyCH<sub>2</sub>OH** required 3 days to reach >80% conversion and other reasons, such as transesterification, might be responsible for the reduced stereocontrol. From the available data there is thus no evidence for the formation of pyridylmethoxide complexes with ligands 4.L3 or 4.L6 even by *in situ* reaction of the bisalkoxide species with pyridylmethanol.

**Table 4.VI.** Stereocontrol by *in-situ* formation of pyridylmethoxide species.

Catalyst	PyCH <sub>2</sub> OH added		$P_m$ (4.X/4.Xb) <sup>a</sup>	$P_m$ (4.X) <sup>b</sup>
	0 equiv	1 equiv		
<b>4.1b</b>	0.48 <sup>c</sup>	0.59	0.60	0.72 <sup>c</sup>
<b>4.2b</b>	0.47 <sup>c</sup>	0.58	0.57	0.67 <sup>c</sup>
<b>4.3b</b>	0.33	0.45		
<b>4.5b</b>	0.46	0.59	0.59	0.71
<b>4.6b</b>	0.43	0.46		

<sup>a</sup>  $P_m$  value expected for a 1:1 mixture of **4.X** and **4.Xb**. <sup>b</sup>  $P_m$  value of **4.X**. <sup>c</sup> taken from ref. <sup>7</sup>.

### Mechanism of stereocontrol.

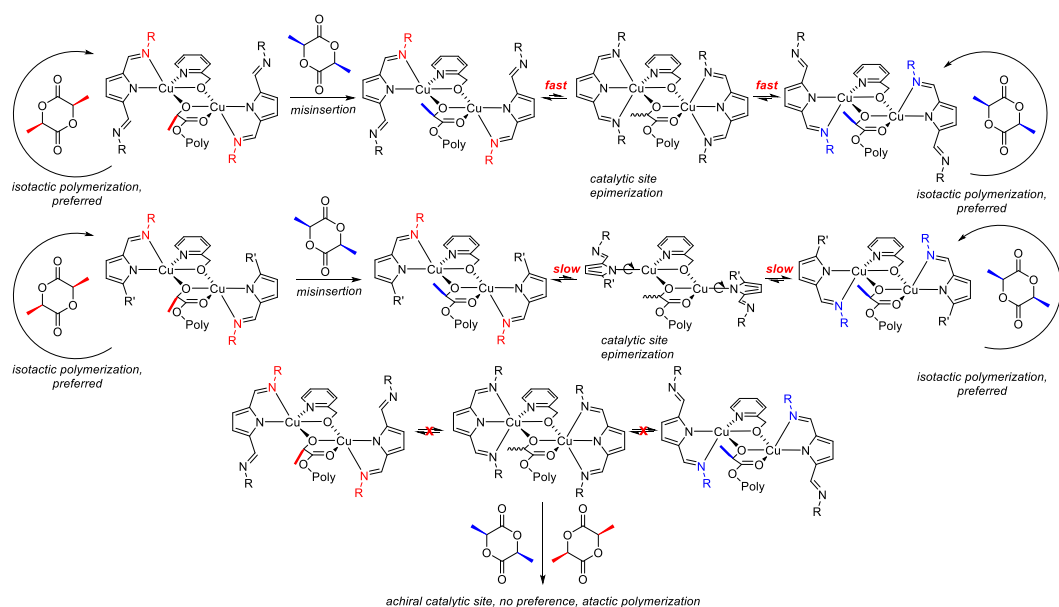
Stereocontrol in **4.1** has been shown to follow a chain-end control mechanism.<sup>7</sup> This is further supported by the fact that stereocontrol was not affected by enforced chain-transfer in immortal polymerizations, neither for **4.1** and **4.2**,<sup>7</sup> nor for **4.8–4.10** (Table 4.S4). Monoiminopyrrolide complexes **4.8–4.10** showed the expected isotactic bias for polymerization, but the obtained  $P_m$  values are notably lower than the ones obtained with the respective diiminopyrrolide complexes **4.1** and **4.2** (Table 4.V). Stereocontrol was lower for methyl-substituted **4.10** than for hydrogen-substituted **4.8**, indicating that steric factors are not primarily responsible for the reduced stereocontrol. The mechanism proposed for **4.1/4.1a** involves adaptation of the chiral catalytic site to chain-end chirality and that the chirality of the catalytic site participates in or even dominates enantiomer selection for the next insertion.<sup>6h,7</sup> Such a "catalytic-site mediated chain-end control mechanism" was initially proposed by Okuda for heterotactic control in scandium complexes,<sup>24</sup> but also observed by Jones for zirconium.<sup>25</sup> Based on the high flexibility of the coordination environment observed in the crystal structures of **4.1/4.1a–4.11/4.11b**, the chiral coordination environment is likely to adapt to the chirality of the chain-end. Adaptation of the catalytic site to chain-end chirality (i. e. catalytic-site epimerization) is probably fast in **4.1**, **4.2** or **4.5**, since it requires only coordination of the pending imino substituent, possibly passing through a tridentate intermediate similar to complex **4.7** via an associative mechanism (Scheme 4.9, top). Monoiminopyrrolide complexes **4.8–4.10**, on the other hand, require dissociation and rotation around the Cu-pyrrole bond or Berry pseudo-rotation of a trigonal-bipyramidal intermediate, both likely to be more difficult considering the ligands involved. The presence of the 5-methyl substituent in **4.10** slows these isomerizations even more. Hindered catalytic-site epimerization and thus the possibility of mismatches between chain end and catalytic site are thus probably responsible for the reduced stereocontrol in **4.8–4.10** (Scheme 4.9, middle).

The involvement of the catalytic site in monomer selection is further supported by polymerizations with **4.7**. The bromobenzyl complex **4.7** surprisingly provided only atactic PLA ( $P_m = 0.53$ , Table 4.V). In this it deviates from the otherwise strictly followed observation that pyridylmethoxide-containing catalysts provide isotactic PLA. Compared to other changes in the ligand substitution pattern in **4.1-4.10**, which led to minor variations of the  $P_m$  value (0.59 – 0.71), the electronic and steric impact of replacing hydrogen by bromine in the *para*-position of the iminobenzyl substituent should be negligible. The atypical polymerization behavior correlates with its atypical crystal structure: Complex **4.7** is the only example in which a tridentate coordination of the diiminopyrrolide ligand was observed. The catalytic site in **4.7** contains octahedral copper centers with an imino group coordinated above and below the equatorial plane (Fig. 4.3). Regardless of chain-end chirality, the catalytic site is thus achiral and will not prefer one enantiomer over the other (Scheme 4.9, bottom). The fact that the only catalyst with an achiral coordination environment is also the only pyridylmethoxide complex not showing preference for isotactic monomer insertion strongly supports that the catalytic site is responsible for monomer selection even if the chiral information is derived from the chain-end.<sup>26</sup>

## Conclusions

The reaction mechanism proposed for isotactic selectivity in iminopyrrolide complexes is supported by the results obtained in varying the ligand substitution pattern. As found for **4.1** and **4.2**, the nature of the bridging alkoxide ligand in the dinuclear active species is of utmost importance for stereocontrol: a pyridylmethoxide ligand in the active species enables stereocontrol, while the more flexible/less coordinating polymerylalkoxide group does not. Reduced stereocontrol in the absence of a pending imine and loss of stereocontrol in complex **7** displaying an achiral catalytic site support the participation of the catalytic site in monomer stereoselection (catalytic-site mediated chain-end control). In combination, these results define the essential requirements to obtain isotactic selectivity in dinuclear copper (and eventually other metal) complexes: a bridging ligand of sufficient rigidity and stability as well as a flexible, chiral catalytic site.

The results presented herein also show that further optimization of diiminopyrrolide copper complexes is limited: Smaller steric variations do not show notable improvement in stereocontrol, while bulkier ligand systems prevent the introduction of the pyridylmethoxide group required for stereocontrol. It seems thus unlikely that further modifications of this ligand system will provide significantly improved catalysts and future work in our group will aim at incorporating the above requirements into new catalytic systems.



**Scheme 4.9.**

## Experimental section

**General considerations.** All reactions were carried out using Schlenk or glove box techniques under nitrogen atmosphere.  $\text{Cu}(\text{OiPr})_2$ ,<sup>27</sup>  $\text{Cu}(\text{OMe})_2$ ,<sup>27</sup> 1*H*-pyrrole-2,5-dicarbaldehyde,<sup>28</sup> 1*H*-pyrrole-2-methyl-5-carbaldehyde,<sup>29</sup> 1*H*-pyrrole-2-chloro-5-carbaldehyde,<sup>29</sup> 4.L3,<sup>8</sup> 4.L8,<sup>9</sup> and 4.L9,<sup>10</sup> were prepared according to literature. Solvents were dried by passage through activated aluminum oxide (MBraun SPS), de-oxygenated by repeated extraction with nitrogen, and stored over molecular sieves.  $\text{C}_6\text{D}_6$  was dried over molecular sieves. *rac*-Lactide (98%) was purchased from Sigma–Aldrich, purified by 3x recrystallization from dry ethyl acetate and kept at  $-30^\circ\text{C}$ . All other chemicals were purchased from common commercial suppliers and used

without further purification.  $^1\text{H}$  and  $^{13}\text{C}$  NMR spectra were acquired on Bruker Advance 300 and 400 spectrometers. Chemical shifts were referenced to the residual signals of the deuterated solvents ( $\text{CDCl}_3$ :  $^1\text{H}$ :  $\delta$  7.26 ppm,  $^{13}\text{C}$ :  $\delta$  77.16). Some  $^{13}\text{C}$  NMR chemical shifts were determined using HSQC spectra. Elemental analyses were performed by the Laboratoire d'analyse élémentaire (Université de Montréal). Molecular weight analyses were performed on a Waters 1525 gel permeation chromatograph equipped with three Phenomenex columns and a refractive index detector at 35 °C. THF was used as the eluent at a flow rate of 1.0 mL·min<sup>-1</sup> and polystyrene standards (Sigma–Aldrich, 1.5 mg·mL<sup>-1</sup>, prepared and filtered (0.2 mm) directly prior to injection) were used for calibration. Obtained molecular weights were corrected by a Mark-Houwink factor of 0.58.<sup>30</sup> All UV-Vis measurements were done in degassed and anhydrous toluene or  $\text{CH}_2\text{Cl}_2$  at ambient temperature in a sealed quartz cell on a Cary 500i UV-Vis-NIR Spectrophotometer.

**[2,5-Bis((1-naphtyl)aldimino)pyrrole], 4.L4.** 1*H*-pyrrole-2,5-dicarbaldehyde (0.5 g, 4.1 mmol) was dissolved in ethanol (25 ml). 1-Naphtylamine (1.2 g, 8.2 mmol) was added and the reaction was heated to reflux overnight. Cooling to ambient temperature resulted in a yellow precipitate which was filtered off, washed with cold ethanol and dried under vacuum (1.22 g, 80%).

$^1\text{H}$  NMR ( $\text{CDCl}_3$ , 300 MHz):  $\delta$  10.51 (s, 1H, NH), 8.51–8.37 (m, 4H, (N=C)H and Ar), 7.92–7.83 (m, 2H, Ar), 7.75 (d,  $J$  = 8 Hz, 2H, Ar), 7.58–7.51 (m, 4H, Ar), 7.48 (dd,  $J$  = 8, 7 Hz, 2H, Ar), 7.10 (d,  $J$  = 7 Hz, 2H, Ar), 6.81 (s, 2H, pyrrole).  $^{13}\text{C}\{^1\text{H}\}$  NMR ( $\text{CDCl}_3$ , 75 MHz):  $\delta$  149.4 ((N=)CH), 149.0 (1-naphtyl), 134.5 (2/5-pyrrole), 134.16 (5-naphtyl), 129.0 (naphtyl), 127.8 (naphtyl), 126.6 (naphtyl), 126.2 (naphtyl), 126.1 (naphtyl), 126.0 (naphtyl), 124.1 (naphtyl), 117.1 (2-naphtyl), 113.0 (3/4-pyrrole). ESI-HRMS ( $m/z$ ):  $[\text{M}+\text{H}]^+$  ( $\text{C}_{26}\text{H}_{20}\text{N}_3$ ) calcd 374.1652; found 374.1659.

**[2,5-Bis(cyclohexylaldimino)pyrrole], 4.L5.** 1*H*-pyrrole-2,5-dicarbaldehyde (0.50 g, 4.1 mmol) was dissolved in ethanol (25 ml). A catalytic amount of formic acid and cyclohexylamine (0.81 g, 8.2 mmol) were added and the reaction was stirred

overnight at ambient temperature. The solvent was removed from the brown solution under vacuum, resulting in a red oil (0.35 g, 30%).

$^1\text{H}$  NMR ( $\text{CDCl}_3$ , 400 MHz):  $\delta$  8.07 (s, 2H, (N=C)H), 6.41 (s, 2H, pyrrole), 3.10 (tt,  $J = 10, 4$  Hz, 2H, NCH), 1.86 – 1.76 (m, 4H,  $\text{CH}_2$ ), 1.75 – 1.61 (m, 6H,  $\text{CH}_2$ ), 1.49 (ddd,  $J = 15, 12, 3$  Hz, 4H,  $\text{CH}_2$ ), 1.41 – 1.19 (m, 6H,  $\text{CH}_2$ ).  $^{13}\text{C}\{^1\text{H}\}$  NMR ( $\text{CDCl}_3$ , 101 MHz):  $\delta$  148.8 ((N=C)), 133.0 (2,5-pyrrole), 114.0 (3,4-pyrrole), 69.7 (NCH), 34.7 ( $\text{CH}_2$ ), 25.8 ( $\text{CH}_2$ ), 25.0 ( $\text{CH}_2$ ). ESI-HRMS (m/z):  $[\text{M}+\text{H}]^+$  ( $\text{C}_{18}\text{H}_{28}\text{N}_3$ ) calcd 286.2277; found 286.2272.

**[2,5-Bis((diphenyl)aldimino)pyrrole], 4.L6.** 1*H*-pyrrole-2,5-dicarbaldehyde (0.50 g, 4.1 mmol) was dissolved in dry ether (25 ml), treated with 2.5 g of  $\text{K}_2\text{CO}_3$  and diphenylamine (1.5 g, 8.2 mmol). The reaction stirred overnight at ambient temperature. The brown suspension was filtered and the solvent removed under vacuum. The residue was treated with hexane (20 ml), resulting in an orange crystalline powder, which was separated by filtration and dried under vacuum (0.28 g, 15%).

$^1\text{H}$  NMR ( $\text{CDCl}_3$ , 300 MHz):  $\delta$  8.19 (s, 2H, (N=C)H), 7.43–7.15 (m, 20H, Ph), 6.48 (s, 2H, pyrrole), 5.57 (s, 2H, NCH), 5.22 (s, 1H, NH).  $^{13}\text{C}\{^1\text{H}\}$  NMR (75 MHz,  $\text{CDCl}_3$ ):  $\delta$  151.3 ((N=C)), 145.8 (*ipso*-Ph), 143.6 (*ipso*-Ph), 133.0 (2,5-pyrrole), 128.6 (*o*-Ph), 128.0 (*o*-Ph), 127.7 (*m*-Ph), 127.2 (*m*-Ph), 127.1 (*p*-Ph), 127.0 (*p*-Ph), 115.4 (3,4-pyrrole), 59.9 (NCH). ESI-HRMS (m/z):  $[\text{M}+\text{H}]^+$  ( $\text{C}_{32}\text{H}_{28}\text{N}_3$ ) calcd 454.2277; found 454.2286.

**[2,5-Bis((4-bromobenzyl)aldimino)pyrrole], 4.L7.** 1*H*-pyrrole-2,5-dicarbaldehyde (0.5 g, 4.1 mmol) was dissolved in dry toluene (25 ml).  $\text{MgSO}_4$  (5 g), a catalytic amount of Amberlyst 15 and 4-bromobenzylamine (1.5 g, 8.2 mmol) were added. The reaction was stirred overnight at ambient temperature. The light yellow suspension was filtered and the solvent removed under vacuum. The residue was treated with hexane (20 ml), resulting in a dark brown oil. The oil was separated by decantation and dried under vacuum to give 0.43 g (23%) of a 1:1 mixture of 4.L7 and 2-

carboxaldehyde-5-((4-bromobenzyl)aldimino)pyrrole. Purification attempts were unsuccessful and the mixture was used without purification in further synthesis.

2,5-Bis((4-bromobenzyl)aldimino)pyrrole:  $^1\text{H}$  NMR ( $\text{CDCl}_3$ , 400 MHz):  $\delta$  8.14 (s, 2H, (N=C)H), 7.45 (d,  $J = 8$  Hz, 4H, m-Ph), 7.17 (d,  $J = 8$  Hz, 4H, o-Ph), 6.53 (s, 2H, pyrrole), 4.67 (s, 4H,  $\text{CH}_2$ ).  $^{13}\text{C}\{^1\text{H}\}$  NMR ( $\text{CDCl}_3$ , 101 MHz):  $\delta$  152.6 ((N=)CH), 138.5 (2,5-pyrrole), 138.1 (*ipso*-Ph), 132.0 (m-Ph), 130.1 (o-Ph), 121.4 (C-Br), 115.7 (3,4-pyrrole), 64.1 ( $\text{CH}_2$ ). ESI-HRMS (m/z):  $[\text{M}+\text{H}]^+$  ( $\text{C}_{20}\text{H}_{18}\text{Br}_2\text{N}_3$ ) calcd 457.9862; found 457.9860.

2-carbaldehyde-5-((4-bromobenzyl)aldimino)pyrrole:  $^1\text{H}$  NMR ( $\text{CDCl}_3$ , 400 MHz):  $\delta$  9.60 (s, 1H, COH), 8.22 (s, 1H, (N=C)H), 7.45 (d,  $J = 8$  Hz, 2H, m-Ph), 7.17 (d,  $J = 8$ , 2H, o-Ph), 6.94 (d,  $J = 3$  Hz, 1H, pyrrole), 6.58 (d,  $J = 3$  Hz, 1H, pyrrole), 4.72 (s, 2H,  $\text{CH}_2$ ).  $^{13}\text{C}\{^1\text{H}\}$  NMR ( $\text{CDCl}_3$ , 101 MHz):  $\delta$  180.40 (COH), 152.3 ((N=)CH), 138.5 (2,5-pyrrole), 138.1 (*ipso*-Ph), 132.1 (2,5-pyrrole), 132.00 (o-Ph), 130.1 (m-Ph), 121.4 (C-Br), 120.89 (3,4-pyrrole), 115.2 (3,4-pyrrole), 64.3 ( $\text{CH}_2$ ). ESI-HRMS (m/z):  $[\text{M}+\text{H}]^+$  ( $\text{C}_{13}\text{H}_{12}\text{BrN}_2\text{O}$ ) calcd 291.0128; found 291.0141.

**[2-methyl-5-((L(-)-alpha-methylbenzyl)aldimino)pyrrole], 4.L10.** Analogous to 4.L7, from 1*H*-pyrrole-2-methyl-5-carbaldehyde (1.0 g, 9.2 mmol), dry toluene (25 ml), 5g  $\text{MgSO}_4$ , a catalytic amount of Amberlyst 15 and L(-)-alpha-methylbenzylamine (1.1 g, 9.2 mmol) to yield a light yellow oil which was purified by silica gel chromatography (0-30% EtOAc in hexane) (0.47 g, 25%).

$^1\text{H}$  NMR ( $\text{CDCl}_3$ , 400 MHz) :  $\delta$  8.06 (s, 1H, (N=C)H), 7.42–7.30 (m, 4H, Ph), 7.27–7.21 (m, 1H, Ph), 6.39 (d,  $J = 3$  Hz, 1H, 3-pyrrole), 5.93 (d,  $J = 3$  Hz, 1H, 2-pyrrole), 4.45 (q,  $J = 6$  Hz, 1H,  $\text{CH}(\text{Me})$ ), 2.27 (s, 3H, pyrrole- $\text{CH}_3$ ), 1.57 (d,  $J = 6$  Hz, 3H,  $\text{CH}(\text{CH}_3)$ ).  $^{13}\text{C}\{^1\text{H}\}$  NMR ( $\text{CDCl}_3$ , 75 MHz):  $\delta$  149.9 ((N=)C), 145.4 (*ipso*-Ph), 142.4 (2-pyrrole) (HSQC), 128.5 (o-Ph), 126.9 (m-Ph), 126.7(p-Ph), 115.1 (5-pyrrole), 110.5 (2-pyrrole), 108.3 (3-pyrrole), 68.7 ( $\text{CH}(\text{Me})\text{Ph}$ ), 24.5 (Me), 13.3 ( $\text{CH}_3$ -pyrrole). ESI-HRMS (m/z):  $[\text{M}+\text{H}]^+$  ( $\text{C}_{14}\text{H}_{17}\text{N}_2$ ) calcd 213.1386; found 213.1386.

**[2-chloro-5-((L(-)alpha-methylbenzyl)aldimino)pyrrole], 4.L11.** Analogous to 4.L7, from 1*H*-pyrrole-2-chloro-5-carbaldehyde (1.0 g, 7.7 mmol), dry toluene (25 ml), 5g MgSO<sub>4</sub>, a catalytic amount of Amberlyst 15 and L(-)-alpha-methylbenzylamine (0.93 g, 7.7 mmol) to yield a light yellow powder (0.52 g, 29%).

<sup>1</sup>H NMR (CDCl<sub>3</sub>, 400 MHz): δ 7.80 (s, 1H, (N=C)*H*), 7.38 – 7.31 (m, 4H, Ph), 7.30 – 7.23 (m, 1H, Ph), 7.04 (br s, 1H, NH), 6.49 (d, *J* = 3 Hz, 1H, pyrrole), 6.10 (d, *J* = 3 Hz, 1H, pyrrole), 4.50 (q, *J* = 6 Hz, 1H, CH(Me)Ph), 1.57 (d, *J* = 6 Hz, 3H, Me). <sup>13</sup>C {<sup>1</sup>H} NMR (CDCl<sub>3</sub>, 101 MHz): δ 148.4 ((N=C)), 144.2 (*ipso*-Ph), 130.0 (2-pyrrole), 128.8 (o-Ph), 127.4 (m-Ph), 126.7 (p-Ph), 125.4 (5-pyrrole), 118.3 (4-pyrrole), 110.0 (3-pyrrole), 66.5 (CH(Me)Ph), 24.2 (Me). ESI-HRMS (m/z): [M+H]<sup>+</sup> (C<sub>13</sub>H<sub>14</sub>ClN<sub>2</sub>) calcd 233.0840; found 233.0849.

**(4.L1)<sub>2</sub>Cu, 4.1c.** To a suspension of copper diisopropoxide (105 mg, 0.58 mmol) in dichloromethane (15 mL) is added 4.L1 (420 mg, 1.28 mmol) under stirring. Stirring is continued for 1 day, after which the suspension is filtered. The filtrate is concentrated and layered with hexane to yield crystalline **4.1c** after several days (112 mg, 25%).

UV-vis (CH<sub>2</sub>Cl<sub>2</sub>, 9.9·10<sup>-5</sup> M or 9.9·10<sup>-6</sup> M) [ $\lambda_{\max}$ , nm ( $\epsilon$ , mol<sup>-1</sup> cm<sup>2</sup>): 364 (27100)]. Anal. Calcd for C<sub>44</sub>H<sub>44</sub>CuN<sub>6</sub>: C, 73.36; H, 6.16; N, 11.67; Found: C, 72.88; H, 6.28; N, 11.39.

**[(4.L1)ClCu<sub>2</sub>( $\mu$ -O, $\kappa$ <sub>N</sub>-OC<sub>2</sub>H<sub>4</sub>NMe<sub>2</sub>)<sub>2</sub>], 4.1e.** Complex **4.1e** was obtained as an undesired side product in the preparation of **4.1** using chloride-contaminated Cu(OR)<sub>2</sub> starting material. (0.006 g, 6%).

Anal. Calcd for C<sub>30</sub>H<sub>42</sub>ClCu<sub>2</sub>N<sub>5</sub>O<sub>2</sub>: C, 54.00; H, 6.34; N, 10.50; Found: C, 54.72; H, 6.39; N, 10.30.

**(4.L2)<sub>2</sub>Cu<sub>2</sub>, 4.2d.** To a suspension of copper diisopropoxide (136 mg, 0.75 mmol) in dichloromethane (15 mL) is added 4.L2 (495 mg, 1.64 mmol) under stirring. Stirring is continued at ambient temperature for 1 day, after which the solution is filtered. The filtrate is concentrated and layered with hexane to yield 210 mg (77%) of **4.2d**.



$^1\text{H}$  NMR ( $\text{CDCl}_3$ , 400 MHz, 298 K):  $\delta$  7.97 (s, 4H, N=CH), 7.15 (m, 12H, Ar), 7.05 (m, 8H, Ar), 6.60 (s, 4H, 3,4-pyrrole), 4.39 (s, 8H,  $\text{NCH}_2$ ).  $^{13}\text{C}$  NMR ( $\text{CDCl}_3$ , 400 MHz, 298 K):  $\delta$  159.3 (N=CH), 141.0 (*ipso*-Ar), 138.8 (2,5-pyrrole), 128.3 (*m*-Ar), 128.0 (*o*-Ar), 127.0 (*p*-Ar), 118.0 (3,4-pyrrole), 63.9 (=N- $\text{CH}_2$ ). UV-vis ( $\text{CH}_2\text{Cl}_2$ ,  $3.4 \cdot 10^{-5}$  M or  $6.9 \cdot 10^{-6}$  M) [ $\lambda_{\text{max}}$ , nm ( $\epsilon$ ,  $\text{mol}^{-1} \text{cm}^2$ ): 318 (20200), 332 (20100), 374 (23000), 500 (sh). Anal. Calcd for  $\text{C}_{40}\text{H}_{36}\text{Cu}_2\text{N}_6$ : C, 66.01; H, 4.99; N, 11.55; Found: C, 66.65; H, 4.82; N, 11.63.

**[(4.L3) $_2$ Cu $_2$ ( $\mu$ -O, $\kappa$  $_N$ -OC $_2$ H $_4$ NMe $_2$ ) $_2$ ], 4.3b.** Cu(OMe) $_2$  (38 mg, 0.30 mmol) was suspended in toluene (3 ml). Dimethylaminoethanol (60  $\mu$ l, 0.60 mmol) was added to the blue suspension, which was left to stir for 45 min. A freshly prepared orange solution of **4.L3** (100 mg, 0.30 mmol) in toluene (2 ml) was added dropwise, resulting in a dark green solution. The reaction was stirred 24 hours at RT, filtered to remove trace impurities, concentrated to 1/3 of the volume, diluted with hexane (18 ml) and kept at  $-30^\circ\text{C}$  for 4 hours, resulting in green crystals. The crystals were separated by decantation and washed with hexane ( $3 \times 10$  ml) (0.024g, 17%).

UV-vis (toluene,  $2.3 \cdot 10^{-5}$  M) [ $\lambda_{\text{max}}$ , nm ( $\epsilon$ ,  $\text{mol}^{-1} \text{cm}^2$ ): 296 (sh), 382 (48400). Anal. Calcd for  $\text{C}_{52}\text{H}_{64}\text{Cu}_2\text{N}_8\text{O}_2$ : C, 65.04; H, 6.72; N, 11.67; Found: C, 65.22; H, 6.91; N, 11.84.

**(4.L3) $_2$ Cu $_2$ , 4.3d.** To a stirred green suspension of copper diisopropoxide (436 mg, 2.4 mmol) in THF (40 mL) at  $50^\circ\text{C}$ , a THF solution of **4.L3** (658 mg, 2 mmol) is added. The colour changes to dark brown and heating is continued for 74 h. After cooling to RT the suspension was filtered. The residue was extracted dichloromethane and layered with hexane to yield 258 mg (33%) of **4.3d**.

$^1\text{H}$  NMR ( $\text{CDCl}_3$ , 400 MHz, 298 K):  $\delta$  7.87 (s, 4H, N=CH), 6.91 (s, 12H, Ar), 6.69 (s, 4H, 3,4-pyrrole), 1.82 (s, 24H, Me).  $^{13}\text{C}$  NMR ( $\text{CDCl}_3$ , 101 MHz, 298 K):  $\delta$  159.7 (N=CH), 149.5 (*ipso*-Ar), 141.9 (2,5-pyrrole), 129.6 (*m*-Ar), 128.1 (*o*-Ar), 124.3 (*p*-Ar), 119.2 (3,4-pyrrole), 18.2 (Me). UV-vis ( $\text{CH}_2\text{Cl}_2$ ,  $6.2 \cdot 10^{-5}$  M or  $6.2 \cdot 10^{-6}$  M) [ $\lambda_{\text{max}}$ , nm ( $\epsilon$ ,  $\text{mol}^{-1} \text{cm}^2$ ): 386 (59000), 550 (sh, <1500). Anal. Calcd for  $\text{C}_{44}\text{H}_{44}\text{N}_6\text{Cu}_2$ : C, 67.41; H, 5.66; N, 10.72; Found: C, 67.10; H, 5.58; N, 10.57.

**(4.L4)<sub>2</sub>Cu, 4.4c.** To a suspension of copper diisopropoxide (111 mg, 0.61 mmol) in toluene (16 mL) 4.L4 (500 mg, 1.34 mmol) is added. After stirring for 3 days, the suspension is filtered off and the light brown-golden residue extracted with dichloromethane. The solvent is removed and the residue recrystallized from diffusion of hexane into dichloromethane (195 mg, 44%).

UV-vis (CH<sub>2</sub>Cl<sub>2</sub>, 6.2·10<sup>-5</sup> M or 6.2·10<sup>-6</sup> M) [ $\lambda_{\max}$ , nm ( $\epsilon$ , mol<sup>-1</sup> cm<sup>2</sup>): 376 (111500)].  
Anal. Calcd for C<sub>52</sub>H<sub>36</sub>CuN<sub>6</sub>: C, 77.26; H, 4.49; N, 10.40; Found: C, 76.67; H, 4.63; N, 9.98.

**[(4.L4)ClCu<sub>2</sub>( $\mu$ -O, $\kappa$ <sub>N</sub>-OC<sub>2</sub>H<sub>4</sub>NMe<sub>2</sub>)<sub>2</sub>], 4.4e.** Analogous to **4.3b**, from Cu(OMe)<sub>2</sub> (34 mg, 0.27 mmol) in toluene (3 mL), 2-pyridinemethanol (52  $\mu$ L, 0.54 mmol), **4.L4** (100 mg, 0.27 mmol) in toluene (2 mL). The filtered and concentrated (1/3 of the volume) green solution was diluted with hexane (18 mL) and kept at -30 °C for 4 h. The oily residue was dissolved in DCM and layered with hexane (1:3), yielding green X-ray quality crystals (0.026 g, 29%).

UV-vis (toluene, 3.4·10<sup>-5</sup>M) [ $\lambda_{\max}$ , nm ( $\epsilon$ , mol<sup>-1</sup> cm<sup>2</sup>): 317 (13600), 403 (24000)].  
Anal. Calcd for C<sub>34</sub>H<sub>38</sub>ClCu<sub>2</sub>N<sub>5</sub>O<sub>2</sub>: C, 57.42; H, 5.39; N, 9.85; Found: C, 61.13; H, 5.56; N, 10.03. (Elemental analysis does not agree. No purification attempted.)

**[(4.L5)<sub>2</sub>Cu<sub>2</sub>( $\mu$ -O, $\kappa$ <sub>N</sub>-OCH<sub>2</sub>Py)<sub>2</sub>], 4.5.** Analogous to **4.3b**, from Cu(OMe)<sub>2</sub> (44 mg, 0.35 mmol) in toluene (3 mL), 2-pyridinemethanol (67  $\mu$ L, 0.70 mmol), **4.L5** (100 mg, 0.35 mmol) in toluene (2 mL). The filtered and concentrated (1/3 of the volume) green solution was diluted with hexane (18 mL) and kept at -30 °C for 4 h. Decantation and washing with hexane (3 x 10 mL) afforded 36 mg (22%) of green X-ray quality crystals.

UV-vis (toluene, 3.4·10<sup>-5</sup>M) [ $\lambda_{\max}$ , nm ( $\epsilon$ , mol<sup>-1</sup> cm<sup>2</sup>): 315 (45500), 368 (41500)].  
Anal. Calcd for C<sub>48</sub>H<sub>64</sub>Cu<sub>2</sub>N<sub>8</sub>O<sub>2</sub>·C<sub>6</sub>H<sub>14</sub>: C, 64.97; H, 7.88; N, 11.22; Found: C, 64.31; H, 7.67; N, 11.28. (One molecule of hexane was found in the X-ray structure.)

**[(4.L5)<sub>2</sub>Cu<sub>2</sub>( $\mu$ -O, $\kappa$ <sub>N</sub>-OC<sub>2</sub>H<sub>4</sub>NMe<sub>2</sub>)<sub>2</sub>], 4.5b.** Analogous to **4.3b**, from Cu(OMe)<sub>2</sub> (44 mg, 0.35 mmol) in toluene (3 mL), dimethylaminoethanol (70  $\mu$ L, 0.70 mmol), **4.L5**

(100 mg, 0.35 mmol) in toluene (2 mL). The filtered and concentrated (1/3 of the volume) green solution was diluted with hexane (18 mL) and kept at  $-30\text{ }^{\circ}\text{C}$  for 4 h. Decantation and washing with hexane (3 x 10 mL) afforded 29 mg (19%) of green X-ray quality crystals.

UV-vis (toluene,  $2 \cdot 10^{-5}\text{M}$ ) [ $\lambda_{\text{max}}$ , nm ( $\epsilon$ ,  $\text{mol}^{-1}\text{ cm}^2$ ): 341 (sh), 357 (25200), 374 (sh). Anal. Calcd for  $\text{C}_{44}\text{H}_{72}\text{Cu}_2\text{N}_8\text{O}_2 \cdot \text{C}_6\text{H}_{14}$ : C, 62.66; H, 9.05; N, 11.69; Found: C, 62.04; H, 9.55; N, 11.45. (One molecule of hexane was found in the X-ray structure.)

**[(4.L6)<sub>2</sub>Cu<sub>2</sub>( $\mu$ -O, $\kappa$ <sub>N</sub>-OC<sub>2</sub>H<sub>4</sub>NMe<sub>2</sub>)<sub>2</sub>], 4.6b.** Analogous to **4.3b**, from Cu(OMe)<sub>2</sub> (28 mg, 0.22 mmol) in toluene (3 mL), dimethylaminoethanol (44  $\mu\text{L}$ , 0.44 mmol), **4.L6** (100 mg, 0.22 mmol) in toluene (2 mL). The filtered and concentrated (1/3 of the volume) green solution was diluted with hexane (18 mL) and kept at  $-30\text{ }^{\circ}\text{C}$  for 4 h. Decantation and washing with hexane (3 x 10 mL) afforded 46 mg (35%) of green X-ray quality crystals.

UV-vis (toluene,  $2.3 \cdot 10^{-5}\text{M}$ ) [ $\lambda_{\text{max}}$ , nm ( $\epsilon$ ,  $\text{mol}^{-1}\text{ cm}^2$ ): 295 (sh), 352 (sh), 363 (27100), 392 (sh). Anal. Calcd for  $\text{C}_{72}\text{H}_{72}\text{Cu}_2\text{N}_8\text{O}_2$ : C, 71.56; H, 6.01; N, 9.27; Found: C, 71.43; H, 6.29 N, 9.19.

**[(4.L6)ClCu<sub>2</sub>( $\mu$ -O, $\kappa$ <sub>N</sub>-OCH<sub>2</sub>Py)<sub>2</sub>], 4.6e.** Analogous to **4.3b**, from Cu(OMe)<sub>2</sub> (28 mg, 0.22 mmol) in toluene (3 mL), 2-pyridinemethanol (42  $\mu\text{L}$ , 0.44 mmol), **4.L6** (100 mg, 0.22 mmol) in toluene (2 mL). The filtered and concentrated (1/3 of the volume) green solution was diluted with hexane (18 mL) and kept at  $-30\text{ }^{\circ}\text{C}$  for 4 h. The oily residue was dissolved in DCM and layered with hexane (1:3), yielding green X-ray quality crystals (0.026 g, 29%).

UV-vis (toluene,  $2 \cdot 10^{-6}\text{M}$ ) [ $\lambda_{\text{max}}$ , nm ( $\epsilon$ ,  $\text{mol}^{-1}\text{ cm}^2$ ): 323 (10750), 338 (sh), 381 (27100), 394 (45700) Anal. Calcd for  $\text{C}_{44}\text{H}_{38}\text{ClCu}_2\text{N}_5\text{O}_2$ : C, 63.57; H, 4.61; N, 8.42; Found: C, 63.54; H, 5.05; N, 8.33.

**[(4.L7)<sub>2</sub>Cu<sub>2</sub>( $\mu$ -O, $\kappa$ <sub>N</sub>-OCH<sub>2</sub>Py)<sub>2</sub>], 4.7.** Analogous to **4.3b**, from Cu(OMe)<sub>2</sub> (28 mg, 0.22 mmol) in toluene (3 mL), 2-pyridinemethanol (42  $\mu\text{L}$ , 0.44 mmol), **4.L7** (100 mg, 0.22 mmol) in toluene (2 mL). The filtered and concentrated (1/3 of the volume)

green solution was diluted with hexane (18 mL) and kept at  $-30\text{ }^{\circ}\text{C}$  for 4 h. Decantation and washing with hexane (3 x 10 mL) afforded 22 mg (16%) of green X-ray quality crystals.

UV-vis (toluene,  $2 \cdot 10^{-6}\text{M}$ ) [ $\lambda_{\text{max}}$ , nm ( $\epsilon$ ,  $\text{mol}^{-1}\text{ cm}^2$ ): 301 (30200), 349 (15500), 373 (sh), 395 (sh). Anal. Calcd for  $\text{C}_{52}\text{H}_{44}\text{Br}_4\text{Cu}_2\text{N}_8\text{O}_2$ : C, 49.58; H, 3.52; N, 8.90; Found: C, 49.31; H, 3.57; N, 8.78.

**[(4.L7)<sub>2</sub>Cu<sub>2</sub>( $\mu$ -O,<sub>K<sub>N</sub></sub>-OC<sub>2</sub>H<sub>4</sub>NMe<sub>2</sub>)<sub>2</sub>], 4.7b.** Analogous to **4.3b**, from Cu(OMe)<sub>2</sub> (28 mg, 0.22 mmol) in toluene (3 mL), dimethylaminoethanol (44  $\mu$ L, 0.44 mmol), **4.L7** (100 mg, 0.22 mmol) in toluene (2 mL). The filtered and concentrated (1/3 of the volume) green solution was diluted with hexane (18 mL) and kept at  $-30\text{ }^{\circ}\text{C}$  for 4 h. Decantation and washing with hexane (3 x 10 mL) afforded very few green X-ray quality crystals.

**[(4.L8)<sub>2</sub>Cu<sub>2</sub>( $\mu$ -O,<sub>K<sub>N</sub></sub>-OC<sub>2</sub>H<sub>4</sub>NMe<sub>2</sub>)<sub>2</sub>], 4.8b.** Analogous to **4.3b**, from Cu(OMe)<sub>2</sub> (63 mg, 0.50 mmol) in toluene (3 mL), dimethylaminoethanol 1 (100  $\mu$ L, 1.00 mmol), **4.L8** (100 mg, 0.50 mmol) in toluene (2 mL). The filtered and concentrated (1/3 of the volume) green solution was diluted with hexane (18 mL) and kept at  $-30\text{ }^{\circ}\text{C}$  for 4 h. Decantation and washing with hexane (3 x 10 mL) afforded 76 mg (44%) of green X-ray quality crystals.

UV-vis (toluene,  $2.3 \cdot 10^{-5}\text{M}$ ) [ $\lambda_{\text{max}}$ , nm ( $\epsilon$ ,  $\text{mol}^{-1}\text{ cm}^2$ ): 344 (12900); 427 (1960), 481 (sh). Anal. Calcd for  $\text{C}_{34}\text{H}_{46}\text{Cu}_2\text{N}_6\text{O}_2$ : C, 58.52; H, 6.64; N, 12.04; Found: C, 58.19; H, 6.98; N, 12.05.

**[(4.L9)<sub>2</sub>Cu<sub>2</sub>( $\mu$ -O,<sub>K<sub>N</sub></sub>-OCH<sub>2</sub>Py)<sub>2</sub>], 4.9.** Analogous to **4.3b**, from Cu(OMe)<sub>2</sub> (68 mg, 0.54 mmol) in toluene (3 mL), 2-pyridinemethanol (105  $\mu$ L, 1.10 mmol), **4.L9** (100 mg, 0.54 mmol) in toluene (2 mL). The filtered and concentrated (1/3 of the volume) green solution was diluted with hexane (18 mL) and kept at  $-30\text{ }^{\circ}\text{C}$  for 4 h. Decantation and washing with hexane (3 x 10 mL) afforded 74 mg (38%) of green X-ray quality crystals.

UV-vis (toluene,  $2.3 \cdot 10^{-5} \text{M}$ ) [ $\lambda_{\text{max}}$ , nm ( $\epsilon$ ,  $\text{mol}^{-1} \text{cm}^2$ ): 346 (8170), 423 (1100), 492 (sh). Anal. Calcd for  $\text{C}_{36}\text{H}_{34}\text{Cu}_2\text{N}_6\text{O}_2$ : C, 60.92; H, 4.83; N, 11.84; Found: C, 60.62; H, 4.65; N, 12.00.

**[(4.L9)<sub>2</sub>Cu<sub>2</sub>( $\mu$ -O, $\kappa$ <sub>N</sub>-OC<sub>2</sub>H<sub>4</sub>NMe<sub>2</sub>)<sub>2</sub>], 4.9b.** Analogous to **4.3b**, from Cu(OMe)<sub>2</sub> (68 mg, 0.54 mmol) in toluene (3 mL), dimethylaminoethanol (109  $\mu$ L, 1.10 mmol), **4.L9** (100 mg, 0.54 mmol) in toluene (2 mL). The filtered and concentrated (1/3 of the volume) green solution was diluted with hexane (18 mL) and kept at  $-30^\circ \text{C}$  for 4 h. Decantation and washing with hexane (3 x 10 mL) afforded 75 mg (42%) of green X-ray quality crystals.

UV-vis (toluene,  $2.3 \cdot 10^{-5} \text{M}$ ) [ $\lambda_{\text{max}}$ , nm ( $\epsilon$ ,  $\text{mol}^{-1} \text{cm}^2$ ): 349 (11400), 427 (1470), 474 (sh). Anal. Calcd for  $\text{C}_{32}\text{H}_{42}\text{Cu}_2\text{N}_6\text{O}_2$ : C, 57.38; H, 6.32; N, 12.55; Found: C, 57.17; H, 6.57; N, 12.44.

**[(4.L10)<sub>2</sub>Cu<sub>2</sub>( $\mu$ -O, $\kappa$ <sub>N</sub>-OCH<sub>2</sub>Py)<sub>2</sub>], 4.10.** Analogous to **4.3b**, from Cu(OMe)<sub>2</sub> (59 mg, 0.47 mmol) in toluene (3 mL), 2-pyridinemethanol (91  $\mu$ L, 0.94 mmol), **4.L10** (100 mg, 0.47 mmol) in toluene (2 mL). The filtered and concentrated (1/3 of the volume) green solution was diluted with hexane (18 mL) and kept at  $-30^\circ \text{C}$  for 4 h. Decantation and washing with hexane (3 x 10 mL) afforded 41 mg (22%) of green X-ray quality crystals.

UV-vis (toluene,  $2 \cdot 10^{-6} \text{M}$ ) [ $\lambda_{\text{max}}$ , nm ( $\epsilon$ ,  $\text{mol}^{-1} \text{cm}^2$ ): 347 (61600), 375 (sh), 433 (sh). Anal. Calcd for  $\text{C}_{40}\text{H}_{42}\text{Cu}_2\text{N}_6\text{O}_2$ : C, 62.73; H, 5.53; N, 10.97; Found: C, 62.62; H, 5.71; N, 11.27.

**[(4.L10)<sub>2</sub>Cu<sub>2</sub>( $\mu$ -O, $\kappa$ <sub>N</sub>-OC<sub>2</sub>H<sub>4</sub>NMe<sub>2</sub>)<sub>2</sub>], 4.10b.** Analogous to **4.3b**, from Cu(OMe)<sub>2</sub> (59 mg, 0.47 mmol) in toluene (3 mL), dimethylaminoethanol (94  $\mu$ L, 0.94 mmol), **4.L10** (100 mg, 0.47 mmol) in toluene (2 mL). The filtered and concentrated (1/3 of the volume) green solution was diluted with hexane (18 mL) and kept at  $-30^\circ \text{C}$  for 4 h. Decantation and washing with hexane (3 x 10 mL) afforded 58 mg (34%) of green X-ray quality crystals.

UV-vis (toluene,  $2 \cdot 10^{-6} \text{M}$ ) [ $\lambda_{\text{max}}$ , nm ( $\epsilon$ ,  $\text{mol}^{-1} \text{cm}^2$ ): 334 (sh), 375 (109600), 387 (sh). Anal. Calcd for  $\text{C}_{36}\text{H}_{50}\text{Cu}_2\text{N}_6\text{O}_2$ : C, 59.56; H, 6.94; N, 11.58; Found: C, 59.30; H, 7.00; N, 11.33.

**[(4.L11)<sub>2</sub>Cu<sub>2</sub>( $\mu$ -O,<sub>KN</sub>-OCH<sub>2</sub>Py)<sub>2</sub>], 4.11.** Analogous to **4.3b**, from Cu(OMe)<sub>2</sub> (54 mg, 0.43 mmol) in toluene (3 mL), 2-pyridinemethanol (83  $\mu\text{L}$ , 0.86 mmol), **4.L11** (100 mg, 0.43 mmol) in toluene (2 mL). The filtered and concentrated (1/3 of the volume) green solution was diluted with hexane (18 mL) and kept at  $-30 \text{ }^\circ\text{C}$  for 4 h. Decantation and washing with hexane (3 x 10 mL) afforded 33 mg (20%) of green X-ray quality crystals.

UV-vis (toluene,  $2 \cdot 10^{-6} \text{M}$ ) [ $\lambda_{\text{max}}$ , nm ( $\epsilon$ ,  $\text{mol}^{-1} \text{cm}^2$ ): 350 (69200). Anal. Calcd for  $\text{C}_{38}\text{H}_{36}\text{Cl}_2\text{Cu}_2\text{N}_6\text{O}_2$ : C, 56.58; H, 4.50; N, 10.42; Found: C, 56.27; H, 4.45; N, 10.38.

**[(4.L11)<sub>2</sub>Cu<sub>2</sub>( $\mu$ -O,<sub>KN</sub>-OC<sub>2</sub>H<sub>4</sub>NMe<sub>2</sub>)<sub>2</sub>], 4.11b.** Analogous to **4.3b**, from Cu(OMe)<sub>2</sub> (54 mg, 0.43 mmol) in toluene (3 mL), dimethylaminoethanol (87  $\mu\text{L}$ , 0.86 mmol), **4.L11** (100 mg, 0.43 mmol) in toluene (2 mL). The filtered and concentrated (1/3 of the volume) green solution was diluted with hexane (18 mL) and kept at  $-30 \text{ }^\circ\text{C}$  for 4 h. Decantation and washing with hexane (3 x 10 mL) afforded 47 mg (28%) of green X-ray quality crystals.

UV-vis (toluene,  $5 \cdot 10^{-6} \text{M}$ ) [ $\lambda_{\text{max}}$ , nm ( $\epsilon$ ,  $\text{mol}^{-1} \text{cm}^2$ ): 349 (37400). Anal. Calcd for  $\text{C}_{34}\text{H}_{44}\text{Cl}_2\text{Cu}_2\text{N}_6\text{O}_2$ : C, 53.26; H, 5.78; N, 10.96; Found: C, 53.18; H, 6.00; N, 10.96.

***rac*-Lactide polymerization.** In a glove box, the desired amount of *rac*-lactide was placed into a J.-Young tube together with C<sub>6</sub>D<sub>6</sub>. A stock solution of an additive (benzyl alcohol or pyridylmethanol) was added, if required, followed by a stock solution of the catalyst (appr. 20 mM in C<sub>6</sub>D<sub>6</sub>). The reaction was followed by <sup>1</sup>H NMR. The reaction was quenched by addition of appr. 5 equiv of a CDCl<sub>3</sub> solution of acetic acid (5 mM). The volatiles were evaporated and solid polymer samples were stored at  $-80 \text{ }^\circ\text{C}$  for further analysis. Conversion was determined from <sup>1</sup>H NMR by comparison to remaining lactide.  $P_m$  values were determined from homodecoupled <sup>1</sup>H NMR spectra and calculated from  $P_m = 1 - 2 \cdot I_1 / (I_1 + I_2)$ , with  $I_1 = 5.15 - 5.21 \text{ ppm}$

(*rmr*; *mmr/rmm*),  $I_2 = 5.21 - 5.25$  ppm (*mmr/rmm*, *mmm*, *mrn*). The integration of the left multiplet and right multiplet ( $I_1$  and  $I_2$ ) required only one, very reproducible dividing point of the integration, which was always taken as the minimum between the two multiplets.  $P_m$ -values obtained this way were typically consistent to  $\pm 1\%$  over the course of one experiment and  $\pm 3\%$  between different experiments under identical conditions.

**X-ray diffraction.** Single crystals were obtained directly from isolation of the products as described above. Diffraction data were collected on a Bruker Venture METALJET diffractometer (Ga  $K\alpha$  radiation) or a Bruker APEXII with a Cu microsource/Quazar MX using the APEX2 software package.<sup>31</sup> Data reduction was performed with SAINT,<sup>32</sup> absorption corrections with SADABS.<sup>33</sup> Structures were solved by dual-space methods (SHELXT).<sup>34</sup> All non-hydrogen atoms were refined anisotropic using full-matrix least-squares on  $F^2$  and hydrogen atoms refined with fixed isotropic U using a riding model (SHELXL97).<sup>35</sup> Further experimental details can be found in Table 4.VII and in the supporting information (CIF).

**Table 4.VII.** Details of X-ray Diffraction Studies

	<b>4.5</b>	<b>4.7</b>	<b>4.9</b>	<b>4.10</b>
Formula	C <sub>54</sub> H <sub>78</sub> Cu <sub>2</sub> N <sub>8</sub> O <sub>2</sub>	C <sub>52</sub> H <sub>44</sub> Br <sub>4</sub> Cu <sub>2</sub> N <sub>8</sub> O <sub>2</sub>	C <sub>36</sub> H <sub>34</sub> Cu <sub>2</sub> N <sub>6</sub> O <sub>2</sub>	C <sub>87</sub> H <sub>92</sub> Cu <sub>4</sub> N <sub>12</sub> O <sub>4</sub>
$M_w$ (g/mol); $d_{\text{calcd}}$ (g/cm <sup>3</sup> )	998.32; 1.284	1259.66; 1.671	709.77; 1.472	1623.88; 1.376
$T$ (K); F(000)	100; 1064	150; 1252	100; 732	100; 1692
Crystal System	Triclinic	Monoclinic	Monoclinic	Monoclinic
Space Group	$P(-1)$	$P2_1/n$	$P2_1/n$	$P2_1$
Unit Cell: $a$ (Å)	10.5038(5)	11.3879(5)	9.0629(2)	11.0206(4)
$b$ (Å)	15.6228(7)	12.5667(5)	9.7780(3)	14.0549(5)
$c$ (Å)	16.4370(8)	17.7200(8)	18.3574(4)	25.6033(10)
$\alpha$ (°)	84.747(3)	90	90	90
$\beta$ (°)	74.381(2)	99.122(3)	100.225(2)	98.681(2)
$\gamma$ (°)	85.211(3)	90	90	90
$V$ (Å <sup>3</sup> ); $Z$	2581.9(2); 2	2503.81(19); 2	1600.94(7); 2	3920.4(3); 2
$\mu$ (mm <sup>-1</sup> ); Abs. Corr.	1.382; multiscan	7.437; multiscan	7.394; multiscan	6.092; multiscan
$\theta$ range (°); completeness	2.85-70.40; 0.97	3.06-60.52; 0.92	4.26-60.52; 1.00	3.04-51.74; 1.00
collected reflections; $R_\sigma$	105568; 0.0393	31921; 0.0750	29766; 0.0513	135190; 0.0835
unique reflections; $R_{\text{int}}$	9865; 0.0696	5297; 0.1083	3676; 0.1041	17792; 0.0884
$R1(F)$ ( $I > 2\sigma(I)$ )	0.0538	0.1236	0.0397	0.0462
w $R(F^2)$ (all data)	0.1690	0.3339	0.1050	0.1069
GoF( $F^2$ ); Flack-x	1.046; -	1.149; -	1.030; -	0.971; 0.013(4)
Residual electron density	0.503; -0.553	0.844; -0.499	0.820; -0.306	0.389; -0.369



Table 4.VI. continued

	4.11	4.3b	4.5b	4.6b
Formula	C <sub>83</sub> H <sub>80</sub> Cl <sub>4</sub> Cu <sub>4</sub> N <sub>12</sub> O <sub>4</sub>	C <sub>52</sub> H <sub>64</sub> Cu <sub>2</sub> N <sub>8</sub> O <sub>2</sub>	C <sub>50</sub> H <sub>86</sub> Cu <sub>2</sub> N <sub>8</sub> O <sub>2</sub>	C <sub>72</sub> H <sub>72</sub> Cu <sub>2</sub> N <sub>8</sub> O <sub>2</sub>
$M_w$ (g/mol); $d_{\text{calcd.}}$ (g/cm <sup>3</sup> )	1705.55; 1.434	960.18; 1.324	958.34; 1.204	1208.46; 1.315
$T$ (K); F(000)	150; 1756	100; 506	100; 2064	100; 634
Crystal System	Monoclinic	Triclinic	Monoclinic	Triclinic
Space Group	$P2_1$	$P(-1)$	$P2_1/c$	$P(-1)$
Unit Cell: $a$ (Å)	11.0600(3)	8.3826(2)	20.8712(8)	8.9820(2)
$b$ (Å)	14.0679(4)	11.8929(3)	18.6639(7)	12.8014(3)
$c$ (Å)	25.6816(8)	12.1630(4)	16.5276(6)	14.7994(4)
$\alpha$ (°)	90	84.5180(10)	90	108.3040(10)
$\beta$ (°)	98.562(2)	86.8510(10)	124.818(2)	92.065(2)
$\gamma$ (°)	90	87.8100(10)	90	107.3560(10)
$V$ (Å <sup>3</sup> ); $Z$	3951.3(2); 2	1204.54(6); 1	5285.5(4); 8	1526.13(7); 1
$\mu$ (mm <sup>-1</sup> ); Abs. Corr.	6.860; multiscan	5.017; multiscan	4.566; multiscan	4.036; multiscan
$\theta$ range (°); completeness	3.13-60.51; 0.99	3.18-60.74; 0.99	3.05-60.65; 1	3.35-58.20; 0.99
collected reflections; $R_\sigma$	146000; 0.0504	19004; 0.0259	43769; 0.0337	45962; 0.0288
unique reflections; $R_{\text{int}}$	17625; 0.0740	5482; 0.0316	6079; 0.0547	6541; 0.0456
$R1(F)$ ( $I > 2\sigma(I)$ )	0.0443	0.0323	0.0450	0.0397
w $R(F^2)$ (all data)	0.1060	0.0870	0.1298	0.1056
GoF( $F^2$ ); Flack-x	1.009; 0.031(3)	1.039; -	1.076; -	1.055; -
Residual electron density	0.580; -0.067	0.404; -0.249	0.758; -0.216	0.694; -0.388

Table 4.VII. continued

	4.7b	4.8b	4.9b	4.10b
Formula	C <sub>48</sub> H <sub>52</sub> Br <sub>4</sub> Cu <sub>2</sub> N <sub>8</sub> O <sub>2</sub>	C <sub>34</sub> H <sub>46</sub> Cu <sub>2</sub> N <sub>6</sub> O <sub>2</sub>	C <sub>32</sub> H <sub>42</sub> Cu <sub>2</sub> N <sub>6</sub> O <sub>2</sub>	C <sub>36</sub> H <sub>50</sub> Cu <sub>2</sub> N <sub>6</sub> O <sub>2</sub>
$M_w$ (g/mol); $d_{\text{calcd.}}$ (g/cm <sup>3</sup> )	1219.7; 1.638	697.85; 1.382	669.79	725.90; 1.346
$T$ (K); F(000)	150; 1220	105; 732	100; 350	100; 764
Crystal System	Monoclinic	Monoclinic	Triclinic	Monoclinic
Space Group	$P2_1/n$	$P2_1/c$	P(-1)	$P2_1$
Unit Cell: $a$ (Å)	7.9349(2)	10.9223(5)	7.7726(2)	8.0880(4)
$b$ (Å)	16.5630(5)	9.6307(5)	10.9081(3)	11.1949(5)
$c$ (Å)	18.9452(6)	16.2975(8)	11.0963(3)	20.1828(10)
$\alpha$ (°)	90	90	111.8750(10)	90
$\beta$ (°)	96.741(2)	101.935(2)	109.6390(10)	101.373(3)
$\gamma$ (°)	90	90	98.8840(10)	90
$V$ (Å <sup>3</sup> ); $Z$	2472.67(13); 2	1677.27(14); 2	779.04(4); 1	1791.56(15); 2
$\mu$ (mm <sup>-1</sup> ); Abs. Corr.	7.512; multiscan	7.052; multiscan	7.579; multiscan	6.618; multiscan
$\theta$ range (°); completeness	3.09-60.60; 0.99	5.38-60.65; 1	5.55-73.41; 0.99	3.89-60.28; 0.98
collected reflections; $R_{\sigma}$	35512; 0.0322	24021; 0.0212	33194; 0.0203	42810; 0.0815
unique reflections; $R_{\text{int}}$	5637; 0.0479	3834; 0.0326	4707; 0.0295	8066; 0.0733
$R1(F)$ ( $I > 2\sigma(I)$ )	0.1081	0.0312	0.0253	0.0489
w $R(F^2)$ (all data)	0.3023	0.0825	0.0726	0.1059
GoF( $F^2$ ); Flack-x	1.167; -	1.026; -	1.074; -	0.974; 0.006(6)
Residual electron density	0.791; -2.989	0.480; -0.224	0.388; -0.590	0.834; -0.242

**Table 4.VII.** continued

	<b>4.11b</b>	<b>4.1c</b>	<b>4.4c</b>	<b>4.2d</b>
Formula	C <sub>34</sub> H <sub>44</sub> Cl <sub>2</sub> Cu <sub>2</sub> N <sub>6</sub> O <sub>2</sub>	C <sub>44</sub> H <sub>44</sub> CuN <sub>6</sub>	C <sub>104</sub> H <sub>72</sub> Cu <sub>2</sub> N <sub>12</sub>	C <sub>40</sub> H <sub>36</sub> Cu <sub>2</sub> N <sub>6</sub>
$M_w$ (g/mol); $d_{\text{calcd.}}$ (g/cm <sup>3</sup> )	766.73; 1.453	720.39; 1.230	1616.82; 1.399	727.83; 1.425
$T$ (K); F(000)	100; 796	150; 758	150; 838	150; 752
Crystal System	Monoclinic	Orthorhombic	Triclinic	Triclinic
Space Group	$P2_1$	$I222$	$P(-1)$	$P(-1)$
Unit Cell: $a$ (Å)	8.2284(3)	11.4846(6)	12.0028(5)	11.5640(5)
$b$ (Å)	11.4891(4)	11.8990(6)	12.5017(6)	12.2066(5)
$c$ (Å)	18.5757(7)	14.2302(8)	14.1183(7)	13.6507(6)
$\alpha$ (°)	90	90	108.106(2)	65.305(3)
$\beta$ (°)	93.444(2)	90	95.140(2)	86.166(3)
$\gamma$ (°)	90	90	104.308(2)	75.908(3)
$V$ (Å <sup>3</sup> ); $Z$	1752.92(11); 2	1944.63(18); 2	1919.06(16); 1	1696.66(13); 1
$\mu$ (mm <sup>-1</sup> ); Abs. Corr.	7.682; multiscan	3.218; multiscan	1.168; multiscan	7.579; multiscan
$\theta$ range (°); completeness	3.94-60.70; 0.93	4.30-60.69; 0.99	3.34-70.41; 0.99	5.55-73.41; 0.97
collected reflections; $R_\sigma$	46940; 0.0457	16160; 0.0557	79946; 0.0308	71303; 0.0322
unique reflections; $R_{\text{int}}$	7511; 0.0528	2158; 0.0727	7262; 0.0676	7577; 0.0528
$R1(F)$ ( $I > 2\sigma(I)$ )	0.0389	0.0646	0.0420	0.0361
w $R(F^2)$ (all data)	0.0874	0.1865	0.1194	0.0796
GoF( $F^2$ ); Flack-x	1.071; 0.029(5)	1.018; 0.059(11)	1.034; -	1.048; -
Residual electron density	0.496; -0.353	1.157; -0.287	0.600; -0.418	0.364; -0.200

**Table 4.VII.** continued

	<b>4.3d</b>	<b>4.1e</b>	<b>4.4e</b>	<b>4.6e</b>
Formula	C <sub>176</sub> H <sub>176</sub> Cu <sub>8</sub> N <sub>24</sub>	C <sub>30</sub> H <sub>42</sub> ClCu <sub>2</sub> N <sub>5</sub> O <sub>2</sub>	C <sub>34</sub> H <sub>38</sub> ClCu <sub>2</sub> N <sub>5</sub> O <sub>2</sub>	C <sub>132</sub> H <sub>114</sub> Cl <sub>3</sub> Cu <sub>6</sub> N <sub>15</sub> O <sub>6</sub>
$M_w$ (g/mol); $d_{\text{calcd.}}$ (g/cm <sup>3</sup> )	3135.72; 1.341	667.21; 1.410	711.22; 1.378	2493.97; 1.439
$T$ (K); F(000)	100; 3264	100; 1.410	150; 1472	100; 3852
Crystal System	Triclinic	Orthorhombic	Monoclinic	Trigonal
Space Group	$P(-1)$	$P2_12_12_1$	$P2_1/n$	$P3_1$
Unit Cell:				
$a$ (Å)	16.9662(5)	7.7265(3)	8.9264(2)	31.2224(8)
$b$ (Å)	17.0172(5)	10.4915(4)	20.9447(5)	31.2224(8)
$c$ (Å)	27.7039(8)	38.7654(16)	18.3428(4)	10.2301(3)
$\alpha$ (°)	94.9220(10)	90	90	90
$\beta$ (°)	102.9600(10)	90	91.8330(10)	90
$\gamma$ (°)	90.0790(10)	90	90	120
$V$ (Å <sup>3</sup> ); $Z$	7764.3(4); 2	3142.4(2); 4	3427.63(13); 4	8636.6(5); 3
$\mu$ (mm <sup>-1</sup> ); Abs. Corr.	6.106; multiscan	8.006; multiscan	2.536; multiscan	6.647; multiscan
$\theta$ range (°); completeness	3.22-59.38; 1	3.97- 57.76; 1	4.86-72.11; 0.99	2.46-60.80; 0.98
collected reflections; $R_\sigma$	35667; 0.0808	40638; 0.1176	46885; 0.0234	148034; 0.0476
unique reflections; $R_{\text{int}}$	35667; 0.1134	7142; 0.1391	6707; 0.0407	24165; 0.0512
$R1(F)$ ( $I > 2\sigma(I)$ )	0.0818	0.0585	0.0312	0.0330
w $R(F^2)$ (all data)	0.2453	0.1330	0.0886	0.0742
GoF( $F^2$ ); Flack- $x$	1.053; -	1.025; 0.026(9)	1.047; -	0.985; -0.007(2)
Residual electron density	0.766; -0.883	0.400; -0.433	0.324 -0.436	0.353; -0.249

## Supporting Information

This material is available free of charge via the Internet at <http://pubs.acs.org>.

## Corresponding Author

\* Email: [Frank.Schaper@umontreal.ca](mailto:Frank.Schaper@umontreal.ca)

## Notes

The authors declare no competing financial interests.

## Acknowledgment

Funding was supplied the NSERC discovery program (RGPIN-2016-04953) and the Centre for Green Chemistry and Catalysis (FQRNT). We thank D. Kapoor and C. Barcha for participation in the preparation of **4.8-4.11b** during their internship. We thank Marie-Christine Tang and Dr. Alexandra Furtos for support with MALDI-MS and Francine Bélanger and Dr. Todd J. J. Whitehorne for support with X-ray crystallography.

## References Chapter 4

(1) (a) Nagarajan, V.; Mohanty, A. K.; Misra, M. *ACS Sustainable Chemistry & Engineering* **2016**, *4*, 2899-2916. (b) Castro-Aguirre, E.; Iñiguez-Franco, F.; Samsudin, H.; Fang, X.; Auras, R. *Advanced Drug Delivery Reviews* **2016**, *107*, 333-366. (c) Slomkowski, S.; Penczek, S.; Duda, A. *Polym. Adv. Technol.* **2014**, *25*, 436-447. (d) Singhvi, M.; Gokhale, D. *RSC Adv.* **2013**, *3*, 13558-13568. (e) Hottle, T. A.; Bilec, M. M.; Landis, A. E. *Polym. Degrad. Stab.* **2013**, *98*, 1898-1907. (f) Inkinen, S.; Hakkarainen, M.; Albertsson, A.-C.; Södergård, A. *Biomacromolecules* **2011**, *12*, 523-532. (g) Ahmed, J.; Varshney, S. K. *Int. J. Food Prop.* **2011**, *14*, 37-58. (h) Vijayakumar, J.; Aravindan, R.; Viruthagiri, T. *Chem. Biochem. Eng. Q.* **2008**, *22*, 245-264. (i) Tokiwa, Y.; Calabia, B. P. *Can. J. Chem.* **2008**, *86*, 548-555. (j) Drumright, R. E.; Gruber, P. R.; Henton, D. E. *Adv. Mater. (Weinheim, Ger.)* **2000**, *12*, 1841-1846.

(2) Vink, E. T. H.; Rábago, K. R.; Glassner, D. A.; Springs, B.; O'Connor, R. P.; Kolstad, J.; Gruber, P. R. *Macromol. Biosci.* **2004**, *4*, 551-564.

(3) (a) Paul, S.; Zhu, Y.; Romain, C.; Brooks, R.; Saini, P. K.; Williams, C. K. *Chem. Commun. (Cambridge, U. K.)* **2015**, *51*, 6459-6479. (b) dos Santos Vieira, I.; Herres-Pawlis, S. *Eur. J. Inorg. Chem.* **2012**, *2012*, 765-774. (c) Dutta, S.; Hung, W.-C.; Huang, B.-H.; Lin, C.-C. In *Synthetic Biodegradable Polymers*, Rieger, B.; Künkel, A.; Coates, G. W.; Reichardt, R.; Dinjus, E.; Zevaco, T. A., Eds. Springer-Verlag: Berlin, 2011; Vol. pp 219-284. (d) Dijkstra, P. J.; Du, H.; Feijen, J. *Polym. Chem.* **2011**, *2*, 520-527. (e) Buffet, J.-C.; Okuda, J. *Polym. Chem.* **2011**, *2*, 2758-2763. (f) Thomas, C. M. *Chem. Soc. Rev.* **2010**, *39*, 165. (g) Stanford, M. J.; Dove, A. P. *Chem. Soc. Rev.* **2010**, *39*, 486-494. (h) Williams, C. K.; Hillmyer, M. A. *Polym. Rev.* **2008**, *48*, 1-10. (i) Ajellal, N.; Carpentier, J.-F.; Guillaume, C.; Guillaume, S. M.; Helou, M.; Poirier, V.; Sarazin, Y.; Trifonov, A. *Dalton Trans.* **2010**, *39*, 8363. (j) Platel, R. H.; Hodgson, L. M.; Williams, C. K. *Polym. Rev.* **2008**, *48*, 11 - 63. (k) Wu, J.; Yu, T.-L.; Chen, C.-T.; Lin, C.-C. *Coord. Chem. Rev.* **2006**, *250*, 602-626. (l) Dechy-Cabaret, O.; Martin-Vaca, B.; Bourissou, D. *Chem. Rev.* **2004**, *104*, 6147-6176. (m) O'Keefe, B. J.; Hillmyer, M. A.; Tolman, W. B. *J. Chem. Soc., Dalton Trans.* **2001**, 2215-2224. (n) Chisholm, M. H.; Zhou, Z. *J. Mater. Chem.* **2004**, *14*,

3081. (o) Zhong, Z.; Dijkstra, P. J.; Feijen, J. *J. Biomater. Sci., Polym. Ed.* **2004**, *15*, 929-946. (p) Huang, B. H.; Dutta, S.; Lin, C. C. In *Comprehensive Inorganic Chemistry II (Second Edition)*, Poeppelemeier, J. R., Ed. Elsevier: Amsterdam, 2013; Vol. pp 1217-1249. (q) Wheaton, C. A.; Hayes, P. G. *Comments Inorg. Chem.* **2011**, *32*, 127-162. (r) Wheaton, C. A.; Hayes, P. G.; Ireland, B. J. *Dalton Trans.* **2009**, 4832 - 4846. (s) Sutar, A. K.; Maharana, T.; Dutta, S.; Chen, C.-T.; Lin, C.-C. *Chem. Soc. Rev.* **2010**, *39*, 1724-1746. (t) Le Roux, E. *Coord. Chem. Rev.* **2016**, *306*, 65-85. (u) Sauer, A.; Kapelski, A.; Fliedel, C.; Dagorne, S.; Kol, M.; Okuda, J. *Dalton Trans.* **2013**, *42*, 9007-9023. (v) MacDonald, J. P.; Shaver, M. P. In *Green Polymer Chemistry: Biobased Materials and Biocatalysis*, American Chemical Society: 2015; Vol. 1192, pp 147-167. (w) Jianming, R.; Anguo, X.; Hongwei, W.; Hailin, Y. *Des. Monomers Polym.* **2013**, *17*, 345-355. (x) Dagorne, S.; Normand, M.; Kirillov, E.; Carpentier, J.-F. *Coord. Chem. Rev.* **2013**, *257*, 1869-1886. (y) Dagorne, S.; Fliedel, C. In *Modern Organoaluminum Reagents: Preparation, Structure, Reactivity and Use*, Woodward, S.; Dagorne, S., Eds. Springer Berlin Heidelberg: Berlin, Heidelberg, 2013; Vol. pp 125-171. (z) Dagorne, S.; Fliedel, C.; de Frémont, P. In *Encyclopedia of Inorganic and Bioinorganic Chemistry*, John Wiley & Sons, Ltd: 2011; Vol. (aa) Amgoune, A.; Thomas, C. M.; Carpentier, J.-F. *Pure Appl. Chem.* **2007**, *79*, 2013-2030.

(4) (a) Xu, T.-Q.; Yang, G.-W.; Liu, C.; Lu, X.-B. *Macromolecules* **2017**, *50*, 515-522. (b) Bhattacharjee, J.; Harinath, A.; Nayek, H. P.; Sarkar, A.; Panda, T. K. *Chem.-Eur. J.* **2017**, *23*, 9319-9331. (c) Myers, D.; White, A. J. P.; Forsyth, C. M.; Bown, M.; Williams, C. K. *Angew. Chem., Int. Ed.* **2017**, *56*, 5277-5282. (d) Rosen, T.; Popowski, Y.; Goldberg, I.; Kol, M. *Chem.-Eur. J.* **2016**, *22*, 11533-11536. (e) Sun, Y.; Xiong, J.; Dai, Z.; Pan, X.; Tang, N.; Wu, J. *Inorg. Chem.* **2016**, *55*, 136-143. (f) McKeown, P.; Davidson, M. G.; Kociok-Kohn, G.; Jones, M. D. *Chem. Commun. (Cambridge, U. K.)* **2016**, *52*, 10431-10434. (g) Wang, H.; Yang, Y.; Ma, H. *Macromolecules* **2014**, *47*, 7750-7764. (h) Mou, Z.; Liu, B.; Wang, M.; Xie, H.; Li, P.; Li, L.; Li, S.; Cui, D. *Chem. Commun. (Cambridge, U. K.)* **2014**, *50*, 11411-11414. (i) Bakewell, C.; White, A. J. P.; Long, N. J.; Williams, C. K. *Angew. Chem., Int. Ed.*

**2014**, *53*, 9226-9230. (j) Aluthge, D. C.; Patrick, B. O.; Mehrkhodavandi, P. *Chem. Commun. (Cambridge, U. K.)* **2013**, *49*, 4295-4297.

(5) (a) Herber, U.; Hegner, K.; Wolters, D.; Siris, R.; Wrobel, K.; Hoffmann, A.; Lochenie, C.; Weber, B.; Kuckling, D.; Herres-Pawlis, S. *Eur. J. Inorg. Chem.* **2017**, *2017*, 1341-1354. (b) Brown, L. A.; Wekesa, F. S.; Unruh, D. K.; Findlater, M.; Long, B. K. *J. Polym. Sci., Part A: Polym. Chem.* **2017**, *55*, 2824-2830. (c) Delle Chiaie, K. R.; Yablon, L. M.; Biernesser, A. B.; Michalowski, G. R.; Sudyn, A. W.; Byers, J. A. *Polym. Chem.* **2016**, *7*, 4675-4681. (d) Biernesser, A. B.; Delle Chiaie, K. R.; Curley, J. B.; Byers, J. A. *Angew. Chem., Int. Ed.* **2016**, *55*, 5251-5254. (e) Manna, C. M.; Kaur, A.; Yablon, L. M.; Haeffner, F.; Li, B.; Byers, J. A. *J. Am. Chem. Soc.* **2015**, *137*, 14232-14235. (f) Kundys, A.; Plichta, A.; Florjańczyk, Z.; Frydrych, A.; Żurawski, K. *J. Polym. Sci., Part A: Polym. Chem.* **2015**, *53*, 1444-1456. (g) Silvino, A. C.; Rodrigues, A. L. C.; Resende, J. A. L. C. *Inorg. Chem. Commun.* **2015**, *55*, 39-42. (h) Keuchguerian, A.; Mougang-Soume, B.; Schaper, F.; Zargarian, D. *Can. J. Chem.* **2015**, *93*, 594-601. (i) Kang, Y. Y.; Park, H.-R.; Lee, M. H.; An, J.; Kim, Y.; Lee, J. *Polyhedron* **2015**, *95*, 24-29. (j) Giese, S. O. K.; Egevardt, C.; Rüdiger, A. L.; Saj, E. L.; Silva, T. A.; Zawadzki, S. F.; Soares, J. F.; Nunes, G. G. *J. Braz. Chem. Soc.* **2015**, *26*, 2258-2268. (k) Lei, Y.-N.; Zhu, Y.-B.; Gong, C.-F.; Lv, J.-J.; Kang, C.; Hou, L.-X. *J Mater Sci: Mater Med* **2014**, *25*, 273-282. (l) Egevardt, C.; Giese, S. O. K.; da C. Santos, A. D.; Barison, A.; de Sá, E. L.; Filho, A. Z.; da Silva, T. A.; Zawadzki, S. F.; Soares, J. F.; Nunes, G. G. *J. Polym. Sci., Part A: Polym. Chem.* **2014**, *52*, 2509-2517. (m) Manna, C. M.; Kaplan, H. Z.; Li, B.; Byers, J. A. *Polyhedron* **2014**, *84*, 160-167. (n) Biernesser, A. B.; Li, B.; Byers, J. A. *J. Am. Chem. Soc.* **2013**, *135*, 16553-16560. (o) Idage, B. B.; Idage, S. B.; Kasegaonkar, A. S.; Jadhav, R. V. *Mater. Sci. Eng., B* **2010**, *168*, 193-198. (p) Chen, J.; Gorczynski, J. L.; Zhang, G.; Fraser, C. L. *Macromolecules* **2010**, *43*, 4909-4920. (q) Wang, X.; Liao, K.; Quan, D.; Wu, Q. *Macromolecules* **2005**, *38*, 4611-4617. (r) Gorczynski, J. L.; Chen, J.; Fraser, C. L. *J. Am. Chem. Soc.* **2005**, *127*, 14956-14957. (s) McGuinness, D. S.; Marshall, E. L.; Gibson, V. C.; Steed, J. W. *J. Polym. Sci., Part A: Polym. Chem.* **2003**, *41*, 3798-3803. (t) O'Keefe, B. J.; Breyfogle, L. E.; Hillmyer, M. A.; Tolman, W. B. *J. Am. Chem. Soc.* **2002**, *124*, 4384-4393. (u) Gibson, V. C.;



Marshall, E. L.; Navarro-Llobet, D.; White, A. J. P.; Williams, D. J. *J. Chem. Soc., Dalton Trans.* **2002**, 4321-4322. (v) O'Keefe, B. J.; Monnier, S. M.; Hillmyer, M. A.; Tolman, W. B. *J. Am. Chem. Soc.* **2001**, *123*, 339-340. (w) Stolt, M.; Södergård, A. *Macromolecules* **1999**, *32*, 6412-6417. (x) Södergård, A.; Stolt, M. *Macromol. Symp.* **1998**, *130*, 393-402. (y) Kricheldorf, H. R.; Damrau, D.-O. *Macromol. Chem. Phys.* **1997**, *198*, 1767-1774.

(6) (a) Ahn, S. H.; Chun, M. K.; Kim, E.; Jeong, J. H.; Nayab, S.; Lee, H. *Polyhedron* **2017**, *127*, 51-58. (b) Cho, J.; Nayab, S.; Jeong, J. H. *Polyhedron* **2016**, *113*, 81-87. (c) Kwon, K. S.; Cho, J.; Nayab, S.; Jeong, J. H. *Inorg. Chem. Commun.* **2015**, *55*, 36-38. (d) Akpan, E. D.; Ojwach, S. O.; Omondi, B.; Nyamori, V. O. *New J. Chem.* **2016**, *40*, 3499-3510. (e) Routaray, A.; Nath, N.; Maharana, T.; Sahoo, P. K.; Das, J. P.; Sutar, A. K. *J Chem Sci* **2016**, *128*, 883-891. (f) Routaray, A.; Nath, N.; Mantri, S.; Maharana, T.; Sutar, A. K. *Chin. J. Cat.* **2015**, *36*, 764-770. (g) Routaray, A.; Nath, N.; Maharana, T.; Sutar, A. k. *J. Macromol. Sci., Part A: Pure Appl. Chem.* **2015**, *52*, 444-453. (h) Fortun, S.; Daneshmand, P.; Schaper, F. *Angew. Chem., Int. Ed.* **2015**, *54*, 13669-13672. (i) Whitehorne, T. J. J.; Schaper, F. *Can. J. Chem.* **2014**, *92*, 206-214. (j) Whitehorne, T. J. J.; Schaper, F. *Inorg. Chem.* **2013**, *52*, 13612-13622. (k) Whitehorne, T. J. J.; Schaper, F. *Chem. Commun. (Cambridge, U. K.)* **2012**, *48*, 10334-10336. (l) Appavoo, D.; Omondi, B.; Guzei, I. A.; van Wyk, J. L.; Zinyemba, O.; Darkwa, J. *Polyhedron* **2014**, *69*, 55-60. (m) Li, C.-Y.; Hsu, S.-J.; Lin, C.-I.; Tsai, C.-Y.; Wang, J.-H.; Ko, B.-T.; Lin, C.-H.; Huang, H.-Y. *J. Polym. Sci., Part A: Polym. Chem.* **2013**, *51*, 3840-3849. (n) Gowda, R. R.; Chakraborty, D. *J. Molec. Catal. A: Chem.* **2011**, *349*, 86-93. (o) Chen, L.-L.; Ding, L.-Q.; Zeng, C.; Long, Y.; Lü, X.-Q.; Song, J.-R.; Fan, D.-D.; Jin, W.-J. *Appl. Organomet. Chem.* **2011**, *25*, 310-316. (p) Bhunora, S.; Mugo, J.; Bhaw-Luximon, A.; Mapolie, S.; Van Wyk, J.; Darkwa, J.; Nordlander, E. *Appl. Organomet. Chem.* **2011**, *25*, 133-145. (q) John, A.; Katiyar, V.; Pang, K.; Shaikh, M. M.; Nanavati, H.; Ghosh, P. *Polyhedron* **2007**, *26*, 4033-4044. (r) Sun, J.; Shi, W.; Chen, D.; Liang, C. *J. Appl. Polym. Sci.* **2002**, *86*, 3312-3315.

(7) Daneshmand, P.; van der Est, A.; Schaper, F. *ACS Catal.* **2017**, *7*, 6289-6301.

(8) Matsuo, Y.; Mashima, K.; Tani, K. *Organometallics* **2001**, *20*, 3510-3518.

- (9) Kerr, W. J.; Middleditch, M.; Watson, A. J. B. *Synlett* **2011**, 2011, 177-180.
- (10) Lin, M.; Cao, Y.; Pei, H.; Chen, Y.; Wu, J.; Li, Y.; Liu, W. *RSC Adv.* **2014**, 4, 9255-9260.
- (11) Groom, C. R.; Bruno, I. J.; Lightfoot, M. P.; Ward, S. C. *Acta Crystallogr., Sect. B: Struct. Sci.* **2016**, 72, 171-179.
- (12) (a) Adams, H.; Bailey, N. A.; Fenton, D. E.; Moss, S.; Jones, G. *Inorg. Chim. Acta* **1984**, 83, L79-L80. (b) Adams, H.; Bailey, N. A.; Fenton, D. E.; Moss, S.; de Barbarin, C. O. R.; Jones, G. *J. Chem. Soc., Dalton Trans.* **1986**, 693-699.
- (13) Vignesh Babu, H.; Muralidharan, K. *Dalton Trans.* **2013**, 42, 1238-1248.
- (14) (a) Schmid, M.; Guillaume, S. M.; Roesky, P. W. *J. Organomet. Chem.* **2013**, 744, 68-73. (b) Babu, H. V.; Muralidharan, K. *RSC Adv.* **2014**, 4, 6094-6102.
- (15) The structure of all crystalline material was verified by single-crystal X-ray diffraction studies using a fast, low-resolution data collection. The latter allowed to unambiguously assign the structure (i. e. connectivity). A full data set, suitable to yield geometrical data, was collected only once for each structure.
- (16) Hathaway, B. J.; Billing, D. E. *Coord. Chem. Rev.* **1970**, 5, 143-207.
- (17) Halcrow, M. A. *Dalton Trans.* **2003**, 4375-4384.
- (18) Yang, L.; Powell, D. R.; Houser, R. P. *Dalton Trans.* **2007**, 955-964.
- (19) Rakshit, R.; Ghorai, S.; Biswas, S.; Mukherjee, C. *Inorg. Chem.* **2014**, 53, 3333-3337.
- (20) Addison, A. W.; Rao, T. N.; Reedijk, J.; van Rijn, J.; Verschoor, G. C. *J. Chem. Soc., Dalton Trans.* **1984**, 1349-1356.
- (21) Drouin, F.; Oguadinma, P. O.; Whitehorne, T. J. J.; Prud'homme, R. E.; Schaper, F. *Organometallics* **2010**, 29, 2139-2147.
- (22) In agreement with this, average C(R)-N-Cu angles increase in the order R = H < R = CH(=N) < R = Cl. The differences are, however, comparable to or smaller than the margin of error.
- (23) We do not obtain a polymer blend. Due to the protonation of a polymerylalkoxy group by pyridylmethanol, these reactions are by default under immortal polymerisation conditions and rapid chain-transfer between catalytic centers is enforced by the external alcohol. The resulting polymer is thus a homogenous

polymer the isotacticity of which is determined by the averaged  $P_m$  values of **5.1** and **5.1b**.

(24) Ma, H.; Spaniol, T. P.; Okuda, J. *Angew. Chem., Int. Ed.* **2006**, *45*, 7818-7821.

(25) Jones, M. D.; Hancock, S. L.; McKeown, P.; Schafer, P. M.; Buchard, A.; Thomas, L. H.; Mahon, M. F.; Lowe, J. P. *Chem. Commun. (Cambridge, U. K.)* **2014**, *50*, 15967-15970.

(26) Complex **5.7** showed reduced polymer molecular weights which correspond to 2 chains per catalyst dimer. An alternative explanation for the lack of stereocontrol, would thus be that **5.7** is the only complex in which both pyridyl methoxide ligands initiate polymerization. However, there is no rationale for a different reactivity of the pyridyl methoxide ligands in **5.7**. A high polydispersity and MALDI-MS spectra (Fig. 5.S19) indicate that the low polymer molecular weight is rather caused by transesterification reactions.

(27) Singh, J. V.; Baranwal, B. P.; Mehrotra, R. C. *Z. Anorg. Allg. Chem.* **1981**, *477*, 235-240.

(28) Knizhnikov, V. A.; Borisova, N. E.; Yurashevich, N. Y.; Popova, L. A.; Chernyad'ev, A. Y.; Zubreichuk, Z. P.; Reshetova, M. D. *Russ. J. Org. Chem.* **2007**, *43*, 855-860.

(29) Kancharla, P.; Kelly, J. X.; Reynolds, K. A. *J. Med. Chem.* **2015**, *58*, 7286-7309.

(30) Save, M.; Schappacher, M.; Soum, A. *Macromol. Chem. Phys.* **2002**, *203*, 889-899.

(31) *APEX2*, Release 2.1-0; Bruker AXS Inc.: Madison, USA, 2006.

(32) *SAINT*, Release 7.34A; Bruker AXS Inc.: Madison, USA, 2006.

(33) Sheldrick, G. M. *SADABS*, Bruker AXS Inc.: Madison, USA, 1996 & 2004.

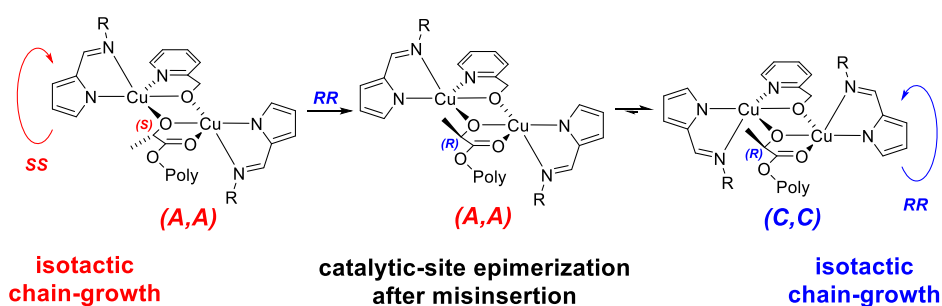
(34) Sheldrick, G. *Acta Crystallogr. Sect. A: Found. Crystallogr.* **2015**, *71*, 3-8.

(35) Sheldrick, G. M. *Acta Crystallogr.* **2008**, *A64*, 112-122.



## Chapter 5 . Catalytic-site-mediated chain-end control in the polymerization of *rac*-lactide with copper iminopyrrolide complexes

Daneshmand, P.; Jiménez-Santiago, J. L.; Aragon-Alberti, M.; Schaper, F. Catalytic-site-mediated chain-end control in the polymerization of *rac*-lactide with copper iminopyrrolide complexes. *Organometallics*, **2018**, *37*, 1751–1759.



Reprinted with permission from *Organometallics*. Copyright 2017 American Chemical Society.

Contributions of F. Schaper: A first draft was provided by me with major modification from Prof. Frank Schaper.

Contributions of J. L. Santiago: Synthesis of two ligands and a copper complex during his internship under my supervision.

Contribution of M. Aragon-Alberti: Synthesis of a ligand during his internship under my supervision.



# Catalytic-site-mediated chain-end control in the polymerization of *rac*-lactide with copper iminopyrrolide complexes

Pargol Daneshmand, José L. Jiménez-Santiago, Maxime Aragon--Alberti, Frank Schaper\*

*Centre in Green Chemistry and Catalysis, Department of Chemistry, Université de Montréal, C. P. 6128 Succ. Centre-Ville, Montréal, QC, H3T 3J7, Canada.*

*Supporting Information Placeholder*

## Abstract

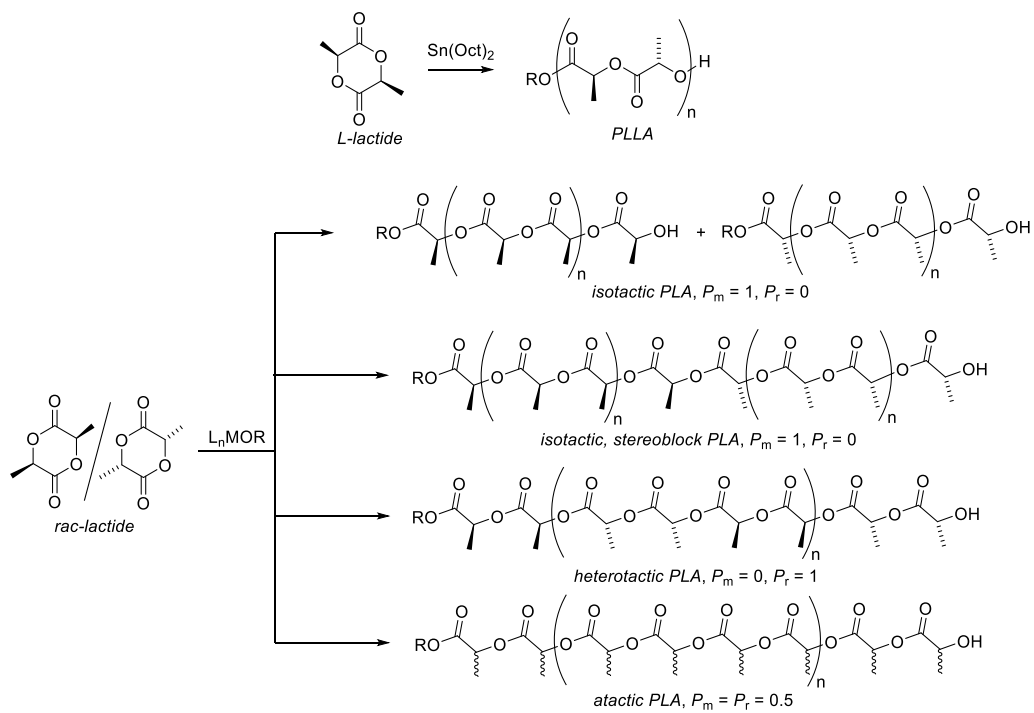
Reaction of copper(II) methoxide with *N*-R-2-iminopyrroles (LH) and pyridylmethanol (R'OH) provided the dinuclear complexes  $\{\text{LCu}(\mu\text{-OR}')\}_2$  (R = naphthyl, CHPh<sub>2</sub>, 2,6-xylyl, 2,6-diisopropylphenyl (diip), or *p*-bromobenzyl). All complexes crystallized as dinuclear compounds with a square-pyramidal coordination geometry around copper and either imine or pyridine (for R = diip) in the apical position. The naphthyl-substituted complex was inactive in *rac*-lactide polymerization at room temperature in benzene. All other complexes showed good activity with apparent rate constants of  $k_{\text{obs}} = 0.16(1) - 1.89(8) \text{ h}^{-1}$  at 2 mM catalyst concentration. All complexes showed a preference for slight isotactic monomer enchainment with  $P_m = 0.60 - 0.68$ . Stereoerror analysis indicate that the chain-end determines stereocontrol. An influence of stereocontrol on the steric bulk of the ligand, on the initial monomer concentration and on the symmetry of the catalytic site support that the chiral information of the chain-end is mediated via the catalytic site (*catalytic-site mediated chain-end control*).

## Introduction

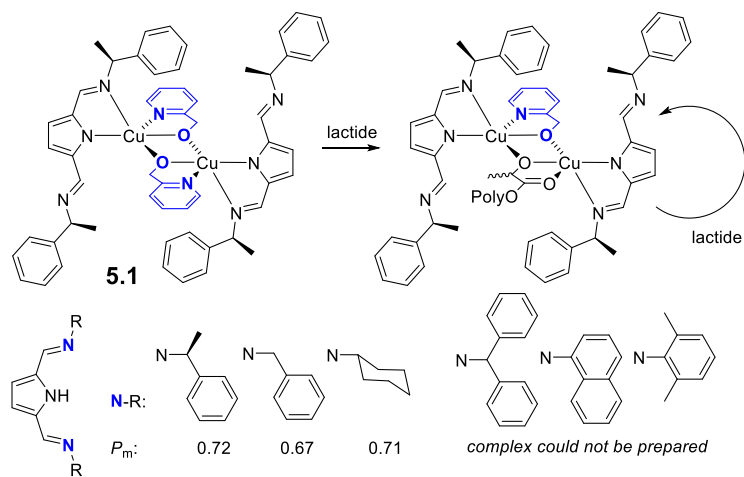
Poly(lactic acid) (PLA) is the most important biodegradable polyester and typically obtained by ring-opening polymerization of lactide, the dimeric anhydride of lactic acid (Scheme 5.1).<sup>1-11</sup> Given its increasing economic importance and the currently unselective polymerization catalysis employed by industry, a large number of academic studies have focused – with varying success – on providing catalyst systems which allow the control of stereochemistry and reactivity in lactide polymerization.<sup>12-38</sup> Unlike the industrially employed polymerization of *L*-lactide, which can only provide isotactic PLLA, polymerization of racemic lactide can give rise to atactic polymer in the absence of stereocontrol. Stereocontrolled polymerization provides isotactic or heterotactic polymer with different degrees of stereoselectivity (Scheme 5.1), of which only isotactic PLA is of current industrial interest. Typically, high degrees of heterotacticity are comparatively easily achieved, while highly active, isoselective polymerization still poses a catalytic challenge.<sup>39-48</sup> Coordination-insertion polymerization catalyzed by a discrete metal alkoxide species is the most employed mechanism.

For various reasons, such as the general biocompatibility and the ease of complex characterization by <sup>1</sup>H NMR, most studies focused on d<sup>0</sup>- or d<sup>10</sup>-metal systems. Mid- to late d<sup>n</sup>-transition metal complexes, on the other hand, have been sparingly studied. Very few studies investigated the performance of Cr,<sup>49</sup> Mn,<sup>50-53</sup> or Co systems.<sup>51, 54, 55</sup> Next to iron,<sup>52, 56-81</sup> copper complexes received the highest attention.<sup>82-104</sup> We have reported that the copper diiminopyrrolide complex **1** polymerizes *rac*-lactide with an isoselectivity of  $P_m = 0.7$  at room temperature (Scheme 5.2).<sup>94</sup> Isoselective stereocontrol was unprecedented for copper complexes. The copper complexes remain dinuclear throughout polymerization and successful stereocontrol depends on the presence of a bridging pyridylmethoxide ligand in the active species (Scheme 5.2).<sup>85</sup>

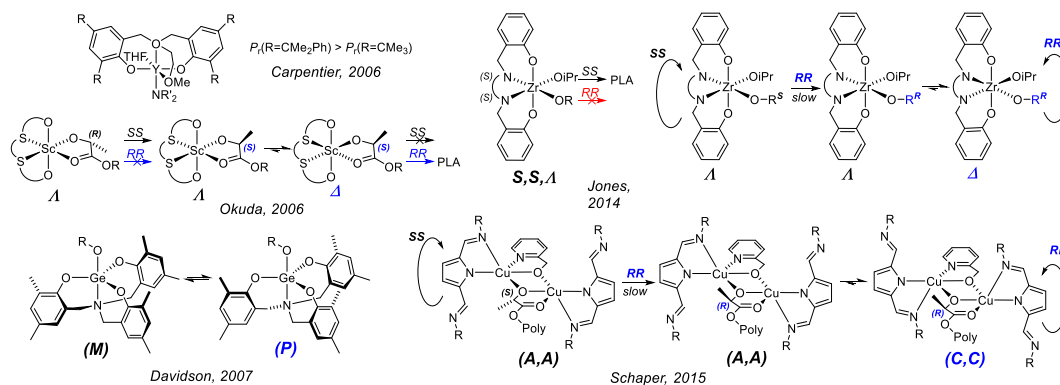




Scheme 5.1.



Scheme 5.2.



**Scheme 5.3.** Catalyst systems showing catalytic-site mediated chain-end control. *RR* and *SS* denote *R,R*- and *S,S*-lactide

The stereocontrol mechanism proposed for lactide polymerization with copper iminopyrrolide complexes was *catalytic-site mediated chain-end control*.<sup>105, 106</sup> In this mechanism the chiral information is derived from the polymer chain end, which in turn determines the configuration of the flexible catalytic site. Monomer selectivity is then either enhanced or even determined by the configuration of the catalytic site. The mechanism is based on initial observations by Carpentier and Okuda that increased flexibility of the ligand/catalytic site led to increased heterotactic stereocontrol (Scheme 5.3).<sup>105, 106</sup> Okuda proposed that heterotactic stereocontrol involves catalytic-site inversion after each insertion step.<sup>105</sup> Davidson proposed that a similar mechanism is in place for  $C_3$ -symmetric germanium and zirconium complexes.<sup>107, 108</sup> Jones obtained isotactic PLA using zirconium complexes with either chiral or achiral ligands.<sup>109, 110</sup> With chiral ligands, the complexes are locked into either  $\Delta$ - or  $\Lambda$ - configuration and stereocontrol follows catalytic-site control. Achiral ligands allow  $\Delta/\Lambda$ -isomerization, and epimerization of the catalytic site after a misinsertion led to stereoblock PLA obtained by (catalytic-site mediated) chain-end control. Copper diiminopyrrolides, such as **5.1**, follow a similar mechanism, in which catalytic-site epimerization is assisted by coordination of the pendant imine (Scheme 5.4). A *catalytic-site mediated chain-end control* combines advantages of the more typical *catalytic-site control* and *chain-end control* mechanisms: (a) Chain-end control and catalytic-site control are often both present in lactide polymerization and – in isotactic catalysts – often with opposing stereoselectivities. (b) Chain-end control

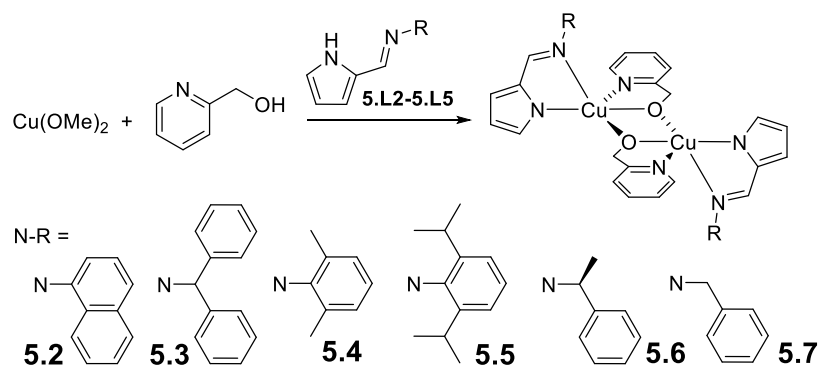
provides longer isotactic blocks with the same degree of control, since only one *r*-diad is introduced per stereoerror. (c) Chain-end control mechanisms are less influenced by fast chain-transfer reactions and thus more suitable for immortal polymerizations. (d) Since monomer selection is governed by the catalytic-site, stereocontrol can thus be more directly influenced than in pure chain-end control. (e) No chiral ligands are required as long as a chiral catalytic site is formed. Despite the advantages of this mechanism, only the very few cases above have been reported, and the stereocontrol mechanism was often more postulated than proven. The same, unfortunately, was also true for diiminopyrrolide complex **5.1**. In the following we will offer further evidence to confirm the existence of this rather unusual stereocontrol mechanism.

## Results and discussion

### *Impact of sterically bulky ligands on stereocontrol.*

Given the strong implication of the catalytic site in the proposed stereocontrol mechanism, a notable influence of the steric bulk provided by the ligand on selectivity would have been expected. Unfortunately, variations of the *N*-substituent in **5.1** either provided complexes with very similar stereocontrol or, for sterically demanding *N*-CHPh<sub>2</sub>, *N*-naphthyl, or *N*-xylyl substituents, the complexes were synthetically not accessible (Scheme 5.2).<sup>84</sup> Influence of ligand steric bulk was thus investigated for the respective *monoiminopyrrolide* complexes, in the expectation that the removal of one imino-substituent would allow the incorporation of a wider range of *N*-substituents.

Synthesis of ligands 5.L2-5.L5 followed either literature protocols or procedures successfully employed for similar ligands (see Experimental Section). The corresponding mono-iminopyrrolide complexes **5.2-5.4** were accessible using the same synthetic protocols employed for **5.1** (Scheme 5.4). In addition, complex **5.5**, containing a *N*-2,6-diisopropylphenyl (diip) substituent was prepared using the same methodology. Monoiminopyrrolide complexes **5.6** and **5.7** with methylbenzyl and benzyl *N*-iminosubstituents have been prepared previously.<sup>85, 94</sup>



#### Scheme 5.4.

All complexes were characterized by X-ray diffraction studies. Previously obtained diimino- and monoiminopyrrolide complexes  $\text{LCu}(\text{OR})$  typically form dinuclear copper complexes with a square-pyramidal coordination geometry around copper. The pyrrolide nitrogen and the bridging alkoxides were always found in the equatorial plane, while either the pyridyl or the imino group occupied the axial position.<sup>84, 85, 94</sup> Complexes **5.2-5.5** follow the same structural pattern (Fig. 5.1): despite  $\tau$  values up to 0.7,<sup>111</sup> the coordination geometry around copper is best described as square-pyramidal with two short Cu-N distances, two short Cu-O distances and one elongated Cu-N distance to the ligand in the apical position (Table 5.I). Complexes **5.2-5.4**, as well as **5.6**,<sup>85</sup> display the imino group in the apical position. The *N*-dipp complex **5** coordinates the pyridyl group in the apical position instead of the imine (Fig. 5.1, Table 5.I). While it is tempting to ascribe this to the increased steric bulk of the diip substituent, coordination of the pyridyl group in the apical position was also favored upon *reducing* the steric bulk from *N*-CH(Me)Ph in **5.6** to *N*-CH<sub>2</sub>Ph in **7**.<sup>84, 85</sup> In general, bond distances and angles do not show any clear dependence on the bulk of the *N*-imino substituent. In concurrence with earlier findings, iminopyrrolide complexes **5.2-5.5** thus show an invariant structural motive (square-pyramidal coordination with the anionic ligands in equatorial positions) combined with a flexibility of the remaining coordination geometry.

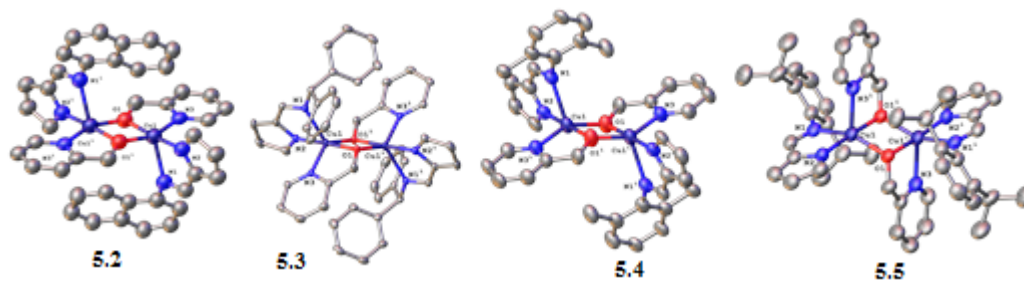


**Figure 5.1.** Crystal structures of **5.2-5.5**. Thermal ellipsoids are drawn at 50% probability (at 30% for **5.2**). Hydrogen atoms, a second independent molecule (**5.4**) and the minor component of *N*-aryl disorder (**5.4**) omitted for clarity.

**Table 5.I.** Bond distances [ $\text{\AA}$ ] and bond angles [deg] in iminopyrrolide copper complexes.

	<b>5.2</b>	<b>5.3</b>	<b>5.4</b> <sup>a</sup>	<b>5.5</b>	<b>5.9</b>	<b>5.6</b> <sup>a,b</sup>	<b>5.7</b> <sup>c</sup>
Cu-N <sub>pyrrole</sub>	1.98(2)	1.936(2)	1.938(7), 1.930(8)	1.952(4)	1.934(8)	1.931(1), 1.935(1)	1.960(2)
Cu-N <sub>imine</sub>	2.37(2)	2.314(2)	2.421(7), 2.374(8)	2.076(4)	2.295(8)	2.317(2), 2.398(1)	2.047(2)
Cu-N <sub>pyridine</sub>	1.953(19)	2.049(2)	2.011(8), 2.000(8)	2.202(4)	2.034(8)	2.022(1), 2.026(1)	2.173(2)
Cu-O <sub>short</sub>	1.942(16)	1.931(1)	1.929(6), 1.925(7)	1.962(3)	1.937(6)	1.927(1), 1.931(1)	1.974(2)
Cu-O <sub>long</sub>	1.976(15)	1.974(1)	1.942(6), 1.953(6)	1.965(3)	1.967(6)	1.951(1), 1.951(1)	1.986(2)
Cu-Cu	3.030(7)	3.018(1)	3.025(3), 2.996(3)	3.0098(12)	3.025(3)	3.0, 3.1	2.992(1)
C6-N <sub>imine-</sub> Cu	139.6(17)	136.4(1)	139, 138 <sup>d</sup>	128.2(3)	134 <sup>d</sup>	137.2(1), 134.8(1)	128.9(2)
$\tau$	0.3	0.7	0.5, 0.5	0.4	0.5	0.4, 0.4	0.6, 0.6
group in apical position	imine	imine	imine, imine	pyridine	imine	imine	pyridine

<sup>a</sup> Two independent molecules in the asymmetric unit. <sup>b</sup> taken from ref. <sup>85</sup>. <sup>c</sup> taken from ref. <sup>84</sup>. <sup>d</sup> averaged value of the observed disorder.

### Lactide polymerization.

Complexes **5.2-5.5** were tested for the polymerization of *rac*-lactide at room temperature in  $C_6D_6$  solution (Table 5.II, Fig. 5.S1, 5.S2). Complex **5.2** was barely active at all and reached less than 10% conversion even after 24 h, while **5.3** showed moderate activity, 6-8 times slower than the less sterically demanding complexes **5.6** or **5.7**, reported previously.<sup>84, 85</sup> Slight curvatures in the semi-logarithmic conversion-time plot (Fig. 5.2) and 83% final conversion for **5.3** indicate that this might be partially due to complex decomposition. Complexes **5.4** and **5.5** on the other hand, showed even higher activities than **5.6** or **5.7** (Fig. 5.2, Table 5.II). Variation of the *ortho*-substituent on the *N*-aryl between methyl and isopropyl did not notably influence activity.

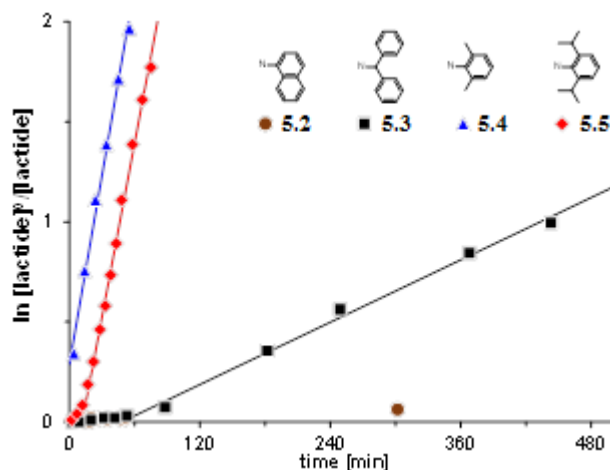


**Figure 5.2.** Semi-logarithmic conversion-time plot for *rac*-lactide polymerizations with **5.2** (circles), **5.3** (squares), **5.4** (triangles) and **5.5** (diamonds).

**Table 5.II.** *Rac*-lactide polymerizations with **5.2-5.5** and **5.9**.<sup>a</sup>

Catalyst	Final conversion (time)	$k_{\text{obs}} [\text{h}^{-1}]$	$M_n^b$	$M_n$ (calc.) <sup>c</sup>	$M_w/M_n$	# chains <sup>d</sup>	$P_m^e$
<b>5.2</b>	4% - 8% (24 – 32 h) <sup>f</sup>						
<b>5.3</b>	83% (27 h)	0.16(1)	12.2 kDa	12.0 kDa	1.6	1.0	0.57
<b>5.4</b>	99% (21 h)	1.89(8)	8.3 kDa	14.3 kDa	1.7	1.7	0.68
<b>5.5</b>	99% (3 h)	1.74(8)	15.9 kDa	14.3 kDa	1.8	0.9	0.65
<b>5.5</b> + 1 Ph <sub>3</sub> COH	95% (2 h)	1.79(3)	10.4 kDa	13.7 kDa	1.3	1.3	0.65
<b>5.6</b> <sup>g</sup>	99% (24 h)	1.29(1)	16.9 kDa	14.3 kDa	2.2	0.8	0.63
<b>5.7</b> <sup>h</sup>	99% (32 h)	1.07(4)	7.0 kDa	14.3 kDa	2.1	2.1	0.60
<b>5.9</b>	99% (23 h)	0.55(1)	11.1 kDa	14.3 kDa	1.6	1.3	0.60

<sup>a</sup> Conditions: C<sub>6</sub>D<sub>6</sub>, RT, [lactide] = 200 mM, [5.L<sub>2</sub>Cu<sub>2</sub>(OR)<sub>2</sub>] = 2 mM. The time of final conversion should not be considered a measure of activity, but just indicates after what time the reaction was quenched. <sup>b</sup>  $M_n$  and  $M_w$  determined by size exclusion chromatography vs. polystyrene standards, with a Mark-Houwink correction factor of 0.58. <sup>c</sup>  $M_n$  expected if one alkoxide per catalyst dimer initiates polymerization, calculated from [lactide]/[cat]·conversion· $M_{\text{lactide}} + M_{\text{ROH}}$ . <sup>d</sup> Number of chains per catalyst dimer, calculated from the ratio of expected and obtained polymer molecular weight. <sup>e</sup>  $P_m$  determined from decoupled <sup>1</sup>H NMR by  $P_m = 1 - 2 \cdot I_1 / (I_1 + I_2)$ , with  $I_1 = 5.20 - 5.25$  ppm (*rmr*, *mmr/rmm*),  $I_2 = 5.13 - 5.20$  ppm (*mmr/rmm*, *mmm*, *mr*). <sup>f</sup> Two experiments. <sup>g</sup> taken from ref. <sup>85</sup>. <sup>h</sup> taken from ref. <sup>84</sup>  $P_m$ -values obtained this way were typically consistent to  $\pm 1\%$  over the course of one experiment and  $\pm 3\%$  between different experiments under identical conditions.

PLA produced with **5.3** and **5.5** shows the molecular weight expected for one polymer chain per catalysts dimer (Table 5.II). The lower polymer molecular weight obtained with complex **5.4** corresponds to 1.7 polymer chains per dimer. The MALDI-MS spectrum of PLA obtained with **5.4** shows however the presence of cyclic oligomers (Fig. 5.S3), which led to the increased number of polymer chains. Stereoerror analysis by <sup>13</sup>C-NMR of PLA produced with **5.4** yielded a ratio of *mr*:*mmr*:*rmm*:*rmr* of 15%:11%:11%:5%, which is the exact ratio expected for chain-end control with a  $P_m$  value of 0.69 (Figure 5.3, Table 5.S1).<sup>112</sup>

Monoiminopyrrolide complexes **5.3-5.5** thus follow the same mechanism as determined for diiminopyrrolide **5.1** in which only one pyridylmethoxide substituent initiates chain growth and the active species is dincuclear.<sup>85, 94</sup>

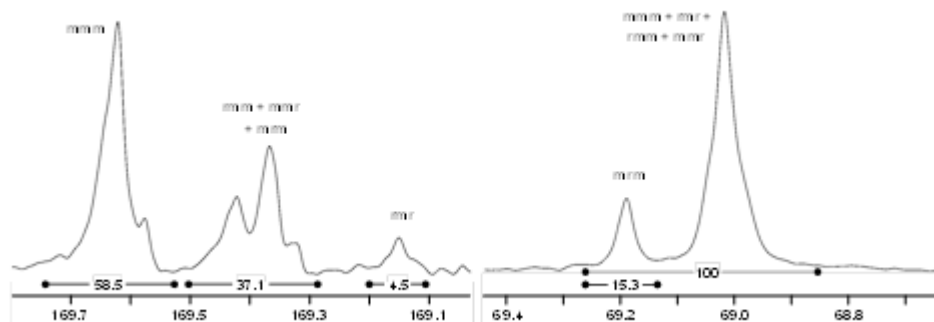


**Figure 5.3.**  $^{13}\text{C}\{^1\text{H}\}$ -NMR of PLA obtained with **5.4**. Left: carbonyl region, right: methine region. Tetrad assignments according to ref. <sup>113, 114</sup>.

As generally observed for iminopyrrolide copper complexes, polymer molecular weight control is relatively poor and polydispersities of 1.6 – 1.8 are surprisingly broad for such well-controlled reactions. Broadened polydispersities are most likely associated with the (reversible) formation of an inactive species. Addition of 1 equiv of trityl alcohol has been shown to enforce fast chain-transfer between inactive and active species without generating additional polymer chains.<sup>85</sup> Addition of  $\text{Ph}_3\text{COH}$  to polymerizations with **5.5** (Fig. 5.S4, 5.S5) consequently reduced polydispersities to 1.3 (Table 5.II).

Complexes **5.3-5.5** all produce isotactically enriched PLA. Replacing H or Me in the *N*-CH(R)Ph substituents of **5.6** and **5.7** by phenyl did not increase isotacticity and **5.3** displayed an even lower  $P_m$  value (Table 5.II). *N*-aryl substituted **5.4** and **5.5**, on the other hand, showed a notable increase in stereocontrol to  $P_m = 0.68$  and  $0.65$ , respectively. Monoiminopyrrolide complexes thus show a clearer and more pronounced dependence of stereocontrol on ligand bulk than diiminopyrrolide complexes (Scheme 5.2), which confirms the participation of the ligand environment on monomer selection.



*Impact of site-epimerization on stereocontrol.*

In the proposed stereocontrol mechanism, a misinsertion is followed by fast catalytic-site inversion and continued isotactic polymerization (Scheme 5.3) and would thus produce an isolated *mrm*-tetrad. Contrary to typical chain-end control, the insertion rate, or more precisely the insertion/isomerization rate ratio, can have an influence on stereocontrol. If insertion occurs before isomerization, an *rmr*-tetrad might be produced, either because the ligand environment is solely responsible for monomer selection or because the chain-end/catalytic-site mismatch decreases stereocontrol. In other words, if epimerization is slow relative to insertion, the catalyst partially behaves as being either under catalytic-site control or under no stereocontrol, both of which provide lower total isotacticities than pure chain-end control (given the same selectivity, catalytic-site control provides up to 10% less isotactic tetrads than chain-end control in lactide polymerization).

Since insertion rate is dependent on monomer concentration, while epimerization is not, one would thus expect that stereocontrol *increases* with conversion since lower lactide concentrations favor epimerization. Isotacticities indeed increase during the polymerization in lactide polymerization with **5.1**,<sup>85</sup> as well as in polymerizations with **5.3-5.5** (Fig. 5.S2 and 5.S5), but the small amount of the changes make it impossible to delineate this effect from chain-end effects at lower chain-lengths. We thus conducted polymerizations with **5.5** at constant catalyst concentration, but varying monomer concentrations (Table 5.S2, Fig. 5.S4). Complex **5.5** was chosen since it was most likely to show slow epimerization and one equiv of Ph<sub>3</sub>COH was added to avoid any influence of reversible or irreversible catalyst decomposition on stereocontrol. At higher lactide concentrations which favor insertion over epimerization, stereocontrol was indeed reduced for 0.67 to 0.63 (Table 5.3, Fig. 5.S5). The observed trend thus supports the necessary involvement of catalytic-site epimerization in the mechanism, although the differences were barely larger than the typical error ( $\pm 2\%$  for  $P_m$  in repeated experiments).

Based on the provided mechanism, polymerization of enantiopure lactide should be faster than *rac*-lactide, since all catalyst would be present in the same isomer enabling

isotactic insertion with the full monomer concentration. In *rac*-lactide polymerization, the catalyst is present 50% in an *SS*-selective and 50% in a *RR*-selective form and half of the monomer can only be incorporated by misinsertion (which is by necessity slower). Polymerizations of **5.5** with *L*-lactide instead of *rac*-lactide showed very similar kinetics with identical induction periods of 11 and 12 min, respectively. As expected, the apparent rate constant for *L*-lactide polymerization was 50% higher (2.85(3) h<sup>-1</sup> for *L*-lactide compared to 1.74(8) h<sup>-1</sup> for *rac*-lactide). This is a somewhat larger difference than expected and translates to an isotacticity of  $P_m = 0.82$  (see supp. Information). While there are possible mechanistic explanations for this, to differentiate between  $P_m = 0.82$  and the observed  $P_m = 0.66$ , rate constants would have to be accurate within  $\pm 10\%$ . The difference is thus most likely due to the experimental error in working with two different batches of lactide.

**Table 5.III.** *rac*-Lactide polymerization with **5.4** at different lactide concentrations. <sup>a</sup>

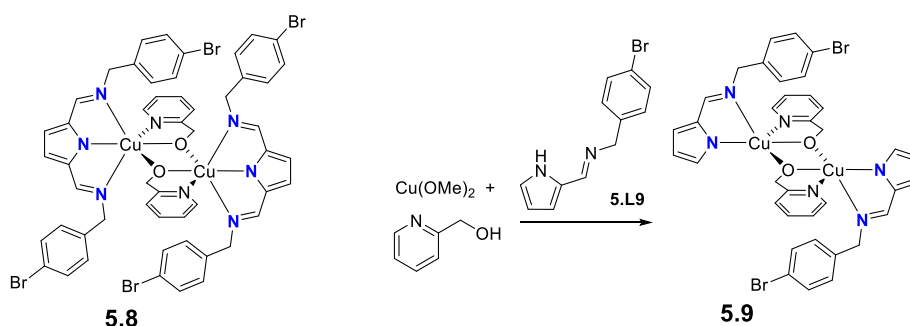
[ <b>5.4</b> ]	[lactide]	$k_{\text{obs}}$ [h <sup>-1</sup> ]	Conversion	$P_m$ <sup>b</sup>
2.0 mM	0.10 M	1.13(2)	98%	0.67
2.0 mM	0.20 M	1.79(3)	95%	0.65
2.0 mM <sup>c</sup>	0.20 M	1.74(8)	99%	0.65
2.0 mM	0.40 M	1.34(5)	97%	0.63

<sup>a</sup> Conditions: C<sub>6</sub>D<sub>6</sub>, in the presence of 2 mM Ph<sub>3</sub>COH. <sup>b</sup>  $P_m$  value averaged for a polymerization degree > 40 lactide units. Typically at polymerization degrees above 40 units the influence of the chain-end became negligible and  $P_m$  values remained constant to  $\pm 1\%$  (c. f. Fig. 5.S5). <sup>c</sup> No Ph<sub>3</sub>COH added.

#### *Impact of catalytic-site symmetry on stereocontrol.*

The proposed stereocontrol mechanism relies on the catalytic site to transfer (and amplify) the chiral information of the chain-end. Accordingly, in the presence of a symmetric catalytic site, no stereocontrol is expected. We have previously reported that **5.8**, carrying a *para*-bromobenzyl *N*-substituent, unexpectedly coordinated both

iminogroups to the copper center which resulted in a  $C_s$ -symmetric catalytic site (Scheme 5.5).<sup>84</sup> The difference in coordination mode was attributed to increased  $\pi$ -stacking interactions in this complex. To distinguish between effects of catalytic site symmetry and effects due to changes in the substitution pattern, such as increased  $\pi$ -stacking interactions, the respective mono-iminopyrrolide **5.9** was prepared (Scheme 5.5). Contrary to its benzyl analogue **5.7**, the crystal structure of **5.9** shows coordination of the imine in the apical position (Fig. 5.4), again indicating that the different coordination isomers observed in solid state are likely very close in energy. Bond lengths and angles are similar to those of **5.2-5.4** and **5.6** (Table 5.I).



### Scheme 5.5.

While **5.9** can provide the same interactions as **5.8**, it cannot form a  $C_s$ -symmetric complex and thus allows us to delineate between the two influences. *Rac*-Lactide polymerization with **5.9** followed clean first order kinetics (Fig. 5.S8, 5.S9) with a rate constant appr. half of that of the respective benzyl-substituted complex **7**. Polymer molecular weight data corresponded to one pyridylmethoxide per catalyst dimer initiating polymerization, but was slightly depressed from that value (Table 5.II). MALDI-MS analysis again indicated the presence of intramolecular transesterification reactions (Fig. 5.S10).

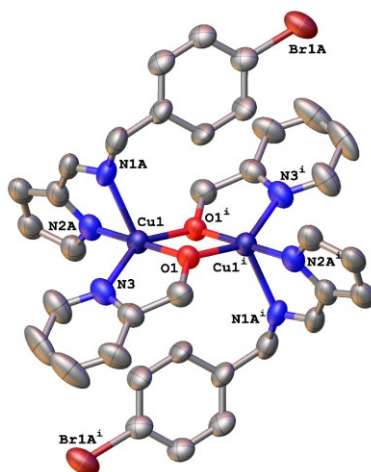


**Figure 5.4.** Crystal structure of **5.9**. Hydrogen atoms and the minor part of the disorder omitted for clarity. Thermal ellipsoids shown at the 50% probability level.

More importantly, monoiminopyrrolide complex **5.9** showed isotactic stereocontrol identical to that of its *N*-benzyl analogue **7** ( $P_m = 0.60$  in both cases, Table 5.II), thus indicating a negligible influence of the *para*-bromosubstituent on stereocontrol. In *rac*-lactide polymerizations with **5.8**, on the other hand, atactic PLA ( $P_m = 0.53$ ) was obtained, with the  $C_s$ -symmetric **5.8** being the only pyridylmethoxide containing complex investigated which did *not* produce isotactically enriched PLA.<sup>84, 85, 94</sup> This strongly supports that the chirality of the catalytic site is responsible for monomer selection, even though stereoerror analysis and other data clearly indicated that the chiral information is provided by the chain-end.

## Conclusion

Investigations into monoiminopyrrolide complexes showed that their lactide polymerization behavior models that of their respective diiminopyrrolide analogues. The observed impact of ligand congestion on stereocontrol, the dependence of stereocontrol on monomer concentration and, most importantly, the absence of stereocontrol if the catalytic site becomes symmetrical, strongly support the presence of a *catalytic-site mediated chain-end control* mechanism in this type of complexes.

Despite the advantages inherent with this stereocontrol mechanism, a successful application will have to rely on establishing the same mechanism in a different catalytic system. Although iminopyrrolide complexes provided the only isotactic

copper complexes reported so far, their inherent weaknesses (poor molecular weight control, sluggish response to steric bulk, limited synthetic variability) were again underlined in this study and make it unlikely that this class of complexes can be improved much further.

## Experimental section

**General considerations.** All reactions were carried out using Schlenk or glove box techniques under nitrogen atmosphere.  $\text{Cu}(\text{OMe})_2$ ,<sup>115</sup> 5.L4,<sup>116</sup> and 5.L5<sup>117</sup> were prepared according to literature. 1*H*-pyrrole-2-dicarbaldehyde was prepared according to literature and recrystallized from hexane at  $-80\text{ }^\circ\text{C}$ .<sup>118</sup> Solvents were dried by passage through activated aluminum oxide (MBraun SPS), de-oxygenated by repeated extraction with nitrogen, and stored over molecular sieves.  $\text{C}_6\text{D}_6$  was dried over molecular sieves. *rac*-Lactide (98%) was purchased from Sigma–Aldrich, purified by 3x recrystallization from dry ethyl acetate and kept at  $-30\text{ }^\circ\text{C}$ . All other chemicals were purchased from common commercial suppliers and used without further purification.  $^1\text{H}$  and  $^{13}\text{C}$  NMR spectra were acquired on Bruker Avance 300 and 400 spectrometers. Chemical shifts were referenced to the residual signals of the deuterated solvents ( $\text{CDCl}_3$ :  $^1\text{H}$ :  $\delta$  7.26 ppm,  $^{13}\text{C}$ :  $\delta$  77.16;  $\text{C}_6\text{D}_6$ :  $^1\text{H}$ :  $\delta$  7.16 ppm,  $^{13}\text{C}$ :  $\delta$  128.38 ppm). Elemental analyses were performed by the Laboratoire d'analyse élémentaire (Université de Montréal). All UV–vis measurements were conducted in anhydrous and degassed toluene at room temperature in a sealed quartz cell on a Cary 500i UV–vis–NIR spectrophotometer.

**2-((naphthyl)aldimino)pyrrole, 5.L2.** 1*H*-pyrrole-2-carbaldehyde (1.0 g, 11 mmol) was dissolved in dry toluene (25 ml).  $\text{MgSO}_4$  (5 g), a catalytic amount of Amberlyst 15 and 1-naphthylamine (1.5 g, 11 mmol) were added. The reaction mixture was stirred overnight at room temperature. The brown suspension was filtered and the solvent was removed under vacuum. The residue was treated with hexane (20 ml), resulting in a brown oil. The oil was separated by decantation and dried under vacuum (1.8 g, 78%). The  $^1\text{H}$  NMR spectra is identical to an alternative preparation published earlier.<sup>119</sup>

$^1\text{H}$  NMR ( $\text{CDCl}_3$ , 400 MHz):  $\delta$  8.35 – 8.27 (m, 2H, (N=C)H and Ar), 7.85 (d,  $J_{\text{HH}} = 7$  Hz, 1H, Ar), 7.70 (d,  $J_{\text{HH}} = 8$  Hz, 1H, Ar), 7.55 – 7.42 (m, 3H, Ar), 7.27 – 7.25 (m, 1H, Ar), 7.05 (d,  $^3J_{\text{HH}} = 7$  Hz, 1H, 5-pyrrole), 7.03 (br s, 1H, NH), 6.76 – 6.72 (m, 1H, 3-pyrrole), 6.38 – 6.31 (m, 1H, 4-Pyrrole).

**2-((benzylhydril)aldimino)pyrrole, 5.L3.** Analogous to 5.L2, from 1*H*-pyrrole-2-carbaldehyde (1.0 g, 11 mmol) and benzhydrylamine (1.9 g, 11 mmol) to yield a brown oil (2.2 g, 81%). The  $^1\text{H}$  NMR spectra is identical to an alternative preparation published earlier.<sup>120</sup>

$^1\text{H}$  NMR ( $\text{CDCl}_3$ , 400 MHz):  $\delta$  8.43 (br s, 1H, NH), 7.97 (s, 1H, (N=C)H), 7.33 – 7.16 (m, 10H, Ph), 6.98 – 6.93 (m, 1H, 5-pyrrole), 6.56 (d,  $^3J_{\text{HH}} = 4$  Hz, 1H, 3-pyrrole), 6.21 (dd,  $^3J_{\text{HH}} = 4, 3$  Hz, 1H, 4-pyrrole), 5.62 (s, 1H, CH).

**2-((4-bromobenzyl)aldimino)pyrrole, 5.L9.** Analogous to 5.L2, from 1*H*-pyrrole-2-carbaldehyde (1.0 g, 11 mmol) and *p*-bromobenzylamine (2.9 g, 16 mmol) to give 2.5 g (91%) a 1:3 mixture of *p*-bromobenzylamine and 5.L9. Purification attempts were unsuccessful and the mixture was used without purification in further synthesis.

$^1\text{H}$  NMR ( $\text{CDCl}_3$ , 300 MHz) :  $\delta$  8.15 (dd,  $J_{\text{HH}} = 2, 1$  Hz, 1H, ((N=C)H), 7.49 – 7.41 (m, 2H, Ar), 7.19 – 7.14 (m, 2H, Ar), 6.90 – 6.86 (m, 1H, 5-pyrrole), 6.53 (dd,  $^3J_{\text{HH}} = 4, ^4J_{\text{HH}} = 1$  Hz, 1H, 3-pyrrole), 6.25 (dd,  $^3J_{\text{HH}} = 4, 3$  Hz, 1H, 4-pyrrole), 4.65 (s, 2H,  $\text{CH}_2$ ).  $^{13}\text{C}\{^1\text{H}\}$  NMR ( $\text{CDCl}_3$ , 75 MHz) :  $\delta$  152.8 (N=C), 138.8 (*ipso*-Ph), 131.7 (*m*-Ph), 130.0 (2-pyrrole), 129.7 (*o*-Ph), 122.1 (5-pyrrole), 121.0 (*p*-Ph), 114.8 (3-pyrrole), 110.1 (4-pyrrole), 63.8 ( $\text{CH}_2$ ). ESI-HRMS ( $m/z$ ):  $\text{M}+\text{H}^+$  ( $\text{C}_{12}\text{H}_{12}\text{BrN}_2$ ) calcd 263.0178; found: 263.0189.

**(5.L2) $_2$ Cu $_2$ ( $\mu$ -O, $\kappa$ <sub>N</sub>-OCH $_2$ Py) $_2$ , 5.2.** Cu(OMe) $_2$  (57 mg, 0.45 mmol) was suspended in toluene (3 ml). 2-pyridylmethanol (87  $\mu$ l, 0.90 mmol) was added to the blue suspension, which was stirred for 45 min. A freshly prepared brown solution of **5.L2** (100 mg, 0.45 mmol) in toluene (2 ml) was added dropwise, resulting in a dark green solution. The reaction was stirred 48 hours at RT, filtered to remove trace impurities, concentrated to 1/3 of the volume, diluted with hexane (18 ml) and kept at  $-30^\circ\text{C}$  for 4 hours, resulting in 31 mg (18%) green X-ray-quality crystals. Samples for elemental analysis were obtained by diffusion of hexane into dichloromethane (1:3).

UV-vis (toluene,  $2.3 \cdot 10^{-6}$  M)  $\lambda_{\text{max}}$ , nm ( $\epsilon$ ,  $\text{mol}^{-1} \text{cm}^2$ ): 355 (25200), 522 (sh), 603 (252), 666 (200). Anal. Calcd for  $\text{C}_{42}\text{H}_{34}\text{Cu}_2\text{N}_6\text{O}_2$ : C, 64.52; H, 4.38; N, 10.75; Found: C, 65.09; H, 4.99; N, 11.33. (Recrystallized twice, final result shown.)

**(5.L3)<sub>2</sub>Cu<sub>2</sub>( $\mu$ -O, $\kappa$ <sub>N</sub>-OCH<sub>2</sub>Py)<sub>2</sub>, 5.3.** Analogous to **5.2**, from Cu(OMe)<sub>2</sub> (48 mg, 0.38 mmol) in toluene (3 mL), 2-pyridylmethanol (73  $\mu$ l, 0.76 mmol), **5.L3** (100 mg, 0.38 mmol) in toluene (2 mL) afforded 32 mg (20%) green X-ray-quality crystals. Samples for elemental analysis were obtained by diffusion of hexane into dichloromethane (1:3).

UV-vis (toluene,  $2 \cdot 10^{-6}$  M)  $\lambda_{\text{max}}$ , nm ( $\epsilon$ ,  $\text{mol}^{-1} \text{cm}^2$ ): 364 (4700), 509 (550), 603 (500), 671 (470). Anal. Calcd for  $\text{C}_{48}\text{H}_{42}\text{Cu}_2\text{N}_6\text{O}_2 \cdot 1/4\text{CH}_2\text{Cl}_2$ : C, 65.62; H, 4.85; N, 9.52; Found: C, 66.03; H, 4.96; N, 9.90.

**(5.L4)<sub>2</sub>Cu<sub>2</sub>( $\mu$ -O, $\kappa$ <sub>N</sub>-OCH<sub>2</sub>Py)<sub>2</sub>, 5.4.** Analogous to **5.2**, from Cu(OMe)<sub>2</sub> (63 mg, 0.50 mmol) in toluene (3 mL), 2-pyridylmethanol (96  $\mu$ l, 1.0 mmol), **5.L4** (100 mg, 0.50 mmol) in toluene (2 mL) afforded 41 mg (23%) green X-ray-quality crystals. Samples for elemental analysis were obtained by diffusion of hexane into dichloromethane (1:3).

UV-vis (toluene,  $2.5 \cdot 10^{-6}$  M)  $\lambda_{\text{max}}$ , nm ( $\epsilon$ ,  $\text{mol}^{-1} \text{cm}^2$ ): 350 (21400), 388 (sh), 542 (780), 607 (800), 664 (675). Anal. Calcd for  $\text{C}_{38}\text{H}_{38}\text{Cu}_2\text{N}_6\text{O}_2 \cdot 1/4\text{CH}_2\text{Cl}_2$ : C, 60.52; H, 5.11; N, 11.07; Found: C, 60.72; H, 5.15; N, 11.36.

**(5.L5)<sub>2</sub>Cu<sub>2</sub>( $\mu$ -O, $\kappa$ <sub>N</sub>-OCH<sub>2</sub>Py)<sub>2</sub>, 5.5.** Analogous to **5.2**, from Cu(OMe)<sub>2</sub> (49 mg, 0.39 mmol) in toluene (3 mL), 2-pyridylmethanol (75  $\mu$ l, 0.78 mmol), **5.L5** (100 mg, 0.39 mmol) in toluene (2 mL) afforded 40 mg (24%) green X-ray-quality crystals. Samples for elemental analysis were obtained by diffusion of hexane into dichloromethane (1:3).

UV-vis (toluene,  $3.6 \cdot 10^{-5}$  M)  $\lambda_{\text{max}}$ , nm ( $\epsilon$ ,  $\text{mol}^{-1} \text{cm}^2$ ): 355 (18500), 388 (sh), 472 (1400), 673 (320). Anal. Calcd for  $\text{C}_{46}\text{H}_{54}\text{Cu}_2\text{N}_6\text{O}_2$ : C, 65.00; H, 6.40; N, 9.89; Found: C, 64.60; H, 6.10; N, 9.78.

**(5.L6)<sub>2</sub>Cu<sub>2</sub>( $\mu$ -O, $\kappa$ <sub>N</sub>-OCH<sub>2</sub>Py)<sub>2</sub>, 5.9.** Analogous to **5.2**, from Cu(OMe)<sub>2</sub> (50 mg, 0.40 mmol) in toluene (3 mL), 2-pyridylmethanol (77  $\mu$ l, 0.80 mmol), **5.L6** (100 mg, 0.40

mmol) in toluene (2 mL). Decantation and washing with hexane (3 x 10 mL) afforded 31 mg (18%) of green X-ray quality crystals.

UV-vis (toluene,  $1.2 \cdot 10^{-5}$  M) [ $\lambda_{\max}$ , nm ( $\epsilon$ , mol<sup>-1</sup> cm<sup>2</sup>)]: 351 (18600), 371 (sh), 490 (1200), 603 (800), 664 (720). Anal. Calcd for C<sub>36</sub>H<sub>32</sub>Br<sub>2</sub>Cu<sub>2</sub>N<sub>6</sub>O<sub>2</sub>: C, 49.84; H, 3.72; N, 9.69; Found: C, 50.06; H, 3.73; N, 9.43.

***rac*-Lactide polymerization.** All manipulations took place in a glove box under nitrogen atmosphere. Stock solutions of the catalysts and BnOH were prepared in dry C<sub>6</sub>D<sub>6</sub> and stored at -30 °C to avoid concentration changes. The desired amount of *rac*-lactide was placed into a J.-Young tube together with C<sub>6</sub>D<sub>6</sub>. A stock solution of benzyl alcohol was added, where required, followed by a stock solution of the catalyst (appr. 20 mM in C<sub>6</sub>D<sub>6</sub>) to give final concentrations of 2.0 mM (of catalyst dimer) and of 0.20 M of lactide. After complete dissolution was assured by shaking, the reaction was followed by <sup>1</sup>H NMR. The reaction was quenched by addition of 5-10 equiv of a CDCl<sub>3</sub> solution of acetic acid (10 mM, drops). The volatiles were evaporated and solid polymer samples were stored at -80 °C for further analysis.

Conversion was determined from <sup>1</sup>H NMR by comparison to remaining lactide.  $P_m$  values were determined from homodecoupled <sup>1</sup>H NMR spectra and calculated from  $P_m = 1 - 2 \cdot I_1 / (I_1 + I_2)$ , with  $I_1 = 5.15 - 5.21$  ppm (*rmr*, *mmr/rmm*),  $I_2 = 5.21 - 5.25$  ppm (*mmr/rmm*, *mmm*, *mrm*). The integration of the left multiplet and right multiplet ( $I_1$  and  $I_2$ ) required only one, very reproducible dividing point of the integration, which was always taken as the minimum between the two multiplets.  $P_m$ -values obtained this way were typically consistent to  $\pm 1\%$  over the course of one experiment and  $\pm 3\%$  between different experiments under identical conditions. Molecular weight analyses were performed on a Waters 1525 gel permeation chromatograph equipped with three Phenomenex columns and a refractive index detector at 35 °C. THF was used as the eluent at a flow rate of 1.0 mL·min<sup>-1</sup> and polystyrene standards (Sigma-Aldrich, 1.5 mg·mL<sup>-1</sup>, prepared and filtered (0.2 mm) directly prior to injection) were used for calibration. Obtained molecular weights were corrected by a Mark-Houwink factor of 0.58.<sup>121</sup>



**X-ray diffraction.** Single crystals were obtained directly from isolation of the products as described above. Diffraction data were collected on a Bruker Venture METALJET diffractometer (Ga K $\alpha$  radiation) using the APEX2 software package.<sup>122</sup> Data reduction was performed with SAINT,<sup>123</sup> absorption corrections with SADABS.<sup>124</sup> Structures were solved by dual-space methods (SHELXT).<sup>125</sup> All non-hydrogen atoms were refined anisotropic using full-matrix least-squares on  $F^2$  and hydrogen atoms refined with fixed isotropic U using a riding model (SHELXL2014).<sup>126</sup> Complexes **5.2**, **5.4**, and **5.9** were found to be twinned. Complex **5.2** diffracted very weakly and a general thermal parameter restraint (RIGU) was necessary in refinement due to the resulting bad data quality. No better crystal could be obtained. Further experimental details can be found in Table 5.IV and in the supporting information (CIF).

**Table 5.IV.** Details of X-ray diffraction experiments.

	5.2	5.3	5.4	5.5	5.9
Formula	C <sub>42</sub> H <sub>34</sub> Cu <sub>2</sub> N <sub>6</sub> O <sub>2</sub>	C <sub>48</sub> H <sub>42</sub> Cu <sub>2</sub> N <sub>6</sub> O <sub>2</sub>	C <sub>38</sub> H <sub>38</sub> Cu <sub>2</sub> N <sub>6</sub> O <sub>2</sub>	C <sub>46</sub> H <sub>54</sub> Cu <sub>2</sub> N <sub>6</sub> O <sub>2</sub>	C <sub>36</sub> H <sub>32</sub> Br <sub>2</sub> Cu <sub>2</sub> N <sub>6</sub> O <sub>2</sub>
$M_w$ (g/mol); $d_{\text{calcd.}}$ (g/cm <sup>3</sup> )	781.83; 1.201	861.95; 1.428	737.82; 1.410	850.03; 1.303	867.57; 1.696
$T$ (K); F(000)	150; 3618	150; 892	150; 764	150; 446	150; 868
Crystal System	Trigonal	Monoclinic	Triclinic	Triclinic	Monoclinic
Space Group	<i>R</i> -3	<i>P</i> 2 <sub>1</sub> / <i>c</i>	<i>P</i> -1	<i>P</i> -1	<i>P</i> 2 <sub>1</sub> / <i>c</i>
Unit Cell: $a$ (Å)	35.261(5)	8.8407(3)	7.9918(7)	10.2561(6)	11.7994(7)
$b$ (Å)	35.261(5)	16.3755(5)	12.0774(12)	10.8248(6)	20.5590(13)
$c$ (Å)	9.0334(17)	14.1657(4)	18.2565(17)	11.7883(7)	7.0097(4)
$\alpha$ (°)	90	90	95.832(5)	65.984(3)	90
$\beta$ (°)	90	102.2090(10)	95.745(5)	83.830(3)	92.497(4)
$\gamma$ (°)	120	90	94.455(5)	65.374(3)	90
$V$ (Å <sup>3</sup> ); $Z$	9727(3); 9	2004.40(11); 2	1737.3(3); 2	1083.67(11); 1	1698.83(18); 2
$\mu$ (mm <sup>-1</sup> ); Abs. Corr.	5.51; multi- scan	5.98; multi-scan	6.83; multi-scan	5.52; multi-scan	8.90; multi-scan
$\theta$ range (°); completeness	2.2–33.6; 0.99	3.6–60.7; 0.98	3.2–61.3; 0.96	3.6–59.9; 0.99	3.3–55.9; 0.99
collected reflections; $R_\sigma$	9578; 0.183	28616; 0.026	67959; 0.126	27019; 0.052	34561; 0.059
unique reflections; $R_{\text{int}}$	1320; 0.251	4539; 0.046	7954; 0.186	4963; 0.079	3889; 0.099
$R1(F)$ ( $I >$ $2\sigma(I)$ )	0.114	0.039	0.126	0.082	0.103
w $R(F^2)$ (all data)	0.299	0.107	0.351	0.233	0.259
GoF( $F^2$ )	1.07	1.11	1.08	1.06	1.08
Residual electron density	0.48, –0.28	0.32, –0.95	1.07, –0.82	1.41, –0.77	1.04, –0.69

**Supporting Information**

Additional tables and figures. Crystal structure data (CIF). The Supporting Information is available free of charge on the ACS Publications website.

**Corresponding Author**

\* Email: Frank.Schaper@umontreal.ca

**Notes**

The authors declare no competing financial interest.

**Acknowledgements**

Funding was supplied by the NSERC discovery program (RGPIN-2016-04953) and the Centre for Green Chemistry and Catalysis (FQRNT). We thank Francine Bélanger for support with X-ray diffraction, Elena Nadezhina for elemental analysis and Marie-Christine Tang, Karine Gilbert and Dr. Alexandra Furtos for support with MALDI-MS. Polymerization with *L*-lactide was proposed by a reviewer.

## References Chapter 5

1. Nagarajan, V.; Mohanty, A. K.; Misra, M., Perspective on Polylactic Acid (PLA) based Sustainable Materials for Durable Applications: Focus on Toughness and Heat Resistance. *ACS Sustainable Chem. Eng.* **2016**, *4*, 2899-2916.
2. Castro-Aguirre, E.; Iñiguez-Franco, F.; Samsudin, H.; Fang, X.; Auras, R., Poly(lactic acid)—Mass production, processing, industrial applications, and end of life. *Adv. Drug Delivery Rev.* **2016**, *107*, 333-366.
3. Slomkowski, S.; Penczek, S.; Duda, A., Polylactides—an overview. *Polym. Adv. Technol.* **2014**, *25*, 436-447.
4. Singhvi, M.; Gokhale, D., Biomass to biodegradable polymer (PLA). *RSC Adv.* **2013**, *3*, 13558-13568.
5. Hottle, T. A.; Bilec, M. M.; Landis, A. E., Sustainability assessments of bio-based polymers. *Polym. Degrad. Stab.* **2013**, *98*, 1898-1907.
6. Inkinen, S.; Hakkarainen, M.; Albertsson, A.-C.; Södergård, A., From Lactic Acid to Poly(lactic acid) (PLA): Characterization and Analysis of PLA and Its Precursors. *Biomacromolecules* **2011**, *12*, 523-532.
7. Ahmed, J.; Varshney, S. K., Polylactides—Chemistry, Properties and Green Packaging Technology: A Review. *Int. J. Food Prop.* **2011**, *14*, 37-58.
8. Vijayakumar, J.; Aravindan, R.; Viruthagiri, T., Recent trends in the production, purification and application of lactic acid. *Chem. Biochem. Eng. Q.* **2008**, *22*, 245-264.
9. Tokiwa, Y.; Calabia, B. P., Biological production of functional chemicals from renewable resources. *Can. J. Chem.* **2008**, *86*, 548-555.
10. Drumright, R. E.; Gruber, P. R.; Henton, D. E., Polylactic Acid Technology. *Adv. Mater. (Weinheim, Ger.)* **2000**, *12*, 1841-1846.
11. Vink, E. T. H.; Rábago, K. R.; Glassner, D. A.; Springs, B.; O'Connor, R. P.; Kolstad, J.; Gruber, P. R., The Sustainability of NatureWorks™ Polylactide Polymers and Ingeo™ Polylactide Fibers: an Update of the Future. *Macromol. Biosci.* **2004**, *4*, 551-564.

12. Paul, S.; Zhu, Y.; Romain, C.; Brooks, R.; Saini, P. K.; Williams, C. K., Ring-opening copolymerization (ROCOP): synthesis and properties of polyesters and polycarbonates. *Chem. Commun. (Cambridge, U. K.)* **2015**, *51*, 6459-6479.
13. dos Santos Vieira, I.; Herres-Pawlis, S., Lactide Polymerisation with Complexes of Neutral N-Donors – New Strategies for Robust Catalysts. *Eur. J. Inorg. Chem.* **2012**, *2012*, 765-774.
14. Dutta, S.; Hung, W.-C.; Huang, B.-H.; Lin, C.-C., Recent Developments in Metal-Catalyzed Ring-Opening Polymerization of Lactides and Glycolides: Preparation of Polylactides, Polyglycolide, and Poly(lactide-co-glycolide). In *Synthetic Biodegradable Polymers*, Rieger, B.; Künkel, A.; Coates, G. W.; Reichardt, R.; Dinjus, E.; Zevaco, T. A., Eds. Springer-Verlag: Berlin, 2011; pp 219-284.
15. Dijkstra, P. J.; Du, H.; Feijen, J., Single site catalysts for stereoselective ring-opening polymerization of lactides. *Polym. Chem.* **2011**, *2*, 520-527.
16. Buffet, J.-C.; Okuda, J., Initiators for the stereoselective ring-opening polymerization of meso-lactide. *Polym. Chem.* **2011**, *2*, 2758-2763.
17. Thomas, C. M., Stereocontrolled ring-opening polymerization of cyclic esters: synthesis of new polyester microstructures. *Chem. Soc. Rev.* **2010**, *39*, 165.
18. Stanford, M. J.; Dove, A. P., Stereocontrolled ring-opening polymerization of lactide. *Chem. Soc. Rev.* **2010**, *39*, 486-494.
19. Williams, C. K.; Hillmyer, M. A., Polymers from Renewable Resources: A Perspective for a Special Issue of Polymer Reviews. *Polym. Rev.* **2008**, *48*, 1-10.
20. Ajellal, N.; Carpentier, J.-F.; Guillaume, C.; Guillaume, S. M.; Helou, M.; Poirier, V.; Sarazin, Y.; Trifonov, A., Metal-catalyzed immortal ring-opening polymerization of lactones, lactides and cyclic carbonates. *Dalton Trans.* **2010**, *39*, 8363.
21. Platel, R. H.; Hodgson, L. M.; Williams, C. K., Biocompatible Initiators for Lactide Polymerization. *Polym. Rev.* **2008**, *48*, 11 - 63.
22. Wu, J.; Yu, T.-L.; Chen, C.-T.; Lin, C.-C., Recent developments in main group metal complexes catalyzed/initiated polymerization of lactides and related cyclic esters. *Coord. Chem. Rev.* **2006**, *250*, 602-626.

23. Dechy-Cabaret, O.; Martin-Vaca, B.; Bourissou, D., Controlled Ring-Opening Polymerization of Lactide and Glycolide. *Chem. Rev.* **2004**, *104*, 6147-6176.
24. O'Keefe, B. J.; Hillmyer, M. A.; Tolman, W. B., Polymerization of lactide and related cyclic esters by discrete metal complexes. *J. Chem. Soc., Dalton Trans.* **2001**, 2215-2224.
25. Chisholm, M. H.; Zhou, Z., New generation polymers: the role of metal alkoxides as catalysts in the production of polyoxygenates. *J. Mater. Chem.* **2004**, *14*, 3081.
26. Zhong, Z.; Dijkstra, P. J.; Feijen, J., Controlled synthesis of biodegradable lactide polymers and copolymers using novel in situ generated or single-site stereoselective polymerization initiators. *J. Biomater. Sci., Polym. Ed.* **2004**, *15*, 929-946.
27. Huang, B. H.; Dutta, S.; Lin, C. C., 1.39 - Main-Group Catalysts for Lactide Polymerization. In *Comprehensive Inorganic Chemistry II (Second Edition)*, Poeppelemeier, J. R., Ed. Elsevier: Amsterdam, 2013; pp 1217-1249.
28. Wheaton, C. A.; Hayes, P. G., Designing cationic zinc and magnesium catalysts for coordination–insertion polymerization of lactide. *Comments Inorg. Chem.* **2011**, *32*, 127-162.
29. Wheaton, C. A.; Hayes, P. G.; Ireland, B. J., Complexes of Mg, Ca and Zn as homogeneous catalysts for lactide polymerization. *Dalton Trans.* **2009**, 4832 - 4846.
30. Sutar, A. K.; Maharana, T.; Dutta, S.; Chen, C.-T.; Lin, C.-C., Ring-opening polymerization by lithium catalysts: an overview. *Chem. Soc. Rev.* **2010**, *39*, 1724-1746.
31. Le Roux, E., Recent advances on tailor-made titanium catalysts for biopolymer synthesis. *Coord. Chem. Rev.* **2016**, *306*, 65-85.
32. Sauer, A.; Kapelski, A.; Fliedel, C.; Dagorne, S.; Kol, M.; Okuda, J., Structurally well-defined group 4 metal complexes as initiators for the ring-opening polymerization of lactide monomers. *Dalton Trans.* **2013**, *42*, 9007-9023.
33. MacDonald, J. P.; Shaver, M. P., Aluminum Salen and Salan Polymerization Catalysts: From Monomer Scope to Macrostructure Control. In *Green Polymer*

*Chemistry: Biobased Materials and Biocatalysis*, American Chemical Society 2015; Vol. 1192, pp 147-167.

34. Jianming, R.; Anguo, X.; Hongwei, W.; Hailin, Y., Review – recent development of ring-opening polymerization of cyclic esters using aluminum complexes. *Des. Monomers Polym.* **2013**, *17*, 345-355.

35. Dagherne, S.; Normand, M.; Kirillov, E.; Carpentier, J.-F., Gallium and indium complexes for ring-opening polymerization of cyclic ethers, esters and carbonates. *Coord. Chem. Rev.* **2013**, *257*, 1869-1886.

36. Dagherne, S.; Fliedel, C., Organoaluminum Species in Homogeneous Polymerization Catalysis. In *Modern Organoaluminum Reagents: Preparation, Structure, Reactivity and Use*, Woodward, S.; Dagherne, S., Eds. Springer Berlin Heidelberg: Berlin, Heidelberg, 2013; pp 125-171.

37. Dagherne, S.; Fliedel, C.; de Frémont, P., Gallium and Indium Compounds in Homogeneous Catalysis. In *Encyclopedia of Inorganic and Bioinorganic Chemistry*, John Wiley & Sons, Ltd 2011.

38. Amgoune, A.; Thomas, C. M.; Carpentier, J.-F., Controlled ring-opening polymerization of lactide by group 3 metal complexes. *Pure Appl. Chem.* **2007**, *79*, 2013-2030.

39. Xu, T.-Q.; Yang, G.-W.; Liu, C.; Lu, X.-B., Highly Robust Yttrium Bis(phenolate) Ether Catalysts for Excellent Isolelective Ring-Opening Polymerization of Racemic Lactide. *Macromolecules* **2017**, *50*, 515-522.

40. Bhattacharjee, J.; Harinath, A.; Nayek, H. P.; Sarkar, A.; Panda, T. K., Highly Active and Iso-Selective Catalysts for the Ring-Opening Polymerization of Cyclic Esters using Group 2 Metal Initiators. *Chem.-Eur. J.* **2017**, *23*, 9319-9331.

41. Myers, D.; White, A. J. P.; Forsyth, C. M.; Bown, M.; Williams, C. K., Phosphasalen Indium Complexes Showing High Rates and Isolelectivities in rac-Lactide Polymerizations. *Angew. Chem., Int. Ed.* **2017**, *56*, 5277-5282.

42. Rosen, T.; Popowski, Y.; Goldberg, I.; Kol, M., Zinc Complexes of Sequential Tetradentate Monoanionic Ligands in the Isolelective Polymerization of rac-Lactide. *Chem.-Eur. J.* **2016**, *22*, 11533-11536.

43. Sun, Y.; Xiong, J.; Dai, Z.; Pan, X.; Tang, N.; Wu, J., Stereoselective Alkali-Metal Catalysts for Highly Isotactic Poly(rac-lactide) Synthesis. *Inorg. Chem.* **2016**, *55*, 136-143.
44. McKeown, P.; Davidson, M. G.; Kociok-Kohn, G.; Jones, M. D., Aluminium salalens vs. salans: "Initiator Design" for the isoselective polymerisation of rac-lactide. *Chem. Commun. (Cambridge, U. K.)* **2016**, *52*, 10431-10434.
45. Wang, H.; Yang, Y.; Ma, H., Stereoselectivity Switch between Zinc and Magnesium Initiators in the Polymerization of rac-Lactide: Different Coordination Chemistry, Different Stereocontrol Mechanisms. *Macromolecules* **2014**, *47*, 7750-7764.
46. Mou, Z.; Liu, B.; Wang, M.; Xie, H.; Li, P.; Li, L.; Li, S.; Cui, D., Isolelective ring-opening polymerization of rac-lactide initiated by achiral heteroscorpionate zwitterionic zinc complexes. *Chem. Commun. (Cambridge, U. K.)* **2014**, *50*, 11411-11414.
47. Bakewell, C.; White, A. J. P.; Long, N. J.; Williams, C. K., Metal-Size Influence in Iso-Selective Lactide Polymerization. *Angew. Chem., Int. Ed.* **2014**, *53*, 9226-9230.
48. Aluthge, D. C.; Patrick, B. O.; Mehrkhodavandi, P., A highly active and site selective indium catalyst for lactide polymerization. *Chem. Commun. (Cambridge, U. K.)* **2013**, *49*, 4295-4297.
49. Balasanthiran, V.; Chatterjee, C.; Chisholm, M. H.; Harrold, N. D.; RajanBabu, T. V.; Warren, G. A., Coupling of Propylene Oxide and Lactide at a Porphyrin Chromium(III) Center. *J. Am. Chem. Soc.* **2015**, *137*, 1786-1789.
50. Daneshmand, P.; Schaper, F., Exploring the reactivity of manganese(iii) complexes with diphenolate-diamino ligands in rac-lactide polymerization. *Dalton Trans.* **2015**, *44*, 20449-20458.
51. Rajashekhar, B.; Chakraborty, D., Co(II) and Mn(II) catalyzed bulk ring-opening polymerization of cyclic esters. *Polym. Bull.* **2014**, *71*, 2185-2203.
52. Idage, B. B.; Idage, S. B.; Kasegaonkar, A. S.; Jadhav, R. V., Ring opening polymerization of dilactide using salen complex as catalyst. *Mater. Sci. Eng., B* **2010**, *168*, 193-198.



53. Kricheldorf, H. R.; Damrau, D.-O., Poly lactones. 44. Polymerizations of L-Lactide Catalyzed by Manganese Salts. *J. Macromol. Sci., Part A: Pure Appl. Chem.* **1998**, *35*, 1875-1887.
54. Tschan, M. J. L.; Guo, J.; Raman, S. K.; Brule, E.; Roisnel, T.; Rager, M.-N.; Legay, R.; Durieux, G.; Rigaud, B.; Thomas, C. M., Zinc and cobalt complexes based on tripodal ligands: synthesis, structure and reactivity toward lactide. *Dalton Trans.* **2014**, *43*, 4550-4564.
55. Shin, S.; Nayab, S.; Lee, H., Polymerizations of methyl methacrylate and rac-lactide by 4-coordinate cobalt(II) complexes supported by N'-substituted N,N',N-bis((1H-pyrazol-1-yl)methyl)amine derivatives. *Polyhedron* **2018**, *141*, 309-321.
56. Duan, R.; Hu, C.; Li, X.; Pang, X.; Sun, Z.; Chen, X.; Wang, X., Air-Stable Salen-Iron Complexes: Stereoselective Catalysts for Lactide and  $\epsilon$ -Caprolactone Polymerization through in Situ Initiation. *Macromolecules* **2017**, *50*, 9188-9195.
57. Delle Chiaie, K. R.; Biernesser, A. B.; Ortuno, M. A.; Dereli, B.; Iovan, D. A.; Wilding, M. J. T.; Li, B.; Cramer, C. J.; Byers, J. A., The role of ligand redox non-innocence in ring-opening polymerization reactions catalysed by bis(imino)pyridine iron alkoxide complexes. *Dalton Trans.* **2017**, *46*, 12971-12980.
58. Herber, U.; Hegner, K.; Wolters, D.; Siris, R.; Wrobel, K.; Hoffmann, A.; Lochenie, C.; Weber, B.; Kuckling, D.; Herres-Pawlis, S., Iron(II) and Zinc(II) Complexes with Tetradentate Bis(pyrazolyl)methane Ligands as Catalysts for the Ring-Opening Polymerisation of rac-Lactide. *Eur. J. Inorg. Chem.* **2017**, *2017*, 1341-1354.
59. Brown, L. A.; Wekesa, F. S.; Unruh, D. K.; Findlater, M.; Long, B. K., BIAN-Fe( $\eta^6$ -C<sub>6</sub>H<sub>6</sub>): Synthesis, characterization, and l-lactide polymerization. *J. Polym. Sci., Part A: Polym. Chem.* **2017**, *55*, 2824-2830.
60. Delle Chiaie, K. R.; Yablon, L. M.; Biernesser, A. B.; Michalowski, G. R.; Sudyn, A. W.; Byers, J. A., Redox-triggered crosslinking of a degradable polymer. *Polym. Chem.* **2016**, *7*, 4675-4681.
61. Biernesser, A. B.; Delle Chiaie, K. R.; Curley, J. B.; Byers, J. A., Block Copolymerization of Lactide and an Epoxide Facilitated by a Redox Switchable Iron-Based Catalyst. *Angew. Chem., Int. Ed.* **2016**, *55*, 5251-5254.

62. Silvino, A. C.; Rodrigues, A. L. C.; Resende, J. A. L. C., Synthesis, structure and application to l-lactide polymerization of a new phenoxy-imine iron(III) complex. *Inorg. Chem. Commun.* **2015**, *55*, 39-42.
63. Manna, C. M.; Kaur, A.; Yablon, L. M.; Haefner, F.; Li, B.; Byers, J. A., Stereoselective Catalysis Achieved through in Situ Desymmetrization of an Achiral Iron Catalyst Precursor. *J. Am. Chem. Soc.* **2015**, *137*, 14232-14235.
64. Kundys, A.; Plichta, A.; Florjańczyk, Z.; Frydrych, A.; Żurawski, K., Screening of metal catalysts influence on the synthesis, structure, properties, and biodegradation of PLA-PBA triblock copolymers obtained in melt. *J. Polym. Sci., Part A: Polym. Chem.* **2015**, *53*, 1444-1456.
65. Keuchguerian, A.; Mougang-Soume, B.; Schaper, F.; Zargarian, D., Lactide polymerization with iron alkoxide complexes. *Can. J. Chem.* **2015**, *93*, 594-601.
66. Kang, Y. Y.; Park, H.-R.; Lee, M. H.; An, J.; Kim, Y.; Lee, J., Dinuclear iron(III) complexes with different ligation for ring opening polymerization of lactide. *Polyhedron* **2015**, *95*, 24-29.
67. Giese, S. O. K.; Egevardt, C.; Rüdiger, A. L.; Saij, E. L.; Silva, T. A.; Zawadzki, S. F.; Soares, J. F.; Nunes, G. G., Catalytic Activity of a Titanium(IV)/Iron(II) Heterometallic Alkoxide in the Ring Opening Polymerization of  $\mu$ -Caprolactone and rac-Lactide. *J. Braz. Chem. Soc.* **2015**, *26*, 2258-2268.
68. Manna, C. M.; Kaplan, H. Z.; Li, B.; Byers, J. A., High molecular weight poly(lactic acid) produced by an efficient iron catalyst bearing a bis(amidinato)-N-heterocyclic carbene ligand. *Polyhedron* **2014**, *84*, 160-167.
69. Lei, Y.-N.; Zhu, Y.-B.; Gong, C.-F.; Lv, J.-J.; Kang, C.; Hou, L.-X., Synthesis, characterization and cytocompatibility of a degradable polymer using ferric catalyst for esophageal tissue engineering. *J Mater Sci: Mater Med* **2014**, *25*, 273-282.
70. Egevardt, C.; Giese, S. O. K.; da C. Santos, A. D.; Barison, A.; de Sá, E. L.; Filho, A. Z.; da Silva, T. A.; Zawadzki, S. F.; Soares, J. F.; Nunes, G. G.,  $\epsilon$ -caprolactone and lactide polymerization promoted by an ionic titanium(IV)/iron(III) polynuclear halo-alkoxide. *J. Polym. Sci., Part A: Polym. Chem.* **2014**, *52*, 2509-2517.

71. Biernesser, A. B.; Li, B.; Byers, J. A., Redox-Controlled Polymerization of Lactide Catalyzed by Bis(imino)pyridine Iron Bis(alkoxide) Complexes. *J. Am. Chem. Soc.* **2013**, *135*, 16553-16560.
72. Chen, J.; Gorczynski, J. L.; Zhang, G.; Fraser, C. L., Iron Tris(dibenzoylmethane–polylactide). *Macromolecules* **2010**, *43*, 4909-4920.
73. Wang, X.; Liao, K.; Quan, D.; Wu, Q., Bulk Ring-Opening Polymerization of Lactides Initiated by Ferric Alkoxides. *Macromolecules* **2005**, *38*, 4611-4617.
74. Gorczynski, J. L.; Chen, J.; Fraser, C. L., Iron Tris(dibenzoylmethane)-Centered Polylactide Stars: Multiple Roles for the Metal Complex in Lactide Ring-Opening Polymerization. *J. Am. Chem. Soc.* **2005**, *127*, 14956-14957.
75. McGuinness, D. S.; Marshall, E. L.; Gibson, V. C.; Steed, J. W., Anionic iron(II) alkoxides as initiators for the controlled ring-opening polymerization of lactide. *J. Polym. Sci., Part A: Polym. Chem.* **2003**, *41*, 3798-3803.
76. O'Keefe, B. J.; Breyfogle, L. E.; Hillmyer, M. A.; Tolman, W. B., Mechanistic Comparison of Cyclic Ester Polymerizations by Novel Iron(III)–Alkoxide Complexes: Single vs Multiple Site Catalysis. *J. Am. Chem. Soc.* **2002**, *124*, 4384-4393.
77. Gibson, V. C.; Marshall, E. L.; Navarro-Llobet, D.; White, A. J. P.; Williams, D. J., A well-defined iron(ii) alkoxide initiator for the controlled polymerisation of lactide. *J. Chem. Soc., Dalton Trans.* **2002**, 4321-4322.
78. O'Keefe, B. J.; Monnier, S. M.; Hillmyer, M. A.; Tolman, W. B., Rapid and Controlled Polymerization of Lactide by Structurally Characterized Ferric Alkoxides. *J. Am. Chem. Soc.* **2001**, *123*, 339-340.
79. Stolt, M.; Södergård, A., Use of Monocarboxylic Iron Derivatives in the Ring-Opening Polymerization of l-Lactide. *Macromolecules* **1999**, *32*, 6412-6417.
80. Södergård, A.; Stolt, M., Ring-opening polymerization of L-lactide by means of different iron compounds. *Macromol. Symp.* **1998**, *130*, 393-402.
81. Kricheldorf, H. R.; Damrau, D.-O., Polylactones, 38. Polymerization of L-lactide with Fe(II) lactate and other resorbable Fe(II) salts. *Macromol. Chem. Phys.* **1997**, *198*, 1767-1774.

82. Kwon, K. S.; Nayab, S.; Jeong, J. H., Synthesis, characterisation and X-ray structure of Cu(II) and Zn(II) complexes bearing N,N-dimethylethylenamine-camphorylimine ligands: Application in the polymerisation of rac-lactide. *Polyhedron* **2017**, *130*, 23-29.

83. Chun, M. K.; Cho, J.; Nayab, S.; Jeong, J. H., Polymerization of rac-Lactide Using Zinc(II) and Copper(II) Complexes of N1,N1-Dimethyl-N2-[(1R)-Myrtenylmethyl]Ethane-1,2-Diamine. *Bull. Korean Chem. Soc.* **2017**, *38*, 1527-1530.

84. Daneshmand, P.; Fortun, S.; Schaper, F., Diiminopyrrolide Copper Complexes: Synthesis, Structures and *rac*-Lactide-Polymerization Activity. *Organometallics* **2017**, *36*, 3860–3877.

85. Daneshmand, P.; van der Est, A.; Schaper, F., Mechanism and stereocontrol in isotactic *rac*-lactide polymerization with copper(II) complexes. *ACS Catal.* **2017**, *7*, 6289-6301.

86. Ahn, S. H.; Chun, M. K.; Kim, E.; Jeong, J. H.; Nayab, S.; Lee, H., Copper(II) complexes containing N,N'-bidentate N-substituted N-(pyridin-2-ylmethyl)amine: Synthesis, structure and application towards polymerization of *rac*-lactide. *Polyhedron* **2017**, *127*, 51-58.

87. Routaray, A.; Nath, N.; Maharana, T.; Sahoo, P. K.; Das, J. P.; Sutar, A. K., Salicylaldimine Copper(II) complex catalyst: Pioneer for ring opening Polymerization of Lactide. *J Chem Sci* **2016**, *128*, 883-891.

88. Mandal, M.; Oppelt, K.; List, M.; Teasdale, I.; Chakraborty, D.; Monkowius, U., Copper(II) complexes with imino phenoxide ligands: synthesis, characterization, and their application as catalysts for the ring-opening polymerization of *rac*-lactide. *Monatsh. Chem.* **2016**, *147*, 1883-1892.

89. Cho, J.; Nayab, S.; Jeong, J. H., Stereoselective polymerisation of *rac*-lactide catalysed by Cu(II) complexes bearing chloro derivatives of N,N'-bis(benzyl)dimethyl-(R,R)-1,2-diaminocyclohexane. *Polyhedron* **2016**, *113*, 81-87.

90. Akpan, E. D.; Ojwach, S. O.; Omondi, B.; Nyamori, V. O., Zn(ii) and Cu(ii) formamidine complexes: structural, kinetics and polymer tacticity studies in the ring-opening polymerization of  $\gamma$ -caprolactone and lactides. *New J. Chem.* **2016**, *40*, 3499-3510.

91. Routaray, A.; Nath, N.; Mantri, S.; Maharana, T.; Sutar, A. K., Synthesis and structural studies of copper(II) complex supported by –ONNO– tetradentate ligand: Efficient catalyst for the ring-opening polymerization of lactide. *Chin. J. Cat.* **2015**, *36*, 764-770.
92. Routaray, A.; Nath, N.; Maharana, T.; Sutar, A. k., Synthesis and Immortal ROP of L-Lactide Using Copper Complex. *J. Macromol. Sci., Part A: Pure Appl.Chem.* **2015**, *52*, 444-453.
93. Kwon, K. S.; Cho, J.; Nayab, S.; Jeong, J. H., Rapid and controlled polymerization of rac-lactide using copper(II) complexes of methyl-naphthalenylmethyl-(R,R)-1,2-diaminocyclohexanes. *Inorg. Chem. Commun.* **2015**, *55*, 36-38.
94. Fortun, S.; Daneshmand, P.; Schaper, F., Isotactic rac-Lactide Polymerization with Copper Complexes: The Influence of Complex Nuclearity. *Angew. Chem., Int. Ed.* **2015**, *54*, 13669-13672.
95. Whitehorne, T. J. J.; Schaper, F., Lactide,  $\beta$ -butyrolactone,  $\delta$ -valerolactone, and  $\epsilon$ -caprolactone polymerization with copper diketiminate complexes. *Can. J. Chem.* **2014**, *92*, 206-214.
96. Appavoo, D.; Omondi, B.; Guzei, I. A.; van Wyk, J. L.; Zinyemba, O.; Darkwa, J., Bis(3,5-dimethylpyrazole) copper(II) and zinc(II) complexes as efficient initiators for the ring opening polymerization of  $\epsilon$ -caprolactone and d,l-lactide. *Polyhedron* **2014**, *69*, 55-60.
97. Whitehorne, T. J. J.; Schaper, F., Square-planar Cu(II) diketiminate complexes in lactide polymerization. *Inorg. Chem.* **2013**, *52*, 13612-13622.
98. Li, C.-Y.; Hsu, S.-J.; Lin, C.-I.; Tsai, C.-Y.; Wang, J.-H.; Ko, B.-T.; Lin, C.-H.; Huang, H.-Y., Air-stable copper derivatives as efficient catalysts for controlled lactide polymerization: Facile synthesis and characterization of well-defined benzotriazole phenoxide copper complexes. *J. Polym. Sci., Part A: Polym. Chem.* **2013**, *51*, 3840-3849.
99. Whitehorne, T. J. J.; Schaper, F., *Nacnac*<sup>Bn</sup>CuOiPr: A strained geometry resulting in very high lactide polymerization activity. *Chem. Commun. (Cambridge, U. K.)* **2012**, *48*, 10334-10336.

100. Gowda, R. R.; Chakraborty, D., Copper acetate catalyzed bulk ring opening polymerization of lactides. *J. Molec. Catal. A: Chem.* **2011**, *349*, 86-93.
101. Chen, L.-L.; Ding, L.-Q.; Zeng, C.; Long, Y.; Lü, X.-Q.; Song, J.-R.; Fan, D.-D.; Jin, W.-J., Bulk solvent-free melt ring-opening polymerization of L-lactide catalyzed by Cu(II) and Cu(II)–Nd(III) complexes of the Salen-type Schiff-base ligand. *Appl. Organomet. Chem.* **2011**, *25*, 310-316.
102. Bhunora, S.; Mugo, J.; Bhaw-Luximon, A.; Mapolie, S.; Van Wyk, J.; Darkwa, J.; Nordlander, E., The use of Cu and Zn salicylaldimine complexes as catalyst precursors in ring opening polymerization of lactides: ligand effects on polymer characteristics. *Appl. Organomet. Chem.* **2011**, *25*, 133-145.
103. John, A.; Katiyar, V.; Pang, K.; Shaikh, M. M.; Nanavati, H.; Ghosh, P., Ni(II) and Cu(II) complexes of phenoxy-ketimine ligands: Synthesis, structures and their utility in bulk ring-opening polymerization (ROP) of l-lactide. *Polyhedron* **2007**, *26*, 4033-4044.
104. Sun, J.; Shi, W.; Chen, D.; Liang, C., The ring-opening polymerization of D,L-lactide catalyzed by new complexes of Cu, Zn, Co, and Ni Schiff base derived from salicylidene and L-aspartic acid. *J. Appl. Polym. Sci.* **2002**, *86*, 3312-3315.
105. Ma, H.; Spaniol, T. P.; Okuda, J., Highly Heteroselective Ring-Opening Polymerization of rac-Lactide Initiated by Bis(phenolato)scandium Complexes. *Angew. Chem., Int. Ed.* **2006**, *45*, 7818-7821.
106. Amgoune, A.; Thomas, C. M.; Roisnel, T.; Carpentier, J.-F., Ring-Opening Polymerization of Lactide with Group 3 Metal Complexes Supported by Dianionic Alkoxy-Amino-Bisphenolate Ligands: Combining High Activity, Productivity, and Selectivity. *Chem.-Eur. J.* **2006**, *12*, 169-179.
107. Chmura, A. J.; Chuck, C. J.; Davidson, M. G.; Jones, M. D.; Lunn, M. D.; Bull, S. D.; Mahon, M. F., A Germanium Alkoxide Supported by a C<sub>3</sub>-Symmetric Ligand for the Stereoselective Synthesis of Highly Heterotactic Polylactide under Solvent-Free Conditions. *Angew. Chem., Int. Ed.* **2007**, *46*, 2280-2283.
108. Chmura, A. J.; Davidson, M. G.; Frankis, C. J.; Jones, M. D.; Lunn, M. D., Highly active and stereoselective zirconium and hafnium alkoxide initiators for

solvent-free ring-opening polymerization of rac-lactide. *Chem. Commun. (Cambridge, U. K.)* **2008**, 1293-1295.

109. Jones, M. D.; Hancock, S. L.; McKeown, P.; Schafer, P. M.; Buchard, A.; Thomas, L. H.; Mahon, M. F.; Lowe, J. P., Zirconium complexes of bipyrrrolidine derived salan ligands for the isoselective polymerisation of rac-lactide. *Chem. Commun. (Cambridge, U. K.)* **2014**, *50*, 15967-15970.

110. Jones, M. D.; Brady, L.; McKeown, P.; Buchard, A.; Schafer, P. M.; Thomas, L. H.; Mahon, M. F.; Woodman, T. J.; Lowe, J. P., Metal influence on the iso- and hetero-selectivity of complexes of bipyrrrolidine derived salan ligands for the polymerisation of rac-lactide. *Chem. Sci.* **2015**, *6*, 5034-5039.

111. Addison, A. W.; Rao, T. N.; Reedijk, J.; van Rijn, J.; Verschoor, G. C., Synthesis, structure, and spectroscopic properties of copper(II) compounds containing nitrogen-sulphur donor ligands; the crystal and molecular structure of aqua[1,7-bis(N-methylbenzimidazol-2[prime or minute]-yl)-2,6-dithiaheptane]copper(II) perchlorate. *J. Chem. Soc., Dalton Trans.* **1984**, 1349-1356.

112. Chamberlain, B. M.; Cheng, M.; Moore, D. R.; Ovitt, T. M.; Lobkovsky, E. B.; Coates, G. W., Polymerization of lactide with zinc and magnesium b-diiminate complexes: stereocontrol and mechanism. *J. Am. Chem. Soc.* **2001**, *123*, 3229-3238.

113. Kasperczyk, J. E., HETCOR NMR study of poly(rac-lactide) and poly(meso-lactide). *Polymer* **1999**, *40*, 5455-5458.

114. Kasperczyk, J. E., Microstructure Analysis of Poly(lactic acid) Obtained by Lithium tert-Butoxide as Initiator. *Macromolecules* **1995**, *28*, 3937-3939.

115. Singh, J. V.; Baranwal, B. P.; Mehrotra, R. C., Synthesis and characterization of some Alkoxide Derivatives of Copper(II). *Z. Anorg. Allg. Chem.* **1981**, *477*, 235-240.

116. Yang, Y.; Liu, B.; Lv, K.; Gao, W.; Cui, D.; Chen, X.; Jing, X., Pyrrolide-Supported Lanthanide Alkyl Complexes. Influence of Ligands on Molecular Structure and Catalytic Activity toward Isoprene Polymerization. *Organometallics* **2007**, *26*, 4575-4584.

117. Yang, Y.; Cui, D.; Chen, X., The behavior of pyrrolyl ligands within the rare-earth metal alkyl complexes. Insertion of C[double bond, length as m-dash]N and

C[double bond, length as m-dash]O double bonds into Ln-[sigma]-C bonds. *Dalton Trans.* **2010**, *39*, 3959-3967.

118. Knizhnikov, V. A.; Borisova, N. E.; Yurashevich, N. Y.; Popova, L. A.; Chernyad'ev, A. Y.; Zubreichuk, Z. P.; Reshetova, M. D., Pincer ligands based on  $\alpha$ -amino acids: I. Synthesis of polydentate ligands from pyrrole-2,5-dicarbaldehyde. *Russ. J. Org. Chem.* **2007**, *43*, 855-860.

119. Simionescu, C. I.; Grigoras, M.; Cianga, I.; Olaru, N., Synthesis of new conjugated polymers with Schiff base structure containing pyrrolyl and naphthalene moieties and HMO study of the monomers reactivity. *European Polymer Journal* **1998**, *34*, 891-898.

120. Wansapura, C. M.; Juyoung, C.; Simpson, J. L.; Szymanski, D.; Eaton, G. R.; Eaton, S. S.; Fox, S., From Planar Toward Tetrahedral Copper(II) Complexes: Structural and Electron Paramagnetic Resonance Studies of Substituent Steric Effects in an Extended Class of Pyrrolate-Imine Ligands. *J. Coord. Chem.* **2003**, *56*, 975-993.

121. Save, M.; Schappacher, M.; Soum, A., Controlled Ring-Opening Polymerization of Lactones and Lactides Initiated by Lanthanum Isopropoxide, 1. General Aspects and Kinetics. *Macromol. Chem. Phys.* **2002**, *203*, 889-899.

122. *APEX2*, Release 2.1-0; Bruker AXS Inc.: Madison, USA, 2006.

123. *SAINTE*, Release 7.34A; Bruker AXS Inc.: Madison, USA, 2006.

124. Sheldrick, G. M. *SADABS*, Bruker AXS Inc.: Madison, USA, 1996 & 2004.

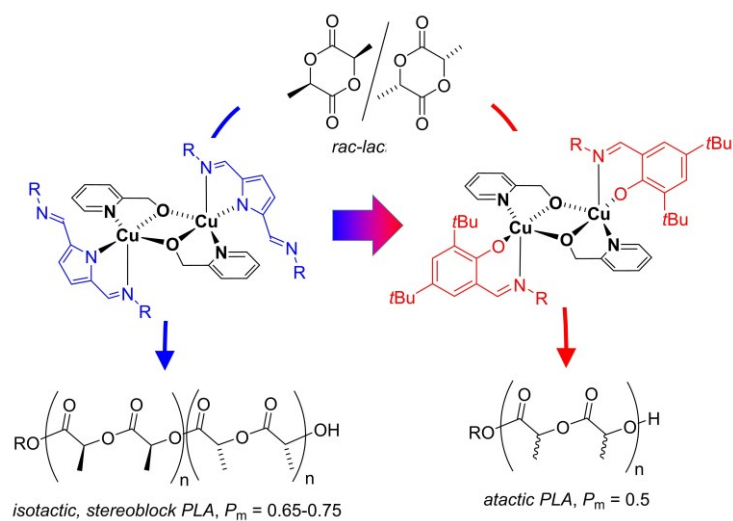
125. Sheldrick, G., SHELXT - Integrated space-group and crystal-structure determination. *Acta Crystallogr. Sect. A: Found. Crystallogr.* **2015**, *71*, 3-8.

126. Sheldrick, G. M., A short history of SHELX. *Acta Crystallogr.* **2008**, *A64*, 112-122.



## Chapter 6 . Dinuclear iminophenoxide copper complexes in *rac*-Lactide polymerisation

Daneshmand, P.; Pinon, L.; Schaper, F. Dinuclear iminophenoxide copper complexes in *rac*-Lactide polymerisation. *Dalton Trans.* **2018**, *in print*.



Reproduced by permission of the Royal Society of Chemistry.

Contributions of F. Schaper: A first draft was provided by me with minor modification from Prof. Frank Schaper.

Contributions of L. Pinon: Synthesis of ligands and initial synthesis of several copper complexes during her internship under my supervision



# Dinuclear iminophenoxide copper complexes in *rac*-Lactide polymerisation

Pargol Daneshmand,<sup>a</sup> Leena Pinon,<sup>a</sup> Frank Schaper<sup>a,\*</sup>

<sup>a</sup> Centre in Green Chemistry and Catalysis, Department of chemistry, Université de Montréal, C. P. 6128 Succ. Centre-Ville, Montréal, QC, H3T 3J7, Canada.

\* Email: Frank.Schaper@umontreal.ca

*Electronic Supplementary Information (ESI) available: Additional graphics and tables, NMR spectra of ligands, and details of X-ray diffraction analysis (CIF).*

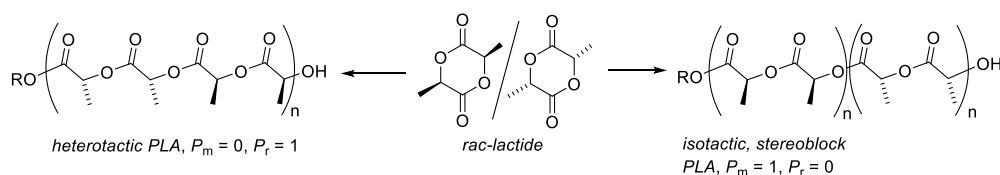
## Abstract

Dinuclear bis(R'-R''-iminomethyl)phenoxide) copper complexes  $6.L_2Cu_2(\mu-OR)_2$  were prepared from the reaction of copper methoxide with ROH and LH (ROH = dimethylaminoethanol or pyridylmethanol, R' = H, 4,6-*t*Bu, 1,3-Cl, R'' = benzyl, cyclohexyl, diphenylmethyl and 2,6-dimethylphenyl). Preparation was complicated by formation of homoleptic  $6.L_2Cu$  and only 9 of the 24 possible combinations could be prepared. All complexes were characterized by single crystal X-ray diffraction studies and crystallized as dinuclear penta-coordinated complexes. Homoleptic complexes  $6.L_2Cu$  were inactive in lactide polymerization at room temperature. Most heteroleptic complexes showed modest to good activities with full conversion in less than 6 h at room temperature. Complexes with R'=H showed poor molecular weight control, complexes with R'=Cl were inactive in polymerization. In pyridylmethoxide-containing complexes, only one alkoxide initiated chain growth. All complexes produced atactic polymer.

## Introduction

In the interest to find sustainable replacements for petroleum-based resources, polylactic acid (PLA) is considered an alternative to polyolefin-based plastics. PLA is obtained by the ring-opening polymerization of lactide, the dimeric anhydride of lactic acid, obtained from the fermentation of corn starch.<sup>1-11</sup> Although lactide is not difficult to polymerize, combining high polymerization

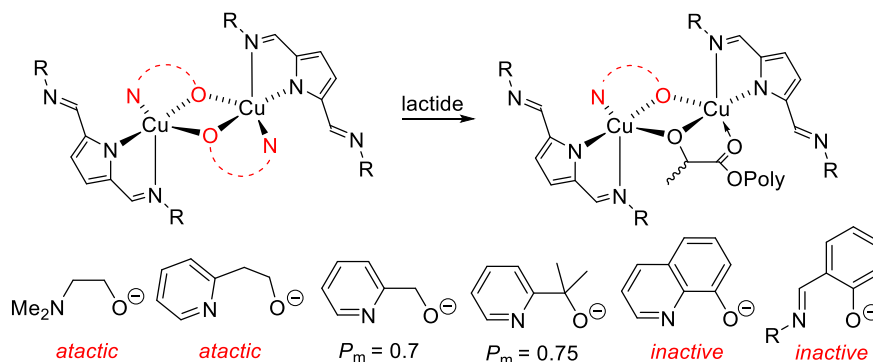
activity with good polymerization control poses a catalytic challenge and attracted academic interest in developing improved catalyst systems, most often based on a coordination-insertion mechanism.<sup>12-38</sup> With regard to stereocontrol, *rac*-lactide has a high tendency towards alternating monomer insertion and highly heterotactic PLA ( $\{RR-SS\}_n$ ,  $P_m = 0$ , Scheme 6.1) was obtained already in early work of Coates on diketiminate zinc catalysts.<sup>39</sup> To obtain the industrially relevant isotactic PLA ( $\{RR\}_n/\{SS\}_n$  or  $\{RR\}_n\{SS\}_n$ ,  $P_m = 1$ ) in combination with high activity and good polymer molecular weight control, was more challenging. Although promising catalyst systems have emerged,<sup>40-49</sup> their optimization remains hindered by the tendency of lactide-polymerization catalysts to react with sometimes catastrophic changes in reactivity upon modification of the ligand framework.



### Scheme 6.1.

Of metal-based catalysts for coordination-insertion polymerization of lactide,  $d^0$ - and  $d^{10}$  metals received the highest attention, while catalysts based on groups 5-11 remained largely unexplored. There are very few reports of catalysts based on Cr,<sup>46</sup> Mn,<sup>50-54</sup> Ni,<sup>55-59</sup> or Co.<sup>52, 60-62</sup> None of these systems could compete in stereocontrol or activity with  $d^0$ - or  $d^{10}$ -metal based catalysts. Complexes based on iron and copper have been studied in somewhat more detail. Several iron complexes showed high activity for coordination-insertion polymerization<sup>63-68</sup> and polymerization activity of iron complexes can be turned on or off by switching their redox state.<sup>69, 70</sup> A recent study reported the first isotactic PLA obtained with iron-based complexes.<sup>71</sup> Copper-based polymerization catalysts are the 2<sup>nd</sup> largest group investigated. The catalysts were either carboxylate salts,<sup>72-74</sup> homoleptic complexes with iminophenoxide-based ligands,<sup>55, 75, 76</sup> or copper(II) salen complexes.<sup>77, 78</sup> None of these complexes were optimized for coordination-insertion polymerization and the

sterically saturated copper centers are not expected to be highly Lewis-acidic. Thus in general only low activities were observed, even in molten polymer. Polymer molecular weight control was often excellent, on the other hand. The one exception with regard to low activities is a copper salen complex, which showed, in the presence of benzyl alcohol, surprising activity in solution (24 h at RT).<sup>78</sup> In 2012, we reported that heteroleptic diketiminate copper(II) alkoxides showed very high activity in *rac*-lactide polymerization in solution (<5 min at RT).<sup>79-81</sup> Perfect molecular weight control, the absence of side reactions, and – unfortunately – also of stereocontrol characterized these catalysts. Jeong’s group reported similarly high activities for *in-situ* generated diamino- or pyridylamino copper(II) alkoxide complexes.<sup>82-86</sup> PLA obtained with these complexes was highly heterotactic, the first time notable stereocontrol was observed in copper-catalyzed lactide polymerization. In 2015, we reported that heteroleptic iminopyrrolide copper alkoxide complexes polymerized lactide with a preference for isotactic monomer insertion, the first time isotactic lactide polymerization was observed for a Cu-based catalyst.<sup>87</sup> The active species is dinuclear and one of the initial pyridylmethoxide ligands does not initiate polymerization, but is retained as a spectator ligand in the complex (Scheme 6.2).<sup>88, 89</sup> The nature of the bridging alkoxide ligand proved to be crucial for stereocontrol and a major impediment in catalyst optimization: Bridges less “rigid” than pyridylmethoxide, such as pyridylethoxide or dimethylaminoethoxide led to loss of stereocontrol. With dimethylaminoethoxide, both alkoxides initiated chain growth. More rigid bridges, such as iminoaryloxides or hydroxyquinoline led to loss of activity (Scheme 6.2).<sup>88</sup>

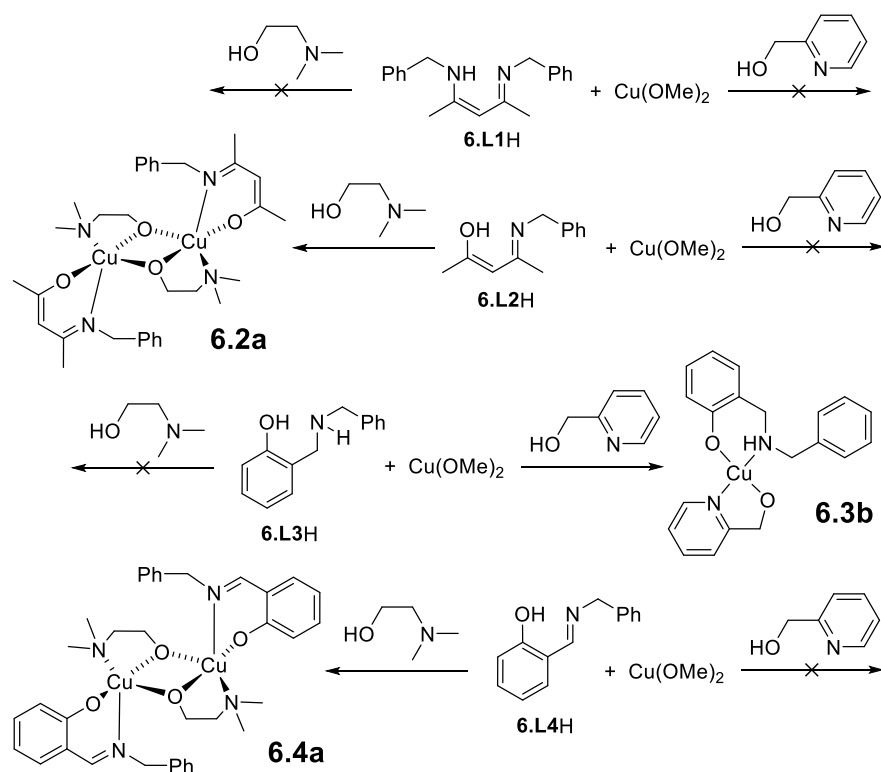


**Scheme 6.2.**

Since stereocontrol seemed to rely on the presence of a pyridylmethoxide bridging ligand, we turned our attention towards possible variations of the spectator ligand. In the following, we describe the preparation of dinuclear pyridylmethoxide complexes with spectator ligands other than iminopyrrolides, in particular heteroleptic iminophenoxide complexes, and their application in the *rac*-lactide polymerization.

## Results and discussion

Four different ligand systems similar to iminopyrroles were targeted for initial exploration in form of their *N*-benzyl substituted derivatives:  $\beta$ -diketimines,  $\beta$ -aminoketones, aminophenols, and iminophenols (Scheme 6.3). We were not able to prepare any heteroleptic copper complexes from the reaction of copper methoxide with **6.L1H** in the presence of either dimethylaminoethanol or pyridylmethanol. Reactions either yielded unidentifiable mixtures or the known homoleptic complex  $(\mathbf{6.L1})_2\text{Cu}$ .<sup>80</sup> Reactions with **6.L2H** in the presence of dimethylaminoethanol yielded the dinuclear complex **6.2a** (Scheme 6.3). No product was obtained with pyridylmethoxide or when the *N*-substituent was cyclohexyl, diphenylmethyl, or xylyl. Complex **6.2a** crystallized as an aminoalkoxide-bridged dimer (Fig. 6.1, Table 6.I). The coordination geometry around copper is square-pyramidal, with a  $\tau$ -value of 0.3.<sup>90</sup> The amine nitrogen is found in the apical position. Cu-N/O bond distances of 1.93-1.99 Å are unremarkable for equatorial atoms in square-pyramidal Cu(II) complexes.



Scheme 6.3.

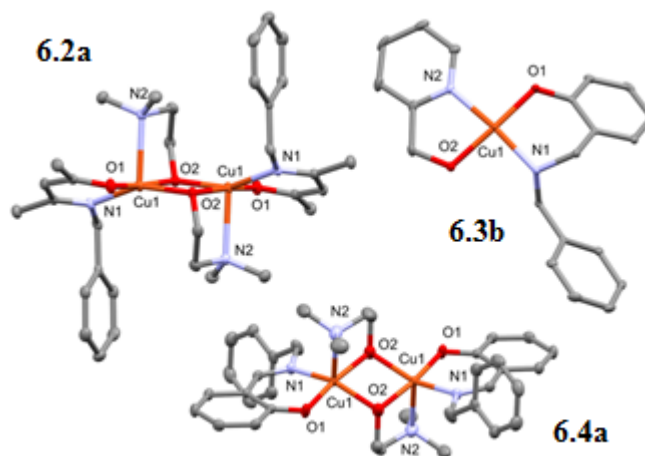


**Figure 6.1.** X-ray structures of **6.2a**, **6.3b** and **6.4a**. Thermal displacements are shown at the 50% probability level. Hydrogen atoms and the minor part of the aminoethoxide disorder in **6.4a** were omitted for clarity.

**Table 6.I.** Bond distances [Å] in crystal structures of **6.2a**, **6.3b** and **6.4a**

	<b>6.2a</b>	<b>6.3b</b>	<b>6.4a</b>
Cu-O1 (ligand)	1.930(1)	1.915(1)	1.913(1) <sup>a</sup>
Cu-N1 (ligand)	1.988(1)	2.029(1)	1.995(2) <sup>a</sup>
Cu-O2 <sub>short</sub> (alkoxide)	1.966(1)	1.929(1)	1.956(2) <sup>a</sup>
Cu-O2 <sub>long</sub> / Cu-N3	1.991(1)	2.512(1)	2.029(1) <sup>a</sup>
Cu-N2	2.341(1)	1.992(1)	2.289(2)
Cu-Cu	2.9922(4)		3.0027(5)
$\tau$	0.3	0.1	0.3
Ligand in apical position	Amine	Pyridylmethanol	Amine

<sup>a</sup> Data only shown for major part of dimethylaminoethoxide disorder.

Complex **6.2a** was active in *rac*-lactide polymerization and reached full conversion in appr. 5 h (Table 6.II). The reaction followed pseudo-first-order kinetics (Fig. 6.S1). As expected for catalyst with an aminoethoxide bridging ligand, the obtained PLA was atactic. We have shown previously that pyridylmethoxide complexes with isotactic stereocontrol can be formed *in situ* from the respective aminoethoxide complexes, which showed no stereocontrol by addition of pyridylmethanol to the polymerization reaction.<sup>87-89</sup> *rac*-Lactide was thus polymerized with **6.2a** in the presence of 1 equiv pyridylmethanol. However no change in the stereochemistry of the polymer was observed (Table 6.II). Polymerizations with **6.2a** and **6.2a**/PyCH<sub>2</sub>OH both showed poor polymer molecular weight control, with polydispersities of 1.7-2.6 and lower than expected polymer molecular weights. It was thus not possible to determine whether added PyCH<sub>2</sub>OH served as a simple chain-transfer reagent in immortal polymerization or whether it was incorporated as a spectator ligand, but without providing stereocontrol. The activity of **6.2a** was appr. twice as high in the presence of PyCH<sub>2</sub>OH. While not investigated in detail, the negative *x*-axis intercept in polymerization with **6.2a** indicates a fast catalyst deactivation at the start of the reaction, which was suppressed in the presence of pyridylmethanol (Fig. 6.S1).



**Table 6.II.** *rac*-lactide polymerizations <sup>a</sup>

Entry	Catalyst	Final conversion	$k_{\text{obs}}$ [h <sup>-1</sup> ]	$M_n^b$	$M_n$ (calc.) <sub>c</sub>	$M_w/M_n$	# chains <sub>d</sub>	$P_m^e$
1	<b>6.2a</b>	97%	0.31(2)	4.3 kDa	14.0 kDa	1.7	3.3	0.48
2	<b>6.2a</b> + 1 PyCH <sub>2</sub> OH	99%	0.61(2)	2.4 kDa	14.1 kDa	2.6	5.8	0.48
3	<b>6.3b</b>	3%	-	-	-	-	-	-
4	<b>6.3b</b> (at 50 °C)	24%	-	0.8 kDa	3.5 kDa	1.3	4.4	0.23
6	<b>6.4a</b>	96%	0.60(0)	7.7 kDa	13.8 kDa	1.2	1.8	0.53
5	<b>6.4c</b> + 5 BnOH	0%	-	-	-	-	-	-
7	<b>6.5a</b>	99%	0.80(1)	5.5 kDa	14.3 kDa	1.5	2.6	0.5
8	<b>6.5a</b> + 1 PyCH <sub>2</sub> OH	97%	1.07(3)	4.3 kDa	14.0 kDa	1.5	3.2	0.49
9	<b>6.6a</b>	36%	-	6.9 kDa	5.2 kDa	1.3	1	0.43
10	<b>6.6b</b>	26%	-	1.4 kDa	3.7 kDa	1.3	2.6	0.35
13	<b>6.8b</b>	97%	0.56(8)	14.5 kDa	14.0 kDa	1.2	1	0.53
15	<b>6.9a</b>	98%	0.82(3)	7.5 kDa	14.1 kDa	1.1	1.9	0.48
16	<b>6.9a</b> + 1 PyCH <sub>2</sub> OH	99%	1.8(0)	4.8 kDa	14.1 kDa	1.2	2.9	0.48
14	<b>6.11b</b>	98%	1.05(12)	15.3 kDa	14.1 kDa	1.3	1.1	0.50
17	<b>6.12b</b>	13%	-	-	-	-	-	-
11	<b>6.16a</b>	15%	-	-	14.4 kDa	-	-	-
12	<b>6.16b</b>	3%	-	-	14.4 kDa	-	-	-

<sup>a</sup> Conditions: C<sub>6</sub>D<sub>6</sub>, RT, [lactide] = 200 mM, [6.L<sub>2</sub>Cu<sub>2</sub>(OR)<sub>2</sub>] = 2 mM. <sup>b</sup>  $M_n$  and  $M_w$  determined by size exclusion chromatography vs. polystyrene standards, with a Mark-Houwink correction factor of 0.58. <sup>c</sup>  $M_n$  expected if one alkoxide per catalyst dimer initiates polymerization, calculated from [lactide]/[cat]·conversion· $M_{\text{lactide}}$  +  $M_{\text{ROH}}$ . <sup>d</sup> Number of chains per catalyst dimer, calculated from the ratio of expected and obtained polymer molecular weight. <sup>e</sup>  $P_m$  determined from decoupled <sup>1</sup>H NMR by  $P_m = 1 - 2 \cdot I_1 / (I_1 + I_2)$ , with  $I_1 = 5.20 - 5.25$  ppm (*rmr*, *mmr/rmm*),  $I_2 = 5.13 - 5.20$  ppm (*mmr/rmm*, *mmm*, *mrm*).

Reaction of the aminophenol ligand **6.L3H** with copper methoxide in the presence of pyridylmethanol afforded complex **6.3b** (Scheme 6.1), which crystallized as a monomeric complex with the square-pyramidal geometry completed by a ancillary pyridylmethanol ligand (Fig. 6.1, Table 6.I). Cu-N/O bond distances are in the expected range. Compared to Cu-N<sub>imino</sub> bond distances (where the *N*-substituent is benzyl), the Cu-N<sub>amino</sub> bond distance is longer by appr. 0.3 Å, as expected for an sp<sup>3</sup>-vs. sp<sup>2</sup>-donor ligand. Complex **6.3b** was essentially inactive for lactide polymerization at room temperature, and reacted sluggishly even at 50 °C (Table 6.II). The obtained PLA was moderately heterotactic ( $P_m = 0.23$ ), but due to possible complex decomposition and the lower than expected polymer molecular weight, the reaction mechanism and the active species are unclear. The inactivity of **6.3b** in polymerization is not due to coordination of pyridylmethanol, which can be added as an external alcohol to polymerizations without any loss of activity. It correlates better with the fact that **6.3b** crystallized as a monomeric, pyridine-coordinated complex. All copper catalysts isolated in our laboratories which showed high activities in coordination-insertion polymerization of lactide formed alkoxide-bridged dimers in the solid state, although excess pyridylmethanol was always present in the reaction mixture. The amino-phenoxide ligand seems to reduce the Lewis acidity of copper sufficiently to discourage the coordination of a bridging alkoxide and likewise of lactide monomer.

Unlike its amino-derivative, we were unable to obtain pyridylmethoxide complexes with the iminophenol ligand **6.L4H**. Instead, the respective homoleptic complex **6.4c**, (**6.L4**)<sub>2</sub>Cu,<sup>91, 92</sup> was obtained (*vide infra*). The respective aminoethoxide complex, **6.4a**, could be prepared readily. Complex **6.4a** crystallizes as the expected dimeric complex with a square-pyramidal coordination around copper and the amine ligand in the apical position (Fig. 6.1, Table 6.I).

Since surprisingly high room temperature activity was reported for a copper(II) salen complex following an activated monomer mechanism,<sup>78</sup> the homoleptic complex **6.4c** was employed for lactide polymerization in the presence of 5 equiv of benzyl alcohol. However, no activity was observed (Table 6.II). The

iminophenol ligand is too acidic to be protonated in sufficient amounts to form active, heteroleptic species,<sup>81</sup> and the complex is not Lewis-acidic enough to catalyse polymerization via an activated monomer mechanism. The heteroleptic complex, on the other hand, showed good activity in lactide polymerization with full conversion in less than 5 h at room temperature. Polymerizations with **6.4a** followed clean first-order kinetics (Fig. 6.2), without any notable induction period or catalyst decomposition. The polydispersity was narrow ( $M_w/M_n = 1.2$ ) and the polymer molecular weight is in good agreement with both alkoxides initiating chain growth. As expected for a catalyst with an aminoethoxide bridging ligand,<sup>87-89</sup> the obtained polymer was atactic.

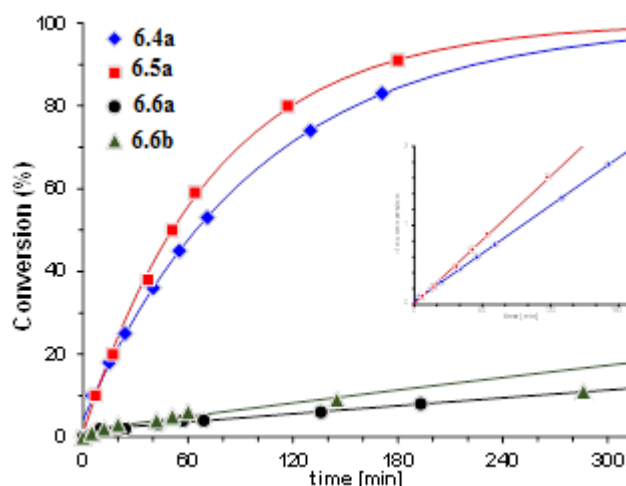
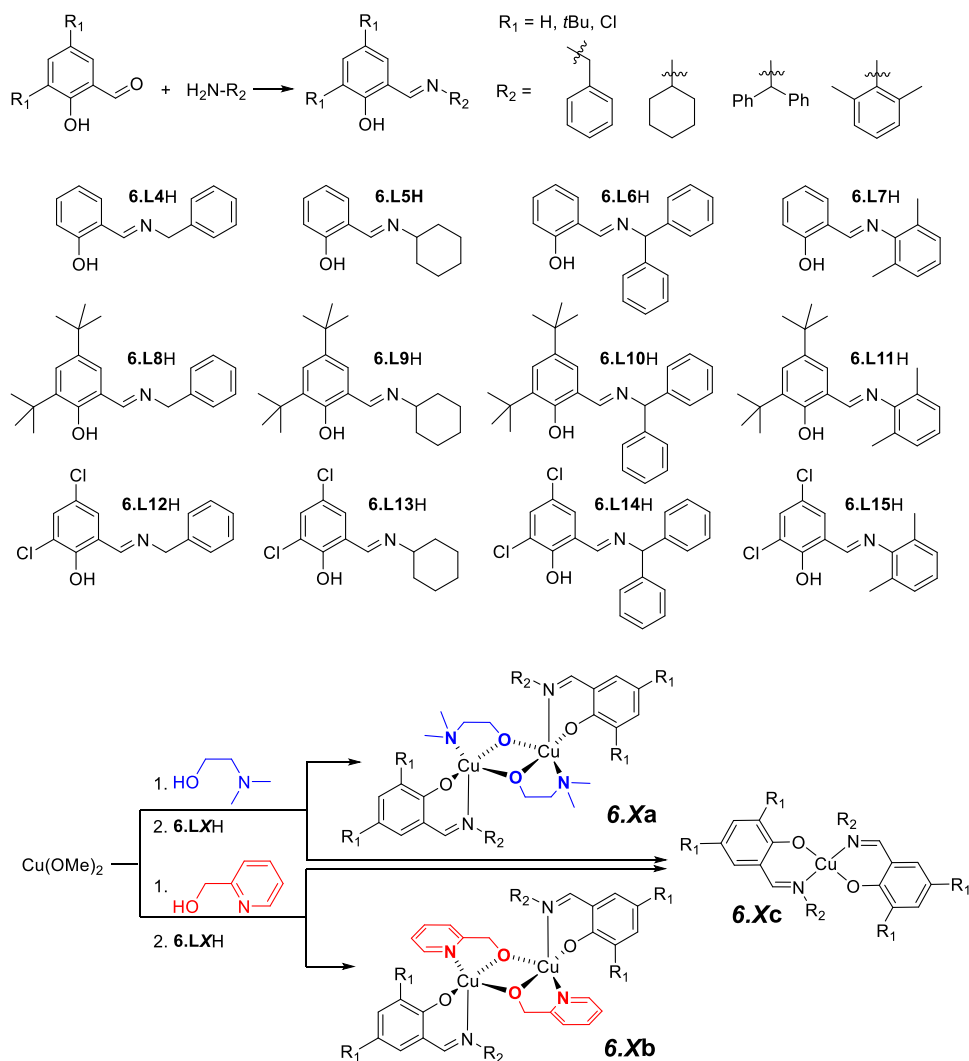


**Figure 6.2.** Conversion-time profiles for rac-lactide polymerization with **6.4a** (diamonds), **6.5a** (squares), **6.6a** (circles) and **6.6b** (triangles). Conditions:  $C_6D_6$ , RT, 0.2 M lactide, 2 mM [cat.]. The inset shows the semi-logarithmic plot. Solid lines represent in both graphics theoretical conversions with the values obtained in linear regression analysis: **6.4a**:  $k_{app} = 0.604(2) \text{ h}^{-1}$ ,  $t_0 = -4 \text{ min}$ , **6.5a**:  $k_{app} = 0.80(1) \text{ h}^{-1}$ ,  $t_0 = -1 \text{ min}$ .

### Iminophenols - ligand and general complex synthesis.

Given the good activity and stereocontrol observed for **6.4a**, we decided to further explore iminophenol ligands for the coordination-insertion polymerization of lactide. All iminophenol ligands, if not already reported, were synthesized through condensation of the salicylaldehyde derivative with

the respective amine, based on a previously reported method (Scheme 6.4, Exp. section).<sup>88</sup> Dinuclear copper complexes  $\{\text{LCu}(\mu\text{OR})\}_2$  were obtained by successive addition of aminoalcohol and the respective iminophenol **6.LXH** to a solution of copper methoxide. Initial addition of (excess) aminoalcohol led to a blue solution. Reaction with the ligand typically formed green solutions, from which the heteroleptic complex with either a dimethylaminoethoxide, **6.Xa**, or pyridylmethoxide, **6.Xb**, bridging ligand could be crystallized (Scheme 6.4). Control of the Schlenk equilibrium proved to be very difficult for iminophenol ligands. In most cases (*vide infra*), dark-brown solutions were obtained after reaction with iminophenol and crystallization – if successful – afforded the homoleptic complexes, **6.Xc** (Scheme 6.4), typically as brown crystals and sometimes accompanied by the respective bisaminoalkoxide complex. Variations of reaction conditions, such as changes of solvent, stoichiometry or order of addition, did not improve the reaction outcome in any of these cases.



Scheme 6.4.

### Salicylaldehyde-based ligands.

Analogous to **6.4a**, reaction of copper(II) methoxide with two equiv of dimethylaminoethanol, followed by addition of the iminophenol ligand lead to green solutions, from which the heteroleptic complexes **6.5a** and **6.6a** crystallized. With the sterically demanding xyllyl *N*-substituent, only the homoleptic complex **6.7c** was obtained. Formation of homoleptic complexes was even more pronounced with the pyridylmethoxide ligand: only with a diphenylmethyl *N*-substituent, **6.L6H**, the heteroleptic complex **6.6b** was obtained. Reactions of **6.L4H**, **6.L5H**, or **6.L7H** afforded dark-brown solutions and after crystallization the homoleptic complexes **6.L<sub>2</sub>Cu 6.4c**, **6.5c** and **6.7c**.

We have noted before that introduction of a pyridylmethoxide bridging ligand is sterically more demanding than that of a dimethylaminoethoxide ligand.<sup>89</sup> Indeed, if salicylaldehyde was used as spectator ligand, i. e. in the absence of any *N*-substituent, copper complexes **6.16a** and **6.16b** were obtained with both bridging ligands (Scheme 6.5, Fig. 6.3). Homoleptic complexes **6.4c-6.7c** were prepared independently from reaction of copper(II) methoxide with two equivalents of iminophenol for characterization purposes (Scheme 6.5, Fig. 6.S2). Preparation of **6.6c** was straightforward and occurred with a yield similar to the other homoleptic complexes. The formation of **6.6b** is thus not due to an inaccessibility of the homoleptic complex.

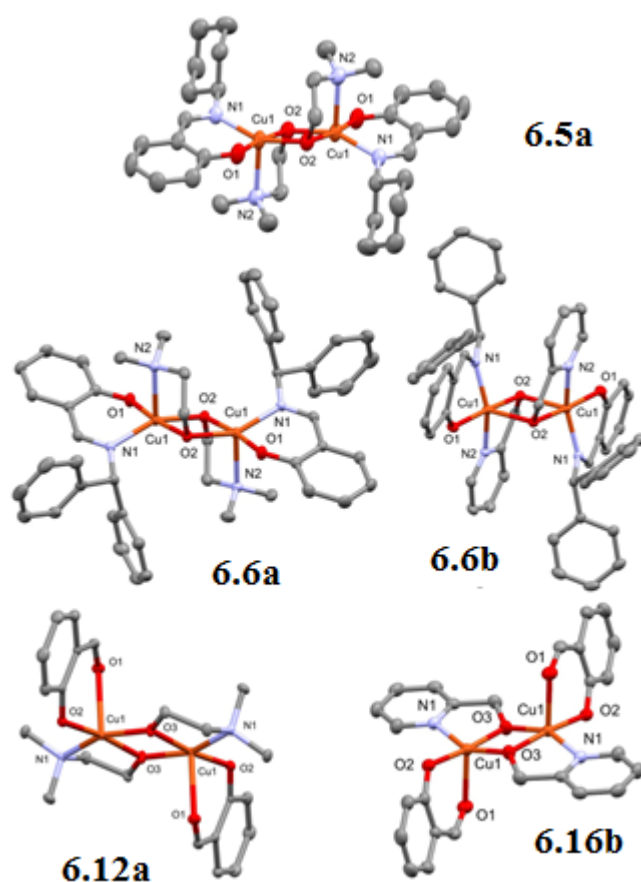
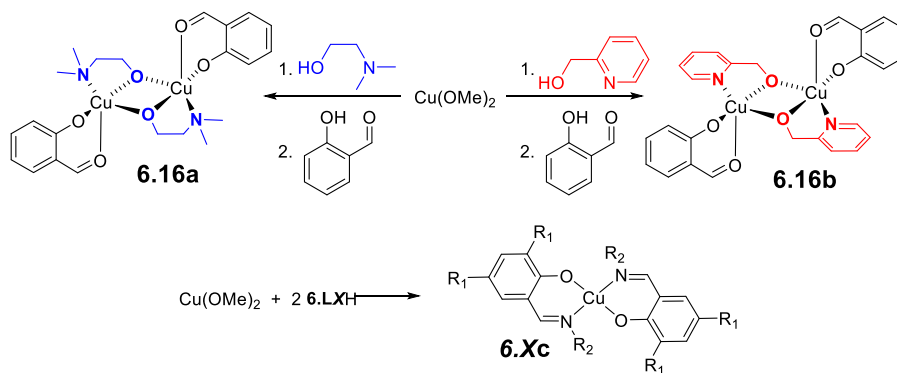


**Figure 6.3.** X-ray structures of **6.5a**, **6.6a**, **6.6b**, and **6.16a** and **6.16b**. Thermal displacements are shown at the 50% probability level. Hydrogen atoms were omitted for clarity. Only one of two independent molecules shown for **6.5a**.



### Scheme 6.5.

As does **6.4a**, heteroleptic complexes **6.5a**, **6.6a**, **6.6b**, **6.16a** and **6.16b** crystallize as dinuclear complexes with bridging aminoalkoxide ligands and with copper in a square-pyramidal geometry (Fig. 6.3, Table 6.III). The latter is confirmed by  $\tau$ -values of 0.3 for all complexes.<sup>90</sup> Consequently, four ligands are found in the equatorial plane with bond distances of appr. 1.9 – 2.0 Å, while one ligand occupies the apical position with an elongated distance of 2.2 – 2.3 Å to the copper center. In **6.4a-6.6a** the amino group of the bridging ligand occupies the apical position and in **6.16a+b** the keto-group of salicylaldehyde. In **6.6b**, on the other hand, the bridging alkoxide is found in the apical position. The structural data does not offer any indication why placement of the alkoxide in the apical position should be favoured for **6.6b**. It should be noted, however, that a bridging alkoxide is likewise observed in the copper bis(pyridylmethoxide) dimer (Fig. 6.S3). Placement of the anionic bridging alkoxide in the weak apical coordination site is thus not a simple consequence of the steric bulk of the diphenylmethyl *N*-substituent. Copper-oxygen and copper-nitrogen distances are in the range expected for five-coordinated Cu(II) complexes.<sup>93</sup> The steric bulk of the *N*-substituent is notable in a Cu-N<sub>imine</sub> distance > 2.0 Å in **6.6a** and **6.6b**, while it remains <2.0 Å in **6.4a** and **6.5a**.

**Table 6.III.** Selected geometric data for heteroleptic copper complexes

	<b>6.5a</b> <sup>a</sup>	<b>6.6a</b>	<b>6.9a</b>	<b>6.10a</b>	<b>6.16a</b>
Cu-O <sub>phenol</sub>	1.915(6), 1.911(6)	1.917(1)	1.910(1)	1.902(2)	1.911(1)
Cu-N <sub>imine/O</sub>	1.992(7), 1.985(7)	2.023(1)	2.025(2)	1.998(2)	2.300(1)
Cu-O <sub>short</sub>	1.965(5), 1.946(6)	1.954(1)	1.932(1)	1.950(2)	1.918(1)
Cu-O <sub>long</sub>	1.987(5), 1.991(6)	2.007(1)	2.116(2)	1.985(2)	1.945(1)
Cu-N <sub>NMe2/py</sub>	2.324(8), 2.322(9)	2.305(1)	2.196(2)	2.422(2)	2.036(1)
Cu-Cu	3.0, 3.0	3.0	3.0	3.0	3.02
$\tau$	0.3, 0.3	0.3	0.7	0.1	0.2
Atom in apical position	Amine, Amine	Amine		Amine	Aldehyde

<sup>a</sup> Two independent molecules in the asymmetric unit. <sup>b</sup> Copper centres crystallographically independent.



**Table 6.III-continued.** Selected geometric data for heteroleptic copper complexes

	<b>6.6b</b>	<b>6.8b</b> <sup>a</sup>	<b>6.11b</b> <sup>b</sup>	<b>6.12b</b> <sup>b</sup>	<b>6.16b</b>
Cu-O <sub>phenol</sub>	1.930(1)	1.926(2), 1.921(2)	1.907(2), 1.891(2)	1.909(3), 1.917(3)	1.906(1)
Cu-N <sub>imine/O</sub>	2.004(1)	1.989(2), 1.986(2)	2.013(2), 2.002(2)	2.014(4), 2.002(4)	2.247(1)
Cu-O <sub>short</sub>	1.947(1)	1.931(2), 1.928(2)	1.945(2), 1.956(2)	1.916(3), 1.919(3)	1.927(1)
Cu-O <sub>long</sub>	2.249(1)	2.226(2), 2.227(2)	1.983(2), 1.980(2)	2.332(3), 2.317(3)	1.949(1)
Cu-N <sub>NMe2/py</sub>	2.009(1)	2.032(2), 2.037(2)	2.239(2), 2.275(2)	1.993(4), 2.009(4)	1.994(2)
Cu-Cu	3.1	3.1, 3.1	3.0	3.1	3.0
$\tau$	0.3	0.3, 0.3	0.3, 0.4	0.2, 0.2	0.3
Atom in apical position	RO <sup>-</sup>	RO <sup>-</sup> , RO <sup>-</sup>	Pyridine, Pyridine	RO <sup>-</sup> , RO <sup>-</sup>	Aldehyde

<sup>a</sup> Two independent molecules in the asymmetric unit. <sup>b</sup> Copper centres crystallographically independent.

All heteroleptic complexes were active for the polymerization of lactide at room temperature in C<sub>6</sub>D<sub>6</sub> solution (Table 6.II). Under typical conditions (2 mM cat., 200 mM *rac*-lactide), polymerizations with **6.4a** and **6.5a** reached completion in less than 5 h (Table 6.II). Polymerizations followed a pseudo-first order rate law with comparable apparent rate constants for both catalysts. Only a negligible induction period was observed before the start of the polymerization (Fig. 6.2). Both complexes provided atactic PLA, which is in agreement with results from iminopyrrolide copper complexes, which require the presence of a pyridylmethoxide bridging ligand for isotacticity. Addition of one equivalent of pyridylmethoxide to polymerizations with **6.5a**, in an attempt to generate **6.5b** *in situ*, was well tolerated, but did not influence stereocontrol. Complexes **6.6a** and **6.6b** reacted only sluggishly and even after 3 days, conversions did not surpass 36% and 26%, respectively (Table 6.II). Salicylaldehyde complexes **6.16a** and **6.16b** were essentially unreactive at

room temperature. Contrary to **6.4a** and **6.5a**, polymerizations with **6.6a** and **6.6b** were moderately heterotactic. The latter might be a consequence of the increased steric bulk of the *N*-substituent or – more likely considering also their low activity – indicative of complex decomposition. The good polymer molecular weight control observed for **6.4a** is unfortunately not retained for its derivatives. Complexes **6.5a**, **6.6a**, and **6.6b** show only mediocre polymer molecular weight control, with polydispersities ranging from 1.3 to 1.5 (Table 6.II). Based on the polymerization behaviour in the analogous iminopyrrolide complexes, we expected only one pyridylmethoxide substituent per catalyst dimer to initiate polymerization, while both aminoethoxide groups should initiate. The low polymer molecular weight control prevents any conclusion whether the same initiator behaviour is followed in iminophenoxide complexes.

#### **4,6-di(*tert*-butyl)salicylaldehyde-based ligands.**

To improve polymer molecular weight control, we investigated iminophenols carrying *tert*-butyl substituents in *ortho*- and *para*-position. As for the salicylaldehyde-based ligands, dimethylaminoethoxide complexes **6.9a** and **6.10a** could be obtained with *N*-cyclohexyl and *N*-diphenylmethyl substituents. Only trace amounts were obtained for **6.10a**, however, which was thus not employed in polymerization. The respective pyridylmethoxide complexes were inaccessible. Surprisingly, the inverse was true for the sterically less demanding *N*-benzyl containing ligand, as well as the sterically more bulky *N*-xylyl ligand, where we could obtain the pyridylmethoxide containing complexes **6.8b** and **6.11b**, but not the respective aminoethoxide complexes. In contrast to salicylaldehyde-based ligands, homoleptic complexes were not obtained as alternative reaction products, although the preparations and structures of **6.8c**,<sup>94</sup> **6.9c**,<sup>94</sup> and **6.11c**<sup>95, 96</sup> have been reported in the literature. Previous preparations of heteroleptic LCu(OR) complexes indicated  $\beta$ -hydride elimination from the alkoxide, followed by decomposition of the Cu(II) hydride as a secondary reaction pathway, in particular for sterically demanding ligands.<sup>80, 89</sup> In some cases Cu(I) reaction products have been isolated,<sup>89</sup> in

others not.<sup>80</sup> A similar decomposition pathway via  $\beta$ -hydride elimination might be in place here.

All isolated complexes crystallized again as dimers with bridging alkoxide ligands (Fig. 6.4, Table 6.III) and a square-pyramidal geometry around copper; the exception being **6.9a**, for which a  $\tau$ -value of 0.7 and the Cu-ligand distances indicate a trigonal-bipyramidal geometry. As in **6.4a-6.6a**, the amine occupies the apical position in **6.10a**. As in **6.6b**, the alkoxide is found in that position in **6.8b**. In **6.11b**, pyridine occupies the apical position. Contrary to most of the structural deviations observed in the complexes studied here, a clear steric motivation exists in this case: placing the bridging alkoxide in the apical position, as in **6.6b** and **6.8b**, would lead for **6.11b** to strong steric interactions between the xyllyl substituent and the bridging pyridylmethanol.

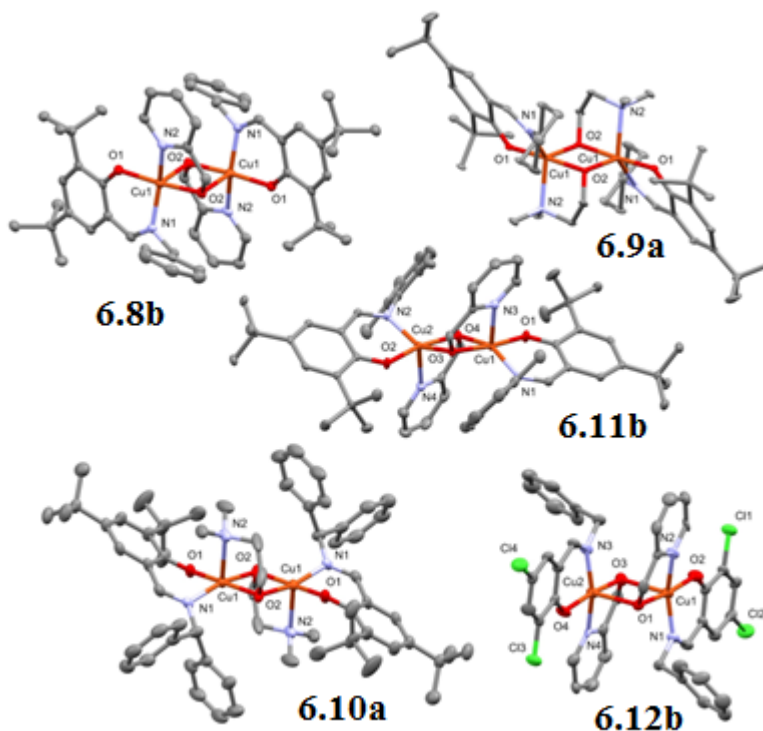


**Figure 6.4.** X-ray structures of **6.8b**, **6.9a**, **6.10a**, and **6.11b** and **6.12b**. Thermal displacements are shown at the 50% probability level. Hydrogen atoms and solvent (**6.8b**) were omitted for clarity. Only one of two independent molecules shown for **6.8b**.

Polymerizations with **6.8b** and **6.11b** showed a notable induction period, while polymerizations with **6.9a** did not (Fig. 6.5). In this, iminophenoxide complexes resemble their iminopyrrolide analogues, where an induction period was associated with the pyridylmethoxide bridging ligand. All polymerizations went to completion in less than 5 h, although some catalyst decomposition was observed for **6.9a**. Polymer molecular weight control was significantly improved and PLA polydispersities were below 1.3 for all catalysts (Table 6.II). More important, the obtained molecular weights indicate that only one pyridylmethoxide ligand initiates chain growth in **6.8b** and **6.11b**, while both alkoxides initiate chain growth in **6.9a**. Iminophenoxide complexes thus follow the same mechanism observed for iminopyrrolide complexes and the active species in polymerizations with **6.8b** and **6.11b** is most likely a pyridylmethoxide-bridged dinuclear compound (Scheme 6.6). However, unlike iminopyrrolide complexes, neither **6.8b**, nor **6.11b** or **6.9a** with pyridylmethoxide added, showed any preference for isotactic polymerization and the obtained PLA was atactic (Table 6.II).

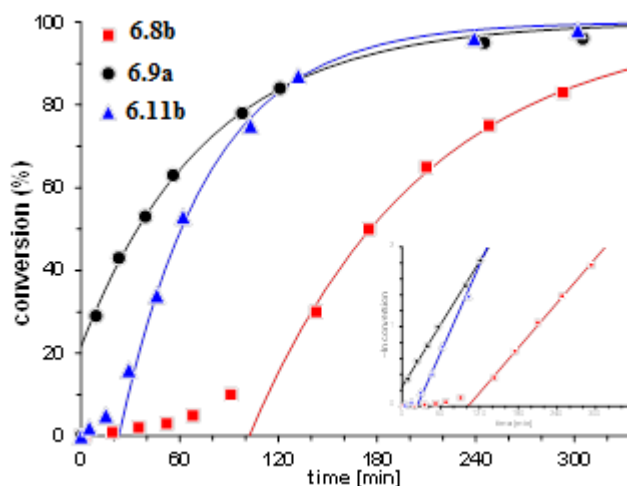
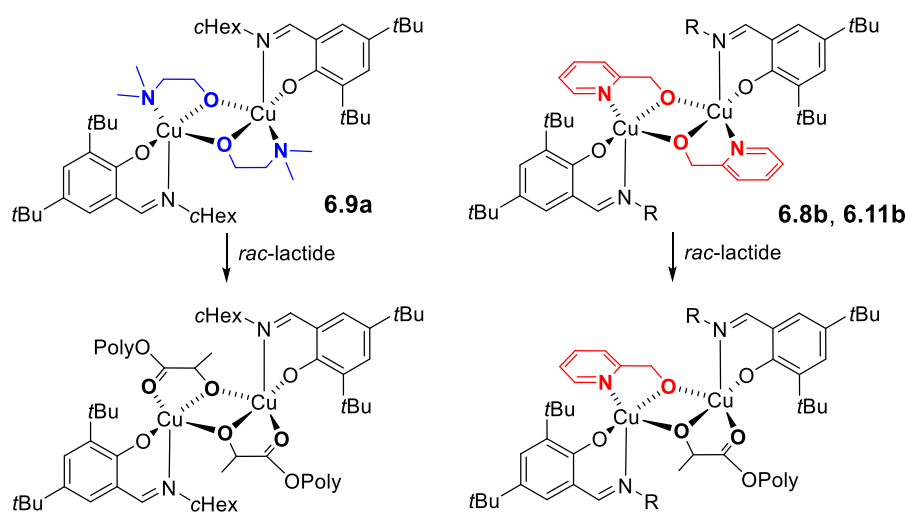


**Figure 6.5.** Conversion-time profiles for *rac*-lactide polymerization with **6.8b** (squares), **6.9a** (circles) and **6.11b** (triangles). Conditions:  $C_6D_6$ , RT, 0.2 M lactide, 2 mM cat.. The inset shows the semi-logarithmic plot. Solid lines represent in both graphics theoretical conversions with the values obtained in linear regression

analysis: **6.8b**:  $k_{app} = 0.57(2) \text{ h}^{-1}$ ,  $t_0 = 102 \text{ min}$ , **6.9a**:  $k_{app} = 0.078(1) \text{ h}^{-1}$ ,  $t_0 = -19 \text{ min}$ , **11b**:  $k_{app} = 1.1(1) \text{ h}^{-1}$ ,  $t_0 = 23 \text{ min}$ .



**Scheme 6.6.**

### 1,3-dichlorosalicylaldehyde-based ligands.

Increased  $\sigma$ -donation from the spectator ligand weakens the coordination of the bridging group. Since stereoselectivity correlated with the “rigidity” of the bridging ligand, increased  $\sigma$ -donation might thus be detrimental for stereocontrol. We investigated iminophenoxide ligands with *ortho*- and *para*-chloro substituents, to reduce  $\sigma$ -donation from the phenoxide ligand. Unfortunately, all attempts to prepare aminoethoxide or pyridylmethoxide complexes with ligands **6.L12H-6.L15H** yielded the homoleptic complexes **6.12c-6.15c** (Fig. 6.S2), with the exception of the *N*-benzyl complex **6.12b**. The solid state structure of complex **6.12b** is very similar to that of **6.8b**. It is tempting to assign a shorter Cu-O<sub>phenoxide</sub> and Cu-N<sub>pyridine</sub> to a higher Lewis-acidity of the copper center, but comparison with all structural data from **6.6b**, **6.8b**, **6.11b**, and **6.12b** does not show a clear correlation between phenoxide ligand  $\sigma$ -donor ability and bond lengths. Unfortunately, complex **6.12b** is essentially inactive in polymerization; either due to decomposition or because monomer was unable to replace the bridging alkoxide. We were thus unable to determine the influence of  $\sigma$ -donation on isotacticity.

## Conclusion

Heteroleptic copper complexes based on 4,6-di(*tert*-butyl)substituted iminophenoxide ligands are successful catalysts for the coordination-insertion polymerization of *rac*-lactide at room temperature. They produce PLA with good activities and high polymer molecular weight control. Their solid-state structures strongly resemble those of the analogous iminopyrrolide complexes and, based on polymer molecular weight data, they form the same dinuclear active species which retains an unreacted pyridylmethoxide ligand. Nevertheless, no stereocontrol was observed, which might be attributed to an increased  $\sigma$ -donation from the spectator ligand. Stereocontrol in dinuclear copper complexes of this type thus seems to require hitting the exact spot of sufficient rigidity/Lewis-acidity in the dinuclear complex to ensure stereocontrol, without encountering loss of activity.

## Experimental

**General considerations.** All reactions were carried out using Schlenk or glove box techniques under nitrogen atmosphere.  $\text{Cu}(\text{OMe})_2$ ,<sup>97</sup> 4,6-di-*tert*-butylsalicylaldehyde,<sup>98</sup> 1,3-dichlorosalicylaldehyde,<sup>98</sup> **6.L2H**,<sup>99</sup> **6.L3H**,<sup>100</sup> **6.L8H**,<sup>101</sup> **6.L9H**,<sup>101</sup> **6.L10H**,<sup>102</sup> and **6.L11H**<sup>103</sup> were prepared according to literature. Solvents were dried by passage through activated aluminum oxide (MBraun SPS), de-oxygenated by repeated extraction with nitrogen, and stored over molecular sieves.  $\text{C}_6\text{D}_6$  was dried over molecular sieves. *rac*-Lactide (98%) was purchased from Sigma–Aldrich, purified by 3x recrystallization from dry ethyl acetate and kept at  $-30\text{ }^\circ\text{C}$ . All other chemicals were purchased from common commercial suppliers and used without further purification.  $^1\text{H}$  and  $^{13}\text{C}$  NMR spectra were acquired on Bruker Avance 300 and 400 spectrometers. Chemical shifts were referenced to the residual signals of the deuterated solvents ( $\text{CDCl}_3$ :  $^1\text{H}$ :  $\delta$  7.26 ppm,  $^{13}\text{C}$ :  $\delta$  77.16). Elemental analyses were performed by the Laboratoire d'analyse élémentaire (Université de Montréal). Molecular weight analyses were performed on a Waters 1525 gel permeation chromatograph equipped with three Phenomenex columns and a

refractive index detector at 35 °C. THF was used as the eluent at a flow rate of 1.0 mL·min<sup>-1</sup> and polystyrene standards (Sigma–Aldrich, 1.5 mg·mL<sup>-1</sup>, prepared and filtered (0.2 mm) directly prior to injection) were used for calibration. Obtained molecular weights were corrected by a Mark-Houwink factor of 0.58.<sup>104</sup> All UV-Vis measurements were done in degassed and anhydrous toluene at RT in a sealed quartz cell on a Cary 500i UV-Vis-NIR Spectrophotometer. <sup>1</sup>H NMR spectra of paramagnetic Cu(II) compounds either provided peaks broadened to an extent that they were indistinguishable from the baseline or they showed one strongly broadened peak, the displacement of which was essentially invariant from the composition of the complex. NMR data is thus not provided for Cu(II) complexes.

**2-((Benzylimino)methyl)phenol, 6.L4H.** A procedure from literature was modified as follows. Salicylaldehyde (1.0 g, 8.2 mmol) was dissolved in dry toluene (25 mL). MgSO<sub>4</sub> (5.0 g), a catalytic amount of Amberlyst 15 and benzylamine (0.88 g, 8.2 mmol) were added. The reaction was refluxed for 4 h. The yellow suspension was filtered and the solvent removed under vacuum. The residue was treated with hexane (20 mL), resulting in a light yellow oil. The oil was separated by decantation and dried under vacuum to give (1.69 g, 98%).

<sup>1</sup>H NMR (CDCl<sub>3</sub>, 400 MHz): δ 8.45 (s, 1H, (N=C)H), 7.40 – 7.23 (m, 7H, Ar), 6.97 (d, *J* = 8 Hz, 1H, Ar), 6.89 (td, *J* = 8, 1 Hz, 1H, Ar), 4.82 (s, 2H, CH<sub>2</sub>).

**2-((Cyclohexylimino)methyl)phenol, 6.L5H.** Analogous to 6.L4H, from salicylaldehyde (1.0 g, 8.2 mmol), dry toluene (25 mL), 5g MgSO<sub>4</sub>, a catalytic amount of Amberlyst 15, cyclohexylamine (0.81 g, 8.2 mmol) and refluxed for 4 hours to yield a light yellow oil (1.64g, 98%).

<sup>1</sup>H NMR (CDCl<sub>3</sub>, 400 MHz): δ 8.36 (s, 1H, (N=C)H), 7.29 (td, *J* = 8, 1 Hz, 1H, Ar), 7.23 (dd, *J* = 8, 1 Hz, 1H, Ar), 6.95 (d, *J* = 8 Hz, 1H, Ar), 6.86 (td, *J* = 8, 1 Hz, 1H, Ar), 3.24 (t, *J* = 10 Hz, 1H, NCH), 1.90 – 1.72 (m, 4H, CH<sub>2</sub>), 1.72 – 1.48 (m, 3H, CH<sub>2</sub>), 1.48 – 1.21 (m, 3H, CH<sub>2</sub>).

**2-((Diphenylmethylimino)methyl)phenol, 6.L6H.** Analogous to 6.L4H, from salicylaldehyde (1.0 g, 8.2 mmol), dry toluene (25 mL), 5g MgSO<sub>4</sub>, a catalytic amount of Amberlyst 15, diphenylmethylamine (1.5 g, 8.2 mmol) and refluxed for 4 hours to yield a light yellow oil (2.21 g, 94%).

<sup>1</sup>H NMR (CDCl<sub>3</sub>, 400 MHz): δ 8.48 (s, 1H, (N=C)H), 7.38 – 7.22 (m, 13H, Ar), 6.99 (d, *J* = 8 Hz, 1H, Ar), 6.89 (td, *J* = 8, 1 Hz, 1H, Ar), 5.63 (s, 1H, CH).

**2-((2,6-Dimethylphenylimino)methyl)phenol, 6.L7H.** Analogous to 6.L4H, from salicylaldehyde (1.0 g, 8.2 mmol), dry toluene (25 mL), 5g MgSO<sub>4</sub>, a catalytic amount of Amberlyst 15, 2,6-xylylamine (1.0 g, 8.2 mmol) and refluxed for 4 hours to yield a light yellow oil (1.82 g, 98%).

<sup>1</sup>H NMR (CDCl<sub>3</sub>, 400 MHz): δ 13.10 (s, 1H, OH), 8.35 (s, 1H, (N=C)H), 7.46 – 7.38 (m, 1H, Ar), 7.36 (dd, *J* = 8, 1 Hz, 1H, Ar), 7.16 – 7.01 (m, 4H, Ar), 6.97 (td, *J* = 8, 1 Hz, 1H, Ar), 2.21 (d, *J* = 8 Hz, 6H, CH<sub>3</sub>).

**1,3-Dichloro-6-((benzylimino)methyl)phenol, 6.L12H.** Analogous to 6.L4H, from 3,5-dichlorosalicylaldehyde (1.0 g, 8.2 mmol), dry toluene (25 mL), 5g MgSO<sub>4</sub>, a catalytic amount of Amberlyst 15, benzylamine (0.88 g, 8.2 mmol) (1.5 g, 8.2 mmol) and refluxed for 4 hours to yield a light yellow oil which was purified by silica gel chromatography (10% EtOAc in hexane) (1.68 g, 73%).

<sup>1</sup>H NMR (CDCl<sub>3</sub>, 300 MHz): δ 8.33 (s, 1H, (N=C)H), 7.43 – 7.27 (m, 6H, Ar), 7.17 (d, *J* = 3 Hz, 1H, Ar), 4.84 (s, 2H, CH<sub>2</sub>); <sup>13</sup>C{<sup>1</sup>H} NMR (CDCl<sub>3</sub>, 75 MHz): δ 163.9 ((N=C), 157.1 (C.OH), 137.0 (ipso-Ph), 132.5 (Ar), 129.2 (Ar), 129.0 (o-Ph), 128.1 (m-Ph), 128.0 (Ar), 123.1 (Ar), 122.7 (Ar), 119.6 (Ar), 62.4 (CH<sub>2</sub>). ESI-HRMS (*m/z*): [M+H]<sup>+</sup> (C<sub>14</sub>H<sub>12</sub>Cl<sub>2</sub>NO) calcd 280.0290; found 280.0290.

**1,3-dichloro-6-((cyclohexylimino)methyl)phenol, 6.L13H.** Analogous to 6.L4H, from 3,5-Dichlorosalicylaldehyde (1.0 g, 8.2 mmol), dry toluene (25 mL), 5g MgSO<sub>4</sub>, a catalytic amount of Amberlyst 15, cyclohexylamine (0.88 g, 8.2 mmol) (1.5 g, 8.2 mmol) and refluxed for 4 hours to yield a light yellow oil which was purified by silica gel chromatography (5% EtOAc in hexane) (1.71 g, 77%).



$^1\text{H}$  NMR ( $\text{CDCl}_3$ , 300 MHz):  $\delta$  8.21 (s, 1H, (N=C)H), 7.40 (d,  $J = 3$  Hz, 1H, o-Ph), 7.11 (d,  $J = 3$  Hz, 1H, m-Ph), 3.37 (tt,  $J = 10$ , 3 Hz, 1H, NCH) 1.95 – 1.85 (m, 4H,  $\text{CH}_2$ ), 1.73 – 1.21 (m, 6H);  $^{13}\text{C}\{^1\text{H}\}$  NMR ( $\text{CDCl}_3$ , 75 MHz):  $\delta$  161.1 ((N=C), 159.7 (C-OH), 132.6 (Ar), 129.0 (Ar), 124.0 (Ar), 121.3 (Ar), 118.7 (Ar), 65.6 (NCH), 34.0 ( $\text{CH}_2$ ), 25.4 ( $\text{CH}_2$ ), 24.2 ( $\text{CH}_2$ ). ESI-HRMS (m/z):  $[\text{M}+\text{H}]^+$  ( $\text{C}_{13}\text{H}_{16}\text{Cl}_2\text{NO}$ ) calcd 272.0603; found 272.0614.

**1,3-dichloro-6-((diphenylmethylimino)methyl)phenol, 6.L14H.** Analogous to 6.L4H, from 3,5-Dichlorosalicylaldehyde (1.0 g, 8.2 mmol), dry toluene (25 mL), 5g  $\text{MgSO}_4$ , a catalytic amount of Amberlyst 15, diphenylmethylamine (0.88 g, 8.2 mmol) (1.5 g, 8.2 mmol) and refluxed for 4 hours to yield a light yellow oil which was purified by silica gel chromatography (5% EtOAc in hexane) (1.76g, 60%).

$^1\text{H}$  NMR ( $\text{CDCl}_3$ , 300 MHz):  $\delta$  8.38 (s, 1H, (N=C)H), 7.42 (d,  $J = 3$  Hz, 1H, o-Ph), 7.39 – 7.26 (m, 10H, Ar), 7.17 (d,  $J = 3$  Hz, 1H, p-Ph), 5.69 (s, 1H, CH);  $^{13}\text{C}\{^1\text{H}\}$  NMR ( $\text{CDCl}_3$ , 75 MHz):  $\delta$  163.5 ((N=C), 156.5 (C-OH), 141.7 (Ar), 132.6 (ipso-Ph), 129.5 (Ar), 129.0 (o-Ph), 127.9 (Ar), 127.6 (m-Ph), 123.1 (Ar), 122.9 (Ar), 119.9 (Ar), 76.4 (CH). ESI-HRMS (m/z):  $[\text{M}+\text{H}]^+$  ( $\text{C}_{20}\text{H}_{16}\text{Cl}_2\text{NO}$ ) calcd 356.0603; found 356.0617.

**1,3-dichloro-6-((2,6-dimethylphenylimino)methyl)phenol, 6.L15H.** Analogous to 6.L4H, from 3,5-dichlorosalicylaldehyde (1.0 g, 8.2 mmol), dry toluene (25 mL), 5g  $\text{MgSO}_4$ , a catalytic amount of Amberlyst 15, 2,6-xylamine (0.88 g, 8.2 mmol) (1.5 g, 8.2 mmol) and refluxed for 4 hours to yield a light yellow oil which was purified by silica gel chromatography (5% EtOAc in hexane) (1.93 g, 80%).

$^1\text{H}$  NMR ( $\text{CDCl}_3$ , 300 MHz):  $\delta$  8.28 (s, 1H, (N=C)H), 7.50 (d,  $J = 3$  Hz, 1H, o-Ph), 7.25 (d,  $J = 3$  Hz, 1H, p-Ph), 7.15 – 7.01 (m, 3H, Ar), 2.20 (s, 6H,  $\text{CH}_3$ );  $^{13}\text{C}\{^1\text{H}\}$  NMR ( $\text{CDCl}_3$ , 75 MHz):  $\delta$  165.3 ((N=C), 156.21 (C-OH), 147.1 (Ar), 133.0 (Ar), 129.9 (Ar), 128.7 (Ar), 128.5 (Ar), 125.9 (Ar), 123.5 (Ar), 123.1 (Ar), 119.9 (Ar), 18.6 ( $\text{CH}_3$ ). ESI-HRMS (m/z):  $[\text{M}+\text{H}]^+$  ( $\text{C}_{15}\text{H}_{14}\text{Cl}_2\text{NO}$ ) calcd 294.0452; found 294.0460.

**[(6.L2)<sub>2</sub>Cu<sub>2</sub>(μ-O,κ<sub>N</sub>-OC<sub>2</sub>H<sub>4</sub>NMe<sub>2</sub>)<sub>2</sub>], 6.2a.** Cu(OMe)<sub>2</sub> (67 mg, 0.53 mmol) was suspended in toluene (3 mL). Dimethylaminoethanol (110 μl, 1.1 mmol) was added to the blue suspension and stirred for 45 min. A freshly prepared colourless solution of **6.L2H** (100 mg, 0.53 mmol) in toluene (2 mL) was added dropwise, resulting in a dark-green solution. The reaction was stirred 24 hours at RT, filtered to remove trace impurities and concentrated to 1/3 of the volume, Green crystals separated on standing, were separated by decantation and washed with ether (3×10 mL) (40 g, 22%).

UV-vis (toluene, 3.5·10<sup>-6</sup>M) [ $\lambda_{\text{max}}$ , nm ( $\epsilon$ , mol<sup>-1</sup> cm<sup>2</sup>): 305 (35000), 385 (5800), 657 (2200). Anal. Calcd for C<sub>32</sub>H<sub>48</sub>Cu<sub>2</sub>N<sub>4</sub>O<sub>4</sub>: C, 56.53; H, 7.12; N, 8.24; Found: C, 56.17; H, 7.48; N, 8.27.

**[(6.L3)Cu(μ-O,κ<sub>N</sub>-OCH<sub>2</sub>Py)], 6.3b.** Analogous to **6.2a**, from Cu(OMe)<sub>2</sub> (59 mg, 0.47 mmol) in toluene (3 mL), 2-pyridinemethanol (91 μL, 0.94 mmol), **6.L3H** (100 mg, 0.47 mmol) in toluene (2 mL). Filtration and concentration (1/3 of the volume) of the green solution, decantation and washing with ether (3 x 10 mL) afforded 27 mg (15%) of green X-ray quality crystals.

UV-vis (toluene, 1.6·10<sup>-5</sup>M) [ $\lambda_{\text{max}}$ , nm ( $\epsilon$ , mol<sup>-1</sup> cm<sup>2</sup>): 294 (sh), 384 (580), 408 (400), 487 (270), 668 (180). Anal. Calcd for C<sub>20</sub>H<sub>20</sub>CuN<sub>2</sub>O<sub>2</sub>: C, 63.47; H, 5.33; N, 8.54; Found: C, 63.53; H, 5.59; N, 8.50.

**(6.L4)<sub>2</sub>Cu<sub>2</sub>(μ-O,κ<sub>N</sub>-OC<sub>2</sub>H<sub>4</sub>NMe<sub>2</sub>)<sub>2</sub>, 6.4a.** Analogous to **6.2a**, from Cu(OMe)<sub>2</sub> (59 mg, 0.47 mmol) in toluene (3 mL), dimethylaminoethanol (95 μL, 0.94 mmol), **6.L4H** (100 mg, 0.47 mmol) in toluene (2 mL). Filtration and concentration (1/3 of the volume) of the green solution, decantation and washing with ether (3 x 10 mL) afforded 30 mg (18%) of green X-ray quality crystals.

UV-vis (toluene, 1.7·10<sup>-5</sup>M) [ $\lambda_{\text{max}}$ , nm ( $\epsilon$ , mol<sup>-1</sup> cm<sup>2</sup>): 303 (sh), 373 (9200), 472 (950), 664 (300). Anal. Calcd for C<sub>36</sub>H<sub>44</sub>Cu<sub>2</sub>N<sub>4</sub>O<sub>4</sub>: C, 59.73; H, 6.13; N, 7.74; Found: C, 59.62; H, 6.52; N, 7.82.

**(6.L4)<sub>2</sub>Cu, 6.4c.** Analogous to **6.2a**, without the addition of alcohol: Cu(OMe)<sub>2</sub> (30 mg, 0.24 mmol) ) was suspended in toluene (3 mL). A freshly prepared

solution of **6.L4H** (100 mg, 0.47 mmol) in toluene (2 mL) was added dropwise. The reaction was stirred for 24 h, filtered to remove trace impurities and concentrated to 1/3 of its volume. Brown crystals separated on standing and were isolated by decantation and washing with hexane (3 x 10 mL) to afford 61 mg (53%) of brown X-ray quality crystals. For the X-ray structure, see Fig. 6.S2. Synthesis<sup>92</sup> and a polymorph<sup>91</sup> of this complex have been reported previously.

UV-vis (toluene,  $2.1 \cdot 10^{-5}$  M) [ $\lambda_{\max}$ , nm ( $\epsilon$ , mol<sup>-1</sup> cm<sup>2</sup>): 307 (sh), 373 (5000), 471 (sh), 644 (300). Anal. Calcd for C<sub>28</sub>H<sub>24</sub>CuN<sub>2</sub>O<sub>2</sub>: C, 69.48; H, 5.00; N, 5.79; Found: C, 69.52; H, 5.30; N, 5.49.

**(6.L5)<sub>2</sub>Cu<sub>2</sub>( $\mu$ -O, $\kappa$ <sub>N</sub>-OC<sub>2</sub>H<sub>4</sub>NMe<sub>2</sub>)<sub>2</sub>, 6.5a.** Analogous to **6.2a**, from Cu(OMe)<sub>2</sub> (62 mg, 0.49 mmol) in toluene (3 mL), dimethylaminoethanol (98  $\mu$ L, 0.98 mmol), **6.L5H** (100 mg, 0.49 mmol) in toluene (2 mL). Filtration and concentration (1/3 of the volume) of the green solution, decantation and washing with ether (3 x 10 mL) afforded 35 mg (20%) of green X-ray quality crystals. For the X-ray structure, see Fig. 6.S2.

UV-vis (toluene,  $8.7 \cdot 10^{-5}$  M) [ $\lambda_{\max}$ , nm ( $\epsilon$ , mol<sup>-1</sup> cm<sup>2</sup>): 317 (sh), 370 (1700), 463 (200), 663 (50). Anal. Calcd for C<sub>34</sub>H<sub>52</sub>Cu<sub>2</sub>N<sub>4</sub>O<sub>4</sub>: C, 57.69; H, 7.40; N, 7.91; Found: C, 57.30; H, 8.02; N, 7.81.

**(6.L5)<sub>2</sub>Cu, 6.5c.** Analogous to **6.4c**, from Cu(OMe)<sub>2</sub> (31 mg, 0.25 mmol), toluene (3 mL), **6.L5H** (100 mg, 0.49 mmol) in toluene (2 mL), 59 mg (50%) of green X-ray quality crystals. For the X-ray structure, see Fig. 6.S2. Synthesis<sup>105</sup> and structure<sup>106</sup> of this complex have been reported previously.

UV-vis (toluene,  $2.1 \cdot 10^{-5}$  M) [ $\lambda_{\max}$ , nm ( $\epsilon$ , mol<sup>-1</sup> cm<sup>2</sup>): 314 (8300), 373 (8700), 467 (sh), 652 (300). Anal. Calcd for C<sub>26</sub>H<sub>32</sub>CuN<sub>2</sub>O<sub>2</sub>: C, 66.71; H, 6.89; N, 5.98; Found: C, 67.00; H, 7.23; N, 5.98.

**(6.L6)Cu<sub>2</sub>( $\mu$ -O, $\kappa$ <sub>N</sub>-OC<sub>2</sub>H<sub>4</sub>NMe<sub>2</sub>)<sub>2</sub>, 6.6a.** Analogous to **6.2a**, from Cu(OMe)<sub>2</sub> (44 mg, 0.35 mmol) in toluene (3 mL), dimethylaminoethanol (70  $\mu$ L, 0.70 mmol), **6.L6H** (100 mg, 0.35 mmol) in toluene (2 mL). Filtration and concentration (1/3 of the volume) of the green solution, decantation and

washing with ether (3 x 10 mL) afforded 28 mg (18%) of green X-ray quality crystals.

UV-vis (toluene,  $3.5 \cdot 10^{-5}$ M) [ $\lambda_{\text{max}}$ , nm ( $\epsilon$ , mol $^{-1}$  cm $^2$ )]: 315 (2300), 349 (sh), 374 (1800), 475 (100). Anal. Calcd for C<sub>48</sub>H<sub>52</sub>Cu<sub>2</sub>N<sub>4</sub>O<sub>4</sub>·1H<sub>2</sub>O: C, 64.48; H, 6.09; N, 6.27; Found: C, 64.11; H, 6.16; N, 6.25.

**(6.L6)<sub>2</sub>Cu<sub>2</sub>( $\mu$ -O, $\kappa$ N-OCH<sub>2</sub>Py)<sub>2</sub>, 6.6b.** Analogous to **6.2a**, from Cu(OMe)<sub>2</sub> (44 mg, 0.35 mmol) in toluene (3 mL), 2-pyridinemethanol (67  $\mu$ L, 0.70 mmol), **6.L6H** (100 mg, 0.35 mmol) in toluene (2 mL). Filtration and concentration (1/3 of the volume) of the green solution, decantation and washing with ether (3 x 10 mL) afforded 24 mg (15%) of green X-ray quality crystals.

UV-vis (toluene,  $1 \cdot 10^{-5}$ M) [ $\lambda_{\text{max}}$ , nm ( $\epsilon$ , mol $^{-1}$  cm $^2$ )]: 318 (6000), 352 (sh), 373 (5000), 474 (300). Anal. Calcd for C<sub>52</sub>H<sub>44</sub>Cu<sub>2</sub>N<sub>4</sub>O<sub>4</sub>·1/2C<sub>4</sub>H<sub>10</sub>O: C, 68.05; H, 5.18; N, 5.88; Found: C, 67.58; H, 4.89; N, 6.29.

**(6.L6)<sub>2</sub>Cu, 6.6c.** Analogous to **6.4c**, from Cu(OMe)<sub>2</sub> (21 mg, 0.17 mmol) in toluene (3 mL), **6.L6H** (100 mg, 0.35 mmol) in toluene (2 mL), 53 mg (49%) of brown X-ray quality crystals.

UV-vis (toluene,  $3.3 \cdot 10^{-5}$ M) [ $\lambda_{\text{max}}$ , nm ( $\epsilon$ , mol $^{-1}$  cm $^2$ )]: 327 (sh), 388 (2700), 671 (200). Anal. Calcd for C<sub>40</sub>H<sub>32</sub>CuN<sub>2</sub>O<sub>2</sub>·1/2C<sub>7</sub>H<sub>8</sub>: C, 76.57; H, 5.32; N, 4.11; Found: C, 76.67; H, 5.78; N, 4.32. For the X-ray structure, see Fig. 6.S2. Synthesis<sup>107</sup> and a polymorph<sup>108</sup> of this complex have been reported previously.

**(6.L7)<sub>2</sub>Cu, 6.7c.** Analogous to **6.4c**, from Cu(OMe)<sub>2</sub> (28 mg, 0.22 mmol) in toluene (3 mL), **6.L7H** (100 mg, 0.44 mmol) in toluene (2 mL). Filtration and concentration (1/3 of the volume) of the brown solution, decantation and washing with hexane (3 x 10 mL) afforded 56 mg (50%) of brown X-ray quality crystals.

UV-vis (toluene,  $2.2 \cdot 10^{-5}$ M) [ $\lambda_{\text{max}}$ , nm ( $\epsilon$ , mol $^{-1}$  cm $^2$ )]: 333 (sh), 411 (3200), 512 (sh), 683 (240). Anal. Calcd for C<sub>30</sub>H<sub>28</sub>CuN<sub>2</sub>O<sub>2</sub>: C, 70.36; H, 5.51; N, 5.47; Found: C, 70.35; H, 5.69; N, 5.54. For the X-ray structure, see Fig. 6.S2. Synthesis<sup>105</sup> of this complex have been reported previously.

**(6.L8)<sub>2</sub>Cu<sub>2</sub>(μ-O,<sub>K</sub>N-OCH<sub>2</sub>Py)<sub>2</sub>, 6.8b.** Analogous to **6.2a**, from Cu(OMe)<sub>2</sub> (39 mg, 0.31 mmol) in toluene (3 mL), 2-pyridinemethanol (60 μL, 0.62 mmol), **6.L8H** (100 mg, 0.31 mmol) in toluene (2 mL). Filtration and concentration (1/3 of the volume) of the green solution, decantation and washing with ether (3 x 10 mL) afforded 26 mg (17%) of green X-ray quality crystals.

UV-vis (toluene, 1.14·10<sup>-5</sup>M) [ $\lambda_{\max}$ , nm ( $\epsilon$ , mol<sup>-1</sup> cm<sup>2</sup>)]: 332 (6200), 400 (sh), 503 (300), 666 (200). Anal. Calcd for C<sub>56</sub>H<sub>68</sub>Cu<sub>2</sub>N<sub>4</sub>O<sub>4</sub>: C, 68.06; H, 6.94; N, 5.67; Found: C, 68.54; H, 7.36; N, 5.41.

**(6.L9)<sub>2</sub>Cu<sub>2</sub>(<sub>K</sub>N-OC<sub>2</sub>H<sub>4</sub>NMe<sub>2</sub>)<sub>2</sub>, 6.9a.** Analogous to **6.2a**, from Cu(OMe)<sub>2</sub> (40 mg, 0.32 mmol) in toluene (3 mL), dimethylaminoethanol (64 μL, 0.64 mmol), **6.L9H** (100 mg, 0.32 mmol) in toluene (2 mL). Filtration and concentration (1/3 of the volume) of the green solution, decantation and washing with ether (3 x 10 mL) afforded 27 mg (18%) of green X-ray quality crystals.

UV-vis (toluene, 1.4·10<sup>-5</sup>M) [ $\lambda_{\max}$ , nm ( $\epsilon$ , mol<sup>-1</sup> cm<sup>2</sup>)]: 324 (8800), 390 (6800), 479 (500). Anal. Calcd for C<sub>50</sub>H<sub>84</sub>Cu<sub>2</sub>N<sub>4</sub>O<sub>4</sub>: C, 64.41; H, 9.08; N, 6.01; Found: C, 64.63; H, 9.87; N, 5.90.

**(6.L10)<sub>2</sub>Cu<sub>2</sub>(μ-O,<sub>K</sub>N-OC<sub>2</sub>H<sub>4</sub>NMe<sub>2</sub>)<sub>2</sub>, 6.10a.** Analogous to **6.2a**, from Cu(OMe)<sub>2</sub> (40 mg, 0.25 mmol) in toluene (3 mL), dimethylaminoethanol (63 μL, 0.50 mmol), **6.L10H** (100 mg, 0.25 mmol) in toluene (2 mL). Filtration and concentration (1/3 of the volume) of the green solution afforded just a few green X-ray quality crystals.

**(6.L11)<sub>2</sub>Cu<sub>2</sub>(μ-O,<sub>K</sub>N-OCH<sub>2</sub>Py)<sub>2</sub>, 6.11b.** Analogous to **6.2a**, from Cu(OMe)<sub>2</sub> (38 mg, 0.30 mmol) in toluene (3 mL), 2-pyridinemethanol (57 μL, 0.60 mmol), **6.L11H** (100 mg, 0.30 mmol) in toluene (2 mL). Filtration and concentration (1/3 of the volume) of the green solution, decantation and washing with ether (3 x 10 mL) afforded 29 mg (19%) of green X-ray quality crystals.

UV-vis (toluene, 3.3·10<sup>-5</sup>M) [ $\lambda_{\max}$ , nm ( $\epsilon$ , mol<sup>-1</sup> cm<sup>2</sup>)]: 334 (sh); 402 (15000), 505 (1200), 662 (300). Anal. Calcd for C<sub>58</sub>H<sub>72</sub>Cu<sub>2</sub>N<sub>4</sub>O<sub>4</sub>: C, 68.54; H, 7.14; N, 5.51; Found: C, 68.41; H, 7.86; N, 5.24.

**(6.L12)<sub>2</sub>Cu<sub>2</sub>(μ-O,κ<sub>N</sub>-OCH<sub>2</sub>Py)<sub>2</sub>, 6.12b.** Analogous to **6.2a**, from Cu(OMe)<sub>2</sub> (45 mg, 0.36 mmol) in toluene (3 mL), 2-pyridinemethanol (70 μL, 0.72 mmol), **6.L12H** (100 mg, 0.36 mmol) in toluene (2 mL). Filtration and concentration (1/3 of the volume) of the green solution, decantation and washing with ether (3 x 10 mL) afforded 18 mg (11%) of green X-ray quality crystals.

UV-vis (toluene, 1.1·10<sup>-5</sup>M) [ $\lambda_{\max}$ , nm ( $\epsilon$ , mol<sup>-1</sup> cm<sup>2</sup>)]: 386 (9000), 484 (sh).  
Anal. Calcd for C<sub>40</sub>H<sub>32</sub>Cl<sub>4</sub>Cu<sub>2</sub>N<sub>4</sub>O<sub>4</sub>: C, 53.29; H, 3.58; N, 6.21; Found: C, 53.57; H, 3.74; N, 6.26.

**(6.L12)<sub>2</sub>Cu, 6.12c.** Analogous to **6.2a**, from Cu(OMe)<sub>2</sub> (23 mg, 0.18 mmol) in toluene (3 mL), **6.L12H** (100 mg, 0.36 mmol) in toluene (2 mL). Filtration and concentration (1/3 of the volume) of the brown solution, decantation and washing with hexane (3 x 10 mL) afforded 60 mg (54%) of brown X-ray quality crystals. For the X-ray structure, see Fig. 6.S2. Elemental analysis differs notably from theoretical values, indicating notable amounts of impurities. No further attempt of purification was attempted.

UV-vis (toluene, 1.1·10<sup>-5</sup>M) [ $\lambda_{\max}$ , nm ( $\epsilon$ , mol<sup>-1</sup> cm<sup>2</sup>)]: 309 (sh), 384 (6800), 470 (sh), 658 (270). Anal. Calcd for C<sub>28</sub>H<sub>20</sub>Cl<sub>4</sub>CuN<sub>2</sub>O<sub>2</sub>: C, 54.08; H, 3.24; N, 4.51; Found: C, 50.50; H, 4.94; N, 6.26.

**(6.L13)<sub>2</sub>Cu, 6.13c.** Analogous to **6.2a**, from Cu(OMe)<sub>2</sub> (24 mg, 0.19 mmol) in toluene (3 mL), **6.L13H** (100 mg, 0.37 mmol) in toluene (2 mL). Filtration and concentration (1/3 of the volume) of the brown solution, decantation and washing with hexane (3 x 10 mL) afforded 68 mg (59%) of brown X-ray quality crystals. For the X-ray structure, see Fig. 6.S2. Synthesis of this complex have been reported previously.<sup>109</sup>

UV-vis (toluene, 1.4·10<sup>-5</sup>M) [ $\lambda_{\max}$ , nm ( $\epsilon$ , mol<sup>-1</sup> cm<sup>2</sup>)]: 301 (sh), 379 (7000), 486 (sh), 671 (300). Anal. Calcd for C<sub>26</sub>H<sub>28</sub>Cl<sub>4</sub>CuN<sub>2</sub>O<sub>2</sub>: C, 51.54; H, 4.66; N, 4.62; Found: C, 51.81; H, 4.84; N, 4.65.

**(6.L12)<sub>2</sub>Cu, 6.14c.** Analogous to **6.5**, from Cu(OMe)<sub>2</sub> (18 mg, 0.14 mmol) in toluene (3 mL), **6.L14H** (100 mg, 0.28 mmol) in toluene (2 mL). Filtration and

concentration (1/3 of the volume) of the brown solution, decantation and washing with hexane (3 x 10 mL) afforded 62 mg (57%) of brown X-ray quality crystals. For the X-ray structure, see Fig. 6.S2.

UV-vis (toluene,  $1.1 \cdot 10^{-5}$  M) [ $\lambda_{\max}$ , nm ( $\epsilon$ , mol<sup>-1</sup> cm<sup>2</sup>): 309 (sh), 381 (6500), 485 (sh), 679 (370). Anal. Calcd for C<sub>40</sub>H<sub>28</sub>Cl<sub>4</sub>CuN<sub>2</sub>O<sub>2</sub>: C, 62.07; H, 3.65; N, 3.62; Found: C, 61.75; H, 3.88; N, 3.68.

**(6.L15)<sub>2</sub>Cu, 6.15c.** Analogous to **6.2a**, from Cu(OMe)<sub>2</sub> (21 mg, 0.17 mmol) in toluene (3 mL), **6.L15H** (100 mg, 0.34 mmol) in toluene (2 mL). Filtration and concentration (1/3 of the volume) of the the green solution afforded just a few green X-ray quality crystals. For the X-ray structure, see Fig. 6.S2.

**(C<sub>7</sub>H<sub>6</sub>O<sub>2</sub>)<sub>2</sub>Cu<sub>2</sub>( $\mu$ -O, $\kappa$ <sub>N</sub>-OC<sub>2</sub>H<sub>4</sub>NMe<sub>2</sub>)<sub>2</sub>, 6.16a.** Analogous to **6.2a**, from Cu(OMe)<sub>2</sub> (103 mg, 0.82 mmol) in toluene (3 mL), dimethylaminoethanol (165  $\mu$ l, 1.64 mmol), salicylaldehyde (100 mg, 0.82 mmol) in toluene (2 mL). Filtration and concentration (1/3 of the volume) of the green solution, decantation and washing with ether (3 x 10 mL) afforded 32 mg (14%) of green X-ray quality crystals.

UV-vis (toluene,  $1.9 \cdot 10^{-5}$  M) [ $\lambda_{\max}$ , nm ( $\epsilon$ , mol<sup>-1</sup> cm<sup>2</sup>): 292 (5000), 319 (4500), 374 (3500), 474 (sh), 675 (350). Anal. Calcd for C<sub>22</sub>H<sub>30</sub>Cu<sub>2</sub>N<sub>2</sub>O<sub>6</sub>: C, 48.43; H, 5.54; N, 5.13; Found: C, 48.15; H, 5.66; N, 5.13.

**(C<sub>7</sub>H<sub>6</sub>O<sub>2</sub>)<sub>2</sub>Cu<sub>2</sub>( $\mu$ -O, $\kappa$ <sub>N</sub>-OCH<sub>2</sub>Py)<sub>2</sub>, 6.16b.** Analogous to **6.2a**, from Cu(OMe)<sub>2</sub> (103 mg, 0.82 mmol) in toluene (3 mL), 2-pyridinemethanol (157  $\mu$ L, 1.64 mmol), salicylaldehyde (100 mg, 0.82 mmol) in toluene (2 mL). Filtration and concentration (1/3 of the volume) of the green solution, decantation and washing with ether (3 x 10 mL) afforded 43 mg (18%) of green X-ray quality crystals.

UV-vis (toluene,  $1.1 \cdot 10^{-4}$  M) [ $\lambda_{\max}$ , nm ( $\epsilon$ , mol<sup>-1</sup> cm<sup>2</sup>): 293 (3000), 330 (2000), 372 (1500), 473 (400), 693 (120). Anal. Calcd for C<sub>26</sub>H<sub>22</sub>Cu<sub>2</sub>N<sub>2</sub>O<sub>6</sub>: C, 53.33; H, 3.79; N, 4.78; Found: C, 53.73; H, 4.17; N, 5.13.

***rac*-Lactide polymerization.** For polymerizations at room temperature in solution, a solution of *rac*-lactide (28 mg, 0.20 mmol) in C<sub>6</sub>D<sub>6</sub> was prepared in a J-Young tube inside the glovebox. If required, external alcohol was added as a stock solution in C<sub>6</sub>D<sub>6</sub>. The desired catalyst (2 μmol, appr. 100 μL of an appr. 20 mM stock solution in C<sub>6</sub>D<sub>6</sub>) was added and the solution completed to 1 mL total volume. Bulk polymerizations were conducted in a pressure tube which was prepared inside the glovebox with the addition of stock solution of the desired catalyst in C<sub>6</sub>D<sub>6</sub>, solid *rac*-lactide and benzyl alcohol (stock solution of 20 mM in C<sub>6</sub>D<sub>6</sub>). The pressure tube was sealed and immersed for 24 h in an oil bath pre-heated to 130 °C. In both cases, polymerization reactions were quenched with 5 equiv of acetic acid (relative to catalyst) in CDCl<sub>3</sub> (5 mM). After determination of conversion and isotacticity, the solvent was evaporated and the polymer stored at –80 °C until GPC analysis.

**X-ray diffraction studies.** Single crystals were obtained described above. Diffraction data was collected either on a Bruker Venture METALJET diffractometer (Ga K $\alpha$  radiation) or a Bruker APEXII (Cu microsource/Quazar MX) with the application of the APEX software package, of SAINT for data reduction and of SADABS for absorption correction. Dual-space refinement (SHELXT) was used to solve structures. All non-hydrogen atoms were refined anisotropic by full matrix-least-squares on  $F^2$  while hydrogen atoms were refined with fixed isotropic U by the application of a riding model (SHELXL97). Additional experimental data can be found in tables 6.IV and 6.S1, and in the supporting information (CIF).



**Table 6.IV.** Details of X-ray Diffraction Studies

	6.2a	6.4a	6.5a	6.6a	6.9a	6.10a	6.16a
Formula	C <sub>32</sub> H <sub>48</sub> Cu <sub>2</sub> N <sub>4</sub> O <sub>4</sub>	C <sub>36</sub> H <sub>44</sub> Cu <sub>2</sub> N <sub>4</sub> O <sub>4</sub>	C <sub>34</sub> H <sub>52</sub> Cu <sub>2</sub> N <sub>4</sub> O <sub>4</sub>	C <sub>48</sub> H <sub>52</sub> Cu <sub>2</sub> N <sub>4</sub> O <sub>4</sub>	C <sub>50</sub> H <sub>84</sub> Cu <sub>2</sub> N <sub>4</sub> O <sub>4</sub>	C <sub>64</sub> H <sub>84</sub> Cu <sub>2</sub> N <sub>4</sub> O <sub>4</sub>	C <sub>22</sub> H <sub>30</sub> Cu <sub>2</sub> N <sub>2</sub> O <sub>6</sub>
$M_w$ (g/mol); $d_{\text{calcd.}}$ (g/cm <sup>3</sup> )	679.8; 1.42	723.8; 1.45	707.9; 1.37	876.0; 1.41	932.3; 1.26	1100.4; 1.21	545.6; 1.52
$T$ (K); F(000)	100; 716	100; 756	125; 634	100; 916	100; 2008	150; 586	100; 1128
Crystal System	Monoclinic	Monoclinic	Triclinic	Monoclinic	Monoclinic	Triclinic	Monoclinic
Space Group	$P2_1/c$	$P2_1/c$	$P(-1)$	$P2_1/n$	$C2/c$	$P(-1)$	$C2/c$
Unit Cell:							
$a$ (Å)	10.2124(4)	9.4481(2)	10.494(2)	9.86980(10)	25.7609(11)	10.9595(5)	20.7678(3)
$b$ (Å)	13.4671(6)	15.9169(4)	11.150(2)	14.7540(2)	9.3613(4)	11.4816(5)	6.11830(10)
$c$ (Å)	11.5479(5)	11.5813(3)	15.860(3)	14.2160(2)	21.0180(9)	12.5663(5)	18.9079(3)
$\alpha$ (°)	90	90	90.01(3)	90	90	82.603(2)	90
$\beta$ (°)	90.5560(10)	107.1780(10)	106.50(3)	92.1850(10)	104.466(2)	88.935(2)	97.71
$\gamma$ (°)	90	90	104.32(3)	90	90	74.196(2)	90
$V$ (Å <sup>3</sup> ); $Z$	1588.12(12); 2	1663.96(7); 2	1719.2(7); 2	2068.61(5); 2	4907.9(4); 4	1508.59(11); 1	2380.76(6); 4
$\mu$ (mm <sup>-1</sup> )	1.984	1.937	6.892	1.663	1.418	4.049	2.538
$\theta$ (°); completeness collected	3.3-72.0; 0.98 30005; 0.010	5.6-72.0; 1 40807; 0.019	2.5-58.3; 0.96 74452; 0.062	5.4-72.1; 1 27872; 0.016	5.3-72.0; 0.99 62412; 0.029	3.1-60.7; 1.0 43024; 0.036	8.6-71.9; 0.98 22853; 0.010
reflections; $R_\sigma$ unique reflections;	3074; 0.022	3260; 0.045	7348; 0.114	4058; 0.028	4796; 0.068	6935; 0.059	2304; 0.022
$R_{\text{int}}$ $R1(F)$ ( $I > 2\sigma(I)$ )	0.027	0.032	0.107	0.033	0.061	0.063	0.023
$wR(F^2)$ (all data)	0.074	0.094	0.329	0.092	0.166	0.169	0.063
GoF( $F^2$ )	1.083	1.091	1.055	1.063	1.055	1.052	1.061
Residual electron density	0.36; -0.31	0.43; -0.35	2.23; -1.94	0.69; -0.38	2.54; -1.18	1.58; -0.50	0.34; -0.29

**Table 6.IV-continued.** Details of X-ray Diffraction Studies

	<b>6.3b</b>	<b>6.6b</b>	<b>6.8b</b>	<b>6.11b</b>	<b>6.12b</b>	<b>6.16b</b>
Formula	C <sub>26</sub> H <sub>27</sub> CuN <sub>3</sub> O <sub>3</sub>	C <sub>52</sub> H <sub>44</sub> Cu <sub>2</sub> N <sub>4</sub> O <sub>4</sub>	C <sub>63</sub> H <sub>76</sub> Cu <sub>2</sub> N <sub>4</sub> O <sub>4</sub>	C <sub>72</sub> H <sub>88</sub> Cu <sub>2</sub> N <sub>4</sub> O <sub>4</sub>	C <sub>40</sub> H <sub>32</sub> Cl <sub>4</sub> Cu <sub>2</sub> N <sub>4</sub> O <sub>4</sub>	C <sub>26</sub> H <sub>22</sub> Cu <sub>2</sub> N <sub>2</sub> O <sub>6</sub>
$M_w$ (g/mol); $d_{\text{calcd}}$ (g/cm <sup>3</sup> )	493.04; 1.432	915.99; 1.462	1080.35; 1.307	1200.54; 1.246	901.57; 1.555	585.53; 1.210
$T$ (K); F(000)	100; 1028	100; 948	100; 1144	100; 1276	150; 1832	100; 596
Crystal System	Monoclinic	Monoclinic	Triclinic	Monoclinic	Monoclinic	Monoclinic
Space Group	$P2_1/c$	$P2_1/n$	$P(-1)$	$P2_1$	$P2_1/n$	$P2_1/n$
Unit Cell:						
$a$ (Å)	11.2111(3)	9.9716(3)	11.8306(4)	11.2710(5)	8.0732(5)	14.8060(2)
$b$ (Å)	10.0858(3)	17.7646(5)	13.9522(5)	25.1487(10)	19.5258(11)	6.79250(10)
$c$ (Å)	20.3125(6)	11.7580(3)	17.0501(6)	11.9113(5)	24.4945(14)	17.3010(3)
$\alpha$ (°)	90	90	102.745(2)	90	90	90
$\beta$ (°)	95.2760(10)	92.5350(10)	90.632(2)	108.617(2)	94.265(3)	112.5270(10)
$\gamma$ (°)	90	90	90.424(2)	90	90	90
$V$ (Å <sup>3</sup> ); $Z$	2287.06(11); 4	2080.79(10); 2	2744.69(17); 2	3199.6(2); 2	3850.5(4); 4	1607.20(4); 2
$\mu$ (mm <sup>-1</sup> )	1.619	1.687	1.353	1.211	7.896	1.924
$\theta$ (°); completeness	3.96-71.99; 0.97	4.98-72.10; 0.99	3.72-71.79; 0.97	4.29-72.00; 0.96	2.52-60.66; 0.99	3.23-72.00; 0.99
collected reflections;	30049; 0.033	27977; 0.015	98116; 0.041	43734; 0.019	98818; 0.034	21072; 0.016
$R_\sigma$						
unique reflections; $R_{\text{int}}$	4360; 0.057	4065; 0.026	10437; 0.120	12091; 0.022	8870; 0.093	3146; 0.026
$R1(F)$ ( $I > 2\sigma(I)$ )	0.033	0.032	0.060	0.026	0.033	0.032
wR( $F^2$ ) (all data)	0.092	0.087	0.166	0.071	0.164	0.090
GoF( $F^2$ )	1.039	1.039	1.063	1.036	1.162	1.098
Residual electron density	0.38; -0.46	0.39; -0.33	1.31; -0.66	0.34; -0.29	0.66; -0.61	0.90; -0.30

## Conflicts of interest

There are no conflicts to declare.

## Acknowledgements

Funding was supplied by the NSERC discovery program (RGPIN-2016-04953) and the Centre for Green Chemistry and Catalysis (FQRNT). We thank Marie-Christine Tang, Louiza Mahrouche and Alexandra Furtos for support with MALDI-MS and Francine Bélanger for support with X-ray crystallography.

## References Chapter 6

1. V. Nagarajan, A. K. Mohanty and M. Misra, *ACS Sustainable Chem. Eng.*, 2016, **4**, 2899-2916.
2. E. Castro-Aguirre, F. Iñiguez-Franco, H. Samsudin, X. Fang and R. Auras, *Advanced drug delivery reviews*, 2016, **107**, 333-366.
3. S. Slomkowski, S. Penczek and A. Duda, *Polymers for Advanced Technologies*, 2014, **25**, 436-447.
4. M. Singhvi and D. Gokhale, *RSC Adv.*, 2013, **3**, 13558-13568.
5. T. A. Hottle, M. M. Bilec and A. E. Landis, *Polymer degradation and stability*, 2013, **2013 v.98 no.9**, pp. 1898-1907.
6. S. Inkinen, M. Hakkarainen, A.-C. Albertsson and A. Södergård, *Biomacromolecules*, 2011, **12**, 523-532.
7. J. Ahmed and S. K. Varshney, *Int. J. Food Prop.*, 2011, **14**, 37-58.
8. J. A. Vijayakumar, R.; Viruthagiri, T. , *Chem. Bio-chem. Eng. Q.*, 2008, **2**, 245-264.
9. Y. Tokiwa and B. P. Calabia, *Can. J. Chem.*, 2008, **86**, 548-555.
10. R. E. Drumright, P. R. Gruber and D. E. Henton, *Advanced Materials*, 2000, **12**, 1841-1846.
11. E. T. H. Vink, K. R. Rábago, D. A. Glassner, B. Springs, R. P. O'Connor, J. Kolstad and P. R. Gruber, *Macromolecular Bioscience*, 2004, **4**, 551-564.
12. S. Paul, Y. Zhu, C. Romain, R. Brooks, P. K. Saini and C. K. Williams, *Chem. Commun. (Cambridge, U. K.)*, 2015, **51**, 6459-6479.
13. I. d. S. Vieira and S. Herres-Pawlis, *European Journal of Inorganic Chemistry*, 2012, **2012**, 765-774.
14. S. Dutta, W.-C. Hung, B.-H. Huang and C.-C. Lin, in *Synthetic Biodegradable Polymers*, eds. B. Rieger, A. Künkel, G. W. Coates, R.

Reichardt, E. Dinjus and T. A. Zevaco, Springer Berlin Heidelberg, Berlin, Heidelberg, 2012, DOI: 10.1007/12\_2011\_156, pp. 219-283.

15. P. J. Dijkstra, H. Du and J. Feijen, *Polym. Chem.*, 2011, **2**, 520-527.

16. J.-C. Buffet and J. Okuda, *Polym. Chem.*, 2011, **2**, 2758-2763.

17. C. M. Thomas, *Chem. Soc. Rev.*, 2010, **39**, 165.

18. M. J. Stanford and A. P. Dove, *Chemical Society Reviews*, 2010, **39**, 486-494.

19. C. K. Williams and M. A. Hillmyer, *Polymer Reviews*, 2008, **48**, 1-10.

20. N. Ajellal, J.-F. Carpentier, C. Guillaume, S. M. Guillaume, M. Helou, V. Poirier, Y. Sarazin and A. Trifonov, *Dalton Trans.*, 2010, **39**, 8363.

21. R. H. Platel, L. M. Hodgson and C. K. Williams, *Polym. Rev.*, 2008, **48**, 11 - 63.

22. J. Wu, T.-L. Yu, C.-T. Chen and C.-C. Lin, *Coord. Chem. Rev.*, 2006, **250**, 602-626.

23. O. Dechy-Cabaret, B. Martin-Vaca and D. Bourissou, *Chem. Rev.*, 2004, **104**, 6147-6176.

24. B. J. O'Keefe, M. A. Hillmyer and W. B. Tolman, *J. Chem. Soc., Dalton Trans.*, 2001, DOI: 10.1039/b104197p, 2215-2224.

25. M. H. Chisholm and Z. Zhou, *Journal of Materials Chemistry*, 2004, **14**, 3081-3092.

26. Z. Zhong, P. J. Dijkstra and J. Feijen, *J. Biomater. Sci., Polym. Ed.*, 2004, **15**, 929-946.

27. B. H. Huang, S. Dutta and C. C. Lin, in *Comprehensive Inorganic Chemistry II (Second Edition)*, ed. J. R. Poeppelemeier, Elsevier, Amsterdam, 2013, DOI: <http://dx.doi.org/10.1016/B978-0-08-097774-4.00146-7>, pp. 1217-1249.

28. C. A. Wheaton and P. G. Hayes, *Comments Inorg. Chem.*, 2011, **32**, 127-162.
29. C. A. Wheaton, P. G. Hayes and B. J. Ireland, *Dalton Transactions*, 2009, DOI: 10.1039/B819107G, 4832-4846.
30. A. K. Sutar, T. Maharana, S. Dutta, C.-T. Chen and C.-C. Lin, *Chem. Soc. Rev.*, 2010, **39**, 1724-1746.
31. E. Le Roux, *Coord. Chem. Rev.*, 2016, **306**, 65-85.
32. A. Sauer, A. Kapelski, C. Fliedel, S. Dagorne, M. Kol and J. Okuda, *Dalton Trans.*, 2013, **42**, 9007-9023.
33. J. P. MacDonald and M. P. Shaver, in *Green Polymer Chemistry: Biobased Materials and Biocatalysis*, American Chemical Society, 2015, vol. 1192, ch. 10, pp. 147-167.
34. R. Jianming, X. Anguo, W. Hongwei and Y. Hailin, *Designed Monomers and Polymers*, 2014, **17**, 345-355.
35. S. Dagorne, M. Normand, E. Kirillov and J.-F. Carpentier, *Coord. Chem. Rev.*, 2013, **257**, 1869-1886.
36. S. F. Dagorne, C.; de Frémont, P., in *In Encyclopedia of Inorganic and Bioinorganic Chemistry*, John Wiley & Sons, Ltd., 2011, DOI: doi:10.1002/9781119951438.eibc2416.
37. S. Dagorne and C. Fliedel, in *Modern Organoaluminum Reagents: Preparation, Structure, Reactivity and Use*, eds. S. Woodward and S. Dagorne, Springer Berlin Heidelberg, Berlin, Heidelberg, 2013, DOI: 10.1007/3418\_2012\_35, pp. 125-171.
38. A. Amgoune, M. Thomas Christophe and J.-F. Carpentier, *Journal*, 2007, **79**, 2013.
39. M. Cheng, A. B. Attygalle, E. B. Lobkovsky and G. W. Coates, *J. Am. Chem. Soc.*, 1999, **121**, 11583-11584.

40. T.-Q. Xu, G.-W. Yang, C. Liu and X.-B. Lu, *Macromolecules*, 2017, **50**, 515-522.
41. D. Myers, A. J. P. White, C. M. Forsyth, M. Bown and C. K. Williams, *Angew. Chem., Int. Ed.*, 2017, **56**, 5277-5282.
42. J. Bhattacharjee, A. Harinath, H. P. Nayek, A. Sarkar and T. K. Panda, *Chem.-Eur. J.*, 2017, **23**, 9319-9331.
43. Y. Sun, J. Xiong, Z. Dai, X. Pan, N. Tang and J. Wu, *Inorg. Chem.*, 2016, **55**, 136-143.
44. T. Rosen, Y. Popowski, I. Goldberg and M. Kol, *Chem.-Eur. J.*, 2016, **22**, 11533-11536.
45. P. McKeown, M. G. Davidson, G. Kociok-Kohn and M. D. Jones, *Chem. Commun. (Cambridge, U. K.)*, 2016, **52**, 10431-10434.
46. V. Balasanthiran, C. Chatterjee, M. H. Chisholm, N. D. Harrold, T. V. RajanBabu and G. A. Warren, *J. Am. Chem. Soc.*, 2015, **137**, 1786-1789.
47. Z. Mou, B. Liu, M. Wang, H. Xie, P. Li, L. Li, S. Li and D. Cui, *Chem. Commun. (Cambridge, U. K.)*, 2014, **50**, 11411-11414.
48. C. Bakewell, A. J. P. White, N. J. Long and C. K. Williams, *Angew. Chem., Int. Ed.*, 2014, **53**, 9226-9230.
49. D. C. Aluthge, B. O. Patrick and P. Mehrkhodavandi, *Chem. Commun. (Cambridge, U. K.)*, 2013, **49**, 4295-4297.
50. H. R. Kricheldorf and D.-O. Damrau, *J. Macromol. Sci., Part A: Pure Appl. Chem.*, 1998, **35**, 1875-1887.
51. B. B. Idage, S. B. Idage, A. S. Kasegaonkar and R. V. Jadhav, *Mater. Sci. Eng., B*, 2010, **168**, 193-198.
52. B. Rajashekhar and D. Chakraborty, *Polym. Bull.*, 2014, **71**, 2185-2203.
53. P. Daneshmand and F. Schaper, *Dalton Trans.*, 2015, **44**, 20449-20458.

54. A. Rathore, H. Kaur and R. Luque, *Journal of Polymer Research*, 2017, **25**, 2.
55. A. John, V. Katiyar, K. Pang, M. M. Shaikh, H. Nanavati and P. Ghosh, *Polyhedron*, 2007, **26**, 4033-4044.
56. L. Ding, W. Jin, Z. Chu, L. Chen, X. Lü, G. Yuan, J. Song, D. Fan and F. Bao, *Inorg. Chem. Commun.*, 2011, **14**, 1274-1278.
57. W.-J. Jin, L.-Q. Ding, Z. Chu, L.-L. Chen, X.-Q. Lü, X.-Y. Zheng, J.-R. Song and D.-D. Fan, *J. Molec. Catal. A: Chem.*, 2011, **337**, 25-32.
58. G. Xiao, B. Yan, R. Ma, W. J. Jin, X. Q. Lu, L. Q. Ding, C. Zeng, L. L. Chen and F. Bao, *Polym. Chem.*, 2011, **2**, 659-664.
59. A. Routaray, S. Mantri, N. Nath, A. K. Sutar and T. Maharana, *Polyhedron*, 2016, **119**, 335-341.
60. M. J. L. Tschan, J. Guo, S. K. Raman, E. Brule, T. Roisnel, M.-N. Rager, R. Legay, G. Durieux, B. Rigaud and C. M. Thomas, *Dalton Trans.*, 2014, **43**, 4550-4564.
61. S. Shin, S. Nayab and H. Lee, *Polyhedron*, 2018, **141**, 309-321.
62. J. Zhang, B. Wang, L. Wang, J. Sun, Y. Zhang, Z. Cao and Z. Wu, *Appl. Organomet. Chem.*, 2018, **32**, e4077.
63. B. J. O'Keefe, S. M. Monnier, M. A. Hillmyer and W. B. Tolman, *J. Am. Chem. Soc.*, 2001, **123**, 339-340.
64. V. C. Gibson, E. L. Marshall, D. Navarro-Llobet, A. J. P. White and D. J. Williams, *J. Chem. Soc., Dalton Trans.*, 2002, DOI: 10.1039/B209703F, 4321-4322.
65. D. S. McGuinness, E. L. Marshall, V. C. Gibson and J. W. Steed, *J. Polym. Sci., Part A: Polym. Chem.*, 2003, **41**, 3798-3803.
66. A. B. Biernesser, B. Li and J. A. Byers, *J. Am. Chem. Soc.*, 2013, **135**, 16553-16560.

67. A. Keuchguerian, B. Mougang-Soume, F. Schaper and D. Zargarian, *Can. J. Chem.*, 2015, **93**, 594–601.
68. L. A. Brown, F. S. Wekesa, D. K. Unruh, M. Findlater and B. K. Long, *J. Polym. Sci., Part A: Polym. Chem.*, 2017, **55**, 2824-2830.
69. C. M. Manna, A. Kaur, L. M. Yablon, F. Haeffner, B. Li and J. A. Byers, *J. Am. Chem. Soc.*, 2015, **137**, 14232-14235.
70. A. B. Biernesser, K. R. Delle Chiaie, J. B. Curley and J. A. Byers, *Angew. Chem., Int. Ed.*, 2016, **55**, 5251-5254.
71. R. Duan, C. Hu, X. Li, X. Pang, Z. Sun, X. Chen and X. Wang, *Macromolecules*, 2017, **50**, 9188-9195.
72. J. Sun, W. Shi, D. Chen and C. Liang, *J. Appl. Polym. Sci.*, 2002, **86**, 3312-3315.
73. R. R. Gowda and D. Chakraborty, *J. Molec. Catal. A: Chem.*, 2011, **349**, 86-93.
74. D. Appavoo, B. Omondi, I. A. Guzei, J. L. van Wyk, O. Zinyemba and J. Darkwa, *Polyhedron*, 2014, **69**, 55-60.
75. S. Bhunora, J. Mugo, A. Bhaw-Luximon, S. Mapolie, J. Van Wyk, J. Darkwa and E. Nordlander, *Appl. Organomet. Chem.*, 2011, **25**, 133-145.
76. C.-Y. Li, S.-J. Hsu, C.-I. Lin, C.-Y. Tsai, J.-H. Wang, B.-T. Ko, C.-H. Lin and H.-Y. Huang, *J. Polym. Sci., Part A: Polym. Chem.*, 2013, **51**, 3840-3849.
77. L.-L. Chen, L.-Q. Ding, C. Zeng, Y. Long, X.-Q. Lü, J.-R. Song, D.-D. Fan and W.-J. Jin, *Appl. Organomet. Chem.*, 2011, **25**, 310-316.
78. A. Routaray, N. Nath, T. Maharana and A. k. Sutar, *J. Macromol. Sci., Part A: Pure Appl. Chem.*, 2015, **52**, 444-453.
79. T. J. J. Whitehorne and F. Schaper, *Chem. Commun. (Cambridge, U. K.)*, 2012, **48**, 10334-10336.
80. T. J. J. Whitehorne and F. Schaper, *Inorg. Chem.*, 2013, **52**, 13612-13622.



81. T. J. J. Whitehorne and F. Schaper, *Can. J. Chem.*, 2014, **92**, 206-214.
82. K. S. Kwon, J. Cho, S. Nayab and J. H. Jeong, *Inorg. Chem. Commun.*, 2015, **55**, 36-38.
83. J. Cho, S. Nayab and J. H. Jeong, *Polyhedron*, 2016, **113**, 81-87.
84. S. H. Ahn, M. K. Chun, E. Kim, J. H. Jeong, S. Nayab and H. Lee, *Polyhedron*, 2017, **127**, 51-58.
85. K. S. Kwon, S. Nayab and J. H. Jeong, *Polyhedron*, 2017, **130**, 23-29.
86. M. K. Chun, J. Cho, S. Nayab and J. H. Jeong, *Bull. Korean Chem. Soc.*, 2017, **38**, 1527-1530.
87. S. Fortun, P. Daneshmand and F. Schaper, *Angew. Chem., Int. Ed.*, 2015, **54**, 13669-13672.
88. P. Daneshmand, A. van der Est and F. Schaper, *ACS Catal.*, 2017, **7**, 6289-6301.
89. P. Daneshmand, S. Fortun and F. Schaper, *Organometallics*, 2017, **36**, 3860-3877.
90. A. W. Addison, T. N. Rao, J. Reedijk, J. van Rijn and G. C. Verschoor, *J. Chem. Soc., Dalton Trans.*, 1984, DOI: 10.1039/DT9840001349, 1349-1356.
91. J. M. Fernández-G, J. Xochitiotzi-Flores, S. Hernández-Ortega, V. Gómez-Vidales and M. Del Rocío Patiño-Maya, *J. Coord. Chem.*, 2010, **63**, 2132-2145.
92. G. C. Percy and D. A. Thornton, *J. Inorg. Nucl. Chem.*, 1972, **34**, 3369-3376.
93. C. R. Groom, I. J. Bruno, M. P. Lightfoot and S. C. Ward, *Acta Crystallogr., Sect. B: Struct. Sci.*, 2016, **72**, 171-179.
94. J. U. Ahmad, M. T. Räisänen, M. Nieger, M. R. Sundberg, P. J. Figiel, M. Leskelä and T. Repo, *Polyhedron*, 2012, **38**, 205-212.

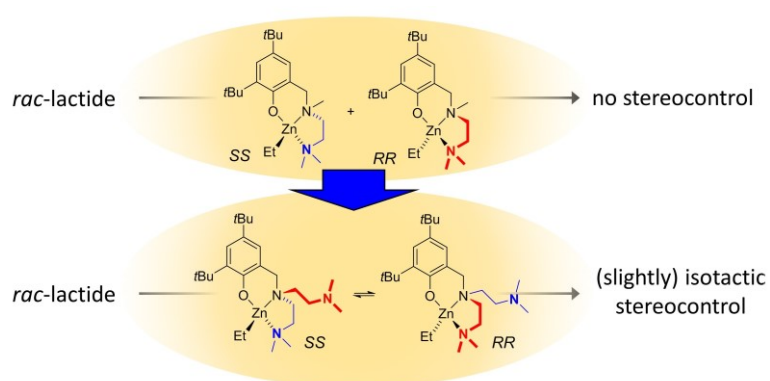
95. A. Mrutu, A. C. Lane, J. M. Drewett, S. D. Yourstone, C. L. Barnes, C. M. Halsey, J. W. Cooley and J. R. Walensky, *Polyhedron*, 2013, **54**, 300-308.
96. V. T. Kasumov, F. Köksal and Y. Zeren, *Spectrochimica Acta Part A: Molecular and Biomolecular Spectroscopy*, 2006, **63**, 330-336.
97. J. V. Singh, B. P. Baranwal and R. C. Mehrotra, *Z. Anorg. Allg. Chem.*, 1981, **477**, 235-240.
98. S. Mondal, S. M. Mandal, T. K. Mondal and C. Sinha, *Spectrochimica Acta Part A: Molecular and Biomolecular Spectroscopy*, 2015, **150**, 268-279.
99. G. N. Ledesma and S. R. Signorella, *Tetrahedron Lett.*, 2012, **53**, 5699-5702.
100. R. V. Stevens and G. S. Bisacchi, *J. Org. Chem.*, 1982, **47**, 2393-2396.
101. J. Uddin Ahmad, M. Nieger, M. R. Sundberg, M. Leskelä and T. Repo, *Journal of Molecular Structure*, 2011, **995**, 9-19.
102. X. Wang, K. Q. Zhao, Y. Al-Khafaji, S. Mo, T. J. Prior, M. R. J. Elsegood and C. Redshaw, *Eur. J. Inorg. Chem.*, 2017, **2017**, 1951-1965.
103. G. Alesso, M. Sanz, M. E. G. Mosquera and T. Cuenca, *Eur. J. Inorg. Chem.*, 2008, **2008**, 4638-4649.
104. M. Save, M. Schappacher and A. Soum, *Macromol. Chem. Phys.*, 2002, **203**, 889-899.
105. S. Yamada, H. Nishikawa and E. Yoshida, Vienna, 1964.
106. T. Hatsue, O. Kazuhide, T. Akira and Y. Shoichiro, *Bull. Chem. Soc. Jpn.*, 1979, **52**, 3522-3527.
107. K. Yamanouchi and S. Yamada, *Bull. Chem. Soc. Jpn.*, 1976, **49**, 163-168.

108. J. M. Fernández-G, O. L. Ruíz-Ramírez, R. A. Toscano, N. Macías-Ruvalcaba and M. Aguilar-Martínez, *Transition Metal Chemistry*, 2000, **25**, 511-517.
109. L. G. Cronenberger, Mrs. T.; Pacheco, H.; Pillon, D. , *Chimica Therapeutica*, 1968, **3**, 87-99.



## Chapter 7 . Configurationally Flexible Zinc Complexes as Catalysts for *rac*-Lactide Polymerisation

Daneshmand, P.; Michalsky, I.; Schaper, F. Configurationally Flexible Zinc Complexes as Catalysts for *rac*-Lactide Polymerisation. *Dalton Trans.* **2018**, *submitted*.



Contributions of F. Schaper: A first draft was provided by me with minor modification from Prof. Frank Schaper.

Contributions of I. Michalsky: Initial synthesis of two zinc complexes during her internship under my supervision



# Configurationally Flexible Zinc Complexes as Catalysts for *rac*-Lactide Polymerisation

Pargol Daneshmand,<sup>a</sup> Ina Michalsky<sup>a</sup> and Frank Schaper<sup>\*a</sup>

<sup>a</sup> Centre in Green Chemistry and Catalysis, Department of chemistry, Université de Montréal, C. P. 6128 Succ. Centre-Ville, Montréal, QC H3T 3J7, Canada.

\* E-mail: Frank.Schaper@umontreal.ca

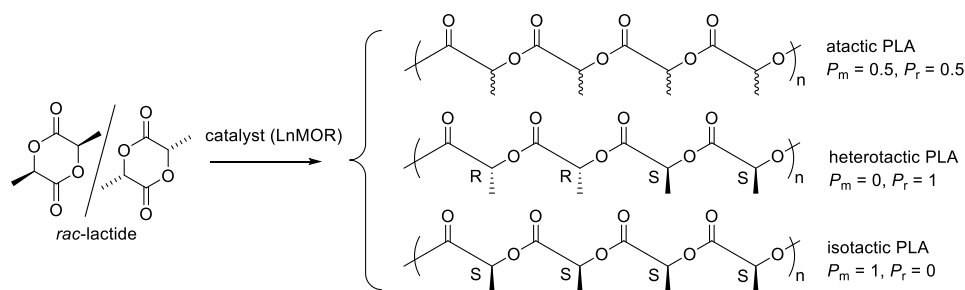
Electronic Supplementary Information (ESI) available: Additional details on polymerisation reactions, X-ray structures and NMR spectra.

## Abstract

Zn(N(SiMe<sub>3</sub>)<sub>2</sub>)<sub>2</sub> was reacted with pyridinemethanol and *R,R-N,N'*-di(methylbenzyl)-2,5-diiminopyrrole (7.L1H) to afford the dimeric complex (7.L1)<sub>2</sub>Zn<sub>2</sub>(μ-OR)<sub>2</sub>. The complex showed moderate activity in *rac*-lactide polymerization to heterotactic polymer (*P*<sub>r</sub>=0.75). 2,4-di-*tert*-butyl-6-aminomethyl-phenol ligands with amino = *N,N,N',N'*-tetramethyldiethylenetriamine (7.L2H) or di-(2-picoly)amine (7.L3H) were reacted with ZnEt<sub>2</sub> to form (7.L2)ZnEt and with Zn(N(SiMe<sub>3</sub>)<sub>2</sub>)<sub>2</sub> to form the respective amide complexes. All complexes, including (7.L1)<sub>2</sub>Zn<sub>2</sub>(μ-OR)<sub>2</sub> were characterised by X-ray diffraction studies. (7.L2)ZnEt was unreactive toward ethanol, but the amide complexes afforded (7.L2)ZnOEt and (7.L3)ZnOEt upon reaction with ethanol, which were used in *rac*-lactide polymerization without isolation. All complexes epimerize readily at room temperature and show apparent C<sub>s</sub>-symmetry in their NMR spectra. The ethoxide complexes were highly active in lactide polymerization, with (7.L3)ZnOEt reaching full conversion in 15 min at 0.5 mM catalyst concentration at room temperature. In both cases, introduction of a second donor arm on the central nitrogen introduced a slight bias for isotactic monomer enchainment (*P*<sub>m</sub> = 0.55-0.60), which for (7.L3)ZnOEt was dependent on catalyst concentration.

## Introduction

Using polylactic acid (PLA) as a green replacement for petroleum based resources has gained a lot of interest recently.<sup>1-10</sup> PLA is prepared through ring opening polymerisation (ROP) of lactide which itself is obtained through fermentation of corn starch.<sup>11-13</sup> Fuelled by its industrial application, controlled lactide polymerisation has become a catalytic challenge.<sup>14-42</sup> To date, there is no catalytic system which can polymerize lactide with high stereocontrol ( $P_m > 95\%$ ) (Scheme 7.1), excellent polymer molecular weight control and good activities under industrially relevant conditions (140 – 180 °C, in the presence of water and lactic acid).



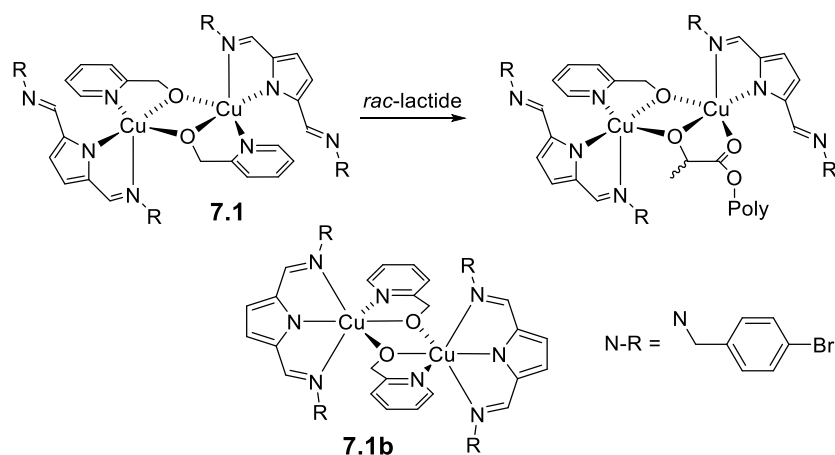
### Scheme 7.1.

The situation is rendered more interesting (and made thoroughly more complicated) by the number of possible mechanistic pathways for lactide polymerisation: In addition to ring-opening polymerisation by anionic or neutral organic initiators, lactide can be polymerized by Lewis-acid activation of the monomer together with a suitable co-initiator (alcohol) or by coordination-insertion polymerisation into a metal alkoxide catalyst. The same mechanistic multitude is observed for isotactic stereocontrol – which seems currently to be the biggest challenge: Not only are the traditional stereocontrol mechanisms, chain-end and catalytic-site control, both observed in lactide polymerisation (sometimes opposing each other), but other mechanisms, such as selective chain transfer, can be operative.<sup>43-45</sup> In this context, there is growing evidence that in some instances a higher flexibility of the catalytic site can be beneficial, which is untypical for “traditional” stereocontrol



mechanisms. Based on initial observations by Ma, Okuda and Carpentier,<sup>46, 47</sup> and follow-up work of Davidson and Jones,<sup>48-51</sup> a *catalytic-site mediated (or ligand mediated) chain-end control* mechanism was proposed. While the chiral information is still derived from the polymer chain end, the latter does not interact directly with the incoming monomer. Rather, the catalytic site adapts its configuration to match the chirality of the chiral chain end, and in turn determines stereochemistry by interaction with the monomer. A flexible and preferably chiral catalytic site is a prerequisite for this mechanism.

We have recently observed this mechanism to be active in copper diiminopyrrolide complexes to provide moderately isotactic PLA.<sup>52-55</sup> The active species of catalyst **7.1** is found to be a dinuclear species, in which the penta-coordinated copper centres are chiral, but can readily epimerize due to the presence of the pendant imino ligand (Scheme 7.2). Stereocontrol seemed to be largely invariant of the nature of the *N*-substituent, but a pyridylmethoxide ligand was essential. The only pyridylmethoxide complex which did not provide isotactic PLA, **7.1b** (Scheme 7.2), showed an octahedrally coordinated copper in its crystal structure and thus an achiral catalytic site, unable to participate in the proposed mechanism.



### Scheme 7.2.

Due to their abundance, low price, non-toxicity and general lack of colour, zinc-based complexes have been expansively investigated in homogenous

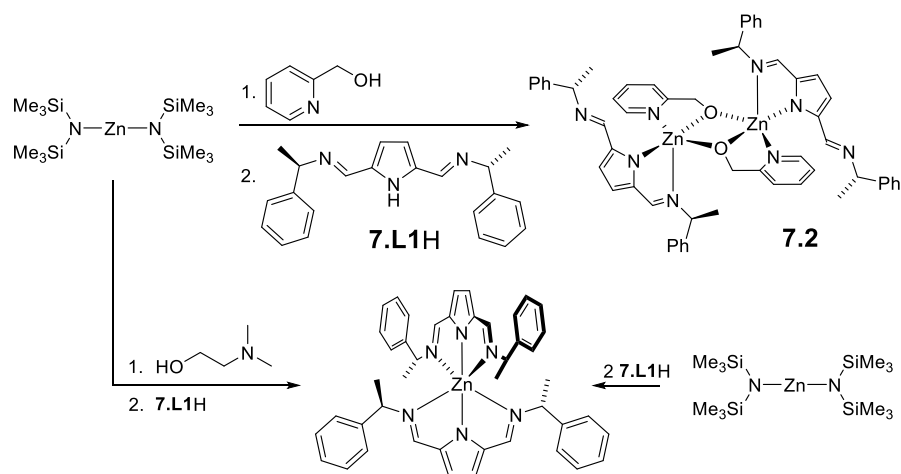
lactide polymerisation from the very beginning.<sup>56, 57</sup> Zinc-based complexes typically show good to excellent activities and good polymer molecular weight control. But despite numerous studies,<sup>14, 15, 17, 20, 24, 26</sup> including our own,<sup>58</sup> stereocontrol toward isotactic PLA was difficult to achieve. Only in recent years, zinc-catalysts with preference for isotactic monomer insertion emerged.<sup>59-73</sup> In the following, we explore if the stereocontrol mechanism observed in copper diiminopyrrolide complexes can be transferred to zinc-based catalysts, either using the identical ligand framework as for copper or by designing a catalyst capable of catalytic site epimerisation.

## Results and discussion

### Diiminopyrrolide complexes

#### Synthesis and structure.

Synthesis of **7.L1H** (Scheme 7.3) has been reported previously.<sup>50</sup> The dimeric complex  $(\mathbf{7.L1})_2\text{Zn}_2(\mu\text{-OCH}_2\text{C}_5\text{H}_4\text{N})_2$ , **7.2**, was obtained similar to the analogous copper(II) complexes by reaction of zinc bis-bis(trimethylsilyl)amide with one equivalent of pyridinemethanol, followed by addition of the ligand **7.L1H** (Scheme 7.3).<sup>50</sup> If dimethylaminoethanol was used instead of pyridinemethanol, the corresponding homoleptic complex  $(\mathbf{7.L1})_2\text{Zn}$  was obtained. For the sake of comparison and characterisation,  $(\mathbf{7.L1})_2\text{Zn}$  was also prepared from reaction of  $\text{Zn}(\text{N}(\text{SiMe}_3)_2)_2$  with two equivalents of **7.L1H** (see Fig. 7.S1 for its crystal structure).



**Scheme 7.3.**

Complex **7.2** crystallised as a dimeric, pentacoordinated complex, with distorted bipyramidal geometry around zinc ( $\tau = 0.7$ ,<sup>74</sup> Fig. 7.1). While  $\tau$ -values can be misleading, this agrees with the observed metal-ligand bond lengths. In the distorted square-pyramidal coordination of **7.1**, the ligand in the apical position showed a notably (0.2-0.3 Å) elongated bond (Table 7.1). In distorted bipyramidal **7.2**, all zinc-ligand bond distances fall all in the range of 2.0-2.1 Å, irrespective of position, and are comparable to what has been reported in literature.<sup>75</sup> Overall though, the structure of **7.2** resembles very strongly that of **7.1** (Table 7.1, Fig. 7.1). Due to the differences in preferred coordination geometry, **7.1** showed a better defined equatorial complex plane with an offset of appr. 0.8 Å between the CuON<sub>2</sub>-planes of each metal centre.<sup>49</sup> The structure of **7.2** is slightly more distorted, with a larger offset (appr. 1.5 Å) between the ZnON<sub>2</sub>-planes.<sup>†</sup>

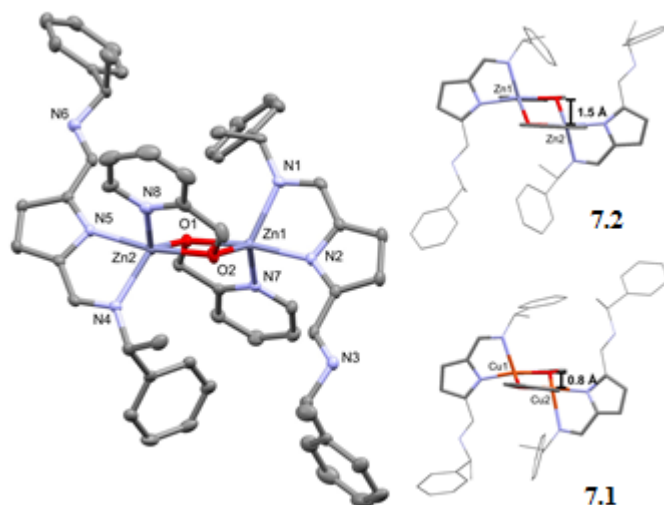


**Figure 7.1.** X-ray structure of **7.2**. Thermal ellipsoids are drawn at the 50% probability level. Hydrogen atoms omitted for clarity.

**Table 7.I.** Selected geometric data for pyridylmethoxide complexes **7.1** and **7.2**<sup>a</sup>

	<b>7.1</b> <sup>b</sup>	<b>7.2</b>
M-N <sub>pyrrole</sub>	1.945(2), 1.964(2)	2.084(2), 2.0896(19)
M-N <sub>imine</sub>	2.294(3), 2.242(3)	2.1205(19), 2.1095(18)
M-O <sub>short</sub>	1.915(2), 1.944(2)	1.9908(16), 1.9850(15)
M-O <sub>long</sub>	1.960(2), 1.960(2)	2.0744(16), 2.0666(17)
M-N <sub>pyridine</sub>	2.025(3), 1.995(3)	2.1084(19), 2.112(2)
M-M	3.025(5)	3.1091(4)
$\tau$	0.6, 0.4	0.7, 0.7

<sup>a</sup> The second values cited refers to the second metal center of the dimer. <sup>b</sup> Taken from ref. 52 for comparison.

The <sup>1</sup>H-NMR spectrum agrees with the unsymmetrical coordination of the ligand observed in the crystal structure: two sets of chemical shifts are obtained for the methylbenzylimino-substituent and the protons of pyrrole and of the methylene group are diastereotopic (Fig. 7.S6).

### ***rac*-Lactide polymerisation.**

Despite the strong structural resemblance between **7.1** and **7.2**, polymerisation results with **7.2** were unsatisfactory and differed strongly from those of **7.1**. At

room temperature and in  $C_6D_6$  solution, complex **7.1** showed slow initiation, followed by pseudo-first order kinetics to produce moderately isotactic PLA after appr. 5 h ( $k_{\text{obs}} = 0.6 \pm 0.1 \text{ h}^{-1}$  at 2 mM catalyst concentration). Complex **7.2**, on the other hand, initiated fast, followed by a slower pseudo-first order regime to reach completion only after 48 h ( $k_{\text{obs}} = 0.15(1) \text{ h}^{-1}$  at 2 mM catalyst concentration, Fig. 7.2) and produced moderately *heterotactic* PLA ( $P_r = 0.75$ ). Polymer weight control is very poor, with appr. 5 chains produced per catalyst dimer and a high polydispersity of 2.4. We thus cannot determine if only one (as in **1**) or if both pyridylmethoxide ligands initiate chain growth.

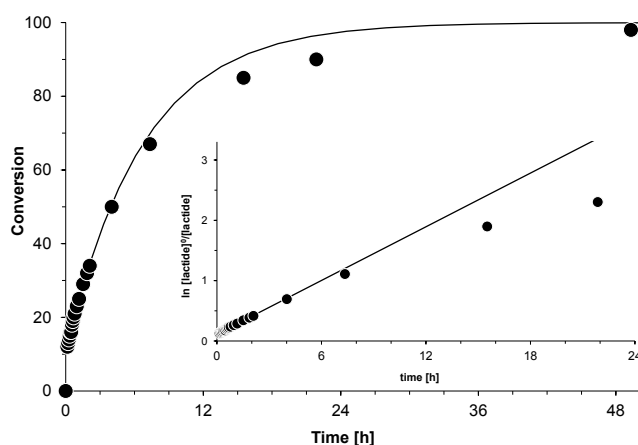
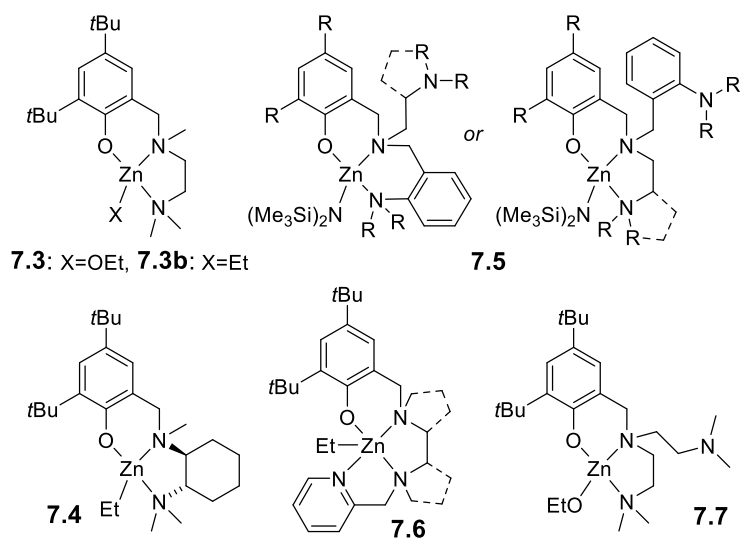


**Figure 7.2.** Conversion-time profile for *rac*-lactide polymerisation with **7.2**. The inset shows the semi-logarithmic plot. Solid lines represent theoretical curves based on linear regression of the linear region in the semi-logarithmic plot.

### Triaminophenolate complexes

Given the poor performance of the diiminopyrrolide complex, we decided to explore if stereocontrol via *site-mediated chain-end control* can be achieved with a ligand better suited for zinc. In 2003, Williams, Hillmyer, Tolman and coworkers reported a tetra-coordinated, monomeric Zn(II) catalyst carrying a diaminophenolate ligand (**7.3**, Scheme 7.4).<sup>76</sup> **7.3** is among the most active zinc-based catalysts reported, reaching full conversion in only 5 min at room temperature with good polymer molecular weight control and low polydispersities. The PLA produced was atactic, however. The high activity was attributed to reversible coordination of the pendant dimethylamino group.

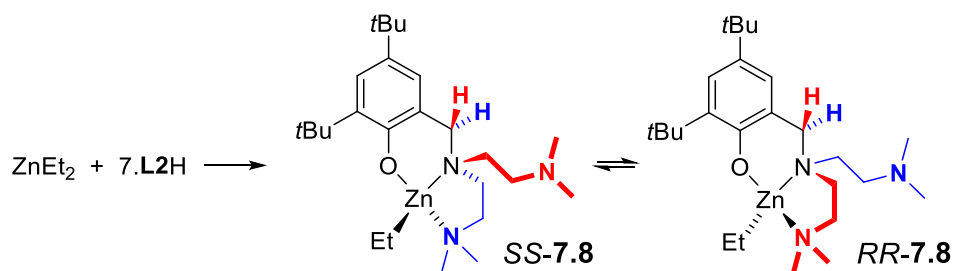
Polyamino-phenolate based ligands have been in the following well studied in zinc-catalysed lactide polymerisation.<sup>59, 62, 69-72, 77-83</sup> Several strategies have been employed to add isotactic stereocontrol to this catalyst system. Mehrkhodavandi introduced chirality into the side arm and replaced the ethylene bridge with a chiral cyclohexylene bridge (**7.4**, Scheme 7.4).<sup>84</sup> The more rigid bridge, however, drastically reduced activity (full conversion in about 40 h), while the resulting PLA remained atactic. Removing the methyl group on the central nitrogen, increased activity, but did not improve on stereocontrol.<sup>81</sup> Ma added an aniline donor arm to the central amine donor (**5**, Scheme 7.4).<sup>69</sup> Stereocontrol correlated with the coordination environment of the zinc centre, with aniline-coordinated complexes providing heterotactic and amine-coordinated complexes providing isotactic PLA. The same group also successfully explored replacing the dimethylamino substituent with chiral or non-chiral cyclic amines to provide isotactic PLA.<sup>71, 72</sup> The results are mechanistically complex and involve catalytic-site control and chain-end control active at the same time. More recently, Kol added a pyridylmethyl donor on the terminal amino group to form a tetradentate ligand with either achiral or chiral spacers (**7.6**, Scheme 7.4). The complexes were highly active in polymerisation and provided isotactic PLA.<sup>70, 73</sup> All these approaches relied on stabilizing a specific environment of the catalytic site. We decided to investigate whether deliberate introduction of flexibility into **7.3**, i. e. providing a stereochemically *unstable* catalytic site, would allow isotactic stereocontrol via a *catalytic-site mediated chain-end control* mechanism. Complex **7.7**, containing identical aminoethyl substituents should preserve the high activity of **7.3**, while exchange of the coordinating arms would invert chirality at the zinc and the central nitrogen atom simultaneously, and would allow facile epimerisation of the complex (Scheme 7.4).



#### Scheme 7.4.

#### Syntheses and structures.

**7.L2H** was prepared by reductive amination of 2-formyl-4,6-*tert*-butylphenol in the presence of  $\text{NaBH}_3(\text{CN})$  and acetic acid in methanol, adapting protocols for similar ligands.<sup>78</sup> It has been previously prepared by reaction of sodium dimethyl amide with the respective chloride substituted precursor.<sup>85</sup> Reaction of zinc diethyl with one equiv of **7.L2H** produced a yellow oil from which colourless crystals of  $(\mathbf{7.L2})\text{ZnEt}$ , **7.8**, could be obtained (Scheme 7.5). The X-ray structure of **7.8** shows a chiral, tetrahedral Zn(II) complex in which only one of the dimethylamino arms is coordinated to the metal (Fig. 7.3). As hypothesised, the additional donor arm does not influence complex geometry, and **7.8** is essentially isostructural to **7.3b** (Scheme 7.4, Table 7.II).<sup>76</sup>



**Scheme 7.5.**

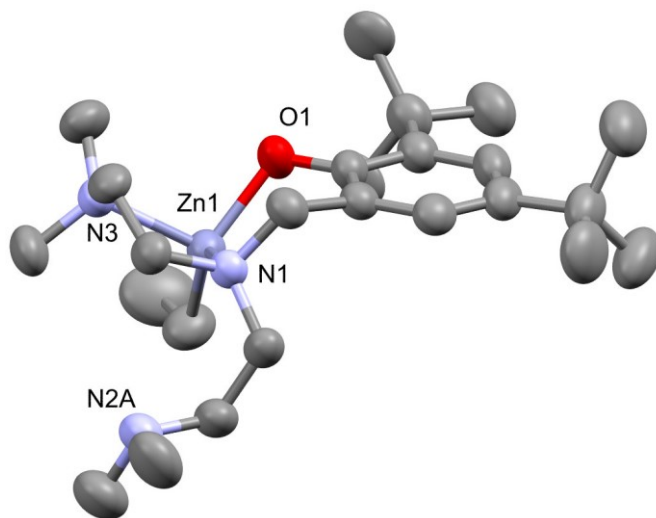


**Figure 7.3.** X-ray structure of **7.8**. Thermal ellipsoids are drawn at the 50% probability level. Hydrogen atoms and minor fractions of disorder in *tert*-butyl and dimethylaminoethylene substituents omitted for clarity.



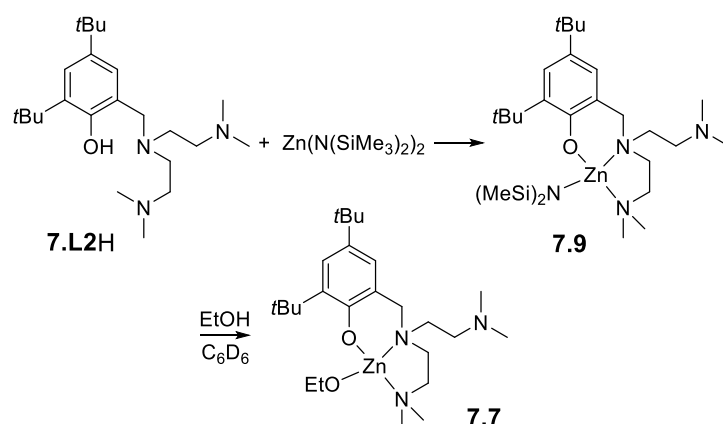
**Table 7.II.** Geometrical details for the X-ray structures of **7.8-7.10**.

	<b>7.8</b>	<b>7.3b</b> <sup>a</sup>	<b>7.9</b>	<b>7.10</b>
Zn-O	1.959(2)	1.956(3)	1.949(2), 1.941(2)	1.972(1)
Zn-N <sub>terminal</sub> <sup>b</sup>	2.159(3)	2.128(3)	2.154(3), 2.158(3)	2.210(1), 2.223(6)
Zn-NR <sub>3</sub>	2.171(3)	2.147(4)	2.118(2), 2.124(2)	2.306(1)
Zn-C/N <sub>amide</sub>	1.977(4)	1.998(4)	1.927(2), 1.933(3)	1.974(1)
O-Zn- C/N <sub>amide</sub>	126.5(1)	128.8(1)	115.6(1), 116.0(1)	120.45(1)
O-Zn-N <sub>terminal</sub> <sub>b</sub>	101.6(1)	99.8(1)	103.4(1), 103.3(1)	95.49(4), 99.7(2)

<sup>a</sup> Taken from ref. 76 <sup>b</sup> N<sub>terminal</sub> : NMe<sub>2</sub> (**7.3b**, **7.8**, **7.9**), pyridine (**7.10**)

The <sup>1</sup>H NMR spectrum of **7.8** displays a higher apparent symmetry than its crystal structure (Fig. 7.S9). The two dimethylamino-capped side arms exchange readily on the NMR time scale and only one singlet is observed for all NMe<sub>2</sub> groups.<sup>§</sup> More importantly, the ArCH<sub>2</sub>N group appears as a singlet with an intensity of 2 at 3.39 ppm. The side arm exchange is thus correlated with an inversion at the zinc centre *and* the central nitrogen, i. e. an epimerisation of the complex, which renders these two protons homotopic (Scheme 7.5). It should be noted that complex **7.3b** shows two distinct singlets for the NMe<sub>2</sub> group and a pair of doublets for ArCH<sub>2</sub>N in its NMR spectrum.<sup>76</sup> Mehrkhodavandi showed that addition of pyridine led to coalescence of the NMe<sub>2</sub> signals, but the ArCH<sub>2</sub>N protons remained diastereotopic.<sup>84</sup> Epimerisation thus does not occur in **7.3b** – even in the presence of Lewis bases – since it would require dissociation of both amine ligands at the same time. As envisioned, the presence of an additional donor arm in **7.8** facilitates epimerisation at the metal centre, a prerequisite for the targeted stereocontrol mechanism.

Williams et al. reported facile transformation of ethyl complex **7.3b** into the desired alkoxide complex **7.3** with ethanol. Unfortunately, the ethyl group in **7.8** was unreactive toward alcoholysis and, even after heating, NMR spectra confirmed the presence of unreacted **7.8** and ethanol. Similar problems were encountered in the reaction of **7.4** with ethanol,<sup>84</sup> and we and others have noticed previously that alcoholysis of the second zinc ethyl bond can be challenging.<sup>58, 86</sup> In fact, the major product of  $\text{ZnEt}_2$  in isopropanol is  $\text{EtZnOiPr}$ .<sup>87</sup> Zinc amide complexes are a commonly employed alternative pathway to prepare heteroleptic zinc alkoxides.<sup>56</sup> Complex **7.9** was thus prepared by addition of 1 equiv  $\text{Zn}(\text{N}(\text{SiMe}_3)_2)_2$  to a toluene solution of **7.L2H**, and formed colourless crystals after recrystallisation from hexane (Scheme 7.6).



### Scheme 7.6.

The X-ray structure of **7.9** shows the same distorted tetrahedral coordination with one uncoordinated amine ligand as in **7.8** (Fig. 7.4, Table 7.II). The  $^1\text{H}$  NMR spectrum of **7.9** likewise showed a single singlet for the aryl methylene group and one singlet for all dimethylamino groups, in agreement with fast exchange of coordinated and uncoordinated dimethylamine ligand, coupled with an epimerisation of the metal centre (Fig. 7.S10). Only one signal is observed for the trimethylsilyl substituents.  $\text{Zn-N}_{\text{amide}}$  rotation is thus fast on the NMR time scale, but this process is not connected with complex epimerisation.

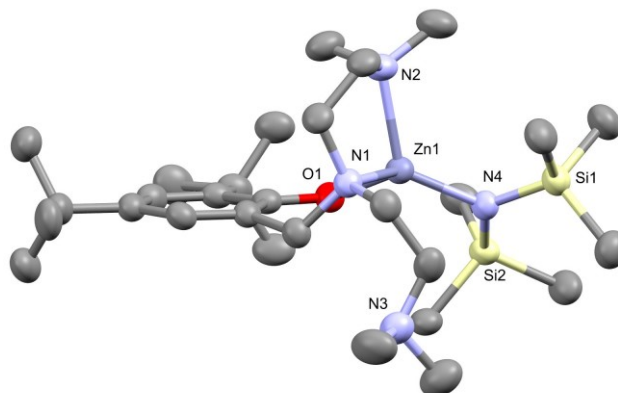


**Figure 7.4.** X-ray structure of **7.9**. Thermal ellipsoids are drawn at the 50% probability level. Hydrogen atoms and the second, independent molecule in the asymmetric unit omitted for clarity.

The desired catalyst **7.7**, containing an alkoxide as a suitable initiator for *rac*-lactide polymerisation, was prepared by the addition of 1 equiv of ethanol to a  $C_6D_6$  solution of **7.9** (Scheme 7.6). The reaction was followed by  $^1H$  NMR to ensure clean conversion to the alkoxide complex. The reaction was complete before the first NMR spectrum was taken ( $< 10$  min, Fig. 7.S8). As for the amide complexes, only a one singlet is observed for the dimethylamine groups and the arylmethylene group, respectively, indicating fast epimerisation at the metal centre. After  $^1H$  NMR confirmed full conversion,  $C_6D_6$  solutions of **7.7** were used as stock solutions in polymerisations experiments.

#### ***rac*-Lactide polymerisation.**

Complex **7.7** readily polymerized lactide in  $C_6D_6$  solution at room temperature and reached full conversion after appr. 30 min at 2 mM catalyst concentration (Table 7.III). The catalyst follows clean first-order kinetics, without notable induction period or complex decomposition (Fig. 7.5). The pseudo-first-order rate constant at 2 mM catalyst concentration is  $k_{obs} = 4.1(1) h^{-1}$  (Fig. 7.5). Complex **7** was thus able to retain the high activity of complex **7.3**. The slightly lower rate when compared to **7.3** ( $k_{obs}(\mathbf{7.3}) = 15 h^{-1}$  at  $[\mathbf{7.3}] = 2$  mM)<sup>76</sup> can be partly attributed to the difference in solvent ( $C_6D_6$  here,  $CH_2Cl_2$  for **7.3**) and partly to the presence of two diamino groups in **7**, which make dissociation

of a diamino ligand, speculated to be required for lactide coordination,<sup>76</sup> statistically less likely. Unfortunately, **7.7** shows relatively poor polymer molecular weight control with polydispersities around 2.8 and lower than expected polymer molecular weight. The latter could be improved under immortal polymerisation conditions: in presence of 4 equiv EtOH, **7.7** produced PLA with the expected molecular weight and lower polydispersities. Activity in immortal polymerisation was only half as high (Table 7.III, Fig. 7.S2 and 7.S3), which is surprising since the complex should not be sensitive towards alcohol. PLA produced with **7.7** showed a very slight isotactic bias of  $P_m = 0.55$ . Using our standardised integration protocol (see experimental part),  $P_m$  values are typically consistent to  $\pm 1\%$  through-out a kinetic experiment and to  $\pm 3\%$  in repeated experiments. The small amount of isotacticity observed is thus outside of typically experimental error, but might nevertheless be influenced by transesterification.<sup>58</sup>  $P_m$  values did, however, not show any variation with conversion or time and are thus not due to transesterification reactions (Fig. 7.6).

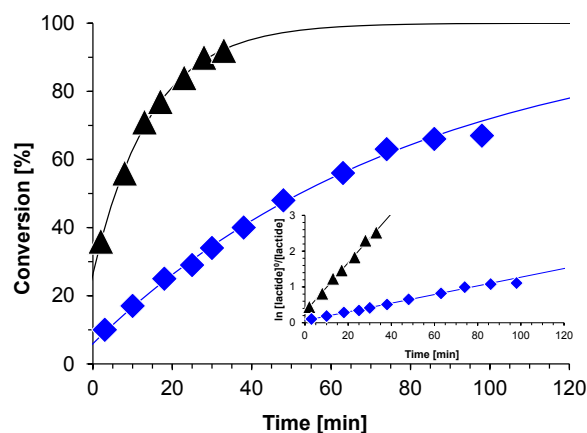


**Figure 7.5.** Conversion-time profiles for rac-lactide polymerisation with **7.7**. Conditions:  $C_6D_6$ , RT, **7.7**:lactide = 1:100. The inset shows the semi-logarithmic plot. Solid lines correspond to theoretical conversions based on rate constants obtained from linear regression: Black triangles:  $[7.7] = 2.0$  mM,  $k_{obs} = 4.1(1)$  h<sup>-1</sup>,  $t_0 = -5$  min, final conversion after >7 h: 99%; blue diamonds:  $[7.7] = 0.5$  mM,  $k_{obs} = 0.73(1)$  h<sup>-1</sup>,  $t_0 = -5$  min, final conversion after >7 h: 67%. The negative axis intercept might indicate

partial catalyst decomposition in the first 5 min of the reaction, inhomogeneous starting conditions or – although unlikely – experimental error.

**Table 7.III.** *rac*-Lactide polymerisation with **7.7** and **7.10**.

Catalyst	[catalyst]	[lactide]	Final conversion	$k_{\text{obs}}$	$M_n^b$	$M_n$ (calc.) <sup>c</sup>	$M_w/M_n$	chains/Zn <sup>d</sup>	$P_m^e$
<b>7.7</b>	2.0 mM	200 mM	99%	4.1(1) h <sup>-1</sup>	6.0 kDa	14.3 kDa	2.8	2.4	0.55
<b>7.7 + 4</b> EtOH	2.0 mM	200 mM	99%	2.5(1) h <sup>-1</sup>	2.7 kDa	2.9 kDa	1.2	5	0.55
<b>7.7</b>	0.5 mM	50 mM	67%	0.73(1) h <sup>-1</sup>	9.1 kDa	9.6 kDa	1.1	1	0.55
<b>7.10</b>	2.0 mM	200 mM	97% 99%	>50 h <sup>-1</sup>	2.4 kDa 9.6 kDa	14.0 kDa 14.3 kDa	1.9 1.1	5.8 1.5	0.49 0.50
<b>7.10</b>	0.5 mM	50 mM	93%	6.9(2) h <sup>-1</sup>	33.8 kDa	13.4 kDa	1.9	0.4	0.55
<b>7.10</b>	0.5 mM	200 mM	96%	12.2(6) h <sup>-1</sup>	32.8 kDa	55.3 kDa	1.7	1.7	0.55
<b>7.10</b>	0.5 mM	500 mM	60%	0.9(1) h <sup>-1</sup>	36.5 kDa	86.4 kDa	1.2	2.7	0.55
<b>7.10</b>	0.3 mM	150 mM	40%	0.25(4) h <sup>-1</sup>	23.2 kDa	27.4 kDa	1.2	1.2	0.60

<sup>a</sup> Conditions: C<sub>6</sub>D<sub>6</sub>, RT. <sup>b</sup>  $M_n$  and  $M_w$  determined by size exclusion chromatography vs. polystyrene standards, with a Mark-Houwink correction factor of 0.58. <sup>c</sup> calculated from [lactide]/([cat]+[EtOH])·conversion· $M_{\text{lactide}} + M_{\text{ROH}}$ . <sup>d</sup> Number of chains per zinc centre, calculated from the ratio of expected and obtained polymer molecular weight. <sup>e</sup>  $P_m$  determined from decoupled <sup>1</sup>H NMR by  $P_m = 1 - 2 \cdot I_1 / (I_1 + I_2)$ , with  $I_1 = 5.20 - 5.25$  ppm (*rmr*, *mmr/rmm*),  $I_2 = 5.13 - 5.20$  ppm (*mmr/rmm*, *mmm*, *mrn*).

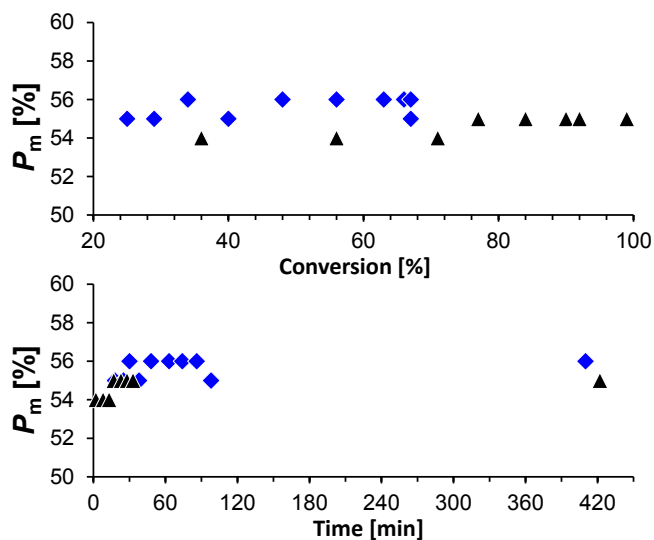
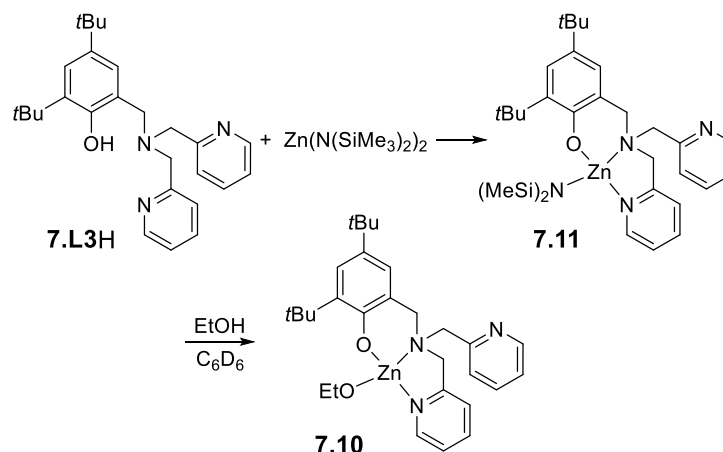


**Figure 7.6.** Variation of polymer microstructure ( $P_m$ ) in dependence of conversion or time in *rac*-lactide polymerisations with **7.7**. Black triangles:  $[7.7] = 2.0$  mM, blue diamonds:  $[7.7] = 0.5$  mM. With  $[7.7] = 0.5$  mM, conversion plateaued at 67%.

To compare the influence of catalytic site epimerisation on stereocontrol, *rac*-lactide polymerisation was investigated with **7.10**, in which the dimethyl amino donors were replaced with pyridyl (Scheme 7.7). Complexes similar to **7.10** have been briefly investigated by Thomas and Carpentier and produced atactic PLA.<sup>78</sup> **7.10** was prepared analogous to **7**: reaction of  $Zn(N(SiMe_3)_2)_2$  and **7.L3H** provided the amide complex **7.11**. Further reaction with ethanol in  $C_6D_6$  afforded **7.10**, which was directly used in polymerisation (Scheme 7.7). In contrast to **7.8** and **7.9**, in the crystal structure of **7.11** both pyridine ligands were coordinated to the metal centre (Fig. 7.7). A  $\tau$ -value of 0.1 would indicate square-pyramidal geometry, but closer inspection of the structure and the respective metal-ligand bond lengths propose distorted bipyramidal geometry as a better description (Table 7.II). The structure of **7.11** does not show mirror-symmetry, despite the coordination of both pyridine ligands, since the geometry of the aryl methylene group forces a bending of the aryl group out of the  $ZnN_2$ -plane toward one of the pyridine ligands. The latter shows a bending of the  $Zn-N_{Pyridine}$  bond out of the mean plane of the pyridine to allow closer contact with the aryl group, indicating favourable  $\pi$ -interactions between the

two aromatic systems (angle between planes =  $34^\circ$ , shortest atom-plane contact =  $3.0 \text{ \AA}$ ).



**Scheme 7.7.**

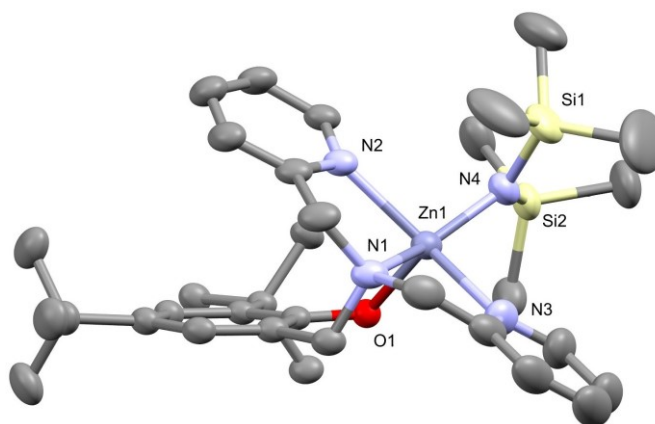
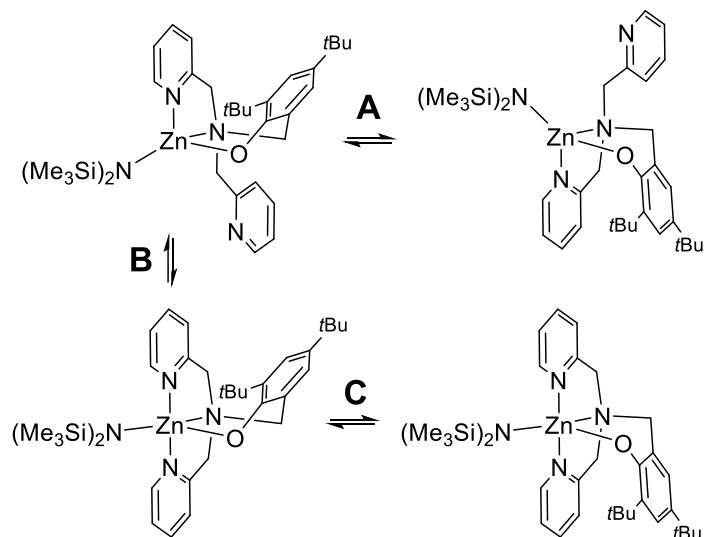


**Figure 7.7.** X-ray structure of **7.11**. Thermal ellipsoids are drawn at the 50% probability level. Hydrogen atoms, and the second, independent molecule in the asymmetric unit omitted for clarity.

The  $^1\text{H}$  NMR spectrum of **7.11** likewise shows indications of stronger interaction of pyridine with the zinc centre. While **7.11** still displays apparent  $C_s$ -symmetry in its  $^1\text{H}$  spectrum, peaks are broadened, indicative of a lower rate of exchange: the  $\text{PyCH}_2$  groups appear as one broadened and one sharp doublet and the  $\text{ArCH}_2$  group is broadened to a large peak between 3.8 – 4.9 ppm (Fig. 7.S12). Only one set of pyridine signals are observed, significantly broadened and coupling is barely visible. **7.11** thus either exists in solution as a tetrahedral

complex and undergoes slow epimerisation (Scheme 7.8, **A**), or it interchanges between a tetrahedral and a five-coordinated species by dissociation/recoordination of a pyridine ligand (**B**), or the complex remains five-coordinated, with a slow “flipping” of the phenolate ring (**C**). All these dynamic processes generate apparent  $C_s$ -symmetry and equalize the two pyridyl moieties. Derivatives of **7.11**, previously reported by Thomas and Carpentier,<sup>78</sup> likewise showed apparent  $C_s$ -symmetry in their NMR spectra. The  $^1\text{H}$  NMR spectra of the respective ethoxide complex **7.10** shows essentially the same features as **7.11**: only one set of peaks for the pyridyl ligands in agreement with apparent  $C_s$  symmetry, but with overall broadened peaks (Fig. 7.S11). Regardless of the exact nature of the dynamic process, it is clear that epimerisation – if it happens at all in **7.10** and **7.11** – is more difficult with pyridyl donors than with dimethylamine ligands.



### Scheme 7.8.

Complex **7.10** was highly active in lactide polymerisation (Table 7.III). Polymerisation was completed in 2 min at ambient temperature at 2 mM catalyst concentration and in appr. 15 min at 0.5 mM, placing **7.10** among the most active zinc-based catalysts (c.f. estimated  $k_{\text{obs}}$  at 2 mM  $[\text{Zn}]$ : **7.3**,<sup>76</sup>  $15 \text{ h}^{-1}$ ; **7.5**,<sup>69</sup>  $10 \text{ h}^{-1}$ ; **7.6**,<sup>73</sup>  $50 \text{ h}^{-1}$ ; **7**,  $4 \text{ h}^{-1}$ ; **7.10**,  $>50 \text{ h}^{-1}$ ). No induction period was observed, but kinetics at 0.5 mM all showed a negative  $x$ -axis intercept,



indicative of catalyst deactivation at the beginning of the reaction (Fig. 7.S4 and 7.S5). The same was observed for **7.7**, but only to an extent still explicable by experimental error. While decomposition did not visually affect polymerisations at catalyst:lactide ratios of 1:100 or 1:400, polymerisations at a ratio of 1:1000 or at catalyst concentrations of 0.3 mM showed curved semi-logarithmic plots and did not reach completion, indicative of catalyst decomposition before the end of the reaction (Fig. 7.S4 and S5). At 0.1 mM catalyst concentration, we did not observe more than 10% conversion. Polymerisation with **7.7** at reduced catalyst concentrations (0.5 mM) also failed to reach completion (Fig. 7.5, Table 7.III).

PLA produced with **7.10**, under conditions identical to those with **7.7**, was atactic. This would be in line with a higher tendency of pyridine to coordinate to zinc and the proposed catalytic-site mediated chain-end control. If the active species is a penta-coordinated zinc complex, the catalytic site is achiral and cannot transfer the chirality of the chain-end to zinc. In diiminopyrrolide copper complexes of type **7.1**, the only complex ever observed to coordinate both iminogroups to form an achiral catalytic site (**7.1b**, Scheme 7.2) was also the only complex of type **7.1** producing atactic PLA.<sup>54, 55</sup> Alternatively, the catalytic site might be slow to epimerize and to adapt to the chain-end, also resulting in loss of the ability to transfer chain-end chirality to the monomer. In the latter case, stereocontrol can be influenced by reaction conditions, since insertion is dependent on monomer concentration, but catalyst epimerisation is not. At lower monomer concentrations, the ratio of epimerisation vs. insertion rate will thus be higher. If lactide concentration was reduced from 200 to 50 mM, while keeping the lactide:catalyst ratio constant, stereocontrol indeed increased to  $P_m = 0.55$  (Table 7.III). Closer investigation revealed, however, that this effect was not due to reduced lactide concentration, but rather due to reduced catalyst concentrations: Increasing lactide concentration to 200 or even to 500 mM, while keeping the catalyst concentration at 0.5 mM, did not affect stereocontrol, which remained constant at  $P_m = 0.55$  (Table 7.III). On the other hand, lowering catalyst concentration to 0.3 mM increased stereocontrol further

to  $P_m = 0.60$ . For **7.7**, lowering of catalyst concentration did not affect stereocontrol (Table 7.III). There are several mechanistic explanations for a negative impact of catalyst concentration on stereocontrol, such as chain-exchange between centres in a catalytic-site control mechanism or the formation of dinuclear species with different reactivities. Given the overall low isoselectivity of **7.7** and **7.10**, in particular when compared to **7.5** and **7.6**, and the mediocre polymer molecular weight control, we did not investigate this issue further.

## Conclusions

The application of the ligand system which provided isotactic copper-based polymerisation catalysts to zinc, afforded a complex of surprisingly similar structure, but strongly different polymerisation reactivity. Metals with coordination geometries closer to copper might show more similar reactivity, but our attempts to prepare the respective iron, cobalt or manganese complexes have not been successful so far.

For aminophenolate-based complexes, the counterintuitive approach to provide additional flexibility to the catalytic site and enable fast epimerisation was successful in introducing a slight isotactic bias in one of the most active zinc-based catalysts. While the low isotacticity and poor polymer molecular weight control do not encourage further optimisation of this ligand system in particular, these results underline that lactide polymerisation often defies the axiom that successful control requires a rigid environment of the catalytic site and that catalytic sites with flexible conformation or even flexible configuration might offer an alternative approach to achieve stereocontrol.

## Experimental

**General considerations.** All reactions were carried out using Schlenk or glove box techniques under nitrogen atmosphere.  $\text{Zn}(\text{N}(\text{SiMe}_3)_2)_2$ ,<sup>88</sup> 2,4-di-*tert*-butylsalicylaldehyde,<sup>89</sup> *N,N,N,N*-tetramethyldiethylenetriamine,<sup>90</sup> and **7.L1H**,<sup>53</sup> were prepared according to literature. Solvents were dried by passage through activated aluminum oxide (MBraun SPS), de-oxygenated by repeated

extraction with nitrogen, and stored over molecular sieves. C<sub>6</sub>D<sub>6</sub> was dried over molecular sieves. *rac*-Lactide (98%) was purchased from Sigma–Aldrich, purified by 3x recrystallisation from dry ethyl acetate and kept at –30 °C. All other chemicals were purchased from common commercial suppliers and used without further purification. <sup>1</sup>H and <sup>13</sup>C NMR spectra were acquired on Bruker Advance 300 and 400 spectrometers. Chemical shifts were referenced to the residual signals of the deuterated solvents (CDCl<sub>3</sub>: <sup>1</sup>H: δ 7.26 ppm, <sup>13</sup>C: δ 77.16; C<sub>6</sub>D<sub>6</sub>: <sup>1</sup>H: δ 7.16 ppm, <sup>13</sup>C: δ 128.06 ppm). Elemental analyses were performed by the Laboratoire d'analyse élémentaire (Université de Montréal). All UV-Vis measurements were performed in degassed and anhydrous toluene at RT in a sealed quartz cell on a Cary 500i UV-Vis-NIR Spectrophotometer.

**2,4-di-*tert*-butyl-6-((*N,N,N',N'*-tetramethyldiethylenetriamine))phenol,**

**7.L2H.**<sup>85</sup> A procedure from literature was adapted as follows:<sup>78</sup> To a brown mixture of 3,5-di-*tert*-butyl-2-hydroxybenzaldehyde (0.50 g, 2.1 mmol), NaBH<sub>3</sub>(CN) (0.16 g, 2.5 mmol) and a few drops of acetic acid in methanol (10 ml), was added a solution of *N,N,N,N*-tetramethyldiethylenetriamine (0.67 g, 4.2 mmol) in methanol (10 ml) dropwise. The reaction was stirred for 48h. The methanol was evaporated and the resulting brown residue was purified by silica gel chromatography (2% MeOH, 1% NEt<sub>3</sub> in CHCl<sub>3</sub>) yielding a light yellow oil (0.62 g, 78%).

<sup>1</sup>H NMR (CDCl<sub>3</sub>, 300 MHz): δ 7.18 (d, *J* = 3 Hz, 1H, Ar), 6.82 (d, *J* = 3 Hz, 1H, Ar), 3.74 (s, 2H, ArCH<sub>2</sub>N), 2.68-2.63 (m, 2H, CH<sub>2</sub>), 2.47-2.43 (m, 2H, CH<sub>2</sub>), 2.19 (s, 12H, N(CH<sub>3</sub>)<sub>2</sub>), 1.40 (s, 9H, CH<sub>3</sub>), 1.27 (s, 9H, CH<sub>3</sub>); <sup>13</sup>C{<sup>1</sup>H} NMR (CDCl<sub>3</sub>, 75 MHz): δ 154.3 (Ar), 140.4 (Ar), 129.8 (Ar), 123.9 (Ar), 122.9 (Ar), 121.9 (Ar), 59.0 (CH<sub>2</sub>), 57.1 (CH<sub>2</sub>), 51.9 (CH<sub>2</sub>), 45.8 (N(CH<sub>3</sub>)<sub>2</sub>), 35.0 (C(CH<sub>3</sub>)<sub>3</sub>), 34.2 (C(CH<sub>3</sub>)<sub>3</sub>), 31.8 (CH<sub>3</sub>), 29.7 (CH<sub>3</sub>). ESI-HRMS (*m/z*): [M+H]<sup>+</sup> (C<sub>23</sub>H<sub>44</sub>N<sub>3</sub>O) calcd 378.3478; found 378.3485.

**2,4-di-*tert*-butyl-6-((di-(2-picoly)amine)phenol, 7.L3H.** A procedure from literature was slightly modified as follows:<sup>78</sup> Analogous to **7.L2H**, from 3,5-di-*tert*-butyl-2-hydroxybenzaldehyde (0.50 g, 2.1 mmol), NaBH<sub>3</sub>(CN) (0.16 g, 2.5

mmol), a few drops of acetic acid, di-(2-picolyl)amine (0.84 g, 4.2 mmol) in methanol (20 ml) stirred for 4 hours to yield a brown residue which was purified by silica gel chromatography (2% MeOH, 1% NEt<sub>3</sub> in CHCl<sub>3</sub>) (0.34 g, 39%).

<sup>1</sup>H NMR (CDCl<sub>3</sub>, 300 MHz): δ 10.62 (s, 1H, OH), 8.56 (ddd, *J* = 6, 2, 1 Hz, 2H, Py), 7.63 (td, *J* = 8, 2 Hz, 2H, Py), 7.37 (d, *J* = 8 Hz, 2H, Py), 7.20 (d, *J* = 3 Hz, 1H, Ar), 7.15 (ddd, *J* = 8, 6, 1 Hz, 2H, Py), 6.87 (d, *J* = 3 Hz, 1H, Ar), 3.87 (s, 4H, PyCH<sub>2</sub>N), 3.80 (s, 2H, ArCH<sub>2</sub>N), 1.45 (s, 9H, CH<sub>3</sub>), 1.26 (s, 9H, CH<sub>3</sub>); <sup>13</sup>C{<sup>1</sup>H} NMR (CDCl<sub>3</sub>, 75 MHz): δ 158.3 (Py), 154.0 (Ar), 149.2 (Py), 140.5 (Ar), 136.7 (Py), 135.7 (Ar), 124.7 (Ar), 123.7 (Py), 123.3 (Ar), 122.4 (Py), 121.8 (Ar), 59.7 (CH<sub>2</sub>), 58.4 (CH<sub>2</sub>), 35.1 (C(CH<sub>3</sub>)<sub>3</sub>), 34.2 (C(CH<sub>3</sub>)<sub>3</sub>), 31.8 (CH<sub>3</sub>), 29.8 (CH<sub>3</sub>). ESI-HRMS (m/z): [M+H]<sup>+</sup> (C<sub>27</sub>H<sub>36</sub>N<sub>3</sub>O) calcd 418.2852; found 418.2857.

**(7.L1)<sub>2</sub>Zn<sub>2</sub>(μ-O,κ<sub>N</sub>-OCH<sub>2</sub>C<sub>6</sub>H<sub>2</sub>N)<sub>2</sub>, 7.2.** Zn(N(SiMe<sub>3</sub>)<sub>2</sub>)<sub>2</sub> (115 mg, 0.304 mmol) was suspended in toluene (3 ml). 2-Pyridinemethanol (28.3 μl, 0.304 mmol) was added to the red suspension, which was left to stir for 45 min. A freshly prepared light orange solution of **7.L1H** (100 mg, 0.304 mmol) in toluene (2 ml) was added dropwise, resulting in a light yellow solution. The reaction was stirred 24 hours at RT, filtered to remove trace impurities, concentrated to 1/3 of the volume resulting in colourless crystals. The crystals were separated by decantation and washed with ether (3×10 ml) (23 mg, 16%).

<sup>1</sup>H NMR (C<sub>6</sub>D<sub>6</sub>, 400 MHz): δ 8.18 (s, 1H, (N=C)H), 7.80 (s, 1H, (N=C)H), 7.35 (s, 1H), 7.29 (bs, 2H, Ph), 7.04 – 6.95 (m, 3H), 6.95 – 6.83 (m, 5H), 6.76 (s, 1H), 6.65 (t, *J* = 8 Hz, 1H), 6.15 (d, *J* = 8 Hz, 1H, pyrrole), 4.64 (d, *J* = 18 Hz, 1H, PyCH<sub>2</sub>), 4.56 (d, *J* = 18 Hz, 1H, PyCH<sub>2</sub>), 4.24 (q, *J* = 7 Hz, 1H, CH), 4.10 (q, *J* = 7 Hz, 1H, CH), 1.50 (d, *J* = 7 Hz, 3H, CH<sub>3</sub>), 1.20 (d, *J* = 7 Hz, 3H, CH<sub>3</sub>); <sup>13</sup>C{<sup>1</sup>H} NMR (C<sub>6</sub>D<sub>6</sub>, 101 MHz): δ 165.2 ((N=C)H), 157.0 (Ar), 154.8 ((N=C)H), 146.7 (Ar), 145.9 (Ar), 144.6 (Ar), 141.6 (Ar), 140.2 (Ar), 137.4 (Ar), 129.3 (Ar), 128.5 (Ar), 127.4 (Ar), 127.0 (Ar), 126.9 (Ar), 126.7 (Ar), 122.0 (Ar), 120.9 (Ar), 116.3 (Ar), 115.7 (Ar), 68.4 (CH<sub>2</sub>), 67.7 (CH), 64.2

(CH), 24.7 (CH<sub>3</sub>), 24.6 (CH<sub>3</sub>). UV-vis (toluene, 2.2·10<sup>-6</sup> M) [ $\lambda_{\max}$ , nm ( $\epsilon$ , mol<sup>-1</sup> cm<sup>2</sup>): 378 (23500), 387 (23800). Anal. Calcd for C<sub>56</sub>H<sub>56</sub>Zn<sub>2</sub>N<sub>8</sub>O<sub>2</sub>: C, 67.00; H, 5.62; N, 11.16; Found: C, 66.34; H, 5.62; N, 10.65.

**(7.L1)<sub>2</sub>Zn.** Zn(HMDS)<sub>2</sub> (115 mg, 0.304 mmol) was suspended in toluene (3 ml). A freshly prepared light orange solution of **7.L1H** (200 mg, 0.608 mmol) in toluene (2 ml) was added dropwise, resulting in a light yellow solution. The reaction was stirred 24 hours at RT, filtered to remove trace impurities, concentrated to 1/3 of the volume resulting in colourless crystals. The crystals were separated by decantation and washed with ether (3×10 ml) and recrystallised two times from a mixture of toluene:hexane (1:3) (53 mg, 24%).

<sup>1</sup>H NMR (C<sub>6</sub>D<sub>6</sub>, 400 MHz):  $\delta$  7.80 (s, 2H, (N=C)H), 7.04 – 6.98 (m, 6H, Ph), 6.93 – 6.86 (m, 4H, Ph), 6.76 (s, 2H, 3,4-Pyrrole), 4.10 (q,  $J$  = 7 Hz, 2H, CH), 1.20 (d,  $J$  = 7 Hz, 6H, CH<sub>3</sub>). UV-vis (toluene, 2.2·10<sup>-6</sup> M) [ $\lambda_{\max}$ , nm ( $\epsilon$ , mol<sup>-1</sup> cm<sup>2</sup>): 376 (20600), 389 (22000), 433 (sh). Despite X-ray quality crystals and repeated re-crystallizations, a satisfactory elemental analysis could not be obtained. The NMR likewise indicates the presence of impurities.

**(7.L2)ZnOEt, 7.7.** To a solution of **7.9** (10 mg, 16  $\mu$ mol) in C<sub>6</sub>D<sub>6</sub> (0.6 ml) in a J-Young tube was added a freshly prepared solution of EtOH in C<sub>6</sub>D<sub>6</sub> (0.20 M) in two portions of appr. 40  $\mu$ L. The reaction was followed by NMR and the amount of the second batch of ethanol was adjusted with regard to remaining **7.9**. After NMR confirmed complete replacement of the amide by ethoxide, the solution used directly in polymerization.

<sup>1</sup>H NMR (C<sub>6</sub>D<sub>6</sub>, 400 MHz):  $\delta$  7.64 (d,  $J$  = 3 Hz, 1H, Ar), 6.94 (d,  $J$  = 3 Hz, 1H, Ar), 3.25 (s, 2H, ArCH<sub>2</sub>), 2.11 (s, 12 H, NMe<sub>2</sub>), 2.01-2.08 (m, 2H, CH<sub>2</sub>), 1.96 (ddd,  $J$  = 13, 9, 4 Hz, 2H, CH<sub>2</sub>), 1.90 (s, 9H, CMe<sub>3</sub>), 1.73 (m, 2H, CH<sub>2</sub>), 1.45 – 1.60 (m, 7H, CH<sub>3</sub> + 2 CH<sub>2</sub>), 1.50 (s, 9H, CMe<sub>3</sub>); <sup>13</sup>C {<sup>1</sup>H} NMR (C<sub>6</sub>D<sub>6</sub>, 101 MHz):  $\delta$  165.4 (Ar), 138.5 (Ar), 134.3 (Ar), 125.5 (Ar), 124.2 (Ar), 121.9 (Ar), 59.9 (CH<sub>2</sub>Ar), 55.9 (CH<sub>2</sub>), 51.2 (CH<sub>2</sub>), 46.3 (NMe<sub>2</sub>), 45.5 (ZnOCH<sub>2</sub>), 35.9 (CMe<sub>3</sub>), 34.2 (CMe<sub>3</sub>), 32.4 (CMe<sub>3</sub>), 32.1 (ZnOCH<sub>2</sub>Me), 30.4 (CMe<sub>3</sub>).

**(7.L2)ZnEt, 7.8.** ZnEt<sub>2</sub> (33 mg, 0.26 mmol) was added to a freshly prepared light yellow solution of **7.L2H** (100 mg, 0.26 mmol) in toluene (5 ml), resulting in an orange solution. The reaction was stirred 24 hours at RT, and filtered to remove trace impurities. The solvent was removed under vacuum and the resulting orange oil was crystallised from hexane (10 ml) at –30 °C. The colourless crystals were separated by decantation and washed with hexane (3x10 ml) (45 mg, 38%).

<sup>1</sup>H NMR (C<sub>6</sub>D<sub>6</sub>, 400 MHz): δ 7.63 (d, *J* = 3 Hz, 1H, Ar), 6.97 (d, *J* = 3 Hz, 1H, Ar), 4.34 (bs, 2H, NCH<sub>2</sub>), 3.39 (s, 2H, ArCH<sub>2</sub>N), 2.50 – 2.40 (m, 2H, NCH<sub>2</sub>), 2.37 – 2.21 (m, 4H, NCH<sub>2</sub>), 1.89 (s, 21H, C(CH<sub>3</sub>)<sub>3</sub> + N(CH<sub>3</sub>)<sub>2</sub>), 1.68 (t, *J* = 8 Hz, 3H, ZnCH<sub>2</sub>CH<sub>3</sub>), 1.49 (s, 9H, C(CH<sub>3</sub>)<sub>3</sub>), 0.45 (q, *J* = 8 Hz, 2H, ZnCH<sub>2</sub>); <sup>13</sup>C{<sup>1</sup>H} NMR (C<sub>6</sub>D<sub>6</sub>, 101 MHz): δ 158.9 (Ar), 149.3 (Ar), 138.4 (Ar), 136.1 (Ar), 123.5 (Ar), 122.2 (Ar), 61.1 (CH<sub>2</sub>), 59.4 (CH<sub>2</sub>), 32.54 (CH<sub>2</sub>), 32.47 (N(CH<sub>3</sub>)<sub>2</sub>), 32.02 (CMe<sub>3</sub>), 31.97 (CMe<sub>3</sub>), 30.4 (CMe<sub>3</sub>), 30.2 (CMe<sub>3</sub>), 23.1 (CH<sub>2</sub>Me), 14.4 (ZnCH<sub>2</sub>). UV-vis (toluene, 1.2·10<sup>-4</sup> M) [ $\lambda_{\max}$ , nm ( $\epsilon$ , mol<sup>-1</sup> cm<sup>2</sup>)]: 302 (2700). Anal. Calcd for C<sub>25</sub>H<sub>47</sub>ZnN<sub>3</sub>O: C, 63.75; H, 10.06; N, 8.92; Found: C, 63.63; H, 10.25; N, 8.84.

**(7.L2)ZnN(SiMe<sub>3</sub>)<sub>2</sub>, 7.9.** Analogous to **7.8**, from Zn(N(SiMe<sub>3</sub>)<sub>2</sub>)<sub>2</sub> (102 mg, 0.265 mmol), **7.L2H** (100 mg, 0.265 mmol) in toluene (5 ml). Filtration, removal of the solvent under vacuum, crystallisation in hexane (10 ml) at –30 °C, decantation and washing with hexane (3x10 ml) afforded 52 mg (32%) of colourless X-ray quality crystals.

<sup>1</sup>H NMR (C<sub>6</sub>D<sub>6</sub>, 400 MHz): δ 7.62 (d, *J* = 3 Hz, 1H, Ar), 6.87 (d, *J* = 3 Hz, 1H, Ar), 3.60 (s, 2H, ArCH<sub>2</sub>N), 2.45 (dt, *J* = 11, 6 Hz, 2H, CH<sub>2</sub>), 2.27 (td, *J* = 11, 6 Hz, 4H, CH<sub>2</sub>), 2.08 – 1.98 (br m, 2H, CH<sub>2</sub>), 1.93 (s, 12H, N(CH<sub>3</sub>)<sub>2</sub>), 1.78 (s, 9H, CH<sub>3</sub>), 1.47 (s, 9H, CH<sub>3</sub>), 0.49 (s, 18H, Si(CH<sub>3</sub>)<sub>3</sub>); <sup>13</sup>C{<sup>1</sup>H} NMR (C<sub>6</sub>D<sub>6</sub>, 101 MHz): δ 164.4 (Ar), 138.1 (Ar), 134.8 (Ar), 126.3 (Ar), 124.9 (Ar), 120.7 (Ar), 62.0 (CH<sub>2</sub>Ar), 56.6 (CH<sub>2</sub>), 53.5 (CH<sub>2</sub>), 46.6 (N(CH<sub>3</sub>)<sub>2</sub>), 35.9 (CMe<sub>3</sub>), 34.2(CMe<sub>3</sub>), 32.3 (CMe<sub>3</sub>), 30.6 (CMe<sub>3</sub>), 7.2 (SiMe<sub>3</sub>). UV-vis (toluene, 7.6·10<sup>-5</sup> M) [ $\lambda_{\max}$ , nm ( $\epsilon$ , mol<sup>-1</sup> cm<sup>2</sup>)]: 302 (4000). Anal. Calcd for

$C_{29}H_{60}N_4OSi_2Zn \cdot 1/3C_6H_{14}$  C, 59.00; H, 10.33; N, 8.88; Found: C, 59.25; H, 10.74; N, 9.16.

**(7.L3)ZnOEt, 7.10.** Analogous to **7**, from a freshly prepared solution of EtOH in  $C_6D_6$  (0.20 M) and **7.11** (10 mg, 16  $\mu$ mol). After NMR confirmed complete replacement of the amide by ethoxide, the solution used directly in polymerization.

$^1H$  NMR ( $C_6D_6$ , 400 MHz):  $\delta$  9.42 (br s, 2H, Py), 7.60 (s, 1H, Ar), 6.97 (s, 1H, Ar), 6.77 (t,  $J = 8$  Hz, 2H, Py), 6.56 (t,  $J = 8$  Hz, 2H, Py), 6.15 (bs, 2H, Py), 3.41 (bs, 2H,  $CH_2$ ), 3.2-3.7 (br, 2H,  $CH_2$ ), 2.75 (bs, 1H), 2.24 (bs, 1H), 1.91 (s, 9H,  $CMe_3$ ), 1.6-1.8 (bm, 2H), 1.51 (s, 9H,  $CMe_3$ ), 1.4 (bm, 3H);  $^{13}C\{^1H\}$  NMR ( $C_6D_6$ , 101 MHz):  $\delta$  165.7 (Ar), 155.6 (Ar), 151.1 (Ar), 139.4 (Ar), 138.5 (Ar), 133.7 (Ar), 125.8 (Ar), 124.3 (Ar), 123.3 (Ar), 122.5 (Ar), 121.6 (Ar), 59.4 ( $CH_2Ar$ ), 58.6 ( $ZnOCH_2$ ), 57.2 ( $CH_2Py$ ), 36.0 ( $C(CH_3)_3$ ), 34.2 ( $C(CH_3)_3$ ), 32.5 ( $CH_3$ ), 32.0 ( $ZnOCH_2CH_3$ ), 30.3 ( $CH_3$ ).

**(7.L3)ZnN(SiMe<sub>3</sub>)<sub>2</sub>, 7.11.** Analogous to **7.8**, from  $Zn(N(SiMe_3)_2)_2$  (92 mg, 0.24 mmol), **7.L3H** (100 mg, 0.24 mmol) in toluene (5 ml). Filtration, removal of the solvent under vacuum, crystallisation in hexane at  $-30$  °C, decantation and washing with hexane (3x10 ml) afforded 54 mg (31%) of colourless X-ray quality crystals, containing 1 equiv co-crystallised hexane.

$^1H$  NMR ( $C_6D_6$ , 400 MHz):  $\delta$  8.78 (bs, 2H, Py), 7.12 (d,  $J = 3$  Hz, 1H, Ar), 6.79 (bs, 2H, Py), 6.62 (d,  $J = 3$  Hz, 1H, Py), 6.50 (bs, 2H, Py), 6.27 (bs, 2H, Py), 3.72 (d,  $J = 14$  Hz, 2H,  $PyCH_2N$ ), 3.45 (d,  $J = 14$  Hz, 2H,  $PyCH_2N$ ), 3.29 (bs, 2H,  $ArCH_2N$ ), 1.68 (s, 9H,  $CH_3$ ), 1.32 (s, 9H,  $CH_3$ ), 0.50 (s, 18H,  $Si(CH_3)_3$ );  $^{13}C\{^1H\}$  NMR ( $C_6D_6$ , 101 MHz): 164.8 (Ar), 154.0 (Py), 149.3 (Py), 137.7 (Py), 137.6 (Ar), 134.0 (Ar), 125.2 (Ar), 123.9 (Ar), 123.1 (Py), 121.8 (Ar), 121.6 (Py), 62.3 ( $CH_2Ar$ ), 61.1 ( $CH_2Py$ ), 35.6 ( $CMe_3$ ), 33.9 ( $CMe_3$ ), 32.4 ( $CMe_3$ ), 30.5 ( $CMe_3$ ), 6.6 ( $SiMe_3$ ). UV-vis (toluene,  $5.7 \cdot 10^{-5}$  M) [ $\lambda_{max}$ , nm ( $\epsilon$ ,  $mol^{-1} cm^2$ ): 296 (4200)]. Anal. Calcd for  $C_{33}H_{52}N_4OSi_2Zn$ : C, 61.70; H, 8.16; N, 8.72; Anal. Calcd for  $C_{33}H_{52}ZnN_4OSi_2 \cdot C_6H_{14}$ : C, 64.30; H, 9.13; N, 7.69; Found: C, 61.99; H, 8.79; N, 8.40. (X-ray structure shows

presence of 1 co-crystallised hexane, which seems to be lost partly on drying. NMR shows the presence of 0.7 hexane, EA analysis samples best agree with 0.2 hexane.)

***rac*-Lactide polymerisation.** In a glove box, the desired amount of *rac*-lactide was placed into a J.-Young tube together with C<sub>6</sub>D<sub>6</sub>. If required, a stock solution of an additive (EtOH, etc.) was added, followed by a stock solution of the catalyst ( $\approx 20$  mM in C<sub>6</sub>D<sub>6</sub>). The reaction was followed by <sup>1</sup>H NMR. The reaction was quenched by addition of  $\approx 5$  equiv of a CDCl<sub>3</sub> solution of acetic acid (5 mM). The volatiles were immediately evaporated and solid polymer samples were stored at  $-80$  °C for further analysis. Conversion was determined from <sup>1</sup>H NMR by comparison to remaining lactide.  $P_m$  values were determined from homodecoupled <sup>1</sup>H NMR spectra and calculated from  $P_m = 1 - 2 \cdot I_1 / (I_1 + I_2)$ , with  $I_1 = 5.15 - 5.21$  ppm (*rmr*, *mmr/rmm*),  $I_2 = 5.21 - 5.25$  ppm (*mmr/rmm*, *mmm*, *mrmm*). The integration of the left multiplet and right multiplet ( $I_1$  and  $I_2$ ) required only one, very reproducible dividing point of the integration, which was always taken as the minimum between the two multiplets.  $P_m$ -values obtained this way were typically consistent to  $\pm 1\%$  over the course of one experiment and  $\pm 3\%$  between different experiments under identical conditions. Molecular weight analyses were performed on *crude reaction products* using a Waters 1525 gel permeation chromatograph equipped with three Phenomenex columns and a refractive index detector at 35 °C. THF was used as the eluent at a flow rate of 1.0 mL·min<sup>-1</sup> and polystyrene standards (Sigma–Aldrich, 1.5 mg·mL<sup>-1</sup>, prepared and filtered (0.2 mm) directly prior to injection) were used for calibration. Obtained molecular weights were corrected by a Mark-Houwink factor of 0.58.<sup>91</sup>

**X-ray diffraction.** Single crystals were obtained directly from isolation of the products as described above. Diffraction data were collected on a Bruker Venture METALJET diffractometer (Ga K $\alpha$  radiation) or a Bruker APEXII with a Cu microsource/Quazar MX using the APEX2 software package.<sup>92</sup> Data reduction was performed with SAINT,<sup>93</sup> absorption corrections with SADABS.<sup>94</sup> Structures were solved by dual-space refinement (SHELXT).<sup>95</sup> All



non-hydrogen atoms were refined anisotropic using full-matrix least-squares on  $F^2$  and hydrogen atoms refined with fixed isotropic U using a riding model (SHELXL97).<sup>96</sup> Further experimental details can be found in Table 7.IV and in the supporting information (CIF).

**Table 7.IV.** Experimental details of X-ray diffraction studies

	7.2	(7.11) <sub>2</sub> Zn	7.8	7.9	7.11
Formula	C <sub>56</sub> H <sub>56</sub> Zn <sub>2</sub> N <sub>8</sub> O <sub>2</sub>	C <sub>44</sub> H <sub>44</sub> ZnN <sub>6</sub>	C <sub>25</sub> H <sub>47</sub> ZnN <sub>3</sub> O	C <sub>29</sub> H <sub>60</sub> ZnN <sub>4</sub> Si <sub>2</sub> O	C <sub>39</sub> H <sub>66</sub> ZnN <sub>4</sub> Si <sub>2</sub> O
$M_w$ (g/mol); $d_{\text{calcd.}}$ (g/cm <sup>3</sup> )	1003.82; 1.312	722.22; 1.236	471.02; 1.125	602.36; 1.115	728.50; 1.155
$T$ (K); F(000)	100; 2096	100; 760	150; 1024	150; 1312	150; 1576
Crystal System	Orthorhombic	Orthorhombic	Monoclinic	Triclinic	Monoclinic
Space Group	$P2_12_12_1$	$P2_12_12$	$P2_1/c$	$P(-1)$	$P2_1/c$
Unit Cell: $a$ (Å)	10.1814(3)	11.4428(7)	9.9872(6)	13.6954(8)	18.8720(5)
$b$ (Å)	13.3856(4)	11.9319(8)	24.3367(16)	13.8027(8)	18.6906(5)
$c$ (Å)	37.3018(12)	14.2169(9)	11.7387(7)	19.6030(11)	12.3226(3)
$\alpha$ (°)	90	90	90	78.331(3)	90
$\beta$ (°)	90	90	102.843(2)	89.408(3)	105.3650(10)
$\gamma$ (°)	90	90	90	81.562(3)	90
$V$ (Å <sup>3</sup> ); $Z$	5083.6(3); 4	1941.1(2); 2	2781.8(3); 4	3589.0(4); 4	4191.18(19); 4
$\mu$ (mm <sup>-1</sup> ); Abs. Corr.	0.956; multiscan	0.725; multiscan	1.350; multiscan	1.115; multiscan	1.010; multiscan
$\theta$ range (°); completeness	3.1-60.7; 0.97	2.7 -60.7; 1.0	5.3-71.4; 0.98	2.8-60; 1.0	3.0-60.6; 1.0
collected reflections; $R_{\sigma}$	114196; 0.0226	21172; 0.0361	31767; 0.0356	90622; 0.0669	70912; 0.0163
unique reflections; $R_{\text{int}}$	11290; 0.0487	4452; 0.0607	5351; 0.0454	16482; 0.0904	9608; 0.0311
$R1(F)$ ( $I > 2\sigma(I)$ )	0.0301	0.0361	0.0586	0.0644	0.0509
$wR(F^2)$ (all data)	0.0765	0.0909	0.2791	0.1660	0.1462
GoF( $F^2$ ); Flack-x	1.054; 0.050(16)	1.120; 0.12(3)	1.271; -	1.021; -	1.044; -
Residual electron density	0.338; -0.391	0.336; -0.302	0.709; -1.162	0.640; -0.380	0.905; -0.751

### Conflicts of interest

There are no conflicts to declare.

### Acknowledgements

Funding was supplied by the NSERC discovery program (RGPIN-2016-04953) and the Centre for Green Chemistry and Catalysis (FQRNT). I. M. contributed during her research internship financed by the DAAD-RISE program. We thank Karine Gilbert and Alexandra Furtos for support with mass spectroscopy and Francine Bélanger for support with X-ray crystallography.

## References Chapter 7

† As an alternative description of the two differing geometries, we can define the equatorial complex plane as containing M, O and N<sub>pyrrol</sub>. The pyridylmethoxide ligands have an angle of 46°-48° with this plane (c. f. 26°-30° in 7.1) and the iminopyrrolide ligands of 53°-62° (c. f. 69°-82° in 7.1).

§ The same spectrum would be expected for a C<sub>s</sub>-symmetric penta-coordinated complex, but it is highly unlikely to observe a higher coordination in solution than in the solid state.

1. V. Nagarajan, A. K. Mohanty and M. Misra, *ACS Sustainable Chem. Eng.*, 2016, **4**, 2899-2916.
2. E. Castro-Aguirre, F. Iñiguez-Franco, H. Samsudin, X. Fang and R. Auras, *Adv. Drug Delivery Rev.*, 2016, **107**, 333-366.
3. S. Slomkowski, S. Penczek and A. Duda, *Polym. Adv. Technol.*, 2014, **25**, 436-447.
4. T. A. Hottle, M. M. Bilec and A. E. Landis, *Polym. Degrad. Stab.*, 2013, **98**, 1898-1907.
5. S. Inkinen, M. Hakkarainen, A.-C. Albertsson and A. Södergård, *Biomacromolecules*, 2011, **12**, 523-532.
6. J. Ahmed and S. K. Varshney, *Int. J. Food Prop.*, 2011, **14**, 37-58.
7. C. K. Williams and M. A. Hillmyer, *Polym. Rev.*, 2008, **48**, 1-10.
8. B. Gupta, N. Revagade and J. Hilborn, *Prog. Polym. Sci.*, 2007, **32**, 455-482.
9. E. T. H. Vink, K. R. Rábago, D. A. Glassner, B. Springs, R. P. O'Connor, J. Kolstad and P. R. Gruber, *Macromol. Biosci.*, 2004, **4**, 551-564.
10. R. E. Drumright, P. R. Gruber and D. E. Henton, *Adv. Mater. (Weinheim, Ger.)*, 2000, **12**, 1841-1846.
11. M. Singhvi and D. Gokhale, *RSC Adv.*, 2013, **3**, 13558-13568.

12. J. Vijayakumar, R. Aravindan and T. Viruthagiri, *Chem. Biochem. Eng. Q.*, 2008, **22**, 245-264.
13. Y. Tokiwa and B. P. Calabia, *Can. J. Chem.*, 2008, **86**, 548-555.
14. B. J. O'Keefe, M. A. Hillmyer and W. B. Tolman, *J. Chem. Soc., Dalton Trans.*, 2001, DOI: 10.1039/b104197p, 2215-2224.
15. O. Dechy-Cabaret, B. Martin-Vaca and D. Bourissou, *Chem. Rev.*, 2004, **104**, 6147-6176.
16. Z. Zhong, P. J. Dijkstra and J. Feijen, *J. Biomater. Sci., Polym. Ed.*, 2004, **15**, 929-946.
17. J. Wu, T.-L. Yu, C.-T. Chen and C.-C. Lin, *Coord. Chem. Rev.*, 2006, **250**, 602-626.
18. A. Amgoune, C. M. Thomas and J.-F. Carpentier, *Pure Appl. Chem.*, 2007, **79**, 2013-2030.
19. R. H. Platel, L. M. Hodgson and C. K. Williams, *Polym. Rev.*, 2008, **48**, 11 - 63.
20. C. A. Wheaton, P. G. Hayes and B. J. Ireland, *Dalton Trans.*, 2009, 4832 - 4846.
21. N. Ajellal, J.-F. Carpentier, C. Guillaume, S. M. Guillaume, M. Helou, V. Poirier, Y. Sarazin and A. Trifonov, *Dalton Trans.*, 2010, **39**, 8363.
22. M. D. Jones, in *Heterogenized Homogeneous Catalysts for Fine Chemicals Production*, eds. P. Barbaro and F. Liguori, Springer Netherlands, 2010, vol. 33, pp. 385-412.
23. M. K. Kiesewetter, E. J. Shin, J. L. Hedrick and R. M. Waymouth, *Macromolecules*, 2010, **43**, 2093-2107.
24. M. J. Stanford and A. P. Dove, *Chem. Soc. Rev.*, 2010, **39**, 486-494.
25. A. K. Sutar, T. Maharana, S. Dutta, C.-T. Chen and C.-C. Lin, *Chem. Soc. Rev.*, 2010, **39**, 1724-1746.

26. C. M. Thomas, *Chem. Soc. Rev.*, 2010, **39**, 165.
27. J.-C. Buffet and J. Okuda, *Polym. Chem.*, 2011, **2**, 2758-2763.
28. S. Dagorne, C. Fliedel and P. de Frémont, in *Encyclopedia of Inorganic and Bioinorganic Chemistry*, John Wiley & Sons, Ltd, 2011, DOI: 10.1002/9781119951438.eibc2416.
29. P. J. Dijkstra, H. Du and J. Feijen, *Polym. Chem.*, 2011, **2**, 520-527.
30. S. Dutta, W.-C. Hung, B.-H. Huang and C.-C. Lin, in *Synthetic Biodegradable Polymers*, eds. B. Rieger, A. Künkel, G. W. Coates, R. Reichardt, E. Dinjus and T. A. Zevaco, Springer-Verlag, Berlin, 2011, pp. 219-284.
31. C. A. Wheaton and P. G. Hayes, *Comments Inorg. Chem.*, 2011, **32**, 127-162.
32. I. dos Santos Vieira and S. Herres-Pawlis, *Eur. J. Inorg. Chem.*, 2012, **2012**, 765-774.
33. J.-F. Carpentier, B. Liu and Y. Sarazin, in *Advances in Organometallic Chemistry and Catalysis*, John Wiley & Sons, Inc., 2013, DOI: 10.1002/9781118742952.ch28, pp. 359-378.
34. S. Dagorne and C. Fliedel, in *Modern Organoaluminum Reagents: Preparation, Structure, Reactivity and Use*, eds. S. Woodward and S. Dagorne, Springer Berlin Heidelberg, Berlin, Heidelberg, 2013, DOI: 10.1007/3418\_2012\_35, pp. 125-171.
35. S. Dagorne, M. Normand, E. Kirillov and J.-F. Carpentier, *Coord. Chem. Rev.*, 2013, **257**, 1869-1886.
36. B. H. Huang, S. Dutta and C. C. Lin, in *Comprehensive Inorganic Chemistry II (Second Edition)*, ed. J. R. Poeppelemeier, Elsevier, Amsterdam, 2013, DOI: 10.1016/B978-0-08-097774-4.00146-7, pp. 1217-1249.
37. R. Jianming, X. Anguo, W. Hongwei and Y. Hailin, *Des. Monomers Polym.*, 2013, **17**, 345-355.

38. A. Sauer, A. Kapelski, C. Fliedel, S. Dagorne, M. Kol and J. Okuda, *Dalton Trans.*, 2013, **42**, 9007-9023.
39. S. M. Guillaume, E. Kirillov, Y. Sarazin and J.-F. Carpentier, *Chem.-Eur. J.*, 2015, **21**, 7988-8003.
40. J. P. MacDonald and M. P. Shaver, in *Green Polymer Chemistry: Biobased Materials and Biocatalysis*, American Chemical Society, 2015, vol. 1192, ch. 10, pp. 147-167.
41. S. Paul, Y. Zhu, C. Romain, R. Brooks, P. K. Saini and C. K. Williams, *Chem. Commun. (Cambridge, U. K.)*, 2015, **51**, 6459-6479.
42. E. Le Roux, *Coord. Chem. Rev.*, 2016, **306**, 65-85.
43. T. M. Ovitt and G. W. Coates, *J. Am. Chem. Soc.*, 2002, **124**, 1316-1326.
44. H. Du, A. H. Velders, P. J. Dijkstra, J. Sun, Z. Zhong, X. Chen and J. Feijen, *Chem.-Eur. J.*, 2009, **15**, 9836-9845.
45. K. Press, I. Goldberg and M. Kol, *Angew. Chem., Int. Ed.*, 2015, **54**, 14858-14861.
46. H. Ma, T. P. Spaniol and J. Okuda, *Angew. Chem., Int. Ed.*, 2006, **45**, 7818-7821.
47. A. Amgoune, C. M. Thomas, T. Roisnel and J.-F. Carpentier, *Chem.-Eur. J.*, 2006, **12**, 169-179.
48. A. J. Chmura, C. J. Chuck, M. G. Davidson, M. D. Jones, M. D. Lunn, S. D. Bull and M. F. Mahon, *Angew. Chem., Int. Ed.*, 2007, **46**, 2280-2283.
49. A. J. Chmura, M. G. Davidson, C. J. Frankis, M. D. Jones and M. D. Lunn, *Chem. Commun. (Cambridge, U. K.)*, 2008, 1293-1295.
50. M. D. Jones, S. L. Hancock, P. McKeown, P. M. Schafer, A. Buchard, L. H. Thomas, M. F. Mahon and J. P. Lowe, *Chem. Commun. (Cambridge, U. K.)*, 2014, **50**, 15967-15970.

51. M. D. Jones, L. Brady, P. McKeown, A. Buchard, P. M. Schafer, L. H. Thomas, M. F. Mahon, T. J. Woodman and J. P. Lowe, *Chem. Sci.*, 2015, **6**, 5034-5039.
52. S. Fortun, P. Daneshmand and F. Schaper, *Angew. Chem., Int. Ed.*, 2015, **54**, 13669-13672.
53. P. Daneshmand, A. van der Est and F. Schaper, *ACS Catal.*, 2017, **7**, 6289-6301.
54. P. Daneshmand, S. Fortun and F. Schaper, *Organometallics*, 2017, **36**, 3860–3877.
55. P. Daneshmand, J. L. Jiménez-Santiago, M. Aragon--Alberti and F. Schaper, *Organometallics*, 2018, **in print**, 10.1021/acs.organomet.1028b00196.
56. M. Cheng, A. B. Attygalle, E. B. Lobkovsky and G. W. Coates, *J. Am. Chem. Soc.*, 1999, **121**, 11583-11584.
57. T. M. Ovitt and G. W. Coates, *J. Am. Chem. Soc.*, 1999, **121**, 4072-4073.
58. F. Drouin, P. O. Oguadinma, T. J. J. Whitehorne, R. E. Prud'homme and F. Schaper, *Organometallics*, 2010, **29**, 2139-2147.
59. L. Wang and H. Ma, *Dalton Trans.*, 2010, **39**, 7897.
60. C.-Y. Sung, C.-Y. Li, J.-K. Su, T.-Y. Chen, C.-H. Lin and B.-T. Ko, *Dalton Trans.*, 2012, **41**, 953-961.
61. M. Honrado, A. Otero, J. Fernández-Baeza, L. F. Sánchez-Barba, A. n. Lara-Sánchez, J. Tejada, M. a. P. Carrión, J. Martínez-Ferrer, A. Garcés and A. M. Rodríguez, *Organometallics*, 2013, **32**, 3437-3440.
62. H. Wang and H. Ma, *Chem. Commun. (Cambridge, U. K.)*, 2013, **49**, 8686-8688.
63. S. Abbina and G. Du, *ACS Macro Lett.*, 2014, **3**, 689-692.

64. M. Honrado, A. Otero, J. Fernández-Baeza, L. F. Sánchez-Barba, A. Garcés, A. n. Lara-Sánchez and A. M. Rodríguez, *Organometallics*, 2014, **33**, 1859-1866.
65. Z. Mou, B. Liu, M. Wang, H. Xie, P. Li, L. Li, S. Li and D. Cui, *Chem. Commun. (Cambridge, U. K.)*, 2014, **50**, 11411-11414.
66. H. Wang, Y. Yang and H. Ma, *Macromolecules*, 2014, **47**, 7750-7764.
67. M. Honrado, A. Otero, J. Fernández-Baeza, L. F. Sánchez-Barba, A. Garcés, A. Lara-Sánchez, J. Martínez-Ferrer, S. Sobrino and A. M. Rodríguez, *Organometallics*, 2015, **34**, 3196-3208.
68. Y. Sun, Y. Cui, J. Xiong, Z. Dai, N. Tang and J. Wu, *Dalton Trans.*, 2015, **44**, 16383-16391.
69. Y. Yang, H. Wang and H. Ma, *Inorg. Chem.*, 2015, **54**, 5839-5854.
70. T. Rosen, Y. Popowski, I. Goldberg and M. Kol, *Chem.-Eur. J.*, 2016, **22**, 11533-11536.
71. H. Wang, Y. Yang and H. Ma, *Inorg. Chem.*, 2016, **55**, 7356-7372.
72. C. Kan, J. Hu, Y. Huang, H. Wang and H. Ma, *Macromolecules*, 2017, **50**, 7911-7919.
73. D. E. Stasiw, A. M. Luke, T. Rosen, A. B. League, M. Mandal, B. D. Neisen, C. J. Cramer, M. Kol and W. B. Tolman, *Inorg. Chem.*, 2017, **56**, 14366-14372.
74. A. W. Addison, T. N. Rao, J. Reedijk, J. van Rijn and G. C. Verschoor, *J. Chem. Soc., Dalton Trans.*, 1984, DOI: 10.1039/DT9840001349, 1349-1356.
75. C. R. Groom, I. J. Bruno, M. P. Lightfoot and S. C. Ward, *Acta Crystallogr., Sect. B: Struct. Sci.*, 2016, **72**, 171-179.
76. C. K. Williams, L. E. Breyfogle, S. K. Choi, W. Nam, V. G. Young, M. A. Hillmyer and W. B. Tolman, *J. Am. Chem. Soc.*, 2003, **125**, 11350-11359.

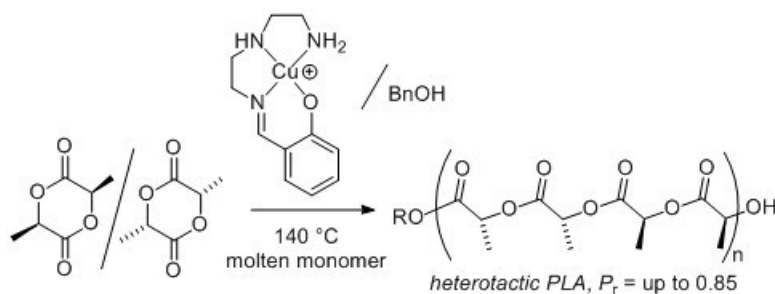


77. P. D. Knight, A. J. P. White and C. K. Williams, *Inorg. Chem.*, 2008, **47**, 11711-11719.
78. Z. Zheng, G. Zhao, R. Fablet, M. Bouyahyi, C. M. Thomas, T. Roisnel, O. Casagrande Jr and J.-F. Carpentier, *New J. Chem.*, 2008, **32**, 2279-2291.
79. S. Yann, P. Valentin, R. Thierry and C. Jean-François, *Eur. J. Inorg. Chem.*, 2010, **2010**, 3423-3428.
80. V. Poirier, T. Roisnel, J.-F. Carpentier and Y. Sarazin, *Dalton Trans.*, 2011, **40**, 523-534.
81. T. Ebrahimi, E. Mamleeva, I. Yu, S. G. Hatzikiriakos and P. Mehrkhodavandi, *Inorg. Chem.*, 2016, **55**, 9445-9453.
82. D. Jedrzkiewicz, D. Kantorska, J. Wojtaszak, J. Ejfler and S. Szafert, *Dalton Trans.*, 2017, **46**, 4929-4942.
83. S. M. Kirk, P. McKeown, M. F. Mahon, G. Kociok-Köhn, T. J. Woodman and M. D. Jones, *Eur. J. Inorg. Chem.*, 2017, **2017**, 5417-5426.
84. G. Labourdette, D. J. Lee, B. O. Patrick, M. B. Ezhova and P. Mehrkhodavandi, *Organometallics*, 2009, **28**, 1309-1319.
85. S. C. Marinescu, T. Agapie, M. W. Day and J. E. Bercaw, *Organometallics*, 2007, **26**, 1178-1190.
86. M. Cheng, D. R. Moore, J. J. Reczek, B. M. Chamberlain, E. B. Lobkovsky and G. W. Coates, *J. Am. Chem. Soc.*, 2001, **123**, 8738-8749.
87. R. J. Herolds, L. Aggarwal and V. Neff, *Can. J. Chem.*, 1963, **41**, 1368.
88. D. Y. Lee and J. F. Hartwig, *Org. Lett.*, 2005, **7**, 1169-1172.
89. S. Mondal, S. M. Mandal, T. K. Mondal and C. Sinha, *Spectrochimica Acta Part A: Molecular and Biomolecular Spectroscopy*, 2015, **150**, 268-279.
90. M. Savva, P. Chen, A. Aljaberi, B. Selvi and M. Spelios, *Bioconjugate Chem.*, 2005, **16**, 1411-1422.

91. M. Save, M. Schappacher and A. Soum, *Macromol. Chem. Phys.*, 2002, **203**, 889-899.
92. *APEX2*, Release 2.1-0; Bruker AXS Inc.: Madison, USA, 2006.
93. *SAINTE*, Release 7.34A; Bruker AXS Inc.: Madison, USA, 2006.
94. G. M. Sheldrick *SADABS*, Bruker AXS Inc.: Madison, USA, 1996 & 2004.
95. G. Sheldrick, *Acta Crystallogr. Sect. A: Found. Crystallogr.*, 2015, **71**, 3-8.
96. G. M. Sheldrick, *Acta Crystallogr.*, 2008, **A64**, 112-122.

## Chapter 8 . Tetradentate aminophenolate copper complexes in *rac*-lactide polymerization

Daneshmand, P.; Randimbiarisolo, A.; Schaper, F. Tetradentate aminophenolate copper complexes in *rac*-lactide polymerization. *Can. J. Chem.* **2018**, *submitted*.



Contributions of F. Schaper: A first draft was provided by me with minor modification from Prof. Frank Schaper.

Contributions of A. Randimbiarisolo: Synthesis of ligands under my supervision.



# Tetradentate aminophenolate copper complexes in *rac*-lactide polymerization

Pargol Daneshmand, Aurélie Randimbiarisolo, Frank Schaper\*

*Centre in Green Chemistry and Catalysis, Département de chimie, Université de Montréal, 2900 Boul. E.-Montpetit, Montréal, QC, H3T 1J4, Canada*

\* [Frank.Schaper@umontreal.ca](mailto:Frank.Schaper@umontreal.ca)

## Abstract

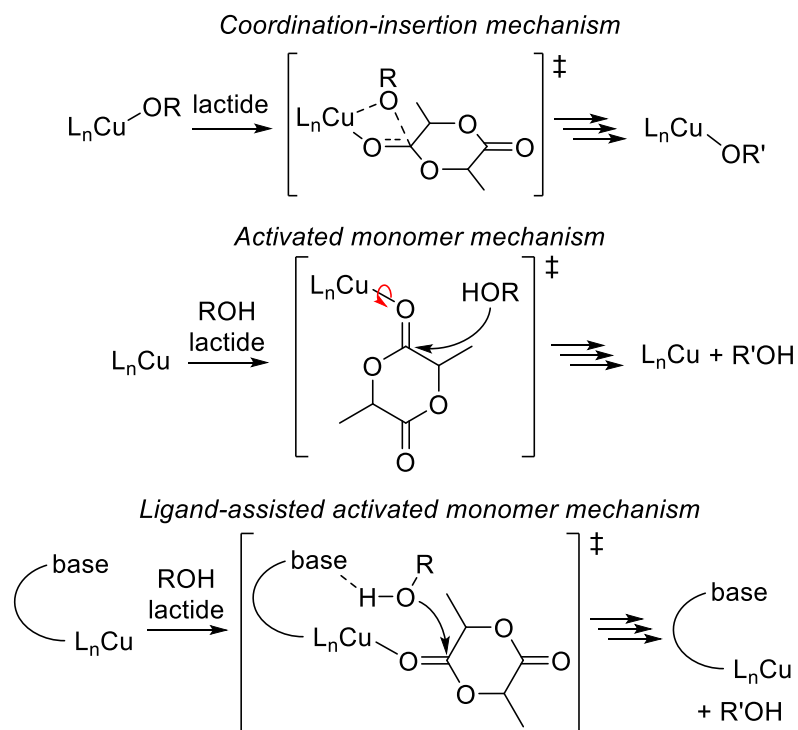
Copper(II) nitrate complexes of 2-(((2-((2-aminoethyl)amino)ethyl)imino)methyl)phenol, 2-(((2-((2-aminoethyl)amino)ethyl)imino)methyl)-4,6-dichlorophenol, 2-(((2-(piperazin-1-yl)ethyl)imino)methyl)phenol and (2,4-di-tert-butyl-6-(((2-(piperazin-1-yl)ethyl)imino)methyl)phenol), as well as a copper(II) acetate complex of 2-(((2-(piperidin-1-yl)ethyl)imino)methyl)phenol have been prepared and characterized by X-ray diffraction studies. In combination with benzyl alcohol, all complexes are active in *rac*-lactide polymerization at 140 °C in molten monomer to provide moderately heterotactic PLA. Most complexes showed complicated reaction kinetics, indicative of two interconverting active species. Molecular weight control was poor and a strong tendency toward intramolecular transesterification led to oligomeric products. There was no indication that the basic site of the ligand is participating in the polymerization reaction by deprotonation of the alcohol nucleophile.

## Introduction

Poly(lactic acid) (PLA), produced from ring-opening polymerization of lactide, is one of the most important biopolymers today.<sup>1-7</sup> Controlled polymerization of lactide has become a catalytic challenge,<sup>7-33</sup> but combining isotactic stereocontrol, polymer molecular weight control with high activity and catalyst stability remains difficult to achieve. Most studies – including our own – focus on coordination-insertion polymerization of lactide, since the tight four-membered metallacycle of the insertion

transition state is likely to be highly influenced by the ligand environment, which in turn would allow control over relative reactivities (Scheme 8.1). A major drawback of lactide polymerization by a coordination-insertion mechanism is the inherent lability of the metal alkoxide catalyst towards protonation. Most coordination-insertion polymerization catalysts thus do not or would not survive conditions currently employed in the industrial production of PLA, i. e. the presence of notable amounts of water and lactic acid at temperatures of 140 °C and above. An alternative pathway to ring-opening polymerization of lactide is Lewis-acid activation of the monomer (Scheme 8.1). Since metal alkoxides are not required, the mechanism typically tolerates protic substances, as long as the spectator ligand is not protonated easily. Polymerizations by an activated-monomer mechanism are, however, more difficult to control, since the nucleophilic attack occurs at some distance from the metal center and since the activated-monomer complex is highly flexible. Lewis-acid-catalyzed lactide polymerizations thus typically show only low to moderate stereocontrol, typically to heterotactic PLA and mainly due to the interaction of the chiral polymeryl alcohol with the monomer without much influence from the catalytic site. In 2013, Sarazin and Carpentier explained an increased activity in rare-earth-based catalysts with a “*ligand-assisted activated monomer mechanism*”.<sup>34</sup> A basic site at the ligand can interact with the alcohol nucleophile by hydrogen bonding, thus facilitating the nucleophilic attack on the monomer (Scheme 8.1). This parallels work by Bourissou and Maron on sulfonic acid-catalyzed caprolactone polymerization, where they showed that sulfonic acid acts as Brønsted acid and base at the same time.<sup>35</sup> In contrast to ordinary activation of the monomer, interaction with the catalytic site now requires a well-defined and relatively rigid geometry. In a series of excellent publications, Wu and coworkers employed this concept in lactide polymerizations with phenolate complexes of group 1 metals, mostly sodium and potassium.<sup>36-42</sup> They could show that phenolate is not incorporated in the polymer chain and acts (mostly) as spectator ligand. The bulky environment (crown-ether coordination around the metal center, highly substituted phenolates) constricts the environment sufficiently to allow stereocontrol, remarkably toward isotactic PLA.

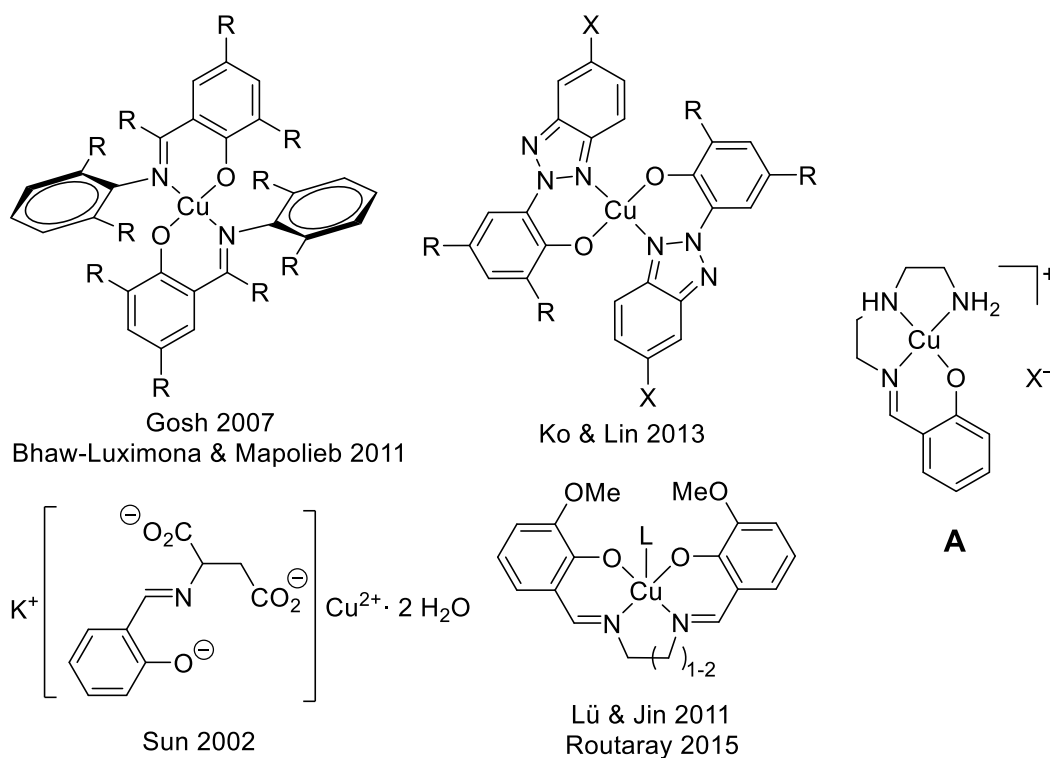
The catalysts are itself achiral (although chirality at the metal is possible in the transition state) and the stereocontrol mechanism was found to be chain-end control.



**Scheme 8.1.**

In the following we explore the possibility to apply this stereocontrol mechanism to copper(II) complexes. Iminophenolate Schiff-base ligands provide highly stable six-membered metallacycles and are one of the most common motifs in coordination chemistry. Iminophenolate copper complexes have been employed in lactide polymerization previously, but typical as homoleptic diphenolate complexes or in form of salen ligands, which can be considered their cyclic analogs (Scheme 8.2).<sup>43-47</sup> Here we investigate heteroleptic complexes of tetradentate ligand **8.L1** with a weakly coordinating anion (**A**, Scheme 8.2). Formation of a cationic complex should increase activity in an activated-monomer mechanism and the dissociation of the terminal amino ligand upon coordination of the monomer (claimed, for example, in similar tridentate zinc complexes)<sup>48-49</sup> will liberate a basic site available for interaction with the alcohol nucleophile. It should be noted that zinc complexes with similar tetradentate linear triaminophenolate ligands have been recently employed by Kol for

isotactic lactide polymerization.<sup>50</sup> These complexes followed a coordination-insertion mechanism, however, different from the mechanism targeted here.

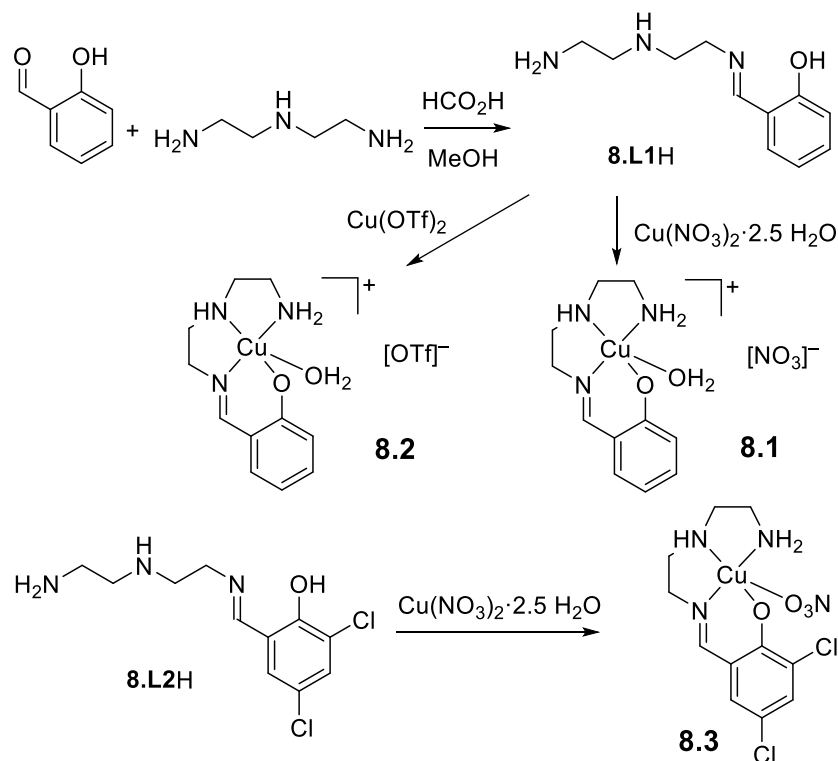


## Scheme 8.2.

## Results and discussions

Copper complexes of type **A** have been reported for a variety of anions. Structurally characterized (**8.L1**)CuX complexes have been reported for  $X^- = \text{PF}_6^-$ ,  $\text{ClO}_4^-$ ,  $\text{Br}^-$ , and  $\text{Cl}^-$ .<sup>51-56</sup> We were most interested in the respective nitrate complex, (**8.L1**)Cu(NO<sub>3</sub>), **8.1**, which was prepared by reaction of copper nitrate with **8.L1H** in methanol (Scheme 8.3). Complex **8.1** crystallizes as a monomeric, cationic complex with square-pyramidal geometry. A water molecule replaced the anion and occupies the apical position (Fig. 8.1, Table 8.I). The respective triflate complex **8.2** was prepared analogously and is practically isostructural (Scheme 8.3, Fig. 8.1, Table 8.I). Reaction with chloro-substituted ligand **8.L2H** provided **8.3**. In **8.3**, the nitrate anion instead of water is coordinated to Cu and bridges two copper centers to form a 1D coordination polymer. Crystal quality was bad for **8.3** and the structure should not be considered more than proof of connectivity.





Scheme 8.3.

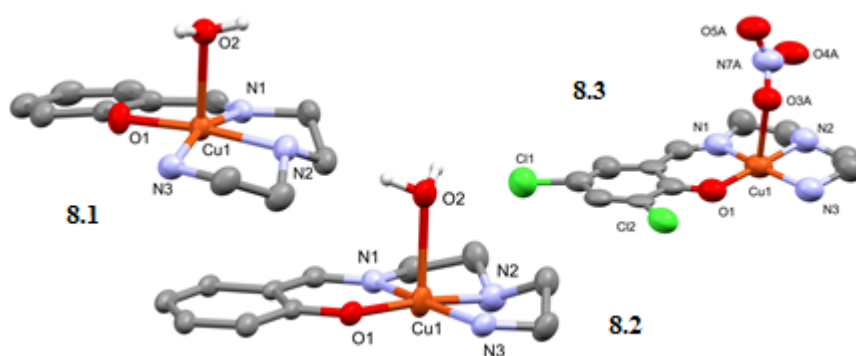


**Figure 8.1.** X-ray structures of **8.1** (left), **8.2** (middle) and **8.3** (right). Thermal ellipsoids are drawn at 50% probability. Hydrogen atoms other than those of water, non-coordinated anions, the second independent molecule for **8.3**, and the minor fraction of the disordered nitrate in **8.3** omitted for clarity.

**Table 8.I.** Bond lengths in the X-ray structures of **8.1-8.6**

	<b>8.1</b>	<b>8.2</b>	<b>8.3</b>	<b>8.4</b>	<b>8.5</b>	<b>8.6</b>
Cu-O <sub>Phenol</sub>	1.924(2)	1.906(6)	1.91(2)	1.921(3)	1.909(13)	1.923(11)
Cu-N(=C)	1.944(3)	1.939(7)	1.97(2)	1.931(4)	1.942(15)	1.920(13)
Cu-N' <sup>a</sup>	2.014(3)	1.995(8)	1.97(2)	2.079(4)	2.067(16)	2.094(14)
Cu-N'' <sup>a</sup>	2.011(3)	2.009(7)	2.03(2)			
Cu-X			2.50(1), 2.72(2)	1.998(3), 2.440(4), (2.618(4))	1.987(13), (2.769(14))	1.942(10), 2.275(11), (2.721(12))
Cu-OH <sub>2</sub> /O(H)Me	2.320(2)	2.425(6)			2.352(13)	
$\tau$	0.1	0.1		0.1	0.1	0.2

<sup>a</sup> N' : first amino group. N'' : second amino group

Complexes **8.1** and **8.2** were tested for the polymerization of *rac*-lactide at 140 °C in molten monomer with benzyl alcohol as a co-initiator. **8.1** showed only low to moderate activity, requiring 24 h to complete conversion. Conversion-time plots of an experiment in which the pressure tube was opened and aliquots taken (Fig. 8.2, squares; Tables 8.II and 8.S1, entry 7) and the results of separate experiments quenched at a given time (Fig. 8.2, diamonds; Table 8.S1, entries 1-6) show very similar conversions. Introduction of ambient atmosphere during sampling thus does not seem to influence the reaction. To test this, polymerizations were conducted in the presence of 5 equiv acetic acid or 5 equiv water (Tables 8.II and S1, entries 11 and 12). Activity was unaffected by acetic acid and even increased upon addition of water (Fig. 8.S1). Polymer molecular weight analysis would normally provide evidence whether water was just tolerated or act as a chain-transfer reagent. However, polymer molecular weights for **8.1** were much lower than expected (Tables 8.II and 8.S1). MALDI-MS spectra confirmed the presence of cyclic oligomers (Fig. 8.S12), indicative of intramolecular transesterification, and polymer molecular weights could thus not be used for mechanistic interpretations. The same tendency for intramolecular transesterification was observed for all other catalysts in this study,

which generally produced oligomers instead of polymers (Tables 8.II and 8.S1, Fig. 8.S12-8.S15).

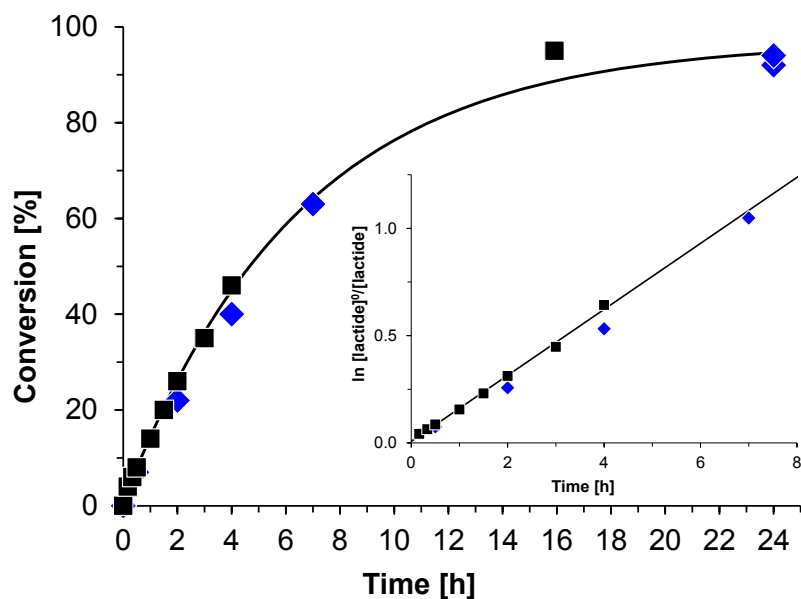


**Figure 8.2.** Conversion-time plot for the polymerization of *rac*-lactide with **8.1**/benzyl alcohol at 140 °C. lactide: **8.1**:BnOH = 100:1:1. Black squares: single experiment with aliquots taken at desired times. Reaction was exposed to air during sampling. Blue diamonds: Series of 5 independent polymerization experiments quenched after 2, 4, 7 and 24 h. Reactions were not exposed to air. The inset shows the semi-logarithmic plot. Solid lines are theoretical conversions using the apparent first-order rate constant determined from the linear region of the semi-logarithmic plot.

**Table 8.II.** Summary of *rac*-lactide polymerizations with **8.1-8.6**/1 equiv benzyl alcohol <sup>a</sup>

Catalyst	LA:Cu:ROH <sup>b</sup>	Additive	Conversion <sup>c</sup>	$k_{\text{obs}}$ [h <sup>-1</sup> ] <sup>d</sup>	$M_w/M_n$ <sup>e</sup>	#chains <sup>f</sup>	$P_r$ <sup>g</sup>
<b>8.1</b>	100:1:1		94-96%	0.15(1)	2.9	17	0.65-0.85
<b>8.1</b>	100:1:1	5 H <sub>2</sub> O	96%	0.37(1)	1.7	17	0.7-0.85
<b>8.1</b>	100:1:1	1-4 [NEt <sub>3</sub> R]X	93-97%	0.37(1)- 0.43(4)	1.6-1.8	9-18	0.6-0.85
<b>8.2</b>	100:1:1		95%	0.13(2)	1.5	9	0.8-0.85
<b>8.3</b>	100:1:1		95%	0.081(3), 0.26(4)	2.3	28	0.8-0.85
<b>8.4</b>	100:1:2 <sup>h</sup>		94-99%	0.16(1), 0.52(2)	1.3-1.4	12	0.6-0.75
<b>8.4</b>	50:1:2 <sup>h</sup>		97%	0.57(3)	1.7	12	0.85-0.9
<b>8.4</b>	200:1:2 <sup>h</sup>		94%	0.072(4), 0.15	1.1	>100	0.75-0.8
<b>8.5</b>	100:1:2 <sup>h</sup>		94-96%	0.10(1), 0.28(2)	1.5-2.0	15-27	0.8
<b>8.6</b>	100:1:1		95-96%	0.14(1), 0.34(4)	2.6-2.9	12-17	0.75-0.8

<sup>a</sup> See Table 8.S1 for all polymerization data. <sup>b</sup> LA = *rac*-lactide, ROH = total amount of alcohol present, i. e. co-crystallized alcohol + benzyl alcohol added. <sup>c</sup> Final conversion after overnight reaction. This value does not represent reactivity. <sup>d</sup> Determined by linear regression of the semi-logarithmic plot. Two values are provided if two linear regions were identified. In this case, the lower value always describes the rate at the beginning of the reaction. <sup>e</sup> Determined by GPC, see experimental section. <sup>f</sup> Number of polymer chains per Cu calculated from (conversion\*[lactide]/[catalyst]\* $M_{\text{lactide}}$ )/ $M_n$ (GPC). <sup>g</sup> Determined from decoupled <sup>1</sup>H NMR, see experimental section. <sup>h</sup> Crystal structure contains co-crystallized methanol.

Activities in polymerizations following an activated monomer-mechanism typically increase with increasing concentration of the alcohol nucleophile. Addition of 2, 4, or 8 equiv of benzyl alcohol indeed led to the expected increase in reactivity, but the increase was not linear and showed saturation behaviour (Fig. 8.3, Table 8.S1, entries 8-10). While we did not investigate this in detail, it is possible that the alcohol pre-coordinates either to the copper center or via hydrogen-bonding with basic sites at the ligand. Saturation of the pre-coordination equilibrium would account for the observed Michaelis-Menten kinetics. While all kinetic traces could be fitted to a first-order rate law for conversions  $<70\%$ , conversions at later stages of the reaction were higher than expected, which will be discussed later.<sup>57</sup>

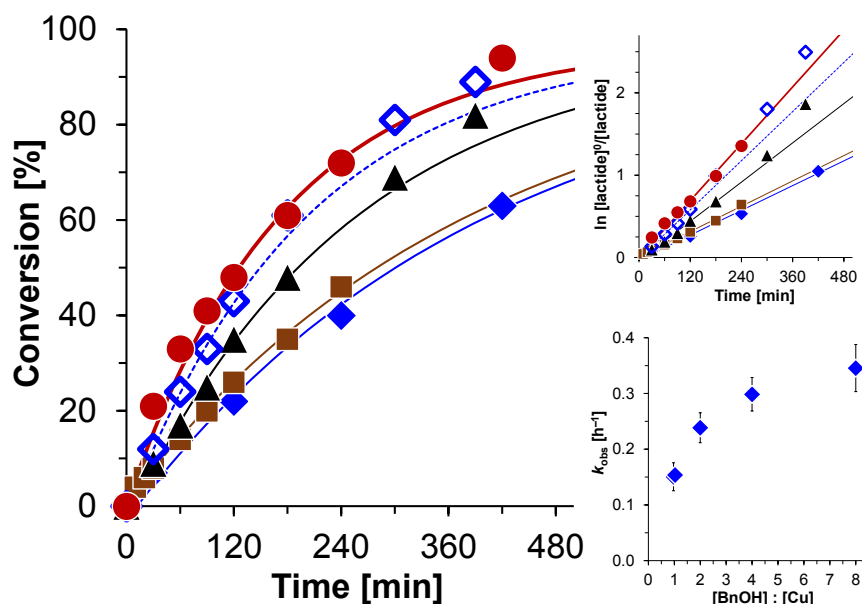


**Figure 8.3.** *rac*-Lactide polymerization with **8.1**/BnOH with different ratios of benzyl alcohol. Conditions: 140 °C, neat monomer, lactide: **8.1** = 100:1, BnOH: **8.1** = 1 (blue diamonds, 5 separate experiments), 1 (brown squares), 2 (black triangles), 4 (blue hollow diamonds), and 8 (red circles). The solid lines are theoretical conversions based on the pseudo-first-order rate constant determined from the linear region of the semilogarithmic plot (conversion  $<70\%$ ). Left: Conversion-time plots, Upper Right: Semilogarithmic plots, Lower Right: Dependence of the observed pseudo-first-order rate constant on benzyl alcohol concentration.

Triflate complex **2** likewise polymerized lactide with essentially identical activity, but showed a pronounced induction period (Fig. 8.4, Tables 8.II and 8.S1, entry 17). To further test the influence of the anion, polymerizations with **8.1** were conducted in the presence of 1 or 4 equiv of  $[\text{NEt}_4]\text{Cl}$  or  $[\text{NEt}_3\text{H}][\text{TsO}]$  ( $[\text{TsO}]^-$  = tosylate, Fig. 8.5, Tables 8.II and 8.S1, entries 13-16). As in **8.2**, the presence of a more coordinating anion resulted in an observable induction period (conversions are below those of **8.1** without added salt for  $t < 60$  min), but final activities were 3 times higher than without addition of salt ( $k_{\text{obs}} = 0.4 \text{ h}^{-1}$ ). Given that both ammonium salts and 4-fold different concentrations yield virtually identical kinetic traces, the observed increase in activity is most likely due to a rate increase of **8.1** under those conditions. In combination with the positive deviation of conversion from the theoretical curves observed above and the higher activity in presence of water, this indicates that **8.1** slowly converts into a more active state and that this conversion is more efficient under more polar conditions.

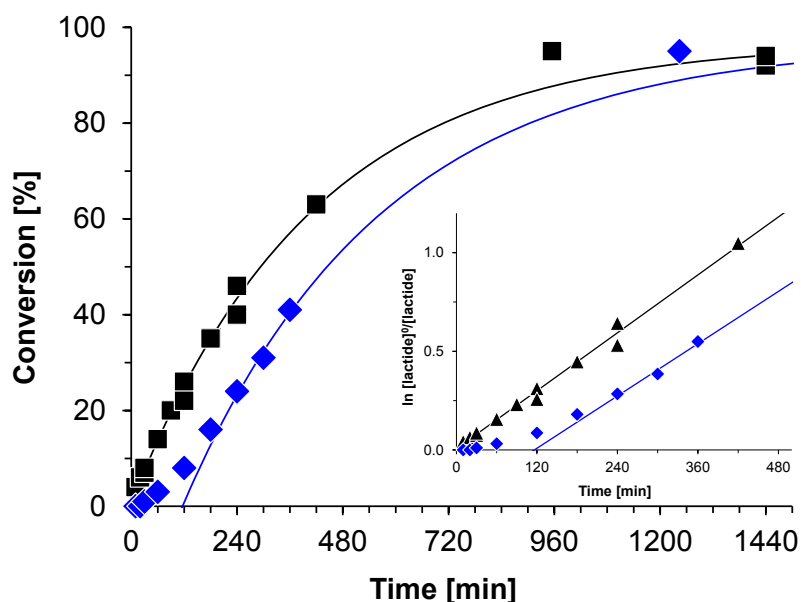


**Figure 8.4.** Conversion-time plot for the polymerization of rac-lactide with **8.2** (blue diamonds). Data for **8.1** under identical conditions is provided for comparison (black squares). Conditions: 140 °C, lactide:[Cu]:BnOH = 100:1:1. The inset shows the semilogarithmic plot. Solid lines represent theoretical conversions based on the

pseudo-first-order rate constant determined by linear regression of the semilogarithmic plots.

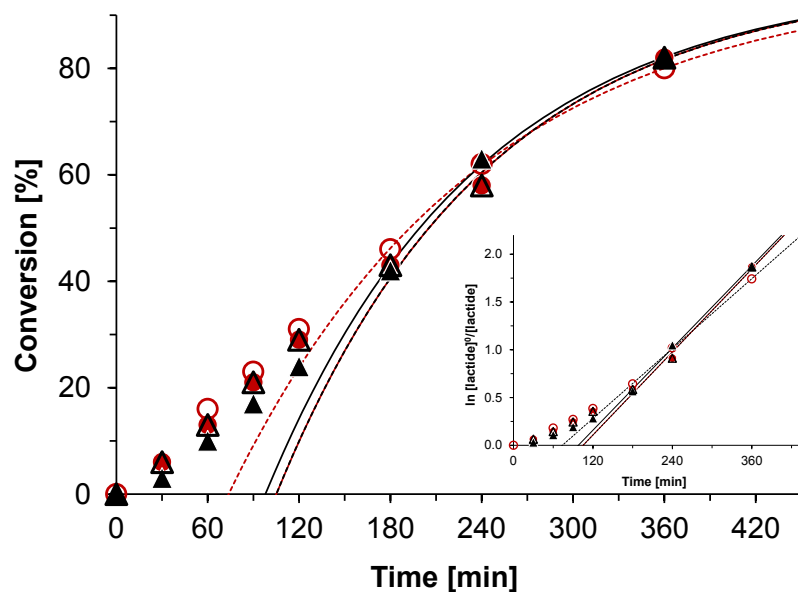


**Figure 8.5.** Conversion-time plot for the polymerization of *rac*-lactide with **8.1** in the presence of ammonium salts: 1 equiv  $[\text{NEt}_4]\text{Cl}$  (black triangle), 4 equiv  $[\text{NEt}_4]\text{Cl}$  (hollow triangle), 1 equiv  $[\text{NEt}_3\text{H}][\text{TsO}]$  (red circle), 4 equiv  $[\text{NEt}_3\text{H}][\text{TsO}]$  (hollow circle). Conditions: 140 °C, lactide: $[\text{Cu}]$ :BnOH = 100:1:1. The inset shows the semilogarithmic plot. Solid lines represent theoretical conversions based on the pseudo-first-order rate constant determined by linear regression of the semilogarithmic plots for  $t > 120$  min.

Kinetics of polymerizations with **8.3**, with a dichloro-substituted phenolate ligand, supported this interpretation. Conversion-time plots of **8.3** in the presence of either 1 or 4 equivalents of benzyl alcohol are close to linear (Fig. 8.6, Tables 8.II and 8.S1, entries 18+19). There is no mechanistic explication for a zero-order dependence on lactide concentration, in particular since the immediate and consistent colour change of the reaction mixture indicates that **8.3** dissolves readily in lactide monomer. The semilogarithmic plot for both reactions does not show the gradual increase to a linear regime expected for first-order reactions with an induction period either, but rather two linear regimes with different rate constants (Fig. 8.6). **8.1** and **8.3** thus slowly

convert from a state of lower reactivity (active immediately or with very short induction periods) to a state of higher reactivity throughout the reaction, which occurs at an earlier stage for **8.3**.

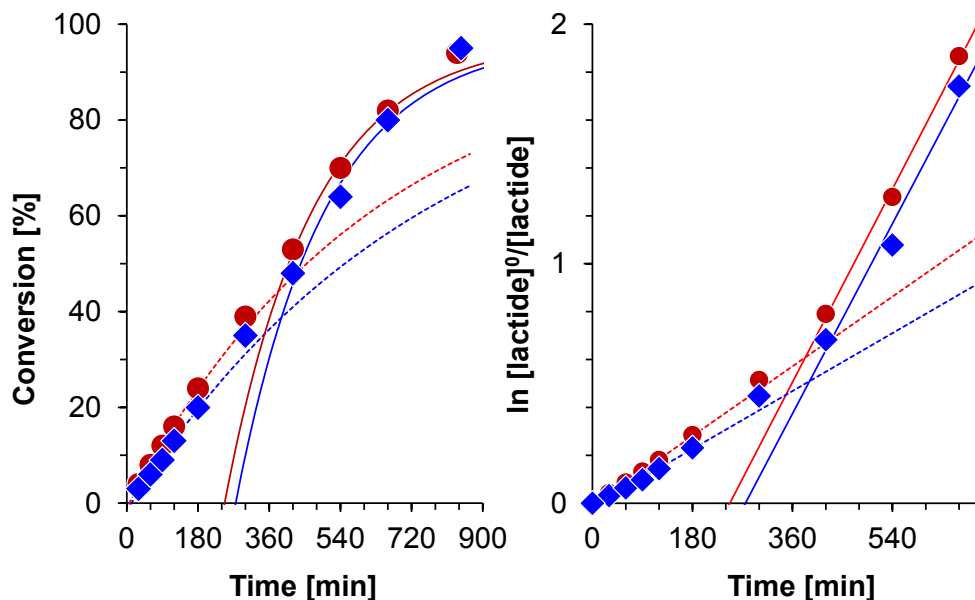
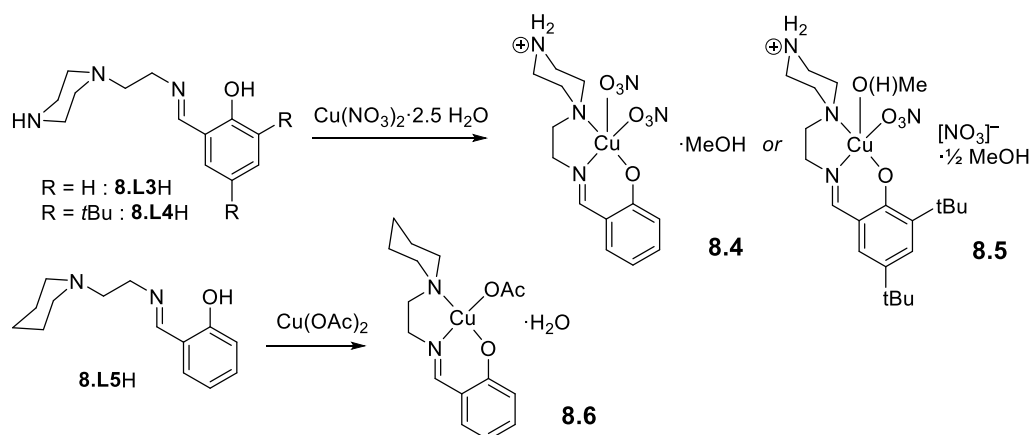


**Figure 8.6.** Conversion-time plot and the semilogarithmic plot for *rac*-lactide polymerizations with **8.3**. Conditions: lactide:3:BnOH = 100:1:1 (blue diamonds), 100:1:4 (red circles).

Polymerizations with **8.1-8.3** all afforded moderately heterotactic PLA ( $P_r = 0.7-0.85$ , Table 8.II). Heterotacticities differed notably between different experiments under otherwise similar conditions, but there was no clear correlation between stereocontrol and either the catalyst employed, addition of benzyl alcohol or ammonium salts (Table 8.S1). To investigate in more detail the influence of a basic group on the ligand on catalyst reactivity, the ethylene diamine moiety was replaced by piperazine (**8.L3H**, Scheme 8.4). Although sterically similar, coordination of both amino groups in piperazine would enforce an unfavourable boat-conformation, and consequently in structurally characterized copper complexes with **8.L3** or ligands similar to **8.L3** the ligand was tridentate.<sup>58-68</sup> Complexes **8.4** and **8.5** were prepared analogous to **8.1**. In addition, **8.6** was prepared, which is sterically similar but does not contain a basic group on the ligand. Reaction with copper(II) nitrate did not afford crystalline material upon reaction with **8.L4H** (even in the presence of base), but **8.6** was readily



obtained with an acetate counteranion (Scheme 8.4). Complexes **8.4** and **8.5** also crystallized as monomeric complexes with square-pyramidal coordination geometry. A derivative structure of **8.4** with nitrate replaced by a water ligand has been reported previously.<sup>62</sup> **8.6** forms a 1D coordination polymer by bridging coordination of the acetate anion, similar to the structure of **8.3**. In all three complexes, there is a weak interaction with a second oxygen on the nitrate or acetate anion. **8.4** and **8.5** were obtained as the nitric acid adducts with an additional anion and a protonated terminal amino group on the piperazine. This is in accordance with all other structurally characterized copper complexes of ligands of type **8.L5**.<sup>58-68</sup> Several attempts to prepare the nitric-acid-free complex by introducing bases in the reaction failed to provide crystalline material. The anion is coordinated in an equatorial position. The apical position is either occupied by a second anion or methanol, with the elongation of the bond length expected for the ligand in the apical position (Table 8.I).



**Scheme 8.4.**

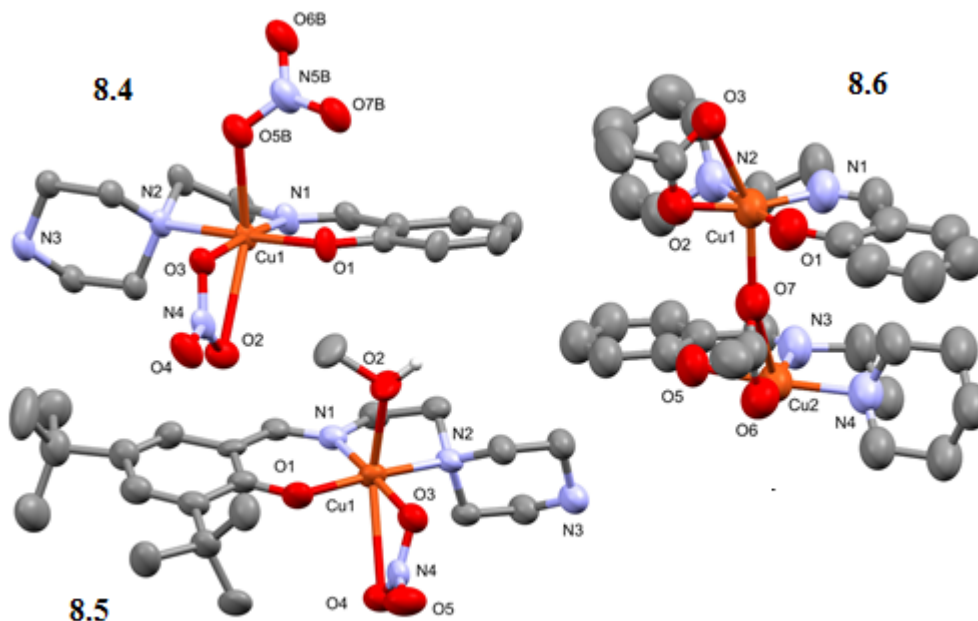


**Figure 8.7.** X-ray structures of **8.4-8.6**. Thermal ellipsoids drawn at 50% probability level. Hydrogen atoms, the second independent molecule in 5 and the anion disorder in 4 omitted for clarity.

The kinetic profile of *rac*-lactide polymerizations with **8.4** showed again an apparent linear conversion-time plot, which deviates significantly from the sigmoidal curve expected for a simple induction period. Conversions from four independent kinetic experiments and from four separate experiments quenched at a given polymerization time agree remarkably well with each other (Fig. 8.8, Tables 8.II and 8.S1, entries 21-30), indicating again that sample-taking did not influence polymerization and that the observed deviations from simple first-order behaviour are reproducible. The semilogarithmic plot shows again two linear regimes, in agreement with slow transformation from one active species into another (Fig. 8.8). Activities somewhat increase with addition of benzyl alcohol (Fig. 8.S2-8.S4, Table 8.S1, entries 20,31-33), but the saturation behaviour is even more pronounced than in **8.1**. Polymerizations at lower and increased catalyst loading yield reduced or increased rate constants for the slow regime at the beginning of the reaction as well as for the fast regime at the end of the reaction (Fig. 8.S5-8.S7, Tables 8.II and 8.S1, entries 34+35). Given the two regimes present, the quality of the data is insufficient to

determine the actual reaction order in catalyst with confidence, but the obtained data agrees reasonably well with a linear dependence on catalyst concentration with a “dead” concentration of 0.3 mol% catalyst (Fig. 8.S7). At **8.4**:lactide = 1:50, the reaction follows pure first-order kinetics (Fig. 8.S5, 8.S6), eventual for the trivial reason that the reaction already reached 90% conversion at the time the second active species typically starts to be noticeable in the reaction kinetics.

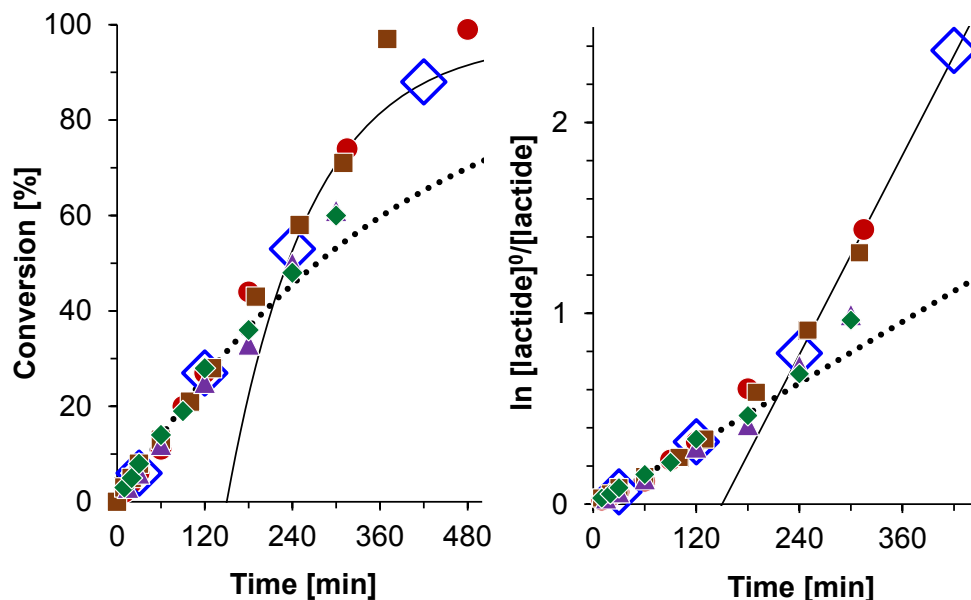


**Figure 8.8.** Conversion-time plot and the semilogarithmic plot for *rac*-lactide polymerizations with **8.4**. Conditions: lactide:4:BnOH = 100:1:1. Hollow diamonds are independent reactions quenched after 0.5, 2, 4, and 7 h without exposing the reaction to air. In the remaining four experiments samples were taken in the desired intervals, exposing the reaction to air. Two reactions were conducted with twice (diamonds) or half (triangles) the total amount of reactants to verify the influence of external impurities.

Polymerizations with **8.4** showed the same moderate heterotacticity as **8.1-8.3** with  $P_r = 0.7-0.8$ . Polymerizations were conducted in the presence of base (1 equiv of triethylamine, pyridine, or *t*BuOK per **8.4**) to ensure that the ammonium group on piperazine is available for interaction with the alcohol (Fig. 8.S8+8.S9, Table 8.S1, entries 36-38). An induction period was observed for triethylamine and pyridine, to lead afterwards to faster conversion than without added base. Polymerizations

showed slightly higher stereocontrol in the presence of pyridine and triethylamine ( $P_r = 0.73$ - $0.87$ , Table 8.II, 8.S1), but lower stereocontrol for *t*BuOK ( $P_r = 0.5$ - $0.7$ ), which would be suspected to be most effective in deprotonating the ammonium group. The slightly increased stereocontrol can thus not be correlated with liberation of a basic side on the ligand.

Introduction of *tert*-butyl substituents at the *ortho*- and *para*-position of the phenolate ligand in **8.5** leads to a minor reduction in activity (approx. 2/3 compared to **8.4**), but otherwise identical polymerization behaviour (Fig. 8.S10 and 8.S11, Tables 8.II and 8.S1, entries 39-41). Stereocontrol was only slightly increased with the more bulky phenolate ligand ( $P_r = 0.75$ - $0.85$ ). Polymerizations with **6**, carrying a tridentate ligand without additional basic site, show the same general polymerization behaviour as **8.1**-**8.5** (Fig. 8.9, Tables 8.II and 8.S1, entries 42-44). Coordination/dissociation of the 3<sup>rd</sup> amino group is thus not responsible for the existence of two active species. Rate constants identical in the range of error to those of **8.4** and unaffected stereocontrol of  $P_r = 0.75$ - $0.80$  further support that the 3<sup>rd</sup> amino group in **8.4** does not participate in the polymerization.

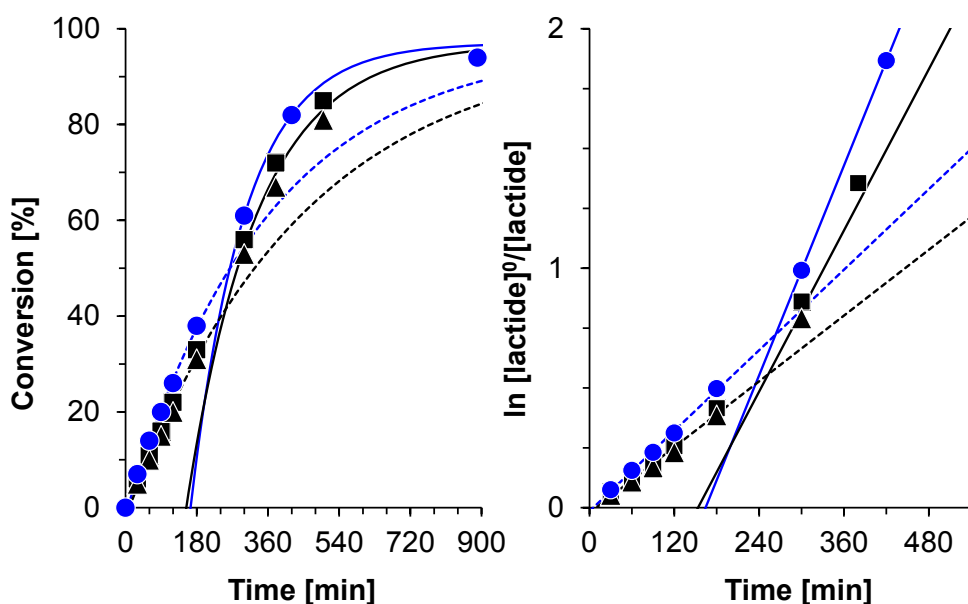


**Figure 8.9.** Conversion-time plot and the semilogarithmic plot for *rac*-lactide polymerizations with **8.6**. Conditions: lactide:6:BnOH = 100:1:1 (squares, triangles),

100:1:4 (circles). Lines represent theoretical conversions calculated from the pseudo-first-order rate constants obtained from the linear regions of the semilogarithmic plot.

## Conclusions

While the structure of the active species is not known, close to identical activities and polymerization kinetics of complexes with diethylenetriamine, piperazineethyleneamine and piperidineethyleneamine substituents propose a tridentate coordination of the ligand in the active species. However, there is no evidence that a basic site facilitates polymerization via a *ligand-assisted chain-end control* mechanism in these complexes.

Complexes **8.1-8.6** show up to 85% heterotacticity, an impressive stereocontrol for polymerizations at 140 °C and unprecedented for copper complexes. The high amount of intramolecular transesterification observed for all complexes, however, and the at best mediocre activity argues against the suitability of this catalyst system for lactide polymerization in general. Given the fact that copper diketimate complexes with a *bidentate* ligand, square-planar geometry and notable steric bulk oriented below and above the complex plane did not show any evidence of transesterification reactions even under monomer-starved conditions,<sup>69-70</sup> it can be argued that ligands which permit square-pyramidal coordination might not provide a constricted enough coordination environment to avoid transesterification reactions.

## Experimental section

**General.** 4,6-di-*tert*-Butylsalicylaldehyde,<sup>71</sup> 1,3-dichlorosalicylaldehyde,<sup>71</sup> **8.L1H**,<sup>54</sup> **8.L3H**,<sup>66</sup> **8.L4H**,<sup>72</sup> and **8.L5H**,<sup>73</sup> were prepared according to literature. *rac*-Lactide (98%) was purchased from Sigma–Aldrich, purified by 3x recrystallization from dry ethyl acetate and kept at –30 °C. All other chemicals were purchased from common commercial suppliers and used without further purification. <sup>1</sup>H and <sup>13</sup>C NMR spectra were acquired on Bruker Avance 300 and 400 spectrometers. Chemical shifts were referenced to the residual signals of the deuterated solvents (CDCl<sub>3</sub>: <sup>1</sup>H: δ 7.26 ppm, <sup>13</sup>C: δ 77.16). Proton and carbon signals of minor isomers are respectively reported in brackets. Abbreviations for peak multiplicities are s (singlet), d (doublet), t (triplet), q (quadruplet), qu (quintuplet), m (multiplet) and br (broad). Certain <sup>13</sup>C NMR

chemical shifts values were extracted from HSQC and HMBC spectra. Elemental analyses were performed by the Laboratoire d'analyse élémentaire (Université de Montréal). All UV-Vis measurements were done in MeOH at RT in a sealed quartz cell on a Cary 500i UV-Vis-NIR Spectrophotometer.

**2-(2-(2-aminoethylamino)ethylimino)methyl)-4,6-dichlorophenol, 8.L2H.** A procedure from literature was adapted as follows:<sup>72</sup> To a yellow solution of 1,3-dichlorosalicylaldehyde (1.00 g, 5.2 mmol) in ethanol (10 mL) was added dropwise a solution of diethylenetriamine (540 mg, 5.2 mol) in ethanol (10 mL), followed by the addition of 5 drops of formic acid. The obtained yellow solution was refluxed for 1 hour. The solvent was removed under vacuum to yield a yellow oil (1.26 g, 87%).

<sup>1</sup>H NMR (CDCl<sub>3</sub>, 300 MHz): δ 8.22 (br s, 1H, H<sup>3</sup>), 7.37 (dd, *J* = 3, 3 Hz, 1H, H<sup>1</sup>), 7.12 (d, *J* = 3 Hz, 0.6H, H<sup>2</sup>), [7.08 (d, *J* = 3 Hz, 0.4H, H<sup>2</sup>)], 3.67 (br s, 2H, H<sup>4</sup>), 2.97 (br s, 2H, H<sup>5</sup>), 2.80 (t, *J* = 6 Hz, 2H, H<sup>7</sup>), 2.68 (t, *J* = 6 Hz, 2H, H<sup>6</sup>); <sup>13</sup>C{<sup>1</sup>H} NMR (CDCl<sub>3</sub>, 75 MHz): δ 164.5 (HSQC, CH<sup>3</sup>), [158.3 (HMBC, C-OH)], 157.8 (HMBC, C-OH) [132.6 (CH<sup>1</sup>)], 132.2 (CH<sup>1</sup>), [129.1, CH<sup>2</sup>], 129.0 (CH<sup>2</sup>), 123.3 (CCl<sup>1</sup>), 122.4 (2C, CCl<sup>2</sup> + C(C=N)), 58.1 (CH<sup>4</sup>), 52.4 (CH<sup>6</sup>), 49.8 (CH<sup>5</sup>), 41.9 (CH<sup>7</sup>), [41.6 (CH<sup>7</sup>)]. ESI-HRMS (*m/z*): [M+H]<sup>+</sup> (C<sub>11</sub>H<sub>16</sub>Cl<sub>2</sub>N<sub>3</sub>O) calcd 276.0670; found 276.0675.

**[(8.L1)Cu][NO<sub>3</sub>]<sub>2</sub>·H<sub>2</sub>O, 8.1.** Cu(NO<sub>3</sub>)<sub>2</sub>·2.5 H<sub>2</sub>O (112 mg, 0.48 mmol) was added to a freshly prepared yellow solution of 2-(2-(2-aminoethylamino)ethylimino)methylphenol (**8.L1H**) (100 mg, 0.48 mmol) in methanol (10 mL). After stirring the suspension for 30 min, the obtained dark blue solution was left to slowly evaporate to yield blue crystals. The crystals were recrystallized from a minimum amount of boiling methanol (38 mg, 23%).

UV-vis (MeOH, 5·10<sup>-6</sup> M) [ $\lambda_{\max}$ , nm ( $\epsilon$ , mol<sup>-1</sup> cm<sup>2</sup>)]: 266 (33310), 362 (104300), 577 (3300). Anal. Calcd for C<sub>11</sub>H<sub>18</sub>CuN<sub>4</sub>O<sub>5</sub>·H<sub>2</sub>O: C, 35.92; H, 5.48; N, 15.23; Found: C, 35.77; H, 5.09; N, 15.88.

**[(8.L1)Cu][CF<sub>3</sub>SO<sub>3</sub>], 2.** Analogous to **8.1**, from Cu(CF<sub>3</sub>SO<sub>3</sub>)<sub>2</sub> (174 mg, 0.48 mmol), 2-(2-(2-aminoethylamino)ethyl)iminomethylphenol (**8.L1H**) (100 mg, 0.48 mmol) in methanol (10 mL) stirred 30 min. The obtained blue solution was left to slowly

evaporate to yield very few purple crystals, which were used without characterization other than X-ray studies.

**[(8.L2)Cu][NO<sub>3</sub>], 8.3.** Analogous to **8.1**, from Cu(NO<sub>3</sub>)<sub>2</sub>·2.5 H<sub>2</sub>O (85 mg, 0.36 mmol), 2-(2-(2-aminoethylamino)ethyl)iminomethyl)-4,6-dichlorophenol (**8.L2H**) (100 mg, 0.36 mmol) in ethanol (10 mL) stirred 30 min to yield dark blue oil. The oil was crystallized from boiling ethanol (3 mL), to yield dark blue crystals which were then re-crystallized from a minimum amount of boiling ethanol (13 mg, 9%).

UV-vis (MeOH, 5·10<sup>-6</sup> M) [ $\lambda_{\max}$ , nm ( $\epsilon$ , mol<sup>-1</sup> cm<sup>2</sup>): 267 (90000), 359 (25000), 570 (1000). Anal. Calcd for C<sub>11</sub>H<sub>14</sub>Cl<sub>2</sub>CuN<sub>4</sub>O<sub>4</sub>·EtOH: C, 34.95; H, 4.51; N, 12.54; Found: C, 34.84; H, 3.95; N, 12.75.

**[(8.L3)Cu][NO<sub>3</sub>]<sub>2</sub>·MeOH, 8.4.** Analogous to **8.1**, from Cu(NO<sub>3</sub>)<sub>2</sub>·2.5 H<sub>2</sub>O (100 mg, 0.43 mmol), 2-((2-(piperazin-1-yl)ethyl)iminomethyl)phenol (**8.L3H**) (100 mg, 0.43 mmol) in methanol (10 mL) stirred 30 min. The desired complex directly crystallized out of the dark green solution (65 mg, 33%).

UV-vis (MeOH, 7.5·10<sup>-6</sup> M) [ $\lambda_{\max}$ , nm ( $\epsilon$ , mol<sup>-1</sup> cm<sup>2</sup>): 278 (76900), 300 (sh), 374 (22100), 632 (200). Anal. Calcd for C<sub>13</sub>H<sub>19</sub>CuN<sub>5</sub>O<sub>7</sub>·CH<sub>3</sub>OH: C, 37.13; H, 5.12; N, 15.46; Found: C, 36.74; H, 5.01; N, 15.43.

**[(8.L4)Cu(MeOH)][NO<sub>3</sub>]<sub>2</sub>·½MeOH, 8.5.** Analogous to **8.1**, from Cu(NO<sub>3</sub>)<sub>2</sub>·2.5 H<sub>2</sub>O (67 mg, 0.29 mmol), 2,4-di-tert-butyl-6-((2-(piperazin-1-yl)ethyl)iminomethyl)phenol (**8.L4H**) (100 mg, 0.29 mmol) in methanol (10 mL) refluxed 1 h to yield dark green crystals. The crystals were re-crystallized from a minimum amount of boiling methanol and washed with hexane (3 x 5 mL). (18 mg, 10%)

UV-vis (MeOH, 2.5·10<sup>-6</sup> M) [ $\lambda_{\max}$ , nm ( $\epsilon$ , mol<sup>-1</sup> cm<sup>2</sup>): 280 (173600), 316 (41400), 390 (45200), 632 (600). Anal. Calcd for C<sub>22</sub>H<sub>39</sub>CuN<sub>5</sub>O<sub>8</sub>·½ C<sub>6</sub>H<sub>14</sub>: C, 49.39; H, 7.50; N, 11.47; Found: C, 49.66; H, 7.12; N, 11.86. (Replacement of methanol by hexane assumed during drying and washing for EA.)

**[(8.L5)Cu(OH<sub>2</sub>)] [AcO]·H<sub>2</sub>O, 8.6.** Analogous to **8.1**, from Cu(OAc)<sub>2</sub> (78 mg, 0.43 mmol), 2-((2-(piperidin-1-yl)ethyl)iminomethyl)phenol (**8.L5H**) (100 mg, 0.43 mmol) in methanol (10 mL) stirred 30 min. The obtained green solution was left to

slowly evaporate to yield green crystals. The crystals were recrystallized from a minimum amount of boiling methanol. (36 mg, 23%)

UV-vis (MeOH,  $7.5 \cdot 10^{-6}$  M) [ $\lambda_{\text{max}}$ , nm ( $\epsilon$ , mol $^{-1}$  cm $^2$ ): 272 (81400), 306 (sh), 378 (22000)]. Anal. Calcd for C<sub>16</sub>H<sub>24</sub>CuN<sub>2</sub>O<sub>4</sub>·H<sub>2</sub>O: C, 47.11; H, 6.92; N, 6.87; Found: C, 47.59; H, 6.71; N, 6.68.

***rac*-Lactide polymerization.** In a glove box, the desired amount of *rac*-lactide was placed into a pressure tube together with the catalyst. If required, a highly concentrated stock solution of an additive (BnOH, etc.) in toluene was added. The pressure tubes were then placed in a preheated oil bath at 140 °C. In kinetic experiments, samples were taken at specific time intervals, dissolved in CDCl<sub>3</sub>, filtered through a short silica plug to remove copper catalyst, which was rinsed with additional CDCl<sub>3</sub>, and studied by <sup>1</sup>H NMR. After drying, polymers were stored at –80 °C for further analysis.

Conversion was determined from <sup>1</sup>H NMR by comparison to remaining lactide.  $P_r$  values were determined from homodecoupled <sup>1</sup>H NMR spectra and calculated from  $P_r = 2 \cdot I_1 / (I_1 + I_2)$ , with  $I_1 = 5.20 - 5.25$  ppm (*rmr*, *mmr/rmm*),  $I_2 = 5.13 - 5.20$  ppm (*mmr/rmm*, *mmm*, *mrmm*). The integration of the left multiplet and right multiplet ( $I_1$  and  $I_2$ ) required only one, very reproducible dividing point of the integration, which was always taken as the minimum between the two multiplets. Nevertheless,  $P_r$  values showed a much higher variability than typically observed in these polymerizations. Investigations indicated incomplete removal of Cu(II) as the source of the high variations. Molecular weight analyses were performed on a Waters 1525 gel permeation chromatograph equipped with three Phenomenex columns and a refractive index detector at 35 °C. THF was used as the eluent at a flow rate of 1.0 mL·min<sup>-1</sup> and polystyrene standards (Sigma–Aldrich, 1.5 mg·mL<sup>-1</sup>, prepared and filtered (0.2 mm) directly prior to injection) were used for calibration. Obtained molecular weights were corrected by a Mark-Houwink factor of 0.58.<sup>74</sup>

**X-ray diffraction studies.** Crystal for X-ray diffraction were obtained from synthesis as described above. Diffraction data were collected on a Bruker Venture METALJET diffractometer (Ga K $\alpha$  radiation) or a Bruker APEX II microsource (Cu K $\alpha$ )



radiation).<sup>75</sup> Data reduction was performed with SAINT,<sup>76</sup> absorption corrections with SADABS.<sup>77</sup> Structures were solved by dual-space refinement (SHELXT).<sup>78</sup> All non-hydrogen atoms were refined anisotropic using full-matrix least-squares on  $F^2$  and hydrogen atoms refined with fixed isotropic U using a riding model (SHELXL97).<sup>79</sup> Further experimental details can be found in Table 8.3 and the supporting information (CIF). All crystals but **1** and **4** were weakly diffracting and yielded poor structural data. Structures should be considered as proof of connectivity mainly.

**Table 8.III.** Details of X-ray Diffraction Studies

	8.1	8.2	8.3
Formula	C <sub>11</sub> H <sub>18</sub> CuN <sub>4</sub> O <sub>5</sub>	C <sub>12</sub> H <sub>18</sub> CuF <sub>3</sub> N <sub>3</sub> O <sub>5</sub> S	C <sub>11</sub> H <sub>14</sub> Cl <sub>2</sub> CuN <sub>4</sub> O <sub>4</sub>
$M_w$ (g/mol).	349.83	436.89	400.70
$T$ (K); F(000)	150; 724	150; 1784	150; 812
Crystal System	Monoclinic	Monoclinic	Triclinic
Space Group	$P2_1/c$	$P2_1/n$	$P(-1)$
Unit Cell: $a$ (Å)	9.1046(4)	20.6661(8)	7.1434(7)
$b$ (Å)	14.6096(6)	7.2817(3)	10.8066(13)
$c$ (Å)	10.8435(4)	24.2161(9)	19.909(2)
$\alpha$ (°)	90	90	96.025(8)
$\beta$ (°)	102.117(2)	109.637(2)	90.517(8)
$\gamma$ (°)	90	90	98.325(9)
$V$ (Å <sup>3</sup> ); $Z$	1410.21(10); 4	3432.2(2); 8	1511.8(3); 4
$\mu$ (mm <sup>-1</sup> ).	8.542	3.511	10.067
Absorption correction	multiscan	multiscan	multiscan
$\theta$ range (°)	4.3-60.9	2.4-72	3.6-42.4
Completeness	1.0	1.0	0.96
Collected refl.; $R_\sigma$	17672; 0.0380	122587; 0.1259	7438; 0.1500
Unique refl.; $R_{\text{int}}$	3198; 0.0567	72266; 0.1724	3106; 0.1205
$R1(F)$ ( $I > 2\sigma(I)$ )	0.0530	0.1071	0.1648
w $R(F^2)$ (all data)	0.1139	0.3005	0.4410
GoF( $F^2$ ); Flack-x	1.15; -	1.04; -	1.04; -
Res. electron density	0.35; -0.45	2.81; -1.91	1.21; -0.67

**Table 8.III-continued.** Details of X-ray Diffraction Studies

	8.4	8.5	8.6
Formula	C <sub>14</sub> H <sub>23</sub> CuN <sub>5</sub> O <sub>8</sub>	C <sub>45</sub> H <sub>82</sub> Cu <sub>2</sub> N <sub>10</sub> O <sub>17</sub>	C <sub>16</sub> H <sub>24</sub> CuN <sub>2</sub> O <sub>4</sub>
$M_w$ (g/mol).	452.91	1162.28	371.91
$T$ (K); F(000)	150; 940	150; 2464	150; 1560
Crystal System	Monoclinic	Orthorhombic	Monoclinic
Space Group	$P2_1/n$	$Pna2_1$	$P2_1/c$
Unit Cell: $a$ (Å)	9.5497(5)	20.8207(13)	9.7008(10)
$b$ (Å)	14.8857(7)	8.3864(6)	18.6698(17)
$c$ (Å)	13.4561(6)	33.203(2)	23.501(3)
$\alpha$ (°)	90	90	90
$\beta$ (°)	98.530(3)	90	101.775(7)
$\gamma$ (°)	90	90	90
$V$ (Å <sup>3</sup> ); Z	1891.68(16); 4	5797.5(7); 4	4166.7(7); 8
$\mu$ (mm <sup>-1</sup> ).	6.543	4.353	5.751
Absorption correction	multiscan	multiscan	multiscan
$\theta$ range (°)	2.6-60.7	3.9-59.9	2.7-42.0
Completeness	1.0	0.98	0.99
Collected refl.; $R_\sigma$	25277; 0.0670	45433; 0.1881	23048; 0.1223
Unique refl.; $R_{int}$	4351; 0.0935	12938; 0.1750	4372; 0.1797
$R1(F)$ ( $I > 2\sigma(I)$ )	0.0812	0.1461	0.1289
wR( $F^2$ ) (all data)	0.2140	0.4089	0.3823
GoF( $F^2$ ); Flack-x	1.04; -	1.13; 0.43(2)	1.20; -
Res. electron density	0.72; -0.88	2.97; -0.76	0.92; -0.47

**Acknowledgements**

Funding was supplied by the NSERC discovery program (RGPIN-2016-04953) and the Centre for Green Chemistry and Catalysis (FQRNT). We thank Francine Bélanger for support with X-ray diffraction, Elena Nadezhina for elemental analysis, Marie-Christine Tang and Dr. Alexandra Furtos for MALDI analyses, and Dr. Antoine Douchez for support with 2D NMR. J. L. Jimenez Santiago contributed during his MITACS internship to ligand synthesis.

## References Chapter 8

- (1) Nagarajan, V.; Mohanty, A. K.; Misra, M. *ACS Sustainable Chem. Eng.* **2016**, *4*, 2899-2916.
- (2) Castro-Aguirre, E.; Iñiguez-Franco, F.; Samsudin, H.; Fang, X.; Auras, R. *Adv. Drug Delivery Rev.* **2016**, *107*, 333-366.
- (3) Slomkowski, S.; Penczek, S.; Duda, A. *Polym. Adv. Technol.* **2014**, *25*, 436-447.
- (4) Singhvi, M.; Gokhale, D. *RSC Adv.* **2013**, *3*, 13558-13568.
- (5) Hottle, T. A.; Bilec, M. M.; Landis, A. E. *Polym. Degrad. Stab.* **2013**, *98*, 1898-1907.
- (6) Inkinen, S.; Hakkarainen, M.; Albertsson, A.-C.; Södergård, A. *Biomacromolecules* **2011**, *12*, 523-532.
- (7) Ahmed, J.; Varshney, S. K. *Int. J. Food Prop.* **2011**, *14*, 37-58.
- (8) Paul, S.; Zhu, Y.; Romain, C.; Brooks, R.; Saini, P. K.; Williams, C. K. *Chem. Commun. (Cambridge, U. K.)* **2015**, *51*, 6459-6479.
- (9) MacDonald, J. P.; Shaver, M. P. In *Green Polymer Chemistry: Biobased Materials and Biocatalysis*, American Chemical Society: 2015, pp 147-167.
- (10) Guillaume, S. M.; Kirillov, E.; Sarazin, Y.; Carpentier, J.-F. *Chem.-Eur. J.* **2015**, *21*, 7988-8003.
- (11) Sauer, A.; Kapelski, A.; Fliedel, C.; Dagherne, S.; Kol, M.; Okuda, J. *Dalton Trans.* **2013**, *42*, 9007-9023.
- (12) Jianming, R.; Anguo, X.; Hongwei, W.; Hailin, Y. *Des. Monomers Polym.* **2013**, *17*, 345-355.
- (13) Huang, B. H.; Dutta, S.; Lin, C. C. In *Comprehensive Inorganic Chemistry II (Second Edition)*, Poeppelmeier, J. R., Ed. Elsevier: Amsterdam, 2013; pp 1217-1249.
- (14) Dagherne, S.; Normand, M.; Kirillov, E.; Carpentier, J.-F. *Coord. Chem. Rev.* **2013**, *257*, 1869-1886.
- (15) Dagherne, S.; Fliedel, C. In *Modern Organoaluminum Reagents: Preparation, Structure, Reactivity and Use*, Woodward, S.; Dagherne, S., Eds. Springer Berlin Heidelberg: Berlin, Heidelberg, 2013; Vol. pp 125-171.

- (16) Carpentier, J.-F.; Liu, B.; Sarazin, Y. In *Advances in Organometallic Chemistry and Catalysis*, John Wiley & Sons, Inc.: 2013; Vol. pp 359-378.
- (17) dos Santos Vieira, I.; Herres-Pawlis, S. *Eur. J. Inorg. Chem.* **2012**, 2012, 765-774.
- (18) Wheaton, C. A.; Hayes, P. G. *Comments Inorg. Chem.* **2011**, 32, 127-162.
- (19) Dutta, S.; Hung, W.-C.; Huang, B.-H.; Lin, C.-C. In *Synthetic Biodegradable Polymers*, Rieger, B.; Künkel, A.; Coates, G. W.; Reichardt, R.; Dinjus, E.; Zevaco, T. A., Eds. Springer-Verlag: Berlin, 2011; Vol. pp 219-284.
- (20) Dijkstra, P. J.; Du, H.; Feijen, J. *Polym. Chem.* **2011**, 2, 520-527.
- (21) Dagorne, S.; Fliedel, C.; de Frémont, P. In *Encyclopedia of Inorganic and Bioinorganic Chemistry*, John Wiley & Sons, Ltd: 2011; Vol.
- (22) Buffet, J.-C.; Okuda, J. *Polym. Chem.* **2011**, 2, 2758-2763.
- (23) Thomas, C. M. *Chem. Soc. Rev.* **2010**, 39, 165.
- (24) Sutar, A. K.; Maharana, T.; Dutta, S.; Chen, C.-T.; Lin, C.-C. *Chem. Soc. Rev.* **2010**, 39, 1724-1746.
- (25) Stanford, M. J.; Dove, A. P. *Chem. Soc. Rev.* **2010**, 39, 486-494.
- (26) Kiesewetter, M. K.; Shin, E. J.; Hedrick, J. L.; Waymouth, R. M. *Macromolecules* **2010**, 43, 2093-2107.
- (27) Jones, M. D. In *Heterogenized Homogeneous Catalysts for Fine Chemicals Production*, Barbaro, P.; Liguori, F., Eds. Springer Netherlands: 2010; Vol. 33, pp 385-412.
- (28) Ajellal, N.; Carpentier, J.-F.; Guillaume, C.; Guillaume, S. M.; Helou, M.; Poirier, V.; Sarazin, Y.; Trifonov, A. *Dalton Trans.* **2010**, 39, 8363.
- (29) Wheaton, C. A.; Hayes, P. G.; Ireland, B. J. *Dalton Trans.* **2009**, 4832 - 4846.
- (30) Amgoune, A.; Thomas, C. M.; Carpentier, J.-F. *Pure Appl. Chem.* **2007**, 79, 2013-2030.
- (31) Wu, J.; Yu, T.-L.; Chen, C.-T.; Lin, C.-C. *Coord. Chem. Rev.* **2006**, 250, 602-626.
- (32) Dechy-Cabaret, O.; Martin-Vaca, B.; Bourissou, D. *Chem. Rev.* **2004**, 104, 6147-6176.

- (33) O'Keefe, B. J.; Hillmyer, M. A.; Tolman, W. B. *J. Chem. Soc., Dalton Trans.* **2001**, 2215-2224.
- (34) Liu, B.; Roisnel, T.; Maron, L.; Carpentier, J.-F.; Sarazin, Y. *Chem.-Eur. J.* **2013**, *19*, 3986-3994.
- (35) Susperregui, N.; Delcroix, D.; Martin-Vaca, B.; Bourissou, D.; Maron, L. *J. Org. Chem.* **2010**, *75*, 6581-6587.
- (36) Zhang, J.; Xiong, J.; Sun, Y.; Tang, N.; Wu, J. *Macromolecules* **2014**, *47*, 7789-7796.
- (37) Dai, Z.; Sun, Y.; Xiong, J.; Pan, X.; Wu, J. *ACS Macro Lett.* **2015**, *4*, 556-560.
- (38) Xiong, J.; Zhang, J.; Sun, Y.; Dai, Z.; Pan, X.; Wu, J. *Inorg. Chem.* **2015**, *54*, 1737-1743.
- (39) Sun, Y.; Xiong, J.; Dai, Z.; Pan, X.; Tang, N.; Wu, J. *Inorg. Chem.* **2016**, *55*, 136-143.
- (40) Chen, C.; Cui, Y.; Mao, X.; Pan, X.; Wu, J. *Macromolecules* **2017**, *50*, 83-96.
- (41) Cui, Y.; Chen, C.; Sun, Y.; Wu, J.; Pan, X. *Inorg. Chem. Front.* **2017**, *4*, 261-269.
- (42) Chen, C.; Jiang, J.; Mao, X.; Cong, Y.; Cui, Y.; Pan, X.; Wu, J. *Inorg. Chem.* **2018**, *57*, 3158-3168.
- (43) Sun, J.; Shi, W.; Chen, D.; Liang, C. *J. Appl. Polym. Sci.* **2002**, *86*, 3312-3315.
- (44) John, A.; Katiyar, V.; Pang, K.; Shaikh, M. M.; Nanavati, H.; Ghosh, P. *Polyhedron* **2007**, *26*, 4033-4044.
- (45) Bhunora, S.; Mugo, J.; Bhaw-Luximon, A.; Mapolie, S.; Van Wyk, J.; Darkwa, J.; Nordlander, E. *Appl. Organomet. Chem.* **2011**, *25*, 133-145.
- (46) Li, C.-Y.; Hsu, S.-J.; Lin, C.-I.; Tsai, C.-Y.; Wang, J.-H.; Ko, B.-T.; Lin, C.-H.; Huang, H.-Y. *J. Polym. Sci., Part A: Polym. Chem.* **2013**, *51*, 3840-3849.
- (47) Routaray, A.; Nath, N.; Maharana, T.; Sutar, A. k. *J. Macromol. Sci., Part A: Pure Appl. Chem.* **2015**, *52*, 444-453.
- (48) Williams, C. K.; Breyfogle, L. E.; Choi, S. K.; Nam, W.; Young, V. G.; Hillmyer, M. A.; Tolman, W. B. *J. Am. Chem. Soc.* **2003**, *125*, 11350-11359.
- (49) Labourdette, G.; Lee, D. J.; Patrick, B. O.; Ezhova, M. B.; Mehrkhodavandi, P. *Organometallics* **2009**, *28*, 1309-1319.

- (50) Rosen, T.; Popowski, Y.; Goldberg, I.; Kol, M. *Chem.-Eur. J.* **2016**, *22*, 11533-11536.
- (51) Zhu, H. L.; Li, S. Y.; He, W. M.; Yu, K. B. *Z. Kristallogr. - New Cryst. Struct.* **2002**, *217*, 599.
- (52) Plyuta, N. I.; Rusanova, J. A.; Petrusenko, S. R.; Omelchenko, I. V. *Acta Crystallogr., Sect. E: Struct. Rep. Online* **2014**, *70*, m330-m331.
- (53) Dieng, M.; Barry, A. H.; Gaye, M.; Sall, A. S.; Perez-Lourido, P.; Valencia-Matarranz, L. *Acta Crystallogr., Sect. E: Struct. Rep. Online* **2011**, *67*, m830-m831.
- (54) Bhunia, A.; Manna, S.; Mistri, S.; Paul, A.; Manne, R. K.; Santra, M. K.; Bertolasi, V.; Chandra Manna, S. *RSC Adv.* **2015**, *5*, 67727-67737.
- (55) Liu, G. X.; Ren, X. M.; Xu, H.; Tang, C. Y.; Wu, G. H.; CunChen, Y. *Chin. Chem. Lett.* **2004**, *15*, 1105.
- (56) Cusmano Priolo, F.; Rotondo, E.; Rizzardi, G.; Bruno, G.; Bombieri, G. *Acta Crystallogr., Sect. C* **1983**, *39*, 550-552.
- (57) The typically explanation for this is a long induction period. However, kinetic fits using this presumption are incongruent, yielding widely varying, even negative induction periods. Neither do conversion-time plots show the inflection point typically present in first-order reactions with an induction period. I. e. the rate in the early stages of the reaction does not increase in the early stages of reaction.
- (58) Xu, R.-B.; Xu, X.-Y.; Wang, M.-Y.; Wang, D.-Q.; Yin, T.; Xu, G.-X.; Yang, X.-J.; Lu, L.-D.; Wang, X.; Lei, Y.-J. *J. Coord. Chem.* **2008**, *61*, 3306-3313.
- (59) Chakraborty, J. *J. Korean Chem. Soc.* **2011**, *55*, 199.
- (60) Maxim, C.; Tuna, F.; Madalan, A. M.; Avarvari, N.; Andruh, M. *Crystal Growth & Design* **2012**, *12*, 1654-1665.
- (61) Gurumoorthy, P.; Mahendiran, D.; Prabhu, D.; Arulvasu, C.; Rahiman, A. K. *RSC Adv.* **2014**, *4*, 42855-42872.
- (62) Pait, M.; Kundu, B.; Kundu, S. C.; Ray, D. *Inorg. Chim. Acta* **2014**, *418*, 30-41.
- (63) Maity, T.; Saha, D.; Bhunia, S.; Brandao, P.; Das, S.; Koner, S. *RSC Adv.* **2015**, *5*, 82179-82191.



- (64) Ishani, M.; Prateeti, C.; Jaydeep, A.; Hulya, K.; Ennio, Z.; Antonio, B.; Antonio, F.; Debasis, D. *ChemistrySelect* **2016**, *1*, 615-625.
- (65) Mistri, S.; Paul, A.; Bhunia, A.; Manne, R. K.; Santra, M. K.; Puschmann, H.; Manna, S. C. *Polyhedron* **2016**, *104*, 63-72.
- (66) Kumari, S.; Mahato, A. K.; Maurya, A.; Singh, V. K.; Kesharwani, N.; Kachhap, P.; Koshevoy, I. O.; Haldar, C. *New J. Chem.* **2017**, *41*, 13625-13646.
- (67) Nesterova, O. V.; Nesterov, D. S.; Krogul-Sobczak, A.; Guedes da Silva, M. F. C.; Pombeiro, A. J. L. *J. Molec. Catal. A: Chem.* **2017**, *426*, 506-515.
- (68) Das, M.; Kumar Kundu, B.; Tiwari, R.; Mandal, P.; Nayak, D.; Ganguly, R.; Mukhopadhyay, S. *Inorg. Chim. Acta* **2018**, *469*, 111-122.
- (69) Whitehorne, T. J. J.; Schaper, F. *Chem. Commun. (Cambridge, U. K.)* **2012**, *48*, 10334-10336.
- (70) Whitehorne, T. J. J.; Schaper, F. *Inorg. Chem.* **2013**, *52*, 13612-13622.
- (71) Mondal, S.; Mandal, S. M.; Mondal, T. K.; Sinha, C. *Spectrochim. Acta, Part A* **2015**, *150*, 268-279.
- (72) Kilic, A.; Tegin, I.; Tas, E.; Ziyadanogullan, R. *J. Iran. Chem. Soc.* **2011**, *8*, 68-77.
- (73) Liu, R.-P.; Duan, M.-Y.; Li, J.; Su, Z.-P.; Zhang, J.-H.; Zhang, F.-X. *J. Struct. Chem.* **2011**, *52*, 935-940.
- (74) Save, M.; Schappacher, M.; Soum, A. *Macromol. Chem. Phys.* **2002**, *203*, 889-899.
- (75) *Apex2*, Release 2.1-0; Bruker AXS Inc.: Madison, USA, 2006.
- (76) *Saint*, Release 7.34A; Bruker AXS Inc.: Madison, USA, 2006.
- (77) Sheldrick, G. M. *Sadabs*, Bruker AXS Inc.: Madison, USA, 1996 & 2004.
- (78) Sheldrick, G. *Acta Crystallogr. Sect. A: Found. Crystallogr.* **2015**, *71*, 3-8.
- (79) Sheldrick, G. M. *Acta Crystallogr.* **2008**, *A64*, 112-122.



## **Chapter 9 . Conclusions**



For the last seventy years, polymers based on fossil resources are used in our everyday life. Their accumulation in the environment increasingly becomes a matter of concern. Biodegradable polymers have become a suitable and green replacement, as their production minimizes the use of fossil resources and their degradation removes them from the environment. One popular biodegradable polymer used to date is polylactic acid (PLA), which has been the main focus of my Ph.D. Even though the pros of using PLA outweigh its cons, costs and lack of public knowledge regarding its disposal is still a concern, they compete with *reusable materials*, such as bags made out of textiles.

As outlined in the introduction, many metal-based catalysts have been used to polymerize lactide to polylactic acid. Most catalysts are either main-group metals, such as aluminum, or come from  $d^0$ - or  $d^{10}$ - transition metal groups, such as zirconium or zinc. Next to iron, copper is the most studied  $d^n$ - metal for the ring-opening polymerization of lactide. All investigations conducted prior to our recent studies have reported copper catalysts that produce atactic or heterotactic PLA.

Our main catalyst consists of a dimeric Cu(II) complex with two diiminopyrrolide ligands. The two copper centers are linked by two pyridylmethoxide or dimethylaminoethoxide bridges, the first leading to the formation of an isotactic PLA ( $P_m = 0.73$ ), the latter producing atactic PLA ( $P_m = 0.50$ ). Kinetic studies as well as the data obtained for the molecular weights of the produced polymer chains indicated that the two complexes form different active species in the polymerization. Since the difference in behavior between these two complexes arises from the bridging alcohols, different bridges were used, ranging from highly flexible to highly rigid to study their effect on stereocontrol. Unfortunately, the catalyst faced a lot of limitations with regard to the nature of the bridging ligand: Rigid bridges, such as 8-hydroxyquinoline, completely suppressed the activity of the complex, while more flexible ligands, such as pyridylethoxide, removed stereocontrol. The only bridging alcohol that led to increased isotacticity was dimethyl-2-pyridylmethoxide, with just a bit higher rigidity/steric bulk than pyridylmethoxide.

After we gained a better understanding about the effect of the bridging alcohol on activity and stereocontrol, we investigated the ligand framework. The diiminopyrrolide ligand used in these catalysts contains two imine arms. X-ray structures obtained for these catalysts clearly showed that in all complexes with such ligand systems (with the exception of an *N*-4-bromobenzylamine-substituted ligand) one imine arm is coordinated to the metal while the other one is not. The mechanism proposed for the catalysts is a “ligand mediated chain-end control mechanism”, which is based on the coordination/dissociation of the imine groups to the Cu(II) center, leading to the epimerization of the metal. Thus a copper center that shows a preference for one enantiomer (e.g. (*S,S*)-lactide), upon a miss-insertion will change chirality through epimerization, and will then show preference for the opposite enantiomer, e.g. (*R,R*)-lactide.

We attempted to reproduce this reactivity with spectator ligands other than iminopyrroles. So far we have only been able to study  $\beta$ -ketoimine and phenoxyimine ligands. The former provided an active dimeric Cu(II) complex with an *N*-benzylamine substituent. PLA produced with this complex was atactic, with much lower than expected molecular weights and very high polydispersities. Changing the ligand framework to a bulky phenoxide led to good molecular weight control and moderate to narrow polydispersities. However, these complexes did not provide isotactic polymer.

Alternatively to changing the ligand frame, we have also tried to change the metal center and study the effect of other metals such as zinc, iron and cobalt on the activity and stereocontrol of the catalysts bearing diiminopyrrolide ligands. We have only been able to isolate a dimeric diiminopyrrolide pyridylmethoxide complex with zinc(II) as the metal center. Unfortunately, unlike the copper catalysts, much lower than expected molecular weights and only heterotactic PLA was obtained.

Since all results obtained pointed to the importance of the epimerization of the metal center in order to obtain stereocontrol, 2,4-di-*tert*-butyl-6-aminomethyl-phenol ligands with amino = *N,N,N',N'*-tetramethyldiethylenetriamine or di-(2-picoly)amine were used. Unfortunately we were not able to obtain the desired catalysts in the

presence of copper. However we were able to isolate the desired zinc complexes. Both catalysts proved to epimerize fast on the NMR time scale, reaching full conversion in around 15 min and 2 min respectively, which placed them among the fastest zinc catalysts known to date. Although our idea to introduce stereocontrol by enabling facile epimerization of the catalytic site succeeded, the obtained PLA is only slightly isotactic ( $P_m = 0.60$ ). Modification of the ligand is required to be able to reach high degrees of isotacticity that have already been reported for zinc catalysts by other groups such as Ma and Kol.

All the complexes discussed until now are active at room temperature in solution. We have also been able to prepare two groups of monomeric catalysts based on manganese (one of the few manganese complexes to show a coordination-insertion mechanism in the ROP of *rac*-lactide) and copper with phenolate based ligands. Both groups are only active in bulk polymerization, yielding polymer chains with much lower than expected molecular weights and no stereocontrol. Unfortunately studying the mechanism of the ROP of lactide in bulk polymerization at 140 °C is much more complicated than in solution. Since the polymers obtained have not shown any interesting results, we have not studied these catalysts in more depth.

In conclusion, to date many catalysts have shown very impressive behavior in the ROP of lactide, both regarding activity and stereocontrol. Even though we have only been able to reach a maximum  $P_m$  value of 75% for copper catalysts, studying the behavior of these dimeric catalysts with an unusual stereocontrol mechanism has brought us a lot of insight into the ROP of lactide. Unfortunately our ligand systems had the limitation of not being able to be modified without losing activity. I believe at this point we should focus on designing ligand systems that are able to provide the needed rigidity, steric bulk, as well as being able to epimerize the metal center in order to obtain very high degrees of stereocontrol.

Cu(II) catalysts have gained a lot of interest due to their nontoxicity and high abundancy. Nevertheless the elucidation of clear mechanistic pathway is challenging due to their paramagnetic nature, making the most common characterization technique, NMR, inaccessible. Through a combination of EPR, X-ray and UV-studies

on a large library of complexes, as well as careful characterization of the final product, the mechanism of this Cu-catalyzed reaction has been identified. These results are important for future mechanistic studies on copper based catalysts. This thesis has offered a complete mechanistic study on dimeric Cu(II) catalysts in *rac*-lactide polymerization that have also been the first copper catalysts to show a catalytic-site mediated chain-end control mechanism. All copper alkoxide complexes active in lactide polymerization have been dimeric in the solid state based on X-ray and solution based on EPR (since all kinetics show a linear dependence on catalyst concentration, there is no monomer-dimer equilibrium present under this conditions). This is due to the requirement of an open coordination site for the monomer, the facility of alkoxide groups to act as bridging ligands and the flexible coordination geometry of copper which allows either tetra- or penta-coordinated complexes. The requirement for a chiral catalyst to obtain stereocontrol was proven by the synthesis of a penta-coordinated dimeric Cu(II) complex bearing a diiminopyrrolo scaffold, having both imine arms coordinated to the metal center. In combination with the use of achiral ligands and the  $^{13}\text{C}$  NMR data, this confirmed the presence of a catalytic-site mediated chain-end control mechanism. Results obtained from the kinetic studies conducted in the presence of an added external alcohol and EPR spectroscopy point to the presence of a monomeric deactivated species in the course of the polymerization. Based on these different results we propose a new pathway to synthesize isotactic PLA by the application of a chiral catalyst containing a flexible ligand system, able to epimerize and adapt itself to the chirality of the last inserted lactide monomer. As a proof of concept that this idea can be adapted to other ligand/metal systems, we studied aminophenolate derivatives with Zn(II). There is no absolute requirement that a catalytic-site mediated chain-end control requires a dinuclear catalytic site. However, it might have an influence: In the case of copper, the dinuclear species has a clearly defined mean catalyst plane with a chiral orientation of the imino ligands. It is not clear if in a mononuclear complex the catalytic site would have the same amplifying influence on stereoselectivity. In the zinc-based species, we see dependence of stereocontrol on catalyst concentration, indicating that monomer/dimer equilibria are of importance here. These are very



fundamental questions in lactide polymerization and both systems, in particular the zinc one, require further studies. It is also unclear which effect the nuclearity of the catalyst has on activity.

A great challenge that chemists in the field of lactide polymerization face is the design of catalysts that can resist the harsh conditions of industrial lactide polymerization while still be able to provide isotactic PLA. To date only a few examples in literature present catalysts with such capacity. It is important for me to develop such catalysts with copper, due to its nontoxicity and abundancy, and since it has already shown a decent degree of isotacticity in solution. Cu(II) is stable in air and in the presence of the correct robust ligand it could be a good candidate for industry. I would aim to prepare these complexes from already available and stable Cu(II) salts such as  $\text{Cu}(\text{NO}_3)_2$ . The goal would be to design ligand frameworks that are easy to prepare and that can provide rigid transition states via the formation of hydrogen bonds with the incoming external alcohol (ligand assisted activated monomer mechanism) in order to obtain isotactic stereocontrol. 2,4-di-*tert*-butyl-6-aminomethyl-phenol ligand with either *N,N,N',N'*-tetramethylethylenetriamine or *N,N*-dimethyl-*N'*-((pyridine-2-yl)methyl)ethane-1,2-diamine as its *N*-substituent would be my starting point in this investigation. The nitrogen of dimethylamine has a higher capacity to do hydrogen bond with the external alcohol, while the pyridine would be more strongly coordinated to the copper center (Figure 9.1).

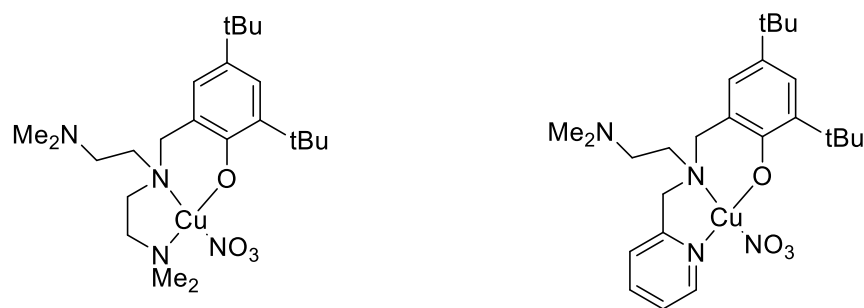


**Figure 9.1.** Proposed air stable copper complexes for *rac*-lactide polymerization.



## **Annexes**



## Supporting information Chapter 2

Daneshmand, P.; Schaper F. Exploring the Reactivity of Manganese(III) Complexes with Diphenolate-diamino Ligands in *rac*-Lactide Polymerization. *Dalton Trans.* **2015**, *44*, 20449-20458.

# Lactide Polymerization Catalyzed by Manganese Complexes

*Pargol Daneshmand, Frank Schaper\**

*Centre in Green Chemistry and Catalysis, Department of chemistry, Université de Montréal, C. P. 6128 Succ. Centre-Ville, Montréal, QC, H3T 3J7, Canada*

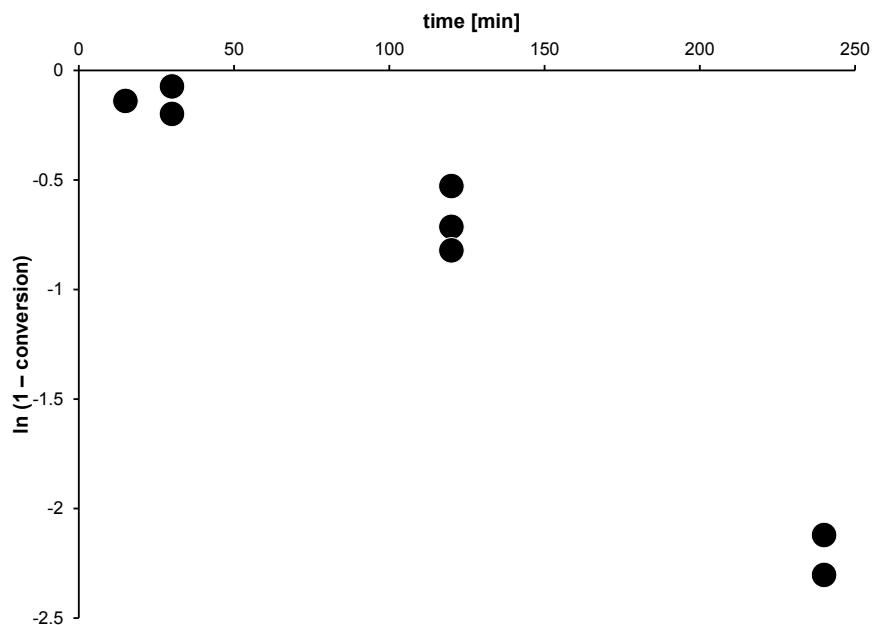


**Figure 2.S1.** Linearized plot (assuming a reaction 1<sup>st</sup> order in lactide) for polymerizations with **2.5a**·MeOH.

**Table 2.S1.** Conversions of all *rac*-lactide polymerization experiments <sup>a</sup>

Catalyst	Alcohol added	Reaction time [min]	Conversion [%]			
			run 1	run 2	run 3	run 4
<b>2.3a</b>		120	49 <sup>c</sup>	53 <sup>d</sup>		
<b>2.3a</b>		240	52 <sup>c</sup>	43 <sup>d</sup>		
<b>2.3a</b>		360	91 <sup>c</sup>	47 <sup>c</sup>	56 <sup>d</sup>	51 <sup>d</sup>
<b>2.3b</b>		240	38	71 <sup>c</sup>		
<b>2.3b</b>		360	48	81 <sup>c</sup>		
<b>2.4a</b> ·MeOH		15	8	7		
<b>2.4a</b> ·MeOH		30	56 <sup>b</sup>	7	5	10
<b>2.4a</b> ·MeOH		60	6			
<b>2.4a</b> ·MeOH		120	7			
<b>2.4a</b> ·MeOH	1 MeOH	15	7	4	18	
<b>2.4a</b> ·MeOH	1 MeOH	30	5	0	0	8
<b>2.4a</b> ·MeOH	2 MeOH	5	4			

<b>2.4a</b> ·MeOH	2 MeOH	15	49	18	4	8
<b>2.4a</b> ·MeOH	2 MeOH	30	47	14		
<b>2.4a</b> ·MeOH	2 MeOH	60	48	17	61	
<b>2.4a</b> ·MeOH	2 MeOH	90	17	27		
<b>2.4a</b> ·MeOH	2 MeOH	120	39	88		
<b>2.4a</b> ·MeOH	2 MeOH	240	30			
<b>2.4a</b> ·MeOH	5 BnOH	60	16	22		
<b>2.4a</b> ·MeOH	5 BnOH	120	32			
<b>2.4a</b> ·MeOH	5 BnOH	240	43			
<b>2.4a</b> ·MeOH	15 BnOH	30	65	37		
<b>2.4a</b> ·MeOH	35 BnOH	30	89	59		
<b>2.4a</b> ·MeOH	95 BnOH	30	97	90		
<b>2.4a</b> ·MeOH	1 NaOMe	60	27			
<b>2.4a</b> ·MeOH	1 NaOMe	120	13			
<b>2.4b</b> ·MeOH	2 MeOH	5	3			
<b>2.4b</b> ·MeOH	2 MeOH	15	4	5		
<b>2.4b</b> ·MeOH	2 MeOH	30	5	4	4	
<b>2.4b</b> ·MeOH	2 MeOH	60	3	7	4	
<b>2.4b</b> ·MeOH	1 NaOMe	120	1			
<b>2.5a</b> ·MeOH		15	13			
<b>2.5a</b> ·MeOH		30	18	7		
<b>2.5a</b> ·MeOH		120	51	41 <sup>c</sup>	56 <sup>d</sup>	
<b>2.5a</b> ·MeOH		240	88	90 <sup>c</sup>	88 <sup>d</sup>	70 <sup>e</sup>
<b>2.5a</b> ·MeOH	5 BnOH	30	17			
<b>2.5a</b> ·MeOH	5 BnOH	60	19	27		
<b>2.5a</b> ·MeOH	5 BnOH	120	30			
<b>2.5a</b> ·MeOH	5 BnOH	240	95			
NaOMe		360	29	38		

<sup>a</sup> Conditions: *rac*-lactide : catalyst = 200:1, sealed tube under N<sub>2</sub>, neat monomer, 130 °C. <sup>b</sup> Outlier, not reported in the main text. <sup>c</sup> *rac*-lactide : catalyst = 100:1. <sup>d</sup> *rac*-lactide : catalyst = 300:1. <sup>e</sup> *rac*-lactide : catalyst = 1000:1.

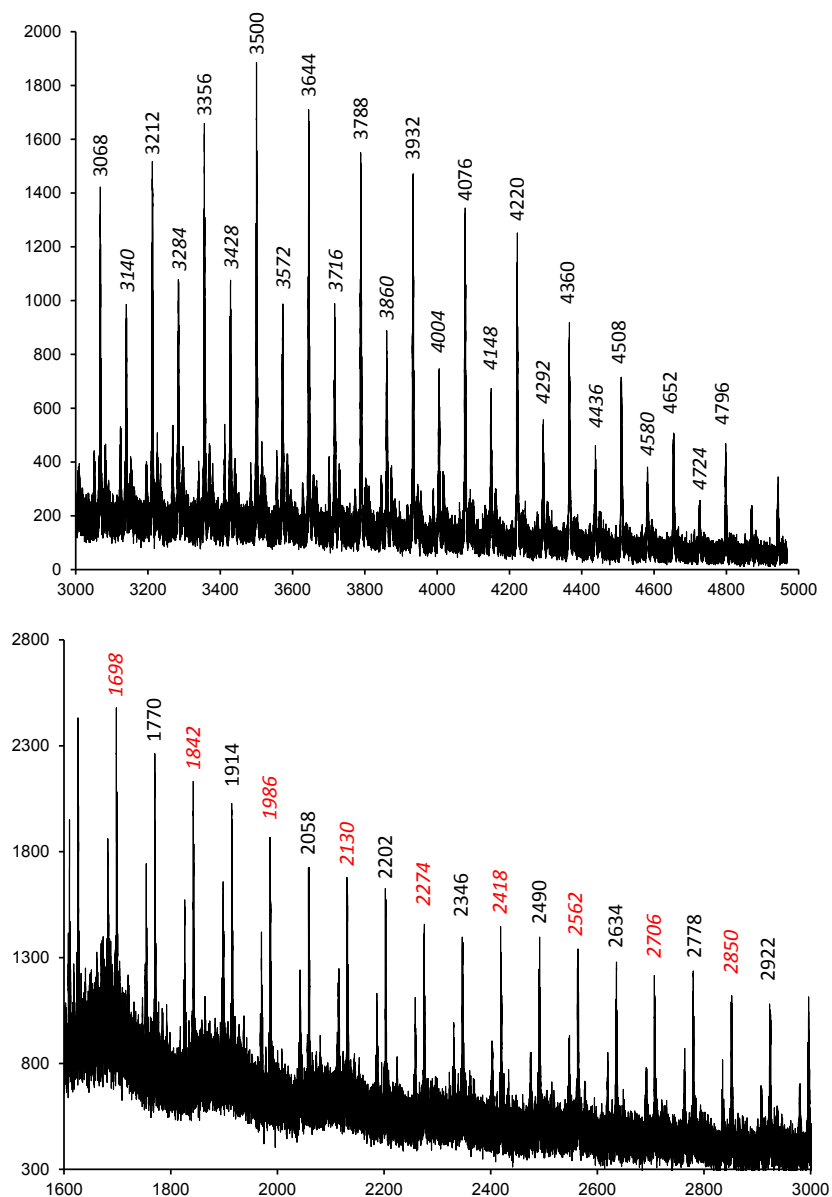


**Figure 2.S2.** MALDI spectra of polymerizations with **2.5a**·MeOH, lactide:catalyst = 100. Top: after 2 h, bottom: after 4 h. Numbers in italics correspond to  $m/z = (n+0.5) \cdot M(\text{lactide})$ , thus polymer resulting from transesterification reactions.  $\text{Na}^+$  was added to the matrix and incorporated in the polymer ion. A second small series with  $\Delta m/z = -16$  was attributed to polymer containing  $\text{Li}^+$  instead of  $\text{Na}^+$ .



**Table 2.S2.** Comparison of calculated elemental analyses from X-ray structural analysis and combustion analyses after drying. Most data indicate partial or total loss of co-crystallized solvent on drying.

Compound	Formula according to X-ray structure	Proposed formula after drying	Combustion analysis
<b>2.3a</b>	$C_{35}H_{57}MnN_2O_3 \cdot MeOH$	$C_{35}H_{57}MnN_2O_3 \cdot MeOH$	C, 67.00;
	C, 67.47; H, 9.60; N, 4.37	C, 67.47; H, 9.60; N, 4.37	H, 9.26; N, 4.44
<b>2.3b</b>		$C_{19}H_{21}Cl_4MnN_2O_3$	C, 43.35;
		C, 43.71; H, 4.05; N, 5.37.	H, 3.67; N, 5.38
<b>2.4a</b> · MeOH	$C_{36}H_{50}ClMnN_2O_2(MeOH) \cdot H_2O$	$C_{36}H_{50}ClMnN_2O_2(MeOH)_{0.5}$	C, 67.72;
	C, 65.04; H, 8.26; N, 4.10	C, 67.53; H, 8.07; N, 4.31.	H, 8.14; N, 4.29
<b>2.4b</b> · MeOH	$C_{21}H_{18}Cl_5MnN_2O_3 \cdot 2 MeOH$	$C_{21}H_{18}Cl_5MnN_2O_3$	C, 43.49;
	C, 42.99; H, 4.08; N, 4.36	C, 43.60; H, 3.14; N, 4.84	H, 2.95; N, 4.62
<b>2.5a</b> · MeOH	$C_{38}H_{57}MnN_2O_4 \cdot MeOH$	$C_{38}H_{57}MnN_2O_4$	C, 69.10;
	C, 67.61; H, 8.87; N, 4.04	C, 69.07; H, 8.69; N, 4.24	H, 8.58; N, 4.34



## Supporting information Chapter 3

Daneshmand, P.; van der Est, A.; Schaper, F. Mechanism and Stereocontrol in Isotactic *rac*-Lactide Polymerization with Copper(II) complexes. *ACS Catal.* **2017**, *7*, 6289–6301.

# Mechanism and Stereocontrol in Isotactic *rac*-Lactide Polymerization with Copper(II) Complexes

*Pargol Daneshmand,<sup>a</sup> Art van der Est,<sup>b</sup> Frank Schaper<sup>a,\*</sup>*

<sup>a</sup> *Centre in Green Chemistry and Catalysis, Department of Chemistry, Université de Montréal, C. P. 6128 Succ. Centre-Ville, Montréal, QC, H3T 3J7, Canada.* <sup>b</sup> *Department of Chemistry, Brock University, St. Catharines, ON, L2S 3A1, Canada.* \* *Email: Frank.Schaper@umontreal.ca*

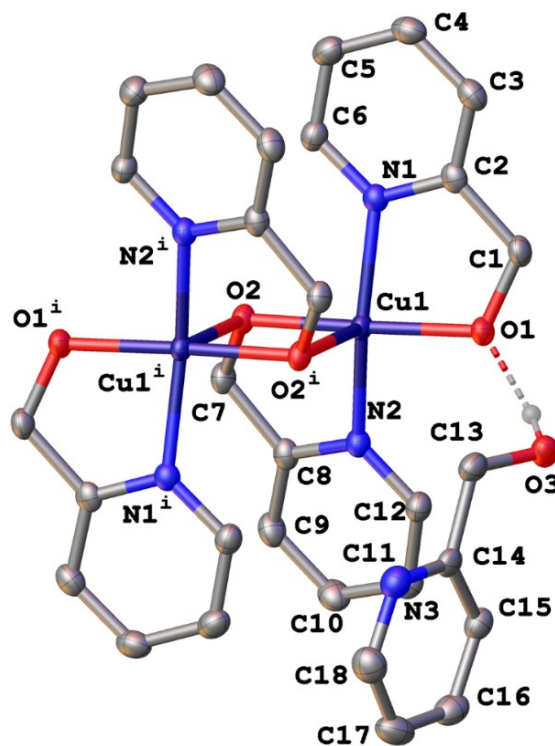


**Figure 3.S1.** Crystal structure of **3.3**. Thermal ellipsoids displayed at the 50% probability level. Hydrogen atoms omitted for clarity.

**Table 3.S1.** Polymerizations with **3.3**.

[ <b>3.3</b> ] <sup>a</sup> (mM)	[lactide] /[ <b>3</b> ]	Addi- tive	[Add.] /[ <b>3.3</b> ]	Conv. (%)	time (h)	$k_{\text{obs}}$ (h <sup>-1</sup> )	$M_n$ , GPC <sup>b</sup> (g/mol)	$M_n$ , calc <sup>c</sup> (g/mol)	chains/ dimer <sup>d</sup>	$M_w/M_n$	$P_m$ <sup>e</sup>
2	100			30	24.5	0.16(1)					0.42- 0.43 0.51- 0.54
2	100			98	28.5	1.07(9)	5800	7200	2.4	2	0.54
2	100			97	3.5		4400	7100	3.2	2.7	0.55
2	100	3.L1	2	0	48						
2	100	3.L1	2	2	48						
2	100	(3.L1) <sub>2</sub>									
2	100	Cu	0.5	4	48						

Conditions: C<sub>6</sub>D<sub>6</sub>, ambient temperature. <sup>a</sup> Concentrations and ratios provided per catalyst dimer, i. e. for 3.L<sub>2</sub>Cu<sub>2</sub>(OR)<sub>2</sub>. <sup>b</sup>  $M_n$  and  $M_w$  determined by size exclusion chromatography vs. polystyrene standards, with a Mark-Houwink correction factor of 0.58. <sup>c</sup>  $M_n$  expected if all alkoxides initiate polymerization, calculated from  $[\text{lactide}]/(2 \cdot [\text{cat.}] + [\text{ROH}]) \cdot \text{conversion} \cdot M_{\text{lactide}} + M_{\text{ROH}}$ . <sup>d</sup> Number of chains per catalyst dimer, calculated from the ratio of expected and obtained polymer molecular weight. <sup>e</sup>  $P_m$  determined from decoupled <sup>1</sup>H NMR by  $P_m = 1 - 2 \cdot I_1/(I_1 + I_2)$ , with  $I_1 = 5.20 - 5.25$  ppm (*rmm*, *mmr/rmm*),  $I_2 = 5.13 - 5.20$  ppm (*mmr/rmm*, *mmm*, *mrm*).

### Variability of the induction period

The observed differences in the induction period were reason for concern, since they cannot be explained by typical polymerization mechanisms. The length of the induction period should depend on the rate of the first insertion(s) into **3.1**. Instead, we found induction periods varying between 4 – 54 min (Table 3.S2). There was no correlation between catalyst concentration, lactide concentration, presence of benzyl alcohol (*vide infra*),  $M_w/M_n$  or other experimental conditions with the length of the induction period. A typical source of experimental error is the presence of protic impurities in the reactions, which might liberate small amounts of pyridyl methanol under formation of inactive hydroxyl copper species. To test the influence free pyridyl methanol has on reaction kinetics, polymerizations were conducted with **3.1** in presence of 0.5 to 2 equiv of pyridyl methanol per catalyst dimer (Fig. 3.S2, Table 3.S3, entries 33-36).

**Table 3.S2.** Induction periods observed in polymerizations with **3.1**.

[ <b>3.1</b> ] / mmol	[lactide] / mmol	[BnOH] / mmol	Induction period <sup>a</sup>	$M_w/M_n$
1	100	0	-15 min	1.5
1	100	0	4 min	1.1
1	300	0	54 min	-
2	200	0	19 min	1.3
2	200	0	21 min	1.7
3	300	0	26 min	-
3	300	0	24 min	1.3
2	200	0.5	57 min	1.1
2	200	1	59 min	1.3
2	200	2	9 min	1.1
1	200	2	72 min	-
2	200	4	7 min	1.1
2	200	8	3 min	1.2

<sup>a</sup> Defined as the intercept of the linear regression line with the *x*-axis in ln conv vs. time plots.

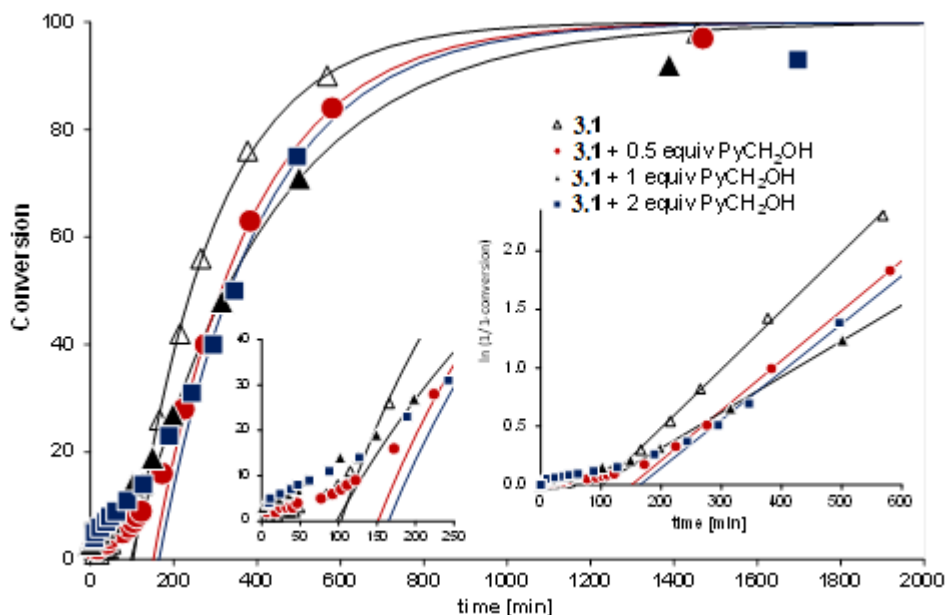


**Figure 3.S2.** Conversion-time profiles of *rac*-lactide polymerizations with **3.1** in the presence of pyridyl methanol.  $[\text{Pyridyl methanol}]/[\mathbf{1}] = 0$  (hollow triangle), 0.5 (circle), 1 (triangle), or 2 (square). Conditions:  $[\mathbf{3.1}] = 2 \text{ mM}$ , lactide/**3.1** = 100:1,  $\text{C}_6\text{D}_6$ , RT.

Increasing amounts of pyridyl methanol led to an increased induction period and slightly reduced rate constants. Notable was also that there was a steep start of polymerization activity in the first 5-10 minutes, which then leveled out for the length of the induction period. These polymerizations were also the only cases where a conversion/time-dependent change in isoselectivity was observed. A reduced isotacticity at low conversions (mostly) recovered at the end of the reaction to the value for typically observed **3.1**. Both effects were more pronounced at higher pyridyl methanol concentrations. The changed reaction kinetics suggest the presence of different active species in the presence of pyridyl methanol. As a chelating alcohol pyridyl methanol might displace the imino pyrrole ligand, at least in small amounts, to generate the homoleptic bis(pyridylmethoxide) complex, **3.3**, and free Ligand **3.L1**. Complex **3.3** was slightly more active in lactide polymerization than **3.1**, with no notable induction period and produced essentially atactic polymer ( $P_m = 0.42 - 0.55$ , Table 3.S1). The proposed effect of free pyridyl methanol on the polymerization is summarized in Figure 3.S3: Free pyridyl methanol (liberated by reaction of **3.1**

with protic impurities), may react with **3.1** to form **3.3**, which does not show an induction period and immediately initiates polymerization to atactic PLA. Since activation of **3.1** is slow, this is the only polymer formed at the beginning of the reaction. After several insertion steps, **3.L1** most likely reacts with the growing polymer chain, to reform **3.1** and polymeryl alcohol, leading to the quenching of the fast initial polymerization. Pyridyl methanol remaining in solution will quench any species obtained by initiation, reforming **3.1** and liberating polymeryl alcohol, and thus prolonging the induction period. Variations of the induction period are thus likely to be the consequence of protic impurities and should not be taken into consideration for the reaction mechanism.

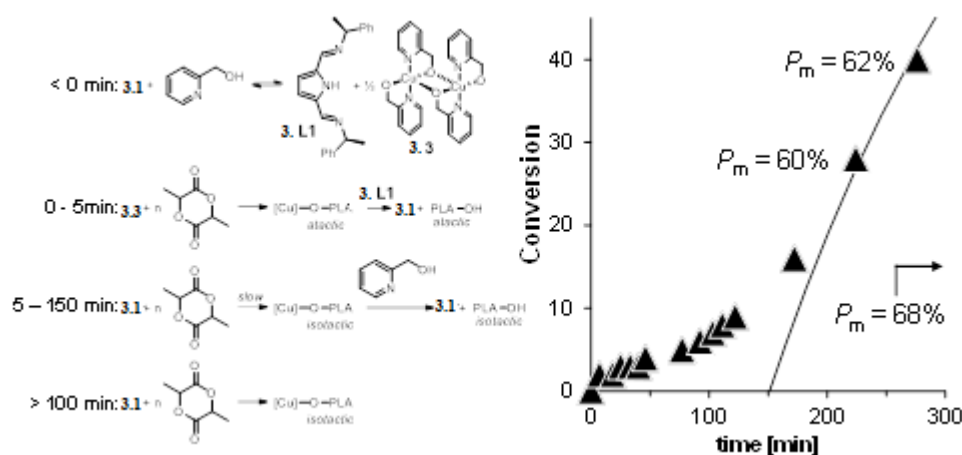


**Figure 3.S3.** Conversion-time plot for rac-lactide polymerization with **3.1** + 0.5 PyCH<sub>2</sub>OH (conditions identical to those in Fig. 3.1).

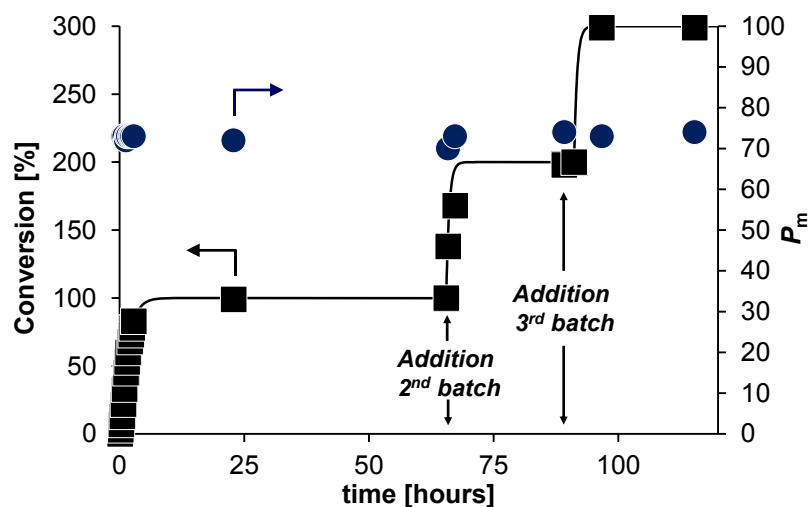


**Figure 3.S4.** Stability of **3.1** under polymerization conditions. Conversion: squares, left axis. Isotacticity ( $P_m$ ): circles, right axis. Conditions:  $[3.1] = 3 \text{ mM}$ ,  $\text{C}_6\text{D}_6$ , RT, lactide additions: 100 equiv at  $t = 0 \text{ h}$ , 100 equiv at  $t = 72 \text{ h}$ , 200 equiv at  $t = 96 \text{ h}$ .

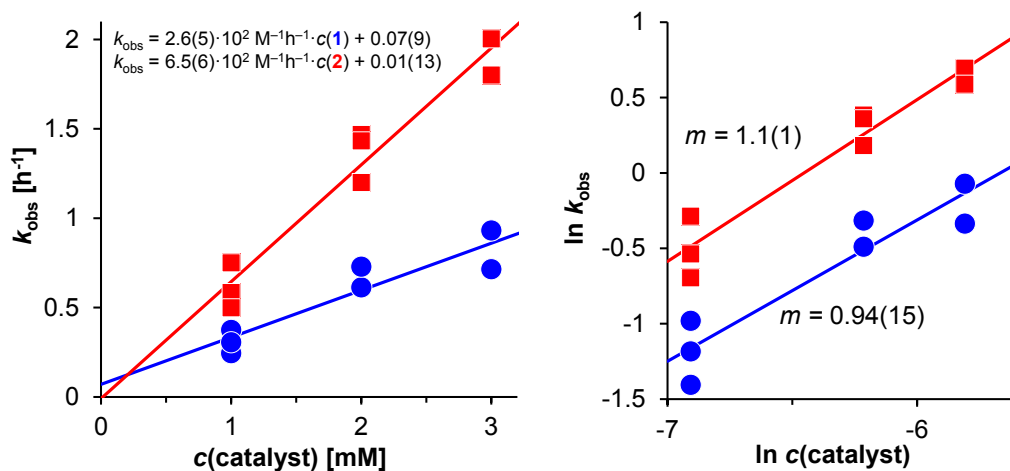


**Figure 3.S5.** Dependence of pseudo-first order rate constants on the concentration of **3.1** or **3.2**. Left: Plot of  $k_{\text{obs}}$  vs.  $[3.1]$  or  $[3.2]$ , respectively, shows a linear relationship. Right: Double-logarithmic plot, the slope confirms first-order dependence on catalyst concentration.



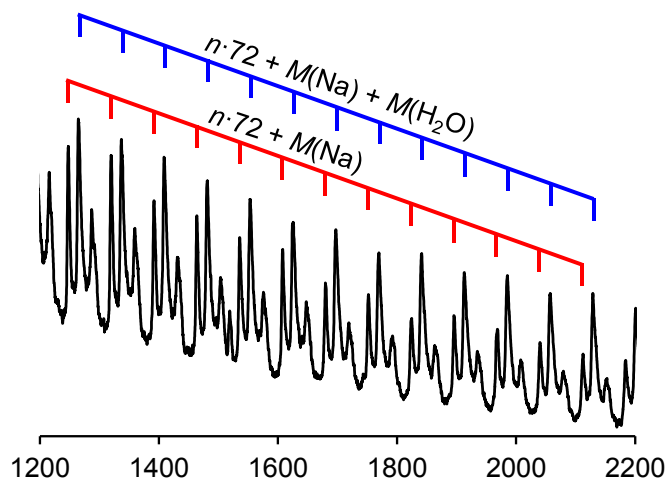


**Figure 3.S6.** MALDI of PLA obtained with **3.2** ( $[3.2] = 2 \text{ mM}$ ,  $[\text{lactide}] = 200 \text{ mM}$ ). A series of  $m/z$  for cyclic oligomers ( $n \cdot 72 + M(\text{Na})$ , in red) and of hydrolysis products ( $n \cdot 72 + M(\text{Na}) + M(\text{H}_2\text{O})$ , in blue) is observed, together with small peaks of an unidentified series of  $(n \cdot 72 + M(\text{Na}) + 40$  or  $n \cdot 72 + 63)$ .

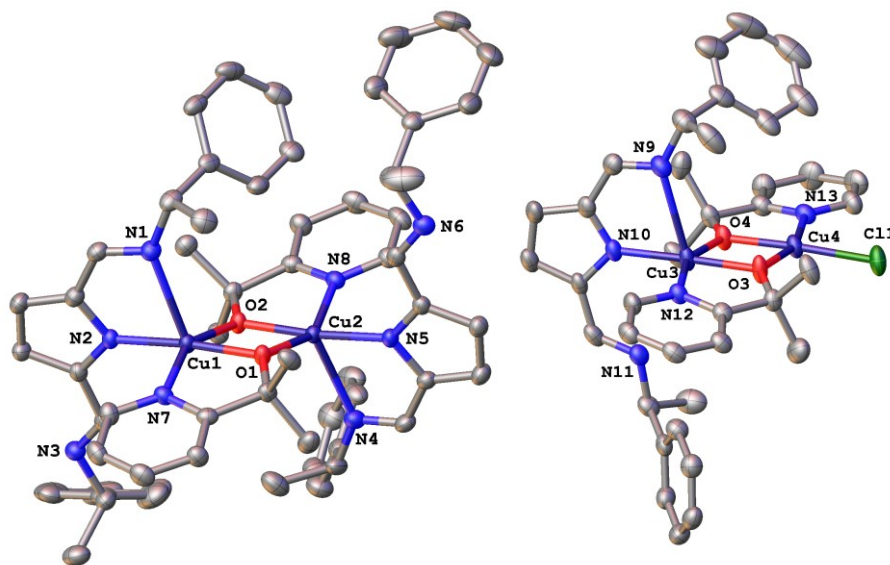
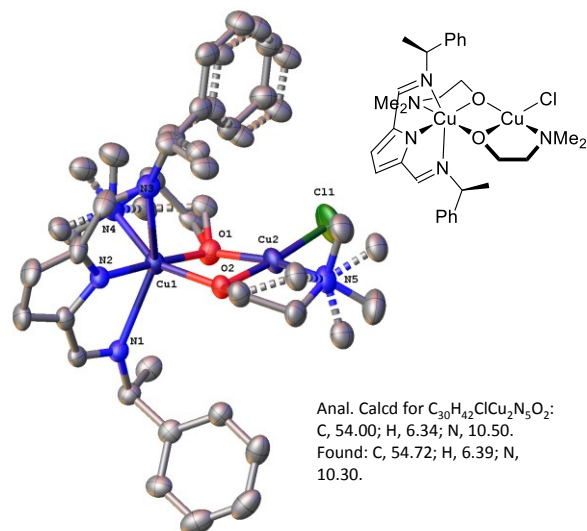


**Figure 3.S7.** Crystal structure of both co-crystallized complexes in **3.5**. Thermal ellipsoids are drawn at the 50% probability level. Hydrogen atoms omitted for clarity.



The co-cocrystallized chloro complex is unlikely to influence polymerization behaviour. An analogous complex with dimethylamino ethoxide as the bridging ligand (see below) was isolated and characterized previously.<sup>1</sup> The complex did not show any activity in lactide polymerization (no conversion after 48 h, 2 mM catalyst, 200 mM lactide, RT,  $C_6D_6$ ).

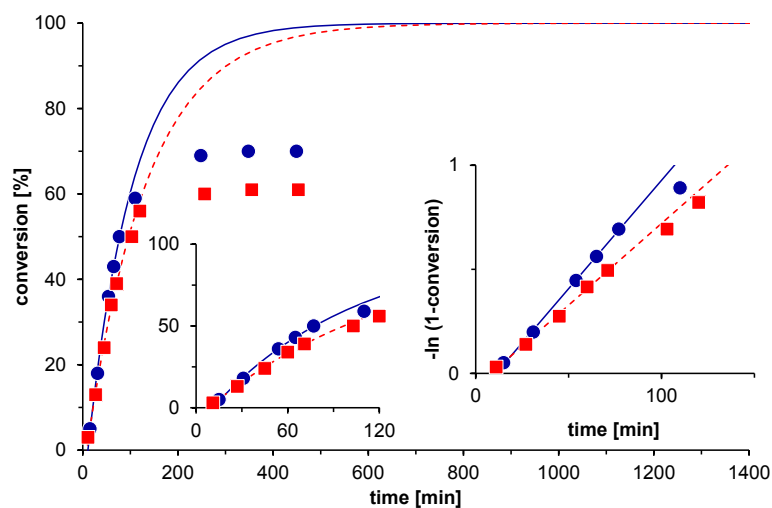


**Figure 3.S8.** Conversion-time profiles of polymerizations with **3.8**.

Conditions: 2 mM **3.8**, 200 mM *rac*-lactide,  $C_6D_6$ , RT (circles); idem + 4 mM  $Ph_3COH$  (squares).

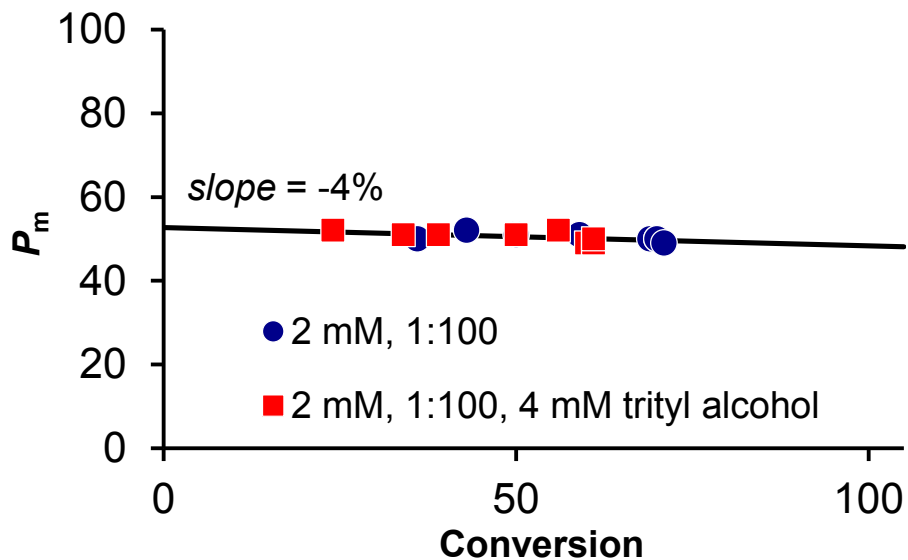


**Figure 3.S9.** Stereocontrol in polymerizations with 3.8.

Conditions: 2 mM 3.8, 200 mM *rac*-lactide,  $C_6D_6$ , RT (circles); idem + 4 mM  $Ph_3COH$  (squares).

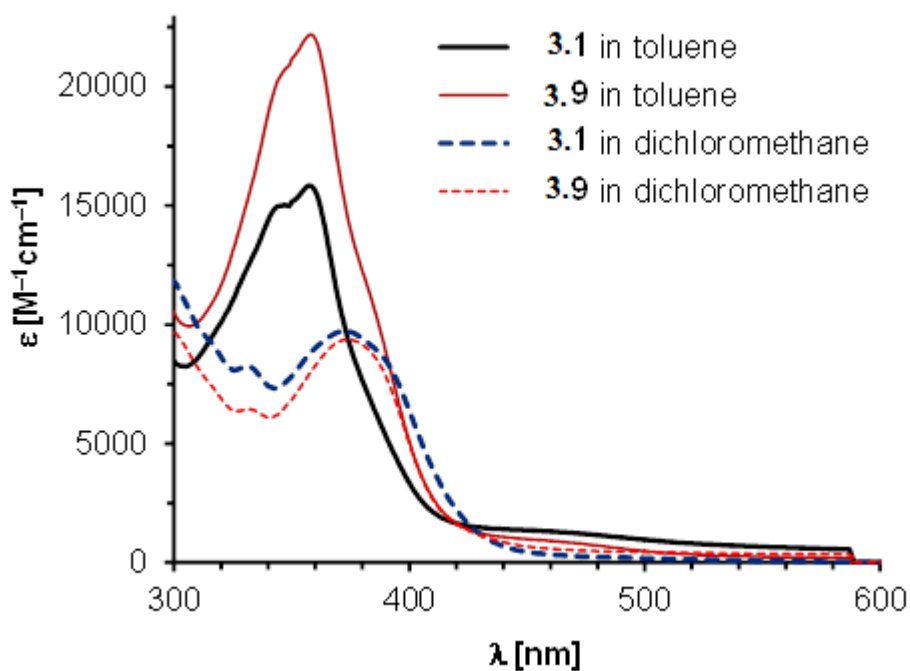


**Figure 3.S10.** UV/vis spectra of 3.1 and 3.9 in either toluene (thick lines) or dichloromethane (thin, dotted lines)

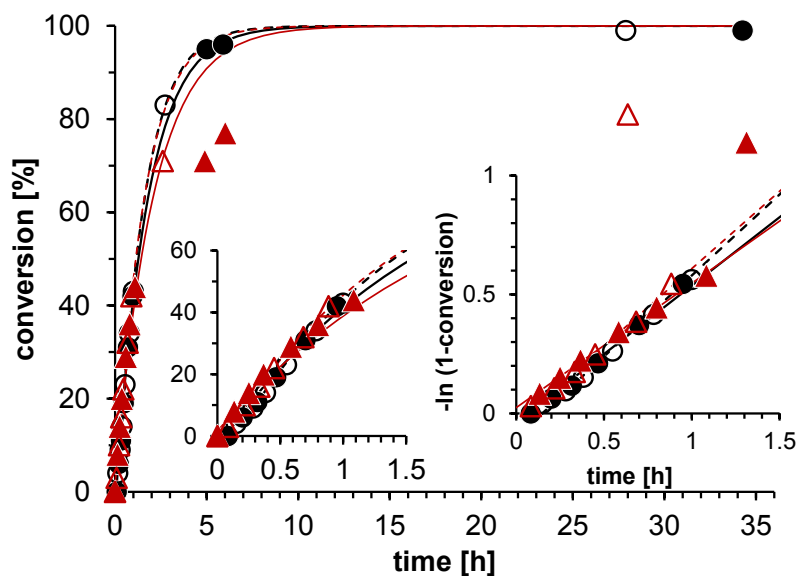


**Figure 3.S11.** Conversion-time profiles of polymerizations with **3.9** (black circles) and **3.10** (red triangles). Conditions: [**3.9**], [**3.10**] = 2 mM, [lactide] = 200 mM, C<sub>6</sub>D<sub>6</sub>, RT. Evidence for catalyst decomposition in polymerizations with **3.10**.

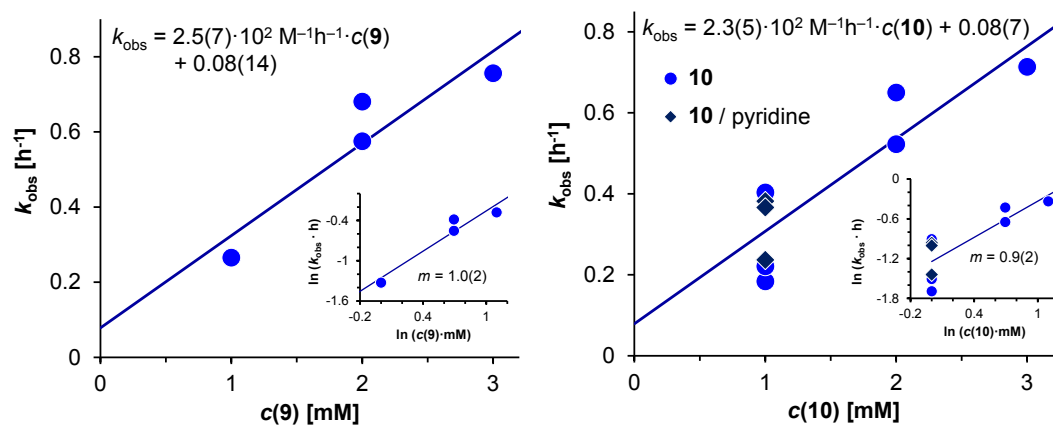


**Figure 3.S12.** Dependence of pseudo-first order rate constants on concentration of **3.9** or **3.10**. Left: Plot of  $k_{\text{obs}}$  vs. [**3.9**] with linear regression. The inset shows the log-log plot of pseudo-first order rate constants vs. catalyst concentration, with a slope of 1.0(2). Right: Plot of  $k_{\text{obs}}$  vs. [**3.10**] (circles) and [**3.10**] in the presence of pyridine (diamonds). The linear regression uses displayed values. The inset shows the log-log plot of pseudo-first order rate constants vs. catalyst concentration and yields a slope of 0.9(2). Results agree with first-order dependence on catalyst concentration for **3.9** and **3.10**.

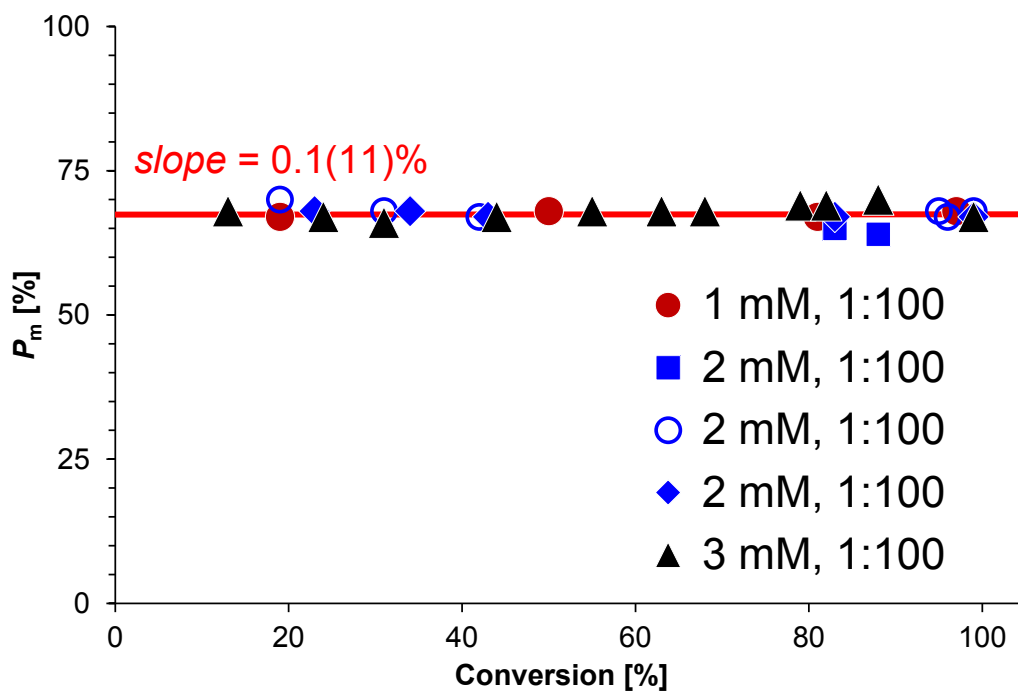


**Figure 3.S13.** Dependence of stereocontrol ( $P_m$ ) on conversion in polymerizations with 3.9.

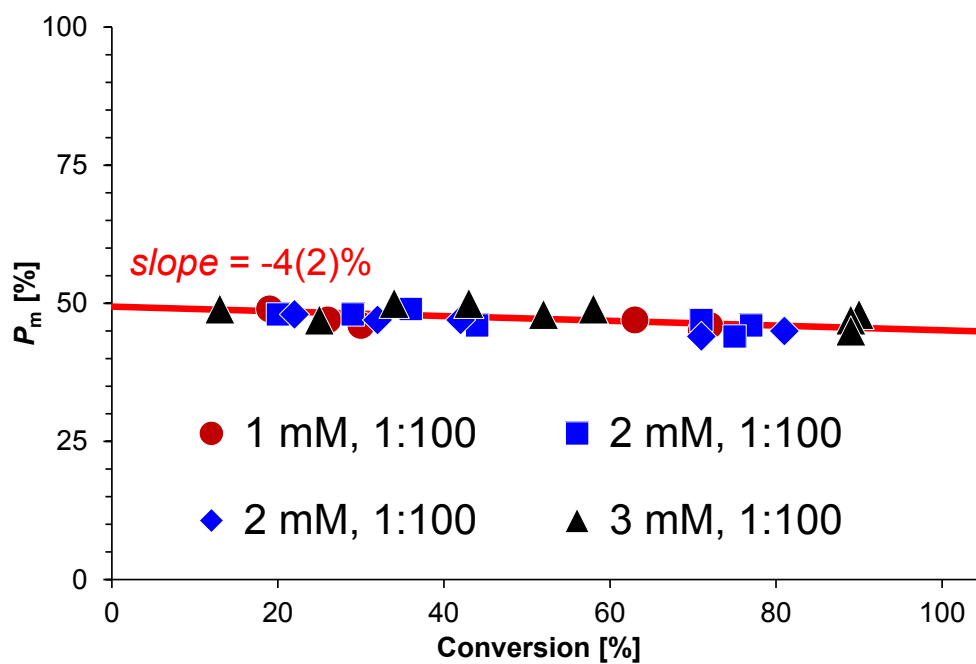


**Figure 3.S14.** Dependence of stereocontrol ( $P_m$ ) on conversion polymerizations with 3.10.

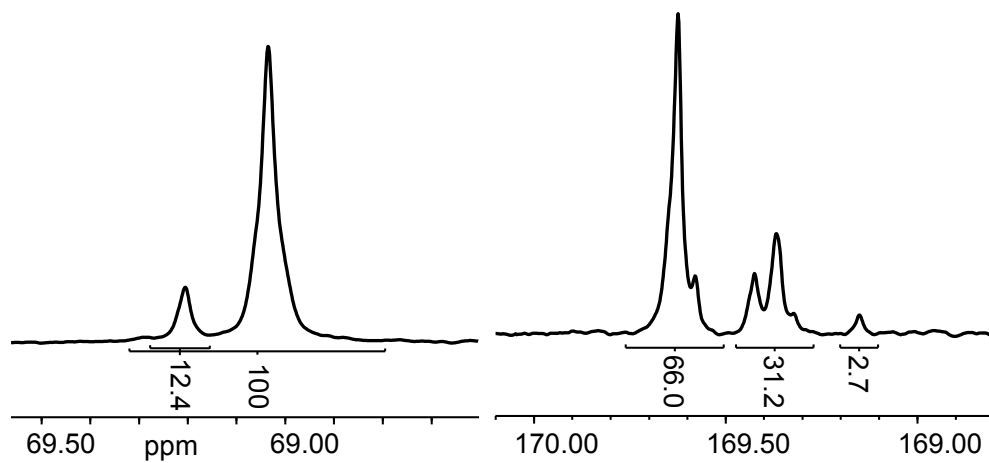


**Figure 3.S15.**  $^{13}\text{C}\{^1\text{H}\}$ -NMR of the methine and the carbonyl region of PLA produced with **3.6**. Data was obtained on a Bruker AV500 spectrometer.

Table 3.S3. Polymerizations with 3.1

Entry	[3.1] <sup>a</sup> (mM)	[lactide] / [3.1]	Additive	[additive] / [3.1]	Conversion (%)	time (h)	$k_{\text{obs}}$ (h <sup>-1</sup> )	$M_{\text{n, GPC}}$ <sup>b</sup> (g/mol)	$M_{\text{n, calc}}$ <sup>c</sup> (g/mol)	chains / dimer <sup>d</sup>	$M_{\text{w}}/M_{\text{n}}$	$P_{\text{m}}$ <sup>e</sup>
1	1	100			97	29	0.375(4)	10000	7100	1.4	1.5	0.73±0.01
2	1	100			94	28.5	0.245(5)	25600	6900	0.5	1.1	0.71-0.75
3	1	100			98	26.5		24400	7200	0.6	1.2	n. d.
4	1	100			97	21		18000	7100	0.8	1.2	0.73
5	1	300			99	20	0.306(5)				0	0.69-0.73
6	2	100			99	23	0.61(1)	10500	7200	1.4	1.7	0.70-0.72
7	2	100			99	23.5	0.73(1)	30400	7200	0.5	1.3	0.72-0.76
8	2	100			99	20.5		23400	7200	0.6	1.3	0.71
9	2	100			99	26.5	0.052(7)	20200	7200	0.7	1.3	0.7
10	3	100			99	16	0.93(5)	26800	7200	0.5	1.3	0.70-0.74
11	3	100			99	23	0.71(2)				0	0.73
12		+ 100 <sup>f</sup>			+ 99 <sup>f</sup>	+ 23.5 <sup>f</sup>					0	0.73
13		+ 200 <sup>f</sup>			+ 99 <sup>f</sup>	+ 24 <sup>f</sup>		400	14400	151	145	0.73
14	2	100	PhCH <sub>2</sub> OH	0.25	99	23	0.35(1)	13200	6400	1.1	1.1	0.67-0.72
15	2	100	PhCH <sub>2</sub> OH	0.5	99	23	0.287(5)	10700	5800	1.3	1.1	0.65-0.71
16	2	100	PhCH <sub>2</sub> OH	1	89	2.5	0.89(1)			2	1.1	0.70-0.72
17	2	100	PhCH <sub>2</sub> OH	2	99	20	0.618(4)	6600	4400	3.1	1.1	0.67-0.71
18	2	100	PhCH <sub>2</sub> OH	4	98	26	0.56(1)	4700	3700	7.2	1.2	0.68-0.70
19	2	100	PhCH <sub>2</sub> OH	4	98	17	0.185(7)	2000	2500	6.8	1.1	0.70-0.71
20	1	200	PhCH <sub>2</sub> OH	2	98	21	0.46(2)	2100	2500			0.64-0.72
21	2	100	Ph <sub>3</sub> COH	0.5	98	22	0.58(1)	12000	7200	1.2	1.2	0.68-0.71
22	2	100	Ph <sub>3</sub> COH	0.5	98	21.5	0.96(1)	15500	7200	0.9	1.2	0.71
23	2	100	Ph <sub>3</sub> COH	0.5	99	22		15500	7200	0.9	1.2	0.71
24	2	100	Ph <sub>3</sub> COH	1	98	22.5		10300	7200	1.4	1.3	0.70-0.73
25	2	100	Ph <sub>3</sub> COH	1	98	22.5	0.8	13000	7200	1.1	1.3	0.64-0.73
26	2	100	Ph <sub>3</sub> COH	1	98	22	0.76(3)	14500	7200	1	1.2	0.70-0.72

Table 3.S3 continued...

Entry	[3.1] <sup>a</sup> (mM)	[lactide] /[3.1]	Additive	[additive] /[3.1]	Conversion (%)	time (h)	$k_{\text{obs}}$ (h <sup>-1</sup> )	$M_{\text{n, GPC}}^{\text{b}}$ (g/mol)	$M_{\text{n, calc}}^{\text{c}}$ (g/mol)	chains / dimer <sup>d</sup>	$M_{\text{w}}/M_{\text{n}}$	$P_{\text{m}}^{\text{e}}$
27	2	100	Ph <sub>3</sub> COH	2	98	22	0.82(1)	14000	7200	1	1.2	0.7
28	2	100	Ph <sub>3</sub> COH	2	98	22	0.50(1)	9400	7200	1.5	1.2	0.68-0.71
29	2	100	Ph <sub>3</sub> COH	2	98	22		13700	7200	1	1.2	0.72
30	2	100	pyridine	5	98	38	0.270(5)	11900	7200	1.2	1.2	0.65-0.71
31	2	100	pyridine	5	98	25	0.364(8)	12300	7200	1.2	1.2	0.71-0.72
32	2	100	pyridine	10	0	24						
33	2	100	PyCH <sub>2</sub> OH	0	98	24.5	0.30(1)	11600	7200	1.2	1.3	0.68-0.71
34	2	100	PyCH <sub>2</sub> OH	0.5	97	24.5	0.256(4)	7900	5700	1.8	1.2	0.60-0.68
35	2	100	PyCH <sub>2</sub> OH	1	92	23	0.183(4)	5200	4500	2.6	1.2	0.45-0.63
36	2	100	PyCH <sub>2</sub> OH	2	93	28.5	0.25(2)	3700	3500	3.6	1.2	0.38-0.64
37	1	100	CH <sub>2</sub> Cl <sub>2</sub> <sup>g</sup>	1	50	29		9300	3700	0.8	1.2	0.6
38	2	100	CH <sub>2</sub> Cl <sub>2</sub> <sup>g</sup>	1	99	25				0.8	1.4	0.60-0.61
39	2	100	CH <sub>2</sub> Cl <sub>2</sub> <sup>g</sup>	1	99	25.5		17400	7200	0.8	1.5	0.55-0.60
40	3	100	CH <sub>2</sub> Cl <sub>2</sub> <sup>g</sup>	1	99	22	0.82(1)	17300	7200	0.8	1.7	0.56-0.60
41	3	100	CH <sub>2</sub> Cl <sub>2</sub> <sup>g</sup>	1	99	22.5	0.73(1)	17300	7200	0.9	1.7	0.59
42	2	100	CH <sub>2</sub> Cl <sub>2</sub> as solvent		79	24.5	0.2	16700	7200	0.8	1.4	0.39-0.49
43	2	100	THF as solvent		92	5.5	0.4	2200	5800	5.3	1.2	0.44-0.50

Conditions: C<sub>6</sub>D<sub>6</sub>, ambient temperature. <sup>a</sup> Concentrations and ratios provided per catalyst dimer, i. e. for 3.L<sub>2</sub>Cu<sub>2</sub>(OR)<sub>2</sub>. <sup>b</sup>  $M_{\text{n}}$  and  $M_{\text{w}}$  determined by size exclusion chromatography vs. polystyrene standards, with a Mark-Houwink correction factor of 0.58. <sup>c</sup>  $M_{\text{n}}$  expected if all alkoxides initiate polymerization, calculated from  $[\text{lactide}]/(2 \cdot [\text{cat.}] + [\text{ROH}]) \cdot \text{conversion} \cdot M_{\text{lactide}} + M_{\text{ROH}}$ . <sup>d</sup> Number of chains per catalyst dimer, calculated from the ratio of expected and obtained polymer molecular weight. <sup>e</sup>  $P_{\text{m}}$  determined from decoupled <sup>1</sup>H NMR by  $P_{\text{m}} = 1 - 2 \cdot I_1/(I_1 + I_2)$ , with  $I_1 = 5.20 - 5.25$  ppm (*rmr*, *mmr/rmm*),  $I_2 = 5.13 - 5.20$  ppm (*mmr/rmm*, *mmm*, *mrm*). <sup>f</sup> Three batches of *rac*-lactide were added successively. <sup>g</sup> Complex contained co-crystallized dichloromethane.



Table 3.S4. Polymerizations with 3.2.

Entry	[3.2] <sup>a</sup> (mM)	[lactide] / [3.2]	Additive	[additive] / [3.2]	Conversion (%)	time (h)	$k_{\text{obs}}$ (h <sup>-1</sup> )	$M_{\text{n, GPC}}^{\text{b}}$ (g/mol)	$M_{\text{n, calc}}^{\text{c}}$ (g/mol)	chains / dimer <sup>d</sup>	$M_{\text{w}}/M_{\text{n}}$	$P_{\text{m}}^{\text{e}}$
1	1	100		0	98	17	0.75(2)	3100	7200	4.6	1.1	0.46-0.48
2	1	100		0	96	17.5	0.58(1)	5800	7000	2.4	1.2	0.46-0.49
3	1	300		0	62	19.5	0.50(2)					
4	2	100		0	99	4	1.47(9)	3100 <sup>f</sup>	7200	4.6	1.1	0.48-0.50
5	2	100		0	99	4	1.43(6)	6600	7200	2.2	1.2	0.48-0.49
6	2	100		0	99	26	1.20(6)	6000	7200	2.4	1.3	0.44-0.47
7	3	100		0	99	4	1.80(4)	3100	7200	4.6	1.2	0.45-0.48
8	3	100		0	95	15.5	2.00(4)	6900	6900	2	1.5	0.45-0.50
9	1	200	pyridine	1	81	34	0.55(3)					0.41-0.44
10	1	200	pyridine	5	57	32	0.26(1)					0.39-0.41
11	1	200	pyridine	10	70	27	0.289(7)					0.45-0.50
12	1	100	PhCH <sub>2</sub> OH	4	98	26	1.4(1)	1400	2500	10.3	1.3	0.47-0.50
13	2	100	PhCH <sub>2</sub> OH	0.25	97	3.5	1.47(1)	6000	6300	2.3	1.3	0.46-0.48
14	2	100	PhCH <sub>2</sub> OH	0.5	99	24	1.19(3)	5100	5800	2.8	1.2	0.44-0.46
15	2	100	PhCH <sub>2</sub> OH	1	98	18	0.92(4)	5200	4800	2.8	1.1	0.43-0.46
16	2	100	PhCH <sub>2</sub> OH	2	96	24.5	0.67(3)	2600	3600	5.3	1.1	0
17	2	100	PhCH <sub>2</sub> OH	2	99	20	1.06(4)	2800	3700	5.1	1.1	0.45-0.46
18	2	100	PhCH <sub>2</sub> OH	4	94	16.5	0.6	1700	2400	8.2	1.1	0.45-0.48
19	1	200	PyCH <sub>2</sub> OH	0.5	83	20.5	0.355(3)					0.47-0.51
20	1	200	PyCH <sub>2</sub> OH	1	99	19.5	0.636(5)					0.57-0.66
21	2	100	PyCH <sub>2</sub> OH	1	99	32.5	1.4(1)	5200	4900	2.8	1.2	0.59-0.60
22	2	100	PyCH <sub>2</sub> OH	1	96	27.5	0.900(2)	6300	4700	2.2	1.2	0.58-0.59
23	2	100	PyCH <sub>2</sub> OH	1	95	20.5	0.54(1)	5500	4700	2.5	1.2	0.58-0.60
24	2	100	PyCH <sub>2</sub> OH	1.5	95	27.5	0.62(1)	5600	4000	2.5	1.2	0.61-0.63

Table 3.S4 continued...

Entry	[3.2] <sup>a</sup>	[lactide]	Additive	[additive]	Conversion (%)	time (h)	$k_{\text{obs}}$ (h <sup>-1</sup> )	$M_{\text{n, GPC}}$ <sup>b</sup> (g/mol)	$M_{\text{n, calc}}$ <sup>c</sup> (g/mol)	chains / dimer <sup>d</sup>	$M_{\text{w}}/M_{\text{n}}$	$P_{\text{m}}$ <sup>e</sup>
	(mM)	/ [3.2]		/ [3.2]								
25	2	100	PyCH <sub>2</sub> OH	2.3	98	19	0.5	4600	3400	3.1	1.2	0.61-0.66
26	2	100	Hydroxy-quinoline	0	98	26.5	0.392(7)	5400	7200	2.6	1.2	
27	2	100	Hydroxy-quinoline	0.5	50	25	0.2	3000	3000	2.4	1.1	0.41-0.44
28	2	100	Hydroxy-quinoline	1	0	24						
29	2	100	CH <sub>2</sub> Cl <sub>2</sub> as solvent	0	88	5.5		7300	6400	1.8	1.1	0.32-0.44
30	2	100	THF as solvent	0	63	5.5		1500	4600	6	1.2	0.39-0.47

Conditions: C<sub>6</sub>D<sub>6</sub>, ambient temperature. <sup>a</sup> Concentrations and ratios provided per catalyst dimer, i. e. for 3.L<sub>2</sub>Cu<sub>2</sub>(OR)<sub>2</sub>. <sup>b</sup>  $M_{\text{n}}$  and  $M_{\text{w}}$  determined by size exclusion chromatography vs. polystyrene standards, with a Mark-Houwink correction factor of 0.58. <sup>c</sup>  $M_{\text{n}}$  expected if all alkoxides initiate polymerization, calculated from  $[\text{lactide}]/(2 \cdot [\text{cat.}] + [\text{ROH}]) \cdot \text{conversion} \cdot M_{\text{lactide}} + M_{\text{ROH}}$ . <sup>d</sup> Number of chains per catalyst dimer, calculated from the ratio of expected and obtained polymer molecular weight. <sup>e</sup>  $P_{\text{m}}$  determined from decoupled <sup>1</sup>H NMR by  $P_{\text{m}} = 1 - 2 \cdot I_1 / (I_1 + I_2)$ , with  $I_1 = 5.20 - 5.25$  ppm (*rmr*, *mmr/rmm*),  $I_2 = 5.13 - 5.20$  ppm (*mmr/rmm*, *mmm*, *rrm*). <sup>f</sup> Value not shown in Fig. 3.2.

Table 3.S5. Polymerizations with 3.5, 3.6, 3.8 - 3.11

Entry	Catalyst	[cat.] <sup>a</sup>	[lactide] / [cat.]	Additive (equiv / [cat])	Conversion (%)	time (h)	$k_{\text{obs}}$ (h <sup>-1</sup> )	$M_{\text{n, GPC}}^{\text{b}}$ (g/mol)	$M_{\text{n, calc}}^{\text{c}}$ (g/mol)	chains/dimer <sup>d</sup>	$M_{\text{w}}/M_{\text{n}}$	$P_{\text{m}}^{\text{e}}$
1	<b>3.5</b>	2 mM	100		0	21						
2	<b>3.5</b>	3 mM	100		0	26.5						
3	<b>3.6</b>	2 mM	100		97	26.5	0.132(7)	14800	7100	0.9	1.1	0.73-0.75
4	<b>3.6</b>	2 mM	100		98	17		23100	7200	0.6	1.2	0.75
	<b>3.1 +</b>											
5	<b>3.2</b>	2 mM	100		99	26	0.868(9)	12500	7200	1.2	1.2	0.55-0.58
6	<b>3.8</b>	2 mM	100		71	25	0.62(1)	6800	5200	1.5	1.2	0.49-0.52
7	<b>3.8</b>	2 mM	100	Ph <sub>3</sub> COH (2)	61	7.5	0.47(1)	6100	4500	1.5	1.1	0.49-0.52
8	<b>3.9</b>	1 mM	100		97	31	0.265(4)	11200	7100	1.3	1.5	0.67-0.68
9	<b>3.9</b>	2 mM	100		99	34.5	0.58(2)	7300	7200	2	1.4	0.67-0.70
10	<b>3.9</b>	2 mM	100		99	28	0.68(1)	27900	7200	0.5	1.4	0.67-0.68
11	<b>3.9</b>	2 mM	100		88	46.5		13000	6400	1	1.2	0.64-0.65
12	<b>3.9</b>	3 mM	100		99	23	0.76(3)	7000	7200	2	1.5	0.66-0.70
13	<b>3.9</b>	1 mM	200	PhCH <sub>2</sub> OH (2)	98	21	0.51(1)					0.61-0.66
14	<b>3.9</b>	2 mM	100	PhCH <sub>2</sub> OH (4)	99	26.5	0.501(6)	2700	2500	5.2	1.2	0.64-0.70
15	<b>3.10</b>	1 mM	25		90	32	0.18(3)					
16	<b>3.10</b>	1 mM	25		91	29.5	0.22(1)					
17	<b>3.10</b>	1 mM	100		72	30.5	0.40(1)	3500	5300	3	1.1	0.45-0.47
18	<b>3.10</b>	2 mM	100		75	34.5	0.52(1)	3300	5500	3.3	1.1	0.44-0.49
19	<b>3.10</b>	2 mM	100		81	28	0.65(2)	7300	5900	1.6	1.3	0.44-0.47
20	<b>3.10</b>	3 mM	100		89	22.5	0.71(1)	6000	6500	2.1	1.1	0.45-0.50
21	<b>3.10</b>	1 mM	200	PyCH <sub>2</sub> OH(0.5)	41	20.5	0.216(9)					0.46-0.49

Table 3.S5 continued...

Entry	Catalyst	[cat.] <sup>a</sup>	[lactide] /[cat.]	Additive (equiv /[cat])	Conversion (%)	time (h)	$k_{\text{obs}}$ (h <sup>-1</sup> )	$M_{n, \text{GPC}}$ (g/mol)	$M_{n, \text{calc}}$ (g/mol)	chains/ dimer <sup>d</sup>	$M_w/M_n$	$P_m$ <sup>e</sup>
22	<b>3.10</b>	1 mM	200	PyCH <sub>2</sub> OH (1)	83	19.5	0.395(1)					0.55-0.60
23	<b>3.10</b>	2 mM	100	PyCH <sub>2</sub> OH (1)	97	33	0.78(1)	4800	4800	2.9	1.1	0.58-0.60
24	<b>3.10</b>	2 mM	100	PyCH <sub>2</sub> OH (1)	95	25.5	0.47(2)					0.49-0.58
25	<b>3.10</b>	1 mM	200	Pyridine (1)	55	34	0.382(4)					0.40-0.45
26	<b>3.10</b>	1 mM	200	Pyridine (5)	53	32	0.366(12)					0.39-0.42
27	<b>3.10</b>	1 mM	200	Pyridine (10)	50	27	0.237(7)					0.37-0.41
28	<b>3.11</b>	1 mM	100		95	20	0.288(9)	11000	6900	1.2	1.3	0.62-0.64
29	<b>3.11</b>	1 mM	200		98	24.5	0.461(5)					0.57-0.58
30			+200	2 <sup>nd</sup> batch	95	+24						
31			+25	3 <sup>rd</sup> batch	94	+25						
32	<b>3.11</b>	2 mM	100		99	10	1.29(1)	16900	7200	0.8	2.2	0.62-0.64
33	<b>3.11</b>	3 mM	100		99	13.5	1.10(5)					0.59-0.61
34			+100	2 <sup>nd</sup> batch	99	+25						0.60-0.63
35			+200	3 <sup>rd</sup> batch	99	+24		17100	14400	1.7	2.4	0.62-0.65
36	<b>3.11</b>	2 mM	100	PyCH <sub>2</sub> OH(0.25)	99	6	1.32(6)	8500	6400	1.7	1.3	0.60-0.65
37	<b>3.11</b>	2 mM	100	PyCH <sub>2</sub> OH(0.5)	99	6	1.35(4)	7900	5800	1.8	1.3	0.59-0.64
38	<b>3.11</b>	2 mM	100	PyCH <sub>2</sub> OH (1)	99	17	0.88(1)	6800	4900	2.1	1.1	0.62-0.66
39	<b>3.11</b>	2 mM	100	PyCH <sub>2</sub> OH (2)	99	19.5	1.13(4)	4200	3700	3.4	1.1	0.58-0.61
40	<b>3.11</b>	2 mM	100	PyCH <sub>2</sub> OH (4)	99	18	0.69(1)	2600	2500	5.5	1.1	0.56-0.59

Conditions: C<sub>6</sub>D<sub>6</sub>, ambient temperature. <sup>a</sup> Concentrations and ratios provided per catalyst dimer, i. e. for 3.L<sub>2</sub>Cu<sub>2</sub>(OR)<sub>2</sub>. <sup>b</sup>  $M_n$  and  $M_w$  determined by size exclusion chromatography vs. polystyrene standards, with a Mark-Houwink correction factor of 0.58. <sup>c</sup>  $M_n$  expected if all alkoxides initiate polymerization, calculated from  $[\text{lactide}]/(2 \cdot [\text{cat.}] + [\text{ROH}]) \cdot \text{conversion} \cdot M_{\text{lactide}} + M_{\text{ROH}}$ . <sup>d</sup> Number of chains per catalyst dimer, calculated from the ratio of expected and obtained polymer molecular weight. <sup>e</sup>  $P_m$  determined from decoupled <sup>1</sup>H NMR by  $P_m = 1 - 2 \cdot I_1/(I_1 + I_2)$ , with  $I_1 = 5.20 - 5.25$  ppm (*rmr*, *mmr/rmm*),  $I_2 = 5.13 - 5.20$  ppm (*mmr/rmm*, *mmm*, *mrm*).

### Additional details on complex purification

Several complexes gave unsatisfying elemental analysis ( $\Delta C = 0.8\text{-}2\%$ ), even though crystalline material was obtained and structures were verified by X-ray diffraction for each batch of catalyst. Analytically pure samples were obtained by recrystallisation from dichloromethane/hexane mixtures, but elemental analysis and NMR indicated the presence of remaining dichloromethane in some cases despite prolonged drying. An X-ray structure of a dichloromethane adduct of **3.1** was obtained in one case. Co-crystallized dichloromethane was shown to negatively effect stereocontrol (see section on solvent dependence). Where NMR or elemental analysis indicated the presence of dichloromethane, polymerization experiments were thus performed using the crystalline material obtained prior to recrystallisation, even if elemental analysis indicated slight impurities.

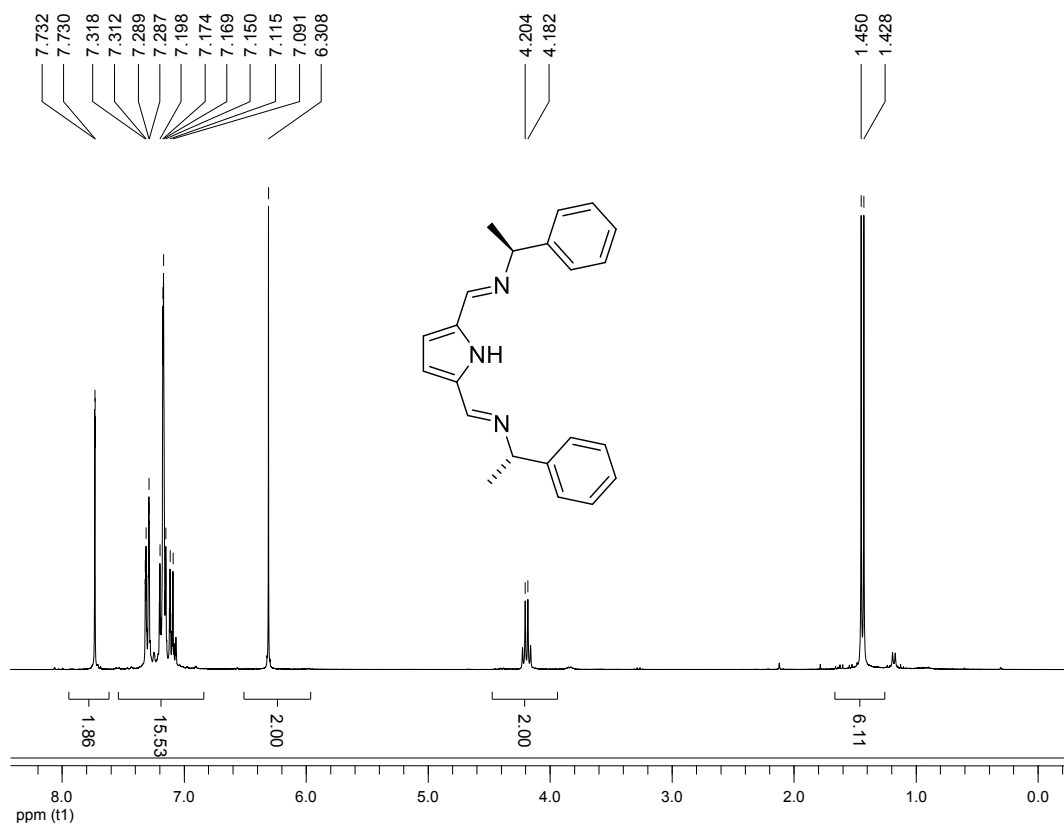


**Figure 3.S16.**  $^1\text{H-NMR}$  of **3.L1** in  $\text{C}_6\text{D}_6$ .

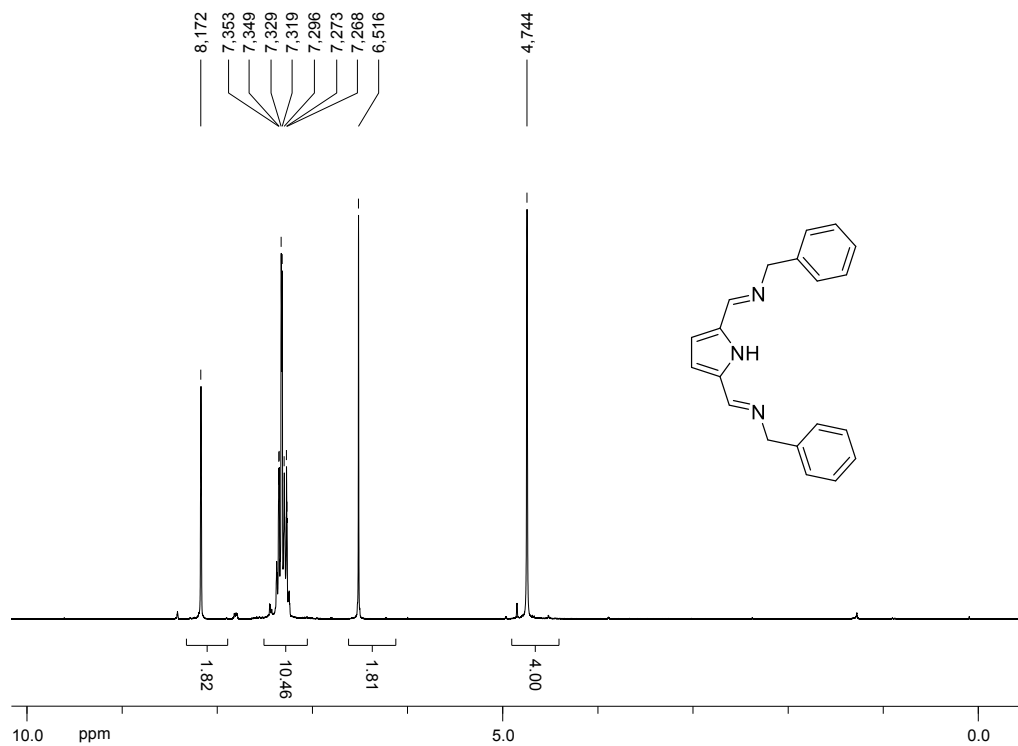


**Figure 3.S17.**  $^1\text{H-NMR}$  of 3.L2 in  $\text{C}_6\text{D}_6$ .

1. Daneshmand, P.; Fortun, S.; Schaper F. Diiminopyrrolide Copper Complexes: Synthesis, Structures and *rac*-Lactide-Polymerization Activity. *Organometallics*, **2017**, *36*, 3860–3877.

## Supporting information Chapter 4

Daneshmand, P.; Fortun, S.; Schaper F. Diiminopyrrolide Copper Complexes: Synthesis, Structures and *rac*-Lactide-Polymerization Activity. *Organometallics*, **2017**, *36*, 3860–3877.

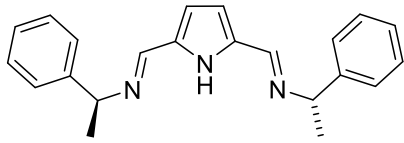
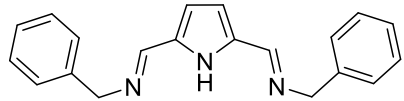
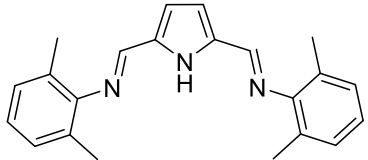
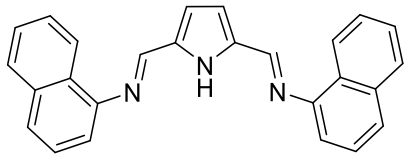
### Diiminopyrrolide Copper Complexes: Synthesis, Structures and *rac*-Lactide- Polymerization Activity

*Pargol Daneshmand, Solène Fortun, Frank Schaper\**

*Centre in Green Chemistry and Catalysis, Department of chemistry, Université de Montréal, C. P. 6128 Succ. Centre-Ville, Montréal, QC, H3T 3J7, Canada*

**Table 4.S1.** Reaction conditions under which **4.1c**, **4.2d**, **4.3d**, or **4.4c** were obtained.

All reaction products were identified by X-ray diffraction (rapid data collection for compound identification).

Ligand	Product	Solvent	Cu(OiPr) <sub>2</sub> : 4.L	Yield
	(4.L1) <sub>2</sub> Cu, <b>4.1c</b>	CH <sub>2</sub> Cl <sub>2</sub>	0.45	25%
	(4.L1) <sub>2</sub> Cu, <b>4.1c</b>	Et <sub>2</sub> O	0.9	< 5%
	(4.L2) <sub>2</sub> Cu <sub>2</sub> , <b>4.2d</b>	THF	0.9	46%
	(4.L2) <sub>2</sub> Cu <sub>2</sub> , <b>4.2d</b>	THF, 50 °C	1.2	24%
	(4.L2) <sub>2</sub> Cu <sub>2</sub> , <b>4.2d</b>	CH <sub>2</sub> Cl <sub>2</sub>	0.45	77%
	(4.L2) <sub>2</sub> Cu <sub>2</sub> , <b>4.2d</b>	Et <sub>2</sub> O	0.9	26%
	(4.L2) <sub>2</sub> Cu <sub>2</sub> , <b>4.2d</b>	Et <sub>2</sub> O	1.2	18%
	(4.L2) <sub>2</sub> Cu <sub>2</sub> , <b>4.2d</b>	Toluene	0.9	40%
	(4.L3) <sub>2</sub> Cu <sub>2</sub> , <b>4.3d</b>	CH <sub>2</sub> Cl <sub>2</sub>	0.9	< 5%
	(4.L3) <sub>2</sub> Cu <sub>2</sub> , <b>4.3d</b>	THF, 50 °C	1.2	33%
	(4.L3) <sub>2</sub> Cu <sub>2</sub> , <b>4.3d</b>	Et <sub>2</sub> O	0.9	10%
	(4.L4) <sub>2</sub> Cu, <b>4.4c</b>	THF	1.2	43%
	(4.L4) <sub>2</sub> Cu, <b>4.4c</b>	MeCN	1.2	7
	(4.L4) <sub>2</sub> Cu, <b>4.4c</b>	Toluene	1.0	37%
	(4.L4) <sub>2</sub> Cu, <b>4.4c</b>	Toluene	0.45	44%



**Table 4.S2.** Bond distances (Å) and angles (°) in homoleptic Cu(I) complexes **4.2d** and **4.3d**.

	<b>4.2d</b>	<b>4.3d</b>
Cu-N <sub>pyrrole</sub>	1.8834(16) – 1.9055(15)	1.890(4) – 1.918(5)
Cu-N <sub>imine, trans-pyrrole</sub>	1.8918(16) – 1.9042(16)	1.906(5) – 1.922(5)
Cu-N <sub>imine, cis-pyrrole</sub>	2.4795(17) – 2.3919(16)	2.358(5) – 2.495(5)
Cu-Cu	2.6004(4)	2.600(11) – 2.608(1)
N <sub>py</sub> -Cu-N <sub>imine, trans</sub>	174.54(7) – 177.94(7)	166.7(2) – 170.5(2)

**Table 4.S3.** Bond distances (Å) and angles (°) in mixed ligand complexes **4.1e**, **4.4e** and **4.6e**.

	<b>4.1e</b>	<b>4.4e</b>	<b>4.6e<sup>a</sup></b>		
Cu-N <sub>pyrrole</sub>	1.926(5)	1.9306(14)	1.927(3)	1.918(3)	1.908(3)
Cu-N <sub>imine, 1</sub>	2.505(5)	2.6491(15)	2.586(3)	2.592(3)	2.709(3)
Cu-N <sub>imine, 2</sub>	3.16	3.02	3.120(2)	2.971(3)	2.848(3)
(L)Cu-N <sub>pyridine/amine</sub> <sub>b</sub>	2.089(6)	2.0469(15)	2.016(3)	2.006(2)	1.991(3)
(L)Cu-O <sub>short</sub> <sup>b</sup>	1.933(5)	1.9285(13)	1.914(2)	1.922(2)	1.927(2)
(L)Cu-O <sub>long</sub> <sup>b</sup>	1.969(4)	1.9468(12)	1.986(2)	1.949(2)	1.937(2)
(Cl)Cu-O <sub>short</sub> <sup>b</sup>	1.899(4)	1.9108(12)	1.898(2)	1.900(2)	1.905(2)
(Cl)Cu-O <sub>long</sub> <sup>b</sup>	1.902(5)	1.9249(13)	1.921(2)	1.928(2)	1.923(2)
Cu-Cl	2.207(2)	2.2028(5)	2.2062(9)	2.1981(9)	2.2073(9)
Cu-Cu	3.0047(14)	3.0237(3)	3.0268(6)	3.0208(6)	3.0159(6)
N <sub>py/am.</sub> -Cu-N <sub>imine</sub>	97.1(2), 102.8(2)	98.05(5), 104.21(6)	77.80(9), 103.94(10)	86.64(9), 102.99(9)	92.45(9), 97.63(10)

<sup>a</sup> Complex **6** contains three independent molecules in the asymmetric unit. <sup>b</sup> (L)Cu signifies the copper atom containing a coordinated diiminopyrrole ligand, (Cl)Cu the copper atom with a coordinated chloride ligand.

**Table 4.S4.** Details of *rac*-lactide polymerizations with **4.5-4.11** and **4.3b-4.11b**.

#	Catalyst	[Catalyst] <sub>a</sub>	[Lactide]	Additive	conversion, time	$k_{\text{obs}}$ [h <sup>-1</sup> ]	$P_m$ <sup>b</sup>	$M_n$ (g/mol) <sup>c</sup>	$M_{n, \text{calc}}$ (g/mol) <sup>d</sup>	$M_w/M_n$	chains/dimer <sup>e</sup>
	<b>4.1</b> <sup>f</sup>	2 mM	200 mM		99%, 23 h	0.61(1)	0.71	10500	7200	1.7	1.4
	<b>4.1</b> <sup>f</sup>	2 mM	200 mM		99%, 24 h	0.73(1)	0.74	30400	7200	1.3	0.5
	<b>4.2</b> <sup>f</sup>	2 mM	200 mM		99%, 35 h	0.58(2)	0.68	7300	7200	1.4	2
	<b>4.2</b> <sup>f</sup>	2 mM	200 mM		99%, 28 h	0.68(1)	0.67	27900	7200	1.4	0.5
1	<b>4.5</b>	1 mM	100 mM		97%, 23 h	0.54(1)	0.71	14800	7100	1.2	1
2	<b>4.5</b>	2 mM	200 mM		99%, 23 h	1.75(2)	0.71	17300	7200	1.5	0.8
3	<b>4.5</b>	2 mM	200 mM		82%, 1 h	1.94(3)	n.d.				
4	<b>4.8</b>	1 mM	200 mM		98%, 24 h	0.46(1)	0.58				
			+200 mM		95%, 90 h		0.57				
			+25 mM		94%, 120 h		0.57				
5	<b>4.8</b>	1 mM	100 mM		95%, 20 h	0.29	0.64	11000	6900	1.3	1.3
6	<b>4.8</b>	2 mM	200 mM		99%, 10 h	1.29(1)	0.64	16900	7200	2.2	0.8
7	<b>4.8</b>	3 mM	300 mM		99%, 14 h	1.10(3)	0.60				
			+100 mM		99%, 62 h		0.62				
			+200 mM		99%, 90 h		0.65	17100	15000	2.4	1.7
8	<b>4.8</b>	2 mM	200 mM	0.5 mM BnOH	99%, 6 h	1.41(5)	0.64	8500	6500	1.3	1.7
9	<b>4.8</b>	2 mM	200 mM	1 mM BnOH	99%, 6 h	1.40(5)	0.64	7900	5800	1.3	1.8
10	<b>4.8</b>	2 mM	200 mM	2 mM BnOH	99%, 17 h	0.94(1)	0.62	6800	4900	1.1	2.1

11	<b>4.8</b>	2 mM	200 mM	4 mM BnOH	99%, 20 h	1.13(4)	0.61	4200	3700	1.1	3.4
12	<b>4.8</b>	2 mM	200 mM	8 mM BnOH	99%, 18 h	0.74(2)	0.58	2600	2500	1.1	5.5
13	<b>4.9</b>	1 mM	200 mM		99%, 18 h	1.00(2)	0.60				
14	<b>4.9</b>	1 mM	100 mM		71%, 21 h	0.32(1)	0.59	5600	5200	1.5	1.8
15	<b>4.9</b>	2 mM	200 mM		99%, 32 h	1.07(4)	0.60	7000	7200	2	2.1
16	<b>4.9</b>	3 mM	300 mM		99%, 2 h	3.36(25)	0.62				
			+100 mM		98%, 42 h		0.60				
			+100 mM		99%, 64 h		0.64				
			+200 mM		99%, 91 h		0.74	16400	16700	2.3	2
17	<b>4.9</b>	2 mM	200 mM	8 mM BnOH	97%, 16 h	0.62(2)	0.56	2200	2400	1.2	6.4
18	<b>4.10</b>	2 mM	200 mM		99%, 27 h	0.52(3)	0.59	12500	7200	1.5	1.1
19	<b>4.10</b>	2 mM	200 mM	2 mM BnOH	99%, 27 h	0.63(2)	0.60	5500	4900	1.2	2.6
20	<b>4.11</b>	2 mM	200 mM		76%, 390 h	0.0021(2)	0.44	1600	5600	1.2	6.9
	<b>4.1b<sup>f</sup></b>	2 mM	200 mM		99%, 24 h	1.43(6)	0.48	6600	7200	1.2	2.2
	<b>4.1b<sup>f</sup></b>	2 mM	200 mM		99%, 26 h	1.20(6)	0.46	6000	7200	1.3	2.4
	<b>4.2b<sup>f</sup></b>	2 mM	200 mM		75%, 35 h	0.52(1)	0.46	3300	5500	1.1	3.3
	<b>4.2b<sup>f</sup></b>	2 mM	200 mM		81%, 28 h	0.65(2)	0.46	7300	5900	1.3	1.6
21	<b>4.3b</b>	2 mM	200 mM		95%, 75 h	0.046(1)	0.33	8600	6900	1.4	1.6
22	<b>4.3b</b>	2 mM	200 mM	2 mM PyCH <sub>2</sub> OH	86%, 75 h	0.04	0.45	6500	4200	1.2	1.9
23	<b>4.5b</b>	1 mM	200 mM		55%, 28 h	0.41(1)	0.45				

24	<b>4.5b</b>	2 mM	200 mM		88%, 28 h	0.82(6)	0.46	5600	4300	1.2	2.3
25	<b>4.5b</b>	1 mM	200 mM	0.5 mM PyCH <sub>2</sub> OH	79%, 3 h	0.66(1)	0.53				
26	<b>4.5b</b>	1 mM	200 mM	1 mM PyCH <sub>2</sub> OH	88%, 3 h	0.80(1)	0.60				
27	<b>4.5b</b>	2 mM	200 mM	2 mM PyCH <sub>2</sub> OH	98%, 3 h	1.73(16)	0.58	5000	4800	1.3	2.8
28	<b>4.6b</b>	2 mM	200 mM		81%, 23 h	0.074(2)	0.43	6500	5900	1.2	1.8
29	<b>4.6b</b>	2 mM	200 mM	2 mM PyCH <sub>2</sub> OH	59%, 44 h	decomp.	0.46	3600	2900	1.2	2.4
30	<b>4.8b</b>	1 mM	200 mM		99%, 25 h	0.83(2)	0.47				
31	<b>4.8b</b>	1 mM	100 mM		99%, 4 h	1.34(5)	0.45	2500	7200	1.5	5.7
32	<b>4.8b</b>	2 mM	200 mM		99%, 34 h	1.41(1)	0.46	3200	7200	1.3	4.5
33	<b>4.8b</b>	3 mM	300 mM		99%, 3 h	1.52(4)	0.46				
			+100 mM		99%, 63 h		0.46				
			+200 mM		99%, 89 h		0.48	8500	14400	2.4	3.4
34	<b>4.8b</b>	2 mM	200 mM	0.5 mM BnOH	99%, 3 h	2.16(2)	0.46	2100	6500	1.3	6.8
35	<b>4.8b</b>	2 mM	200 mM	1 mM BnOH	99%, 3 h	2.28(7)	0.44	1800	5800	1.3	8.0
36	<b>4.8b</b>	2 mM	200 mM	2 mM BnOH	99%, 17 h	1.48(1)	0.43	3200	4900	1.2	4.5
37	<b>4.8b</b>	2 mM	200 mM	4 mM BnOH	99%, 4.5 h	1.58(12)	0.44	2400	3700	1.2	6.0
38	<b>4.8b</b>	2 mM	200 mM	8 mM BnOH	99%, 18 h	0.93(3)	0.45	2100	2500	1.2	6.8
39	<b>4.9b</b>	1 mM	200 mM		99%, 18 h	0.48(1)	0.46				
40	<b>4.9b</b>	1 mM	100 mM		98%, 20 h	0.45(1)	0.46	3300	7200	1.4	4.3

41	<b>4.9b</b>	2 mM	200 mM		99%, 32 h	0.80(2)	0.46	3900	7200	1.3	3.7
42	<b>4.9b</b>	3 mM	300 mM		99%, 4 h	1.50(7)	0.47				
43	<b>4.9b</b>	3 mM	400 mM		99%, 64 h		0.50				
44	<b>4.9b</b>	3 mM	600 mM		99%, 91 h		0.53	8900	14400	2.2	3.2
45	<b>4.9b</b>	2 mM	200 mM	8 mM BnOH	99%, 17 h	0.67(3)	0.40	1900	2500	1.2	7.6
46	<b>4.10b</b>	2 mM	200 mM		97%, 4 h	1.00(3)	0.44	7100	7100	1.3	2.0
47	<b>4.10b</b>	2 mM	200 mM		97%, 26 h	0.89(2)	0.48				
48	<b>4.10b</b>	2 mM	200 mM		98%, 4 h	n.d.	0.49				
49	<b>4.10b</b>	2 mM	200 mM	0.4 mM BnOH	98%, 28 h	0.93(1)	0.46				
50	<b>4.10b</b>	2 mM	200 mM	2 mM BnOH	97%, 26 h	0.62(1)	0.44				
51	<b>4.11b</b>	2 mM	200 mM		64%, 16 d	0.0027(3)	0.43	3500	4700	1.4	2.7

Conditions: C<sub>6</sub>D<sub>6</sub>, ambient temperature. <sup>a</sup> Concentrations and ratios provided per catalyst dimer, i. e. for 4.L<sub>2</sub>Cu<sub>2</sub>(OR)<sub>2</sub>. <sup>b</sup>  $P_m$  determined from decoupled <sup>1</sup>H NMR by  $P_m = 1 - 2 \cdot I_1 / (I_1 + I_2)$ , with  $I_1 = 5.20 - 5.25$  ppm (*rmr*, *mmr/rmm*),  $I_2 = 5.13 - 5.20$  ppm (*mmr/rmm*, *mmm*, *mrmm*). <sup>c</sup>  $M_n$  and  $M_w$  determined by size exclusion chromatography vs. polystyrene standards, with a Mark-Houwink correction factor of 0.58. <sup>d</sup>  $M_n$  expected if all alkoxides initiate polymerization, calculated from  $[\text{lactide}] / (2 \cdot [\text{cat.}] + [\text{ROH}]) \cdot \text{conversion} \cdot M_{\text{lactide}} + M_{\text{ROH}}$ . <sup>e</sup> Number of chains per catalyst dimer, calculated from the ratio of expected and obtained polymer molecular weight. <sup>f</sup> Values taken from ref. 7 for comparison.

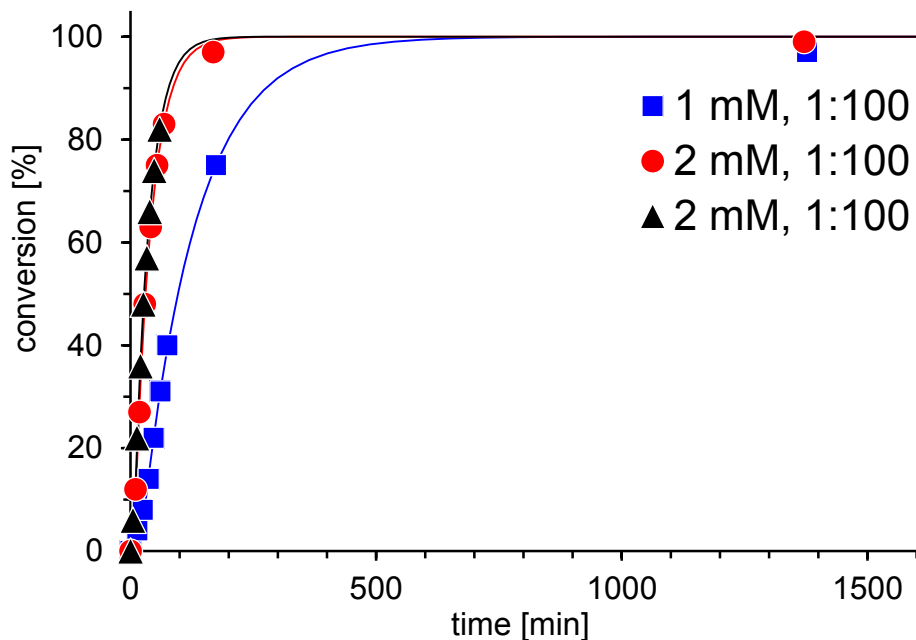


**Figure 4.S1.** Conversion-time plots for *rac*-lactide polymerizations with 4.5.

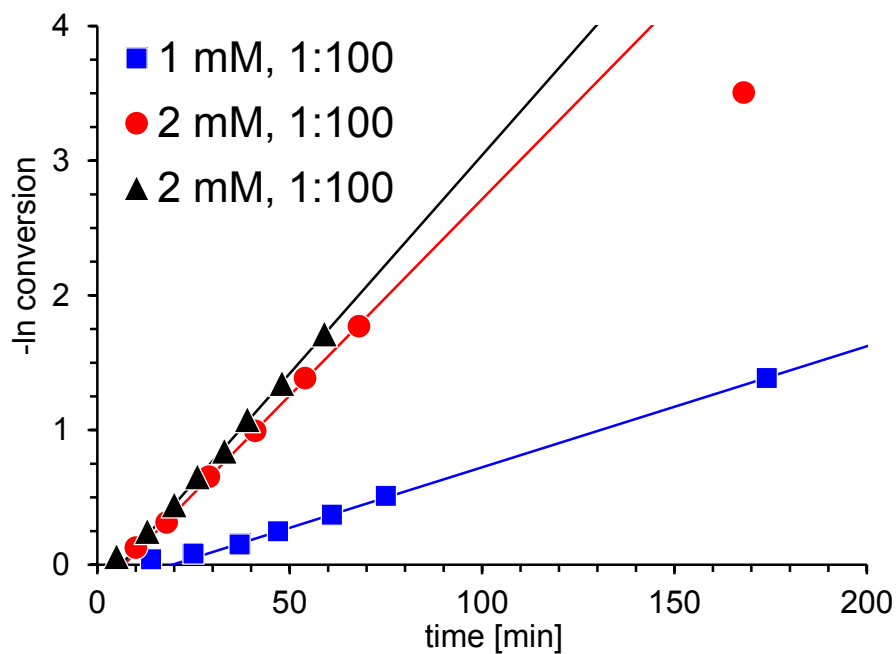


**Figure 4.S2.** Linearized conversion-time plots for *rac*-lactide polymerizations with 4.5.

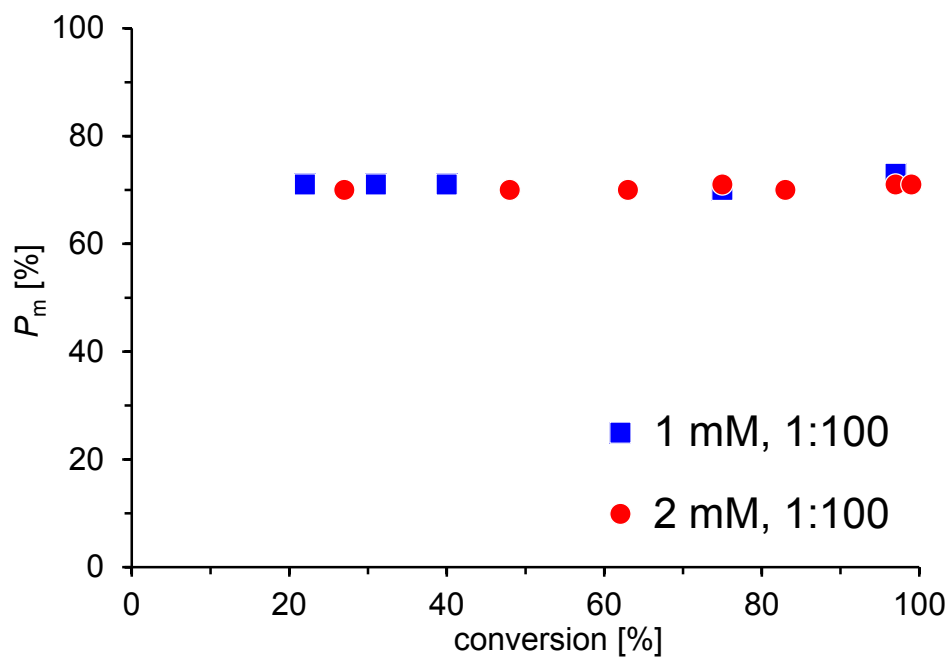


**Figure 4.S3.** Isotacticity ( $P_m$ ) versus conversion in *rac*-lactide polymerizations with 4.5.

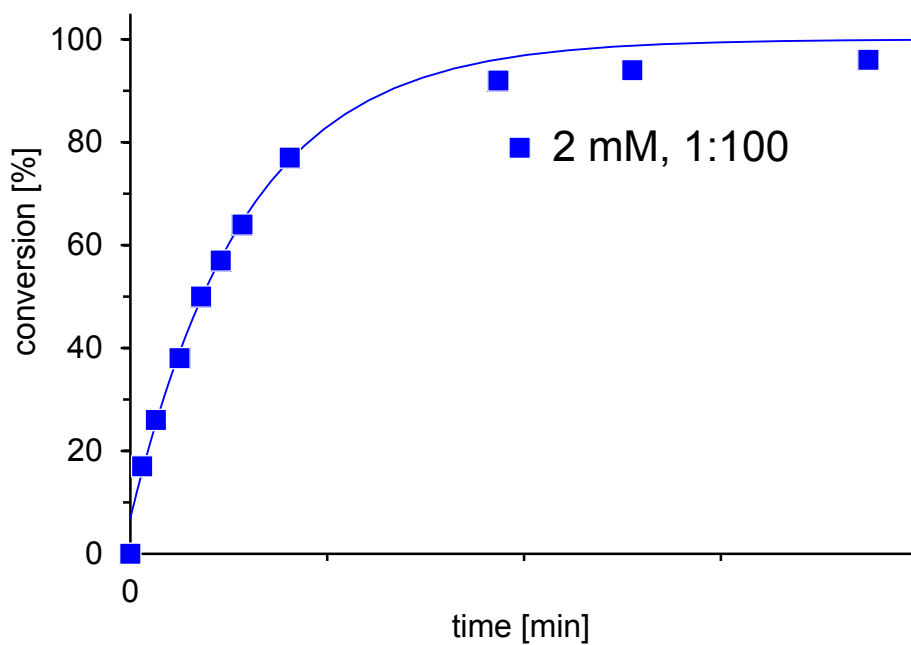


**Figure 4.S4.** Conversion-time plots for *rac*-lactide polymerizations with 4.7.

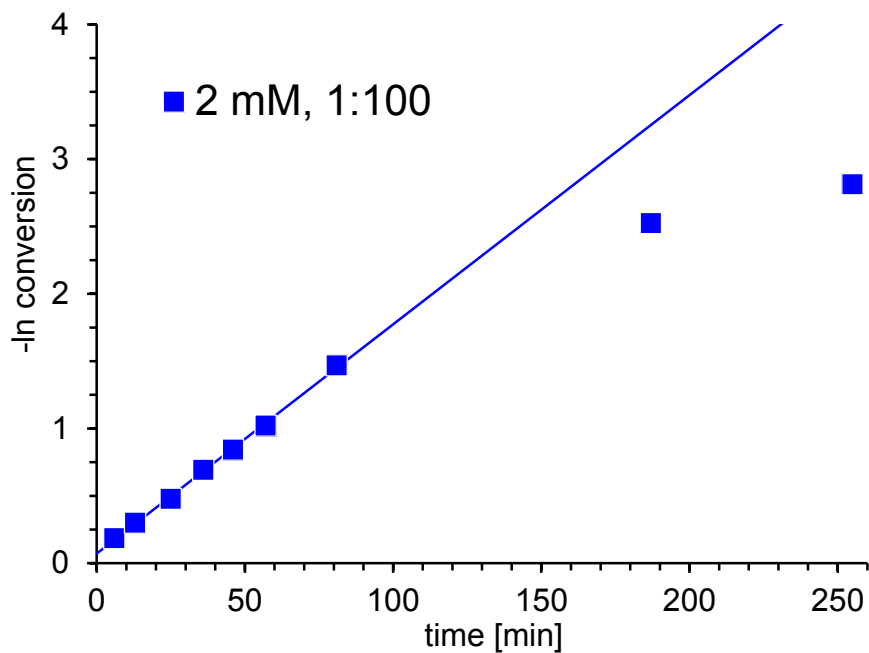


**Figure 4.S5.** Linearized conversion-time plots for *rac*-lactide polymerizations with 4.7.

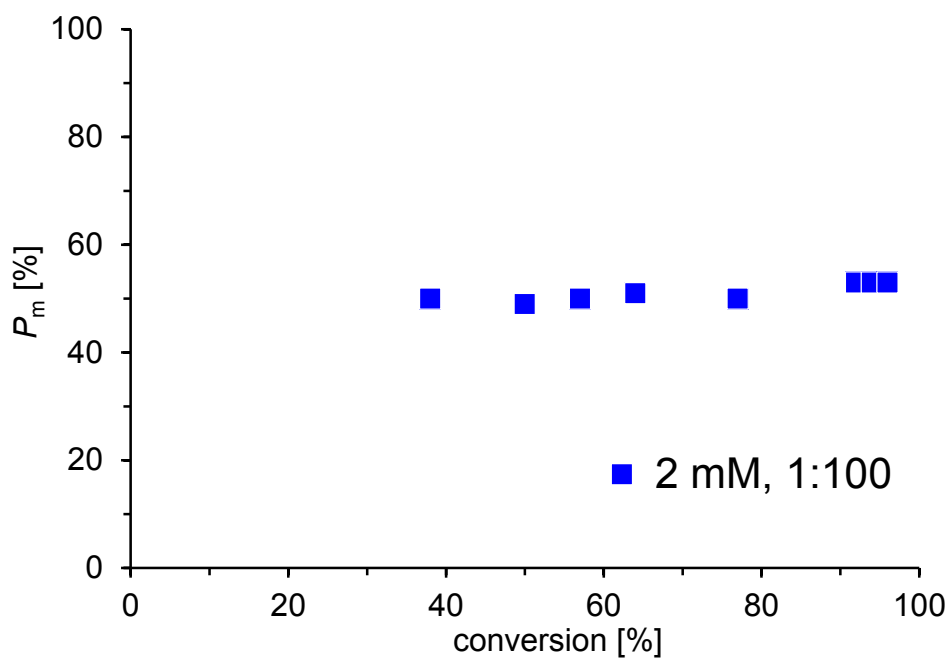


**Figure 4.S6.** Isotacticity ( $P_m$ ) versus conversion in *rac*-lactide polymerizations with 4.7.



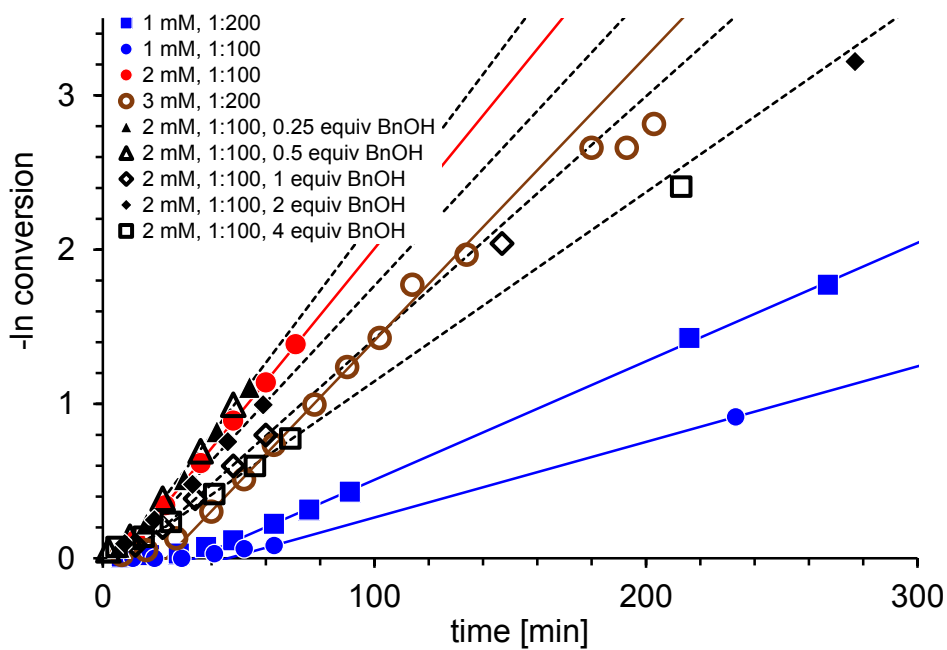


**Figure 4.S7.** Linearized conversion-time plots for *rac*-lactide polymerizations with 4.8.

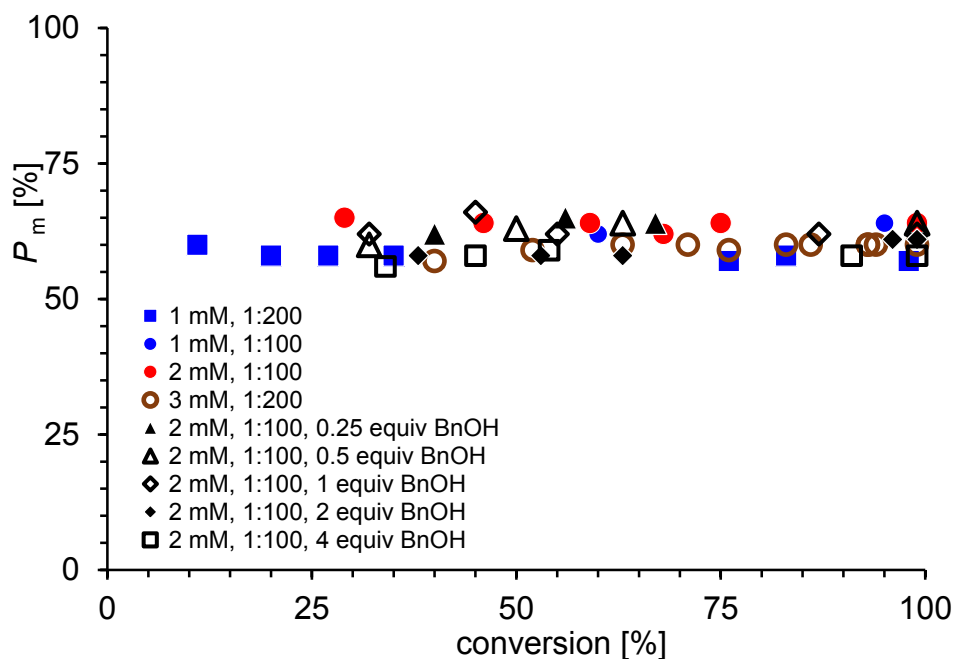


**Figure 4.S8.** Isotacticity ( $P_m$ ) versus conversion in *rac*-lactide polymerizations with 4.8.

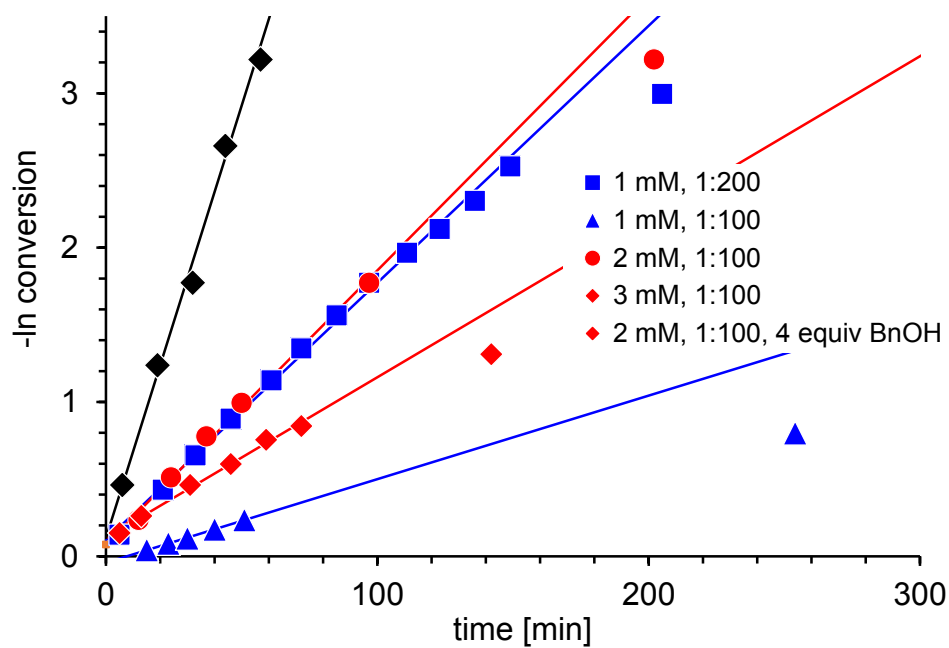


**Figure 4.S9.** Linearized conversion-time plots for *rac*-lactide polymerizations with 4.9.

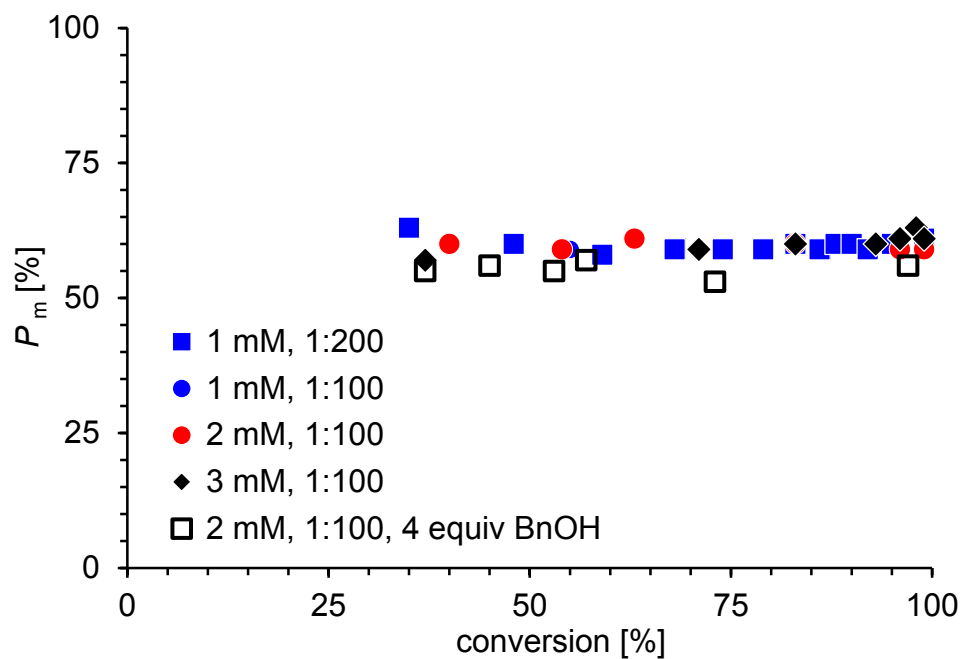


**Figure 4.S10.** Isotacticity ( $P_m$ ) versus conversion in *rac*-lactide polymerizations with 4.9.

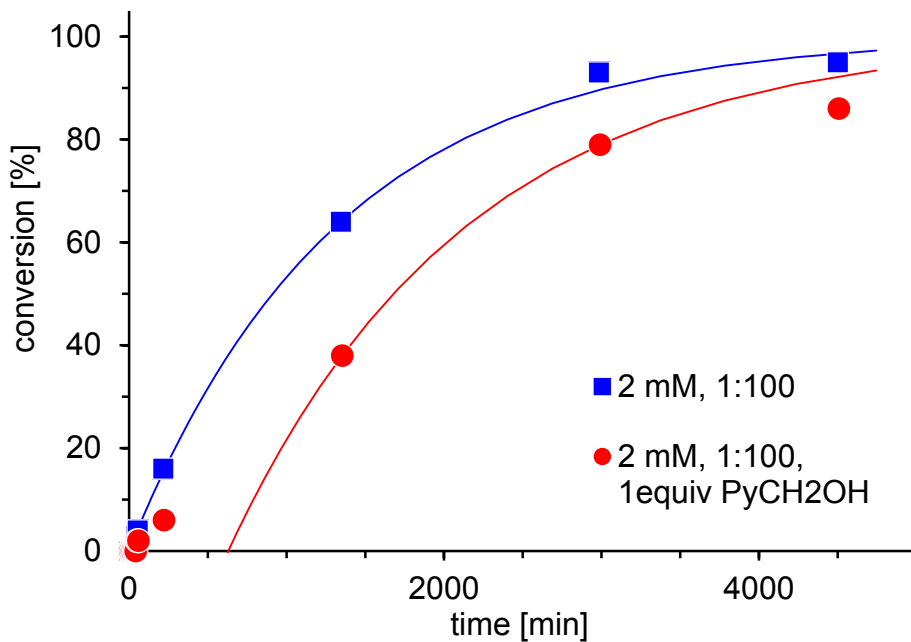


Figure 4.S11. Conversion-time plots for *rac*-lactide polymerizations with 4.3b.

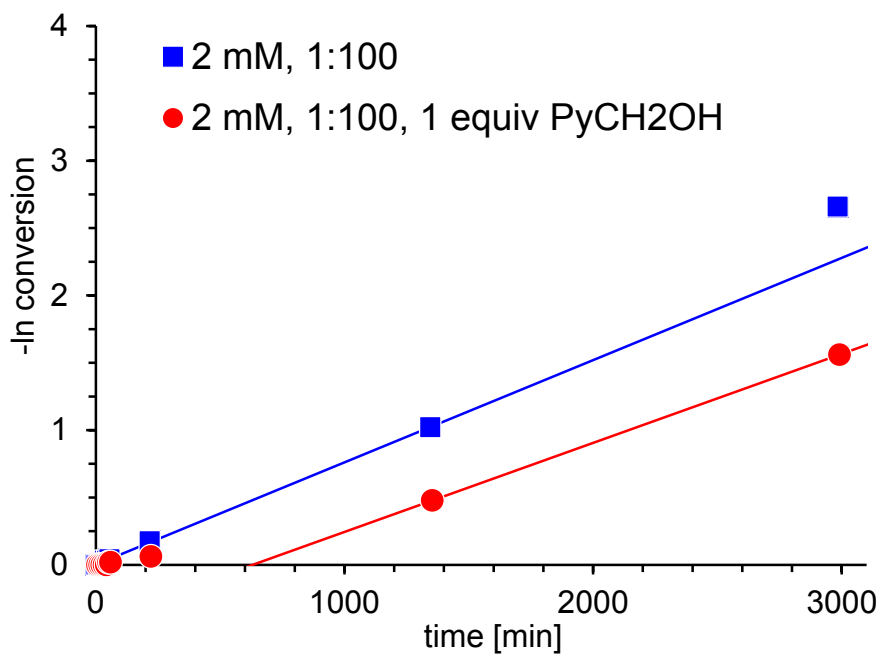


Figure 4.S12. Linearized conversion-time plots for *rac*-lactide polymerizations with 4.3b.

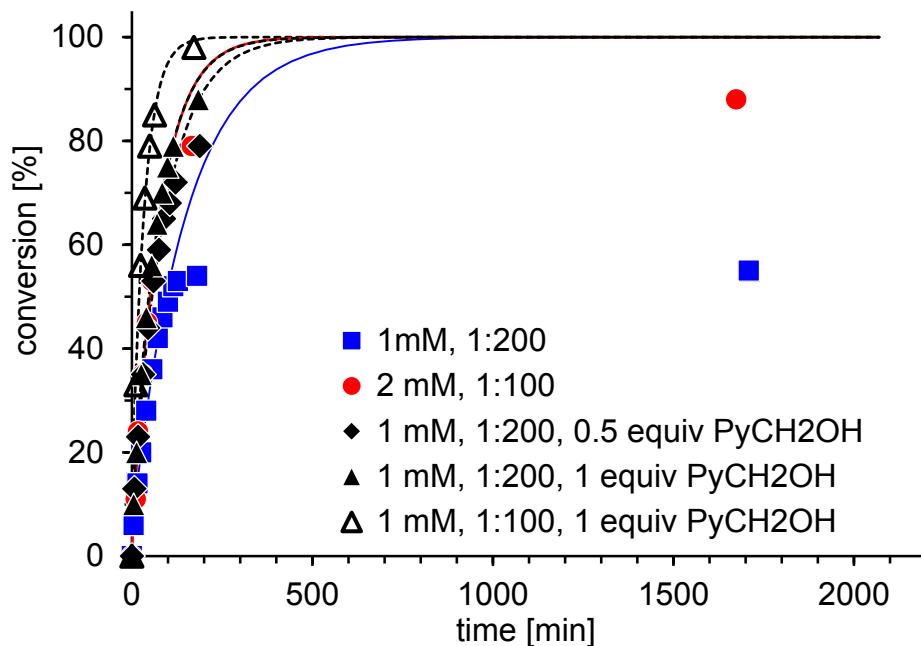


Figure 4.S13. Conversion-time plots for *rac*-lactide polymerizations with **4.5b**.

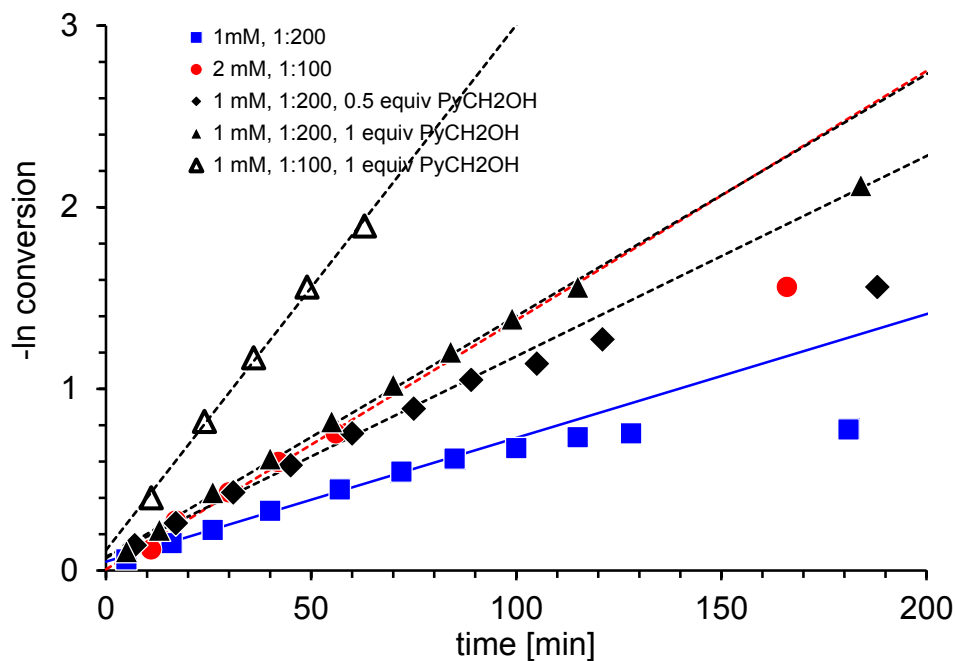
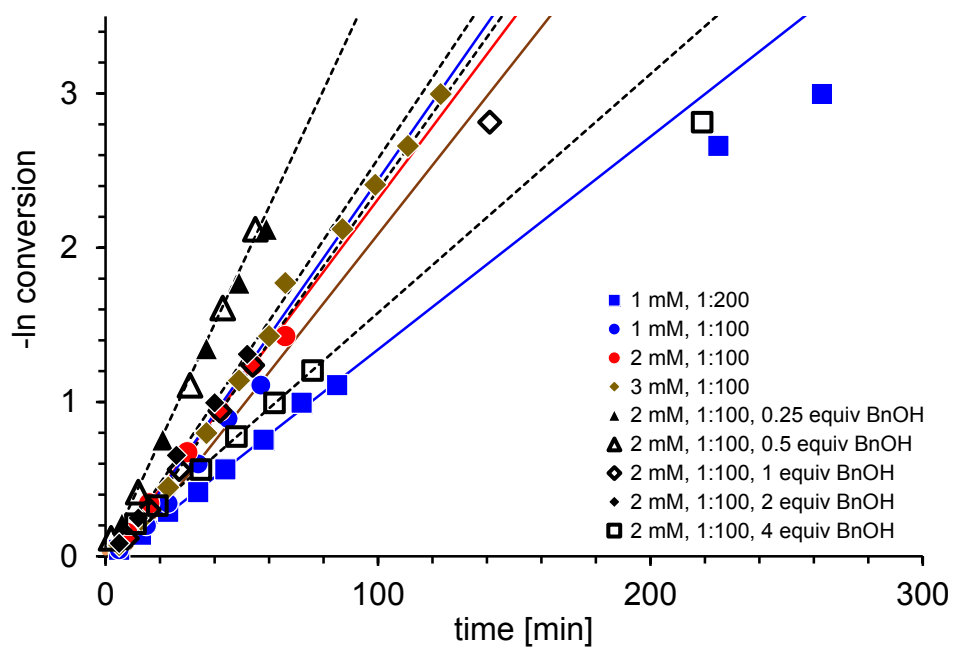
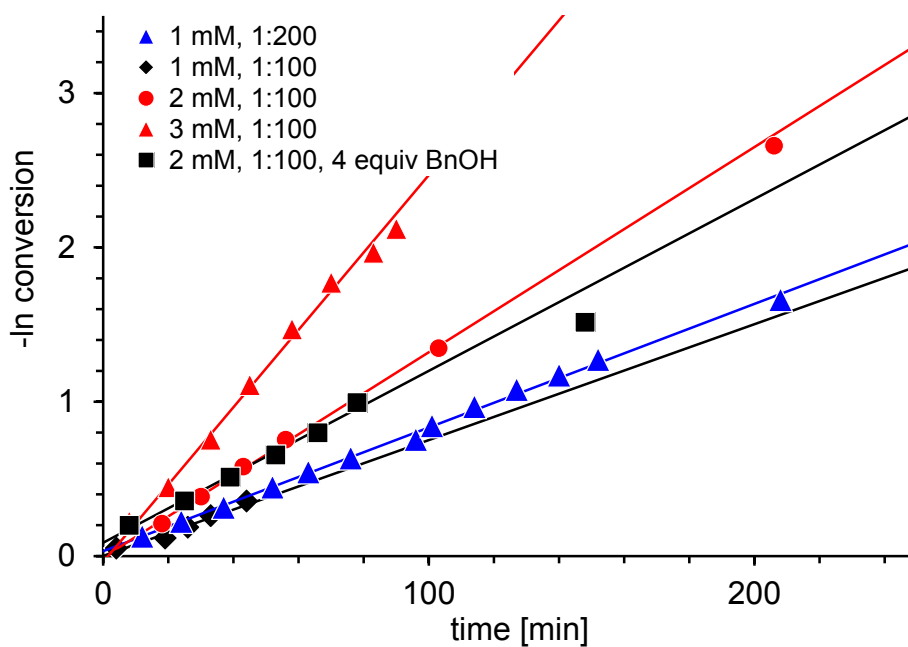


Figure 4.S14. Linearized conversion-time plots for *rac*-lactide polymerizations with **4.5b**.



**Figure 4.S15.** Linearized conversion-time plots for *rac*-lactide polymerizations with 4.8b.



**Figure 4.S16.** Linearized conversion-time plots for *rac*-lactide polymerizations with 4.9b.

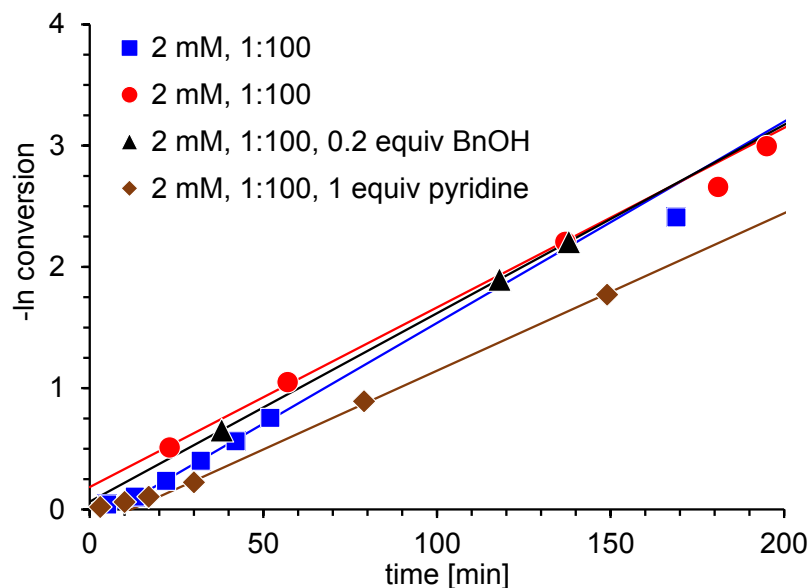


**Figure 4.S17.** Linearized conversion-time plots for *rac*-lactide polymerizations with **4.10b**.

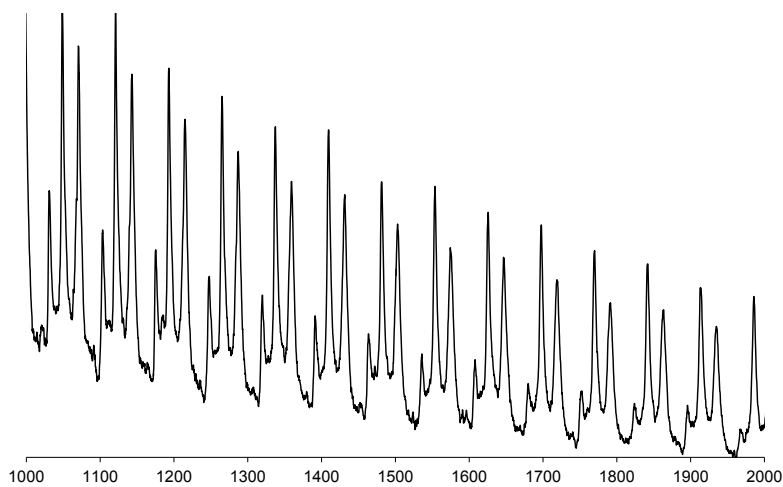


**Figure 4.S18.** MALDI spectra of PLA produced with **4.8**.

A series of  $m/z = n \cdot 72 + M(\text{Na}^+)$  is indicative of cyclic esters due to intramolecular transesterification and a series of  $m/z = n \cdot 72 + M(\text{Na}^+) + M(\text{H}_2\text{O})$  is observed. The latter is likely a product of PLA degradation or opening of the cyclic esters by water. A third series with  $m/z = n \cdot 72 + 2M(\text{Na}^+) + M(\text{OH}^-)$  is observed, which is identical to the series before, only that the carboxylic acid group is present as its sodium carboxylate salt.

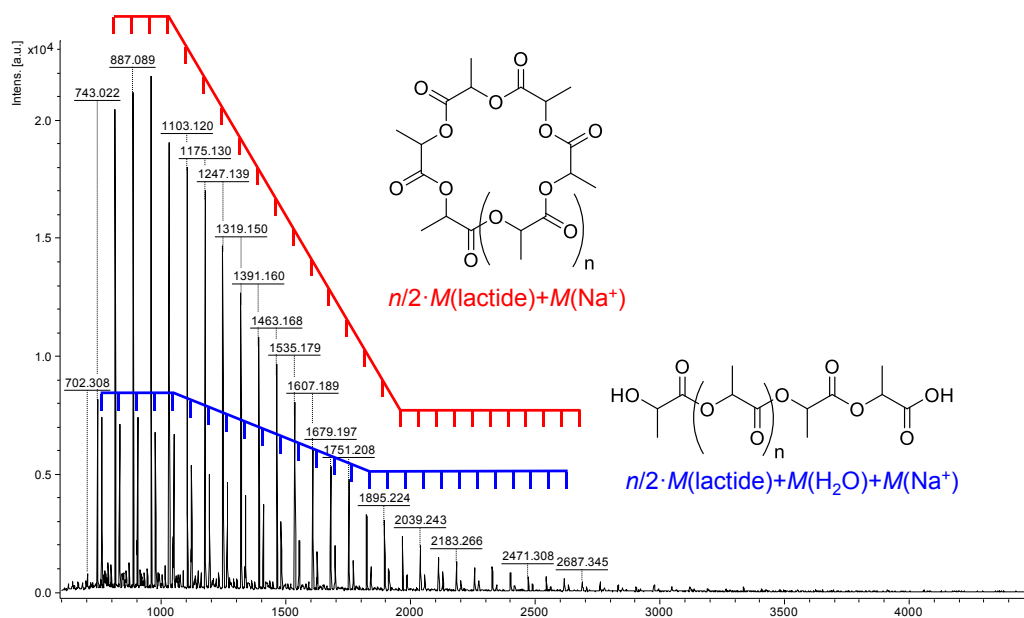


**Figure 4.S19.** MALDI spectra of PLA produced with 4.7.

The red series of  $m/z = n \cdot 72 + M(\text{Na}^+)$  is indicative of cyclic esters due to intramolecular transesterification. The blue series of  $m/z = n \cdot 72 + M(\text{Na}^+) + M(\text{H}_2\text{O})$  indicate short, formally water-initiated chains and is likely product of PLA degradation.

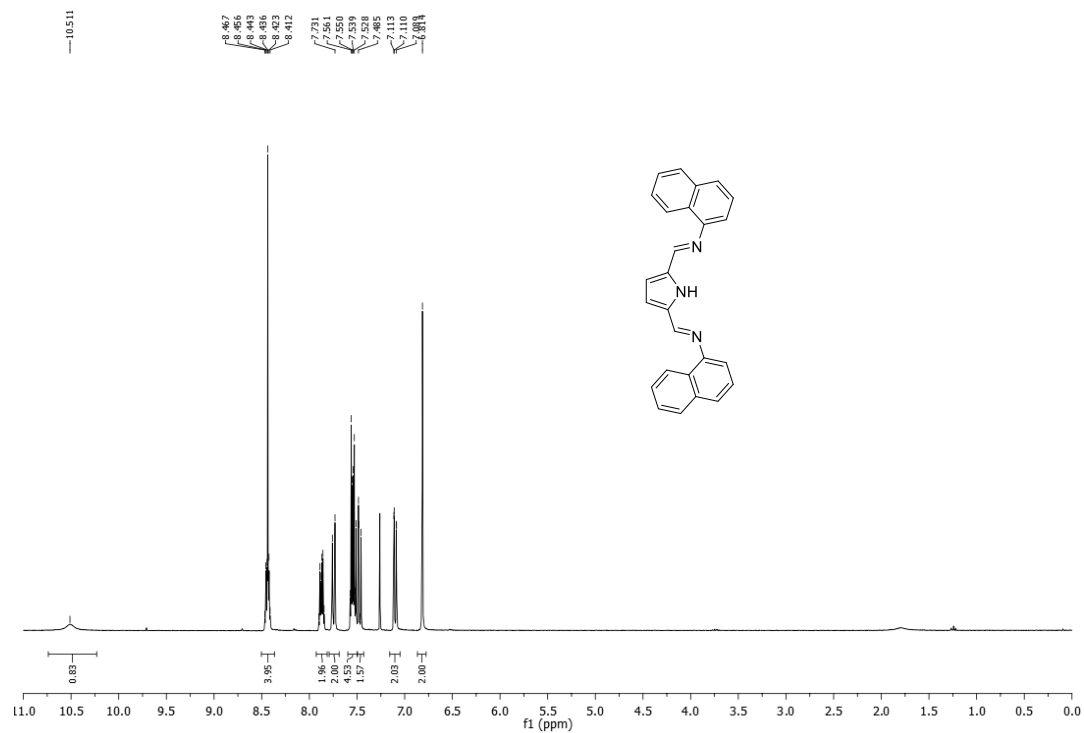


Figure 4.S20.  $^1\text{H-NMR}$  spectra of 4.L4 in  $\text{CDCl}_3$

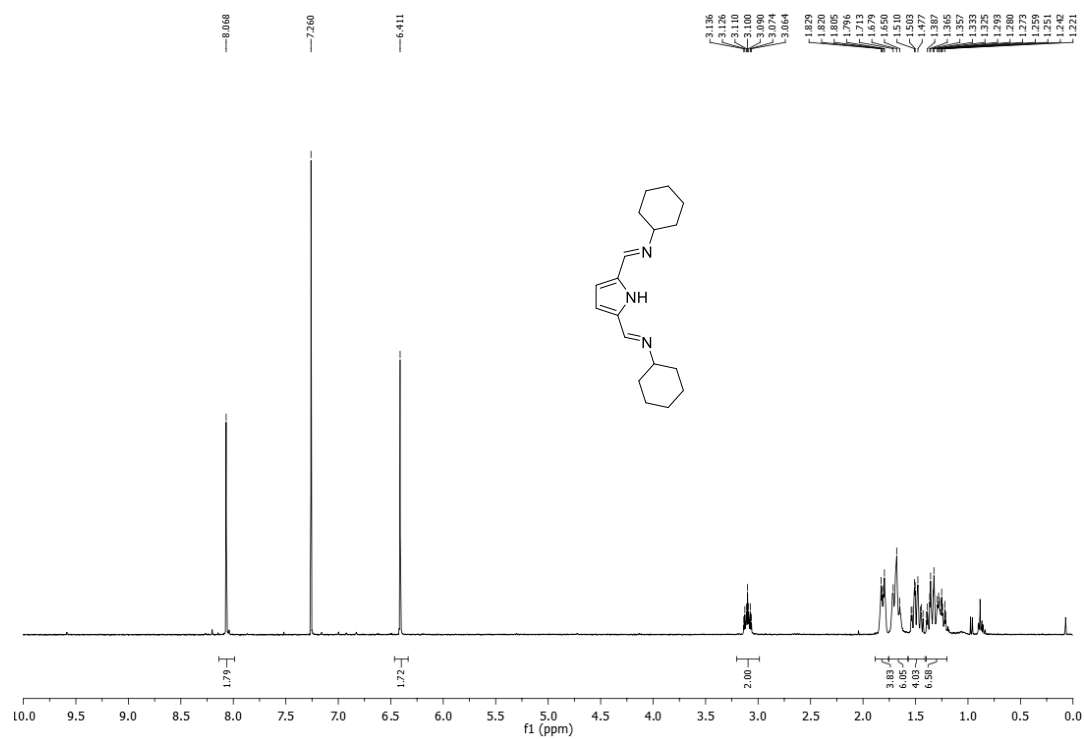
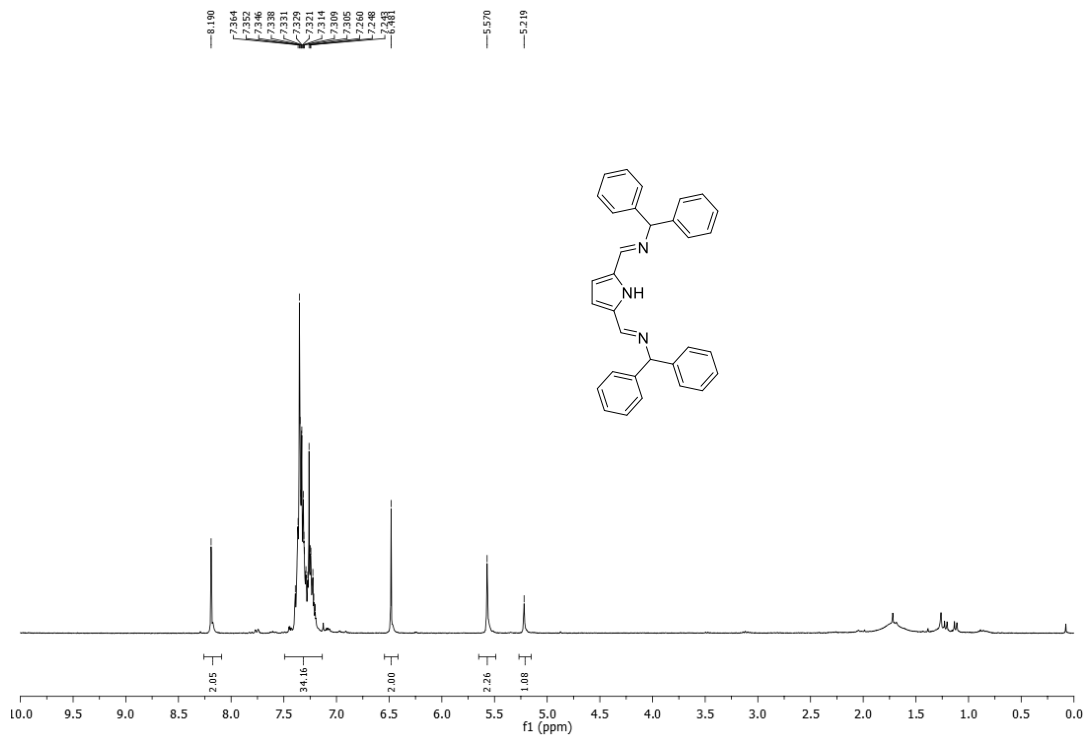
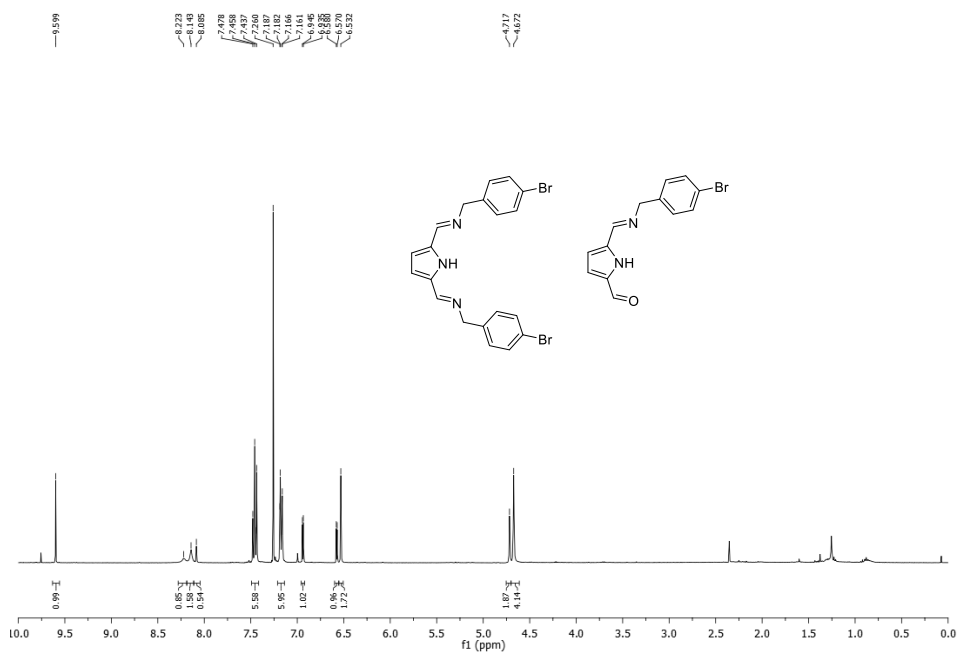


Figure 4.S21.  $^1\text{H-NMR}$  spectra of 4.L5 in  $\text{CDCl}_3$





**Figure 4.S22.**  $^1\text{H-NMR}$  spectra of 4.L6 in  $\text{CDCl}_3$



**Figure 4.S23.**  $^1\text{H-NMR}$  spectra of 4.L7 in  $\text{CDCl}_3$ . Purification attempts of the 1:1 mixture of 4.L7 and 2-carboxaldehyde-5-((4-bromobenzyl)aldimino)pyrrole obtained were unsuccessful and the mixture was used without purification in further synthesis.

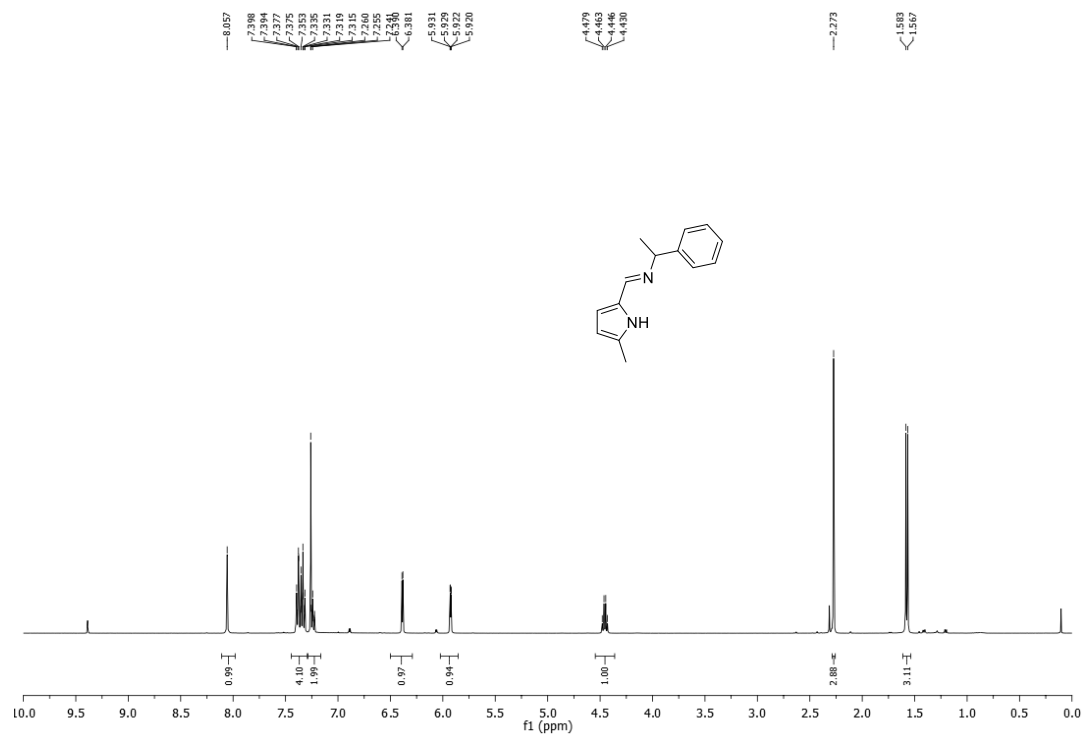


Figure 4.S24.  $^1\text{H-NMR}$  spectra of 4.L10 in  $\text{CDCl}_3$

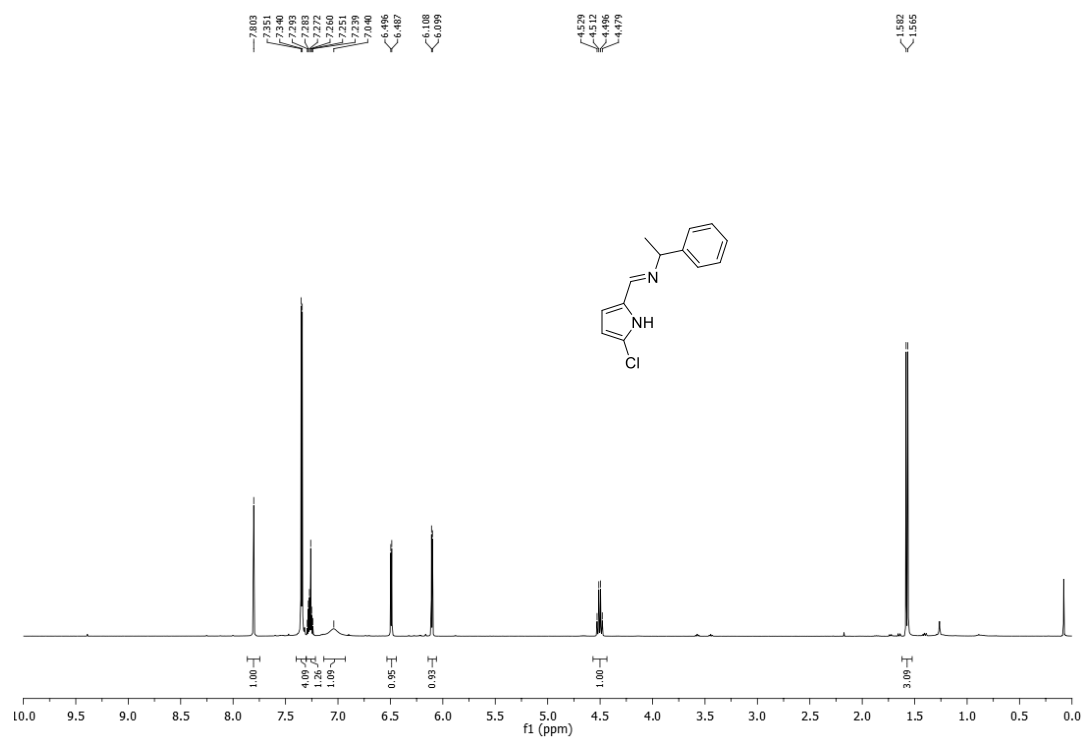


Figure 4.S25.  $^1\text{H-NMR}$  spectra of 4.L11 in  $\text{CDCl}_3$

## Supporting information Chapter 5

Daneshmand, P.; Jiménez-Santiago, J. L.; Aragon--Alberti, M.; Schaper, F. Catalytic-site-mediated chain-end control in the polymerization of *rac*-lactide with copper iminopyrrolide complexes. *Organometallics*, **2018**, *37*, 1751–1759.

### Catalytic-site-mediated chain-end control in the polymerization of *rac*-lactide with copper iminopyrrolide complexes

*Pargol Daneshmand, José L. Jiménez-Santiago, Maxime Aragon--Alberti, Frank Schaper\**

*Centre in Green Chemistry and Catalysis, Department of Chemistry, Université de Montréal, C. P. 6128 Succ. Centre-Ville, Montréal, QC, H3T 3J7, Canada.*

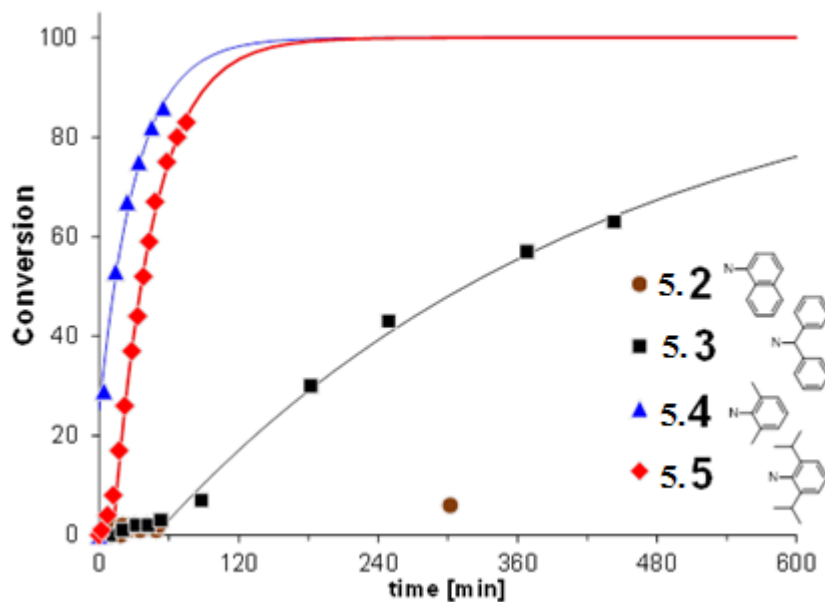


**Figure 5.S1.** Conversion-time plot for *rac*-lactide polymerizations with 5.2-5.5. Conditions:  $C_6D_6$ , RT, [lactide] = 200 mM,  $[5.L_2Cu_2(OR)_2]$  = 2 mM.

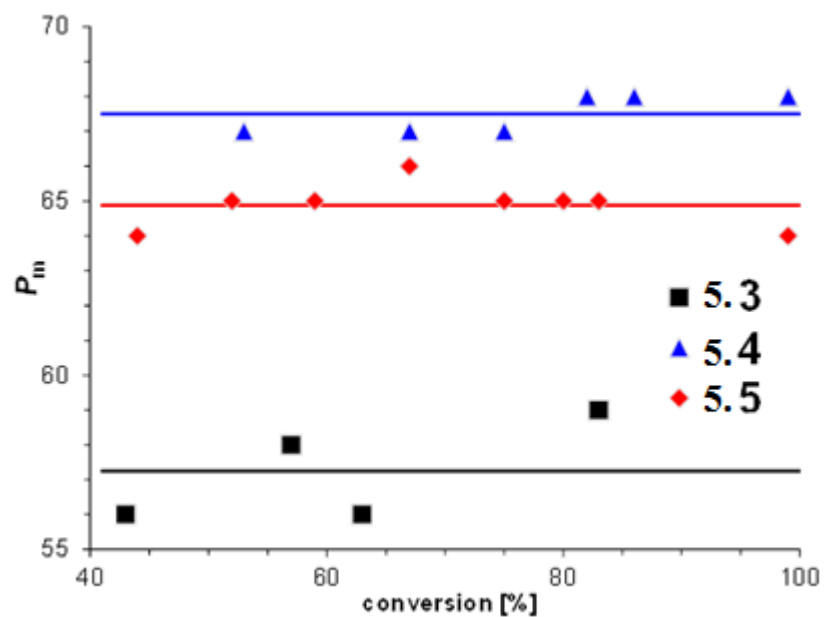


**Figure 5.S2.** Stereocontrol ( $P_m$ ) dependence on conversion for 5.3 (squares), 5.4 (triangles), 5.5 (diamonds). Solid lines indicate the averaged  $P_m$  value.

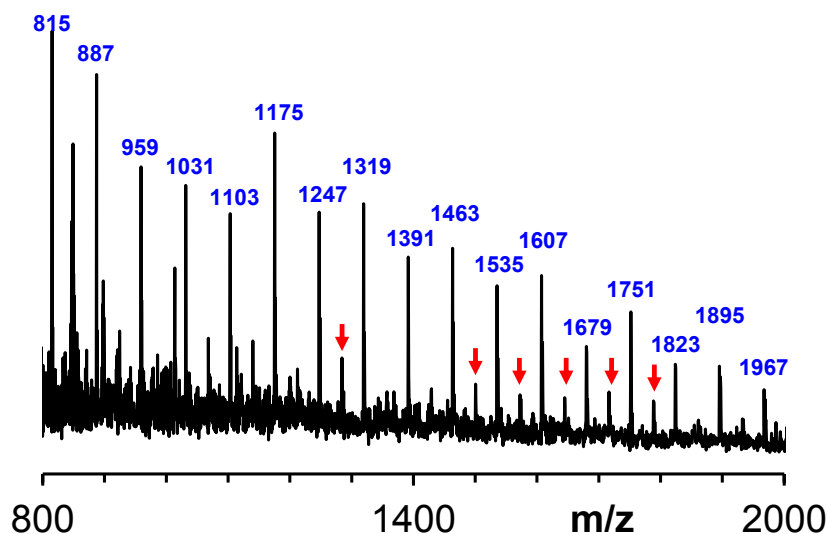


**Figure 5.S3.** MALDI-MS spectrum of PLA obtained with **5.4**.

Blue numbers indicate a series of  $m/z = n/2 \cdot M(\text{lactide}) + M(\text{Na})$  indicative of cyclic oligomers resulting from intramolecular transesterification. The red arrows indicate small peaks corresponding to  $m/z = n/2 \cdot M(\text{lactide}) + M(\text{PyCH}_2\text{OH}) + M(\text{Na})$  indicative of intermolecular transesterification. Matrix: dithranol with NaCl added to facilitate ionization.

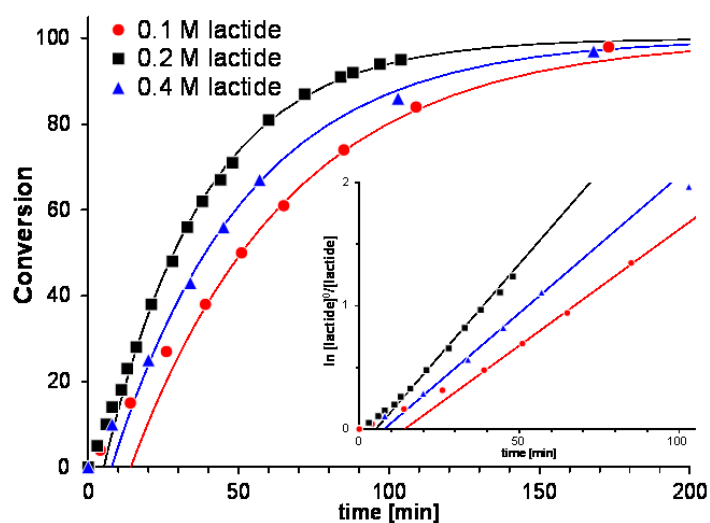


**Figure 5.S4.** Conversion-time plot for *rac*-lactide polymerizations with **5.5** + 1 equiv  $\text{Ph}_3\text{COH}$ . Conditions:  $\text{C}_6\text{D}_6$ , RT,  $[\text{lactide}] = 100\text{--}400$  mM,  $[\text{5.L}_2\text{Cu}_2(\text{OR})_2] = 2$  mM,  $[\text{Ph}_3\text{COH}] = 2$  mM. The inset shows the semi-logarithmic plot.

**Table 5.S1.** Simulation of stereoerrors via chain-end control or catalytic-site control mechanism

Tetrad	<sup>13</sup> C NMR	Best fit for chain-end control	Best fit for catalytic-site control
		$P_m = 0.692$	$\alpha = 0.791$
<i>mmm</i>	0.585	0.585	0.587
<i>mmr</i>	0.109	0.107	0.083
<i>rmm</i>	0.109	0.107	0.083
<i>mr<sup>m</sup>m</i>	0.153	0.154	0.165
<i>rmr</i>	0.045	0.047	0.083

$[mmr]/[rmm]$  determined from the combined peak in the carbonyl region ( $[mr<sup>m</sup>m] + [mmr] + [rmm]$ ) by subtraction of  $[mr<sup>m</sup>m]$  determined from the methine region and under the assumption that  $[mmr] = [rmm]$ . Theoretical distributions calculated according to Chamberlain, B. M.; Cheng, M.; Moore, D. R.; Ovitt, T. M.; Lobkovsky, E. B.; Coates, G. W. *J. Am. Chem. Soc.* **2001**, *123*, 3229 for chain-end control and to Ovitt, T. M.; Coates, G. W. *J. Am. Chem. Soc.* **2002**, *124*, 1316 for catalytic-site control.

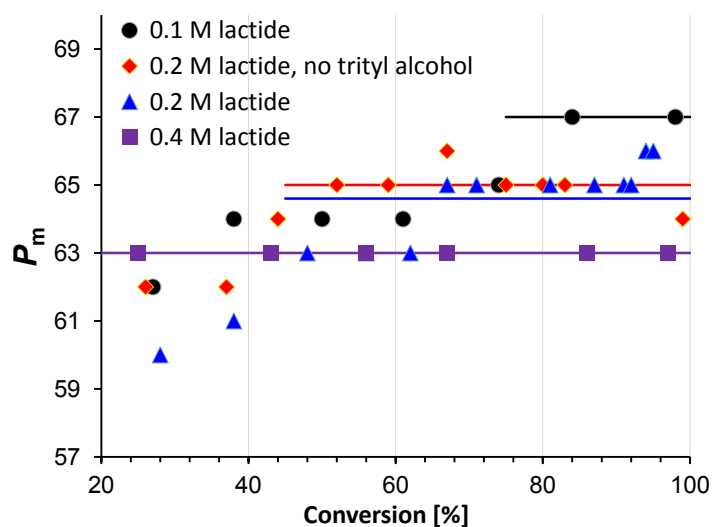


**Figure 5.S5.** Stereocontrol dependence on conversion for *rac*-lactide polymerization with **5.5**+Ph<sub>3</sub>COH at different lactide concentrations. The solid lines indicate the averaged  $P_m$  value. (Values at polymerization degrees < 40 were not considered, to avoid an influence of chain-end tetrads on the  $P_m$ -value.)

### ***L*-Lactide polymerization**

In the proposed mechanism, the catalytic site adapts to the chirality of the polymer chain. In *rac*-lactide polymerization, 50% of the catalyst is thus present in the *R*-induced form, **5.5<sup>R</sup>**, 50% in the *S*-induced form, **5.5<sup>S</sup>**. The apparent rate constant is a mixture of stereocorrect insertion,  $k_m$ , and stereoerror insertion,  $k_r$ :

$$\begin{aligned} v_{rac} &= k_{rac}[LA] = k_m[\mathbf{5.5^R}][RR] + k_r[\mathbf{5.5^R}][SS] + k_m[\mathbf{5.5^S}][SS] + k_r[\mathbf{5.5^S}][RR] \\ &= \frac{k_m + k_r}{2}[\mathbf{5.5}][LA] \\ &\Rightarrow \frac{k_{rac}}{[\mathbf{5.5}]} = \frac{k_m + k_r}{2} \\ &\left( [\mathbf{5.5^R}] = [\mathbf{5.5^S}] = [\mathbf{5.5}]/2, \quad [SS] = [RR] = [LA]/2 \right) \end{aligned}$$

In *L*-lactide polymerization,  $[\mathbf{5.5^R}] = 0$ ,  $[\mathbf{5.5^S}] = [\mathbf{5.5}]$ , and  $[RR] = 0$ ,  $[SS] = [LA]$ , thus

$$v_L = k_L[LA] = k_m[\mathbf{5.5}][LA] \Rightarrow k_L/[\mathbf{5.5}] = k_m$$

From  $k_{rac} = 1.7 \text{ h}^{-1}$ ,  $k_L = 2.8 \text{ h}^{-1}$ , and  $[\mathbf{5.5}] = 2.0 \text{ mM}$ , we obtain  $k_m = 1.4 \text{ h}^{-1}\text{mM}^{-1}$  and  $k_r = 0.3 \text{ h}^{-1}\text{mM}^{-1}$ . These constants would result in an isoselectivity of  $P_m = k_m / (k_m + k_r) = 82\%$ .

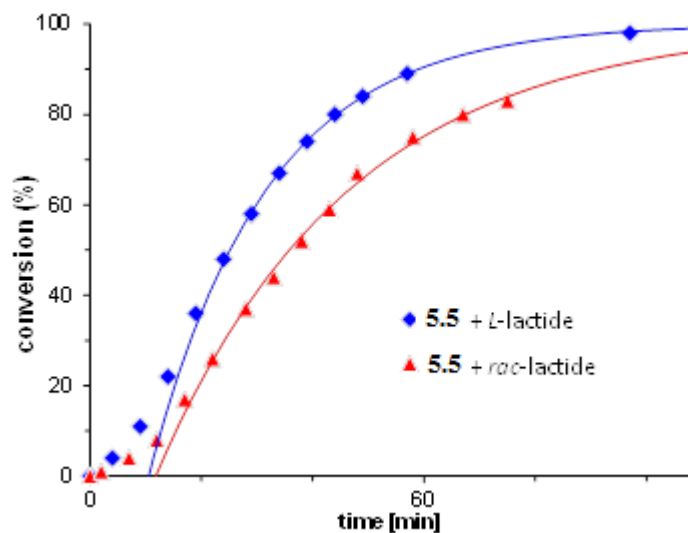


**Figure 5.S6.** Conversion-time plot for *rac*-lactide (blue diamonds) and *L*-lactide polymerizations (red triangles) with **5.5**.

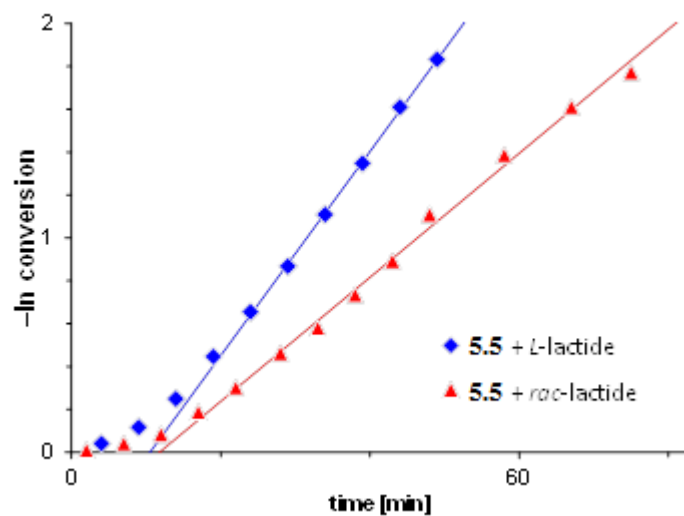


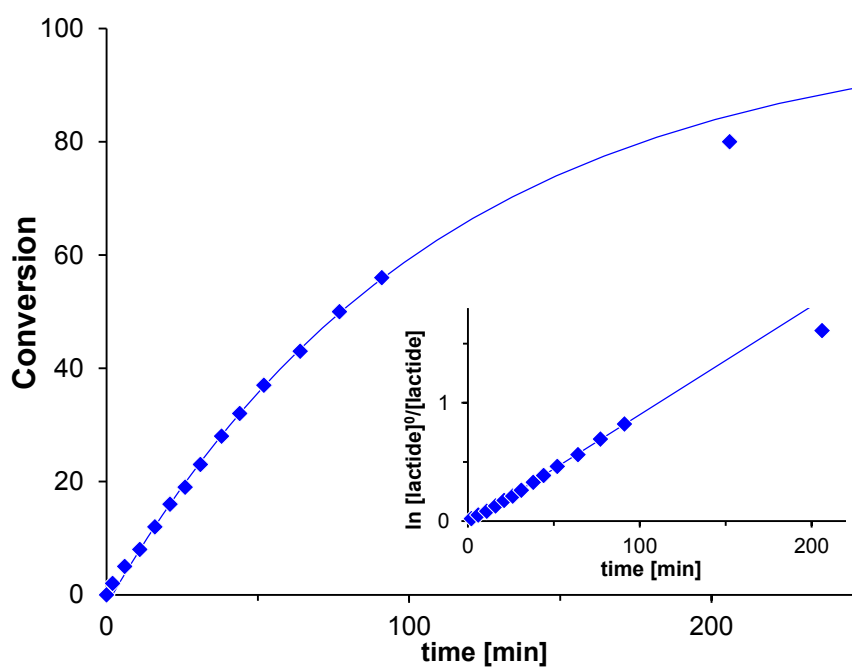
**Figure 5.S7.** Semi-logarithmic conversion-time plot for *rac*-lactide (blue diamonds) and *L*-lactide polymerizations (red triangles) with **5.5**. The solid lines are calculated from  $k_{app}$  and  $t_0$  obtained from linear regression of the semi-logarithmic plot ( $k_{app} = 2.85(3) \text{ h}^{-1}$  and  $t_0 = 12 \text{ min}$  for *L*-lactide). Conditions:  $\text{C}_6\text{D}_6$ , RT,  $[\text{lactide}] = 200 \text{ mM}$ ,  $[\text{5.L}_2\text{Cu}_2(\text{OR})_2] = 2 \text{ mM}$ .



**Table 5.S2.** *Rac*-lactide polymerizations with **5.5** at variable lactide concentration. <sup>a</sup>

[Catalyst]	[lactide]	Final conversion	$k_{\text{obs}}$ [h <sup>-1</sup> ]	$M_n$ <sup>b</sup>	$M_n$ (calc.) <sup>c</sup>	$M_w/M_n$	# chains <sup>d</sup>	$P_m$ <sup>e</sup>
2.0 mM	0.10 M	98% (3 h)	1.13(3)	5.1 kDa	7.1 kDa	1.8	1.4	0.67
2.0 mM	0.20 M	95% (2 h)	1.79(3)	10.4 kDa	13.7 kDa	1.3	1.3	0.65
2.0 mM	0.40 M	97% (3 h)	1.34(5)	12.5 kDa	27.9 kDa	2.5	2.3	0.63

<sup>a</sup> Conditions: C<sub>6</sub>D<sub>6</sub>, RT, [Ph<sub>3</sub>COH] = [5.L<sub>2</sub>Cu<sub>2</sub>(OR)<sub>2</sub>] = 2 mM. <sup>b</sup>  $M_n$  and  $M_w$  determined by size exclusion chromatography vs. polystyrene standards, with a Mark-Houwink correction factor of 0.58. <sup>c</sup>  $M_n$  expected if one alkoxide per catalyst dimer initiates polymerization, calculated from [lactide]/[cat]·conversion· $M_{\text{lactide}}$  +  $M_{\text{ROH}}$ . <sup>d</sup> Number of chains per catalyst dimer, calculated from the ratio of expected and obtained polymer molecular weight. <sup>e</sup>  $P_m$  determined from decoupled <sup>1</sup>H NMR by  $P_m = 1 - 2 \cdot I_1 / (I_1 + I_2)$ , with  $I_1 = 5.20 - 5.25$  ppm (*mmr*, *mmr/rmm*),  $I_2 = 5.13 - 5.20$  ppm (*mmr/rmm*, *mmm*, *mrmm*).

**Figure 5.S8.** Conversion-time plot for *rac*-lactide polymerizations with **5.9**.

Conditions: C<sub>6</sub>D<sub>6</sub>, RT, [lactide] = 200 mM, [5.L<sub>2</sub>Cu<sub>2</sub>(OR)<sub>2</sub>] = 2 mM. The inset shows the semi-logarithmic plot.

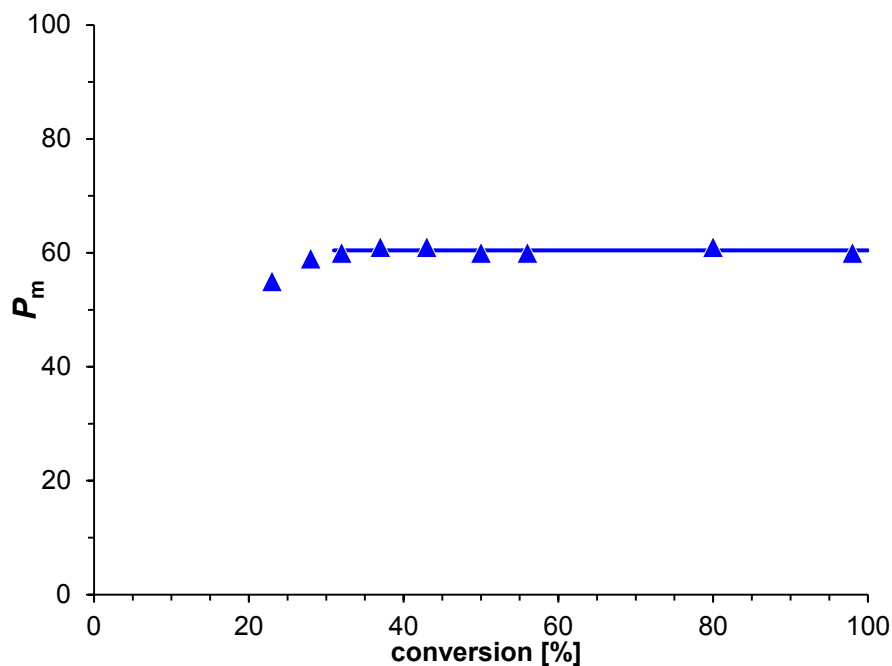


**Figure 5.S9.** Stereocontrol dependence on conversion for *rac*-lactide polymerization with **5.9**. The solid lines indicates the averaged  $P_m$  value. (Values at conversions lower than 30% were not considered in the calculation of the average due to chain-end effects in short polymer chains.)

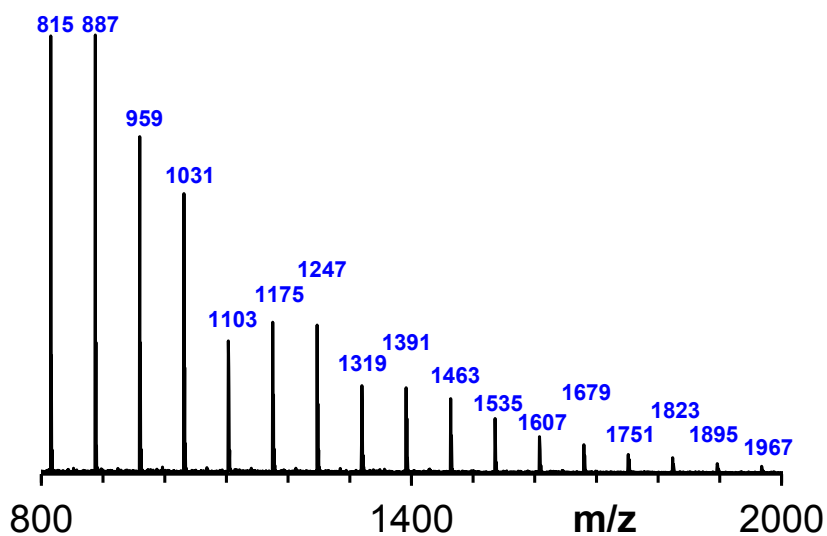


**Figure 5.S10.** MALDI-MS spectrum of PLA obtained with **5.9**. Numbers indicate a series of  $m/z = n/2 \cdot M(\text{lactide}) + M(\text{Na})$  indicative of cyclic oligomers resulting from intramolecular transesterification. Matrix: dithranol with NaCl added to facilitate ionization.

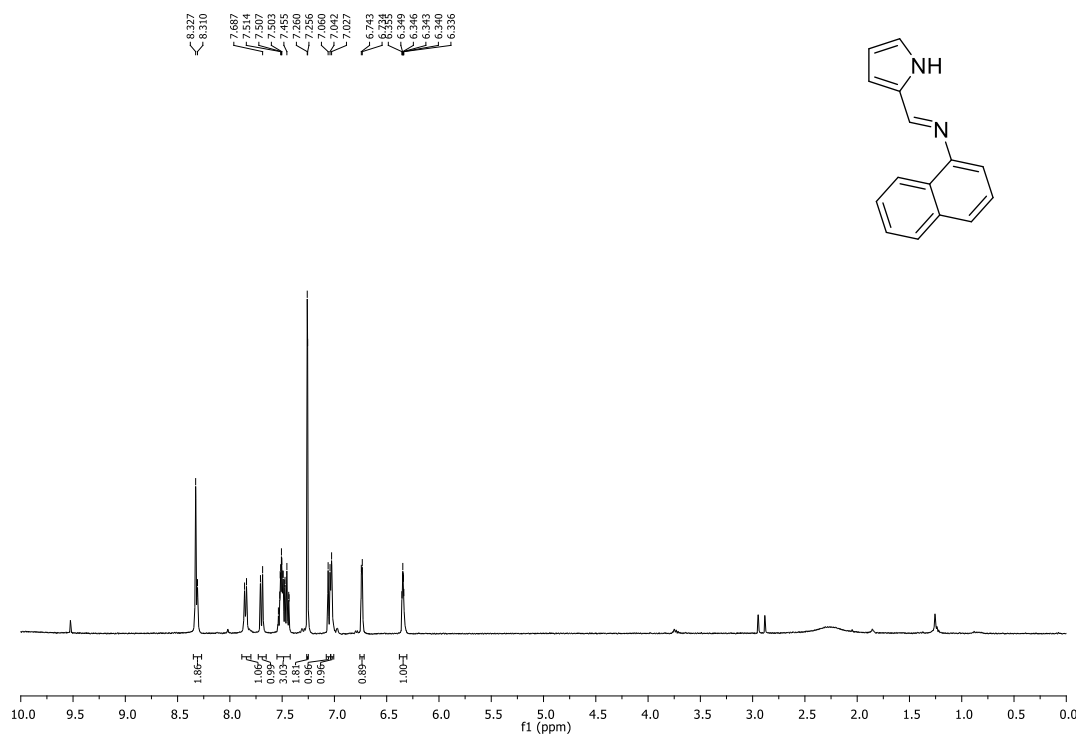


Figure 5.S11. <sup>1</sup>H-NMR spectra of 5.L2 in CDCl<sub>3</sub> (400 MHz).

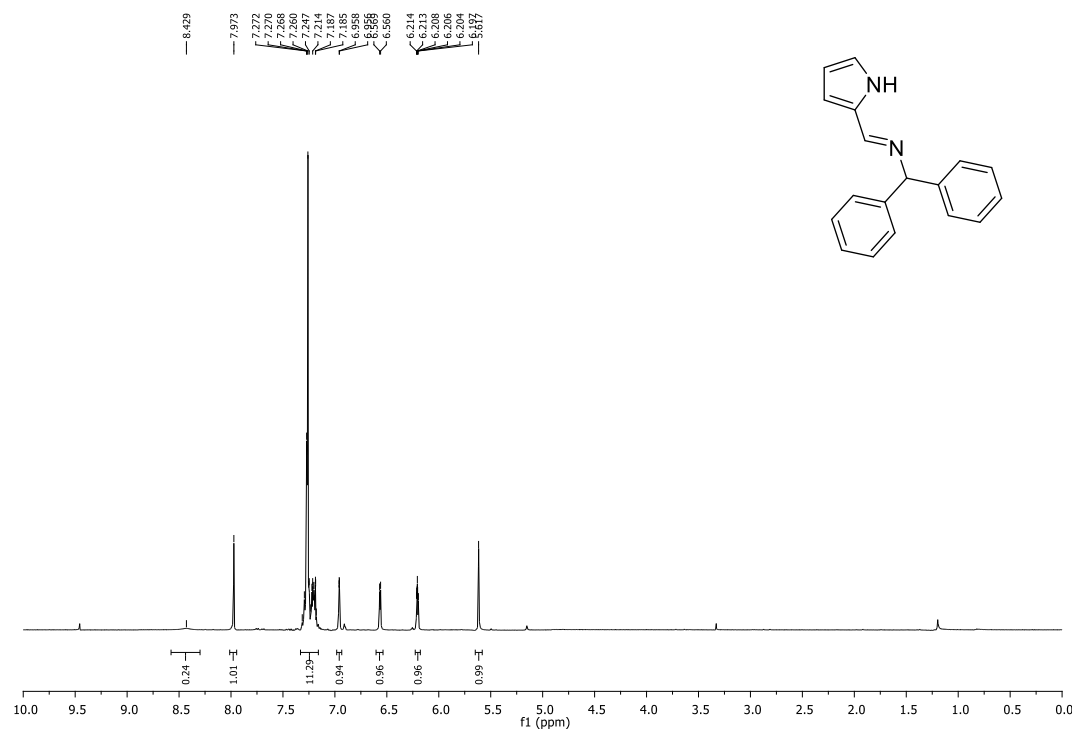
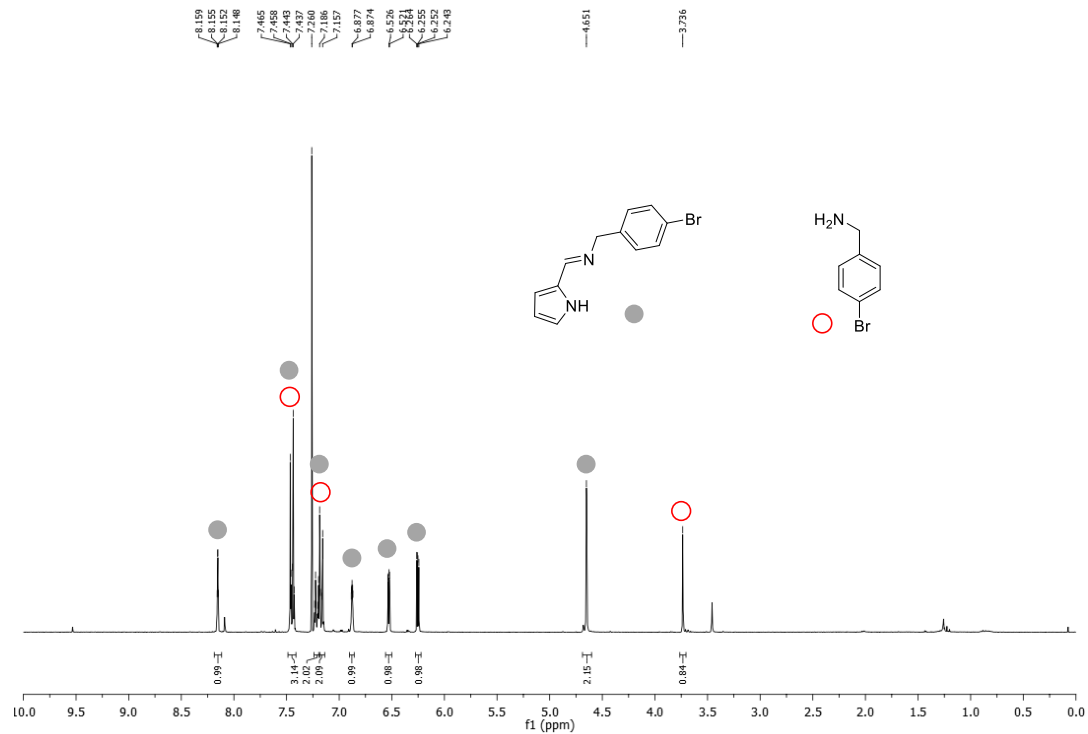


Figure 5.S12. <sup>1</sup>H-NMR spectra of 5.L3 in CDCl<sub>3</sub> (400 MHz).



**Figure 5.S13.**  $^1\text{H-NMR}$  spectra of 5.L9 (3:1 mixture with the free amine) in  $\text{CDCl}_3$  (400 MHz).

## Supporting information Chapter 6

Daneshmand, P.; Pinon, L.; Schaper, F. Dinuclear iminophenoxide copper complexes in *rac*-Lactide polymerisation. *Dalton Trans.* **2018**, *in print*.

## Dimeric iminophenoxide copper complexes in *rac*-Lactide polymerization

*Pargol Daneshmand, Leena Pinon, Frank Schaper\**

*Centre in Green Chemistry and Catalysis, Department of chemistry, Université de Montréal, C. P. 6128 Succ. Centre-Ville, Montréal, QC, H3T 3J7, Canada. Email: Frank.Schaper@umontreal.ca*

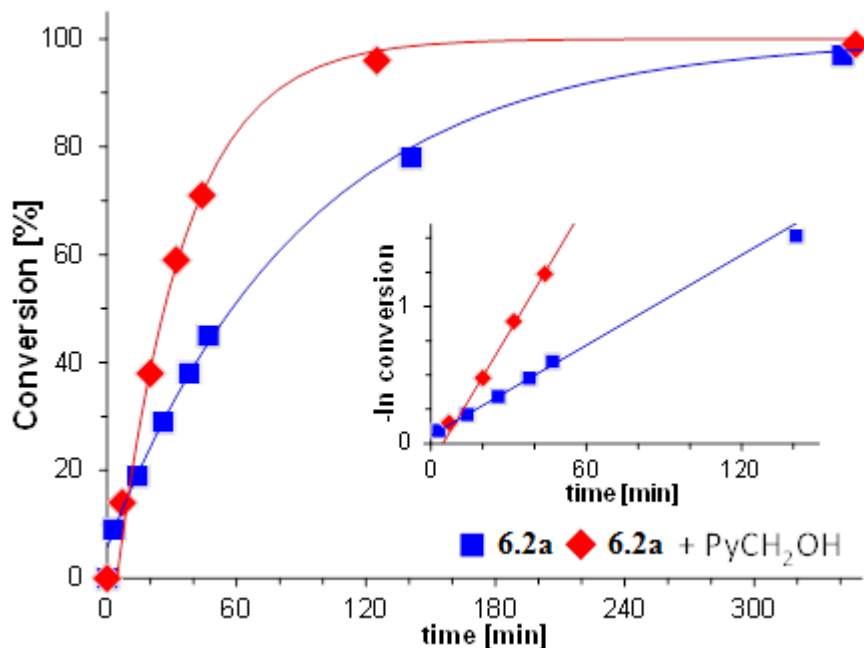


**Figure 6.S1.** Kinetics of *rac*-lactide polymerization with **6.2a** without (blue squares) and with addition of 1 equiv pyridylmethanol (red diamonds). Linear regression provided  $k_{\text{app}} = 0.69(2) \text{ h}^{-1}$  and  $t_0 = -4 \text{ min}$  (**6.2a**) and  $k_{\text{app}} = 1.9(1) \text{ h}^{-1}$  and  $t_0 = 5 \text{ min}$  (**6.2a**/PyCH<sub>2</sub>OH). Conditions: C<sub>6</sub>D<sub>6</sub>, RT, [lactide] = 200 mM, [6.L<sub>2</sub>Cu<sub>2</sub>(OR)<sub>2</sub>] = 2 mM.

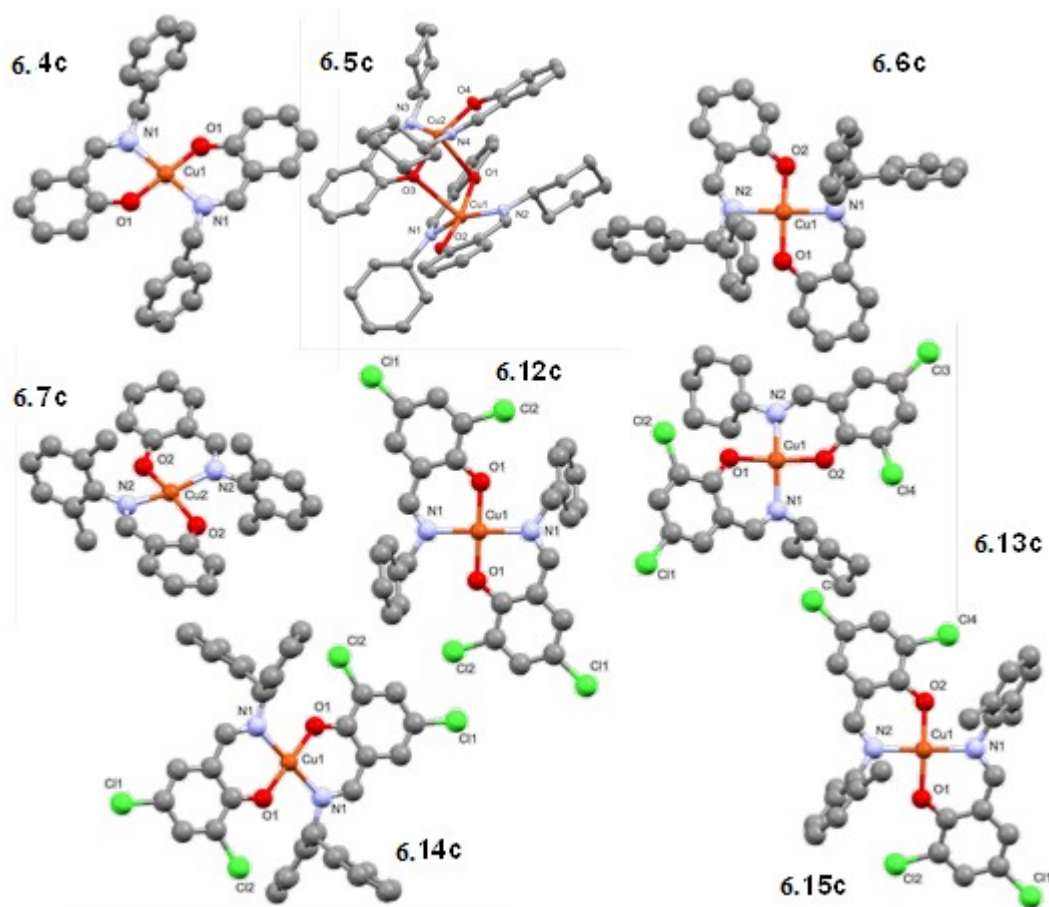


**Figure 6.S2.** X-ray structures of homoleptic bis(iminoaryloxy) copper complexes **6.4c-6.7c** and **6.12c-6.15c**.

The structure of **6.5c** has been reported before.<sup>1</sup> Complex **6.5c**, the only dimeric complex, is also the only crystal with a green colour. All other crystals have brownish colours. For **6.4c**<sup>2</sup> and **6.6c**<sup>3</sup>, the structure of a polymorph has been reported.

**Table 6.S1.** Experimental details of X-ray diffraction studies of the homoleptic complexes.

	<b>6.4c</b>	<b>6.5c</b>	<b>6.6c</b>	<b>6.7c</b>	<b>6.12c</b>	<b>6.13c</b>	<b>6.14c</b>	<b>6.15c</b>
Formula	C <sub>28</sub> H <sub>24</sub> CuN <sub>2</sub> O <sub>2</sub>	C <sub>26</sub> H <sub>32</sub> CuN <sub>2</sub> O <sub>2</sub>	C <sub>40</sub> H <sub>32</sub> CuN <sub>2</sub> O <sub>2</sub>	C <sub>30</sub> H <sub>28</sub> CuN <sub>2</sub> O <sub>2</sub>	C <sub>28</sub> H <sub>20</sub> Cl <sub>4</sub> CuN <sub>2</sub> O <sub>2</sub>	C <sub>26</sub> H <sub>28</sub> Cl <sub>4</sub> CuN <sub>2</sub> O <sub>2</sub>	C <sub>40</sub> H <sub>28</sub> Cl <sub>4</sub> CuN <sub>2</sub> O <sub>2</sub>	C <sub>37</sub> H <sub>32</sub> Cl <sub>4</sub> CuN <sub>2</sub> O <sub>2</sub>
<i>M<sub>w</sub></i> (g/mol)	484.03	468.07	636.21	512.08	621.80	605.84	773.98	741.98
<i>T</i> (K); F(000)	150; 502	100; 1976	110; 1324	100; 1068	150; 630	130; 1244	150; 395	150; 762
Crystal System	Monoclinic	Monoclinic	Monoclinic	Monoclinic	Monoclinic	Monoclinic	Triclinic	Monoclinic
Space Group	<i>P</i> 2 <sub>1</sub> /n	<i>P</i> 2 <sub>1</sub> /n	<i>P</i> 2 <sub>1</sub> /n	<i>P</i> 2/n	<i>P</i> 2 <sub>1</sub> /c	<i>P</i> 2 <sub>1</sub> /c	<i>P</i> (-1)	<i>P</i> 2 <sub>1</sub>
Unit Cell: <i>a</i> (Å)	10.1218(3)	21.3119(6)	17.4037(5)	14.3106(5)	10.5290(4)	14.7942(4)	8.4189(3)	11.0291(3)
<i>b</i> (Å)	9.0847(2)	9.3432(3)	10.2071(3)	12.1062(5)	6.0011(2)	12.6835(4)	8.9201(3)	9.5222(3)
<i>c</i> (Å)	12.4074(3)	23.0794(7)	18.7364(5)	14.6604(6)	20.1597(8)	14.0429(4)	12.4839(4)	16.5393(5)
<i>α</i> (°)	90	90	90	90	90	90	72.893(1)	90
<i>β</i> (°)	107.042(1)	99.239(1)	111.805(1)	96.816(2)	99.976(1)	91.930(1)	72.331(1)	96.603(1)
<i>γ</i> (°)	90	90	90	90	90	90	87.649(1)	90
<i>V</i> (Å <sup>3</sup> )	1090.81(5)	4536.0(2)	3090.2(2)	2521.9(2)	1254.54(8)	2633.6(1)	852.56(5)	1725.46(9)
<i>μ</i> (mm <sup>-1</sup> ); <i>Z</i>	5.555; 2	1.549; 8	4.012; 4	4.824; 4	7.436; 2	7.067; 4	5.553; 1	5.467; 2
<i>θ</i> (°); completeness	3.2-60.6; 1.0	5.1-71.9; 1.0	2.2-60.8; 0.99	3.6-60.6; 1	3.7-60.7; 1.0	2.6-54.2; 0.95	3.4-60.7; 1.0	3.5-60.6; 0.77
collected reflections; <i>R<sub>σ</sub></i>	27675; 0.026	122428; 0.018	68961; 0.024	43808; 0.038	18642; 0.022	19086; 0.034	20783; 0.036	87742; 0.019
unique reflections; <i>R<sub>int</sub></i>	2492; 0.052	8881; 0.040	7097; 0.045	5818; 0.060	2879; 0.042	4639; 0.034	3881; 0.060	6152; 0.030
<i>R</i> 1( <i>F</i> ) ( <i>I</i> > 2σ( <i>I</i> ))	0.080	0.035	0.047	0.051	0.032	0.047	0.044	0.025
w <i>R</i> ( <i>F</i> <sup>2</sup> ) (all data)	0.253	0.100	0.134	0.130	0.086	0.123	0.124	0.066
Go <i>F</i> ( <i>F</i> <sup>2</sup> ); Flack- <i>x</i>	1.068; -	1.034; -	1.052; -	1.054; -	1.099; -	1.040; -	1.080; -	1.13; -0.011(3)
Residual electron density	0.80; -1.54	0.42; -0.43	0.68; -0.60	1.08; -0.52	0.26; -1.08	0.41; -0.80	0.48; -1.11	0.24; -0.56



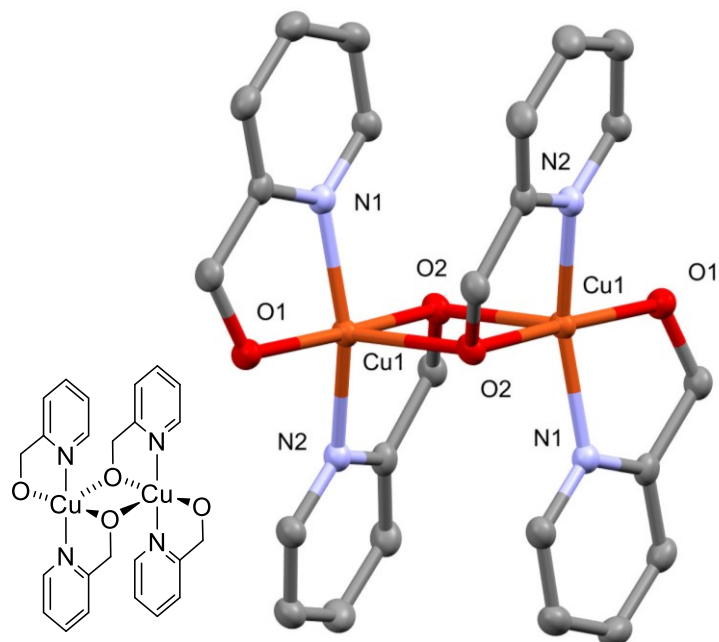


**Figure 6.S3.** X-ray structure of bis(pyridylmethoxide)copper. Thermal displacements are shown at the 50% probability level. Hydrogen atoms were omitted for clarity.

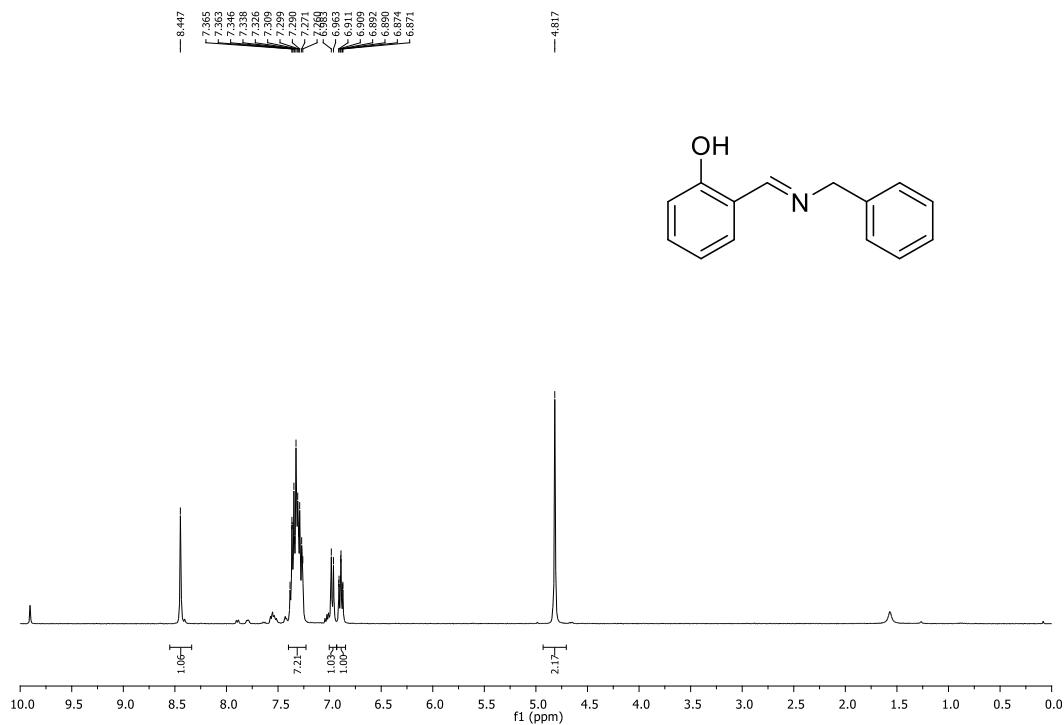


**Figure 6.S4.** <sup>1</sup>H-NMR spectra of 6.L4H in CDCl<sub>3</sub> (400 MHz).

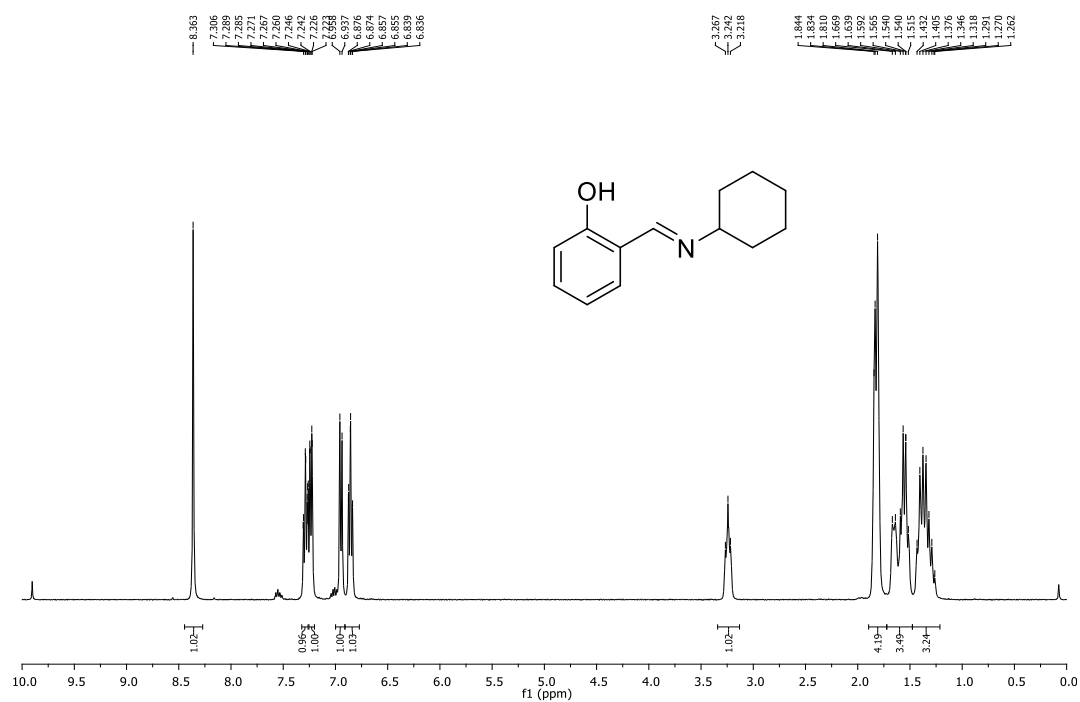


**Figure 6.S5.**  $^1\text{H-NMR}$  spectra of **6.L5H** in  $\text{CDCl}_3$  (400 MHz).

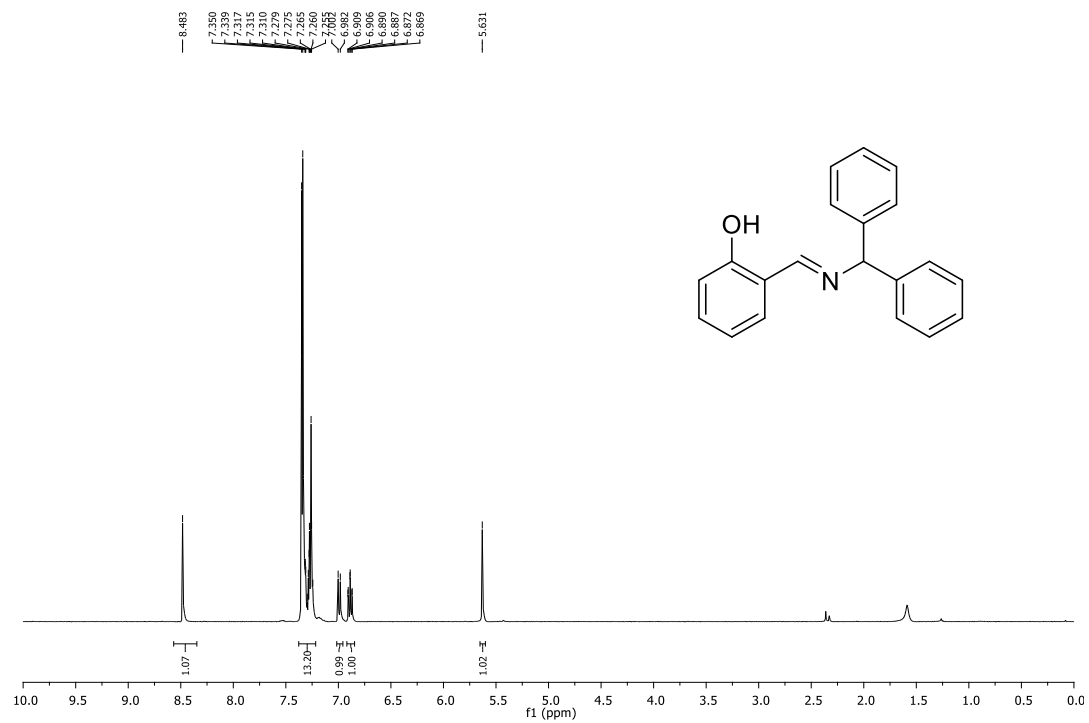


**Figure 6.S6.**  $^1\text{H-NMR}$  spectra of **6.L6H** in  $\text{CDCl}_3$  (400 MHz).

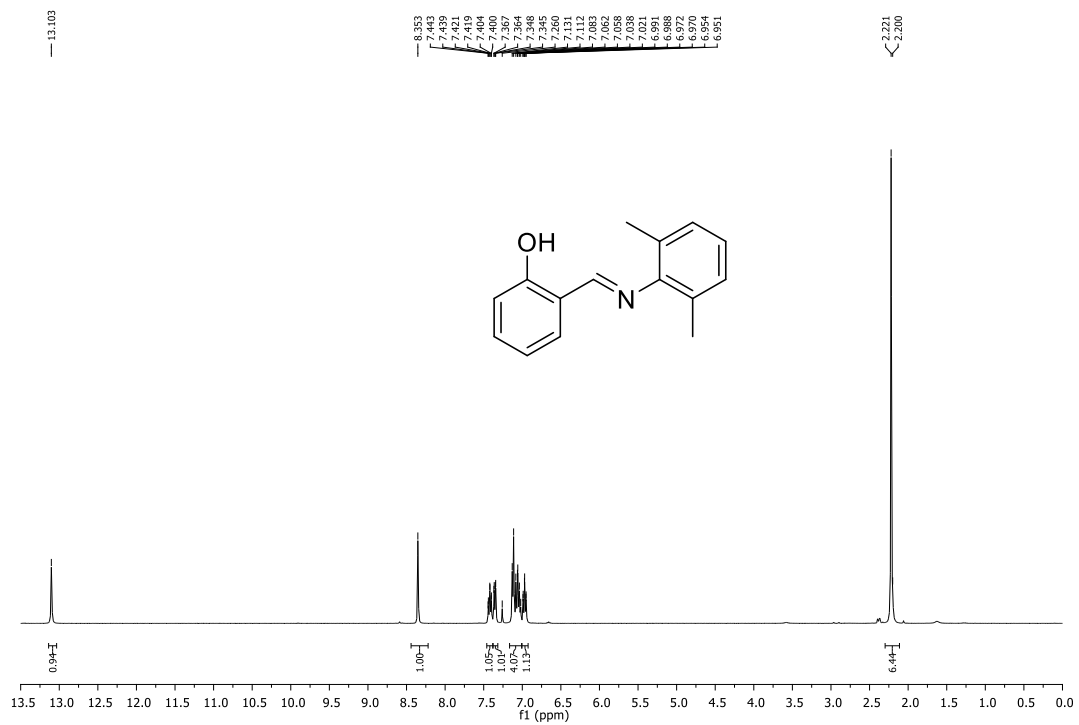


Figure 6.S7. <sup>1</sup>H-NMR spectra of 6.L7H in CDCl<sub>3</sub> (400 MHz).

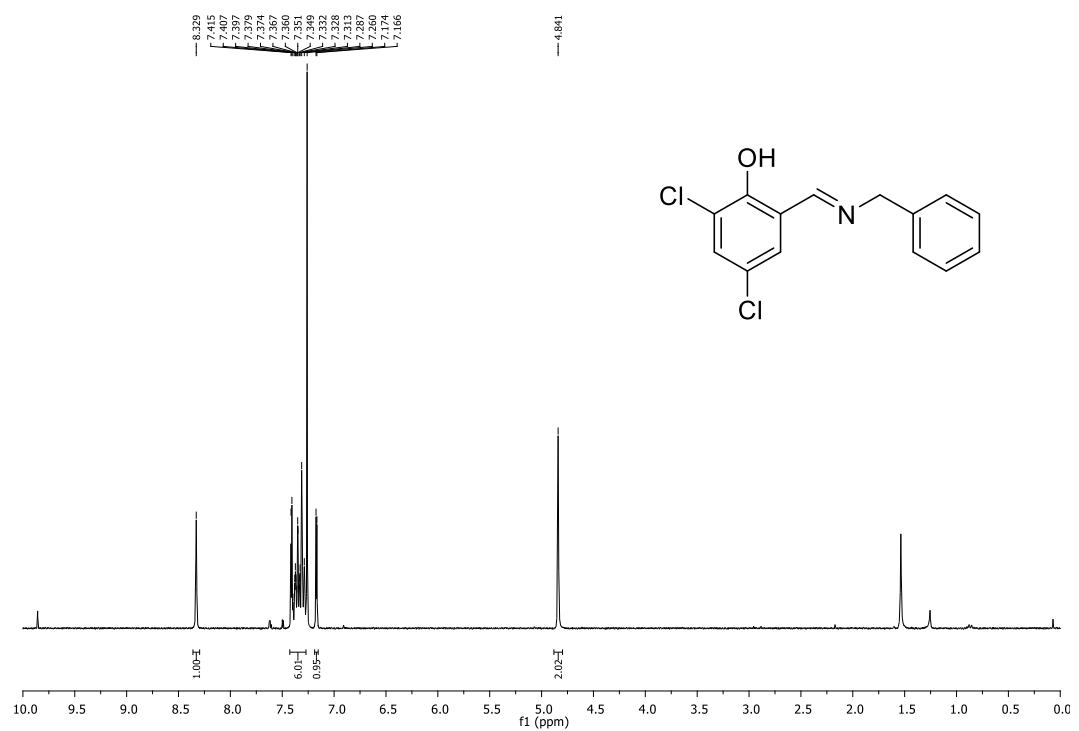


Figure 6.S8. <sup>1</sup>H-NMR spectra of 6.L12H in CDCl<sub>3</sub> (400 MHz).

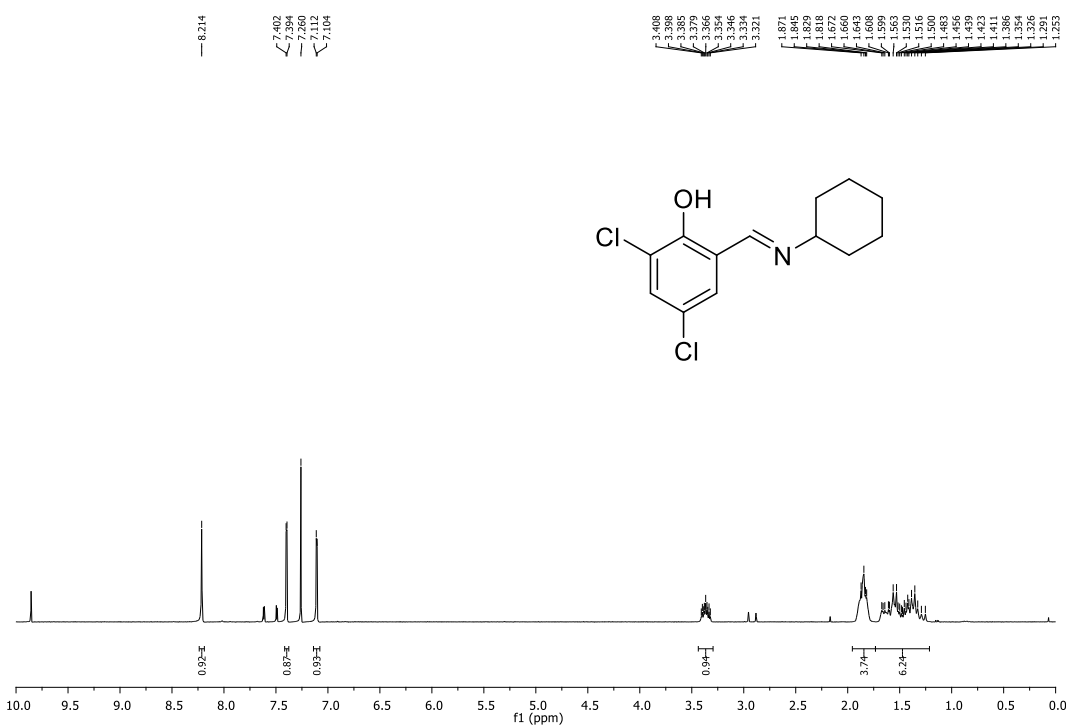


Figure 6.S9. <sup>1</sup>H-NMR spectra of 6.L13H in CDCl<sub>3</sub> (400 MHz).

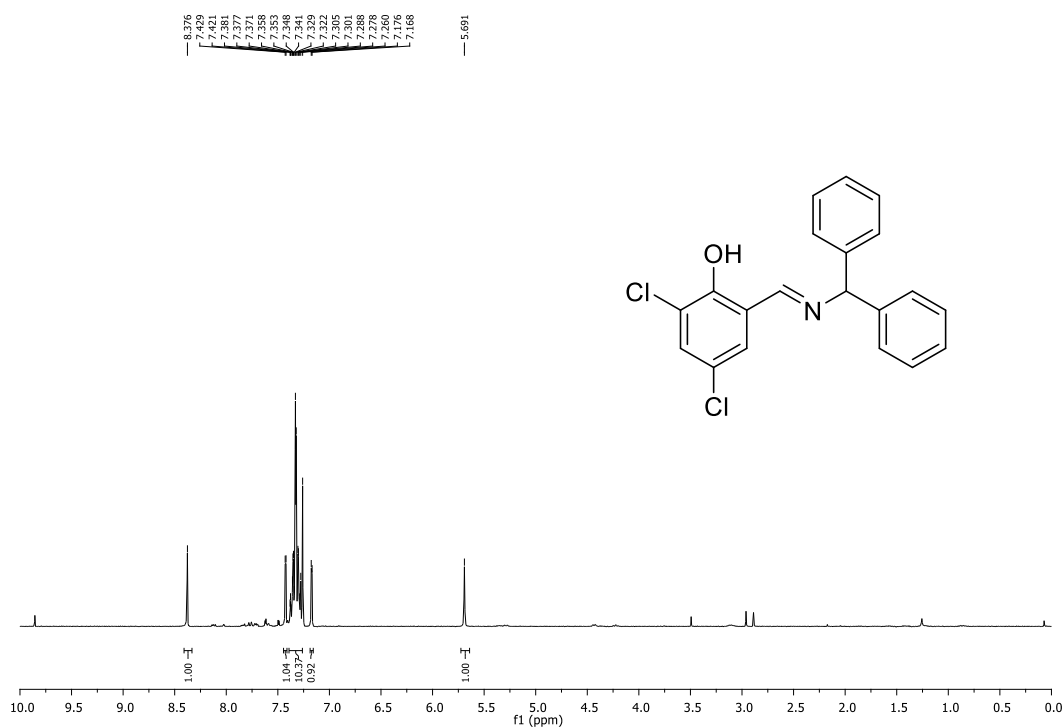
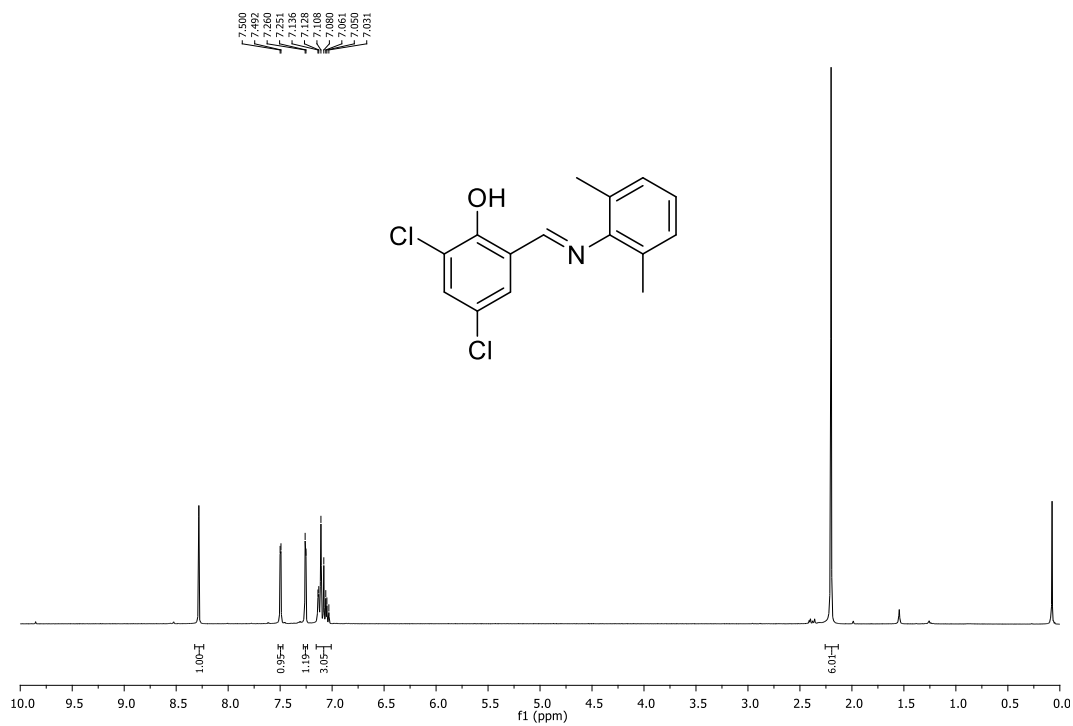


Figure 6.S10. <sup>1</sup>H-NMR spectra of 6.L14H in CDCl<sub>3</sub> (400 MHz).



**Figure 6.S11.**  $^1\text{H-NMR}$  spectra of **6.L15H** in  $\text{CDCl}_3$  (400 MHz).

1. T. Hatsue, O. Kazuhide, T. Akira and Y. Shoichiro, *Bull. Chem. Soc. Jpn.*, 1979, **52**, 3522.
2. J. M. Fernández-G, J. Xochitiotzi-Flores, S. Hernández-Ortega, V. Gómez-Vidales and M. Del Rocío Patiño-Maya, *J. Coord. Chem.*, 2010, **63**, 2132.
3. J. M. Fernández-G, O. L. Ruíz-Ramírez, R. A. Toscano, N. Macías-Ruvalcaba and M. Aguilar-Martínez, *Transition Metal Chemistry*, 2000, **25**, 511.



## Supporting information Chapter 7

Daneshmand, P.; Michalsky, I.; Schaper, F. Configurationally Flexible Zinc Complexes as Catalysts for *rac*-Lactide Polymerisation. *Dalton Trans.* **2018**, *Submitted*.

## Configurationally Flexible Zinc Complexes as Catalysts for *rac*-Lactide Polymerisation

*Pargol Daneshmand, Ina Michalsky, Frank Schaper\**

*Centre in Green Chemistry and Catalysis, Department of chemistry, Université de Montréal, C. P. 6128 Succ. Centre-Ville, Montréal, QC, H3T 3J7, Canada.*

*\* [Frank.Schaper@umontreal.ca](mailto:Frank.Schaper@umontreal.ca)*

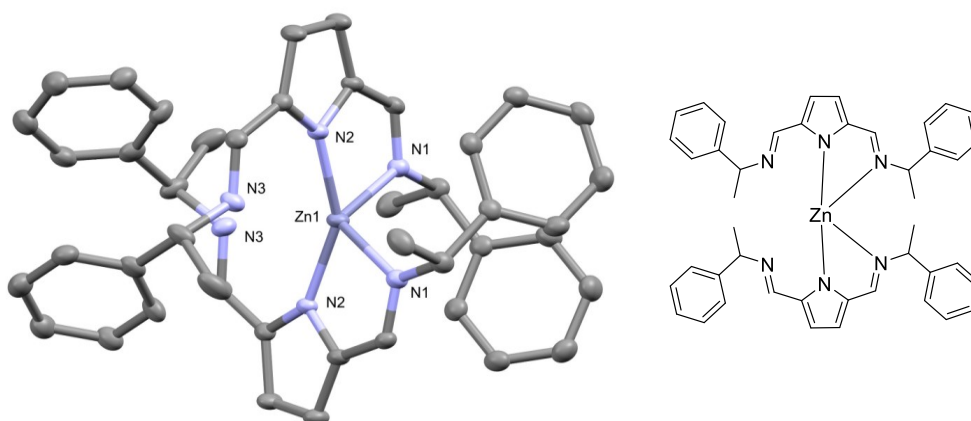


**Figure 7.S1.** Crystal structure of  $(7.L1)_2Zn$ .

Thermal ellipsoids displayed at the 50% probability level. Hydrogen atoms omitted for clarity.

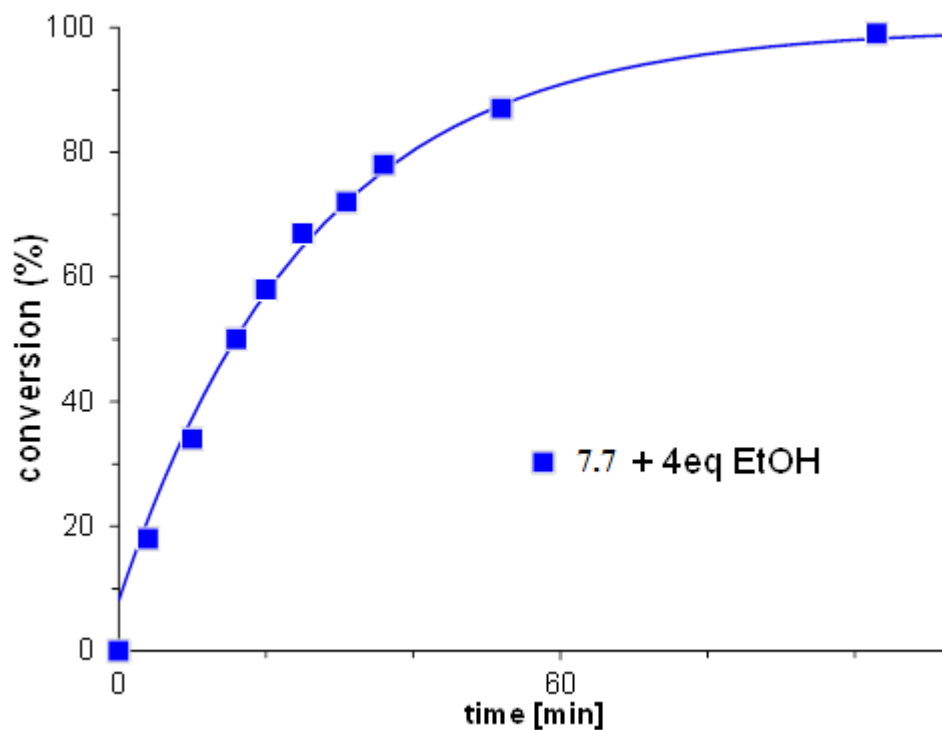


**Figure 7.S2.** Conversion-time plots for *rac*-lactide polymerizations with **7.7** + 4eq EtOH.



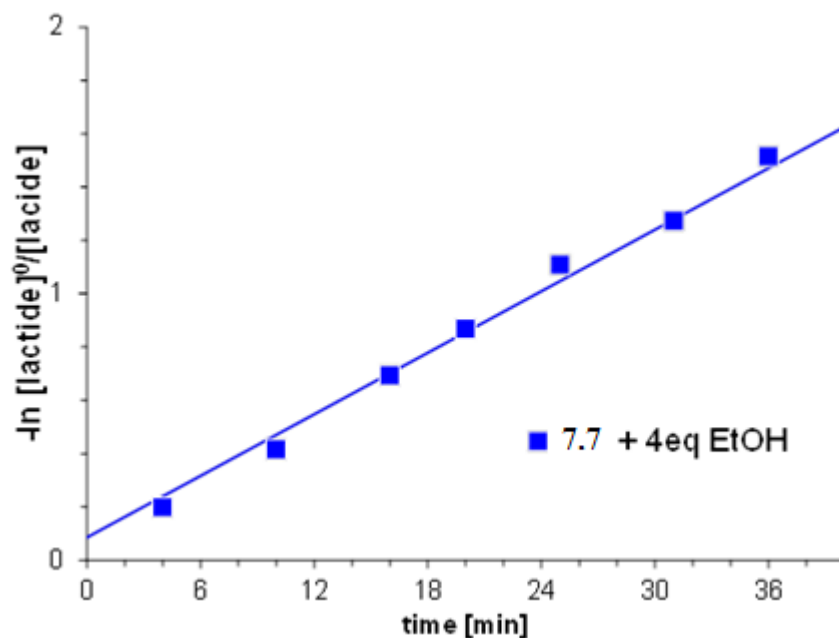


**Figure 7.S3.** Linearized conversion-time plots for *rac*-lactide polymerizations with 7.7 + 4eq EtOH.

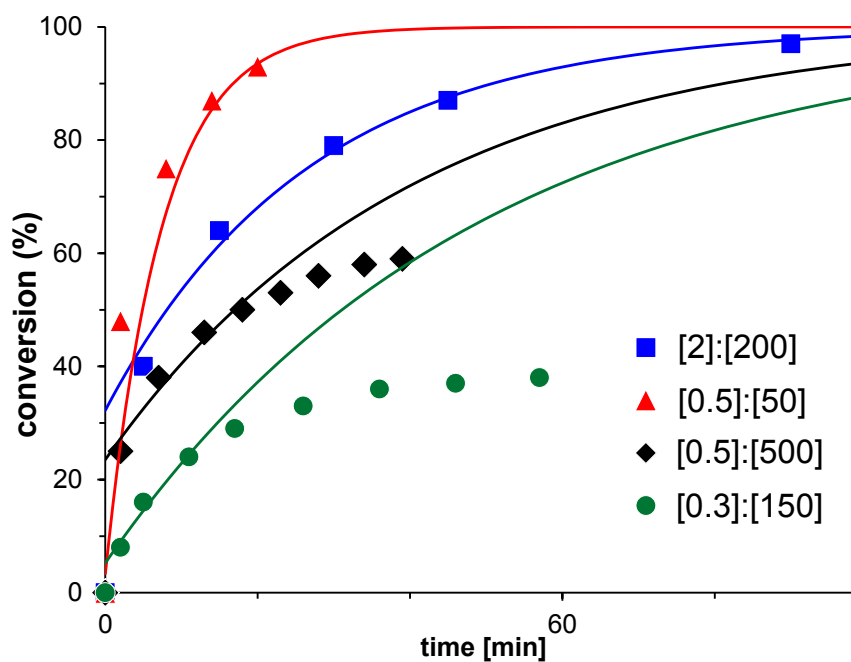


**Figure 7.S4.** Conversion-time plots for *rac*-lactide polymerizations with 7.10 at different catalyst and lactide concentrations at RT in C<sub>6</sub>D<sub>6</sub> ([7.10] = 2, 0.5, 0.3 mM).

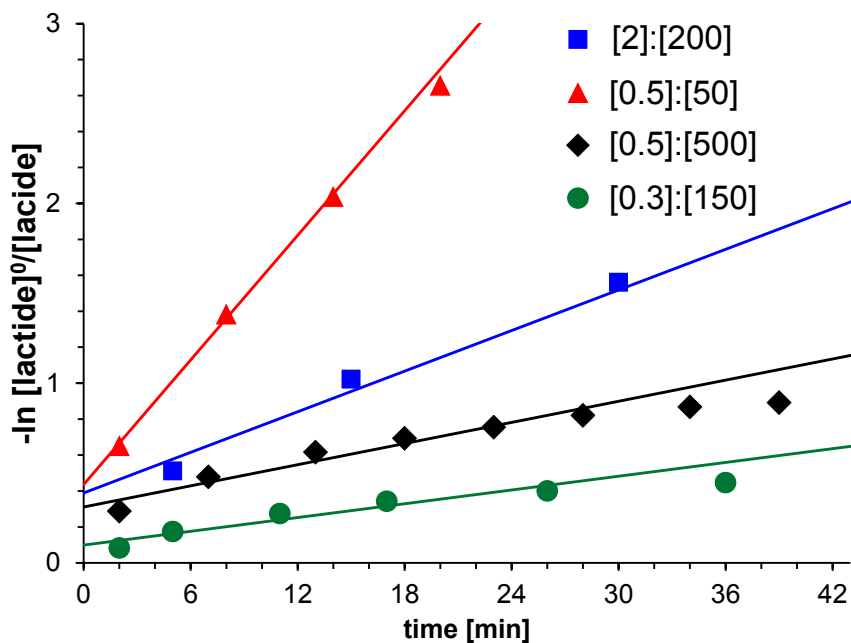


**Figure 7.S5.** Linearized conversion-time plots for *rac*-lactide polymerizations with **7.10** at different catalyst or lactide concentrations at RT in  $C_6D_6$  ( $[7.10] = 2, 0.5, 0.3$  mM).

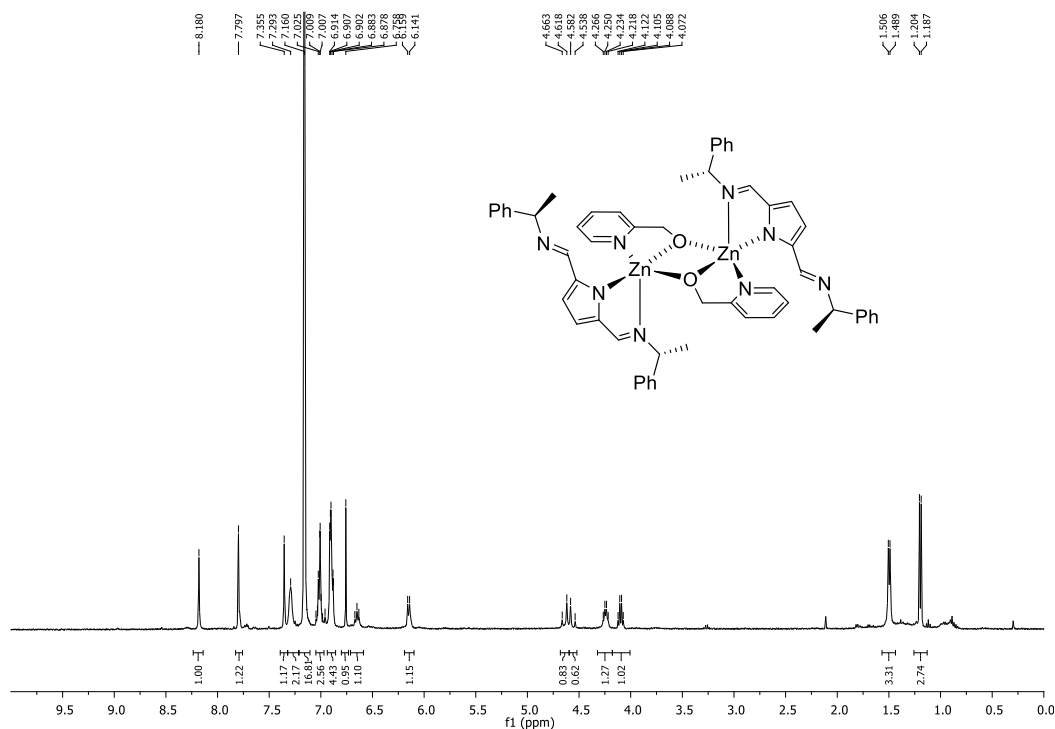


**Figure 7.S6.**  $^1H$ -NMR (400 MHz) spectra of **7.2** in  $C_6D_6$ .

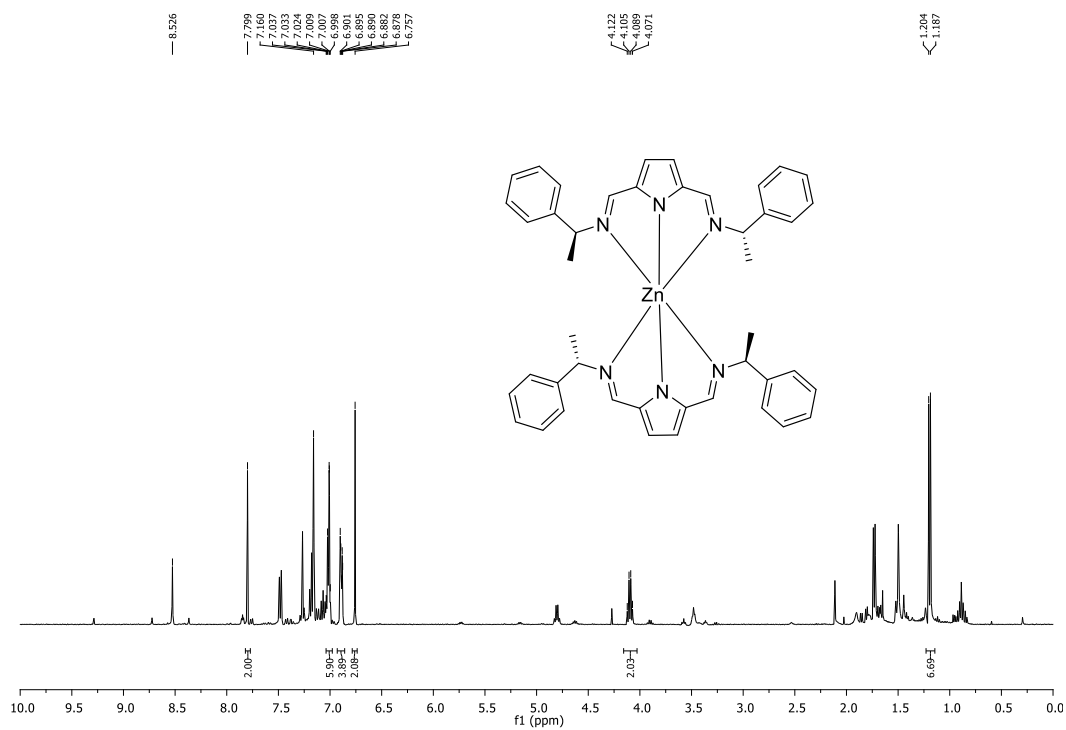


Figure 7.S7.  $^1H$ -NMR (400 MHz) spectra of  $(7.L1)_2Zn$  in  $C_6D_6$ .

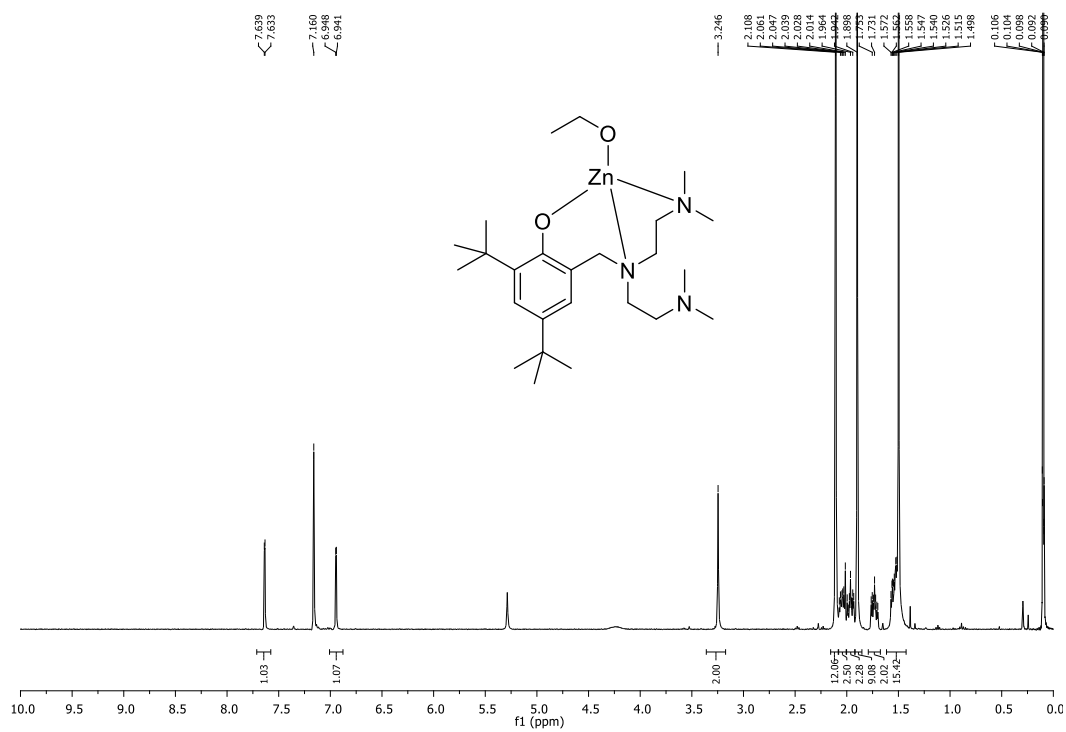
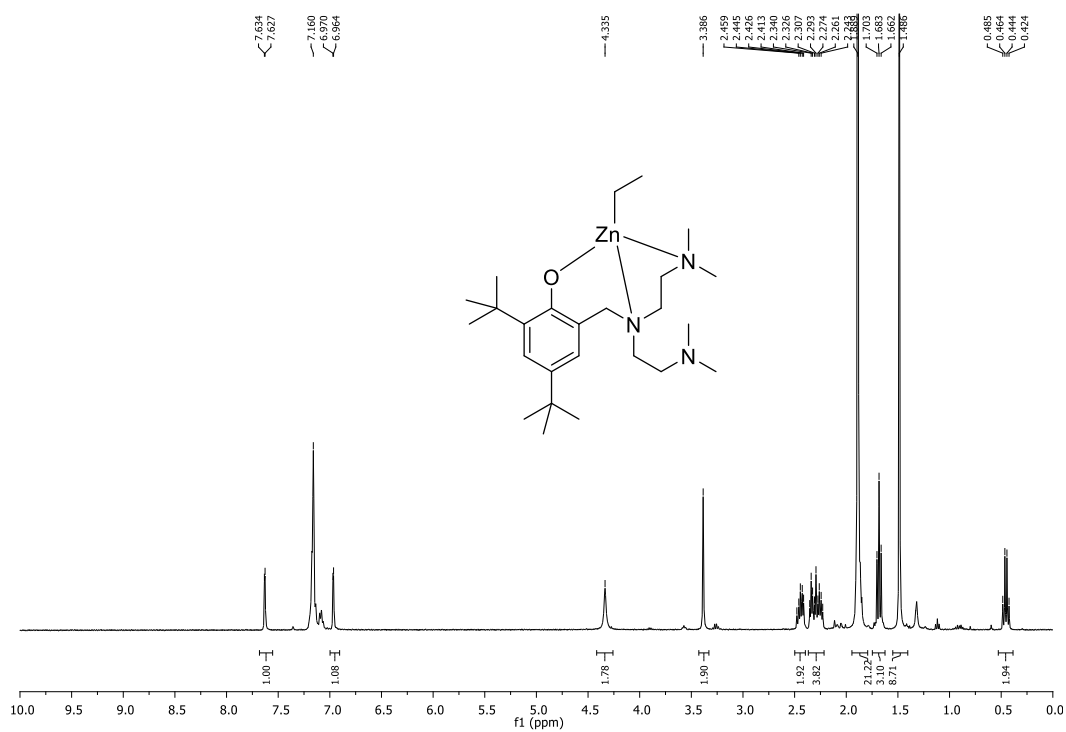
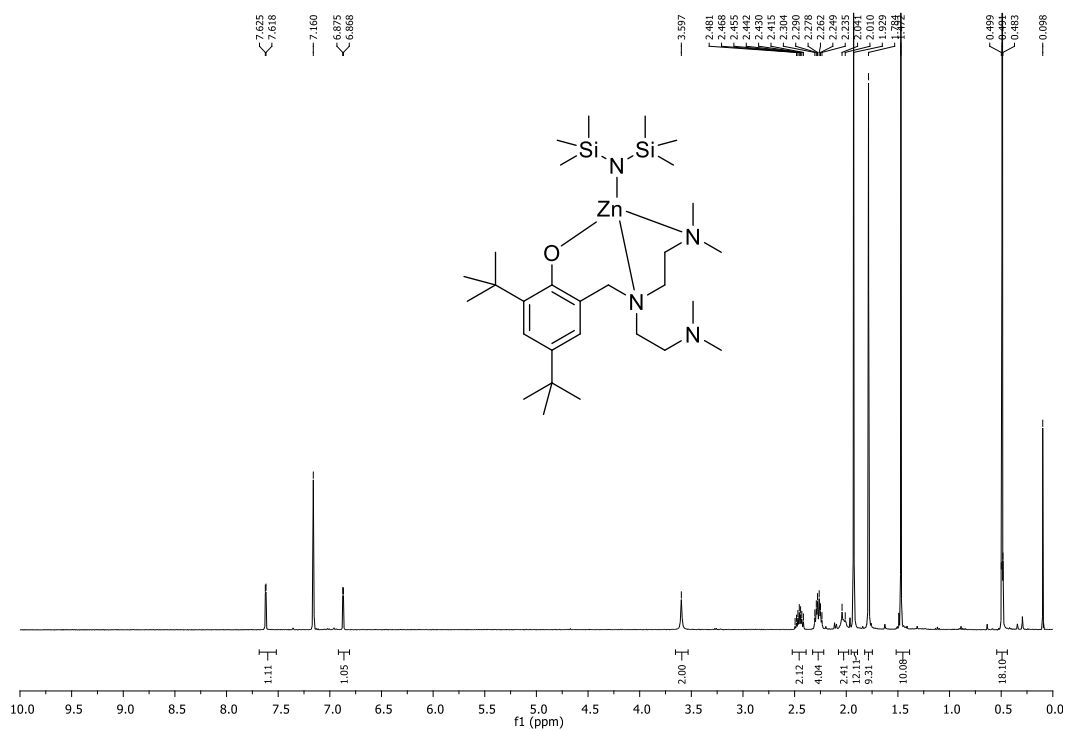


Figure 7.S8.  $^1H$ -NMR (400 MHz) spectra of **7.7** in  $C_6D_6$ .



**Figure 7.S9.**  $^1\text{H-NMR}$  (400 MHz) spectra of **7.8** in  $\text{C}_6\text{D}_6$ .



**Figure 7.S10.**  $^1\text{H-NMR}$  (400 MHz) spectra of **7.9** in  $\text{C}_6\text{D}_6$ .

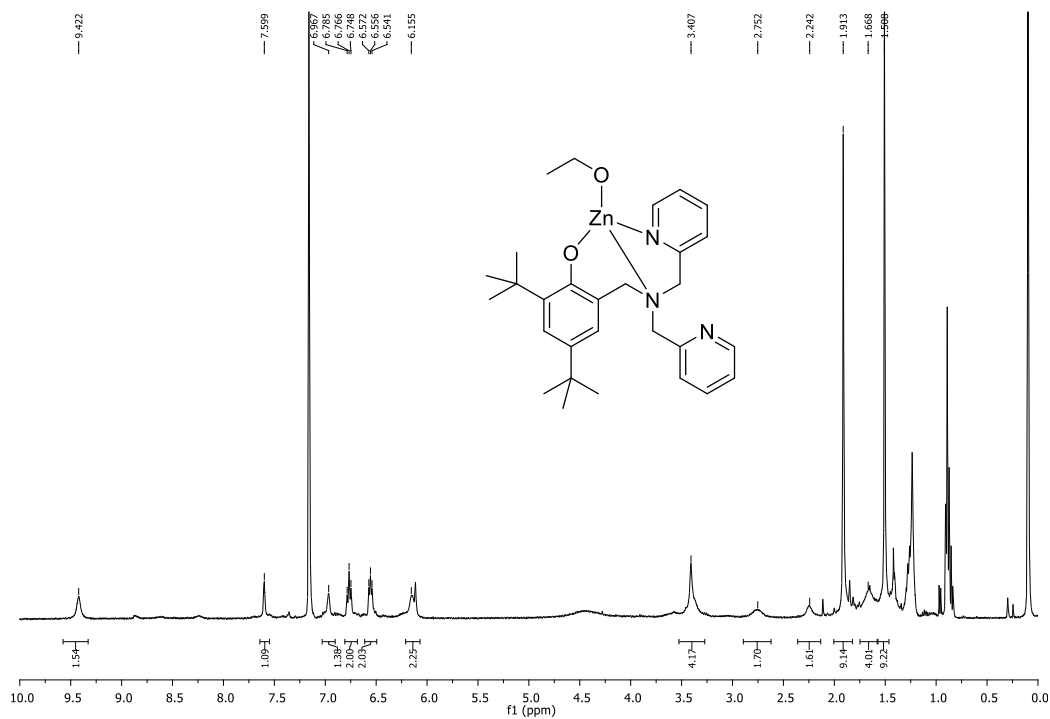


Figure 7.S11.  $^1\text{H-NMR}$  (400 MHz) spectra of **7.10** in  $\text{C}_6\text{D}_6$ .

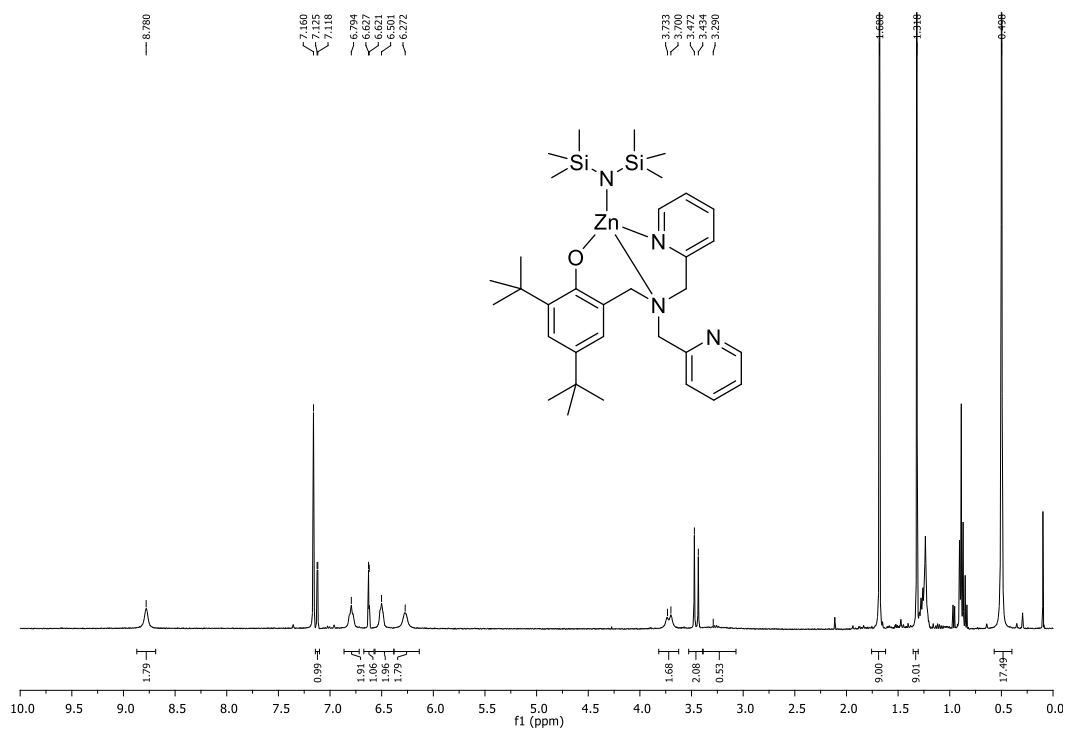


Figure 7.S12.  $^1\text{H-NMR}$  (400 MHz) spectra of **7.11** in  $\text{C}_6\text{D}_6$ .

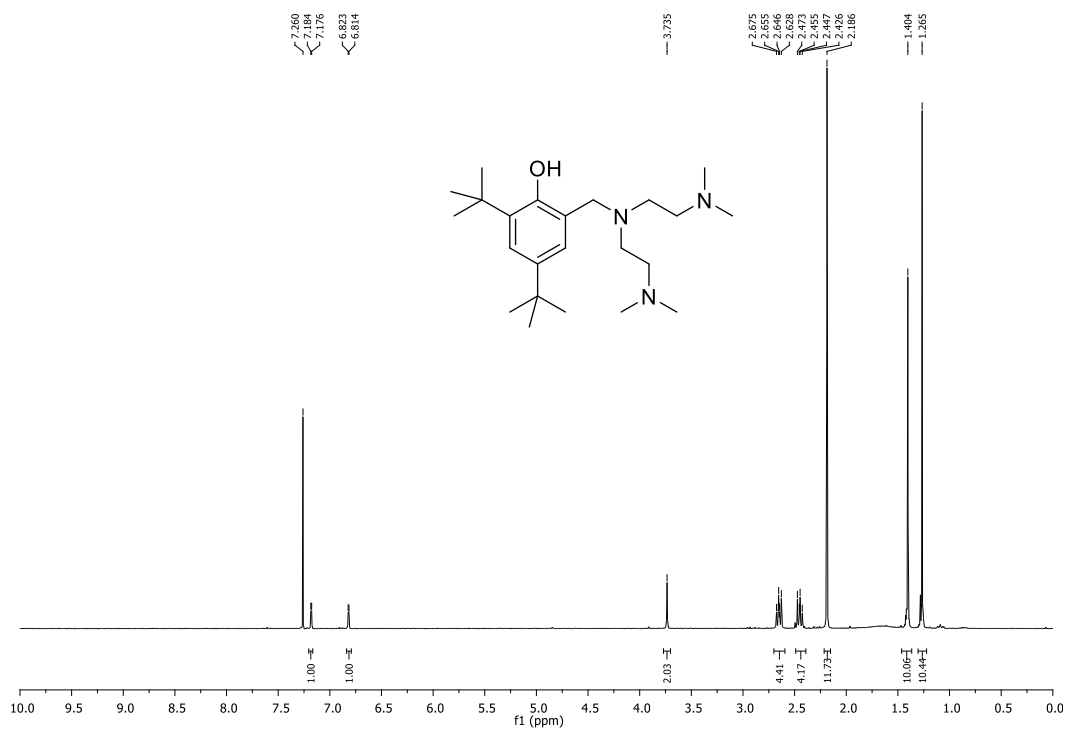


Figure 7.S13.  $^1\text{H-NMR}$  (300 MHz) spectra of 7.L2 in  $\text{CDCl}_3$ .

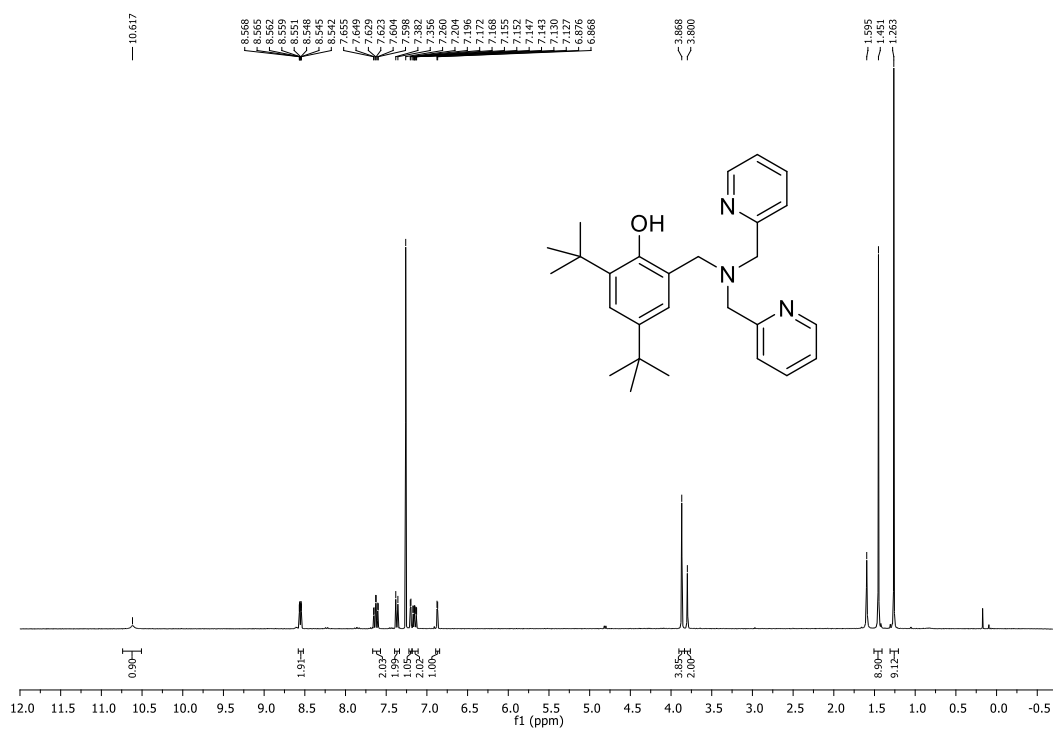


Figure 7.S14.  $^1\text{H-NMR}$  (300 MHz) spectra of 7.L3 in  $\text{CDCl}_3$ .

## Supporting information Chapter 8

Daneshmand, P.; Randimbiarisolo, A.; Schaper, F. Tetradentate aminophenolate copper complexes in *rac*-lactide polymerization. *Can. J. Chem.* **2018**, *Submitted*.

### Tetradentate aminophenolate copper complexes in *rac*-lactide polymerization

*Pargol Daneshmand, Aurélie Randimbiarisolo, Frank Schaper\**

*Centre in Green Chemistry and Catalysis, Département de chimie, Université de Montréal, 2900 Boul. E.-Montpetit, Montréal, QC, H3T 1J4, Canada*

*\* Frank.Schaper@umontreal.ca*

**Table 8.S1.** Details of *rac*-lactide polymerizations at 140 °C in molten monomer with **8.1-8.6**

#	Catalyst	Additive	LA:Cat.:BnO H <sup>a</sup>	LA:RO H <sup>a</sup>	Conversion	Time	$k_{obs}$ [h <sup>-1</sup> ] <sup>b</sup>	$P_r$	$M_n$ <sup>c</sup> [g/mol]	$M_n(\text{calc})$ [g/mol] <sup>d</sup>	$M_w/M_n$
1	8.1		100:1:1	100:1	7%	0.5 h	0.15(1)				
2	8.1		100:1:1	100:1	22%	2 h	(see above) <sup>e</sup>	0.74			
3	8.1		100:1:1	100:1	40%	4 h	(see above) <sup>e</sup>	0.78			
4	8.1		100:1:1	100:1	63%	7 h	(see above) <sup>e</sup>	0.63			
5	8.1		100:1:1	100:1	92%	24 h	(see above) <sup>e</sup>				
6	8.1		100:1:1	100:1	94%	24 h	(see above) <sup>e</sup>	0.7	800	13500	2.9
7	8.1		100:1:1	100:1	95%		0.15(1)	0.65- 0.85			
8	8.1		100:1:2	100:2	96%		0.24(1)	0.75	600	6900	2
9	8.1		100:1:4	100:4	95%		0.30(1)	0.75- 0.8	600	3400	1.8
10	8.1		100:1:8	100:8	94%		0.35(1)		500	1700	1.7
11	8.1	5 equiv H <sub>2</sub> O	100:1:1	100:1	96%	21 h	0.37(1)	0.7- 0.85	800	13800	1.7
12	8.1	5 equiv AcOH	100:1:1	100:1	94%	23 h	0.19(1)	0.65- 0.75	700	13500	1.7
13	8.1	1 equiv [Et <sub>4</sub> N]Cl	100:1:1	100:1	95%	21 h	0.43(2)	0.60- 0.75	800	13700	1.6
14	8.1	4 equiv [Et <sub>4</sub> N]Cl	100:1:1	100:1	94%	6 h	0.43(4)	0.55- 0.7	1600	13500	1.6
15	8.1	1 equiv [Et <sub>3</sub> NH][OTs]	100:1:1	100:1	97%	21 h	0.43(4)	0.75- 0.85	800	14000	1.8
16	8.1	4 equiv [Et <sub>3</sub> NH][OTs]	100:1:1	100:1	93%	21 h	0.37(1)	0.75- 0.8	800	13400	1.7



17	8.2	100:1:1	100:1	95%	21 h	0.13(2)	0.85	1500	13700	1.5
18	8.3	100:1:1	100:2 <sup>f</sup>	95%	14 h	0.081(3), 0.26(4)	0.8- 0.85	500	6800	2.3
19	8.3	100:1:4	100:5 <sup>f</sup>	94%	14 h	0.097(2), 0.27(1)		600	2700	2
20	8.4	100:1:0	100:1 <sup>f</sup>	94%		0.13(1)		3500	13500	1.2
21	8.4	100:1:1	100:2 <sup>f</sup>	6%	0.5 h	0.16(1), 0.52(2)				
22	8.4	100:1:1	100:2 <sup>f</sup>	27%	2 h	(see above) <sup>e</sup>	0.75			
23	8.4	100:1:1	100:2 <sup>f</sup>	53%	4 h	(see above) <sup>e</sup>	0.65			
24	8.4	100:1:1	100:2 <sup>f</sup>	88%	7 h	(see above) <sup>e</sup>	0.6			
25	8.4	100:1:1	100:2 <sup>f</sup>	94%	24 h	(see above) <sup>e</sup>	0.55			
26	8.4	100:1:1	100:2 <sup>f</sup>	97%	24 h	(see above) <sup>e</sup>	0.55			
27	8.4	100:1:1	100:2 <sup>f</sup>	99%	8 h	(see above) <sup>e</sup>				
28	8.4	100:1:1	100:2 <sup>f</sup>	97%	6 h	(see above) <sup>e</sup>	0.7- 0.85			
29	8.4	100:1:1 <sup>g</sup>	100:2 <sup>f</sup>	96%	20 h	(see above) <sup>e</sup>	0.75	9200	6900	1.4
30	8.4	100:1:1 <sup>h</sup>	100:2 <sup>f</sup>	96%	21 h	(see above) <sup>e</sup>	0.7	1200	6900	1.3
31	8.4	100:1:2	100:3 <sup>f</sup>	94%	21 h	0.23(1)	0.7-0.8	1800	4500	1.5
32	8.4	100:1:4	100:5 <sup>f</sup>	93%	20 h	0.17(1)	0.65- 0.75	1900	2700	1.5
33	8.4	100:1:8	100:9 <sup>f</sup>	97%	23 h	0.24(1)	0.75- 0.9	900	1600	1.6
34	8.4	50:1:1	50:2 <sup>f</sup>	97%	24 h	0.57(3)	0.85- 0.9	600	3500	1.7

35	8.4		200:1:1	200:2 <sup>f</sup>	94%	23 h	0.072(4),0.15	0.75-0.8	200	13500	1.1
36	8.4	1 equiv pyridine	100:1:1	100:2 <sup>f</sup>	93%	22 h	0.77(10)	0.8-0.85	500	6700	1.5
37	8.4	1 equiv <i>t</i> BuOK	100:1:1	100:2 <sup>f</sup>	97%	22 h	0.40(5)	0.5-0.7	500	7000	4
38	8.4	1 equiv NEt <sub>3</sub>	100:1:1	100:2 <sup>f</sup>	95%	22 h	0.40(3)	0.75-0.85	700	6800	1.1
39	8.5		100:1:1	100:2 <sup>f</sup>	94	21 h	0.10(1), 0.28(2)	0.8	500	6800	2
40	8.5		100:1:1	100:2 <sup>f</sup>	96	24 h	(see above) <sup>e</sup>		900	6900	1.5
41	8.5		100:1:4	100:5 <sup>f</sup>	93	15 h	0.14(1), 0.35(4)	0.75	700	2700	2.1
42	8.6		100:1:1	100:1	95%	20 h	0.14(1), 0.34(4)	0.8	800	13700	2.6
43	8.6		100:1:1	100:1	96%	20 h	(see above) <sup>e</sup>		1200	13800	2.9
44	8.6		100:1:4	100:4	94%	23 h	0.17(1), 0.44	0.75	1200	3400	2.2

<sup>a</sup> LA = *rac*-lactide.  $P_r$  values were determined from homodecoupled <sup>1</sup>H NMR spectra and calculated from  $P_r = 2 \cdot I_1 / (I_1 + I_2)$ , with  $I_1 = 5.15 - 5.21$  ppm (*rmr*, *mmr/rmm*),  $I_2 = 5.21 - 5.25$  ppm (*mmr/rmm*, *mmm*, *mrmm*). The integration of the left multiplet and right multiplet ( $I_1$  and  $I_2$ ) required only one, very reproducible dividing point of the integration, which was always taken as the minimum between the two multiplets. <sup>b</sup> Determined by linear regression of the linear regions in the semilogarithmic plot. If two linear regions could be identified, both values were provided. The second rate constants for reactions at higher conversion was typically determined only with a limited amount of data points. <sup>c</sup> Determined from GPC analysis against polystyrene standards and a Mark-Houwink factor of 0.58 (see experimental). <sup>d</sup> Calculated from conversion $\cdot n(\text{lactide})/n(\text{ROH})+M(\text{ROH})$ . <sup>e</sup> Several experiments combined in the linear regression analysis. <sup>f</sup> Catalyst contained co-crystallized methanol or ethanol. <sup>g</sup> Half of the normally used amount of lactide in the same experimental setup. <sup>h</sup> Twice the normally used amount of lactide in the same experimental setup.

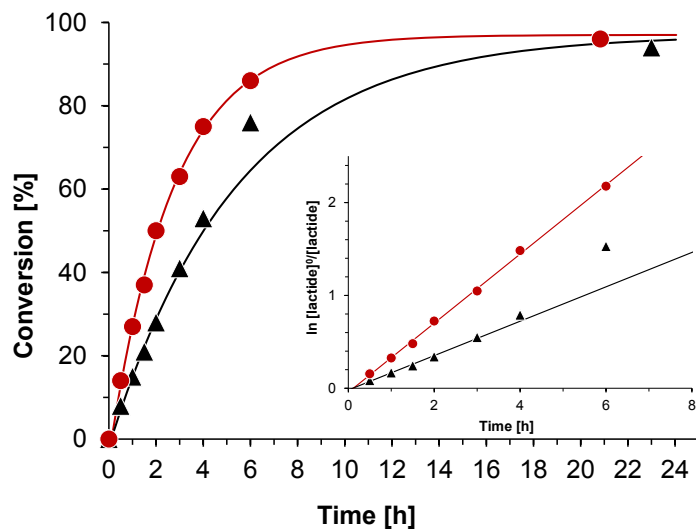


**Figure 8.S1.** Conversion-time plots for the polymerization of *rac*-lactide with **8.1**/benzyl alcohol at 140 °C. [lactide]:[ **8.1**]:[BnOH] = 100:1:1. Black triangles: in the presence of 5 equiv of acetic acid (relative to **8.1**),  $k_{\text{obs}} = 0.19(1) \text{ h}^{-1}$ . Red circles: in the presence of 5 equiv of water (relative to **8.1**),  $k_{\text{obs}} = 0.37(1) \text{ h}^{-1}$ .

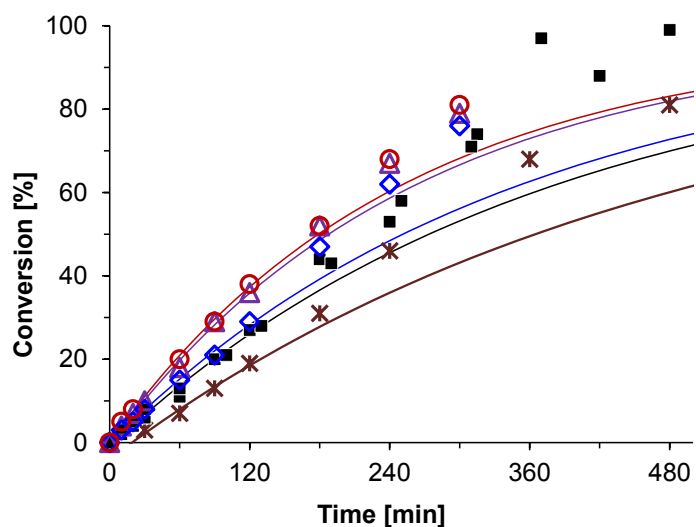


**Figure 8.S2.** Conversion-time plot for *rac*-lactide polymerizations with **8.4** at 140 °C in the presence of different amounts of benzyl alcohol. Conditions: lactide:Cu = 100:1, BnOH:Cu = 0 (stars), 1 (squares, combined data of several experiments), 2 (triangles), 4 (diamonds), and 8 (circles). The solid lines represent theoretical conversions with the pseudo-first-order rate constant determined from the linear region of the semilogarithmic plot at the beginning of the reaction.

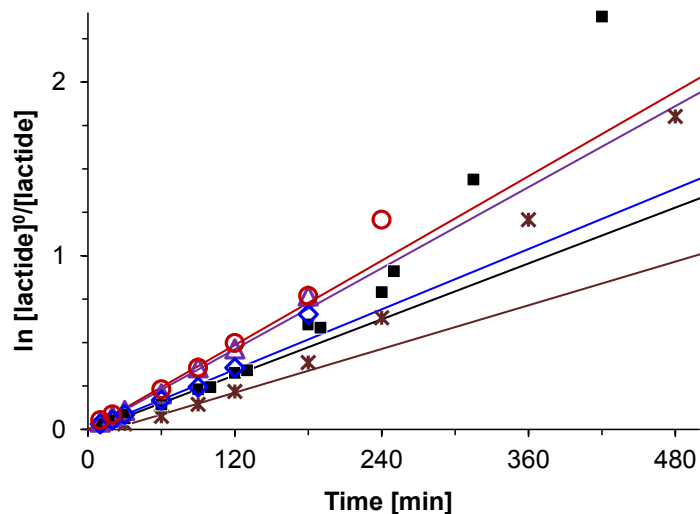


**Figure 8.S3.** Semilogarithmic conversion-time plot for *rac*-lactide polymerizations with **8.4** at 140 °C in the presence of different amounts of benzyl alcohol. Conditions: lactide:Cu = 100:1, BnOH:Cu = 0 (stars), 1 (squares, combined data of several experiments), 2 (triangles), 4 (diamonds), and 8 (circles). The solid line represent theoretical conversions with the pseudo-first-order rate constant determined from the linear region of the semilogarithmic plot at the beginning of the reaction.

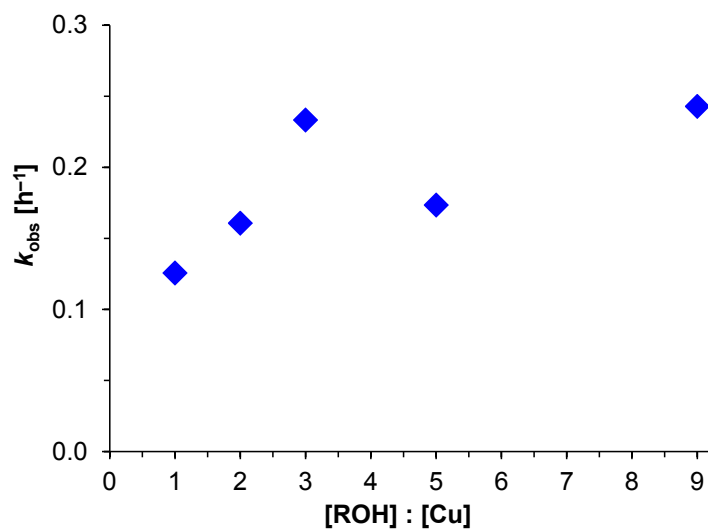


**Figure 8.S4.** Dependence of the pseudo-first-order rate constants for *rac*-lactide polymerizations with **8.4** at 140 °C on the amount of alcohol present. **8.4** contains 1 equiv MeOH in its crystal structure. No addition of alcohol thus represents ROH:Cu = 1:1.

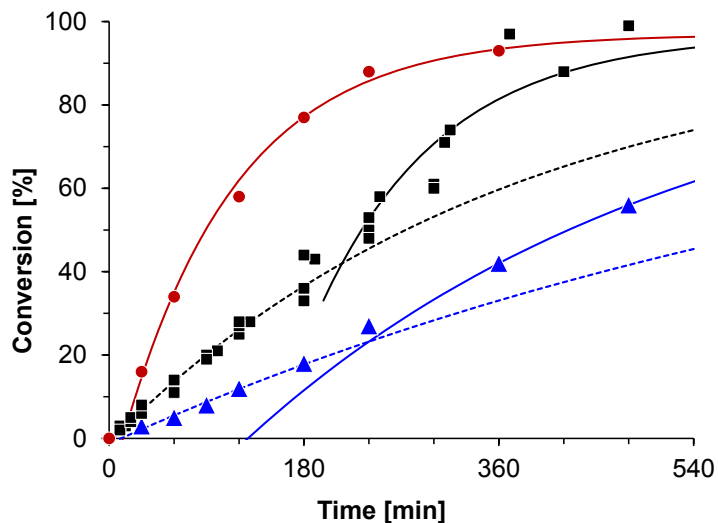


**Figure 8.S5.** Conversion-time plot for *rac*-lactide polymerizations with **8.4** at 140 °C at different lactide:catalyst ratios. Conditions: lactide:Cu:BnOH = 200:1:1 (triangles), 100:1:1 (squares, combined data of several experiments), 50:1:1 (circles). The solid line represent theoretical conversion with the pseudo-first-order rate constant determined from the linear regions of the semilogarithmic plot.

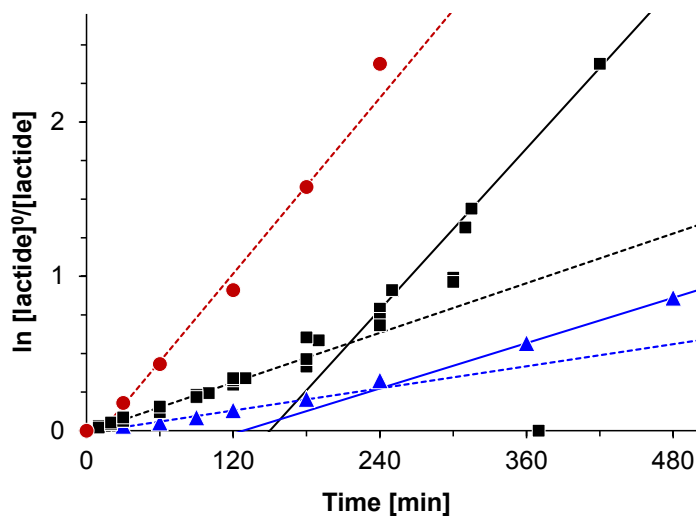


**Figure 8.S6.** Semilogarithmic conversion-time plot for *rac*-lactide polymerizations with **8.4** at 140 °C at different lactide:catalyst ratios. Conditions: lactide:Cu:BnOH = 200:1:1 (triangles), 100:1:1 (squares, combined data of several experiments), 50:1:1 (circles). The lines represent theoretical conversion with the pseudo-first-order rate constant determined from the linear regions.

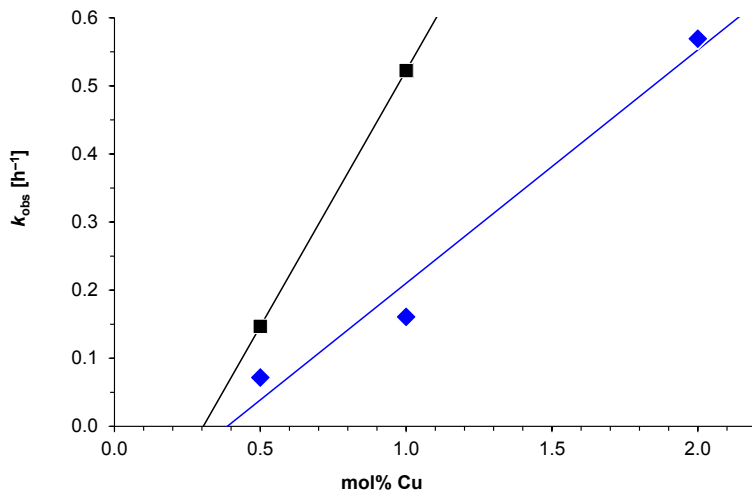


**Figure 8.S7.** Dependence of the pseudo-first order rate constants on the ratio of **8.4**:lactide in lactide polymerizations with **8.4** at 140 °C. Diamonds: rate constants determined from the slower, initial part of the reaction, squares: rate constants determined from the later, faster part of the reaction.

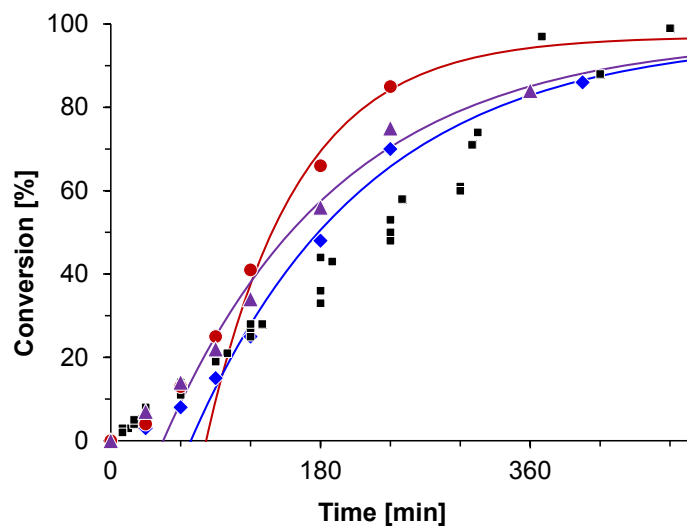


**Figure 8.S8.** Conversion-time plots for *rac*-lactide polymerizations with **8.4** at 140 °C with the addition of bases. Conditions: lactide: **8.4**:BnOH:base = 100:1:1:1, base = none (squares, combined data of several experiments), NEt<sub>3</sub> (diamonds), pyridine (circles), or KO*t*Bu (triangles). The solid lines represent theoretical conversions with the pseudo-first-order rate constant determined from the linear regions of the semilogarithmic plot after the induction period.

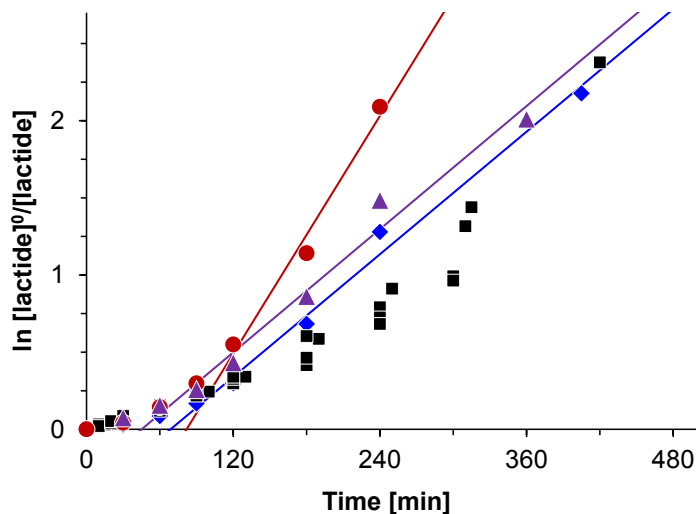


**Figure 8.S9.** Semilogarithmic conversion-time plots for *rac*-lactide polymerizations with **8.4** at 140 °C with the addition of bases. Conditions: lactide: **8.4**:BnOH:base = 100:1:1:1, base = none (squares, combined data of several experiments), NEt<sub>3</sub> (diamonds), pyridine (circles), or KOtBu (triangles). The solid lines represent theoretical conversions with the pseudo-first-order rate constant determined from the linear regions of the semilogarithmic plot after the induction period.

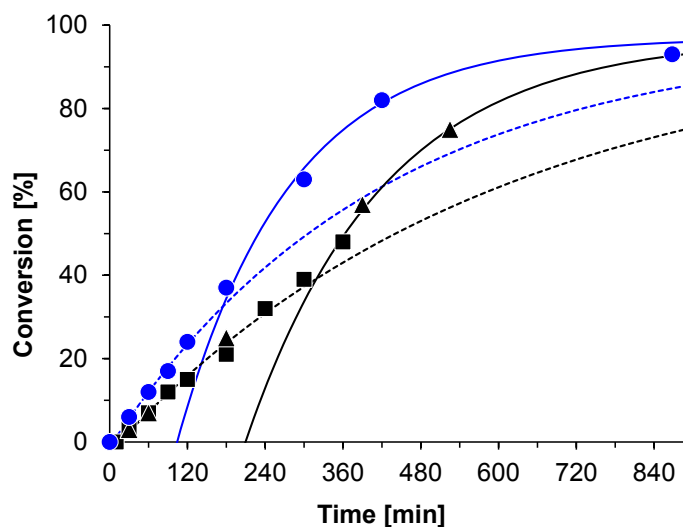


**Figure 8.S10.** Conversion-time plots for *rac*-lactide polymerizations with **8.5** at 140 °C. Conditions: lactide: **8.5**:BnOH = 100:1:1 (squares, triangles), 100:1:4 (circles). The solid lines represent theoretical conversions with the pseudo-first-order rate constant determined from the linear regions of the semilogarithmic plot.

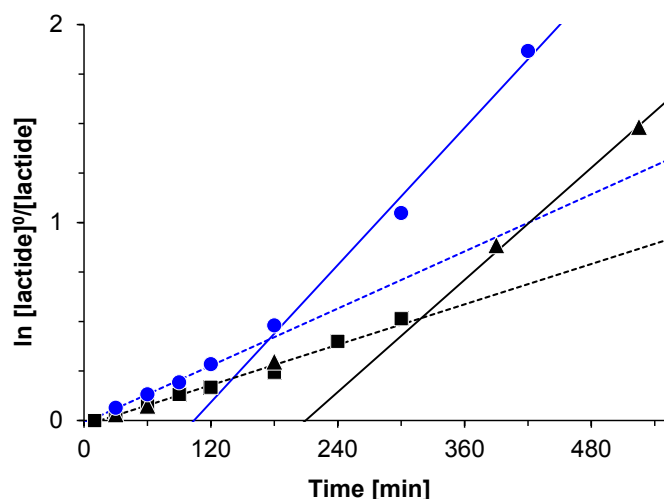


**Figure 8.S11.** Semilogarithmic conversion-time plots for *rac*-lactide polymerizations with **8.5** at 140 °C. Conditions: lactide: **8.5**:BnOH = 100:1:1 (squares, triangles), 100:1:4 (circles). The solid lines represent theoretical conversions with the pseudo-first-order rate constant determined by linear regression from the linear regions of the semilogarithmic plot.

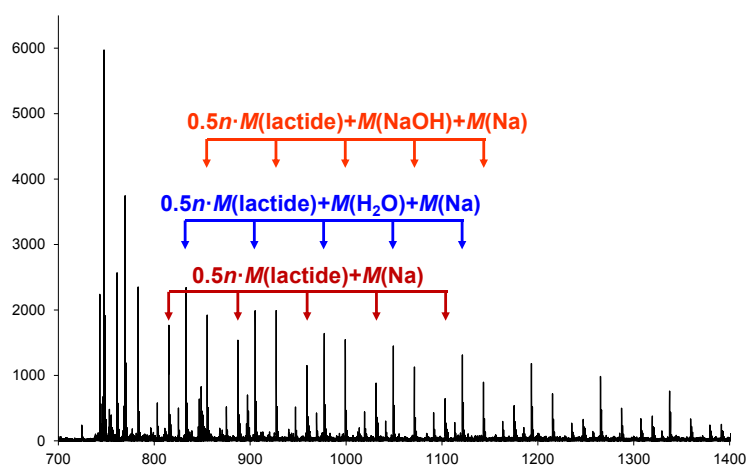


**Figure 8.S12.** MALDI-MS of PLA produced with **8.1**. The red series of  $m/z = 0.5n \cdot M(\text{lactide}) + M(\text{Na})$  is indicative of cyclic oligomers formed by intramolecular transesterification. The blue series of  $m/z = 0.5n \cdot M(\text{lactide}) + M(\text{Na}) + M(\text{H}_2\text{O})$  are hydroxyl-terminated linear oligomers, either from initiation by water or – most likely – from opening of cyclic oligomers by water under MS conditions. A smaller series of  $m/z = 0.5n \cdot M(\text{lactide}) + M(\text{H}) + M(\text{MeOH})$  is likewise visible, as is a series of  $m/z = 0.5n \cdot M(\text{lactide}) + M(\text{NaOH}) + M(\text{Na})$ .



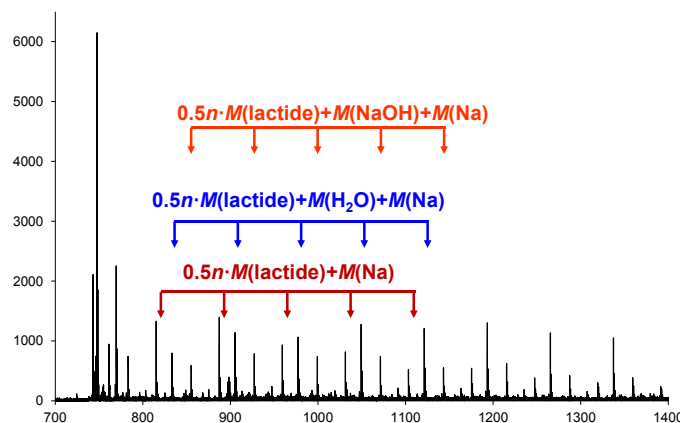


**Figure 8.S13.** MALDI-MS of PLA produced with **8.3**. The red series of  $m/z = 0.5n \cdot M(\text{lactide}) + M(\text{Na})$  is indicative of cyclic oligomers formed by intramolecular transesterification. The blue series of  $m/z = 0.5n \cdot M(\text{lactide}) + M(\text{Na}) + M(\text{H}_2\text{O})$  are hydroxyl-terminated linear oligomers, either from initiation by water or – most likely – from opening of cyclic oligomers by water under MS conditions. Accompanied by the same series after deprotonation of the carboxylate with  $m/z = 0.5n \cdot M(\text{lactide}) + M(\text{NaOH}) + M(\text{Na})$ .

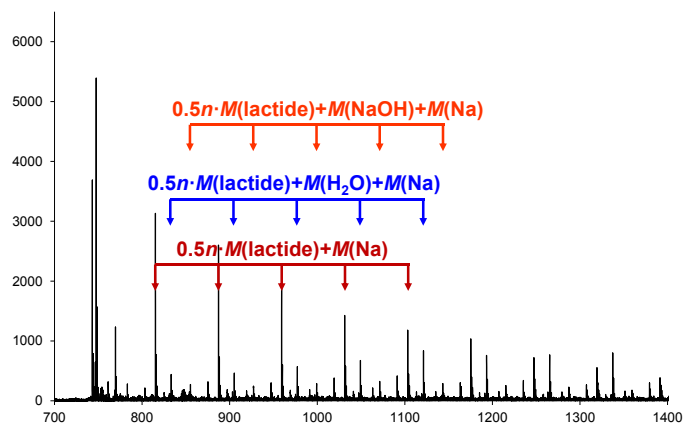


**Figure 8.S14.** MALDI-MS of PLA produced with **8.5**. The red series of  $m/z = 0.5n \cdot M(\text{lactide}) + M(\text{Na})$  is indicative of cyclic oligomers formed by intramolecular transesterification. The blue series of  $m/z = 0.5n \cdot M(\text{lactide}) + M(\text{Na}) + M(\text{H}_2\text{O})$  are hydroxyl-terminated linear oligomers, either from initiation by water or – most likely – from opening of cyclic oligomers by water under MS conditions. A smaller series of  $m/z = 0.5n \cdot M(\text{lactide}) + M(\text{H}) + M(\text{MeOH})$  is likewise visible, as is a series of  $m/z = 0.5n \cdot M(\text{lactide}) + M(\text{NaOH}) + M(\text{Na})$ .

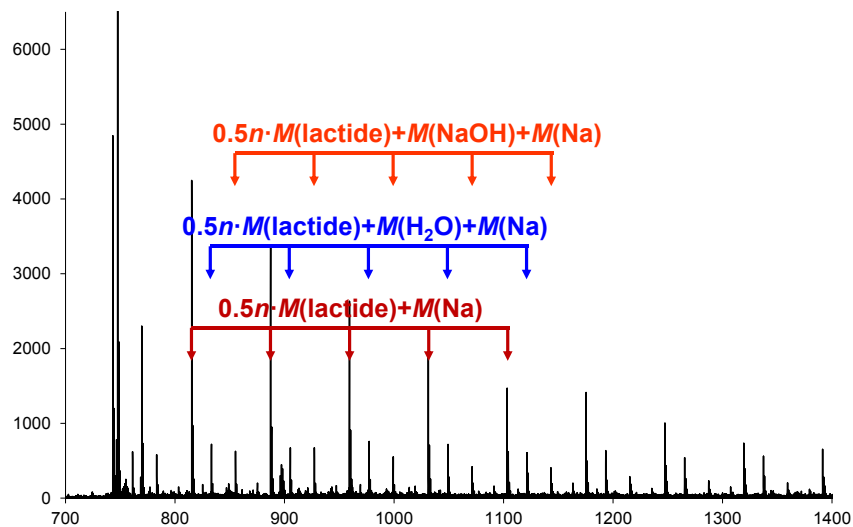


**Figure 8.S15.** MALDI-MS of PLA produced with **8.6**. The red series of  $m/z = 0.5n \cdot M(\text{lactide}) + M(\text{Na})$  is indicative of cyclic oligomers formed by intramolecular transesterification. The blue series of  $m/z = 0.5n \cdot M(\text{lactide}) + M(\text{Na}) + M(\text{H}_2\text{O})$  are hydroxyl-terminated linear oligomers, either from initiation with water or – most likely – from opening of cyclic oligomers by water under MS conditions. Also visible is the deprotonated linear chain with  $m/z = 0.5n \cdot M(\text{lactide}) + M(\text{NaOH}) + M(\text{Na})$ .

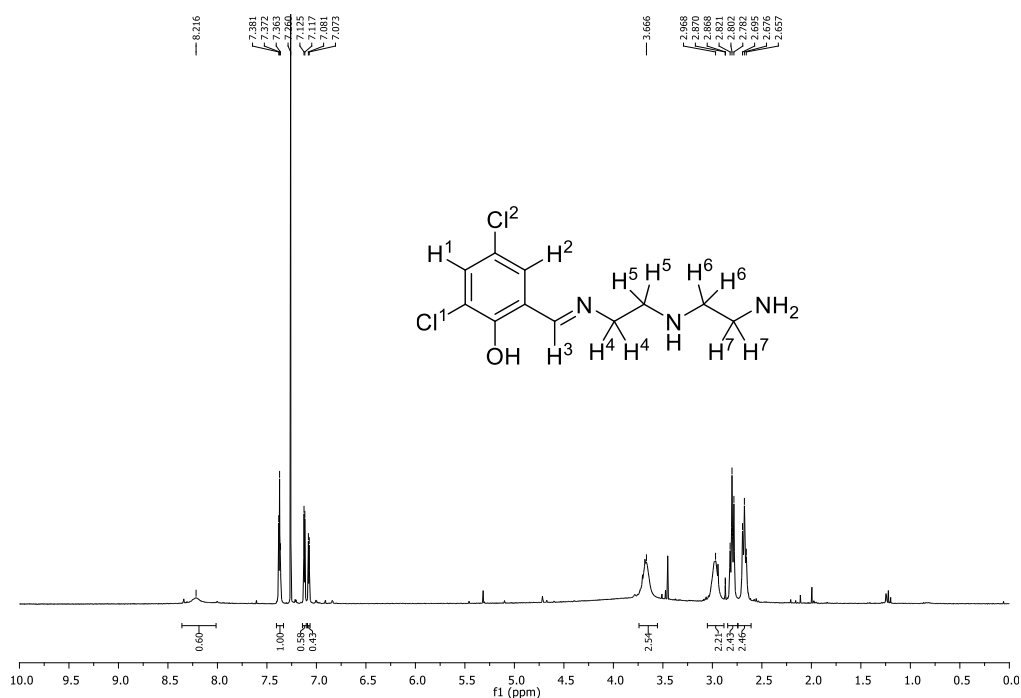


**Figure 8.S16.**  $^1\text{H}$  NMR spectrum (300 MHz) of ligand **8.L2H** in  $\text{CDCl}_3$ .



